

**UNIVERSIDAD DE SEVILLA
ESCUELA SUPERIOR DE INGENIEROS**



TESIS DOCTORAL

**ANALYSIS AND EXPERIMENTAL
CHARACTERIZATION OF NONLINEAR
CIRCUITS APPLIED TO WIRELESS
COMMUNICATIONS SYSTEMS**

**AUTOR: María José Madero Ayora
DIRECTOR: Dr. Carlos Crespo Cadenas**

Sevilla, 2008

**UNIVERSIDAD DE SEVILLA
ESCUELA SUPERIOR DE
INGENIEROS**



TESIS DOCTORAL

**ANALYSIS AND EXPERIMENTAL
CHARACTERIZATION OF NONLINEAR
CIRCUITS APPLIED TO WIRELESS
COMMUNICATIONS SYSTEMS**

MARÍA JOSÉ MADERO AYORA

2008

**UNIVERSIDAD DE SEVILLA
DEPARTAMENTO DE TEORÍA DE LA SEÑAL
Y COMUNICACIONES
ESCUELA SUPERIOR DE INGENIEROS**

TESIS DOCTORAL

**ANALYSIS AND EXPERIMENTAL
CHARACTERIZATION OF NONLINEAR
CIRCUITS APPLIED TO WIRELESS
COMMUNICATIONS SYSTEMS**

AUTOR: María José Madero Ayora
Ingeniero de Telecomunicación

DIRECTOR: Carlos Crespo Cadenas
Profesor Titular del Depto. de Teoría de la Señal y
Comunicaciones. Universidad de Sevilla

Sevilla, 2008

Firma del Director de la Tesis

Fdo.: Prof. Dr. Carlos Crespo Cadenas

Firma del Doctorando

Fdo.: María José Madero Ayora

A mi familia.

To my family.

AGRADECIMIENTOS

Quisiera expresar mi más sincero agradecimiento a todas las personas que han contribuido a la realización de esta Tesis, y en especial:

En primer lugar y ante todo, al Prof. Carlos Crespo, por haberme dado la oportunidad de unirme al Grupo de Sistemas de Radiocomunicación y compartir conmigo su experiencia y profundos conocimientos investigadores, por su apoyo en mi formación docente, y por su paciencia, accesibilidad y entusiasmo al dirigir esta Tesis.

Al Prof. Javier Reina, a quien también considero responsable de la formación docente e investigadora recibida, por su inestimable ayuda y generosidad.

Al Prof. José Ignacio Acha, Director del Departamento de Teoría de la Señal y Comunicaciones de la Universidad de Sevilla, por la confianza depositada en mí durante estos años.

A los Profs. Thomas J. Brazil y José Carlos Pedro, por el tiempo dedicado a evaluar esta Tesis. Mi especial agradecimiento al Prof. Thomas J. Brazil y a todo su equipo de investigación, por su cálida acogida y su ayuda durante mi estancia en University College Dublin.

A todos los miembros del Departamento de Teoría de la Señal y Comunicaciones de la Universidad de Sevilla, por la educación recibida de ellos como estudiante, y por sus consejos y compañerismo en la actualidad. Entre ellos, quisiera expresar mi especial gratitud al Prof. Justo Calvo, mi mentor en el Programa de Formación de Profesores Noveles, y al Prof. Rubén Martín, por sugerirme la realización de los estudios de doctorado.

Agradezco la financiación recibida de la Comisión Interministerial de Ciencia y Tecnología (CICYT), a través de los proyectos TIC2001-0751-C04-04 y TEC2004-06451-

C05-03, y la Ayuda de movilidad recibida de la Universidad de Sevilla que hizo posible mi estancia de investigación en Dublín.

Hago también extensivo mi agradecimiento a José Alberto Villegas, Guadalupe Toscano, Laura Vergillos, Carlos Matabuena, Ana Belén Madera, y Pedro Robustillo, entre otros, por contribuir en la implementación de la plataforma de medidas.

Quisiera dar las gracias a todos mis amigos, por estar siempre a mi lado a lo largo de todas las experiencias que hemos vivido juntos.

No puedo terminar sin expresar lo enormemente agradecida que me siento hacia mi familia. En particular, por supuesto, a mis padres, Vicente Madero y María José Ayora, y a mi hermano, Vicente, por sus constantes ánimos y cariño. A ellos está dedicada esta Tesis.

ACKNOWLEDGEMENTS

I would like to express my sincere gratefulness to all the people that have contribute to the fulfillment of this Thesis, and specially:

First and foremost, to Prof. Carlos Crespo, for giving me the opportunity to join the Radiocommunication Systems Group and sharing with me his expertise and research insight, for his support in my training as a teacher, and for his patience, accessibility and enthusiasm while supervising this Thesis.

To Prof. Javier Reina, to whom I also considered responsible of my instruction as a teacher and researcher, for his invaluable help and generosity.

To Prof. José Ignacio Acha, Head of the Signal Theory and Communications Department of the University of Seville, for having trusted in me during these years.

To Profs. Thomas J. Brazil and José Carlos Pedro, for taking the time to evaluate this Thesis. Special thanks to Prof. Thomas J. Brazil and all his research team, for their warm welcome and assistance during my stay at University College Dublin.

To everybody at the Signal Theory and Communications Department of the University of Seville, for the education received from them as a student, and for their advice and comradeship nowadays. Among them, I would like to express my special gratitude to Prof. Justo Calvo, my mentor in the Training Programm for Novice Teachers, and Prof. Rubén Martín, for suggesting me to enrol on the doctoral studies.

I gratefully acknowledge the financial support provided by the Spanish National Board of Scientific and Technological Research (CICYT) under projects TIC2001-0751-C04-04 and TEC2004- 06451-C05-03, and the grant received from the University of Seville that made possible my research stay in Dublin.

Special thanks must go also to José Alberto Villegas, Guadalupe Toscano, Laura Vergillos, Carlos Matabuena, Ana Belén Madera, and Pedro Robustillo, among others,

for contributing to the implementation of the characterization setup.

I wish to thank all my friends for being always by my side through all the experiences we have lived together.

I cannot finish without saying how grateful I am to my family. Particular thanks, of course, to my parents, Vicente Madero and María José Ayora, and to my brother, Vicente, for their constant encouragement and love. To them I dedicate this Thesis.

Introducción

Durante los últimos años hemos sido testigos de la consolidación de las tecnologías inalámbricas y móviles, en lo que ha venido a llamarse la “sociedad de la información”. La enorme presencia de las redes inalámbricas ha sido posible gracias a destacados logros en el campo del hardware. En el área de las comunicaciones móviles, por ejemplo, el establecimiento de la Tercera Generación de sistemas celulares y la inminente llegada de los sistemas de Cuarta Generación han impulsado el estudio de nuevas técnicas para dar respuesta a la demanda de mayores tasas de transferencia de información, número de usuarios y movilidad. Cuando se desean mayores tasas de transferencia es necesario emplear formatos de modulación más complejos, normalmente con cada vez mayores anchos de banda [1]. El aumento en el número de usuarios hace necesario minimizar la distorsión introducida por los circuitos inalámbricos para evitar interferencias de las señales de unos usuarios con las de otros en el espectro limitado que les ha sido asignado [2]. Por último, la búsqueda de movilidad exige sistemas altamente integrados en los que son prioritarios un bajo consumo y coste [3].

De entre los más de un millón de transistores que contienen los dispositivos inalámbricos de bolsillo hoy en día, sólo una pequeña fracción opera en el rango de RF y el resto realiza procesado de baja frecuencia de la señal de banda base, puesto que la mayor parte de los sistemas actuales están basados en procesadores digitales de señal (DSPs¹) [4], [5], [6]. Sin embargo, la sección de RF analógica sigue siendo el cuello de botella del transceptor completo [7]. De entre los bloques básicos que se incluyen en

¹Al final del documento se puede encontrar una lista completa de las abreviaturas y símbolos que se han usado en esta Tesis.

un enlace típico transmisor-receptor para comunicaciones inalámbricas destacan los amplificadores y mezcladores, que pueden dar lugar a importantes efectos no lineales. La operación no lineal no es fácil de describir analíticamente, por lo que obtener diseños optimizados es complejo. Entre los efectos de la distorsión no lineal, es necesario tener en cuenta la distorsión de intermodulación y el recrecimiento espectral, puesto que estos efectos no se pueden eliminar mediante filtrado y producen interferencia de canal adyacente [8].

El diseño asistido por ordenador (CAD) juega un papel primordial como parte del proceso de síntesis de circuitos no lineales, cuya principal motivación es desarrollar productos competitivos en el menor tiempo posible [9]. Puesto que no existen ni métodos ni modelos universales para los circuitos no lineales, cada modelo y cada técnica de simulación resultarán adecuados sólo para aplicaciones específicas [10]. Sin embargo, dos de las herramientas más extendidas para el análisis de sistemas no lineales son el Balance Armónico [11], [12] y la representación mediante series de Volterra [13], [14], [15], [16]. El Balance Armónico es una técnica iterativa para analizar el régimen permanente con especial aplicación en el caso general de circuitos no lineales. Debido a las limitaciones prácticas que presentan los desarrollos en series de Volterra para circuitos fuertemente no lineales o de gran tamaño, el Balance Armónico es el método preferido en esos casos. Puede verse como una extensión del análisis fasorial para el caso no lineal y se ha convertido en una herramienta madura en el caso de entradas senoidales que incluyen todas las herramientas CAD comerciales más importantes. Presenta excelentes propiedades de convergencia cuando se combina con los algoritmos de Newton-Raphson para la resolución de los sistemas de ecuaciones no lineales a los que se da lugar. La principal restricción para las técnicas clásicas de Balance Armónico es que el tipo de excitaciones que pueden manejar de forma eficiente se limita a señales periódicas y cuasi-periódicas con un número limitado de componentes frecuenciales.

Una figura de mérito que se ha venido empleando en el diseño de circuitos para los sistemas de comunicaciones inalámbricas actuales es la relación de potencia en el canal adyacente (ACPR). Sin embargo, la evaluación precisa de esta cantidad, y otras características relacionadas, en amplificadores y mezcladores excitados por señales moduladas digitalmente resulta una tarea con una complejidad computacional elevada que hace ineficientes las técnicas clásicas de Balance Armónico. Por ello, se han propuesto métodos de envolvente [17], [18], [19] o algoritmos de Balance Armónico orientados a modulación [20], que tratan específicamente este problema y permiten el análisis eficiente de circuitos con un gran número de líneas espectrales. A pesar de esto, sigue siendo necesario disponer de métodos alternativos que consigan una mayor reducción del tiempo de computación.

Por otro lado, la representación en series de Volterra se ha empleado para describir una amplia variedad de fenómenos no lineales. Normalmente se acepta que la aplicación de las series de Volterra se limita al estudio de sistemas débilmente no lineales y bajas distorsiones. Sin embargo, las series de Volterra permiten obtener expresiones cerradas que describen el comportamiento del sistema, frente a otras técnicas basadas en algoritmos de iteración numérica. Este tipo de información resulta de gran interés para llegar a comprender los mecanismos que producen los efectos de memoria [21].

Normalmente, los requisitos mencionados para los circuitos inalámbricos están contrapuestos. Por ejemplo, para un amplificador de potencia en el transmisor o receptor, la eficiencia suele disminuir a medida que se va ganando linealidad en el circuito y, por tanto, disminuye la distorsión. La solución de compromiso consiste en aplicar técnicas especiales para linealizar las características del amplificador sin degradar la eficiencia [22], [23]. Sin embargo, un incremento en el ancho de banda suele conducir a esquemas de linealización ineficaces debido al comportamiento dependiente del ancho de banda o efectos de memoria que presentan los amplificadores de potencia [24], [25].

Un asunto a tener en cuenta finalmente es que la mayor parte de los modelos para dispositivos no lineales se obtienen a partir de medidas. En este trabajo se revisan los procedimientos para la caracterización no lineal y sus figuras de mérito asociadas, dado el importante papel que juegan. Puesto que los dispositivos no lineales no cumplen con el principio de superposición, su respuesta presentará características diferentes en función de cuál sea la excitación empleada [26]. Por eso, se consideran principalmente tres tipos de entradas: un único tono, dos tonos y señales moduladas de espectro continuo. De entre ellas, las medidas de intermodulación de dos tonos ocupan una posición destacada y comprender sus particularidades centra la atención de muchos investigadores [27], [28], [29]. Por un lado, se puede emplear una prueba de dos tonos con separación variable entre los tonos para la caracterización experimental de los efectos de memoria, siendo aconsejables medidas tanto de la magnitud como de la fase de los productos de intermodulación. Por otro lado, partiendo de una prueba de dos tonos es posible predecir el comportamiento de las componentes de distorsión para señales multitono [30] y para modulaciones más complejas [31].

La presente Tesis pretende dar una visión amplia y detallada sobre el análisis de circuitos no lineales para comunicaciones inalámbricas. Partiendo de una revisión del estado del arte de los métodos de análisis no lineal, los enfoques estudiados incluyen la aplicación del algoritmo de Newton Simplificado a la solución de circuitos débilmente no lineales [32]. La aplicación de este método constituye una herramienta novedosa adecuada para el análisis de circuitos que contengan tanto amplificadores como mezcladores [33]. Como ventaja adicional del método de Newton Simplificado,

se demuestra que permite la obtención de expresiones teóricas para modelar la dependencia con la frecuencia de banda base de la distorsión de intermodulación en amplificadores con memoria [34], de forma análoga a la representación mediante series de Volterra. La contribución final que se presentará consiste en un modelo basado en impedancias para amplificadores con transistores FET o amplificadores comerciales, propuesto para tener en cuenta los efectos de memoria en la intermodulación sin importar cuál sea su naturaleza [35].

El objetivo principal de esta Tesis consiste en contribuir al estudio y desarrollo de nuevas técnicas de análisis para sistemas no lineales aplicados a comunicaciones inalámbricas. Este objetivo general se puede dividir en los siguientes:

- Desarrollo de una herramienta de análisis para circuitos débilmente no lineales bajo señales de comunicaciones moduladas digitalmente de banda estrecha.
- Estudio de la dependencia del ancho de banda o efectos de memoria de la distorsión de intermodulación.
- Caracterización experimental de la distorsión no lineal y los efectos de memoria en amplificadores de potencia de RF.

Métodos basados en envolventes para sistemas no lineales de comunicaciones inalámbricas

Método de las Envolventes de Corriente

El Método de las Envolventes de Corriente (EC) [18] fue presentado por Borich *et al.* en 1999 como una herramienta eficiente para la simulación de circuitos de comunicaciones operados en régimen débilmente no lineal. Este método puede considerarse una extensión eficiente del Método de las Corrientes No Lineales (NC) [13] para señales de comunicaciones digitales.

Para conseguir una reducción considerable del tiempo de simulación, se asume un comportamiento no lineal débil de los circuitos. Aunque los dispositivos amplificadores de microondas se emplean cada vez más próximos a la saturación para conseguir mayores potencias de salida y mejor eficiencia, sigue siendo necesaria una alta linealidad para que obtener mejores prestaciones del sistema. Por eso, en muchos casos los circuitos de comunicaciones inalámbricos se operan en un régimen débilmente no lineal. Los métodos basados en Balance Armónico o los métodos híbridos

en tiempo-frecuencia convergen de manera más rápida para los circuitos débilmente no lineales que para el caso fuertemente no lineal debido al menor número de iteraciones que son necesarias. Sin embargo, no se llega a explotar directamente la característica cuasi-lineal, de modo que la mejora en la velocidad de simulación sólo es modesta. En el método EC se consigue una mejora significativa del tiempo de simulación asumiendo una excitación de banda estrecha y una no linealidad débil.

Para la aplicación de este método se formula el problema a partir de las ecuaciones procedentes del análisis nodal modificado del circuito equivalente para el dispositivo a tratar. Se considera que las tensiones nodales del circuito vienen dadas por una suma de tensiones incrementales:

$$v(t) = V_0 + v_1(t) + \dots + v_n(t), \quad (0.1)$$

donde la tensión V_0 representa la componente de continua. Los elementos no lineales se representan a través de series de potencias alrededor del punto de polarización con un número finito N de términos:

$$\begin{aligned} i_g(t) &= \sum_{k=1}^N g_k v^k(t), \\ i_c(t) &= \sum_{k=0}^N c_k v^k(t) \frac{dv_c(t)}{dt}, \\ i(t) &= \sum_{k=1}^N g_{k0} v^k(t) + \sum_{l=1}^N g_{0l} u^l(t) + \sum_{k=1}^N \sum_{l=1}^3 g_{kl} v^k(t) u^l(t). \end{aligned} \quad (0.2)$$

De acuerdo con la suposición débilmente no lineal, se asume que las no linealidades de los elementos son suficientemente suaves para que las corrientes de las conductancias, las capacidades y las fuentes dependientes se puedan aproximar por los primeros términos de sus desarrollos en series de potencias. En el método EC se extienden los sumatorios hasta $N = 3$.

Las corrientes de excitación del circuito serán señales moduladas de banda estrecha de la forma:

$$i_s(t) = \text{Re} \{ \tilde{i}_s(t) e^{j\omega_c t} \}. \quad (0.3)$$

En este caso, cualquier variable del circuito toma la siguiente forma para la iteración de orden n :

$$x_n(t) = \frac{1}{2} \sum_{h=-n}^n \tilde{x}_n(h, t) e^{jh\omega_c t}, \quad (0.4)$$

donde $\tilde{x}_n(h, t)$ es la envolvente compleja de la señal alrededor del h -ésimo armónico de ω_c . Nótese que estamos extendiendo los sumatorios hasta n , puesto que se aplica el método NC y las corrientes no lineales que se emplean no superan el orden n coincidente con la iteración realizada. Puesto que las componentes de $x_n(h, t)$ centradas en

$-\omega_c, \dots, -n\omega_c$ son los complejos conjugados de aquellas centradas en $\omega_c, \dots, n\omega_c$, es habitual tratar sólo con frecuencias positivas, cuya representación en el dominio de la frecuencia es:

$$X_n(\omega) = \sum_{h=0}^n \tilde{X}_{n,h}(\omega - h\omega_c). \quad (0.5)$$

En el método EC se realizan dos suposiciones básicas: la primera de ellas consiste en realizar un tratamiento cuasi-periódico de las envolventes complejas alrededor de cada armónico de ω_c , es decir, aproximar las envolventes complejas por señales periódicas representando cada envolvente compleja $\tilde{x}_n(h, t)$ mediante un número discreto de sinusoides e introducir una representación mediante series de Fourier.

Bajo esta suposición, el sistema de ecuaciones en el dominio de la frecuencia equivalente al que se resuelve en el método NC puede expresarse:

$$\begin{aligned} \mathbf{Y}(\omega) \tilde{\mathbf{V}}_{n,h}(\omega - h\omega_c) &= \tilde{\mathbf{I}}_{n,h}(\omega - h\omega_c) \\ n = 1, \dots, N, \quad h = 0, \dots, H, \end{aligned} \quad (0.6)$$

donde $\mathbf{Y}(\omega)$ es la matriz de admitancias de los nodos del subcircuito lineal aumentado, formado por todos los elementos lineales junto con los términos lineales de la representación en series de potencias de los elementos no lineales. $\tilde{\mathbf{V}}_{n,h}(\omega - h\omega_c)$ e $\tilde{\mathbf{I}}_{n,h}(\omega - h\omega_c)$ son los vectores con las envolventes complejas de las tensiones de los nodos y de las corrientes de excitación para la n -ésima iteración, evaluadas alrededor del h -ésimo armónico. En principio, es posible resolver directamente el sistema de ecuaciones (0.6) para encontrar $\tilde{\mathbf{V}}_{n,h}(\omega - h\omega_c)$, aunque éste no es un enfoque eficiente. Las envolventes deben ser muestreadas para largos intervalos de tiempo, lo que suele dar lugar a varios miles de componentes frecuenciales y supondría tener que realizar la evaluación y factorización de $\mathbf{Y}(\omega)$ en miles de puntos de frecuencia.

Por eso, la segunda suposición que se tiene en cuenta en este método se basa en el hecho de que, si la excitación es de banda estrecha, el espectro de las formas de onda del circuito se concentra en bandas estrechas alrededor de $h\omega_c$. Así, es posible realizar una expansión en serie de Taylor con un orden bajo de la representación en frecuencia de la matriz de admitancia alrededor de cada armónico de ω_c sin cometer un error significativo. En este método se considera que una aproximación de primer orden es suficiente en general, es decir:

$$\begin{aligned} \mathbf{Y}(\omega) &\simeq \mathbf{Y}(h\omega_c) + \mathbf{\Omega}_h \mathbf{Y}'(h\omega_c), \quad h = 0, \dots, n \\ \mathbf{\Omega}_h &= \text{diag}(\omega - h\omega_c) \end{aligned} \quad (0.7)$$

aunque se pueden tener en cuenta desarrollos en serie de mayor orden si se desea mayor precisión al predecir los cambios con la frecuencia de modulación que se producen en las componentes de distorsión, es decir, para tratar los efectos de la memoria de manera más rigurosa.

Si se sustituye (0.7) en (0.6) y se realiza una transformada inversa de Fourier para recuperar las expresiones de las tensiones de los nodos en el dominio de la frecuencia, se obtiene la siguiente expresión:

$$\left[\mathbf{Y}(h\omega_c) - j\mathbf{Y}'(h\omega_c)\frac{d}{dt} \right] \tilde{\mathbf{v}}_n(h, t) = \tilde{\mathbf{i}}_n(h, t), \quad (0.8)$$

$$n = 1, \dots, N, \quad h = 0, \dots, n$$

donde $\tilde{\mathbf{v}}_n(h, t)$ es el vector solución con las formas de onda de las envolventes complejas de las tensiones alrededor de hf_c para la corriente no lineal de orden n -ésimo. La aplicación de esta ecuación (0.8) constituye el método de las Envolventes de Corriente. Para cada n y cada h , (0.8) es un sistema de ecuaciones diferenciales lineales en las envolventes complejas de las tensiones de los nodos. Cuando se aplica este algoritmo hasta $N = H = 3$, en total aparecen doce sistemas de ecuaciones, aunque algunos tienen soluciones triviales y otros no resultan de interés. Finalmente, sólo es necesario resolver cuatro sistemas de ecuaciones.

Las envolventes de corriente que aparecen en el lado derecho de (0.8) se obtienen de sustituir en las expresiones de las corrientes no lineales del método NC la representación en función de las envolventes complejas de las tensiones de los nodos que hemos adoptado, (0.4), y después recoger todos los términos centrados en la frecuencia $h\omega_c$. Los resultados de este procedimiento son los siguientes:

- Para la solución del primer orden ($n = 1$), la envolvente de corriente es la envolvente de la fuente de señal original del circuito.
- Para el segundo orden ($n = 2$), hay dos envolventes de corriente correspondientes a la componente de banda base y a la componente centrada en $2\omega_c$. Las expresiones que toman las envolventes de corrientes del segundo orden para los distintos tipos de elementos no lineales son las siguientes:

– Para una conductancia no lineal:

$$\tilde{i}_2(0, t) = -\frac{g_2}{2} |\tilde{v}_1(1, t)|^2 \quad (0.9)$$

$$\tilde{i}_2(2, t) = -\frac{g_2}{2} \tilde{v}_1^2(1, t)$$

– Para una fuente de corriente dependiente de dos tensiones:

$$\tilde{i}_2(0, t) = -\left[\frac{g_{20}}{2} |\tilde{v}_1(1, t)|^2 + \frac{g_{02}}{2} |\tilde{u}_1(1, t)|^2 + \frac{g_{11}}{2} \text{Re}\{\tilde{v}_1(1, t)\tilde{u}_1^*(1, t)\} \right] \quad (0.10)$$

$$\tilde{i}_2(2, t) = -\left[\frac{g_{20}}{2} \tilde{v}_1^2(1, t) + \frac{g_{02}}{2} \tilde{u}_1^2(1, t) + \frac{g_{11}}{2} \tilde{v}_1(1, t)\tilde{u}_1(1, t) \right]$$

- En el caso de una capacidad no lineal se ha tenido en cuenta que las derivadas pueden aproximarse actuando sólo sobre las portadoras (despreciando la variación de las envolventes frente a la de la portadora) por lo suponen la multiplicación de la contribución por el término $j\hbar\omega_c$. De este modo, resultan las expresiones:

$$\begin{aligned}\tilde{i}_2(0, t) &= -\frac{c_1}{4} \frac{d}{dt} (|\tilde{v}_1(1, t)|^2) \approx 0 \\ \tilde{i}_2(2, t) &\approx -j\omega_c \frac{c_1}{2} \tilde{v}_1^2(1, t)\end{aligned}\quad (0.11)$$

- Para el tercer orden ($n = 3$) hay también dos envolventes de corriente correspondientes a la componente fundamental y la componente centrada en $3\omega_c$. Sin embargo, la componente fundamental es la de mayor interés práctico. Las expresiones de las envolventes de corriente del tercer orden son las siguientes:

- Para una conductancia no lineal:

$$\begin{aligned}\tilde{i}_3(1, t) &= -\left[\frac{3g_3}{4} \tilde{v}_1^2(1, t) \tilde{v}_1^*(1, t) + 2g_2 \tilde{v}_1(1, t) \tilde{v}_2(0, t) + g_2 \tilde{v}_1^*(1, t) \tilde{v}_2(2, t) \right] \\ \tilde{i}_3(3, t) &= -\left[\frac{g_3}{4} \tilde{v}_1^3(1, t) + g_2 \tilde{v}_1(1, t) \tilde{v}_2(2, t) \right]\end{aligned}\quad (0.12)$$

- Para una fuente de corriente dependiente de dos tensiones:

$$\begin{aligned}\tilde{i}_3(1, t) &= -\left\{ \frac{3g_{30}}{4} \tilde{v}_1^2(1, t) \tilde{v}_1^*(1, t) + \frac{3g_{03}}{4} \tilde{u}_1^2(1, t) \tilde{u}_1^*(1, t) + \right. \\ &\quad 2g_{20} \left[\frac{1}{2} \tilde{v}_1^*(1, t) \tilde{v}_2(2, t) + \tilde{v}_1(1, t) \tilde{v}_2(0, t) \right] + \\ &\quad \left. 2g_{02} \left[\frac{1}{2} \tilde{u}_1^*(1, t) \tilde{u}_2(2, t) + \tilde{u}_1(1, t) \tilde{u}_2(0, t) \right] + \right. \\ g_{11} &\left[\frac{1}{2} \tilde{v}_1^*(1, t) \tilde{u}_2(2, t) + \tilde{v}_1(1, t) \tilde{u}_2(0, t) + \frac{1}{2} \tilde{u}_1^*(1, t) \tilde{v}_2(2, t) + \tilde{u}_1(1, t) \tilde{v}_2(0, t) \right] + \\ &\quad \frac{g_{21}}{4} [\tilde{v}_1^2(1, t) \tilde{u}_1^*(1, t) + 2|\tilde{v}_1(1, t)|^2 \tilde{u}_1(1, t)] + \\ &\quad \left. \frac{g_{12}}{4} [\tilde{u}_1^2(1, t) \tilde{v}_1^*(1, t) + 2|\tilde{u}_1(1, t)|^2 \tilde{v}_1(1, t)] \right\}\end{aligned}\quad (0.13)$$

$$\begin{aligned}\tilde{i}_3(3, t) &= -\left\{ \frac{g_{30}}{4} \tilde{v}_1^3(1, t) + \frac{g_{03}}{4} \tilde{u}_1^3(1, t) + \frac{g_{21}}{4} \tilde{v}_1^2(1, t) \tilde{u}_1(1, t) + \right. \\ &\quad \frac{g_{12}}{4} \tilde{u}_1^2(1, t) \tilde{v}_1(1, t) + g_{20} \tilde{v}_1(1, t) \tilde{v}_2(2, t) + g_{02} \tilde{u}_1(1, t) \tilde{u}_2(2, t) + \\ &\quad \left. \frac{g_{11}}{2} [\tilde{v}_1(1, t) \tilde{u}_2(2, t) + \tilde{u}_1(1, t) \tilde{v}_2(2, t)] \right\}\end{aligned}\quad (0.14)$$

– Para una capacidad no lineal:

$$\begin{aligned}\tilde{i}_3(1, t) &\approx -j\omega_c \left[\frac{c_2}{4} \tilde{v}_1^2(1, t) \tilde{v}_1^*(1, t) + c_1 \tilde{v}_1(1, t) \tilde{v}_2(0, t) + \frac{c_1}{2} \tilde{v}_1^*(1, t) \tilde{v}_2(2, t) \right] \\ \tilde{i}_3(3, t) &\approx -j3\omega_c \left[\frac{c_2}{12} \tilde{v}_1^3(1, t) + \frac{c_1}{2} \tilde{v}_1(1, t) \tilde{v}_2(2, t) \right]\end{aligned}\quad (0.15)$$

Para resolver el sistema de ecuaciones diferenciales lineales de las envolventes complejas de (3.32) se muestrean las formas de onda de las envolventes en M puntos a lo largo del intervalo de tiempo $(M - 1)\Delta t$, donde el paso de tiempo Δt se elige de forma adecuada. Al aplicar, por ejemplo, el método de discretización de Backward-Euler, resulta el proceso iterativo:

$$\begin{aligned}[j\mathbf{Y}'(h\omega_c) - \Delta t \cdot \mathbf{Y}(h\omega_c)] \tilde{\mathbf{v}}_n(h, t_{k+1}) &= \\ j\mathbf{Y}'(h\omega_c) \tilde{\mathbf{v}}_n(h, t_k) - \Delta t \cdot \tilde{\mathbf{i}}_n(h, t_{k+1}), & \\ \tilde{\mathbf{v}}_n(h, t_0) = 0, \quad n = 1, \dots, N, \quad h = 0, \dots, n.\end{aligned}\quad (0.16)$$

Se pueden emplear otras fórmulas de integración de mayor orden con similares resultados. Las matrices de coeficientes $[j\mathbf{Y}'(h\omega_c) - \Delta t \cdot \mathbf{Y}(h\omega_c)]$ son poco densas y se factorizan una sola vez al principio del proceso de iteración. Se puede observar que sólo es necesario almacenar y factorizar cuatro de estas matrices. Por tanto, una vez que las matrices de coeficientes se han factorizado, casi todo el tiempo de simulación se emplea en resolver sistemas lineales de ecuaciones triangulares poco densos. Esto produce una reducción bastante considerable del tiempo de simulación.

La limitación principal de este método surge de la aproximación débilmente no lineal que se ha tomado, por lo que el rango dinámico de aplicación del método se ve afectado. Al comparar los resultados obtenidos mediante el método EC con los del Balance Armónico, se observa que ambos coinciden bastante bien para niveles bajos de potencia de entrada pero el método EC empieza a separarse de la solución a medida que el amplificador se adentra en la zona de saturación y su ganancia empieza a comprimirse. Esto ocurre porque en la región de saturación los desarrollos en series de potencia de orden bajo que se han empleado no describen adecuadamente el comportamiento del dispositivo. Para superar esta limitación y mejorar la precisión del método de [18], en [36], [19] se propone un nuevo método de envolventes de corriente con rango dinámico extendido (NEC) en el que también se representa la salida del circuito como una suma de tensiones incrementales, aunque ahora cada una de estas tensiones es la solución de un circuito lineal variante en el tiempo excitado por una corriente no lineal. Para cada paso del proceso iterativo es necesario actualizar los valores de los elementos del circuito (cuya topología se mantiene invariante), además de las corrientes de excitación no lineales. Las principales ventajas de esta nueva técnica son que presenta buenas propiedades de convergencia y mejor precisión que [18], aunque aumenta el coste computacional.

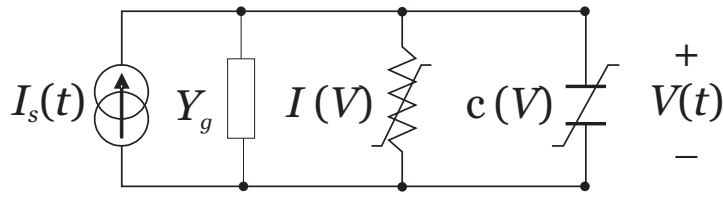


Figure 0.1: Circuito no lineal de un sólo nodo.

Método de Newton Simplificado para circuitos de comunicaciones débilmente no lineales

Una de las contribuciones originales presentadas en esta Tesis es el método de Newton Simplificado (SN) propuesto en [32] para realizar un análisis eficiente de circuitos débilmente no lineales excitados por señales de comunicaciones, que se basa en el método EC. La principal ventaja del método propuesto es la reducción de los tiempos de simulación que supone, al mismo tiempo que se consigue un buen ajuste de las simulaciones con resultados experimentales. Esta necesidad de acelerar las simulaciones proviene del gran coste computacional que suponen las predicciones de ACPR, de gran interés en procesos de diseño y optimización.

Durante décadas se han desarrollado diferentes métodos para evaluar las no-linealidades de los circuitos de microondas que pueden aplicarse también a la predicción de ACPR. Las técnicas de Balance Armónico usando el algoritmo de Newton-Raphson (HB-N) o métodos de relajación (HB-R) son ejemplos de métodos de simulación muy eficientes cuando se consideran señales periódicas o cuasi-periódicas y circuitos no lineales generales [37], [38] y [39]. Los métodos basados en envolventes suelen aplicar la aproximación de un comportamiento débilmente no lineal y resultan más eficientes para señales de comunicaciones que el empleo de las técnicas de Balance Armónico clásicas.

En este apartado se presenta un nuevo enfoque para el análisis de la distorsión en circuitos débilmente no lineales excitados con señales de RF de banda estrecha manteniendo la simplicidad del método EC, resultando aún más eficiente en tiempo de simulación.

Por claridad, se considera el circuito no lineal de un sólo nodo de la Figura 0.1, que contiene conductancias y capacidades no lineales controladas por tensión y que es excitado por una única fuente. Sean las tensiones $v(t)$ de los nodos del circuito

$$V(t) = V_0 + v_1(t) + \dots + v_n(t) + \delta v_n(t) \quad (0.17)$$

donde la tensión V_0 se corresponde con el término de continua. Los desarrollos en

series de potencias de las fuentes de corriente no lineales, $i(v)$, y las cargas no lineales, $q(v)$, se expresan en este caso alrededor del punto de polarización de dc. Este desarrollo realizado para la dc se mantendrá para todas las iteraciones, de modo que es posible distinguir en cada uno de estos elementos un primer término lineal con las tensiones de los nodos y un segundo término con una dependencia no lineal con dichas tensiones:

- Para una conductancia no lineal:

$$i[v(t)] = \sum_{k=1}^{\infty} g_k v^k(t) = g_1 v(t) + i_{NL}[v(t)] \quad (0.18)$$

- Para una fuente de corriente dependiente de dos tensiones:

$$i[v(t), u(t)] = \sum_{\substack{k,l \\ k+l \geq 1}}^{\infty} g_{kl} v^k(t) u^l(t) = g_{10} v(t) + g_{01} u(t) + i_{NL}[v(t), u(t)] \quad (0.19)$$

- Para una capacidad no lineal:

$$i_c[v(t)] = \frac{d}{dt} \sum_{k=1}^{\infty} q_k v^k(t) = c_1 \frac{dv(t)}{dt} + \frac{dq_{NL}[v(t)]}{dt} \quad (0.20)$$

La tensión del nodo en el circuito del ejemplo satisface la ecuación

$$L[V(t)] + I[V(t)] + \frac{dq[v(t)]}{dt} = I_s + i_s(t), \quad (0.21)$$

con $L[\cdot]$ un operador integro-diferencial que tiene en cuenta los elementos lineales del circuito. Para la tensión continua se resuelve:

$$L[V_0] + I[V_0] = I_s, \quad (0.22)$$

mientras que se tiene la siguiente ecuación para el resto de los términos en la tensión:

$$L[v_1(t) + \delta v_1(t)] + I[v_1(t) + \delta v_1(t)] + \frac{dq[v_1(t) + \delta v_1(t)]}{dt} = i_s(t). \quad (0.23)$$

Omitiendo la dependencia temporal explícita, se obtiene la siguiente ecuación lineal para la primera tensión incremental v_1 :

$$L[v_1] + g_1 v_1 + c_0 \frac{dv_1}{dt} = i_s \quad (0.24)$$

De nuevo, v_1 se calcula del mismo modo que el término lineal en el método NC convencional y en el método NEC. La primera tensión residual δv_1 satisface la ecuación

$$L[\delta v_1] + g_1 \delta v_1 + i_{NL}(v) + c_0 \frac{d\delta v_1}{dt} + \frac{dq_{NL}(v)}{dt} = 0. \quad (0.25)$$

Teniendo en cuenta que $\delta v_1 = v_2 + \delta v_2$, se puede evaluar la segunda tensión incremental v_2 resolviendo la siguiente ecuación lineal:

$$L[v_2] + g_1 v_2 + c_0 \frac{dv_2}{dt} = i_2(\bar{v}_1) \quad (0.26)$$

con

$$i_2(\bar{v}_1) = -i_{NL}(\bar{v}_1) - \frac{dq_{NL}(\bar{v}_1)}{dt} \quad (0.27)$$

Al generalizar estos resultados, se obtiene la siguiente ecuación para calcular cada tensión incremental v_n :

$$L[v_n] + g_1 v_n + c_0 \frac{dv_n}{dt} = i_n(\bar{v}_{n-1}) \quad (0.28)$$

con

$$i_n(\bar{v}_{n-1}) = -[i_{NL}(\bar{v}_{n-1}) - i_{NL}(\bar{v}_{n-2})] - \left[\frac{dq_{NL}(\bar{v}_{n-1})}{dt} - \frac{dq_{NL}(\bar{v}_{n-2})}{dt} \right] \quad (0.29)$$

Podemos observar que en cada iteración se realiza el desarrollo en series de Taylor alrededor del punto de polarización, por lo que en todas ellas se está resolviendo el mismo circuito lineal invariante, formado por los elementos lineales junto con los términos lineales de los elementos no lineales, como en el método EC. En cambio, las corrientes aplicadas difieren de las empleadas en el método NC, ya que en éste las expresiones de las corriente no lineales se obtienen despreciando todos los términos de orden mayor que la iteración que se está contemplando. El motivo de esto es que el método NC fue propuesto para la obtención de las funciones de transferencia no lineales que aparecen en las descripciones en series de Volterra. Por tanto, las corrientes empleadas en el método propuesto suponen una mejor aproximación de las corrientes no lineales reales que las del método NC al contemplar términos de mayor orden.

En resumen, para obtener las tensiones incrementales en un circuito genérico con más de un nodo es necesario resolver el siguiente sistema de ecuaciones:

$$L[\mathbf{v}_n] = \mathbf{i}_n, \quad n = 1, 2, \dots, N. \quad (0.30)$$

donde $L[\cdot]$ representa un operador lineal genérico en forma matricial. Este sistema de ecuaciones integro-diferenciales se obtiene mediante un análisis nodal del subcircuito lineal ampliado. Las fuentes de corriente \mathbf{i}_n que se aplican al circuito lineal invariante en el tiempo de (0.30) son como sigue:

1. En la primera iteración ($n = 1$), la corriente de excitación es la fuente de corriente original.

2. La fuente de corriente no lineal para la segunda iteración ($n = 2$) es

$$i_2 = -i_{NL}(v_1) - \frac{dq_{NL}(v_1)}{dt} = -\sum_{k=2}^{\infty} g_k v_1^k - \frac{d}{dt} \sum_{k=2}^{\infty} \frac{c_{k-1}}{k} v_1^k \quad (0.31)$$

3. Para obtener las fuentes de corriente no lineales de la tercera iteración se tiene en cuenta que:

$$i_3 = -[i_{NL}(v_2 + v_1) - i_{NL}(v_1)] - \left[\frac{dq_{NL}(v_2 + v_1)}{dt} - \frac{dq_{NL}(v_1)}{dt} \right] \quad (0.32)$$

Considerando que la tensión incremental $v_2(t)$ es pequeña comparada con el término lineal $v_1(t)$, la corriente de excitación se puede aproximar por su desarrollo en serie de Taylor de primer orden y expresar

$$i_3 = - \left. \frac{di_{NL}(v)}{dv} \right|_{v=v_1} \cdot v_2 - \left. \frac{d}{dv} \frac{dq_{NL}(v)}{dt} \right|_{v=v_1} \cdot v_2 - \left. \frac{dq_{NL}(v)}{dv} \right|_{v=v_1} \cdot \frac{dv_2}{dt}. \quad (0.33)$$

4. Este procedimiento se podría generalizar para obtener las fuentes de corriente no lineales para la n -ésima iteración

$$i_n = - \left. \frac{di_{NL}(v)}{dv} \right|_{v=v_{n-2}} \cdot v_{n-1} - \left. \frac{d}{dv} \frac{dq_{NL}(v)}{dt} \right|_{v=v_{n-2}} \cdot v_{n-1} - \left. \frac{dq_{NL}(v)}{dv} \right|_{v=v_{n-2}} \cdot \frac{dv_{n-1}}{dt}. \quad (0.34)$$

En el método propuesto el número de iteraciones para el algoritmo de (0.30) se restringe hasta $N = 3$, asumiendo un comportamiento débilmente no lineal.

En el caso de que la excitación aplicada sea una señal de RF modulada de banda estrecha, se puede seguir un procedimiento similar al del método EC y obtener el siguiente sistema lineal de ecuaciones para las envolventes complejas de las tensiones incrementales para el armónico h y la n -ésima iteración:

$$\left[\mathbf{Y}(h\omega_c) - j\mathbf{Y}'(h\omega_c) \frac{d}{dt} \right] \tilde{\mathbf{v}}_n(h, t) = \tilde{\mathbf{i}}_n(h, t). \quad (0.35)$$

Una vez que se han determinado las envolventes complejas de las corrientes no lineales, se pueden muestrear las formas de ondas con un paso temporal Δt y emplear el método de discretización de Backward-Euler para resolver el sistema de ecuaciones (3.76) para cada iteración y cada armónico

$$[j\mathbf{Y}'(h\omega_c) - \Delta t \cdot \mathbf{Y}(h\omega_c)] \tilde{\mathbf{v}}_n(h, t_{k+1}) = j\mathbf{Y}'(h\omega_c) \tilde{\mathbf{v}}_n(h, t_k) - \Delta t \cdot \tilde{\mathbf{i}}_n(h, t_{k+1}). \quad (0.36)$$

Además, la extensión de este procedimiento para incluir más armónicos y términos de mayor orden en el desarrollo en series de potencias de las corrientes no lineales se

puede conseguir de un modo bastante simple. Basta con resolver un cierto número de sistemas de ecuaciones como el de (3.76) para $n = 1, \dots, N$ y $h = 0, \dots, H$, excepto en la última iteración, en la que sólo será necesario considerar el primer armónico para hallar respuestas dentro de la banda de interés y, por lo tanto, sólo habrá que resolver un sistema de ecuaciones.

Para ilustrar la eficiencia del método propuesto, podemos comparar la convergencia de este método con la del método EC de un modo teórico. En términos del conjunto de ecuaciones algebraicas que es necesario resolver, podemos decir que el método EC resulta un método subóptimo puesto que se están despreciando los términos de orden mayor que n en el miembro de la derecha de las ecuaciones. En cambio, el método propuesto implementa un proceso iterativo basado en un algoritmo de Newton Simplificado, en el que el Jacobiano que se calcula para la primera iteración de DC se reutiliza para todas las iteraciones. De este modo, la convergencia del método propuesto resulta algo más lenta que en el algoritmo de Newton-Raphson, aunque la carga computacional de cada iteración es mucho menor, por lo que en términos globales se produce una reducción del tiempo de simulación.

Por otro lado, la principal desventaja del enfoque de Newton Simplificado es que presenta una región de convergencia reducida que produce que, si la solución inicial del proceso iterativo no está lo suficientemente cerca de la solución final, es posible que este método no converja. Es decir, si el circuito que se está analizando tiene un comportamiento fuertemente no lineal la convergencia del método no está garantizada. Sin embargo, se han realizado simulaciones en las que ha sido posible predecir satisfactoriamente el comportamiento no lineal de un amplificador con un nivel de potencia cercano al punto de compresión de 1 dB, donde exhibe un comportamiento no lineal moderado, por lo que no se trata de una restricción demasiado estricta.

Finalmente, es importante resaltar que con este método podemos encontrar una tensión nodal incremental para la envolvente compleja en torno al primer armónico desde la segunda iteración, por lo que únicamente es necesario resolver dos sistemas lineales de ecuaciones para encontrar una corrección a la predicción lineal para la envolvente compleja del primer armónico. Además, la adecuada correspondencia entre el regeneración espectral calculado y el medido permiten una predicción fiable de ACPR.

Métodos de Envolventes de Corrientes para señales de comunicaciones en mezcladores

El análisis no lineal de mezcladores es una de las tareas más exigentes en la simulación de circuitos de microondas, dado su fuerte comportamiento no lineal y la gran

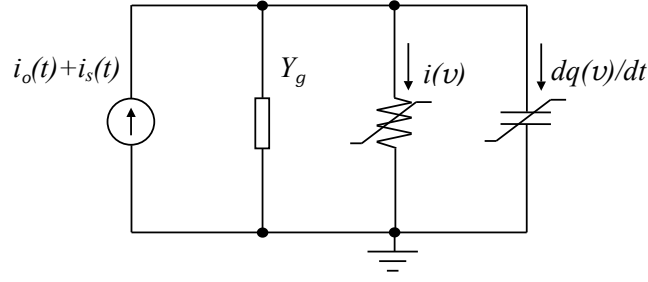


Figure 0.2: Circuito no lineal de un nodo excitado como mezclador.

cantidad de componentes espectrales que se generan. Por tanto, los algoritmos empleados para resolver las ecuaciones no lineales en estos circuitos suelen converger de forma lenta y cada iteración requiere una elevada carga computacional y de almacenamiento. Para el caso de señales de RF moduladas, son necesarios aún más recursos computacionales, haciendo que las técnicas de Balance Armónico no sean eficientes.

Puesto que el oscilador local es normalmente una señal de mayor amplitud que la señal de entrada, es usual considerar la excitación de entrada como una perturbación alrededor de la respuesta del sistema al oscilador local. Ejemplos de estos procedimientos aplicados a mezcladores son los trabajos clásicos de [40] y [41]. Otras generalizaciones del método empleado en éste último que usan series de Volterra variantes en el tiempo han sido presentadas en [42] y [43]. Sin embargo, la naturaleza aleatoria de los datos recomienda simular largas secuencias de símbolos, que dan lugar a cientos de miles de componentes frecuenciales. En [44] y [45], se hace hincapié en la obtención de métodos eficientes para analizar mezcladores con señales moduladas de banda estrecha.

Para exponer los principios teóricos de los métodos estudiados se considera el circuito simple de un sólo nodo de la Figura 0.2, que representa un mezclador y, por tanto, es excitado por dos fuentes de corriente independientes: el oscilador local $i_o(t)$ sinusoidal, que incluye la polarización, y la señal de RF $i_s(t)$. En este caso, la tensión del nodo satisface la ecuación

$$L[v(t)] + i[v(t)] + \frac{dq[v(t)]}{dt} = i_o(t) + i_s(t), \quad (0.37)$$

donde el operador $L[\cdot]$ denota la ecuación integro-diferencial que representa el subcircuito lineal y se representa en el dominio de la frecuencia por la admitancia Y_g .

En primer lugar, la tensión del nodo $v(t)$ se representa como una suma de tensiones incrementales

$$v(t) = v_0(t) + v_1(t) + \dots + v_n(t) + \delta v_n(t) = \bar{v}_n(t) + \delta v_n(t), \quad (0.38)$$

donde ahora $v_0(t)$ es la solución de la ecuación (0.37) cuando sólo está presente la fuente del oscilador local $i_o(t)$, i.e.

$$L[v_0] + i(v_0) + \frac{dq(v_0)}{dt} = i_o. \quad (0.39)$$

De esta forma, el número de componentes frecuenciales a considerar ha sido drásticamente reducido y es fácil conseguir la convergencia de métodos como HB-N. Por tanto, es posible asumir que v_0 es conocida. Entonces, se puede obtener la siguiente ecuación para la primera tensión incremental, si se aproximan $i(v)$ y $q(v)$ por sus desarrollos de primer orden alrededor de v_0 :

$$L[v_1] + g(v_0)v_1 + \frac{d}{dt} [c(v_0)v_1] = i_s. \quad (0.40)$$

La ecuación (3.96) representa un sistema lineal variante en el tiempo de forma cuasi-periódica, para el que se puede hallar la solución empleando el concepto de matrices de conversión [8] y considerar conocidos los términos v_1 y $\bar{v}_1 = v_0 + v_1$.

A continuación, se presentarán dos enfoques para resolver el resto de las iteraciones para $n \geq 2$, que dan lugar a dos métodos distintos para evaluar la distorsión no lineal en mezcladores con señales de comunicaciones:

- **Método NEC para señales de comunicaciones en mezcladores**

Este algoritmo fue propuesto en [46] y puede verse como una extensión del método NEC presentado en [19] para el análisis de señales moduladas digitalmente en mezcladores, por tanto nos referiremos a él como NEC-M. Su principal ventaja frente al Balance Armónico multitono es una reducción del tiempo de computación y un uso más eficiente de los recursos.

A partir de la segunda iteración, en el método NEC-M se resuelven ecuaciones del tipo de:

$$L[v_n] + g(\bar{v}_{n-1})v_n + \frac{d}{dt} [c(\bar{v}_{n-1})v_n] = i_n(\bar{v}_{n-1}), \quad (0.41)$$

donde

$$\begin{aligned} i_n(\bar{v}_{n-1}) &= i_0 + i_s - L[\bar{v}_{n-1}] - i(\bar{v}_{n-1}) - \frac{dq(\bar{v}_{n-1})}{dt} = \\ &= \left\{ g(\bar{v}_{n-2})v_{n-1} + \frac{d}{dt} [c(\bar{v}_{n-2})v_{n-1}] \right\} - \left[i(\bar{v}_{n-1}) - i(\bar{v}_{n-2}) + \frac{dq(\bar{v}_{n-1})}{dt} - \frac{dq(\bar{v}_{n-2})}{dt} \right]. \end{aligned} \quad (0.42)$$

En estas ecuaciones se analiza siempre el mismo circuito variante en el tiempo, linealizado en torno a las formas de onda que toma la tensión en las iteraciones previas, que en este caso no son periódicas sino cuasi-periódicas. Para considerar señales moduladas, se emplean representaciones mediante transformadas

discretas de Fourier (DFT) bidimensionales, es decir,

$$v_n(t) = \frac{1}{2} \sum_{h,m} \tilde{v}_n(h, m, t) e^{j(h\omega_c + m\omega_o)t}. \quad (0.43)$$

De este modo, las variables del algoritmo correspondientes a las tensiones en cada nodo serán vectores columna con $(2H + 1) \times (2M + 1)$ filas, donde H y M son el número de armónicos del oscilador local y de la frecuencia intermedia relevantes, respectivamente. El aumento de complejidad con respecto al caso de una sola entrada es, por tanto, evidente.

- **Método PHB extendido para señales de comunicaciones en mezcladores**

El segundo enfoque consiste en una extensión del método de Balance Armónico Paramétrico (E-PHB) que fue propuesta en [33] para reducir aún más el coste computacional. En este caso, a partir de la segunda iteración se mantienen los desarrollos en serie de $i(v)$ y $q(v)$ en torno a v_0 durante el resto de las iteraciones, de forma similar al enfoque SN. De este modo, para obtener la tensión incremental de la iteración n -ésima es necesario resolver el mismo circuito lineal variante en el tiempo de (0.40), ahora con la corriente

$$\begin{aligned} i_n(\bar{v}_{n-1}) &= i_0 + i_s - L[\bar{v}_{n-1}] - i(\bar{v}_{n-1}) - \frac{dq(\bar{v}_{n-1})}{dt} = \\ &= \left\{ g(v_0)v_{n-1} + \frac{d}{dt} [c(v_0)v_{n-1}] \right\} - \left[i(\bar{v}_{n-1}) - i(\bar{v}_{n-2}) + \frac{dq(\bar{v}_{n-1})}{dt} - \frac{dq(\bar{v}_{n-2})}{dt} \right]. \end{aligned} \quad (0.44)$$

Para el caso de señales moduladas de RF, además, se introducen algunas simplificaciones adicionales con respecto al caso anterior que consisten en emplear un algoritmo de relajación por el que se resuelve cada armónico de la frecuencia intermedia por separado y considerar sólo los términos con $|h| \leq H$ y $0 \leq m \leq M$, obteniendo el resto a partir de ellos. Así, las variables empleadas son vectores columna con sólo $(2H + 1)$ filas, lo que supone una reducción en el coste computacional. Sin embargo, la convergencia del método NEC-M es mejor que la del enfoque E-PHB.

Comparación con medidas experimentales

Técnicas de caracterización no lineal básicas

Mientras para el comportamiento lineal existen figuras de mérito para representar las características observables de los dispositivos bien establecidas, sus equivalentes no

lineales están aún bajo desarrollo y sometidas a debate [26]. Al no cumplir el principio de superposición, la respuesta de un sistema no lineal a una determinada entrada puede variar considerablemente dependiendo del tipo de entrada empleada. Por tanto, es aconsejable emplear entradas similares a las excitaciones esperadas en la operación real. Las señales de prueba más prácticas para los dispositivos no lineales empleados en circuitos de comunicaciones son aquellas con una densidad espectral de potencia (PSD) limitada en banda que contienen gran número de líneas espectrales.

La aproximación más simple a estas señales consiste en concentrar toda la potencia en una sola línea espectral, $x(t) = A_i \cos(2\pi ft)$, dando lugar a la prueba de un tono. En el caso de un dispositivo no lineal, la salida producida ante este estímulo contiene, además de la frecuencia fundamental, nuevas componentes de frecuencia en los armónicos de la entrada:

$$y_{NL}(t) = \sum_{h=0}^{\infty} A_{oh}(f, A_i) \cos[2\pi hft + \phi_{oh}(f, A_i)]. \quad (0.45)$$

A partir de esta salida, las principales figuras de mérito asociadas a las pruebas de un tono son:

- **Conversión AM-AM:** en la que se representa las variaciones de la amplitud de la salida en la frecuencia fundamental al cambiar el nivel de entrada.
- **Punto de compresión de 1 dB, P_{1dB} :** se define como el nivel de potencia para el que la potencia de salida está 1 dB por debajo del valor que se obtendría al extrapolar la característica lineal de pequeña señal.
- **Conversión AM-PM:** representa la variación en la fase de la salida fundamental de un dispositivo no lineal ante una entrada con amplitud variable para una frecuencia fija, ya que las componentes de distorsión no lineales se suman vectorialmente a la salida fundamental. Esta característica es exclusiva de sistemas no lineales dinámicos o con memoria, incluyendo aquellos normalmente llamados sistemas casi sin memoria [47].
- **Distorsión Armónica Total, THD:** se define como el cociente entre la potencia total debida a componentes armónicas y la potencia de la componente fundamental.

Los montajes más comunes para realizar las pruebas de un tono consisten en un generador de onda continua conectado a un Analizador Vectorial de Red (VNA) [48], [49], aunque se puede emplear también un Analizador de Espectros (SA) [50], [51], siendo éste último necesario en caso de realizar una caracterización de THD. Otras

alternativas con equipamiento especial de laboratorio también son posibles, por ejemplo, haciendo uso de Analizadores de Transición de Microondas o de Analizadores Vectoriales de Red No Lineales (NVNA).

Sin embargo, las pruebas de un tono sólo pueden producir componentes espectrales armónicamente relacionadas con la frecuencia de entrada. Para superar este inconveniente se emplean pruebas de dos tonos, donde la señal de entrada está formada por dos tonos de igual amplitud dentro de una cierta banda de interés, $x(t) = A_{i1} \cos(2\pi f_1 t) + A_{i2} \cos(2\pi f_2 t)$. La salida contiene un gran número de productos de mezcla

$$y_{NL}(t) = \sum_{r=1}^{\infty} A_{or} \cos(2\pi f_r t + \phi_{or}), \text{ donde } f_r = m f_1 + n f_2 \text{ y } m, n \in \mathbb{Z}, \quad (0.46)$$

de los cuales, los de orden impar pueden dar lugar a distorsión dentro de la banda si $m + n = 1$. Entre ellos destacan los productos de intermodulación (IM) de orden n -ésimo, IM_n , que dan lugar a la distorsión de intermodulación (IMD). Entre las figuras de mérito asociadas a esta prueba se encuentran:

- **Relación de intermodulación, IMR** , que se define como el cociente entre la potencia de salida a la frecuencia fundamental y la potencia de los productos de IM de tercer orden, IM_3 .
- **Punto de intercepto de tercer orden, IP_3** , que es el punto ficticio que se obtiene cuando la línea extrapolada de pendiente 1 dB/dB de la potencia a la frecuencia fundamental corta la línea extrapolada de pendiente 3 dB/dB de la potencia de IM_3 . También se pueden definir los puntos de intercepto IP_5 o IP_7 .
- **Rango dinámico libre de espurias, SFDR**, que es el cociente entre el nivel de potencia a la salida para la frecuencia fundamental y el ruido o el nivel de potencia de IMD.

Por otro lado, una señal de dos tonos se puede ver como una portadora a frecuencia $f_c = \frac{f_1 + f_2}{2}$ con una modulación de amplitud de doble banda lateral con portadora suprimida (DSB-SC) donde la envolvente compleja es una señal coseno con frecuencia proporcional a la separación entre los tonos $f_m = \frac{\Delta f}{2}$. De este modo, queda patente la relación que existe entre la separación entre los dos tonos y la frecuencia de banda base, haciendo que la medida de IMD con señales de dos tonos variando Δf sean adecuadas para tener en cuenta los efectos de memoria.

El equipo usual para las pruebas de dos tonos es un SA, normalmente junto con dos generadores de señal que dan lugar a los dos tonos que se aplican al dispositivo

bajo prueba (DUT) mediante un combinador o acoplador direccional. De este modo, las fase de los tonos generados están incorreladas [26].

El principal inconveniente de la prueba de dos tonos es la dificultad para evaluar la distorsión en las frecuencias fundamentales. Por eso, es usual emplear señales moduladas limitadas en banda para medir la distorsión cocanal, o incluso otras señales que se les parezcan, como las señales multitono de espectro discreto o el ruido limitado en banda. El espectro de una señal no lineal consiste en agrupaciones de componentes centradas en los diferentes armónicos. Si nos centramos en la distorsión dentro de la banda, las nuevas componentes generadas por la distorsión no lineal dan lugar al recrecimiento espectral. Por eso, las principales figuras de mérito asociadas a este caso son:

- **Relación de intermodulación multitono**, MIMR, que generaliza el concepto de IMR para las señales multitono.
- **Relación de potencia en el canal adyacente (ACPR) y potencia en el canal adyacente (ACP)**: existen varias figuras de mérito aceptadas para caracterizar la interferencia potencial introducida en los canales adyacentes por las componentes del recrecimiento espectral. Entre ellas, podemos mencionar la relación de potencia de canal adyacente total, que se define como el cociente entre la suma de las potencias de los canales adyacentes superior e inferior y la potencia en el canal de interés, o la relación de potencia únicamente en el canal adyacente inferior o superior. Otra alternativa es definir la potencia en el canal adyacente, ACP, para un ancho de banda predefinido o en las bandas correspondientes a los canales adyacentes primero, segundo, etc.
- **Relación de potencia de ruido**, NPR, que es una forma indirecta de caracterizar la distorsión cocanal. En una prueba de potencia de ruido se eliminan las componentes fundamentales en una cierta banda muy estrecha, de forma que las componentes observadas a la salida en esa posición se deben a la distorsión cocanal.
- **Magnitud del Error Vectorial**, EVM, que se define como el error cuadrático medio entre los valores de la envolvente compleja medida y los valores teóricos, para cada uno de los símbolos.

Para la generación de señales de prueba moduladas digitalmente se suelen emplear generadores de formas de onda arbitraria. Las medidas de ACPR se suelen llevar a cabo mediante SAs [52], mientras que las medidas de EVM suelen requerir Analizadores Vectoriales de Señal (VSAs) [53].

Otro concepto indispensable para una completa caracterización del comportamiento de un dispositivo no lineal es la memoria. El término de memoria fue propuesto por Chua [54] para describir que en la salida para un instante t de un sistema influyen no sólo la entrada a ese instante, sino también un rango finito de valores pasados de la señal de entrada para instantes $t - \tau$. La longitud de la memoria viene determinada por el mayor de los retrasos considerados, τ . Al hablar de efectos de memoria en un sistema no lineal estamos describiendo, esencialmente, un comportamiento dinámico del sistema que puede darse en una escala de tiempos similar a la frecuencia de la señal — memoria a corto plazo — o a tasas mucho menores — memoria a largo plazo. Por eso, los sistemas que sólo presentan efectos de memoria a corto plazo son considerados sistemas casi sin memoria por muchos autores [24], para los que las distorsiones de amplitud y fase se modelan mediante conversiones AM-AM y AM-PM estáticas o funciones de transferencia no lineal (NLTF) de valores complejos pero constantes. En cambio, se considera que los sistemas no lineales con efectos de memoria a largo plazo presentan características AM-AM y AM-PM dinámicas y NLTFs dependientes de la frecuencia.

Los efectos de memoria se pueden observar como desplazamientos en la amplitud y la fase de las componentes de IM al cambiar la frecuencia de modulación [24], o también por la presencia de histéresis en las gráficas AM-AM y AM-PM [55]. Otras formas de referirse a estos fenómenos en la literatura es como comportamiento de IMD dependiente del ancho de banda [25], efectos dinámicos del sistema [56], efectos dependientes de la tasa [57] o efectos no cuasi-estáticos (NQS) [9], [58]. Una diferencia entre los productos de IM superior e inferior para una entrada de dos tonos o entre los canales adyacentes superior e inferior para una entrada modulada se conoce como una asimetría, y es otra indicación de la existencia de efectos de memoria. Los efectos de memoria en amplificadores de potencia de RF se clasifican en [27], [58]:

- **Efectos de memoria a corto plazo:** son producidos por las reactancias asociadas al transistor (a través de su modelo circuital) y por las redes de adaptación empleadas, ya que suelen construirse con componentes reactivos o líneas de transmisión.
- **Efectos de memoria a largo plazo:** se producen por tres causas principales, que son los efectos térmicos que se suelen dar para frecuencias de modulación por debajo de 100 kHz, los estados trampa producidos por imperfecciones en los semiconductores que dan lugar a variaciones en la escala de los kilohertzios a los megahertzios y las redes de polarización, que proporcionan caminos de baja impedancia para la dc a la vez que una alta impedancia para la señal de RF.

Tradicionalmente, las hojas de especificaciones de los circuitos de microondas y RF

comerciales muestran el comportamiento no lineal mediante distintas figuras usando un ancho de banda arbitrario para la modulación. Sin embargo, los niveles de IMD variarán mucho en función del ancho de banda de las señales empleadas debido a complejas interacciones dentro del dispositivo no lineal o entre este y el resto del circuito. Estos efectos pueden llegar a hacer que algunos métodos de linealización se vuelvan completamente ineficientes, especialmente los que se basen en reducir la IMD aplicando una excitación que contenga una distorsión similar pero de fase opuesta, como puede ser el caso de la predistorsión digital desde un punto de vista simplificado.

A pesar de todo, la caracterización de los efectos de memoria no es una práctica extendida fuera del campo de la investigación en la actualidad y, aunque se ha propuesto un número reducido de figuras de mérito para cuantificar los efectos de memoria, aún no están bien establecidas.

Descripción de la plataforma de medidas

Como parte de esta Tesis, se ha desarrollado una plataforma para la caracterización automática de dispositivos no lineales, empleando equipamiento de laboratorio estándar de comunicaciones, cuya foto se muestra en la Fig 0.3. Los elementos más destacados del montaje son los siguientes:

- Analizador de espectros ESA E4407B de Agilent, con opción de análisis de modulación.
- Generador de señal SMIQ02B de Rhode & Schwarz, con capacidad para la generación de formas de ondas arbitrarias integrada.
- Generador de señal SMR20 de Rhode & Schwarz.
- Dos fuentes de alimentación de dc: una 6622A de Agilent y una TPS-4000D de Topward Electric Instruments.

Los instrumentos se controlan mediante un software comercial instalado en un PC mediante una interfaz GPIB. También se incluye en el montaje un *test-fixture* para la colocación de los circuitos de microondas que van a ser caracterizados, así como otros elementos que puedan ser necesarios para medidas particulares, como redes de polarización comerciales (*bias-Tees*), filtros, atenuadores, divisores y combinadores de potencia, acopladores direccionales, etc.

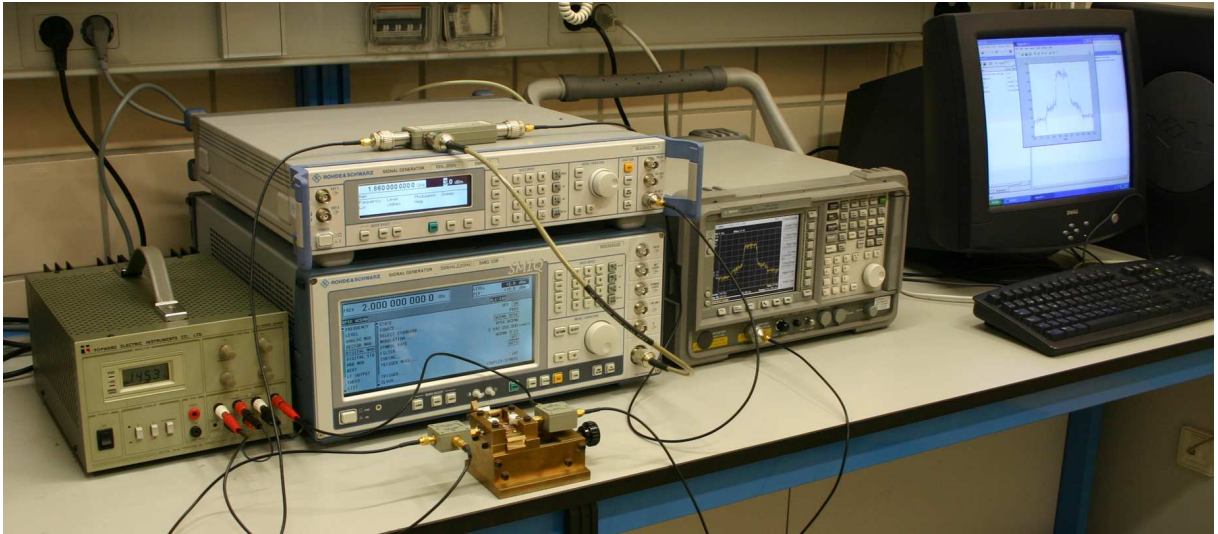


Figure 0.3: Fotografía del equipamiento de la plataforma para la caracterización no lineal de circuitos.

Las principales ventajas del montaje empleado son la velocidad que se consigue gracias a la automatización de las medidas y la simplificación que introduce la interfaz gráfica de usuario diseñada. Otro aspecto positivo es la posibilidad de disponer de forma inmediata de los resultados de medida en el PC, tanto en formato gráfico como numérico, para integrar los datos experimentales de forma fácil con las técnicas de simulación y modelado. En la Figura 0.4 se muestra una captura de pantalla del software diseñado.

Entre las características de las medidas que permite dicha plataforma destaca la posibilidad medir tanto la magnitud como la fase relativa en pruebas de dos tonos, algo aconsejable para una completa caracterización de IMD. Previamente se han propuesto distintos métodos para la medida de la fase de la IMD basados en VNAs [27], [59], [60], o en un Generador Vectorial de Señal y un NVNA [61]. Su principal desventaja es que requieren montajes sofisticados y equipos altamente especializados. Otros métodos propuestos emplean como excitación señales de dos tonos incorrelados estándar [62], [63], o correlados [64], junto con técnicas basadas en el promediado estadístico de ventanas de señal o filtrado espectral. Por último, existen métodos ampliamente aceptados basados en generadores con capacidad para formas de onda arbitrarias y la adquisición de las muestras de salida con osciloscopios digitales [65], VSAs [66], [67], [68] o un SA [69].

El método experimental empleado en la plataforma fue presentado en [70] y sigue esta última tendencia de muestreo de banda ancha, empleando equipos de comunicaciones estándar. Se basa en la generación de dos tonos mediante una señal modulada DSB-SC, gracias a la utilización de un generador de señal con opción de modulación

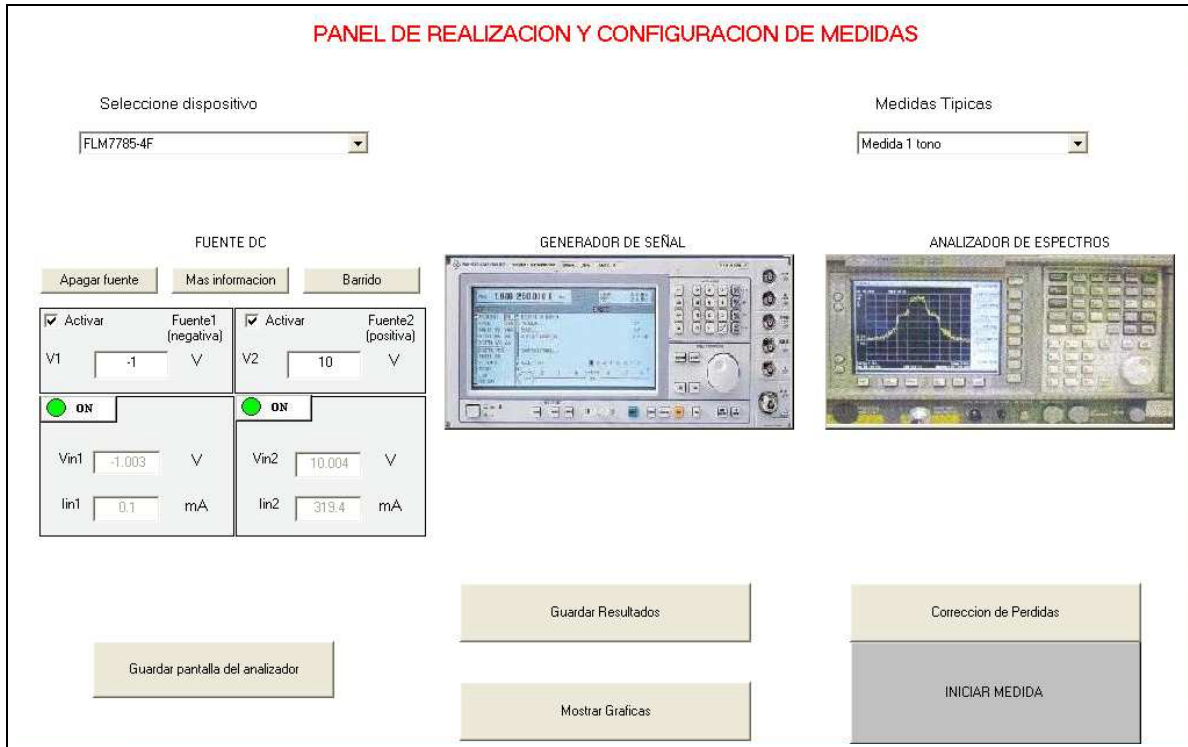


Figure 0.4: Ventana principal del software implementado para controlar el montaje de medidas automatizado.

arbitraria. La ventaja de este método no es sólo el uso de un único generador de señal para producir los dos tonos, sino que la fase relativa entre ellos se puede controlar mediante la definición por software de la señal moduladora. Una limitación que presenta es que existen respuestas generadas por el procesado digital de la señal. Sin embargo, estas respuestas están más de 65 dB por debajo de los tonos y permiten suficiente margen para medir la IM sin error apreciable en las situaciones prácticas. Las muestras de la señal en banda base a la salida son adquiridas en un analizador de espectros con opción de análisis de modulación para recuperar su espectro, que contiene información tanto de la magnitud como de la fase. Por tanto, mediante una transformada de Fourier es posible obtener las fases de los productos de IM con respecto a la de los tonos. Esta es otra de las restricciones del método propuesto, que no es posible medir valores absolutos de la fase, sino relativos a la fase de los tonos. La máxima separación entre los tonos posible de acuerdo con la tasa de muestreo del analizador de espectros es de 10 MHz, pero si se tiene en cuenta que IM3 e IM5 muestran separaciones mayores, de $3\Delta f$ y $5\Delta f$ en cada caso, la separación máxima entre los tonos no debe superar los 3.3 MHz y 2 MHz, respectivamente. Finalmente, se realiza un post-procesado para corregir la fase que elimina el retraso de tránsito de la señal.

Para realizar medidas de la fase de los productos de IM se construyó un amplificador usando una red de polarización diseñada expresamente para mostrar una reso-

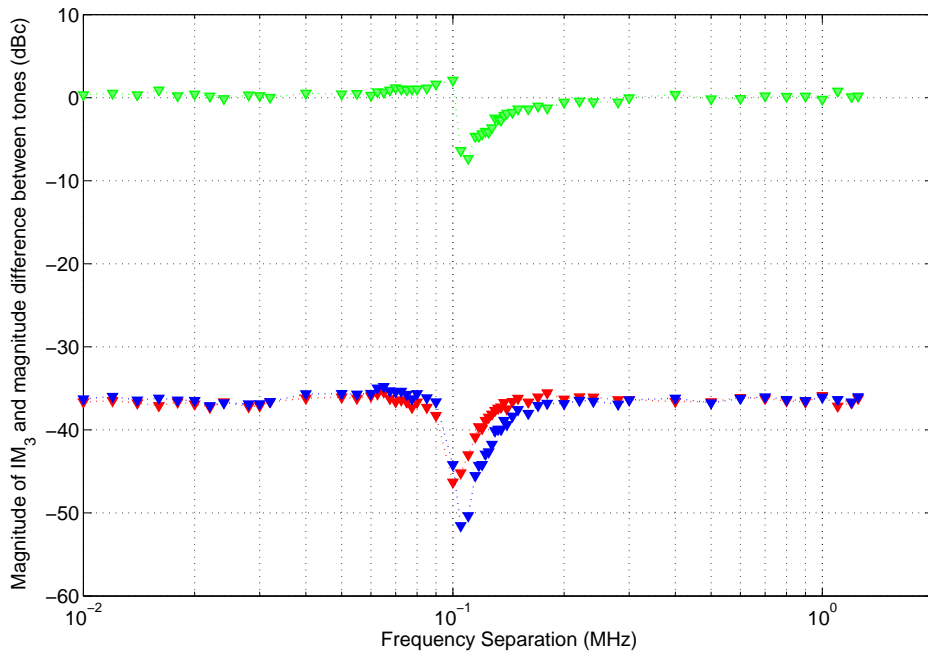


Figure 0.5: Medida de la magnitud de IM3 e IM5 (rojo y azul) y de la diferencia en magnitud entre los tonos (verde). Red de polarización resonante.

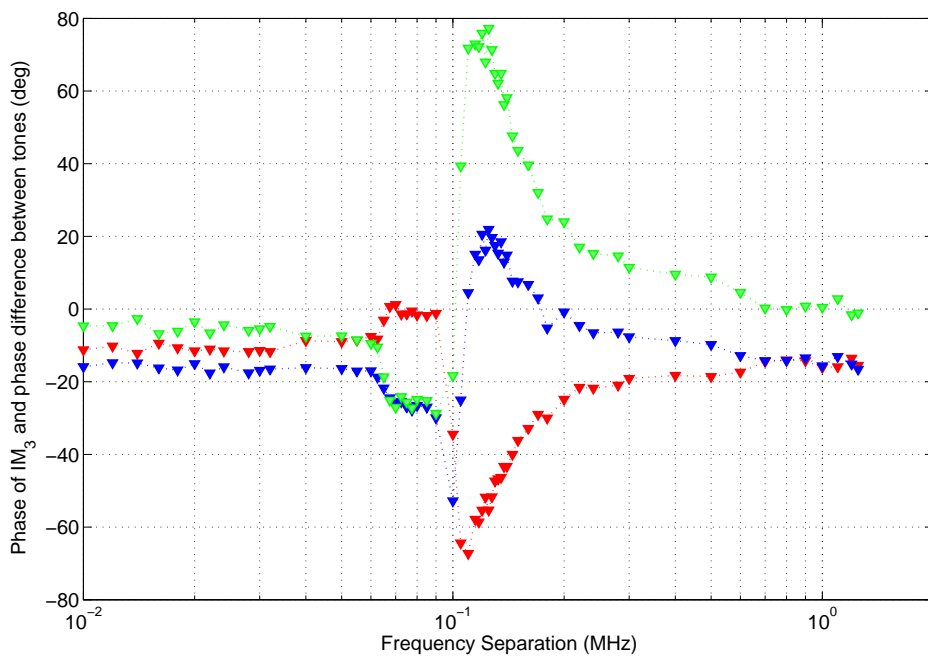


Figure 0.6: Medida de la fase de IM3 e IM5 (rojo y azul) y de la diferencia en fase entre los tonos (verde). Red de polarización resonante.

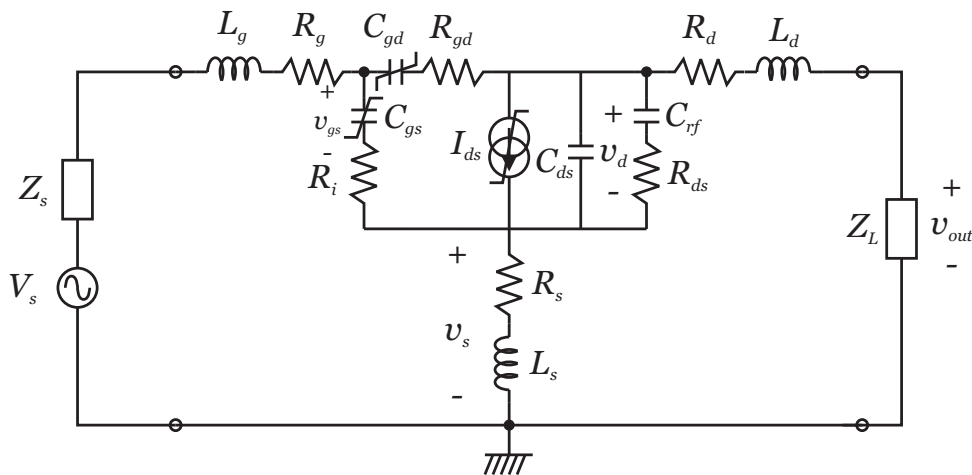


Figure 0.7: Circuito equivalente de tres nodos empleado para el análisis del MESFET CFB0301 de Celeritek y el HEMT EPB018A5-70 de Excellics.

nancia en torno a 130 kHz, de forma que se pudiera observar alguna dependencia de IM3 e IM5 con la frecuencia. Las medidas de la magnitud y la fase de los productos IM3 junto con la diferencia en magnitud y fase entre el producto de IM superior y el inferior se muestran en las Figuras 0.5 y 0.6. Las medidas de la fase de IM3 e IM5 han demostrado ser más adecuadas en muchos casos para detectar efectos dependientes de la frecuencia o asimetrías, enfatizando la importancia de la caracterización en fase de la IMD.

Resultados de los métodos de análisis basados en envolvente

Para demostrar las prestaciones de los métodos descritos en el Capítulo 3, se han aplicado al análisis de circuitos simples de amplificadores y mezcladores basados en un único dispositivo MESFET CFB0301 de Celeritek o HEMT EPB018A5-70 de Excellics. Se ha empleado el circuito equivalente de tres nodos mostrado en la Figura 0.7. Entre los modelos no lineales de gran señal usados para los dispositivos señalados destacan los modelos de Curtice cúbico [71] y Angelov [72]. Entre los elementos del circuito equivalente, R_g , R_s , R_d , L_g , L_s , y L_d forman el circuito extrínseco. Con respecto al circuito intrínseco, R_i es la resistencia intrínseca o resistencia de la región del semiconductor bajo la puerta, entre la fuente y el canal. C_{ds} es la capacidad de drenador a fuente, que viene dominada por la capacidad de metalización y se trata por tanto como una constante. C_{gs} y C_{gd} son las capacidades de puerta a canal. Nótese que las ramas que contienen las parejas R_i - C_{gs} y R_{ds} - C_{rf} introducen una dependencia en frecuencia similar a la de un filtro, por lo que tienen en cuenta efectos NQS o de memoria. I_{ds} es la fuente de corriente no lineal del canal. Se acepta generalmente que la fuente

de no linealidad dominante en los transistores MESFET y HEMT es la corriente de drenador a fuente $I_{ds}(V_{gs}, V_{ds})$ [9], [21], [28], [73], [74].

Los métodos EC y SN tienen en común que ambos analizan el mismo circuito lineal aumentado durante todas sus iteraciones. Por tanto, ambos pueden ser resumidos en el siguiente proceso iterativo:

$$[j\mathbf{Y}'(h\omega_c) - \Delta t \cdot \mathbf{Y}(h\omega_c)] \tilde{\mathbf{v}}_n(h, t_{k+1}) = j\mathbf{Y}'(h\omega_c) \tilde{\mathbf{v}}_n(h, t_k) - \Delta t \cdot \tilde{\mathbf{i}}_n(h, t_{k+1}), \quad (0.47)$$

donde se considera un número de iteraciones N en cada caso. La matriz de admitancias y su primera derivada con respecto a ω para el ejemplo de la Figura 0.7 toman las expresiones siguientes:

$$\mathbf{Y}(h\omega_c) = \begin{pmatrix} Y_{11}(h\omega_c) & Y_{12}(h\omega_c) & Y_{13}(h\omega_c) \\ Y_{21}(h\omega_c) & Y_{22}(h\omega_c) & Y_{23}(h\omega_c) \\ Y_{31}(h\omega_c) & Y_{32}(h\omega_c) & Y_{33}(h\omega_c) \end{pmatrix}, \quad (0.48)$$

con

$$\begin{aligned} Y_{11}(h\omega_c) &= \frac{1 + jh\omega_c R_i C_{gs}}{Z_s + R_g + jh\omega_c L_g} + \frac{jh\omega_c C_{gd} (1 + jh\omega_c R_i C_{gs})}{1 + jh\omega_c R_{gd} C_{gd}} + jh\omega_c C_{gs}, \\ Y_{12}(h\omega_c) &= -\frac{jh\omega_c C_{gd}}{1 + jh\omega_c R_{gd} C_{gd}}, \\ Y_{13}(h\omega_c) &= \frac{1}{Z_s + R_g + jh\omega_c L_g}, \\ Y_{21}(h\omega_c) &= g_{10} - \frac{jh\omega_c C_{gd} (1 + jh\omega_c R_i C_{gs})}{1 + jh\omega_c R_{gd} C_{gd}}, \\ Y_{22}(h\omega_c) &= g_{01} + \frac{1}{Z_L + R_d + jh\omega_c L_d} + \frac{jh\omega_c C_{gd}}{1 + jh\omega_c R_{gd} C_{gd}} + jh\omega_c C_{ds} + \frac{jh\omega_c C_{rf}}{1 + jh\omega_c R_{ds} C_{rf}}, \\ Y_{23}(h\omega_c) &= \frac{1}{Z_L + R_d + jh\omega_c L_d}, \\ Y_{31}(h\omega_c) &= -g_{10} - jh\omega_c C_{gs}, \\ Y_{32}(h\omega_c) &= -g_{01} - jh\omega_c C_{ds} - \frac{jh\omega_c C_{rf}}{1 + jh\omega_c R_{ds} C_{rf}}, \\ Y_{33}(h\omega_c) &= \frac{1}{R_s + jh\omega_c L_s}, \end{aligned} \quad (0.49)$$

y

$$\mathbf{Y}'(h\omega_c) = \begin{pmatrix} Y'_{11}(h\omega_c) & Y'_{12}(h\omega_c) & Y'_{13}(h\omega_c) \\ Y'_{21}(h\omega_c) & Y'_{22}(h\omega_c) & Y'_{23}(h\omega_c) \\ Y'_{31}(h\omega_c) & Y'_{32}(h\omega_c) & Y'_{33}(h\omega_c) \end{pmatrix}, \quad (0.50)$$

con

$$Y'_{11}(h\omega_c) = \frac{jR_i C_{gs}}{Z_s + R_g + jh\omega_c L_g} - \frac{jL_g (1 + jh\omega_c R_i C_{gs})}{(Z_s + R_g + jh\omega_c L_g)^2} +$$

$$\begin{aligned}
& + \frac{jC_{gd}(1 + jh\omega_c R_i C_{gs})}{(1 + jh\omega_c R_{gd} C_{gd})^2} - \frac{h\omega_c R_i C_{gs} C_{gd}}{1 + jh\omega_c R_{gd} C_{gd}} + jC_{gs}, \\
Y'_{12}(h\omega_c) &= -\frac{jC_{gd}}{(1 + jh\omega_c R_{gd} C_{gd})^2}, \\
Y'_{13}(h\omega_c) &= -\frac{jL_g}{(Z_s + R_g + jh\omega_c L_g)^2}, \\
Y'_{21}(h\omega_c) &= -\frac{jC_{gd}(1 + jh\omega_c R_i C_{gs})}{(1 + jh\omega_c R_{gd} C_{gd})^2} + \frac{h\omega_c R_i C_{gs} C_{gd}}{1 + jh\omega_c R_{gd} C_{gd}}, \quad (0.51) \\
Y'_{22}(h\omega_c) &= -\frac{jL_d}{(Z_L + R_d + jh\omega_c L_d)^2} + \frac{jC_{gd}}{(1 + jh\omega_c R_{gd} C_{gd})^2} + jC_{ds} + \frac{jC_{rf}}{(1 + jh\omega_c R_{ds} C_{rf})^2}, \\
Y'_{23}(h\omega_c) &= -\frac{jL_d}{(Z_L + R_d + jh\omega_c L_d)^2}, \\
Y'_{31}(h\omega_c) &= -jC_{gs}, \\
Y'_{32}(h\omega_c) &= -jC_{ds} - \frac{jC_{rf}}{(1 + jh\omega_c R_{ds} C_{rf})^2}, \\
Y'_{33}(h\omega_c) &= -\frac{jL_s}{(R_s + jh\omega_c L_s)^2}.
\end{aligned}$$

Las incógnitas del problema son las envolventes complejas de las tensiones, tal como se expresa en el siguiente vector:

$$\tilde{\mathbf{v}}_{\mathbf{n}}(h, t) = \begin{bmatrix} \tilde{v}_{gs,n}(h, t) \\ \tilde{v}_{ds,n}(h, t) \\ \tilde{v}_{s,n}(h, t) \end{bmatrix}, \quad (0.52)$$

y la tensión de salida es:

$$\tilde{v}_{out,n}(h, t) = \frac{Z_L [\tilde{v}_{ds,n}(h, t) + \tilde{v}_{s,n}(h, t)]}{Z_L + R_d + jh\omega_c L_d}. \quad (0.53)$$

Con el dispositivo MESFET CFB0103 de Celeritek se construyó un amplificador a 2 GHz, usando una polarización $V_{DS} = 2$ V y $I_D = 25$ mA. Se tuvo especial cuidado en el proceso de modelado para obtener una adecuada precisión de las características no lineales. Se consideró únicamente la fuente de corriente no lineal I_{ds} para la que se utilizó un modelo de Angelov con seis coeficientes ($P_2 = 0$), cuyo ajuste se hizo empleando medidas de la magnitud de IMD para dos señales a frecuencias de 150 y 151 MHz siguiendo un enfoque de series dobles de Volterra [42].

Además, se construyó otro amplificador con el HEMT EPB018A5-70 de Excellics, al que se le aplicó una polarización con $V_{GS} = -0.24$ V y $V_{DS} = 2$ V, para obtener una corriente de drenador de 15 mA, mediante sendas bias-Tees ZFBT-6G de Minicircuits. Los valores de los coeficientes de un modelo de gran señal de Curtice cúbico proporcionado por el fabricante para I_{ds} fueron readaptados a un modelo de Angelov de seis

coeficientes (con $\lambda = 1$) debido a que aparecerían imprecisiones no despreciables con el modelo del fabricante. Con este mismo dispositivo HEMT, se construyó también un mezclador de puerta. El punto óptimo de polarización se obtuvo de forma experimental como $V_{GS} = -0.45$ V para la tensión de drenador recomendada $V_{DS} = 2$ V. Se emplearon señales de RF a una frecuencia $f_{RF} = 2$ GHz y del oscilador local a una frecuencia $f_{LO} = 1.86$ GHz con un nivel $P_{LO} = -4.5$ dBm, que se aplicaron mediante un acoplador direccional.

Método de las Envolventes de Corriente

Se empleó el amplificador construido con el MESFET CFB0301 de Celeritek. Se han tenido en cuenta las siguientes corrientes no lineales:

- Para el caso lineal, $n = 1$, sólo se tiene en cuenta la zona de la frecuencia fundamental con $h = 1$:

$$\tilde{\mathbf{i}}_1(1, t) = \begin{bmatrix} \frac{\tilde{v}_g(t)}{Z_s + R_g + j\omega_c L_g} \\ 0 \\ 0 \end{bmatrix}. \quad (0.54)$$

- Para la segunda iteración, $n = 2$, es necesario considerar dos envolventes de corrientes para $h = 0$ y $h = 2$:

$$\tilde{\mathbf{i}}_2(0, t) = \begin{bmatrix} 0 \\ -\tilde{i}_{d,2}(0, t) \\ \tilde{i}_{d,2}(0, t) \end{bmatrix}, \quad (0.55)$$

$$\tilde{\mathbf{i}}_2(2, t) = \begin{bmatrix} 0 \\ -\tilde{i}_{d,2}(2, t) \\ \tilde{i}_{d,2}(2, t) \end{bmatrix}, \quad (0.56)$$

con

$$\tilde{i}_{d,2}(0, t) = \frac{g_{20}}{2} |\tilde{v}_{gs,1}(1, t)|^2 + \frac{g_{02}}{2} |\tilde{v}_{ds,1}(1, t)|^2 + \frac{g_{11}}{2} Re\{\tilde{v}_{gs,1}(1, t)\tilde{v}_{ds,1}^*(1, t)\}, \quad (0.57)$$

$$\tilde{i}_{d,2}(2, t) = \frac{g_{20}}{2} \tilde{v}_{gs,1}^2(1, t) + \frac{g_{02}}{2} \tilde{v}_{ds,1}^2(1, t) + \frac{g_{11}}{2} \tilde{v}_{gs,1}(1, t)\tilde{v}_{ds,1}(1, t). \quad (0.58)$$

- Para la tercera iteración, $n = 3$, de nuevo se consideran dos envolventes de corriente para $h = 1$ y $h = 3$, aunque la última sólo es necesaria porque se busca una predicción del tercer armónico:

$$\tilde{\mathbf{i}}_3(1, t) = \begin{bmatrix} 0 \\ -\tilde{i}_{d,3}(1, t) \\ \tilde{i}_{d,3}(1, t) \end{bmatrix}, \quad (0.59)$$

$$\tilde{\mathbf{i}}_3(3, t) = \begin{bmatrix} 0 \\ -\tilde{i}_{d,3}(3, t) \\ \tilde{i}_{d,3}(3, t) \end{bmatrix}, \quad (0.60)$$

con

$$\begin{aligned} \tilde{i}_{d,3}(1, t) = & \frac{3g_{30}}{4}\tilde{v}_{gs,1}^2(1, t)\tilde{v}_{gs,1}^*(1, t) + \frac{3g_{03}}{4}\tilde{v}_{ds,1}^2(1, t)\tilde{v}_{ds,1}^*(1, t) + \\ & 2g_{20} \left[\frac{1}{2}\tilde{v}_{gs,1}^*(1, t)\tilde{v}_{gs,2}(2, t) + \tilde{v}_{gs,1}(1, t)\tilde{v}_{gs,2}(0, t) \right] + \\ & 2g_{02} \left[\frac{1}{2}\tilde{v}_{ds,1}^*(1, t)\tilde{v}_{ds,2}(2, t) + \tilde{v}_{ds,1}(1, t)\tilde{v}_{ds,2}(0, t) \right] + \\ & g_{11} \left[\frac{1}{2}\tilde{v}_{gs,1}^*(1, t)\tilde{v}_{ds,2}(2, t) + \tilde{v}_{gs,1}(1, t)\tilde{v}_{ds,2}(0, t) + \right. \\ & \left. + \frac{1}{2}\tilde{v}_{ds,1}^*(1, t)\tilde{v}_{gs,2}(2, t) + \tilde{v}_{ds,1}(1, t)\tilde{v}_{gs,2}(0, t) \right] + \\ & \frac{g_{21}}{4} [\tilde{v}_{gs,1}^2(1, t)\tilde{v}_{ds,1}^*(1, t) + 2|\tilde{v}_{gs,1}(1, t)|^2\tilde{v}_{ds,1}(1, t)] + \\ & \frac{g_{12}}{4} [\tilde{v}_{ds,1}^2(1, t)\tilde{v}_{gs,1}^*(1, t) + 2|\tilde{v}_{ds,1}(1, t)|^2\tilde{v}_{gs,1}(1, t)], \end{aligned} \quad (0.61)$$

$$\begin{aligned} \tilde{i}_{d,3}(3, t) = & \frac{g_{30}}{4}\tilde{v}_{gs,1}^3(1, t) + \frac{g_{03}}{4}\tilde{v}_{ds,1}^3(1, t) + \frac{g_{21}}{4}\tilde{v}_{gs,1}^2(1, t)\tilde{v}_{ds,1}(1, t) + \\ & \frac{g_{12}}{4}\tilde{v}_{ds,1}^2(1, t)\tilde{v}_{gs,1}(1, t) + g_{20}\tilde{v}_{gs,1}(1, t)\tilde{v}_{gs,2}(2, t) + g_{02}\tilde{v}_{ds,1}(1, t)\tilde{v}_{ds,2}(2, t) + \\ & \frac{g_{11}}{2} [\tilde{v}_{gs,1}(1, t)\tilde{v}_{ds,2}(2, t) + \tilde{v}_{ds,1}(1, t)\tilde{v}_{gs,2}(2, t)] \end{aligned} \quad (0.62)$$

La Figura 0.8 muestra la salida para la frecuencia fundamental, segundo y tercer armónicos en un rango de potencias de entrada. También se ha probado el amplificador con una señal W-CDMA QPSK correspondiente al 3GPP a 2 GHz, con una tasa de 3.84 Mchip/s y pulso coseno alzado con un factor de roll-off de 0.22. La Figura 0.9 compara el espectro medido a la salida con las simulaciones realizadas mediante el método EC para dos niveles de potencia de entrada, el primero lo suficientemente bajo para que las no linealidades no sean apreciables, y el segundo más cercano al punto de compresión de 1 dB, donde es más apreciable el recrecimiento espectral que produce interferencia de canal adyacente. Todas las simulaciones se ajustan satisfactoriamente a las medidas, por lo que se puede concluir la validez de los métodos basados en envolvente.

Enfoque de Newton Simplificado para circuitos débilmente no lineales

En este caso, se empleó el amplificador basado en el HEMT EPB018A5-70 de Excellics, para el que se han tenido en cuenta los coeficientes tanto de la fuente no lineal de

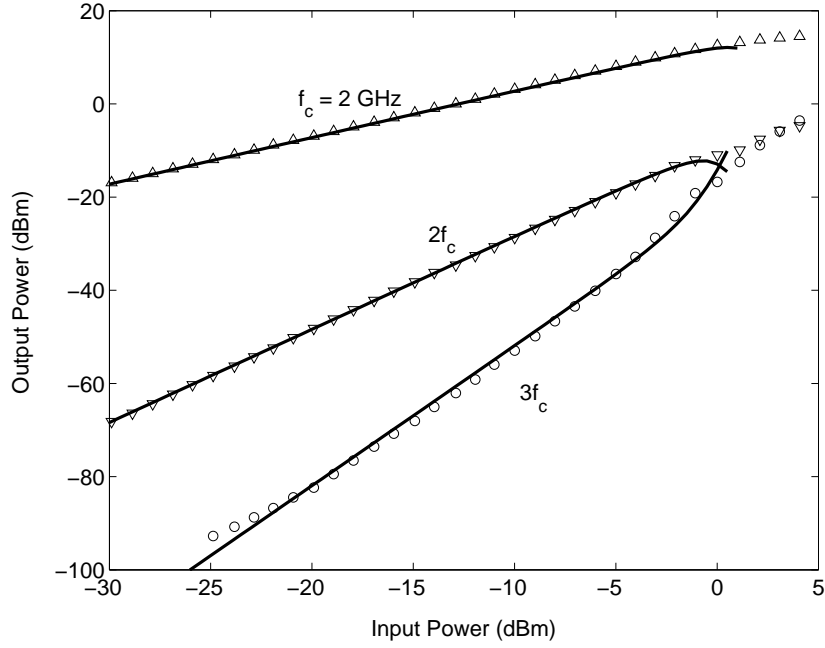


Figure 0.8: Potencia de salida a la frecuencia fundamental y los armónicos segundo y tercero. Puntos, medidas; línea continua: simulaciones con el método EC.

corriente de drenador como de la capacidad no lineal de puerta a fuente. Hasta la segunda iteración, éstos son:

- Para el caso lineal, $n = 1$, sólo se tiene en cuenta la zona de la frecuencia fundamental con $h = 1$:

$$\tilde{\mathbf{i}}_1(1, t) = \begin{bmatrix} \frac{\tilde{v}_g(t)}{Z_s + R_g + j\omega_c L_g} \\ 0 \\ 0 \end{bmatrix}. \quad (0.63)$$

- Para la segunda iteración, $n = 2$, hay que considerar cuatro envolventes de corriente para $h = 0, 1, 2$, y 3:

$$\tilde{\mathbf{i}}_2(h, t) = \begin{bmatrix} -\tilde{i}_{c,2}(h, t) \\ -\tilde{i}_{d,2}(h, t) \\ \tilde{i}_{d,2}(h, t) + \tilde{i}_{c,2}(h, t) \end{bmatrix}, \quad (0.64)$$

con

$$\tilde{i}_{d,2}(0, t) = \frac{g_{20}}{2} |\tilde{v}_{gs,1}(t)|^2 + \frac{g_{02}}{2} |\tilde{v}_{ds,1}(t)|^2 + \frac{g_{11}}{2} \text{Re}\{\tilde{v}_{gs,1}(t)\tilde{v}_{ds,1}^*(t)\} \quad (0.65)$$

$$\begin{aligned} \tilde{i}_{d,2}(1, t) = & \frac{3g_{30}}{4} |\tilde{v}_{gs,1}(t)|^2 \tilde{v}_{gs,1}(t) + \frac{3g_{03}}{4} |\tilde{v}_{ds,1}(t)|^2 \tilde{v}_{ds,1}(t) + \frac{g_{21}}{4} \tilde{v}_{gs,1}^2(t) \tilde{v}_{ds,1}^*(t) + \\ & + \frac{g_{21}}{2} |\tilde{v}_{gs,1}(t)|^2 \tilde{v}_{ds,1}(t) + \frac{g_{12}}{4} \tilde{v}_{ds,1}^2(t) \tilde{v}_{gs,1}^*(t) + \frac{g_{12}}{2} |\tilde{v}_{ds,1}(t)|^2 \tilde{v}_{gs,1}(t) \end{aligned} \quad (0.66)$$

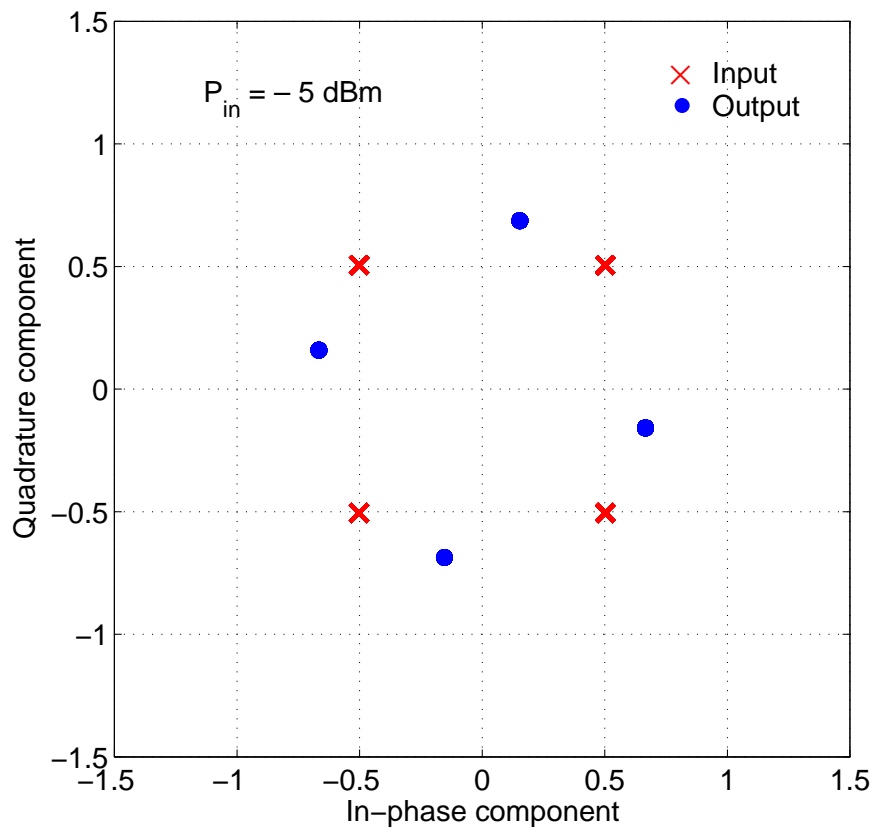
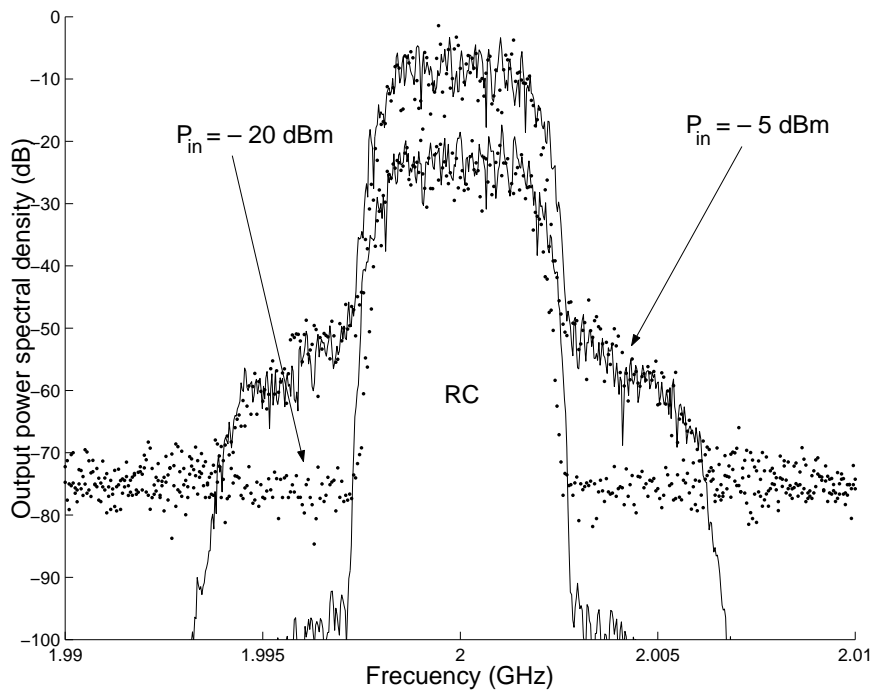


Figure 0.9: Constelación and PSD a la salida de un amplificador MESFET para dos niveles de potencia de entrada con pulsos coseno alzado. Puntos, medidas; línea continua, predicciones con el método EC.

$$\tilde{i}_{d,2}(2, t) = \frac{g_{20}}{2} \tilde{v}_{gs,1}^2(t) + \frac{g_{02}}{2} \tilde{v}_{ds,1}^2(t) + \frac{g_{11}}{2} \tilde{v}_{gs,1}(t) \tilde{v}_{ds,1}(t) \quad (0.67)$$

$$\begin{aligned} \tilde{i}_{d,2}(3, t) &= \frac{g_{30}}{4} \tilde{v}_{gs,1}^3(t) + \frac{g_{03}}{4} \tilde{v}_{ds,1}^3(t) + \\ &+ \frac{g_{21}}{4} \tilde{v}_{gs,1}^2(t) \tilde{v}_{ds,1}(t) + \frac{g_{12}}{4} \tilde{v}_{ds,1}^2(t) \tilde{v}_{gs,1}(t) \end{aligned} \quad (0.68)$$

$$\tilde{i}_{c,2}(0, t) = 0 \quad (0.69)$$

$$\tilde{i}_{c,2}(1, t) = j\omega \frac{c_2}{4} |\tilde{v}_{gs,1}(t)|^2 \tilde{v}_{gs,1}(t) \quad (0.70)$$

$$\tilde{i}_{c,2}(2, t) = j\omega \frac{c_1}{2} \tilde{v}_{gs,1}^2(t) \quad (0.71)$$

$$\tilde{i}_{c,2}(3, t) = j\omega \frac{c_2}{4} \tilde{v}_{gs,1}^3(t) \quad (0.72)$$

La Figura 0.10 muestra la potencia a la salida para el tono superior e IM3 frente a la potencia de entrada para una excitación de dos tonos separados 1 MHz. Se puede observar un buen rango dinámico, incluso cuando sólo se resuelven dos sistemas de ecuaciones hasta la segunda iteración. Los tiempos de simulación en estos casos están por debajo de 2 segundos en un PC Pentium IV. Cuando se considera una señal de comunicaciones W-CDMA de UMTS 3GPP con una tasa de 3.84 Mchip/s, como en la Figura 0.11 la predicción del recrecimiento espectral es adecuada y muestra una buena correspondencia con la del método EC. Cuando sólo se tiene en cuenta hasta la segunda iteración en el enfoque SN se consigue una reducción del 50% del tiempo de computación. La precisión lograda en las predicciones del recrecimiento espectral para un amplio rango dinámico y los reducidos tiempos de simulación permiten realizar simulaciones de ACPR como la mostrada en la Figura 0.12.

Dos enfoques alternativos para señales de comunicaciones en mezcladores

Para comparar las prestaciones de los métodos NEC-M y E-PHB se empleó el mezclador construido con el HEMT EPB018A5-70 de Excellics. La Figura 0.13 muestra los resultados para la ganancia de conversión obtenida con una excitación de dos tonos a 2 y 2.001 GHz, variando la potencia de entrada. Se puede observar que las predicciones de los métodos E-PHB y NEC-M se aproximan mucho a los resultados experimentales, incluso para niveles bastante por encima del punto de compresión de 1 dB. Además, se han hecho predicciones para una señal W-CDMA de UMTS 3GPP a 2 GHz, con una tasa de 3.84 Mchip/s, en la que se ha medido la salida a frecuencia intermedia para diferentes niveles de entrada. La Figura 0.14 muestra el recrecimiento espectral de la salida a frecuencia intermedia. La coincidencia entre los datos medidos y simulados con el enfoque E-PHB es destacable, aún con la reducción computacional

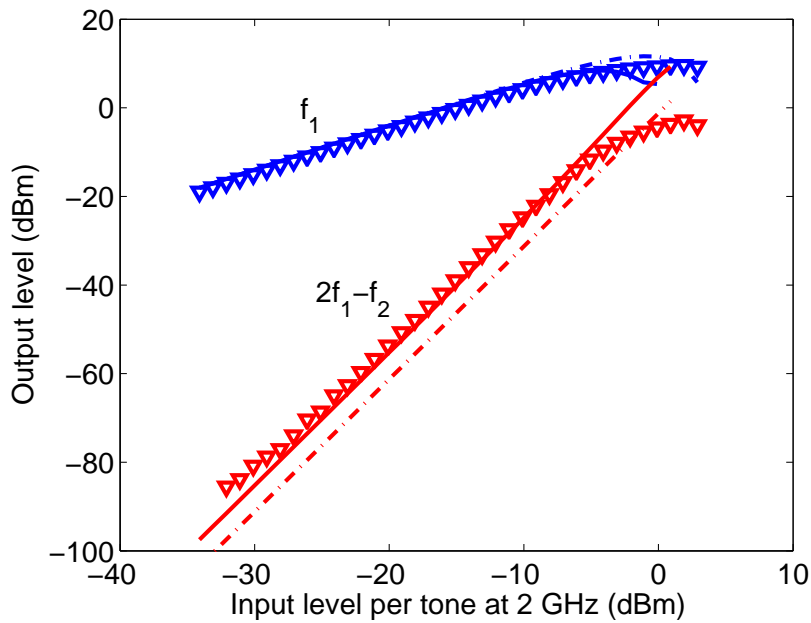


Figure 0.10: Productos de IM para un amplificador HEMT en función de la potencia de entrada. Simulaciones mediante el enfoque SN hasta la tercera iteración (línea continua) y considerando sólo hasta la segunda iteración (línea discontinua). Medidas (triángulos).

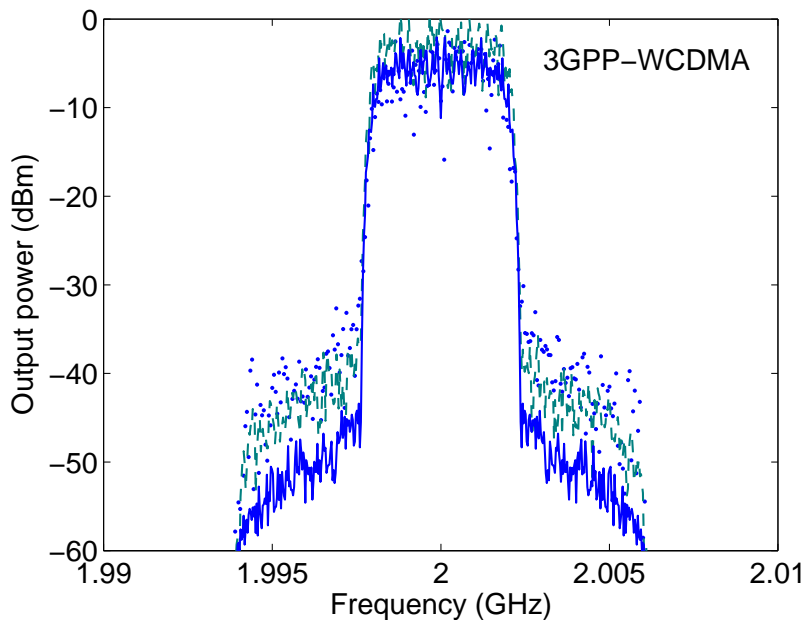


Figure 0.11: Predicción del recrecimiento espectral para una señal W-CDMA de UMTS 3GPP. Se comparan las medidas (puntos) con el enfoque SN hasta la segunda iteración (línea continua) y con el método EC hasta la tercera iteración (línea punteada).

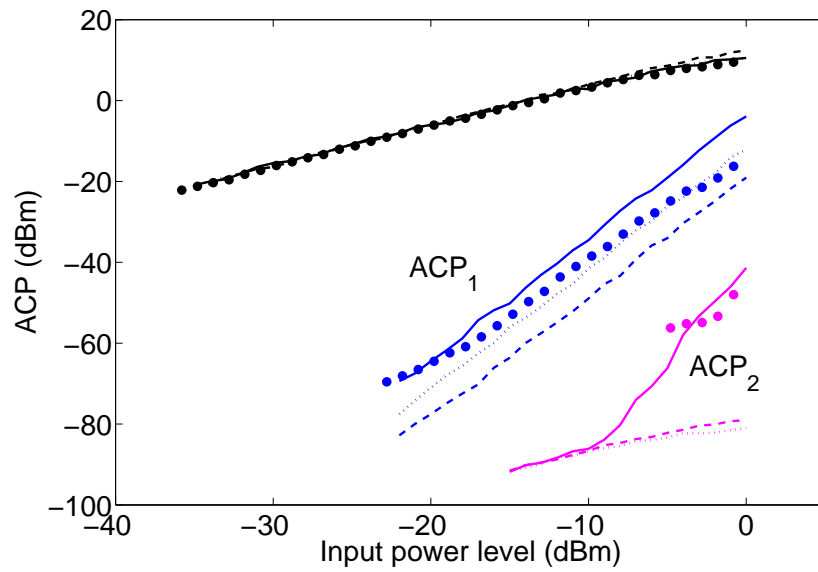


Figure 0.12: Predicción de potencia en el canal y ACP en los los dos primeros canales adyacentes para una señal W-CDMA de UMTS 3GPP frente a la potencia de entrada. Se comparan las medidas (puntos) con el enfoque SN hasta la tercera (línea continua) y segunda iteración (línea discontinua), y con el método EC (línea punteada).

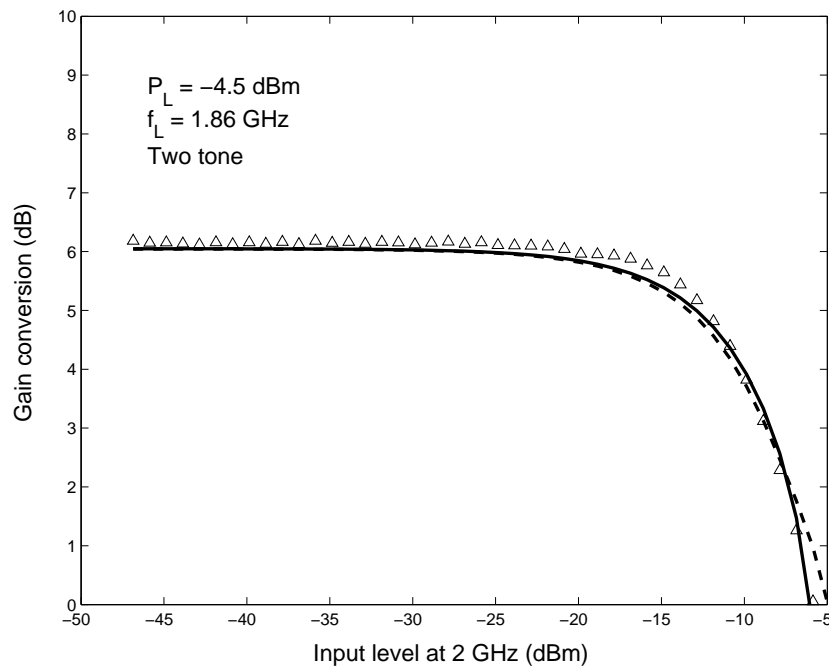


Figure 0.13: Ganancia de conversión de un mezclador de puerta HEMT para una señal de dos tonos. Medidas (triángulos) y resultados de las simulaciones mediante los métodos propuestos (E-PHB: línea continua; NEC-M: línea discontinua).

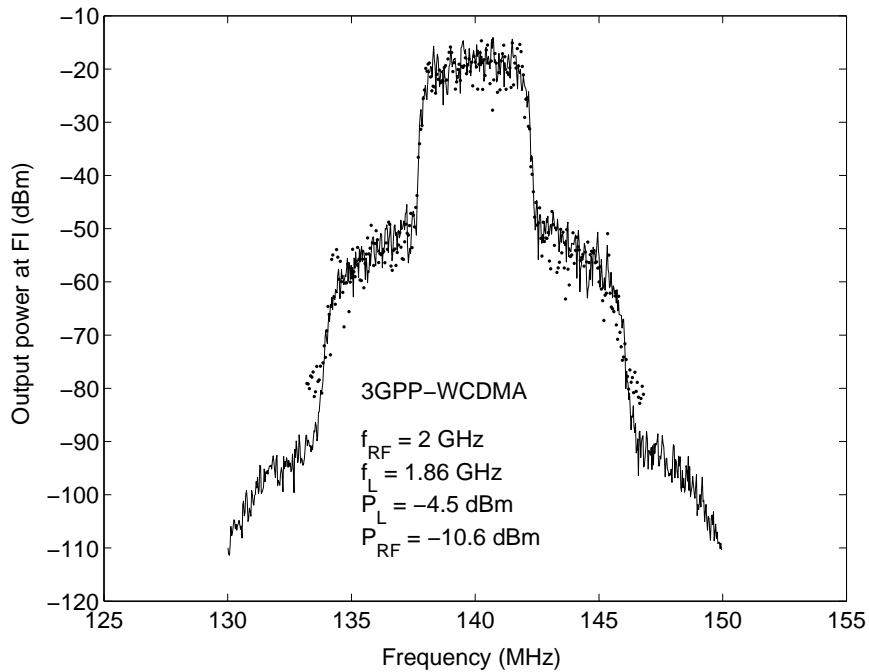


Figure 0.14: Predicción del recrecimiento espectral para una señal W-CDMA de UMTS 3GPP (línea continua) y medidas (puntos). Ancho de banda de resolución: 100 kHz.

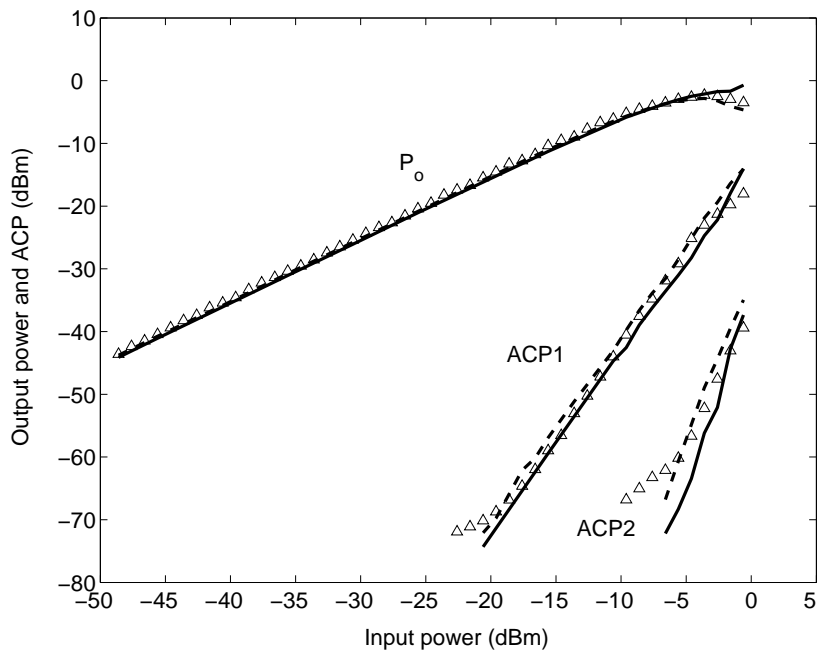


Figure 0.15: Predicción de la potencia cocanal y ACP para una señal W-CDMA de UMTS 3GPP (E-PHB: línea continua y NEC-M: línea discontinua) y medidas (triángulos). Ancho de banda de cálculo: 3.84 MHz.

que supone. Por último, la Figura 0.15 presenta una comparación entre los valores medidos y predichos para la potencia cocanal y el ACP de los dos canales adyacentes superiores e inferiores en un amplio rango de potencias de entrada. El ajuste es muy adecuado, considerando que con el enfoque E-PHB se emplearon unos 5 minutos de tiempo de simulación por nivel de potencia.

Modelado de la distorsión de intermodulación

Los métodos tradicionales de modelado no pueden estimar la dependencia de la IMD con el ancho de banda y, en cambio, es necesario tener en cuenta estos efectos para satisfacer los requisitos exigidos en el diseño de amplificadores cada vez para mayores anchos de banda. Por tanto, está justificada la necesidad de modelo que permitan predecir los efectos de memoria. El método predominante para el análisis teórico del comportamiento débilmente no lineal es la representación mediante series de Volterra, tanto convencionales [28], [21], [75], [76], como dinámicas [59]. El principal motivo es que sus resultados pueden escribirse en expresiones cerradas que contribuyen a la comprensión del fenómeno de la IMD. Estudios de este tipo como [28] o [21] indican que las impedancias de terminación en banda base son las principales causas de las asimetrías y los efectos de memoria observados en los productos de IM. Siguiendo este enfoque, en este trabajo se ha aplicado el enfoque de Newton Simplificado al análisis de la IMD para señales de dos tonos en amplificadores HEMT bajo la suposición de banda estrecha e incluyendo hasta términos de quinto orden. Esto ha permitido hallar expresiones teóricas cerradas para IM3 e IM5.

Enfoque de Newton Simplificado aplicado al análisis de los productos de intermodulación

Para el análisis de los productos de IM en amplificadores HEMT se ha considerado el circuito equivalente simplificado de dos nodos que se muestra en la Figura 0.16, donde sólo se considera la no linealidad principal. Las impedancias de fuente y carga, $Z_s(f)$ y $Z_L(f)$, incluyen los elementos de las redes de polarización y de adaptación. Al aplicar el enfoque SN, tendremos en cuenta que la corriente de drenador se puede escribir $i_{ds}(t) = g_{10}v_g(t) + g_{01}v_d(t) + i_{NL}[v_g(t), v_d(t)]$, donde g_{10} y g_{01} son las conductancias lineales incluidas en el circuito lineal aumentado y el término de la contribución no lineal viene dado por $i_{NL}[v_g(t), v_d(t)] = \sum_{k=2}^{\infty} g_{k0}v_g^k(t) + \sum_{l=2}^{\infty} g_{0l}v_d^l(t) + \sum_{k,l=1}^{\infty} g_{kl}v_g^k(t)v_d^l(t)$, donde las sumas se han truncado suponiendo que $g_{k0} = 0$, $g_{0l} = 0$ para $k, l > 5$ y $g_{kl} = 0$ para $k + l > 3$.

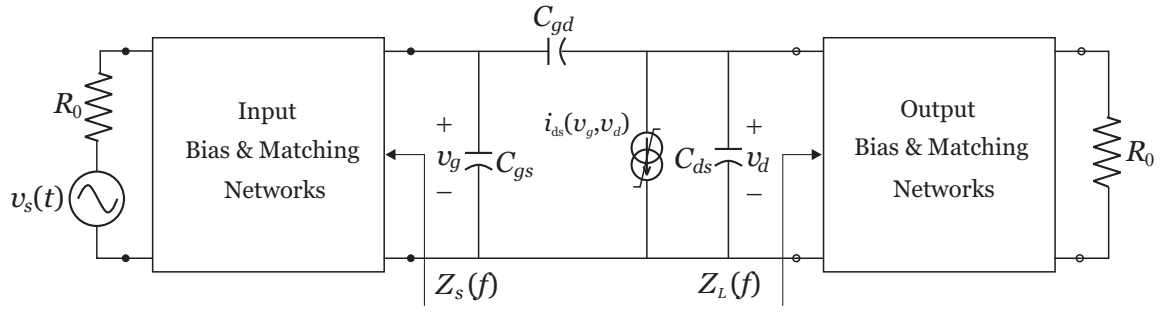


Figure 0.16: Circuito equivalente de dos nodos empleado en el análisis de IM de un amplificador HEMT, donde sólo se ha considerado la no linealidad principal.

Un análisis nodal del circuito cuyas incógnitas son las tensiones de los nodos en el dominio de la frecuencia da lugar a:

$$\mathbf{Y}(f)\mathbf{V}(f) = \mathbf{I}(f), \quad (0.73)$$

donde

$$\mathbf{Y}(f) = \begin{bmatrix} \bar{Y}_s(f) & -j2\pi f C_{gd} \\ Y_{md}(f) & \bar{Y}_L(f) \end{bmatrix}, \quad (0.74)$$

y las siguientes definiciones se han tenido en cuenta:

$$\bar{Y}_L(f) = Y_L(f) + j2\pi f(C_{ds} + C_{gd}) + g_{01}, \quad (0.75)$$

$$Y_{md}(f) = -j2\pi f C_{gd} + g_{10}, \quad (0.76)$$

$$\bar{Y}_s(f) = Y_s(f) + j2\pi f(C_{gs} + C_{gd}). \quad (0.77)$$

Considérese que se aplica una señal de dos tonos de RF expresada mediante su envolvente compleja:

$$v_s(t) = \frac{1}{2} \tilde{v}_s(t) e^{j2\pi f_c t} + \frac{1}{2} \tilde{v}_s^*(t) e^{-j2\pi f_c t}, \quad (0.78)$$

donde

$$\tilde{v}_s(t) = A e^{j2\pi f_m t} + A e^{-j2\pi f_m t} = 2A \cos(2\pi f_m t), \quad (0.79)$$

y se asume banda estrecha, i.e., $m f_m \ll f_c$ para $m \leq 5$. Con esta fuente de excitación, en cualquier paso del algoritmo SN las variables del circuito para la iteración n -ésima tomarán la forma general

$$v_n(t) = \frac{1}{2} \sum_{h=-\infty}^{\infty} \tilde{v}_n(h, t) e^{j2\pi h f_c t} = \frac{1}{2} \sum_{h, m=-\infty}^{\infty} \tilde{v}_n(h, m) e^{j2\pi (h f_c + m f_m) t}. \quad (0.80)$$

Estas señales se aproximarán por señales cuasi-periódicas tomando un número finito de armónicos H .

En el régimen permanente cuasi-periódico, la expresión equivalente en el dominio de la frecuencia para el método SN es $\mathbf{Y}(hf_c + f) \tilde{\mathbf{V}}_n(h, f) = \tilde{\mathbf{I}}_n(h, f)$, para cada iteración n y cada armónico h . Una vez que se ha hallado el punto de reposo del circuito y se han realizado los desarrollos en serie de potencias de las fuentes no lineales, se dejan a circuito abierto todas las fuentes de corriente y se resuelve el análisis nodal del circuito lineal aumentado para la primera iteración ($n = 1$). En este caso sólo existen términos a frecuencias para $h = 1$ y $m = \pm 1$:

$$\begin{aligned}\tilde{v}_{g1}(1, \pm 1) &= H_{g1}A \\ \tilde{v}_{d1}(1, \pm 1) &= H_1A.\end{aligned}\tag{0.81}$$

donde H_{g1} y H_1 son las funciones de transferencia lineales que relacionan las tensiones de entrada con las de los nodos de puerta y drenador, respectivamente, ambas evaluadas a la frecuencia de la portadora f_c .

Para la segunda iteración, se cortocircuita la fuente de corriente externa y se aplican las corrientes no lineales. A partir de la expresión de la corriente no lineal $i_2(t) = -i_{NL}[v_{g1}(t), v_{d1}(t)]$ se obtienen las componentes envolventes de corriente $\tilde{i}_2(h, m)$, de las cuales las más relevantes son las correspondientes a la zona de dc:

$$\begin{aligned}\tilde{i}_2(0, \pm 2) &= -[\gamma_{20}A^2 + 3\gamma_{40}A^4], \\ \tilde{i}_2(0, \pm 4) &= -\frac{3}{4}\gamma_{40}A^4,\end{aligned}\tag{0.82}$$

y de la frecuencia fundamental:

$$\begin{aligned}\tilde{i}_2(1, \pm 1) &= -\left[\frac{9}{4}\gamma_{31}A^3 + \frac{25}{4}\gamma_{51}A^5\right], \\ \tilde{i}_2(1, \pm 3) &= -\left[\frac{3}{4}\gamma_{31}A^3 + \frac{25}{8}\gamma_{51}A^5\right], \\ \tilde{i}_2(1, \pm 5) &= -\frac{5}{8}\gamma_{51}A^5.\end{aligned}\tag{0.83}$$

Las componentes de las tensiones incrementales a las frecuencias $hf_c + mf_m$ se pueden expresar como

$$\begin{aligned}\tilde{v}_{g2}(h, m) &= Z_g(hf_c + mf_m)\tilde{i}_2(h, m) \approx Z_{gh}\tilde{i}_2(h, m), \\ \tilde{v}_{d2}(h, m) &= Z(hf_c + mf_m)\tilde{i}_2(h, m) \approx Z_h\tilde{i}_2(h, m),\end{aligned}\tag{0.84}$$

donde $Z_g(f)$ y $Z(f)$ son las impedancias que relacionan componentes de las corrientes no lineales con las componentes de $v_g(t)$ y $v_d(t)$, respectivamente. Para la zona de dc $Z_g(mf_m) \approx 0$ pero $Z(mf_m) = \bar{Z}_L(mf_m)$, que representa la impedancia de carga vista por la fuente de corriente de drenador a frecuencias de banda base, de forma que se cumplen las relaciones

$$\tilde{v}_{g2}(0, m) = 0,$$

$$\tilde{v}_{d2}(0, m) = \bar{Z}_L(m f_m) \tilde{i}_2(0, m), \quad (0.85)$$

para m par. En otras zonas de frecuencia, se hacen las aproximaciones $Z_g(h f_c + m f_m) \approx Z_g(h f_c) = Z_{gh}$ y $Z(h f_c + m f_m) \approx Z(h f_c) = Z_h$ que implican que la impedancia es plana a la frecuencia fundamental y para sus armónicos. En cambio, presenta variaciones a frecuencias de banda base, lo que se suele dar para las características típicas de la carga y las redes de polarización y de adaptación empleadas en amplificadores de RF.

Las contribuciones de la tensión incremental de segundo orden para la zona de la fundamental resultan:

$$\begin{aligned} \tilde{v}_{d2}(1, \pm 1) &= - \left[\frac{9}{4} \gamma_{31} Z_1 A^3 + \frac{25}{4} \gamma_{51} Z_1 A^5 \right], \\ \tilde{v}_{d2}(1, \pm 3) &= - \left[\frac{3}{4} \gamma_{31} Z_1 A^3 + \frac{25}{8} \gamma_{51} Z_1 A^5 \right], \\ \tilde{v}_{d2}(1, \pm 5) &= - \frac{5}{8} \gamma_{51} Z_1 A^5. \end{aligned} \quad (0.86)$$

Para la tercera iteración es necesario evaluar la corriente no lineal $i_3(t) = - \left[i_{NL} [v_{g1}(t) + v_{g2}(t), v_{d1}(t) + v_{d2}(t)] - i_{NL} [v_{g1}(t), v_{d1}(t)] \right]$. Para ello se realiza una aproximación de la misma mediante un desarrollo en serie de Taylor de primer orden, resultando $i_3(t) = - \left\{ 2g_{20} v_{g1}(t) v_{g2}(t) + g_{11} [v_{d1}(t) v_{g2}(t) + v_{g1}(t) v_{d2}(t)] + 2g_{02} v_{d1}(t) v_{d2}(t) \right\}$. Siguiendo un procedimiento análogo al de la segunda iteración se obtienen las contribuciones de la tensión incremental de drenador de tercer orden.

Como resumen, en la Tabla 0.1 se presentan los términos de la tensión incremental de drenador en la zona de la frecuencia fundamental. Sumando las tensiones incrementales para todas las iteraciones consideradas, se puede expresar la tensión de drenador a las frecuencias de los tonos $f = f_c \pm f_m$ como

$$V_{d_{u,l}} = H_1 A + \left[\frac{9}{4} \gamma_3 + \gamma'_{20} \bar{Z}_L(\pm \Delta f) \right] A^3 + \left[\frac{25}{4} \gamma_5 + 3 \gamma'_{40} \bar{Z}_L(\pm \Delta f) \right] A^5, \quad (0.87)$$

donde la notación V_{d_i}/V_{d_u} se emplea para denotar las frecuencias de los tonos inferior/superior, respectivamente; y los coeficientes γ , que cambian con la polarización pero son constantes con la frecuencia de banda base, están definidos en el Apéndice C. De forma similar, se obtiene IM3 a las frecuencias $f = f_c \pm 3f_m$ como

$$V_{d_{3u,3l}} = \left[\frac{3}{4} \gamma_3 + \gamma'_{20} \bar{Z}_L(\pm \Delta f) \right] A^3 + \left[\frac{25}{8} \gamma_5 + 3 \gamma'_{40} \bar{Z}_L(\pm \Delta f) + \frac{3}{4} \gamma'_{40} \bar{Z}_L(\pm 2 \Delta f) \right] A^5, \quad (0.88)$$

e IM5 a las frecuencias $f = f_c \pm 5f_m$ como

$$V_{d_{5u,5l}} = \left[\frac{5}{8} \gamma_5 + \frac{3}{4} \gamma'_{40} \bar{Z}_L(\pm 2 \Delta f) \right] A^5. \quad (0.89)$$

Table 0.1: Términos de V_{d_n} para la zona de la frecuencia fundamental ($h = 1$)

	$m = \pm 1$
$n = 1$	$H_1 A$
$n = 2$	$-\frac{9}{4}\gamma_{31}Z_1A^3 - \frac{25}{4}\gamma_{51}Z_1A^5$
$n = 3$	$\frac{3}{2}\gamma'_{22}Z_1A^3 + \gamma'_{20}\bar{Z}_L(\pm\Delta f)A^3 +$ $+ [5\gamma'_{42}Z_1 + 3\gamma'_{40}\bar{Z}_L(\pm\Delta f)] A^5$
	$m = \pm 3$
$n = 1$	0
$n = 2$	$-\frac{3}{4}\gamma_{31}Z_1A^3 - \frac{25}{8}\gamma_{51}Z_1A^5$
$n = 3$	$\frac{1}{2}\gamma'_{22}Z_1A^3 + \gamma'_{20}\bar{Z}_L(\pm\Delta f)A^3 +$ $+ [\frac{5}{2}\gamma'_{42}Z_1 + 3\gamma'_{40}\bar{Z}_L(\pm\Delta f) + \frac{3}{4}\gamma'_{40}\bar{Z}_L(\pm 2\Delta f)] A^5$
	$m = \pm 5$
$n = 1$	0
$n = 2$	$-\frac{5}{8}\gamma_{51}Z_1A^5$
$n = 3$	$[\frac{1}{2}\gamma'_{42}Z_1 + \frac{3}{4}\gamma'_{40}\bar{Z}_L(\pm 2\Delta f)] A^5$

Por tanto, las variaciones de IM3 e IM5 sólo dependen de las variaciones de la impedancia de carga banda base con la separación entre los tonos Δf , siendo este termino la fuente principal de los efectos de memoria del dispositivo. Por otro lado, las expresiones (0.87)- (0.89) dan lugar a valores distintos para las frecuencias inferiores y superiores puesto que la impedancia de carga \bar{Z}_L puede tomar valores distintos para las frecuencias de banda base positivas y negativas. Por lo tanto, se obtienen las siguientes expresiones para las asimetrías de IM3 e IM5:

$$A_3 = \frac{1 + \frac{4\gamma'_{20}}{3\gamma_3}\bar{Z}_L(\Delta f) + \left[\frac{25}{6} \frac{\gamma_5}{\gamma_3} + 4 \frac{\gamma'_{40}}{\gamma_3}\bar{Z}_L(\Delta f) + \frac{\gamma'_{40}}{\gamma_3}\bar{Z}_L(2\Delta f) \right] A^2}{1 + \frac{4\gamma'_{20}}{3\gamma_3}\bar{Z}_L^*(\Delta f) + \left[\frac{25}{6} \frac{\gamma_5}{\gamma_3} + 4 \frac{\gamma'_{40}}{\gamma_3}\bar{Z}_L^*(\Delta f) + \frac{\gamma'_{40}}{\gamma_3}\bar{Z}_L^*(2\Delta f) \right] A^2}, \quad (0.90)$$

$$A_5 = \frac{1 + \frac{6\gamma'_{40}}{5\gamma_5}\bar{Z}_L(2\Delta f)}{1 + \frac{6\gamma'_{40}}{5\gamma_5}\bar{Z}_L^*(2\Delta f)}. \quad (0.91)$$

La novedad introducida por estas expresiones es que los resultados propuestos incluyen efectos de quinto orden, dando lugar a una descripción más detallada de la asimetría de IM3 y permitiendo la predicción de IM5.

Para comprobar los resultados de las predicciones proporcionadas por las expresiones anteriores, se han comparado con las medidas realizadas sobre un amplificador HEMT EPB018A5-70 de Excellics. Para poder realizar simulaciones hasta quinto orden fue necesario emplear un modelo de Curtice de cinco coeficientes, en lugar del modelo de Curtice cúbico proporcionado por el fabricante.

En primer lugar se midió el amplificador usando la red de polarización resonante indicada previamente. En las Figuras 0.17 y 0.18 se muestran resultados correspondientes a la asimetría de fase de IM3. La dependencia en frecuencia mostrada por la impedancia de carga de banda base se observa claramente en ambas gráficas, produciendo una asimetría de fase en torno a 130 kHz. Tanto las medidas como la característica calculada muestran también un cambio en la fase a la frecuencia $\frac{\Delta f}{2}$, que indica la contribución de los términos de quinto orden a IM3. Este efecto se describe de forma aproximada mediante el procedimiento propuesto en la Figura 0.17 (línea discontinua), mientras que no es posible cuando se emplea un enfoque convencional basado en series de Volterra como el aplicado en [21] (línea punteada). La coincidencia de las simulaciones con las medidas puede mejorarse usando un modelo más detallado de la red de polarización, incluyendo el factor Q de sus elementos, y unos valores optimizados de los coeficientes γ para mejorar el modelo no lineal del HEMT, como se muestra con línea continua en la Figura 0.17. La Figura 0.18 representa medidas de la asimetría de fase de IM3 para dos valores diferentes de la tensión V_{GS} a una potencia $P_{in} = -12.4$ dBm, en las que se puede observar una inversión en la fase entre

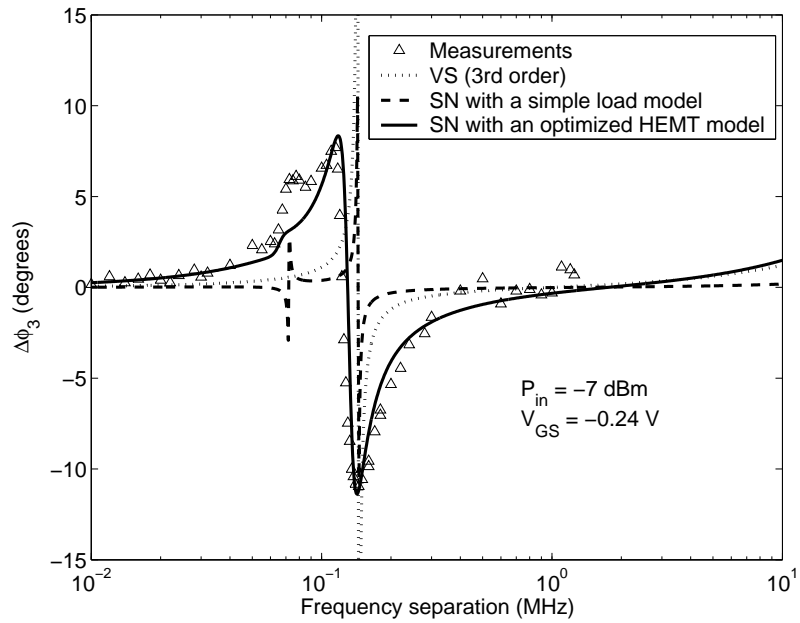


Figure 0.17: Diferencia de fase de IM3 para un amplificador HEMT con red de polarización resonante. Línea punteada: enfoque convencional de series de Volterra. Línea discontinua: enfoque SN con un modelo de carga básico. Línea continua: enfoque SN con un modelo optimizado.

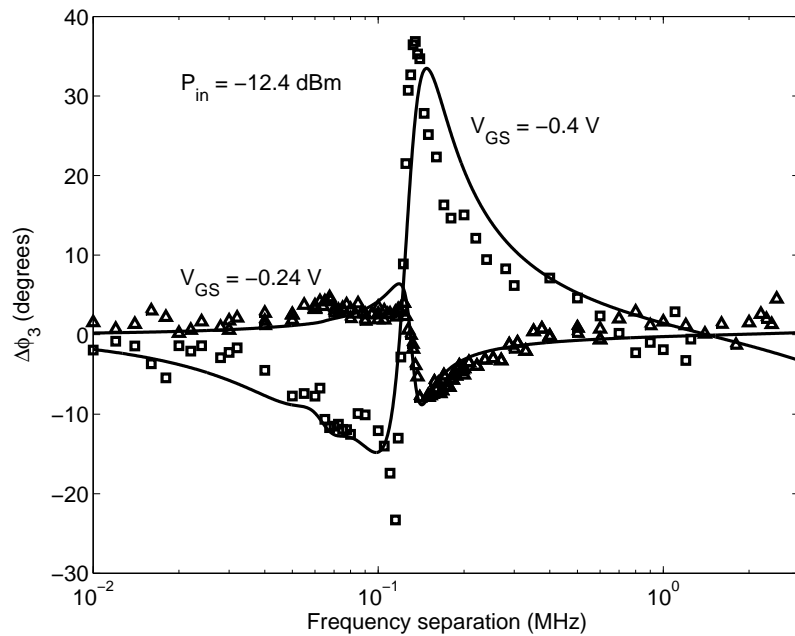


Figure 0.18: Medida de la diferencia de fase de IM3 para el punto de polarización recomendado (triángulos) y para $V_{GS} = -0.4$ V (cuadrados). Línea continua: enfoque SN con modelo optimizado.

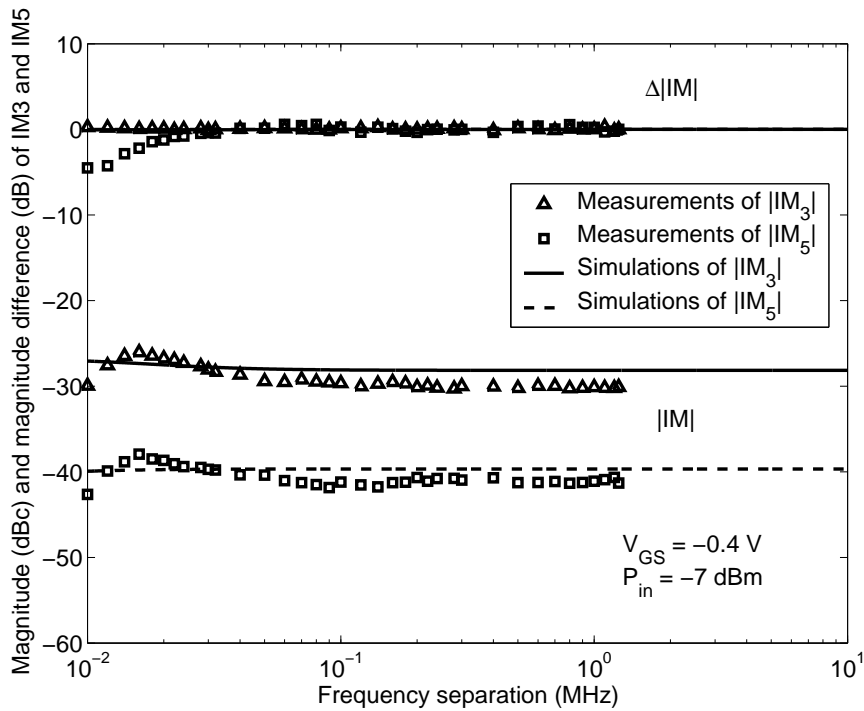


Figure 0.19: Medida de la magnitud y de la diferencia de magnitud de IM3 (triángulos) e IM5 (cuadrados) empleando una bias-Tee comercial. Línea continua: simulaciones con el enfoque SN.

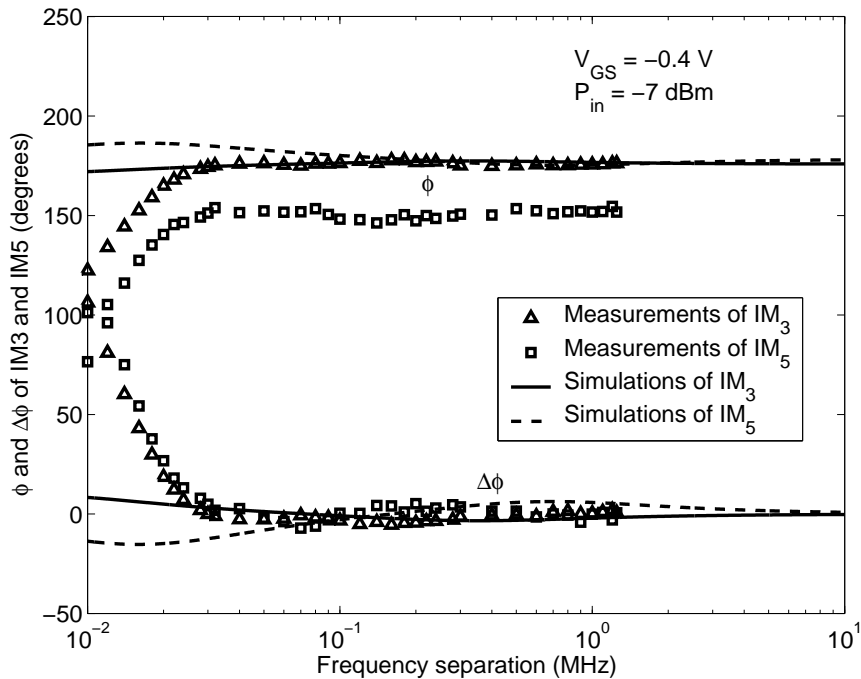


Figure 0.20: Medida de la fase y de la diferencia de fase de IM3 (triángulos) e IM5 (cuadrados) empleando una bias-Tee comercial. Línea continua: simulaciones con el enfoque SN.

ambas polarizaciones y que la asimetría es más pronunciada para la polarización con $V_{GS} = -0.4$ V.

Cuando se polarizó el amplificador usando una bias-Tee comercial ZFBT-6GW de Minicircuits, los resultados obtenidos tanto para la magnitud como para la fase de los productos IM3 e IM5 se muestran en las Figuras 0.19 y 0.20, incluyendo las asimetrías de tercer y quinto orden. En este caso, se extrajo el modelo de la bias-Tee comercial empleada a partir de medidas del parámetro s_{11} en un VNA y la impedancia de carga obtenida se empleó en las simulaciones. Aunque se observa un buen ajuste general con las medidas, existe una desviación evidente para separaciones entre los tonos por debajo de 30 kHz. Esto sugiere que la dependencia con la frecuencia observada en dicha zona podría haber sido causada por efectos de memoria de origen térmico o debidos a estados trampa y de ionización por impacto.

Discusión sobre los resultados teóricos

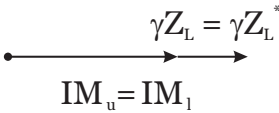
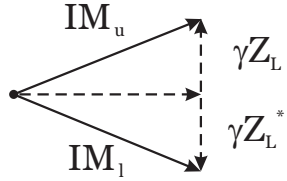
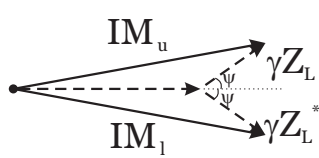
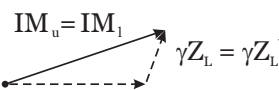
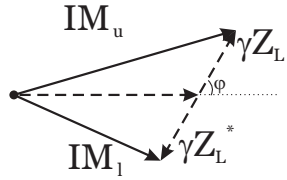
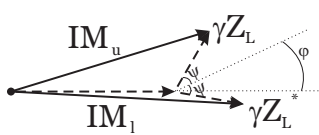
En muchos trabajos, sólo se consideran asimetrías en la magnitud de los productos de IM, sin prestar atención a las asimetrías en la fase. Por otro lado, aunque la existencia de asimetría es otra indicación de efectos de memoria, no todos los sistemas con memoria presentarán asimetrías espectrales. Por eso, se han estudiado las circunstancias que es necesario que se den para que se observen asimetrías en magnitud y/o fase en los productos de IM. Para ello se ha partido de una expresión simplificada que retiene la dependencia con la impedancia de carga de banda base de las expresiones (0.90) and (0.91):

$$F_{asym} = \frac{1 + \gamma \bar{Z}_L}{1 + \gamma \bar{Z}_L^*}. \quad (0.92)$$

En la Tabla 0.2 se ilustran los diferentes escenarios que se pueden dar. Se puede concluir que:

- Si la impedancia de carga de banda base \bar{Z}_L es real no son posibles efectos de memoria ni asimetrías, ni de magnitud ni de fase.
- Si la impedancia de carga de banda base \bar{Z}_L tiene una parte imaginaria no despreciable, el dispositivo siempre presentará asimetría de fase.
- Sólo cuando los coeficientes γ y la impedancia de carga de banda base \bar{Z}_L son complejos aparecerá una asimetría tanto en magnitud como en fase.
- Si los coeficientes γ son despreciables, el término constante dominará los vectores resultantes y no será posible observar asimetrías. En este caso, aunque la variación de la IMD con Δf no sea evidente, el amplificador sigue presentando efectos de memoria.

Table 0.2: Diferentes situaciones de asimetría con respecto a γ y \bar{Z}_L .

$\gamma \in \mathbb{R}$		
$\bar{Z}_L \in \mathbb{R}$	\bar{Z}_L es imaginario puro	$\bar{Z}_L \in \mathbb{C}, \quad \bar{Z}_L = Z e^{j\psi}$
$\bar{Z}_L^* = \bar{Z}_L$ $ F_{asym} = 1, \quad \phi_{asym} = 0$	$\bar{Z}_L^* = -\bar{Z}_L$ $ F_{asym} = 1, \quad \phi_{asym} \neq 0$	$\bar{Z}_L^* = Z e^{-j\psi}$ $ F_{asym} = 1, \quad \phi_{asym} \neq 0$
 <p style="text-align: center;">$\text{IM}_u = \text{IM}_1$ Simetría</p>	 <p style="text-align: center;">Simetría en magnitud Asimetría en fase</p>	 <p style="text-align: center;">Simetría en magnitud Asimetría en fase</p>
$\gamma \in \mathbb{C}, \quad \gamma = \gamma e^{j\varphi}$		
$\bar{Z}_L \in \mathbb{R}$	\bar{Z}_L es imaginario puro	$\bar{Z}_L \in \mathbb{C}, \quad \bar{Z}_L = Z e^{j\psi}$
$\gamma \bar{Z}_L^* = \gamma \bar{Z}_L$ $ F_{asym} = 1, \quad \phi_{asym} = 0$	$\gamma \bar{Z}_L^* = -\gamma \bar{Z}_L$ $ F_{asym} \neq 1, \quad \phi_{asym} \neq 0$	$\gamma \bar{Z}_L = \gamma Z e^{j(\varphi+\psi)}$ $\gamma \bar{Z}_L^* = \gamma Z e^{j(\varphi-\psi)}$ $ F_{asym} \neq 1, \quad \phi_{asym} \neq 0$
 <p style="text-align: center;">$\text{IM}_u = \text{IM}_1$ Simetría</p>	 <p style="text-align: center;">Asimetría en magnitud y en fase</p>	 <p style="text-align: center;">Asimetría en magnitud y en fase</p>

- Si la característica observada en un analizador de espectros presenta asimetría (de magnitud), entonces se puede afirmar que el amplificador tiene memoria. Pero no se puede asegurar que cualquier dispositivo con memoria presente asimetría de magnitud ni que un dispositivo que no presente asimetrías en magnitud no tenga memoria.

Modelo de IM3 basado en impedancia para los efectos de memoria electrotérmicos

Las discrepancias observadas entre las medidas y las predicciones proporcionadas por el enfoque SN para los productos de IM sugieren la necesidad de considerar modelos para los efectos de memoria a largo plazo producidos por causas térmicas, ionización por impacto o estados trampa. Para ello, en [77] se propuso un modelo simplificado basado en la obtención de una impedancia de carga equivalente que pudiera explicar dichas discrepancias. Algunos trabajos recientes que tienen en cuenta los efectos de memoria térmicos lo hacen mediante elementos térmicos en el modelo del transistor [78], [79], [80], [81], o mediante un modelo de comportamiento térmico acoplado al circuito equivalente del dispositivo. Otros efectos de memoria a largo plazo cuyo estudio ha sido afrontado recientemente son los estados trampa, que se suelen modelar mediante funciones de transferencia dependientes de Δf y las tensiones de polarización [82], [83]. El modelo propuesto en este caso trata mediante un modelo eléctrico, el de una hipotética impedancia de carga equivalente, cualquier tipo de efecto de memoria sin importar cuál sea su origen. Dicho modelo se obtiene a partir de la comparación de las medidas experimentales de los productos de IM con las expresiones teóricas obtenidas con el método SN, en las que se han despreciado los efectos de quinto orden. Se ha trabajado con las expresiones siguientes de la magnitud y la fase de los productos IM3 relativas a la de los tonos, puesto que se disponía de medidas de fase relativa:

$$F_3 = \frac{\left[\frac{3}{4}\gamma_3 + \gamma'_{20}\bar{Z}_L(\pm\Delta f) \right] A^2}{H_1 + \left[\frac{9}{4}\gamma_3 + \gamma'_{20}\bar{Z}_L(\pm\Delta f) \right] A^2}, \quad (0.93)$$

Recordemos que el único término dependiente de la frecuencia en estas expresiones es $\bar{Z}_L(\pm\Delta f)$, de modo que la impedancia de carga juega un papel predominante en la generación de los efectos de memoria. La idea básica del enfoque propuesto consiste en extraer los valores de una impedancia de carga equivalente que proporcione un ajuste adecuado de las medidas incluso en presencia de efectos dispersivos de baja frecuencia. Parte de dicha impedancia de carga equivalente será conocida, i.e., los elementos del modelo intrínseco del HEMT conectados al drenador, la impedancia de la red de polarización y la impedancia de salida. Por eso, su valor puede eliminarse e in-

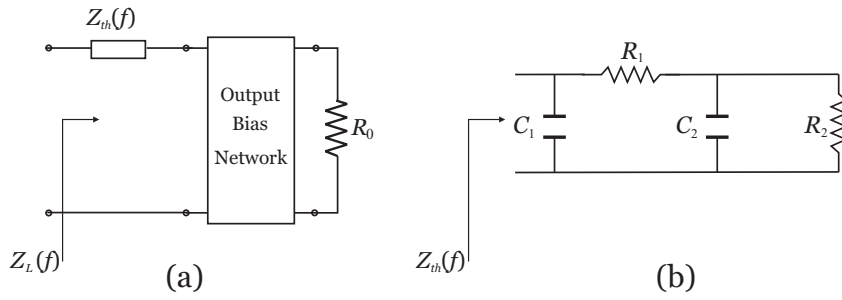


Figure 0.21: Modelo propuesto de la impedancia de carga equivalente \bar{Z}_L (a) y de la impedancia hipotética Z_{th} (b) para el modelo equivalente de un amplificador HEMT utilizado en el análisis.

Introducir el término restante como una impedancia hipotética Z_{th} que tenga en cuenta los efectos electro-térmicos no incluidos en el modelo del dispositivo.

Para ilustrar el procedimiento propuesto, se aplicó a las medidas y el modelo del amplificador construido con el HEMT EPB018A5-70 de Excellics para dos polarizaciones, $V_{GS} = -0.24$ V y $V_{GS} = -0.4$ V, siendo $V_{DS} = 2$ V, y diferentes niveles de entrada que se aplicaron mediante bias-Tee ZFBT-6GW de Minicircuits. Como ya ha sido mencionado, las simulaciones con el enfoque SN sólo ajustan los resultados de las medidas por encima de unos 30 kHz. Por ello, se extrajeron los valores de la impedancia equivalente de carga \bar{Z}_L que producía ajuste perfecto con las medidas en el rango completo y, tras extraer la parte conocida de dicha impedancia, se consiguieron los mejores resultados al modelar la impedancia hipotética Z_{th} debida a efectos electro-térmicos como una impedancia en serie situada entre el modelo intrínseco del amplificador y la red de polarización, tal como se muestra en la Figura 0.21(a). Finalmente, se probaron varias topologías simples de circuitos para Z_{th} , obteniéndose los mejores resultados para un circuito RC en paralelo con dos polos, como el mostrado en la Figura 0.21(b). En todas las pruebas realizadas para distintas condiciones de funcionamiento del amplificador se encontró que el mejor ajuste se producía para la misma configuración de \bar{Z}_L y la misma topología de Z_{th} . En la Figura 0.22 se pueden observar los valores hallados para la impedancia equivalente de carga \bar{Z}_L y para la impedancia hipotética Z_{th} . Aunque los modelos circuitales simples propuestos sólo producen un ajuste moderado, los resultados logrados al introducirlos en las simulaciones de la magnitud y la fase de los productos de IM son más que aceptables, como puede comprobarse de las Figuras 0.23 y 0.24, en los trazos con línea continua. Cabe destacar que los cambios con Δf que caracterizan a los efectos de memoria se observan más claramente en fase que en magnitud. Otra característica a resaltar es que el circuito que modela Z_{th} resulta ser un filtro paso bajo, de manera que juega un papel análogo al de una impedancia térmica como las propuestas en [27] o [78].

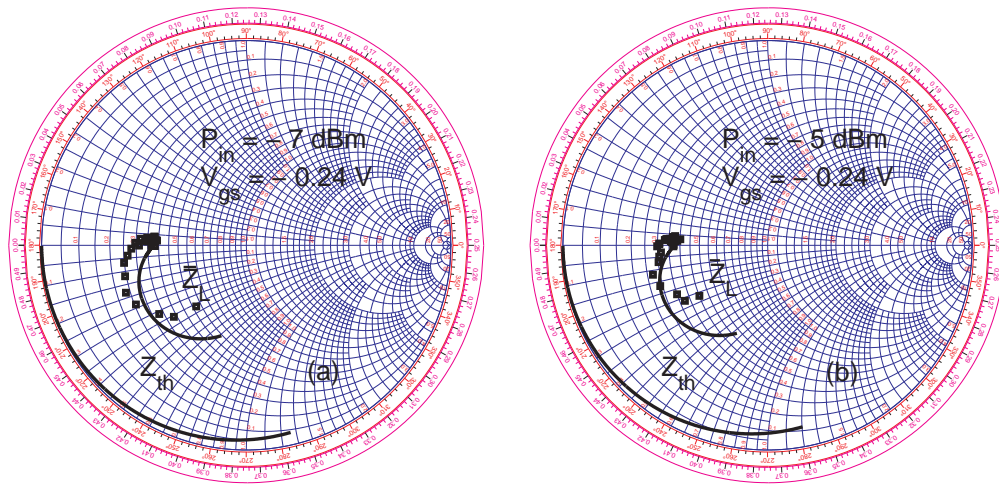


Figure 0.22: Carta de Smith con los valores extraídos de Z_{th} (triángulos) para un amplificador HEMT con $P_{in} = -7$ dBm (a) y $P_{in} = -5$ dBm (b) para una tensión de polarización $V_{GS} = -0.24$ V. La línea continua representa la impedancia del circuito resonante paralelo RC que mejor aproxima los valores extraídos y la impedancia de carga equivalente (\bar{Z}_L) incluyendo este circuito RC.

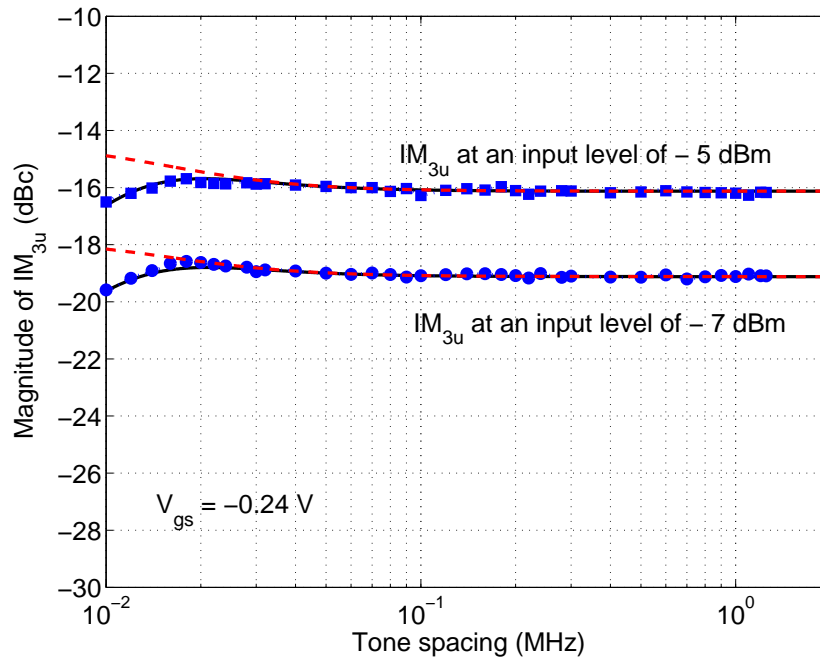


Figure 0.23: Medida de la magnitud de los productos IM3 superiores para un amplificador HEMT con $P_{in} = -7$ dBm (círculos) y $P_{in} = -5$ dBm (cuadrados), con polarización $V_{GS} = -0.24$ V. Predicciones sin Z_{th} (línea discontinua), con los valores extraídos de Z_{th} (línea punteada) y con el modelo circuital escogido (línea continua).

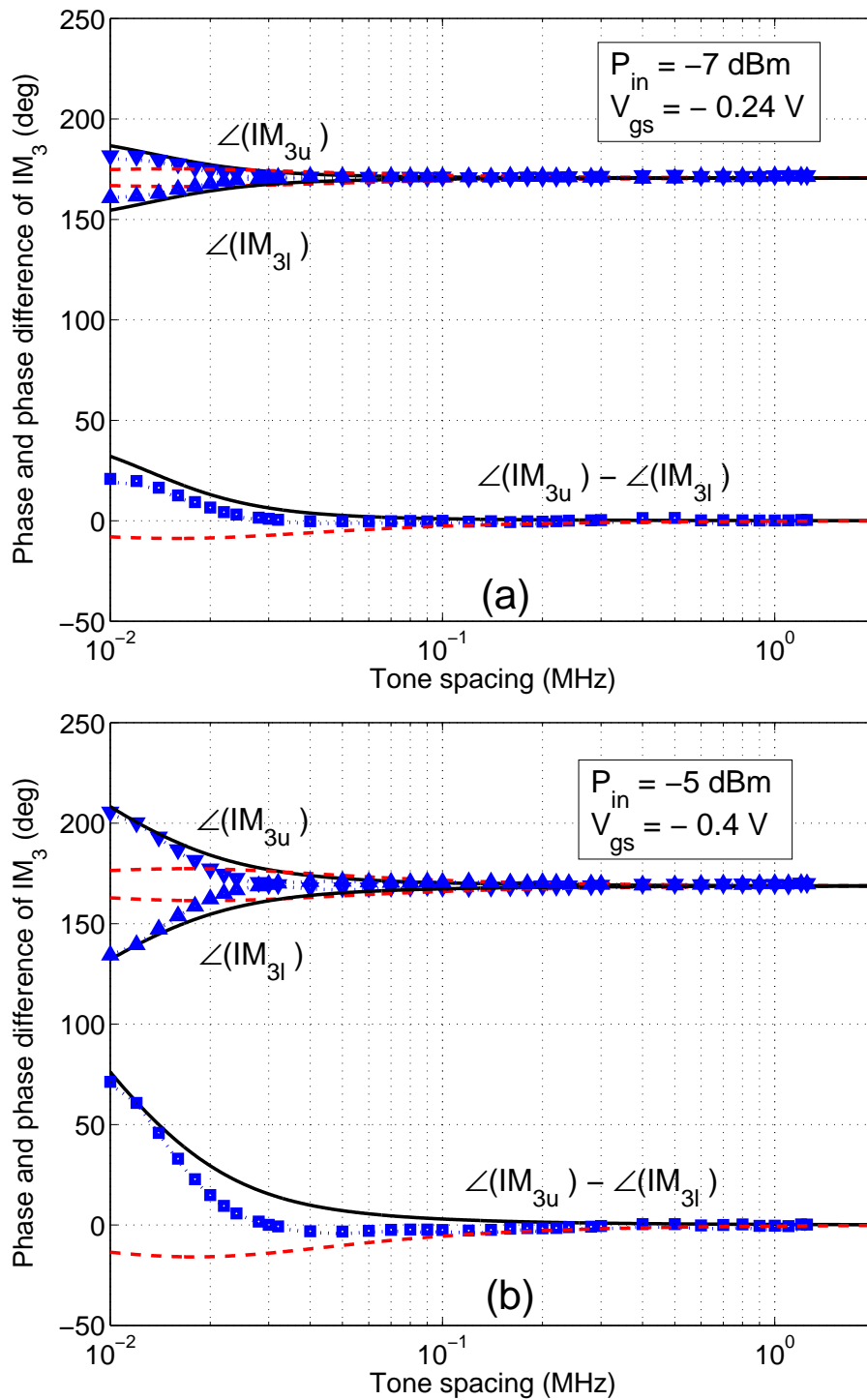


Figure 0.24: Medida de la fase (triángulos) de los productos IM3 y la asimetría de fase (cuadrados) para un amplificador HEMT con $P_{in} = -7$ dBm (círculos) y $P_{in} = -5$ dBm (cuadrados), con polarización $V_{GS} = -0.24$ V. Predicciones sin Z_{th} (línea discontinua), con los valores extraídos de Z_{th} (línea punteada) y con el modelo circuital escogido (línea continua).

Extensión del modelo basado en impedancia para amplificadores comerciales

Los resultados teóricos obtenidos para un dispositivo HEMT se pueden generalizar para amplificadores con circuitos más complejos, para los que se propone la siguiente extensión [84]:

$$V_{3u,3l} = \sum_{\substack{n=3 \\ n\text{-odd}}} [a_n + b_n Z_{eq}(\pm \Delta f)] A^n, \quad (0.94)$$

donde los parámetros a_n y b_n dependen de la frecuencia de portadora, mientras que la impedancia equivalente Z_{eq} modela la dependencia de los productos de IM con la frecuencia. El modelo fue aplicado para el caso de un amplificador comercial MAX2430 de MAXIM, al que se le realizaron medidas de IM3 tanto en magnitud como en fase, tomando cuatro valores para la potencia de entrada entre -25 y -10 dBm y 15 valores para la separación entre los tonos para cada nivel. Las medidas se han ajustado al modelo propuesto mediante un procedimiento de optimización no lineal por mínimos cuadrados, puesto que no se tiene conocimiento de la estructura interna del circuito.

Los valores de la impedancia $Z_{eq}(\Delta f)$ que minimizan el error cuadrático se muestran en la Figura 0.25. Puesto que dicha curva en la carta de Smith resulta similar a la de un circuito resonante paralelo, $Z_{eq}(\Delta f)$ se ha aproximado por la impedancia equivalente de un circuito RLC, tal como se dibuja en trazo continuo sobre la misma figura. Finalmente, se han realizado simulaciones con el modelo incluyendo el circuito resonante propuesto junto con los coeficientes calculados $\{a_n, b_n\}$, cuyos resultados se muestran en las Figuras 0.26 y 0.27 para la asimetría en fase de IM3 y la magnitud del producto IM3 superior, respectivamente. Para conseguir ajustar en este caso el modelo en el elevado rango dinámico de las medidas fue necesario emplear 6 coeficientes $\{a_n, b_n\}$. Como se puede observar, el ajuste entre las medidas y el modelo es muy bueno, incluso cuando el amplificador se opera cerca de saturación.

Conclusiones y líneas futuras de investigación

Después de la investigación llevada a cabo en esta Tesis, en la que el enfoque de Newton Simplificado se podría ver como el hilo común de todas las técnicas propuestas, es posible extraer tres ideas fundamentales:

1. Es posible aplicar un nuevo método de Newton Simplificado para analizar los fenómenos de distorsión en circuitos débilmente no lineales excitados por señales de comunicaciones inalámbricas. El método de Newton Simplificado es un enfoque iterativo basado en la resolución de un circuito lineal aumentado excitado por corrientes no lineales diferentes para cada iteración, al igual que

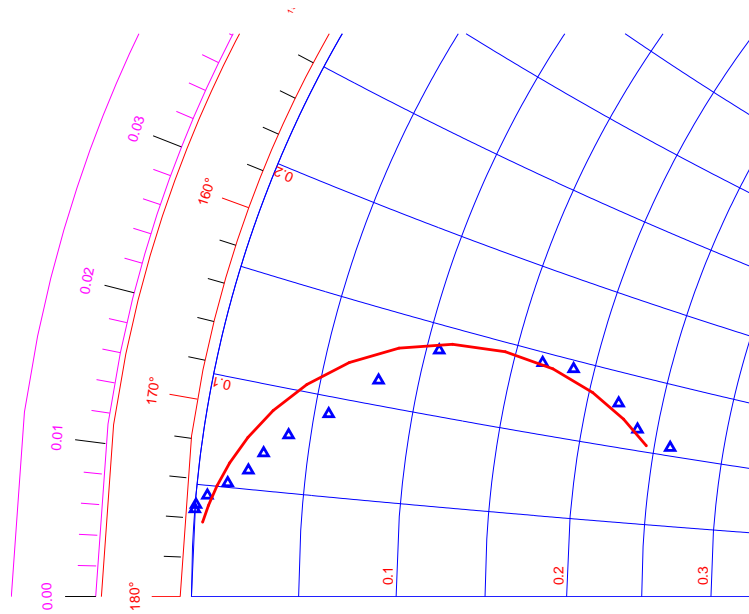


Figure 0.25: Zoom de la carta de Smith con los valores extraídos de $Z_{eq}(\Delta f)$ (triángulos) para un amplificador comercial. Línea continua: impedancia del circuito resonante RLC en paralelo que mejor aproxima los valores extraídos.

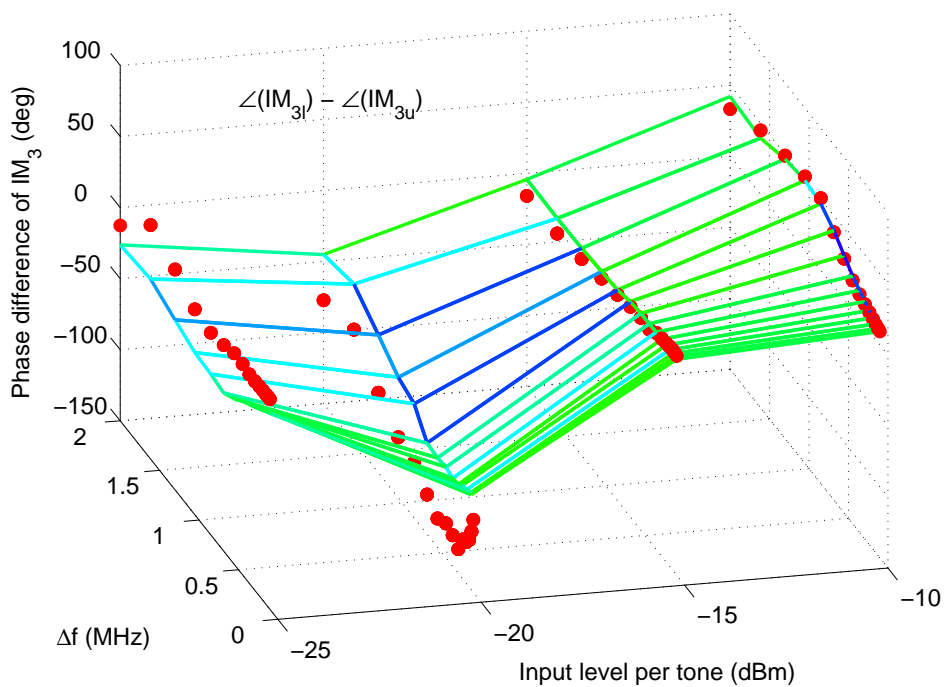


Figure 0.26: Medida de la asimetría de fase de IM3 (puntos) y predicción (malla) usando los valores extraídos de Z_{eq} y 6 parámetros $\{a_n, b_n\}$.

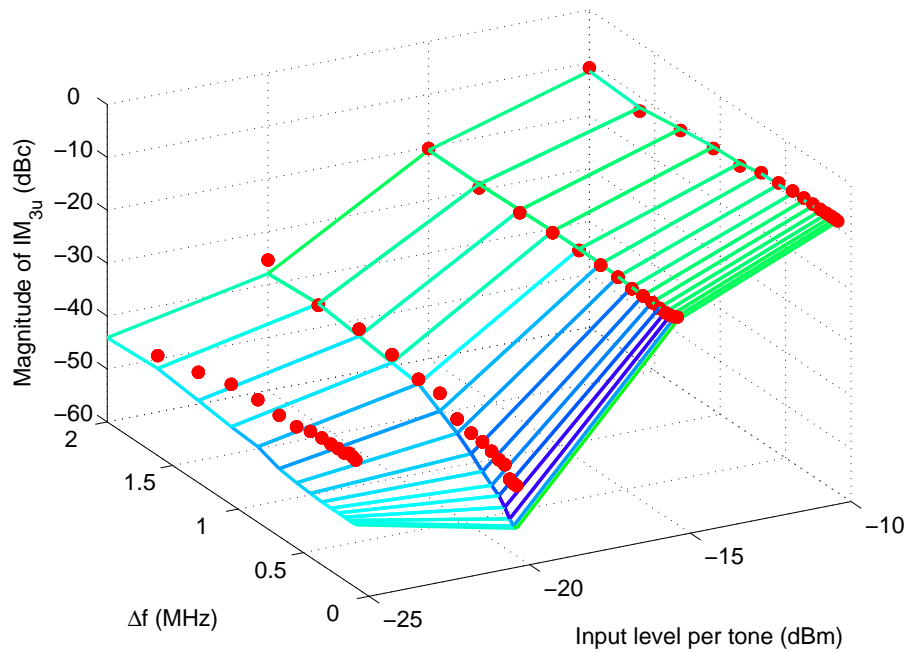


Figure 0.27: Medida de la magnitud del producto IM3 superior (puntos) y predicción (malla) usando los valores extraídos de Z_{eq} y 6 parámetros $\{a_n, b_n\}$.

otros métodos basados en envolvente. Su principal ventaja radica en el hecho de que las corrientes no lineales derivadas mediante este método constituyen una mejor aproximación de la no linealidad real, ya que incluyen términos de mayor orden. A pesar de que la reducida región de convergencia del algoritmo de Newton Simplificado, se han alcanzado predicciones satisfactorias de las características de amplificadores con no linealidades medias. En general, se puede conseguir una reducción del tiempo de computación gracias a la reutilización del Jacobiano, lo que permite simulaciones de ACPR eficientes para un rango amplio de niveles de potencia.

Una aplicación específica de este método se puede diseñar para mezcladores, donde el espectro de salida más complejo aconseja algunas simplificaciones adicionales para reducir el coste computacional y las necesidades de almacenamiento. En este caso, la excitación de entrada es considerada como una perturbación en torno a la respuesta a la gran señal del oscilador local, lo que conduce a la resolución de un subcircuito lineal aumentado que varía periódicamente con el tiempo por medio de la matriz conversión de admitancias.

2. El enfoque de Newton Simplificado se puede usar también para obtener expresiones cerradas para la IMD en amplificadores. Estas expresiones teóricas resultan una alternativa al método convencional de las series de Volterra que tienen la característica de tratarse de un algoritmo de convergencia más rápida sin perder

la posibilidad de generar expresiones cerradas. Esta cualidad permite, no sólo incluir términos de órdenes mayores en la expresión de IM3 que incorporan dependencia con la amplitud a la asimetría de IM3, sino también hacen posible evaluar la magnitud y la fase de IM5. Asimismo, queda patente la influencia de la impedancia de terminación en banda base sobre los efectos de memoria y las asimetrías observadas. Este análisis da lugar a algunas observaciones que permiten comprender mejor el comportamiento de la IM.

3. Es necesario profundizar más en el modelado de gran señal de los circuitos para tener en cuenta los efectos de dispersión a baja frecuencia en las expresiones teóricas de la IMD. Un enfoque prometedor que debería probarse es la extracción de un modelo basado en impedancias tanto para amplificadores FET como comerciales. El uso de una impedancia equivalente dota al modelo de un significado estructural, ya que lo identifica con un elemento circuital con un papel importante en la generación de efectos de memoria, sin importar su naturaleza. Es interesante resaltar que el circuito de impedancia hipotética equivalente modelado para la inclusión de los efectos de memoria de baja frecuencia toma una forma análoga a la de algunas redes dispersivas mencionadas en la literatura.

Algunos de los resultados presentados en esta Tesis son susceptibles de futuras extensiones, al mismo tiempo que se abren nuevas líneas de investigación:

- Sería recomendable extender las estrategias propuestas para mejorar la eficiencia de las técnicas de análisis no lineal al caso de señales moduladas multiportadora, por ejemplo las empleadas en estándares de comunicaciones inalámbricos modernos como son WiMAX o la familia 802.11. Por otro lado, la reducción computacional alcanzada con el método de Newton Simplificado sugiere unos prometedores resultados al ser aplicado para circuitos de muy gran tamaño o sistemas de comunicaciones completos.
- Sería recomendable investigar la aplicación de técnicas para la mejora de la calidad de las medidas realizadas con la herramienta de caracterización diseñada, como la recientemente propuesta en [85] para extender el ancho de banda de los bancos de pruebas de amplificadores de RF.
- Podría ser interesante evaluar las implicaciones de eliminar la suposición de banda estrecha en los resultados obtenidos, de gran importancia para tecnologías como UWB (ultra-wideband).
- La suposición realizada en este trabajo de que las impedancias en un amplificador FET son planas en los anchos de banda estrechos de las señales de comunicaciones en torno a las frecuencias de la fundamental y el segundo armónico

ha sido aplicada con éxito en [86] para la deducción de un modelo de comportamiento basado en series de Volterra, para el que se obtiene una reducción considerable en el número de coeficientes involucrados. Este hecho ha abierto una nueva línea de investigación dirigida al estudio comparativo entre las diferentes estructuras de modelos de comportamiento, su precisión, su efectividad al manejar efectos de memoria o la idoneidad de los procedimientos de identificación de los *kernels* asociados.

- Aún quedan múltiples opciones por explorar con relación a dotar a los modelos circuitales de gran señal de capacidad para modelar los efectos de memoria, incluyendo efectos térmicos, de ionización por impacto o de estados trampa, entre otros fenómenos dispersivos.

ABSTRACT

In this Thesis, a study of nonlinear analysis and experimental characterization techniques for wireless communications systems is made. Starting from a review of the more relevant general-purpose steady-state nonlinear analysis methods, including Harmonic Balance analysis and Volterra series representation with the Nonlinear Currents methods for the obtention on nonlinear transfer functions, evidence is given that classical techniques turn to be inefficient for circuits excited with digital modulations. After that, more efficient envelope-based methods, such as the Envelop [sic] Transient, modulation-oriented Harmonic Balance, and Envelope Currents methods, are presented to specifically address the issue of simulating nonlinear circuits with communications signals.

The Simplified Newton approach is proposed for the analysis of weakly nonlinear communications circuits. This is an iterative approach based on solving an augmented linear subcircuit driven by different nonlinear current sources for each iteration, which result a better approximation for the real nonlinearity than in the Envelope Currents method. It is applied to the study of both weakly nonlinear amplifiers and mixers, obtaining a reduction of the computational time that allows efficient ACPR simulations for a wide range of input power levels. In the case of mixers, a comparison is made between the performance achieved by using an standard Newton approach — the New Envelope Currents method for mixers — and a Simplified Newton approach — the Extended Parametric Harmonic Balance.

Experimental measurements are accomplished, with which the simulation techniques are satisfactorily compared. For this purpose, an explanation on the different kinds of nonlinear characterization techniques and their associated figures of merit is presented, including the concept of memory effects. The proposed measurement setup, which implements a technique for the phase characterization of third- and fifth-order intermodulation products with non-sophisticated communications equip-

ment, is described and illustrated by several examples. Among the characterizations made, the two-tone intermodulation distortion measurements including magnitude and phase, as well as the evaluation of the spectral regrowth and ACPR for UMTS W-CDMA QPSK modulated signals could be remarked.

Additionally to other advantages, it is also demonstrated that the same Simplified Newton approach allows the obtention of closed-form expressions to model the baseband-frequency dependence of the intermodulation distortion in power amplifiers with memory, analogously to Volterra series representation. These theoretical expressions are employed to gain an insight into the impact of the baseband termination impedance, leading to some conditions that need to be met so that an asymmetry in magnitude and/or phase can be observed between the intermodulation products.

Finally, an impedance-based model for the inclusion of electrothermal memory effects in intermodulation (regardless their nature) is presented for FET amplifiers, and then extended for commercial amplifiers with no knowledge of their internal structure. The methodology is based on extracting an equivalent hypothetical load impedance that provides the model with an structural significance. It is shown that there is an analogy between the modelled equivalent impedance circuit and some of the networks found in literature to model low-frequency dispersion phenomena.

CONTENTS

Agradecimientos	i
Acknowledgements	iii
Resumen	v
Abstract	lxi
Contents	lxiii
List of Figures	lxix
List of Tables	lxxv
1 Introduction	1
1.1 Foreword	1
1.2 Aims and scope	5
1.3 Thesis overview	6
2 Steady-State Analysis Methods for Nonlinear Systems	9
2.1 Introduction	9
2.1.1 Frequency-domain methods	12
2.2 Numerical solution of nonlinear equations	13
2.2.1 Newton-Raphson method	13
2.2.2 Convergence criteria	14

2.2.3	Simplified Newton-Raphson methods	15
2.2.4	Continuation methods	18
2.2.5	Discretization	19
2.3	Formulation of the problem	20
2.3.1	Circuit equations: modified nodal analysis	20
2.3.2	Nonlinear circuit elements representation	24
2.4	Harmonic Balance	27
2.4.1	Historical development	27
2.4.2	Harmonic Balance analysis	30
2.4.3	Solution algorithms	36
2.4.3.1	Optimization methods	36
2.4.3.2	Relaxation methods	37
2.4.3.2.1	Splitting	37
2.4.3.2.2	Gauss-Jacobi-Newton Harmonic Relaxation	38
2.4.3.3	Newton's methods or Harmonic Newton	41
2.4.4	Example: Harmonic Balance analysis of a FET amplifier	45
2.4.5	Matrix methods for solving the Harmonic Balance iteration	48
2.4.6	Multitone inputs in Harmonic Balance analysis	51
2.5	Volterra series	54
2.5.1	Volterra series representation	56
2.5.2	Multitone input analysis using Volterra series	60
2.5.3	Volterra series representation of bandpass nonlinear systems with memory	63
2.5.4	Nonlinear transfer functions determination	67
2.5.4.1	Probing or Harmonic Input method	67
2.5.4.2	Nonlinear Currents method	75
2.6	Brief overview of envelope-based methods	82
2.7	Comparison of analysis techniques	83

3	Envelope-based Methods for Nonlinear Wireless Systems	87
3.1	Introduction	87
3.1.1	Modulated signals	89
3.2	Envelop Transient method	90
3.2.1	Multi-rate partial differential equation methods	93
3.3	Modulation-oriented Harmonic Balance	94
3.4	Envelope Currents method	97
3.5	Envelope currents method with extended dynamic range	102
3.6	SN method for weakly nonlinear communications circuits	106
3.7	Envelope Currents methods for communications signals in mixers	115
3.7.1	Introduction	115
3.7.1.1	Parametric Harmonic Balance	116
3.7.2	Description of the procedure	118
3.7.2.1	NEC method for communications signals in mixers	119
3.7.2.2	Extended PHB approach for communication signals in mixers	122
3.7.3	Comparison of NEC-M and E-PHB with other methods	124
4	Comparison with Experimental Measurements	127
4.1	Basic nonlinear characterization techniques	127
4.1.1	One-tone characterization tests	128
4.1.2	Two-tone characterization tests	131
4.1.3	Band-limited continuous spectra characterization tests	133
4.1.4	Memory effects	138
4.2	Measurement setup description	143
4.2.1	Illustrative examples of nonlinear distortion characterization . . .	145
4.3	Results for envelope-based analysis methods	150
4.3.1	Employed large-signal models for MESFET and HEMT devices . .	150

4.3.1.1	Illustrative examples of large-signal modelling	154
4.3.2	Envelope Currents method	159
4.3.3	SN approach for weakly nonlinear communication circuits	164
4.3.4	Two alternate EC approaches for communication signals in mixers	169
4.4	Phase characterization of intermodulation products IM3 and IM5	172
4.4.1	Phase correction considering delay	176
4.4.2	Measurement results	179
5	Modelling of Intermodulation Distortion	185
5.1	Introduction	185
5.2	SN approach applied to the analysis of IM products	186
5.2.1	Discussion about theoretical results	194
5.3	Correspondence of predicted asymmetries with experimental results . .	197
5.4	Impedance-based IM3 model with electrothermal memory effects	203
5.4.1	HEMT amplifier experimental results	206
5.4.2	Memory effects in FET amplifiers including dispersive phenomena	210
5.5	Extension of the impedance-based model for commercial amplifiers . . .	212
5.5.1	Commercial amplifier results	213
6	Conclusions and Suggestions for Future Work	217
6.1	Conclusions	217
6.2	Suggestions for future work	220
A	List of Publications	223
B	Expressions for the nonlinear envelope currents in the SN method	225

C Incremental envelope voltages in the SN analysis of two-tone IM products	229
C.1 First-order iteration: linear iteration	230
C.2 Second-order iteration	230
C.3 Third-order iteration	235
Bibliography	243
List of Abbreviations and Symbols	265

LIST OF FIGURES

1.1	Block diagram of a typical wireless communications transmitter-receiver link.	2
2.1	Newton-Raphson method illustrated.	14
2.2	Parallel-chord method illustrated.	16
2.3	Simplified Newton-Raphson method illustrated.	17
2.4	Example of a linear circuit.	21
2.5	Example of a circuit with nonlinear elements.	23
2.6	Nonlinear circuit elements. (a) Nonlinear conductance. (b) Nonlinear capacitance. (c) Nonlinear current source controlled by voltage.	24
2.7	Nonlinear circuit divided into linear and nonlinear subcircuits.	31
2.8	Circuit interpretation of the splitting method applied to HB.	40
2.9	Circuit interpretation of the block Gauss-Jacobi-Newton method applied to HB.	41
2.10	Circuit interpretation of the Newton's method applied to HB.	44
2.11	Equivalent circuit for the large-signal model of a FET.	45
2.12	Equivalent circuit of a FET amplifier for large-signal HB analysis.	46
2.13	Approximation to $x(t)$ by a succession of rectangular pulses.	57
2.14	Model of nonlinear circuit suggested by the Volterra series representation.	59
2.15	Simplified equivalent circuit of a FET amplifier.	69
2.16	Alternative representation of Figure 2.15, with linear elements in parallel with nonlinear current sources.	70

2.17	Envelope-based simulation process. Picture taken from [87].	83
3.1	Spectrum of a narrowband RF signal after a nonlinear circuit.	90
3.2	Single-node nonlinear circuit.	103
3.3	Different approaches for the simulation of microwave nonlinear circuits. (a) NC method. (b) NEC method.	104
3.4	Single-node nonlinear circuit.	108
3.5	Single-node nonlinear circuit driven as a mixer.	118
4.1	Spectral regrowth observed in a nonlinear system excited by a narrowband modulated stimulus.	135
4.2	Illustration of the output power spectral density of a noise power ratio test.	137
4.3	Photograph of the nonlinear circuits characterization setup.	144
4.4	Diagram of the nonlinear circuits characterization setup.	145
4.5	Main window of the implemented software controlling the automated measurement setup.	146
4.6	Current consumption for a MAXIM 2430 power amplifier versus input power level.	147
4.7	Output power for the fundamental frequency and first harmonics for a MAXIM 2430 power amplifier illustrating AM-AM characterization. . .	148
4.8	Conversion gain measurement for a MAXIM 2430 power amplifier. . . .	148
4.9	Output power at fundamentals and IM3 components versus input level for a MAXIM 2430 power amplifier for a two-tone excitation with $\Delta f = 2$ MHz.	149
4.10	Measurements of in-band power and ACP of a MAXIM 2430 power amplifier with a 3GPP UMTS W-CDMA signal.	149
4.11	Output PSD traces for a MAXIM 2430 power amplifier with a QPSK 3GPP UMTS W-CDMA signal and two power input levels.	150
4.12	Equivalent three-node circuit employed to analyse the MESFET CFB0301 of Celeritek and the HEMT EPB018A5-70 of Excellics.	151
4.13	Measurement setup for large-signal characterization of a MESFET amplifier.	157

4.14	IM products level measured at the input of the SA.	158
4.15	Output power for a MESFET amplifier at the fundamental frequency, second and third harmonics using the EC method.	160
4.16	Power gain of a MESFET amplifier at 2 GHz using the EC method. . . .	161
4.17	Constellation and output PSD of a MESFET amplifier with a raised- cosine filter using the EC method.	162
4.18	Constellation and output PSD of a MESFET amplifier with a root- raised-cosine filter using the EC method.	163
4.19	Power gain of a HEMT amplifier for an input of two-tones using the SN approach.	166
4.20	IM products for a HEMT amplifier as a function of input power level using the SN approach.	166
4.21	Spectral regrowth prediction for a HEMT amplifier with a 3GPP UMTS W-CDMA signal. Comparison of SN with two iterations and EC with three iterations.	167
4.22	Spectral regrowth prediction for a HEMT amplifier with a 3GPP UMTS W-CDMA signal. Comparison of SN and EC both with three iterations. .	167
4.23	Spectral regrowth prediction for a HEMT amplifier with a 3GPP W- CDMA signal and an input level near the 1-dB compression point using SN approach.	168
4.24	ACP prediction for a HEMT amplifier with a 3GPP UMTS W-CDMA signal versus the input level using SN approach.	168
4.25	Conversion gain of the HEMT gate mixer for two-tone input using the E-PHB and NEC approaches.	170
4.26	Two-tone IMD of the HEMT gate mixer versus input power using the E-PHB and NEC approaches.	170
4.27	Spectral regrowth prediction for a 3GPP UMTS W-CDMA signal using the E-PHB approach.	171
4.28	Spectral regrowth prediction of a 3GPP UMTS W-CDMA strong signal applied to a HEMT gate mixer using the E-PHB and NEC approaches. .	171
4.29	In-band power and adjacent channel power prediction for a 3GPP UMTS W-CDMA signal using the E-PHB and NEC approaches.	172

4.30	Proposed setup in [27] for measuring amplitude and phase responses of IM products.	173
4.31	Proposed setup in [59] for measuring amplitude and phase responses of IM products.	173
4.32	Proposed setup in [61] for measuring amplitude and phase responses of IM products.	173
4.33	Equipment setup for two-tone IMD characterization	174
4.34	Schematic diagram of the post-process carried out with the acquired baseband samples.	175
4.35	IM characteristic of a HEMT amplifier without (dotted line) and with predistortion using the measured phase (solid line).	178
4.36	Measured magnitude of IM3 and IM5 for a commercial bias-Tee.	180
4.37	Measured phase of IM3 and IM5 for a commercial bias-Tee.	180
4.38	Measured magnitude of IM3 versus V_{GS} for a commercial bias-Tee.	181
4.39	Measured phase of IM3 versus V_{GS} for a commercial bias-Tee.	181
4.40	Circuit model for the constructed resonant bias network.	182
4.41	Measured magnitude of IM3 for a resonant bias network.	182
4.42	Measured phase of IM3 for a resonant bias network.	183
4.43	Measured magnitude and phase of IM3 versus input power level for a resonant bias network.	183
5.1	Simplified two-node model of a HEMT amplifier with only the most significant nonlinearity.	187
5.2	Asymmetries imply memory effects, but the converse is not true.	197
5.3	Measured and calculated phase of lower IM3 and phase difference at two bias points using a commercial bias-Tee.	198
5.4	Measured and calculated phase of IM3 lower product for a HEMT amplifier with a resonant bias network. Results calculated with the SN method are plotted with a solid line.	200
5.5	Detail of measured and calculated phase difference between IM3 products with resonant bias network.	200

5.6	Phase difference of IM3 for a HEMT amplifier with a higher input level with resonant bias network. Comparison of models.	201
5.7	Measured and simulated phase difference of IM3 for the recommended bias point and for $V_{GS} = -0.4$ V.	201
5.8	Measured and simulated magnitude and magnitude difference of IM3 and IM5 using a commercial bias-Tee.	202
5.9	Measured and simulated phase and phase difference of IM3 and IM5 using a commercial bias-Tee.	202
5.10	Equivalent circuit of a HEMT amplifier, including the proposed model for the equivalent load impedance.	205
5.11	Smith Chart with the extracted values of Z_{th} and its RC circuit model for a HEMT amplifier with a bias voltage $V_{GS} = -0.24$ V.	207
5.12	Measured magnitude of upper IM3 products for a HEMT amplifier at input levels of -7 and -5 dBm and a bias voltage $V_{GS} = -0.24$ V, including predictions.	208
5.13	Measured phase and phase difference of IM3 products for a HEMT amplifier at different input levels and bias voltages, including predictions.	209
5.14	Equivalent circuit of a model including dispersive phenomena.	211
5.15	Zoom in the Smith Chart with the extracted values of Z_{eq} and its RLC circuit model for a commercial amplifier.	213
5.16	Measured and predicted magnitude and magnitude difference of IM3 at an input level of -10 dBm.	215
5.17	Measured and predicted phase and phase difference of IM3 at an input level of -10 dBm.	215
5.18	Measured two-tone phase asymmetries and prediction for a commercial amplifier.	216
5.19	Measured magnitude of upper IM3 products and prediction for a commercial amplifier.	216

LIST OF TABLES

2.1	Comparison of nonlinear microwave circuits techniques.	85
3.1	Comparison between the second-order nonlinear currents for EC and SN approaches	114
5.1	Incremental drain voltage terms for the fundamental frequency zone ($h = 1$)	192
5.2	Different asymmetry situations with respect to γ and \bar{Z}_L	196

INTRODUCTION

1.1 Foreword

During the last years we have witnessed the consolidation of wireless and mobile technologies in what has been called the “information society”. This ubiquity of wireless networks has been possible thanks to remarkable achievements in the field of hardware and technology, which have provided us with the best quality, improved and brand-new services, while maintaining user-friendliness and affordable prices. Regarding mobile communications, for example, the establishment of the Third-Generation cellular systems and the imminent advent of the Fourth-Generation mobile systems have propelled the study of novel techniques in wireless communications in order to give solutions to the challenges associated to the rapid increase in the information transfer rates, the number of users, and their mobility. When higher information transfer rates are desired, more complex modulation formats are required, often with increasingly growing bandwidths [1]. The rise in the number of users urges the need for minimising the distortion introduced by wireless circuits, so that every user’s signals do not interfere with the other’s in the limited spectrum allocated to them [2]. Lastly, the search for mobility demands highly integrated systems where low consumption and cost are top priorities [3].

Among the more than one million transistors contained in today’s pocket wireless devices, only a very small fraction operates in the RF range and the rest perform low-frequency baseband signal processing. This baseband signal processing has undergone a substantial evolution over the last years that has led to the complex modern systems based on digital signal processors (DSPs¹) and microprocessors [4], [5], [6]. However, the analog RF section is still the design bottleneck of the entire transceiver [7]. RF and microwave front-ends used in communications systems re-

¹A complete list of the abbreviations and symbols used in this Thesis can be found at the end of the document.

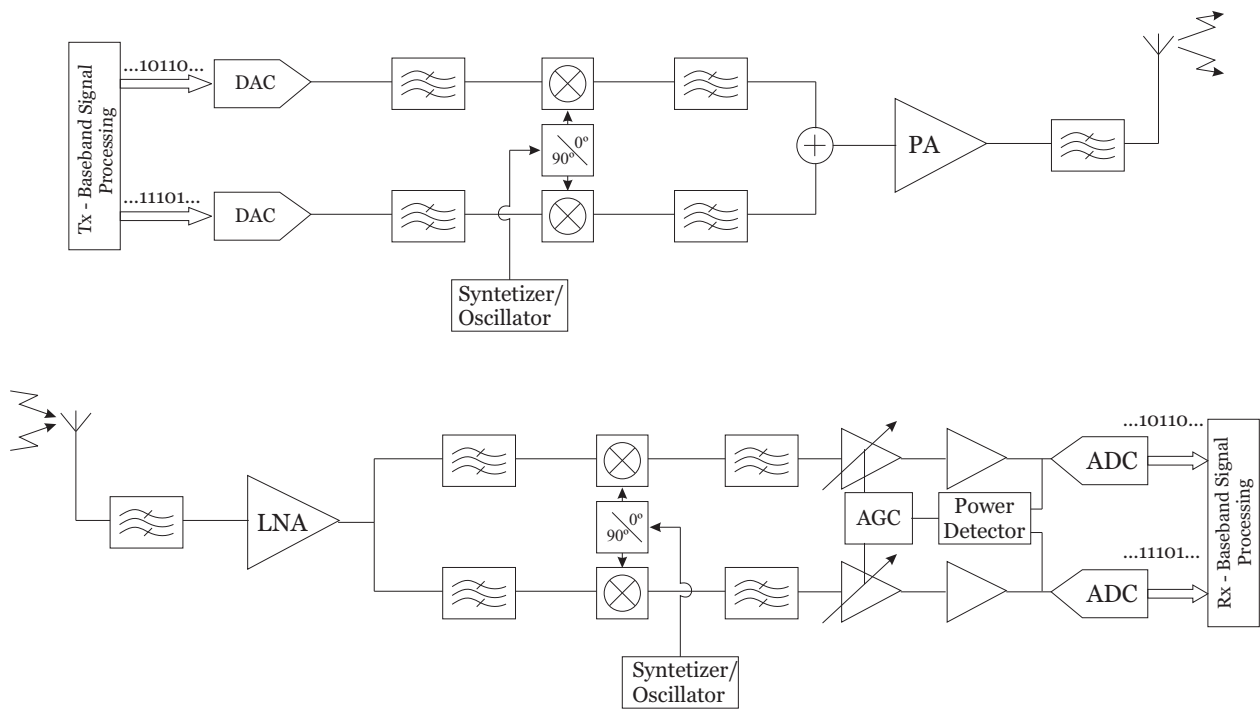


Figure 1.1: Block diagram of a typical wireless communications transmitter-receiver link.

quired diverse types of passive and active circuits, linear and nonlinear. Considering the scenario given by a typical wireless communications transmitter-receiver link, as shown in Figure 1.1, the relevance of two active subsystems is remarked, namely amplifiers and mixers. Since the system’s nonlinear behaviour is heavily dependent on the input signals employed, advanced knowledge of the digital world is more than advisable for the modern RF engineer. Modern wireless communications systems are designed to operate with digital signals that have large bandwidths and high peak-to-average power ratios. Important nonlinear effects are generated in the circuits by the envelope variations of these signals. Nonlinear operation cannot be easily described analytically, therefore optimised designs are complex. In addition to the changes in amplitude and phase shifts typically observed in linear systems, spurious components are generated in nonlinear circuits, distorting the amplifier or mixer behaviour. Among the effects of nonlinear distortion, intermodulation distortion and spectral regrowth should be taken into account since they cannot be eliminated by filtering and produce detrimental adjacent channel interference [8].

Within the field of nonlinear analysis and synthesis, computer-aided design (CAD) plays a key role. The basic motivation for using circuit simulation as part of the design process is to develop competitive products in the shortest possible time [9]. One of the most important drawbacks of nonlinear circuits is that there are neither universal analysis methods nor universal models. Therefore, every model and simulation

technique will perform in a specific application only [10]. However, two of the most extended tools for the analysis of nonlinear systems are Harmonic Balance [11], [12] and Volterra series representation [13], [14], [15], [16]. Harmonic Balance is an iterative technique to analyse the steady state with applicability for the general case of nonlinear circuits. Due to the practical limitations of Volterra series expansion for strongly nonlinear or very large circuits, Harmonic Balance is the preferred method in these cases. It can be seen as an extension of phasor analysis from the linear to the nonlinear field. Harmonic Balance analysis has become a mature tool for nonlinear analysis with sinusoidal inputs and all the major commercial CAD software include it. It presents excellent convergence properties when combine with the Newton-Raphson solution algorithms. The main restriction for standard Harmonic Balance techniques is that the kind of excitation that they can efficiently handle is usually restricted to periodic or quasi-periodic signals with a limited number of frequency components.

Adjacent channel power ratio is being used as a determinant figure of merit in the design of circuits for modern wireless communications systems. However, precise evaluation of this quantity and other related characteristics in nonlinear amplifiers and mixers, when excited by digitally-modulated signals, results a task of a high computational complexity that renders standard Harmonic Balance techniques inefficient. Circuit envelope methods [17], [18], [19] or modulation-oriented Harmonic Balance [20] algorithms have been proposed to specifically address this issue and allow RF designers to efficiently analyse circuits with a large number of spectral lines. Despite that, some alternative methods that achieve a further reduction of the computation time are demanded.

On the other hand, Volterra series representation has been used to described a wide variety of nonlinear phenomena including the nonlinearities in microwave and RF circuits for communications. The application of Volterra series restricted to the study of weakly nonlinear systems and low distortions is widely accepted, due to the cumbersomeness of the high-order nonlinear transfer functions. However, Volterra series enable the obtention of closed-form expressions describing the system behaviour, in contrast with other techniques based on numeric iteration algorithms. This kind of information proves to be of invaluable interest to gain an insight into the mechanisms producing memory effects [21].

The aforementioned specifications for wireless circuits are usually opposed. Take a power amplifier in a transmitter or receiver, for example. In typical power amplifier topologies, the efficiency drops as the circuit is designed for higher linearity and, therefore, lower distortion. The trade-off solution consist in applying special techniques in order to linearise the amplifier characteristics with negligible degradation in efficiency [22], [23]. However, a bandwidth increase to allow higher trans-

fer rates usually leads to ineffective linearization schemes. The reason for this is the bandwidth-dependent behaviour or memory effects exhibited by power amplifiers [24], [25]. These phenomena are the result of complex interactions inside the active devices and with the rest of the circuit, which should be modelled to satisfactorily accomplished the design of high performance amplifiers.

As a final subject to be account for, we should keep in mind that most of the models for nonlinear devices are derived from measurements. The procedures for nonlinear characterization and their associated figures of merit play a fundamental role on the correct specification of electronic devices. Since nonlinear devices do not comply with superposition, their response will present different characteristics depending on the excitation used [26]. Three main inputs are usually considered in nonlinear measurements: single-tone, two-tone and continuous spectra modulated signals. Among them, two-tone intermodulation measurements occupy an outstanding position, and understanding its particularities centres many researchers attention [27], [28], [29]. On the one hand, a two-tone test with varying tone separations can be used for experimental characterization of memory effects, being advisable measurements for both magnitude and phase of the intermodulation products. On the other hand, starting with a two-tone test it is possible to predict the nonlinear distortion components behaviour for multisine signals [30] and more complex modulations [31].

The present Thesis is intended to give a wide and detailed vision on the analysis of nonlinear circuits for wireless communications. Starting from a review of the state-of-the-art nonlinear analysis methods, the studied approaches include the application of the Simplified Newton algorithm to the solution of weakly nonlinear circuits by calculating successive incremental voltages in an iterative process [32]. Although the use of the Simplified Newton algorithm in Harmonic Balance is already well-known [10], [88] and it can be found in literature for other research fields such as antennas and propagation [89] or computer aided simulation of power systems [90], to the best of the author's knowledge, no use has been reported in which it has been combine with an envelope formulation in order to reduce the computation time as required with communications signals. Thus, this constitutes a novel tool suitable for the analysis of circuits including both amplifiers and mixers [33]. As an additional advantage of the Simplified Newton approach, it is demonstrated that it allows the obtention of theoretical expressions to model the baseband-frequency dependence of the intermodulation distortion in power amplifiers with memory [34], analogously to Volterra series representation. The final contribution consists in an impedance-based model for FET and commercial amplifiers, which is proposed in order to account for memory effects in intermodulation, regardless their nature [35]. The explained methodology has been applied to a series of simple examples involving surface mounted amplifiers and mix-

ers in microstrip circuits, for which the correspondence between the predictions of the studied techniques and experimental data is demonstrated.

1.2 Aims and scope

Considering the previous work made in this research field, the basic aim of the present Thesis consist in contributing to the study and development of new analysis techniques for nonlinear systems applied to wireless communications. This general objective can be split into the following primary aims:

- Development of an analysis tool for weakly nonlinear circuits subject to digitally-modulated narrowband communications signals.
- Study of the bandwidth-dependence or memory effects of the intermodulation distortion.
- Experimental characterization of the nonlinear distortion and memory effects in RF power amplifiers.

The problem of the analysis of nonlinear circuits is a large one, with many facets and avenues for research. In order to make the scope of this Thesis reasonable, a series of boundaries have been adopted.

Nonlinear phenomena could be studied in an enormous diversity of systems. The types of systems herein studied are non-autonomous, time-invariant weakly nonlinear circuits consisting of a set of lumped elements and sources. We will consider an element to be lumped if it is accurately modelled with an algebraic function of a finite number of network variables. A non-autonomous circuit is that with, at least, one external input source. When referring to weakly nonlinear circuits, it is assumed that the nonlinear component of the currents and voltages of the circuit is sufficiently small so that the currents in the nonlinear conductances, capacitances and dependent sources used to modelled nonlinear microwave devices can be approximated by means of the first terms of their Taylor-series expansions.

The input signals of interest are bandpass narrowband digitally-modulated communications signals, that is, bandpass signals whose centre frequency is much higher than the occupied bandwidth so that they can be expressed in terms of their complex envelopes. An additional implication of the narrowband restriction for two-tone signals is that the tones separation about the centre frequency cannot exceed a certain limit.

There are three fundamental approaches to nonlinear analysis of communications circuits and systems: system-level or behavioural approaches, circuit-level approaches and device- or physical-level approaches. System-level methods model the input-output relationships for the quantities of interest, typically the complex envelopes of the source and load waveforms, whilst the structural details of the nonlinear circuit are ignored. Circuit-level methods view the nonlinear circuit as the collection of its structural elements, usually conferring this methods a better accuracy and comprehension of the system's behaviour. Finally, physical-level approaches achieve the best accuracy by means of computationally expensive solution of the electromagnetic equations of the real scenario. The present work will be focused on circuit-level techniques, seeking for a convenient trade-off between accuracy and computational cost.

Regarding the variety of semiconductor substrates and construction technologies for the transistors, the used devices will be restricted to GaAs MESFETs and HEMTs because of their relevance in the RF and microwaves field. Therefore, only those large-signal equivalent circuit models especially conceived for GaAs MESFETs and HEMTs will be considered.

1.3 Thesis overview

This Thesis pursued objectives are developed throughout four chapters, whose structure is detailed next.

Chapter 1 has introduced the general field in which this Thesis is framed. The increasing demands on the specifications of designs for wireless communications have been discussed and the key role of power amplifiers has been remarked. The interest for accurate and efficient analysis techniques which enable nonlinear characterization including memory effects has been justified.

Chapter 2 presents a review of the more relevant steady-state methods for the analysis of nonlinear systems, where the Harmonic Balance method and the Volterra series analysis are highlighted. In the first sections, basic ideas regarding the numerical solution of nonlinear equations and the conventions adopted for the formulation of the problem are presented. After that, the Harmonic Balance iterative technique is detailed, paying attention to its various possibilities devised in order to achieve a trade-off between accuracy and computational cost. The proposed solution algorithms and matrix methods for solving the Harmonic Balance iteration are presented. Special considerations required in the case of multitone inputs are pointed out. Afterwards, Volterra series representation of nonlinear systems is presented. Two sections are dedicated to cases of particular interest, namely multitone inputs and bandpass systems

with memory. The methods of Harmonic Input and Nonlinear Currents for the obtention of nonlinear transfer functions are also reviewed. This chapter ends with a brief overview of the characteristics of envelope-based methods and a comparison between the considered techniques.

Chapter 3 is devoted to envelope-based methods specifically devised to efficiently deal with communications signals. The background in the field of envelope-based methods is reviewed. The Envelop [sic] Transient method, Modulation-Oriented Harmonic Balance, and Envelope Currents methods are summarised in a first part. Then, an alternative Simplified Newton approach is presented as one of the main contributions of this Thesis. The Simplified Newton approach is applied to the study of both weakly nonlinear amplifiers and mixers. In the case of mixers, a comparison is made between the performance achieved by using an standard Newton approach — the New Envelope Currents method for mixers — and a Simplified Newton approach — the Extended Parametric Harmonic Balance.

Experimental measurements, with which the simulations techniques are compared, are obtained in Chapter 4. A first definition of the different kinds of nonlinear characterization techniques and their associated figures of merit is presented, including the concept of memory effects. Later, the proposed measurement setup is described and illustrated by several examples. After a brief presentation of the large-signal models employed, the good correspondence of the simulations accomplished by the proposed envelope-based analysis methods with the experimental data is demonstrated by means of some examples. In the last section, a technique for the phase characterization of third- and fifth-order intermodulation products is proposed by using non-sophisticated communications equipment.

In Chapter 5, the Simplified Newton approach is applied to the analysis of two-tone intermodulation products under the assumption that the tone spacing is sufficiently small, i.e., the narrowband assumption. The information derived from the obtained theoretical expressions is then discussed. Once a good correspondence of the predicted intermodulation asymmetries to measurements is shown except for the lower frequency separations, an impedance-based model for the inclusion of electrothermal memory effects is presented for FET amplifiers, and then extended for commercial amplifiers with no knowledge of their internal structure.

Finally, the proposed conclusions and suggestions for future work are gathered.

Three appendixes are included at the end of this dissertation. The first of them is a list of the author's publications related with the present Thesis. Appendix B contains the expressions for the nonlinear envelope currents derived following the Simplified Newton approach. Lastly, Appendix C details the obtention of the incremental en-

velope voltages employed in the analysis of two-tone intermodulation following the Simplified Newton approach.

STEADY-STATE METHODS FOR THE
ANALYSIS OF NONLINEAR CIRCUITS
AND SYSTEMS

2.1 Introduction

Accurate computer simulation has helped to reduce the cost and time required to complete many new integrated circuit products, because a design can be corrected and its performance tuned faster and more economically by using Computer Aided Design (CAD) than by the repeated fabrication and testing of prototypes. However, microwave circuit designers require the computer simulation programs to be efficient computing steady-state quantities, such as harmonic distortion, for nonlinear circuits with a widely spread spectrum response, which often include distributed devices. This is a challenging and important problem that has motivated the work of many researches in the last decades.

Steady-state analysis of microwave circuits is typically of more interest to a designer than transient analysis. This is because microwave systems performance is studied in terms of quantities that are best measured in steady state such as distortion, power, frequency, noise, and transfer characteristics like gain and impedance. For that reason, the methods chosen in this chapter for the analysis of nonlinear circuits are steady-state methods.

In the most general terms, a *steady-state solution* of a differential equation is one that is asymptotically approached as the effect of the initial condition dies out. A differential equation may not have a steady-state solution, or can have any number of steady-state solutions. If there are multiple steady-state solutions, the steady-state that is asymptotically approached will depend on the initial condition. There is a region of attraction for every steady-state solution for which, if the initial condition

is contained in the associated region, then the solution approaches the given steady-state solution. A solution is referred to as being *asymptotically stable* when it returns to a given steady-state solution after being slightly perturbed from the same steady-state solution.

Among the different kinds of steady-state behaviour, we should emphasise the following due to their primary interest. The simplest case is *dc steady state*, where the solution is an equilibrium point of the circuit and does not vary with time. Asymptotically stable linear circuits driven by sinusoidal sources eventually exhibit a *sinusoidal steady-state* solution, which is characterised by being purely sinusoidal except possibly for some dc offset. If the steady-state response of a circuit consists solely of a linear combination of a dc offset and a possible infinite number of harmonically related sinusoids, the circuit is said to be in *periodic steady-state*. Periodic steady-state solution results either from self oscillations or as a response to periodically varying inputs. If a nonlinear circuit is driven by several periodic sources at incommensurate¹ frequencies, it will typically have a *quasiperiodic steady-state* response, consisting of a linear combination of sinusoids at the sum and difference frequencies of a finite set of fundamental frequencies and their harmonics. The fundamental frequencies usually correspond to these of the input signals, though sometimes they are even multiples of them or they result from self oscillations. Quasiperiodic steady-state includes periodic steady-state as a special case. Finally, there are steady-state responses that do not fit into any of the above classifications. These occur, for example, in the case of circuits with noise as the stimulus.

The analysis methods that will be reviewed in this Thesis only compute periodic and quasiperiodic solutions. In addition, these methods do not distinguish between solutions that are asymptotically stable from those that are not, being necessary other methods to determine the stability of the solutions, such as those presented in [91] and [92]. However, in most practical cases, circuits that are carefully designed will achieve a periodic or quasiperiodic steady-state from any condition, assuming that the inputs and outputs are periodic or quasiperiodic.

Among the common tools to simulate analog circuits, we can refer to those based on time-domain transient analysis. It is possible to calculate the steady-state response of these circuits by integrating numerically the differential equations that describe them, starting from a certain initial condition until the transient behaviour dies out. The time-domain transient analysis is the most intuitive method for the computation of the steady-state in nonlinear circuits, since it is the natural domain for human perception. Because of that, both nonlinear models and input excitation signals are described in the time-domain. However, this general approach can become impractical

¹Two frequencies f_p and f_q are said to be incommensurate if their quotient is a rational number.

because it implies a huge computational cost when the ratio of the highest to the lowest frequency present in the steady-state solution is large. In these cases, the number of discretization time-steps used by the numerical integration algorithm will be enormous, because the time interval over which the differential equations must be numerically integrated is set by the lowest frequency, but the size of the time-steps is constrained by the highest frequency response.

An example where the aforementioned disadvantage arises is when we are studying nonlinear circuits excited by multi-carrier signals. Let us consider the most simple example for this case: that of a two-tone input $x(t) = A_1 \cos(2\pi f_1 t) + A_2 \cos(2\pi f_2 t)$, where f_1 and f_2 are relatively large but close frequencies. Taking into account Nyquist theorem, it is necessary to sample the input signal at a sample rate $R_m \geq 2f_2$, although higher rates are advisable. This makes necessary the use of rather narrow time-steps, a fact that would not be a problem provided that the time interval over which we must integrate is short. But, since $f_1 \approx f_2$, the intermodulation product at the difference frequency $f_2 - f_1$ makes necessary to consider an integration time of at least $T = \frac{1}{f_2 - f_1}$, that tends to infinity and implies a very large computational cost.

Conventional transient analysis can be accelerated by exploiting those features typical of each kind of circuit and the applied excitation. This way, authors like Petzold [93] and Kundert [94] suggest approximating the same problem by developing an integration method that follows the envelope of the solution rather than the solution itself. However, there are a wide variety of methods that directly compute the steady-state solution more efficiently than integrating numerically the differential equations that describe the circuit from some initial condition. In the time domain, it is possible to derive faster algorithms if the steady-state problem is recast to one of finding an initial condition for which the solution to the differential equation is immediately the steady-state. These type of problems are called *boundary-value problems*. There are also frequency-domain methods, in which case a finite number of coefficients for the Fourier-series expansion of the steady-state solution are calculated.

The advantage of frequency-domain methods over time-domain methods is their flexibility to incorporate distributed devices easily, since the partial differential equations included in the time-domain definition of distributed devices are transformed into complex algebraic equations in the frequency domain. Their disadvantage is that, if the problem shows a strong nonlinearity, a large number of terms is required in the series expansions so that the frequency-domain methods can be accurate, and this fact makes them inefficient. Nevertheless, several microwave circuits, such as low-noise amplifiers or instrumentation amplifiers, show quite commonly a weakly nonlinear behaviour. This means that distortion levels, though significant, are very small compared to the main signal. In addition, signals applied to most communication circuits

are narrowband signals. In general, time-domain methods cannot exploit features derived from the weakly nonlinear behaviour of this kind of circuits or the narrowband condition of the excitations, consequently they are usually less efficient in these cases.

2.1.1 Frequency-domain methods

In frequency-domain methods, solutions are represented by means of a finite number of coefficients of their Fourier-series expansion. The advantage of this representation is particularly compelling when the steady-state solution is quasiperiodic, as it is usual in the case of weakly nonlinear microwave circuits, since the number of required coefficients to represent this kind of signals will decrease and the approximation made when the Fourier series are truncated will be better fitted. The use of Fourier series to represent solutions implies that only the steady-state behaviour of the system is representable and thus the initial transient behaviour is avoided. Furthermore, the circuit can be simulated even if it is unstable.

On the other hand, the analysis of linear time-invariant circuit devices, regardless they are lumped or distributed components that can be described by a frequency response, proves to be easy in the frequency-domain since it exploits the principle of superposition. Computing the coefficients of the response of nonlinear devices is more difficult than for linear devices, because the principle of superposition no longer applies and each of the coefficients of the response depends on all the coefficients of the stimulus in a more complex way. In practice, the coefficients of the response are calculated approximately by converting frequency-domain representations of voltages and currents into time samples by means of the inverse Fourier transform. Nonlinear devices are more easily evaluated in the time domain and then the results are converted back into the frequency domain by using the forward Fourier transform.

Usually, frequency-domain methods applied to nonlinear circuits are referred to as *Harmonic Balance* methods (HB). The name stems from the employed approach, which is based on balancing the existing currents between the linear and nonlinear circuits. In HB, the nonlinear integro-differential equations describing the circuit are replaced by a system of algebraic nonlinear equations, whose solution is an approximation to the steady-state response of the circuit. These equations are solved iteratively.

HB is sometimes considered a mixed-domain method, because the nonlinear devices are evaluated in the time domain while the linear devices are evaluated in the frequency domain. However, evaluating the nonlinear devices in the time domain is not a fundamental part of the algorithm. Thus, HB can be summarised as just being the method where Kirchhoff's current law is formulated in the frequency domain.

2.2 Numerical solution of nonlinear equations

2.2.1 Newton-Raphson method

Algebraic nonlinear equations are not solvable explicitly. Instead, it is necessary to use some kind of iterative method of successive approximations to the solution, in which the iterative process is repeated until the solution satisfies the equations with an error smaller than a specified tolerance. The approach of the Newton-Raphson method to solve nonlinear equations starts with an initial solution to which some correction terms are added. These are obtained by solving the system of equations generated when the circuit is linearised about a certain solution. In this way, solving the nonlinear problem is converted into solving a sequence of linear problems constructed in such a form that the sum of the partial solutions to all the iterations converges to the solution of the nonlinear problem.

Let us consider the following implicit nonlinear system of equations

$$f(\hat{x}) = \mathbf{0} \quad (2.1)$$

where $\hat{x} \in \mathbb{R}^N$ and $f : \mathbb{R}^N \rightarrow \mathbb{R}^N$ is a Lipschitz continuously differentiable vector-valued function, i.e., $\|f(x, t) - f(y, t)\| \leq K\|x - y\| \quad \forall x, y \in \mathbb{R}^N$ and K is a constant value. By Taylor's expansion, an initial guess $x^{(0)}$ must satisfy

$$f(\hat{x}) = f(x^{(0)}) + \frac{df(x^{(0)})}{dx}(\hat{x} - x^{(0)}) + \mathcal{O}\left((\hat{x} - x^{(0)})^2\right) \quad (2.2)$$

Taking into account that both x and f are N -dimensional vectors, the derivative $\frac{df(x)}{dx}$ can be represented by the Jacobian matrix $J_f(x)$, if it exists.

$$\frac{df(x)}{dx} = J_f(x) = \left[\frac{\partial f_m(x)}{\partial x_n} \right], \quad m, n = 1, 2, \dots, N. \quad (2.3)$$

$\mathcal{O}(\cdot)$ is a function that represents the higher order terms and is such that $\lim_{\alpha \rightarrow 0} \frac{\|\mathcal{O}(\alpha)\|}{\alpha}$ is bounded. Equation (2.2) suggests that if $(\hat{x} - x^{(0)})$ is small, then the root of

$$f_{lin}(x^{(1)}) = f(x^{(0)}) + J_f(x^{(0)})(x^{(1)} - x^{(0)}), \quad (2.4)$$

will be close to \hat{x} , where $f_{lin}(x)$ is the linearised approximation to $f(x)$ (it represents the hyperplane that is tangent to $f(x)$ at $x^{(0)}$). Therefore, an improved approximation to \hat{x} will be the value $x^{(1)}$ that satisfies $f_{lin}(x^{(1)}) = 0$, that is to say,

$$x^{(1)} = x^{(0)} - J_f^{-1}(x^{(0)})f(x^{(0)}). \quad (2.5)$$

This procedure is repeated iteratively until the specified convergence criteria are satisfied.

$$x^{(i+1)} = x^{(i)} - J_f^{-1}(x^{(i)})f(x^{(i)}). \tag{2.6}$$

The sequence generated by (2.6) is illustrated in Figure 2.1 for a one-dimensional case. It converges to \hat{x} if f is continuously differentiable, $J_f(\hat{x})$ is nonsingular and $x^{(0)}$ is sufficiently close to \hat{x} [95] [96]. If the i -th iteration error is defined as $\varepsilon^{(i)} = \|x^{(i)} - \hat{x}\|$ and there are two constants p and $\alpha \neq 0$ such that

$$\lim_{i \rightarrow \infty} \frac{\varepsilon^{(i+1)}}{(\varepsilon^{(i)})^p} = \alpha, \tag{2.7}$$

then p is called the rate or order of convergence. For Newton-Raphson method, when $J_f(x)$ is a Lipschitz function, $p \geq 2$, i.e., the asymptotic convergence is at least quadratic. However, in general, there is no way to assure that the initial value $x^{(0)}$ is sufficiently close to the solution \hat{x} , and consequently convergence can be elusive.

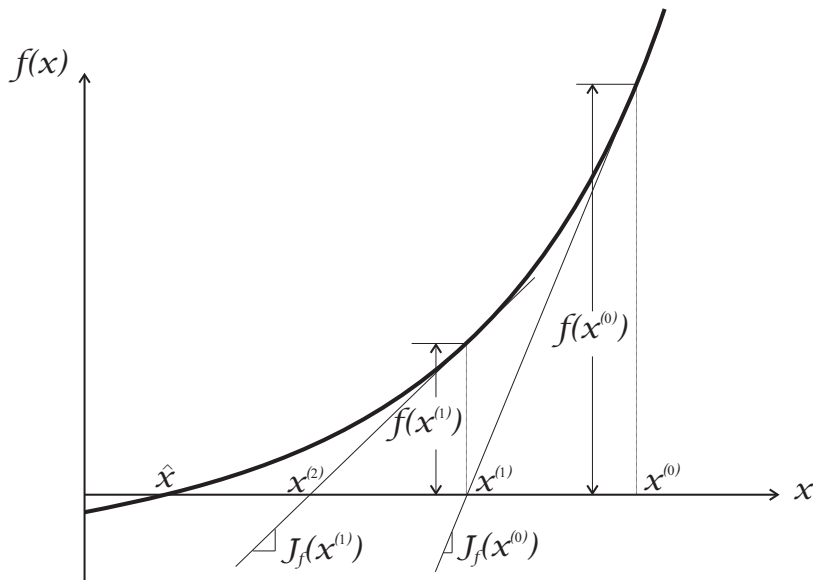


Figure 2.1: Newton-Raphson method illustrated.

2.2.2 Convergence criteria

As a practical matter, it is necessary to terminate the Newton-Raphson iteration after a finite number of iterations. In a general way, the process is stopped when

$$\|f(x^{(i)})\| < \varepsilon_f \tag{2.8}$$

where ε_f is some positive real number. In fact, there are several stop criteria for iterative algorithms, although two largely used error functions are the minimum squared

error, $\|f(x^{(i)}) \cdot f^*(x^{(i)})\|$, and the norm of the error function used in equation (2.8), $\|f(x^{(i)})\|$. In order to see how this convergence criterion affects the error in the solution, let assume that the true solution is \hat{x} and that $\|f(x^{(i)})\| \leq \varepsilon_f$. By expanding f about $x^{(i)}$, it is easy to show that

$$J_f(x^{(i)})[\hat{x} - x^{(i)}] \approx -f(x^{(i)}). \quad (2.9)$$

Therefore, the quantity $\Delta x^{(i)} = -J_f^{-1}(x^{(i)})f(x^{(i)})$ is a first-order estimate of the error in the solution. Notice that this quantity has been previously computed in (2.6), so the additional convergence criterion can be incorporated to directly control the error in the adopted solution:

$$\|\Delta x^{(i)}\| < \varepsilon_x. \quad (2.10)$$

It is recommended to use both convergence criteria, (2.8) and (2.10), for the Newton-Raphson algorithm because if only (2.8) is used it is possible to nearly satisfy (2.1) but still have a large error in the solution, situation that might happen if the Jacobian of the function were an ill-conditioned matrix. Furthermore, if only the criterion (2.10) is used, it is possible to prematurely terminate the iteration process when (2.6) is far from being satisfied because the progress toward the solution in one step is small and that causes Δx to be small. This last situation is referred to as *false convergence*.

2.2.3 Simplified Newton-Raphson methods

Previously defined Newton-Raphson method requires at each iteration, not only the obtention of the N components of $f(x^{(i)})$, but also the construction and factorization of the $(N \times N)$ Jacobian matrix. There are several cases in which these operations can be very expensive computationally. In the case of microwave circuits, for example, the aforementioned situation can be found when highly nonlinear circuits are solved in the frequency domain, since it is necessary to consider a great amount of mixing-frequency terms that generate large size matrices. In addition to this, the construction and factorization of the Jacobian can be avoided under certain circumstances, leading to various simplified Newton-Raphson methods which have been developed over the years to increase the efficiency of the algorithms [10], [32].

The simplified Newton-Raphson methods are related to the *parallel-chord method* [95], in which function f can be replaced at some approximation $x^{(0)}$ of its solution \hat{x} by a linear function

$$f_{lin}(x) = f(x^{(0)}) + \mathbf{A}(x - x^{(0)}), \quad (2.11)$$

with a constant nonsingular matrix \mathbf{A} defining an hyperplane in the multidimensional problem. Note that, if the matrix \mathbf{A} were the Jacobian $J_f(x)$ this expression would be

identical to the one used in the Newton-Raphson method. Therefore, taking the root of $f_{lin}(x)$ as a new approximation $x^{(1)}$ to the solution \hat{x} , and repeating this procedure with a fixed \mathbf{A} , the iteration of the parallel-chord method is obtained (see Figure 2.2)

$$x^{(i+1)} = x^{(i)} - \mathbf{A}^{-1}f(x^{(i)}). \tag{2.12}$$

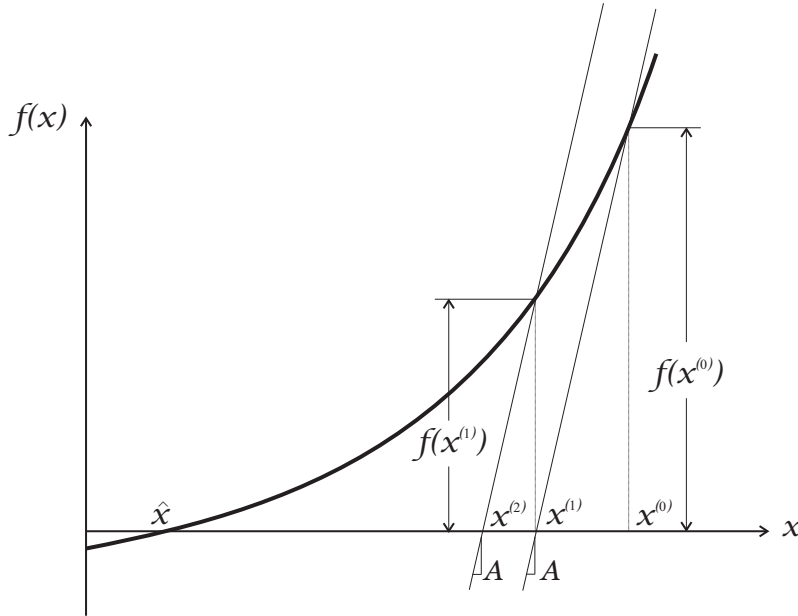


Figure 2.2: Parallel-chord method illustrated.

The crucial point in applying the iteration (2.12) is the proper choice of \mathbf{A} . A particularly simple possibility is $\mathbf{A} = \alpha\mathbf{I}$ with \mathbf{I} the identity matrix of range N and $\alpha \neq 0$ an scalar, so that, in essence, a one-dimensional iteration is applied to each component of f separately. A more sophisticated choice is motivated by the fact that in one dimension the slope $\frac{df(x^{(0)})}{dx}$ of the tangent of f at $x^{(0)}$ is a reasonable selection for α . If we take $\mathbf{A} = J_f(x^{(0)})$, the obtained method is referred to as a simplified Newton-Raphson method. There are many possible choices for the matrix \mathbf{A} in the parallel-chord method, although an underlying requirement for any \mathbf{A} is that the iteration (2.12) be at least locally convergent. This means that when $x^{(0)}$ is sufficiently close to a solution \hat{x} of $f(x) = 0$, then we should be assured that $\lim_{i \rightarrow \infty} x^{(i)} = \hat{x}$.

In this Thesis, we are interested in the simplified Newton-Raphson method in which the Jacobian is formed and factorised only for the first iteration, and then it is reused for the rest of the iterations (see Figure 2.3)

$$x^{(i+1)} = x^{(i)} - J_f^{-1}(x^{(0)})f(x^{(i)}). \tag{2.13}$$

If the function f is nearly linear, then the changes in the Jacobian from iteration to iteration are small and the first Jacobian computed is a close approximation to the real

Jacobian in the subsequent steps. In this case, the simplified method converges to the correct solution. The Jacobian is only used to generate the new solutions of each iteration, but is not used to confirm the convergence, so that the errors derived from the approximations in the Jacobian only affect the rate and region of convergence, not the accuracy of the final solution. The simplified Newton-Raphson method can be considerably faster than the conventional Newton-Raphson method to solve large nearly-linear systems of equations, even though they usually require a greater number of iterations, because each iteration is less expensive computationally. Nevertheless, the region of convergence is often smaller than with the conventional Newton-Raphson method.

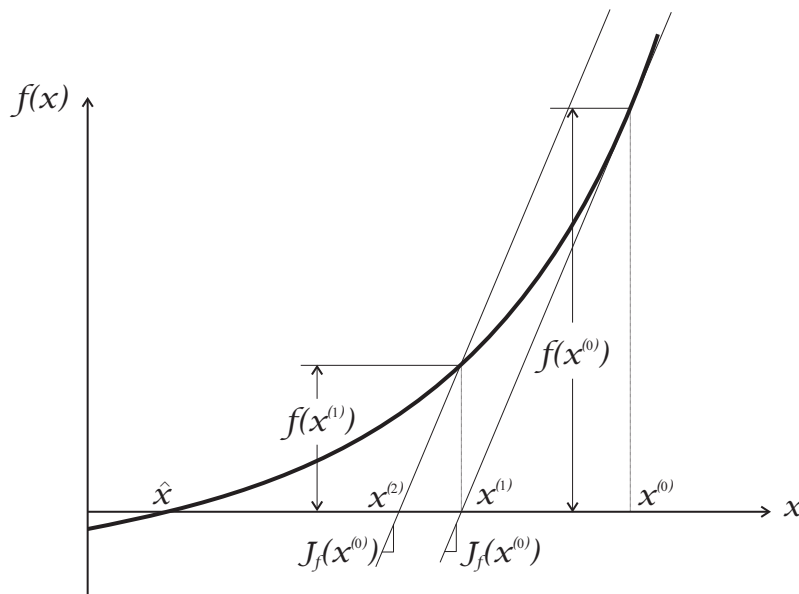


Figure 2.3: Simplified Newton-Raphson method illustrated.

In order to increase the region of convergence over that of the simplified Newton-Raphson method, it is possible to reevaluate the Jacobian every k iterations rather than using the initial Jacobian until the convergence is achieved. This method, referred to as Samănskii's method, may be considered a k -step method, where each iteration is composed of one Newton-Raphson step and $k - 1$ simplified Newton-Raphson steps. Traud and Samănskii [95] demonstrated that the sequence formed by every k -th iteration converges with a rate $k + 1$. Therefore, if $k = 2$, i.e., the Jacobian is updated every other iteration, then cubic convergence is achieved. As expected, this rate of convergence is inferior to that of conventional Newton-Raphson, where the sequence formed by every other iterations converges quartically.

The advantages of the simplified Newton-Raphson iterations are combined with the large region of convergence of the conventional Newton-Raphson method if the

sequence $\{\|f(x^{(i)})\|\}$ is monitored and simplified Newton-Raphson iterations are used while a sufficient reduction in this norm is achieved. If the reduction in an iteration is insufficient, the iteration and the Jacobian should be discarded and a complete Newton-Raphson step should be carried out.

2.2.4 Continuation methods

Continuation methods provide a way for obtaining starting points that are sufficiently close to the real solution to assure convergence in the Newton-Raphson methods. In this case, a dependence with some parameter p is included in the system function

$$f(x, p) = 0 \quad (2.14)$$

where $f(x, 1) = f(x)$, i.e., when the parameter is set to $p = 1$, we consider the particular system for which the solution is desired; while $f(x_0, 0) = 0$, i.e., for $p = 0$ the system has a known solution x_0 . In other words, equation (2.14) can be written as a function of p $f(x(p), p) = 0$.

The aim of this kind of methods is to compute the response of the circuit to a certain excitation when it is initialised with $x^{(0)}(p)$. The solution $x(p)$ can be found for an increasing sequence of values of p , $0 = p_0 < p_1 < p_2 < \dots < p_s = 1$. If $x(p)$ is a continuous function of p , then it is always possible to choose p_s close enough to p_{s-1} so that if $x(p_{s-1})$ is used as a starting point, it is sufficiently close to $x(p_s)$ to assure convergence. Therefore, a finite sequence of problems is generated, the solution to the first of which is known, and such that the solution of each problem is close enough to the solution of the next to be within the region of convergence of the Newton-Raphson method.

The step size $p_s - p_{s-1}$ is adjusted at each step to minimise the total number of Newton iterations. Linear extrapolation is normally used with continuation methods to reduce the number of steps required. After the first steps, a simple form of linear extrapolation can be used based on the solution at the previous two steps.

$$x^{(0)}(p_s) = x^{(0)}(p_{s-1}) + \frac{p_s - p_{s-1}}{p_{s-1} - p_{s-2}} [x^{(0)}(p_{s-1}) - x^{(0)}(p_{s-2})]. \quad (2.15)$$

When computing the dc operating point of a circuit, it is very common to use as a continuation parameter the fraction of the dc source voltages and currents applied to the circuit. In almost all circuit simulators, when all potentials are zero no current flows through any device except sources. Thus, when all sources are turned off, circuits are guaranteed to have a solution with zero potential at every node and zero current through every branch. From this known solution, the source levels can be

slowly increased and the circuit solved at each step, until the desired source levels are attained. Continuation implemented in this manner is generally referred to as *source stepping*.

The advantage of continuation methods is that they guarantee that, if a solution exists, it can be obtained from another one previously calculated. A disadvantage of these methods is that, for some nonlinear systems, it is necessary to complete a large number of continuation steps until the final solution is obtained. Consequently, the continuation methods are usually associated to other methods in order to increase their region of convergence.

2.2.5 Discretization

Nonlinear circuits are modelled by using a system of nonlinear differential equations. However, in general it is not possible to solve numerically systems of nonlinear differential equations directly and discretization is required. Discretization approximates a system of differential equations with a system of difference equations. In other words, the time interval of interest $[0, T]$ is divided into a finite number of possibly nonuniform subintervals with a monotonically increasing sequence of time-points $[t_0, t_1, \dots, t_K]$, where $t_0 = 0$ and $t_K = T$. The subintervals are called time-steps and denoted by $h_k = t_k - t_{k-1}$. At t_k , the solution of the discretised system is an approximation to the solution of the original differential equation. At each time-point, an algebraic system of equations must be solved, thus discretization converts a differential equation into a sequence of algebraic equations. One commonly used approach to get this conversion is to replace the derivatives $\frac{d^n x}{dt^n}$ with one of the following finite-difference approximations:

$$\text{Forward difference: } \frac{d^n x(t_k)}{dt^n} \simeq \frac{1}{h_k^n} \sum_{r=0}^n (-1)^r \binom{n}{r} x(t_{k+n-r}), \quad (2.16)$$

$$\text{Backward difference: } \frac{d^n x(t_k)}{dt^n} \simeq \frac{1}{h_{k+1}^n} \sum_{r=0}^n (-1)^r \binom{n}{r} x(t_{k-r}).$$

For the case of first-order derivatives, the simplest methods of this type are the one-step explicit and implicit Euler algorithms, defined by taking $n = 1$ in the previous expressions

$$\text{Explicit or forward Euler: } \frac{dx(t_k)}{dt} \simeq \frac{x(t_{k+1}) - x(t_k)}{h_k}, \quad (2.17)$$

$$\text{Implicit or backward Euler: } \frac{dx(t_{k+1})}{dt} \simeq \frac{x(t_{k+1}) - x(t_k)}{h_{k+1}},$$

although we can also consider the generalized finite difference expression for one-sided multipoint discretization rules

$$\frac{dx}{dt} = \sum_{r=0}^R \alpha_r x(t_{n-r}). \quad (2.18)$$

Implicit or backward Euler method presents the advantage of being stable even if the differential equations being solved have widely separated time constants. The integration of differential equations is conveniently carried out by applying methods like explicit and implicit Euler starting at t_0 and progressing forward toward t_k because, when computing the solution at t_k , it is only necessary to know the solution at previous values of time.

2.3 Formulation of the problem

2.3.1 Circuit equations: modified nodal analysis

Systematic methods for the formulation of circuit equations are desirable when complicated networks are being analysed. In general, these methods are based on the incidence, cut-set, and loop matrices, which are derived by using topological considerations. Taking into account that electronic circuits generally present much more loops than nodes, it is a common practice to resort to nodal analysis.

As it was mentioned in Section 1.2, in this Thesis we will consider time-invariant nonlinear circuits consisting of an arbitrary set of lumped linear elements such as resistors, capacitances and inductances, lumped nonlinear elements and sources. Traditionally, a lumped device is one whose physical dimensions are much smaller than the wavelength of the signal present in the circuit. In this Thesis, a device is considered lumped if it is accurately modelled with an algebraic function of a finite number of network variables. Any device that is not lumped is distributed. The inclusion of distributed linear elements in the present analysis is relatively straightforward and will be discussed shortly. We will also consider non-autonomous or forced circuits only, that is, circuits with at least one nonconstant periodic or quasiperiodic input source. Formulation of the problem will be based on the circuit equations to be solved, which will be obtained by means of a modified nodal analysis. That is to say, circuit equations are posed in terms of their node voltages, also including as unknowns the currents in inductances, voltage sources and current-controlled elements. To do so, it is necessary that each element of the circuit has an admittance representation in which current is expressed as a function of voltage.

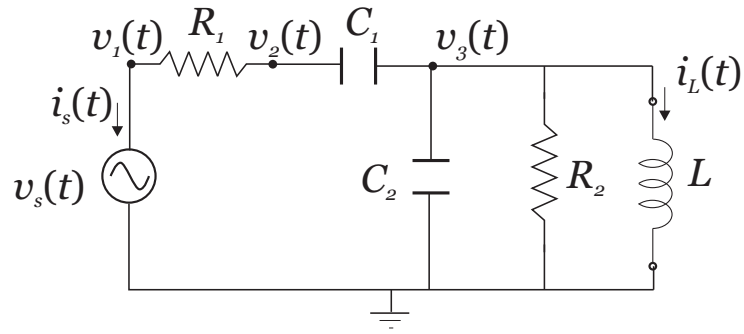


Figure 2.4: Example of a linear circuit.

In order to illustrate the nodal formulation of circuit equations, let us consider the following example based on the circuit shown in Figure 2.4.

Let

$$\mathbf{x}(t) = \begin{bmatrix} v_1(t) \\ v_2(t) \\ v_3(t) \\ i_s(t) \\ i_L(t) \end{bmatrix} \quad (2.19)$$

be the vector of unknown circuit variables which contains the voltages of all the nodes in the circuit, together with the currents through the independent voltage source, $i_s(t)$, and through the inductance, $i_L(t)$. When Kirchhoff's voltage law is taken into account for all the circuit nodes, the following system of equations is obtained, expressed in matrix form:

$$\mathbf{G}\mathbf{x}(t) + \frac{d}{dt}\mathbf{C}\mathbf{x}(t) = \mathbf{b}(t), \quad (2.20)$$

where

$$\mathbf{G} = \begin{pmatrix} \frac{1}{R_1} & -\frac{1}{R_1} & 0 & 1 & 0 \\ -\frac{1}{R_1} & \frac{1}{R_1} & 0 & 0 & 0 \\ 0 & 0 & \frac{1}{R_2} & 0 & 1 \\ 1 & 0 & 0 & 0 & 0 \\ 0 & 0 & 1 & 0 & 0 \end{pmatrix}, \quad \mathbf{C} = \begin{pmatrix} 0 & 0 & 0 & 0 & 0 \\ 0 & C_1 & -C_1 & 0 & 0 \\ 0 & -C_1 & C_1 + C_2 & 0 & 0 \\ 0 & 0 & 0 & 0 & 0 \\ 0 & 0 & 0 & 0 & -L \end{pmatrix} \quad (2.21)$$

$$\text{and } \mathbf{b}(t) = \begin{bmatrix} 0 \\ 0 \\ 0 \\ v_s(t) \\ 0 \end{bmatrix}.$$

Matrix \mathbf{G} includes the contribution of the resistive elements and, in addition, con-

tains connectivity information for the inductor and the independent voltage source. Matrix \mathbf{C} accounts for the reactive elements. And, finally, vector $\mathbf{b}(t)$ involves the independent sources.

It can be observed that the first three equations in the system (2.20) involve node voltages only. When circuit equations can be formulated solely in terms of node voltages, the method is referred to as *nodal analysis*. In the example shown in Figure 2.4, the presence of an ideal voltage source makes necessary to include its branch current as an unknown. Moreover, the inductor current is included as an unknown, because it is more convenient to use a first order differential equation to describe this element rather than adding an integral of the unknowns vector to the left-hand side of (2.20) in order to account for the presence of the inductor. When it is necessary or convenient to include other variables as unknowns besides node voltages, the method is referred to as *modified nodal analysis*.

The advantage of the modified nodal analysis is that it is possible to deduce general rules to construct the matrices and vectors \mathbf{G} , \mathbf{C} and $\mathbf{b}(t)$ directly. These rules can be implemented in computer-aided design programs, being the modified nodal analysis methods adopted in many commercial circuit simulators.

Let now consider the circuit in Figure 2.4 in the frequency domain. The new vector containing the unknowns will be the following:

$$\mathbf{X}(t) = \begin{bmatrix} V_1 \\ V_2 \\ V_3 \\ I_s \\ I_L \end{bmatrix}, \quad (2.22)$$

which includes the complex phasors of each of the node voltages and currents that formed the vector of the unknowns in the time domain. Similarly, let \mathbf{B} denote the phasors corresponding to the sources vector $\mathbf{b}(t)$. It is straightforward to verify that, in the frequency domain, equation (2.20) becomes

$$\mathbf{Y}(\omega)\mathbf{X} = \mathbf{B}, \quad (2.23)$$

where matrix $\mathbf{Y}(\omega)$ is known as *modified node admittance matrix* and it is defined as

$$\mathbf{Y}(\omega) = \mathbf{G} + j\omega\mathbf{C}. \quad (2.24)$$

We can deduce from the previous equations that the inclusion of distributed elements or linear multiport devices is quite straightforward in the frequency domain. It is only necessary to obtain the admittance matrix of the new device and add it to the

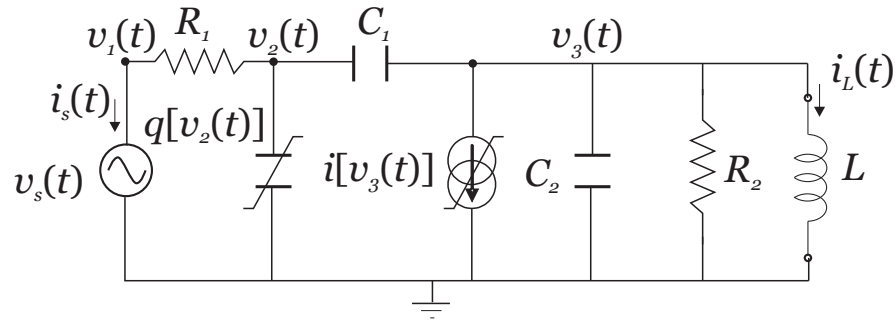


Figure 2.5: Example of a circuit with nonlinear elements.

appropriate elements of $\mathbf{Y}(\omega)$, considering the position inside the circuit where the new device is inserted.

In order to complete the description about the formulation of the problem, let consider that two nonlinear elements are inserted in the circuit of the aforementioned example, as it is shown in Figure 2.5.

In this case, new terms must be added to equation (2.20) in order to include the nonlinear elements, resulting

$$\mathbf{G}\mathbf{x}(t) + \frac{d}{dt}\mathbf{C}\mathbf{x}(t) + \frac{d}{dt}\mathbf{q}[\mathbf{x}(t)] + \mathbf{i}[\mathbf{x}(t)] = \mathbf{b}(t), \quad (2.25)$$

where

$$\mathbf{q}[\mathbf{x}(t)] = \begin{bmatrix} 0 \\ q[v_2(t)] \\ 0 \\ 0 \\ 0 \end{bmatrix} \quad \text{and} \quad \mathbf{i}[\mathbf{x}(t)] = \begin{bmatrix} 0 \\ 0 \\ i[v_3(t)] \\ 0 \\ 0 \end{bmatrix}. \quad (2.26)$$

Vectors $\frac{d}{dt}\mathbf{q}[\mathbf{x}(t)]$ and $\mathbf{i}[\mathbf{x}(t)]$ account for the currents that flow through the nonlinear elements, and the functions \mathbf{i} and \mathbf{q} must be differentiable.

Another way to express the nodal circuit equations that is convenient for the inclusion of distributed elements is given as

$$\frac{d}{dt}\mathbf{q}[\mathbf{x}(t)] + \mathbf{i}[\mathbf{x}(t)] + \int_{-\infty}^t \mathbf{y}(t - \tau)\mathbf{x}(\tau)d\tau = \mathbf{b}(t). \quad (2.27)$$

In this expression, $\mathbf{y}(t)$ is obtained by inverse Fourier transforming the modified node admittance matrix $\mathbf{Y}(\omega)$, in which only the linear elements of the circuit have been included and all the nonlinear elements have been removed.

2.3.2 Nonlinear circuit elements representation

In order to accomplish the nonlinear analysis of an electronic circuit, whose devices include inherent nonlinearities, it is necessary to replace each device with an equivalent model. The more usual nonlinear elements included in the models of the devices which are going to be treated in this Thesis are nonlinear conductances, nonlinear capacitances and nonlinear controlled sources. For all these cases, the current depends nonlinearly on one or more voltages and the elements can be appropriately characterised by a power series about the bias point.

In Figure 2.6(a), a nonlinear conductance is shown whose voltage-current relationship can be expressed as

$$i_G(t) = g[v_G(t)]. \tag{2.28}$$

If V_G and I_G denote the voltage and current in the operation point, respectively, the power series expansion of the function $g[\cdot]$ about the bias point can be written as:

$$i_G(t) = I_G + \sum_{k=1}^{\infty} g_k [v_G(t) - V_G]^k, \tag{2.29}$$

where g_k is the k -th coefficient of the power series. If we make use of the definition of incremental currents and voltages $i_g(t) = i_G(t) - I_G$ and $v_g(t) = v_G(t) - V_G$, equation (2.29) can be reduced to

$$i_g(t) = \sum_{k=1}^{\infty} g_k v_g^k(t). \tag{2.30}$$

In the case of the nonlinear capacitance shown in Figure 2.6(b), we can write current as a function of charge by applying the chain rule

$$i_C(t) = \frac{dq_C(t)}{dt} = \frac{dq_C(t)}{dv_C(t)} \cdot \frac{dv_C(t)}{dt} = C[v_C(t)] \frac{dv_C(t)}{dt}, \tag{2.31}$$

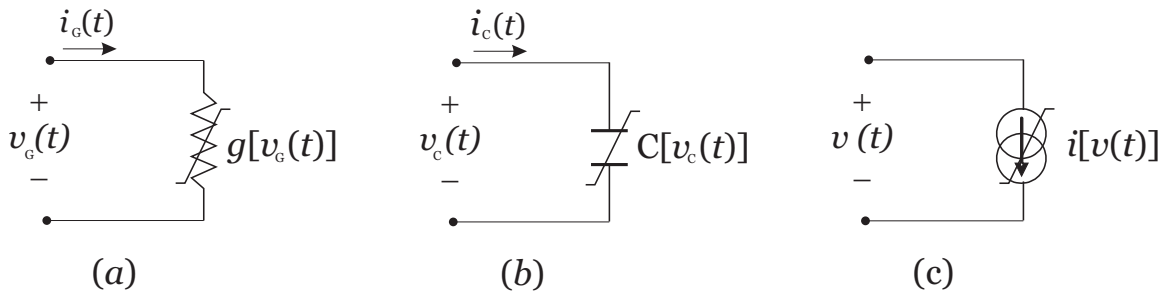


Figure 2.6: Nonlinear circuit elements. (a) Nonlinear conductance. (b) Nonlinear capacitance. (c) Nonlinear current source controlled by voltage.

where $C[v_C(t)]$ is the incremental capacitance. Let assume that the nonlinear capacitance admits a power series expansion about the bias point, then it can be written as:

$$C[v_C(t)] = c_0 + \sum_{k=1}^{\infty} c_k [v_C(t) - V_C]^k = \sum_{k=0}^{\infty} c_k v_c^k(t), \quad (2.32)$$

where $v_c(t) = v_C(t) - V_C$ is the incremental voltage. Current is expressed in terms of the coefficients of the nonlinear capacitance as

$$i_C(t) = \sum_{k=0}^{\infty} c_k v_c^k(t) \frac{dv_C(t)}{dt}. \quad (2.33)$$

In order to write this expression as a function of the incremental voltages and currents, it is enough to rewrite (2.33) in the following equivalent form:

$$i_c(t) - I_C = \sum_{k=0}^{\infty} c_k v_c^k(t) \frac{d[v_c(t) + V_C]}{dt}. \quad (2.34)$$

Taking into account that $I_C = 0$, since it is a dc current, and that V_C is a constant, it can be concluded that

$$i_c(t) = \sum_{k=0}^{\infty} c_k v_c^k(t) \frac{dv_c(t)}{dt}. \quad (2.35)$$

Finally, it is necessary to consider the case of a nonlinear current source voltage-controlled, as the one shown in Figure 2.6(c). For the case of a nonlinear current source controlled by a single voltage, the power series expression for the current is

$$i[v(t)] = \sum_{k=0}^{\infty} g_k v^k(t), \quad (2.36)$$

and for the case of a nonlinearity depending on two voltages, the power series of the current is expressed as

$$i[v(t), u(t)] = \sum_{k=0}^{\infty} \sum_{\substack{l=0 \\ k+l \geq 1}}^{\infty} g_{kl} v^k(t) u^l(t). \quad (2.37)$$

For the nonlinear circuits based on FET devices that have been analysed and whose results will be shown in this Thesis, the main nonlinearity appears in the current that flows through the drain $i_{ds}[v_{gs}, v_{ds}]$ and it has been modelled as a nonlinear controlled source expressed as shown in (2.37), due to the importance of the cross-terms g_{kl} demonstrated in several research papers [97]. Note that in this case, the g_{k0} coefficients are related to the nonlinear controlled source that depends on v_{gs} , while the g_{0l}

are the coefficients of the nonlinear output conductance. Therefore, sometimes the following expression, equivalent to (2.37), that considers separately those effects in three different terms is preferred:

$$i[v(t), u(t)] = \sum_{k=1}^{\infty} g_{k0} v^k(t) + \sum_{l=1}^{\infty} g_{0l} u^l(t) + \sum_{k=1}^{\infty} \sum_{l=1}^{\infty} g_{kl} v^k(t) u^l(t). \quad (2.38)$$

In summary, the typical nonlinear elements in circuits include:

- Nonlinear conductance:

$$i_g(t) = \sum_{k=1}^{\infty} g_k v_g^k(t). \quad (2.39)$$

- Nonlinear capacitance:

$$i_c(t) = \frac{d}{dt} \sum_{k=1}^{\infty} q_k v_c^k(t) = \sum_{k=1}^{\infty} k q_k v_c^{k-1}(t) \frac{dv_c(t)}{dt} = \sum_{k=0}^{\infty} c_k v_c^k(t) \frac{dv_c(t)}{dt}. \quad (2.40)$$

- Dependent nonlinearity:

$$i(t) = i[v(t), u(t)] = \sum_{\substack{k=0 \\ k+l \geq 1}}^{\infty} \sum_{l=0}^{\infty} g_{kl} v^k(t) u^l(t) = \sum_{k=1}^{\infty} g_{k0} v^k(t) + \sum_{l=1}^{\infty} g_{0l} u^l(t) + \sum_{k=1}^{\infty} \sum_{l=1}^{\infty} g_{kl} v^k(t) u^l(t). \quad (2.41)$$

in which v and u denote voltages at different points in the circuit.

Regarding the obtention of the power series coefficients g_k or g_{kl} , in this Thesis the traditional approach based on the Taylor series expansion around the circuit bias point will be used, so that they are defined as:

$$g_k = \frac{1}{k!} \left. \frac{d^k i[v(t)]}{dv^k} \right|_{v=V_{DC}}, \quad (2.42)$$

$$g_{kl} = \frac{1}{k! l!} \left. \frac{\partial^{k+l} i[v(t), u(t)]}{\partial v^k \partial u^l} \right|_{v=V_{DC}, u=U_{DC}}. \quad (2.43)$$

However, an alternative approach is proposed in [98] that uses Chebyshev series expansion instead of Taylor series expansion in order to get the polynomial approximation of the nonlinear functions describing the devices. In this case, although a more complex procedure provides values for the coefficients g_k or g_{kl} which are different from those obtained with equations (2.42) and (2.43), the power series structure is maintained for the nonlinear elements representation. Therefore, equations (2.39)-(2.41) remain applicable.

2.4 Harmonic Balance

2.4.1 Historical development

Harmonic Balance (HB) was originally considered an approximate technique for finding analytically the nearly-sinusoidal solution of a differential equation [99]. Baily formulated HB as a numerical method in 1969 [100]. Since then, it has been reformulated into an accurate method for finding numerically the solution of a differential equation driven by single or multiple sinusoids. The conventional approach begins by partitioning the circuit into linear and nonlinear subcircuits. The linear subcircuit is evaluated in the frequency domain while the nonlinear subcircuit is evaluated in the time domain. The problem then becomes that of finding the voltages on the nodes of both subcircuits that result in Kirchhoff's current law being satisfied in those nodes. In 1974, Egami showed that it is possible to solve these equations by using Newton-Raphson [101]. Gwarek and Kerr solved the equations by using nonlinear relaxation [102] [103], and Nakhla and Vlach used optimization methods [104]. Variations of these approaches have been presented by a large collection of authors [11].

In 1985, Kundert and Sangiovanni-Vincentelli proposed a method, referred to as *Harmonic Relaxation-Newton*, that combines most of the advantages of both relaxation and Newton-Raphson methods; and in 1986 they proposed an alternative relaxation method called *Gauss-Jacobi-Newton Harmonic Relaxation* with superior convergence properties [38].

Until 1984, HB was only used to analyse circuits with a periodic response. That year Ushida and Chua showed that a transform for the quasi-periodic signals present in mixers could be developed by starting from the matrix form of the Discrete Fourier Transform (DFT), but more than the normal number of time-points were needed in the sampled time-domain waveforms [105]. Although this approach allowed HB to be applied in mixers, it had some disadvantages because the extra time samples represented a computational burden and the number of samples in excess required the use of least-squares methods to perform the transformation of signals to and from the time and frequency domains, being this method ill-conditioned. Also in 1984, Gilmore and Rosenbaum [106] [107] presented a completely different transform that exploited sparsity in a spectrum, with which quasiperiodic signals can be analysed because, in practice, this type of signals is zero at almost all harmonics, i.e., the spectrum is sparse.

In 1987, Sorkin, Kundert and Sangiovanni-Vincentelli [108] [109] showed that using equally spaced samples in the time domain leads to ill-conditioning in the transform that could only be remedied by either using more than the theoretical mini-

imum number of time samples or using unequally spaced samples. In addition, an approach based on multidimensional Fast Fourier Transforms (FFTs) was proposed by Bava *et al.* [110] and later presented by Rizzoli [111], [112], Ushida [113], and Heron [39]. Another method for the analysis of nonlinear microwave circuits driven by non-harmonically related generators is the *Spectral Balance*, proposed by Gayral and Ngoya in 1987 [114], [115]. In this method, a generalised Fourier series and the corresponding method to get its complex coefficients are employed, where the involved frequencies have no particular relation.

A significant departure from conventional HB was suggested by Steer and Kahn in 1983 in [116], [117], and developed subsequently by other authors such as Haywood [118], Chang [119], [120], and Närhi [121]. They proposed to evaluate the nonlinear devices directly in the frequency domain. To do so, nonlinearities described by arbitrary continuous functions are modelled over the anticipated operating range with any kind of function that can be expressed by means of the four basic arithmetic operations (addition, subtraction, multiplication, and quotient). Among the methods proposed to approximate the nonlinear devices, we can encounter power series, generalised power series, rational functions or Chebyshev polynomials. This approximation allows us to obtain the output spectrum by using only spectral convolutions. This method, sometimes referred to as *Frequency Domain Spectral Balance*, exhibits as a disadvantage that it is very difficult to approximate accurately strongly nonlinear functions over a wide range with the aforementioned basic methods.

Since the 1990s, a major research interest has been focused on techniques to accelerate the computational time of HB methods. Some of the approaches aiming this objective were based on matrix methods for solving the HB iteration. In [122], Rizzoli presented a technique based on the exploitation of sparse-matrix techniques by setting to zero selected elements of the Jacobian matrix. Nevertheless, we could say that the most successful approaches are those based on Krylov-subspace techniques to iteratively solve the large linear systems of equations derived from each HB iteration. A related issue of this kind of techniques is that of finding the appropriate preconditioning matrix required to achieve good convergence speed. Among the works devoted to this kind of techniques ([123], [124], [125], [126], [127], [128], [129], [130], [131], [132]), that of Rizzoli [125] deserves a special mention. In that work, the *Inexact Newton* technique was introduced. It presents some advantages for solving large-sized nonlinear systems and exhibits the best results when applying a Krylov-subspace iterative solver, the GMRES.

A completely different approach also based on a Krylov technique, is that proposed by Gad in [133], where a reduction of the nonlinear circuit or the nonlinear set of equations is sought instead of reducing the cost of factorising the Jacobian matrix.

In that work, a Krylov-based projection technique is employed to reduce the size of the original set of equations to be solved in the HB analysis, while the accuracy of the solution is preserved because the reduced set of nonlinear equations shares with the original one the first derivatives with respect to the RF excitation level.

Other different approaches to accelerate computational time were proposed. Asai and Makino presented in [134] and [135] a technique which was taken up again by Gourary in [129]. It consisted in exploiting the concept of *Frequency Domain Latency* by using a multirate sampling for the FFT. Filicori introduced in [136] the *Frequency Windowing Harmonic Balance*, a technique in which the circuit equations were decoupled and linearised inside some frequency windows where the admittance of the circuit was assumed almost constant. This approximation leads to an important reduction of the computing effort, although it presents a limited validity range.

At the same time, some researchers proposed the use of different and more sophisticated algorithms for the solution of the HB equations [137], [88], while in [138] the use of the parallel-chords method was proposed as a simple linear-centric modelling approach to speed up the overall run-time.

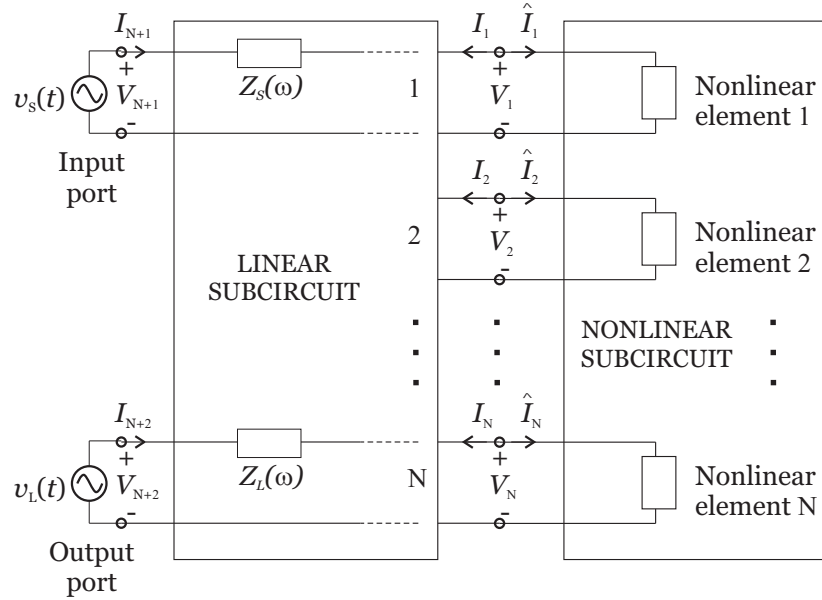
The second issue that has been widely developed during the last fifteen years are the techniques to create an optimum set of unequally spaced samples for the transformation from the time domain to the frequency domain ([139], [10], [140], [141], [142], [127], [128], [143], [144], [145], [146]). Although the approaches presented in those works will be addressed in Section 2.4.6, we will mention here the *Wavelet Harmonic Balance* introduced by Soveiko in 2003 in [146], which is a modification of HB where wavelets instead of Fourier series are used as basis functions to transform the time samples to the frequency domain, with the subsequent increase in sparsity of the matrix and a reduction in computational cost.

More recently, modern wireless communications systems have undergone a significant evolution which has aroused an increasing interest in simulation techniques for systems driven by digitally-modulated carriers. The great number of frequency components which must be taken into account is the main cause of the inefficiency that standard HB methods present with digitally-modulated carriers. Hence, although a considerable part of the proposed techniques for the analysis of nonlinear microwave systems with digitally-modulated carriers are based on HB methods ([20], [45], [17], [130], [18], [147], [19], [148]), they are formulated in terms of the complex envelopes of the involved signals. Section 2.6 and Chapter 3 will be devoted to this kind of techniques.

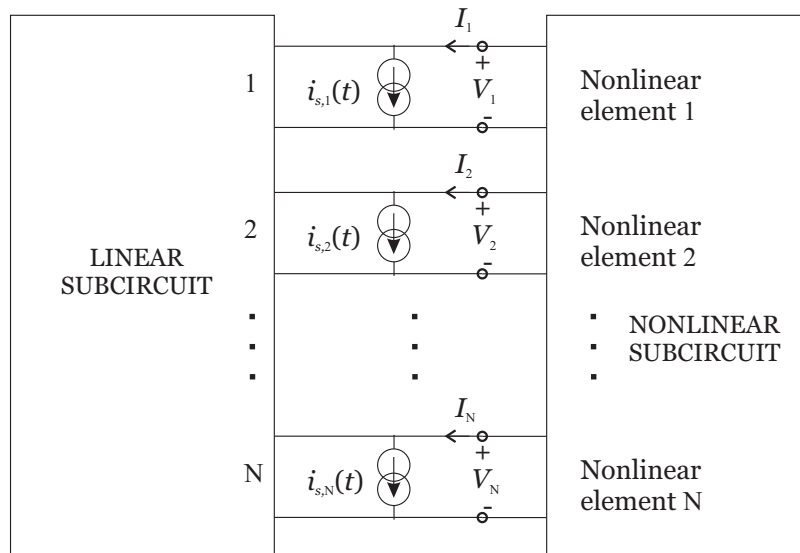
2.4.2 Harmonic Balance analysis

HB can be seen as an extension of phasor analysis from linear to nonlinear differential equations. Recall that phasor analysis is a classical method to obtain the steady-state solution to a system where linear differential equations apply and whose stimulus is a sinusoid of frequency ω_c . It is assumed that the solution has the form $x(t) = \text{Re} [X e^{j\omega_c t}]$, where X is the complex amplitude or phasor of the solution. When we substitute this response in the differential equations and evaluate the derivatives, a system of algebraic equations results, which is solved to obtain the phasor X . When the differential equation is not linear, an approximate solution can be found by using HB. We can assume that the solution is periodic and consists of a linear combination of harmonically related sinusoids. Once this solution is substituted into the differential equations, the resulting expressions can be factored into a sum of purely sinusoidal terms. Due to the orthogonality of sinusoids at different harmonics, the resulting algebraic system of equations can be broken up into a collection of simpler equations, one for each harmonic. The nonlinear equations are solved by finding the coefficients of the sinusoids that produce the balancing of the algebraic currents equation at each harmonic.

In general, microwave and RF circuits have a large number of both linear and nonlinear circuit elements. A convenient way of grouping the circuit elements can be as shown in Figure 2.7(a) to form two subcircuits, one linear and the other nonlinear. The linear subcircuit can be treated as a multiport and described by its Y parameters (which, in turn, can be obtained from the node admittance matrix, as it will be shown later). The nonlinear elements, modelled by their I/V or Q/V characteristics, might be solved directly in the frequency domain, although it would require a complicated Fourier decomposition of each nonlinear function and a convolution of the spectral tones and harmonics applied to the circuit. Instead, it is more convenient to analyse the nonlinear elements in the time domain. Thus, the circuit is reduced to an $(N + 2)$ -port network, with nonlinear elements connected to N ports and voltage sources connected to the other two ports. The $(N + 1)$ -th and $(N + 2)$ -th ports represent the input and output ports in a two-port network. Usually, a sinusoidal source is connected to only one of those ports; however, sources are shown at both ports in Figure 2.7 for generality. The source and load impedances, $Z_s(\omega)$ and $Z_L(\omega)$, are considered included into the linear subcircuit. Because of the nonlinear elements, the port voltages and currents have frequency components at harmonics of the excitation. Although in theory an infinite number of harmonics exist at each port, we shall assume that the dc component and the first H harmonics (i.e., $h = 0, \dots, H$) describe all the voltages and currents adequately.



(a)



(b)

Figure 2.7: Nonlinear circuit divided into linear and nonlinear subcircuits.

The idea of HB is to find a set of port voltage frequency components or, alternatively, port voltage waveforms which give the same currents in both the linear subcircuit equations and the nonlinear subcircuit equations. That is, the currents of the N ports satisfy Kirchhoff's current law

$$\begin{bmatrix} \mathbf{I}_1 \\ \mathbf{I}_2 \\ \vdots \\ \mathbf{I}_N \end{bmatrix} + \begin{bmatrix} \hat{\mathbf{I}}_1 \\ \hat{\mathbf{I}}_2 \\ \vdots \\ \hat{\mathbf{I}}_N \end{bmatrix} = \mathbf{0} \quad (2.44)$$

where each element of the currents vector is in turn a vector with the dc component and the first H harmonics (including their negative counterparts)

$$\mathbf{I}_n = [I_n(-H) \dots I_n(0) \dots I_n(H)]^T, \quad \hat{\mathbf{I}}_n = [\hat{I}_n(-H) \dots \hat{I}_n(0) \dots \hat{I}_n(H)]^T. \quad (2.45)$$

Note that the vectors include both negative-frequency and positive-frequency components. This consideration has been adopted because it is more convenient for the formulation of the main algorithms used to solve the HB equations (see Sections 2.4.3.2.2 and 2.4.3.3), although it presents some drawbacks. Real excitations are being considered, where the negative-frequency components are the complex conjugates of the positive-frequency ones and can be found from their counterparts immediately if needed. Eliminating the negative-frequency components from (2.44) could have reduced its complexity considerably. However, when using the Gauss-Jacobi-Newton or Newton algorithms in HB, the constrain imposed by using only positive-frequency components makes the derivative $\mathbf{J}_F(\mathbf{V})$ unrepresentable in the complex field. The way to circumvent this problem consists in treating separately real and imaginary parts, which implies doubling the number of variables involved and complicates notation considerably. This conversion, however, halves the memory and the number of operations required. It should be kept in mind that the more general internal representation of complex numbers consists in using pairs of numbers stored with floating point or double precision format, which means internally doubling the number of variables involved.

Despite knowing that it is not the most efficient solution, in this Thesis it has been decided to include both negative and positive frequencies and consider complex variables for the sake of simplicity in notation. Further details in derivations for HB methods where the presence of negative frequencies is not required can be found, for example, in [38], [10], and [8], although they are out of the scope of this Thesis.

The linear subcircuit can be analysed by means of its port admittance matrix

$$\begin{bmatrix} \mathbf{I}_1 \\ \vdots \\ \mathbf{I}_N \\ \mathbf{I}_{N+1} \\ \mathbf{I}_{N+2} \end{bmatrix} = \begin{pmatrix} \mathbf{Y}_{1,1} & \cdots & \mathbf{Y}_{1,N} & \mathbf{Y}_{1,N+1} & \mathbf{Y}_{1,N+2} \\ \vdots & \ddots & \vdots & \vdots & \vdots \\ \mathbf{Y}_{N,1} & \cdots & \mathbf{Y}_{N,N} & \mathbf{Y}_{N,N+1} & \mathbf{Y}_{N,N+2} \\ \mathbf{Y}_{N+1,1} & \cdots & \mathbf{Y}_{N+1,N} & \mathbf{Y}_{N+1,N+1} & \mathbf{Y}_{N+1,N+2} \\ \mathbf{Y}_{N+2,1} & \cdots & \mathbf{Y}_{N+2,N} & \mathbf{Y}_{N+2,N+1} & \mathbf{Y}_{N+2,N+2} \end{pmatrix} \begin{bmatrix} \mathbf{V}_1 \\ \vdots \\ \mathbf{V}_N \\ \mathbf{V}_{N+1} \\ \mathbf{V}_{N+2} \end{bmatrix}, \quad (2.46)$$

where each element in the voltage vector is in turn a vector of the form

$$\mathbf{V}_n = [V_n(-H) \dots V_n(0) \dots V_n(H)]^T, \quad (2.47)$$

and the elements of the admittance matrix are diagonal submatrices that correspond to the different harmonics of the fundamental frequency ω_c

$$\mathbf{Y}_{m,n} = \begin{pmatrix} Y_{m,n}(-H\omega_c) & \cdots & 0 & \cdots & 0 \\ \vdots & \ddots & \vdots & \vdots & \vdots \\ 0 & \cdots & Y_{m,n}(0) & \cdots & 0 \\ \vdots & \vdots & \vdots & \ddots & \vdots \\ 0 & \cdots & 0 & \cdots & Y_{m,n}(H\omega_c) \end{pmatrix}. \quad (2.48)$$

The excitation vectors \mathbf{V}_{N+1} and \mathbf{V}_{N+2} have the form

$$\begin{bmatrix} \mathbf{V}_{N+1} \\ \mathbf{V}_{N+2} \end{bmatrix} = \begin{bmatrix} 0 \\ \vdots \\ \frac{V_S}{2} \\ V_{b1} \\ \frac{V_S}{2} \\ \vdots \\ 0 \\ 0 \\ \vdots \\ V_{b2} \\ \vdots \\ 0 \end{bmatrix} \quad (2.49)$$

where V_{b1} and V_{b2} are the dc voltages at ports $N + 1$ and $N + 2$, respectively, and V_S is the excitation voltage at frequency ω_c at the $(N + 1)$ -th port. Equation (2.49) implies that the $(N + 1)$ -th port excitation includes a dc and a fundamental frequency source, while the $(N + 2)$ -th port includes only dc. This is the usual situation; it corresponds, for example, to a FET amplifier that has gate and drain bias and gate excitation.

It is convenient to partition the expression in (2.46) so that it can be written as:

$$\begin{bmatrix} \mathbf{I}_1 \\ \vdots \\ \mathbf{I}_N \end{bmatrix} = \begin{pmatrix} \mathbf{Y}_{1,N+1} & \mathbf{Y}_{1,N+2} \\ \vdots & \vdots \\ \mathbf{Y}_{N,N+1} & \mathbf{Y}_{N,N+2} \end{pmatrix} \begin{bmatrix} \mathbf{V}_{N+1} \\ \mathbf{V}_{N+2} \end{bmatrix} + \begin{pmatrix} \mathbf{Y}_{1,1} & \dots & \mathbf{Y}_{1,N} \\ \vdots & \ddots & \vdots \\ \mathbf{Y}_{N,1} & \dots & \mathbf{Y}_{N,N} \end{pmatrix} \begin{bmatrix} \mathbf{V}_1 \\ \vdots \\ \mathbf{V}_N \end{bmatrix} \quad (2.50)$$

or

$$\mathbf{I} = \mathbf{I}_s + \mathbf{Y}_{N \times N} \mathbf{V}, \quad (2.51)$$

where $\mathbf{Y}_{N \times N}$ is the submatrix formed by the first N rows and columns of \mathbf{Y} , and \mathbf{I}_s represents a set of current sources in parallel with the first N ports. This equation can be illustrated by means of the equivalent circuit shown in Figure 2.7(b), where the external excitation sources in the $(N+1)$ -th and $(N+2)$ -th ports need not be considered further.

As it was explained in Section 2.3.2, the most usual nonlinear elements can be nonlinear capacitances, conductances or controlled sources, all of them voltage-controlled elements. For all the cases, their analysis is carried out in the time domain by inverse Fourier transforming the complex phasor voltage at each port

$$\mathcal{F}^{-1}[\mathbf{V}_n] \rightarrow v_n(t). \quad (2.52)$$

For the case of a nonlinear capacitor, the charge waveform can be expressed as a function of the voltages at all N ports, i.e., $q_n(t) = f_{q_n}[v_1(t), v_2(t), \dots, v_N(t)]$. Applying the Fourier transform gives the charge vectors for the capacitors at each port

$$\mathcal{F}[q_n(t)] \rightarrow \mathbf{Q}_n. \quad (2.53)$$

According to Nyquist's theorem, a function must be evaluated at least $2H$ time samples per period in order to adequately determine the coefficients of the first H harmonics. However, it is advisable to use more samples than necessary, oversampling the waveforms between 2.5 and 2.6 times the number of harmonics to reduce the errors caused by *aliasing*. This way, a vector is constructed with the harmonics of the charge of the nonlinear capacitor at each port

$$\mathbf{Q} = [\mathbf{Q}_1 \dots \mathbf{Q}_N]^T, \text{ where } \mathbf{Q}_n = [Q_n(-H) \dots Q_n(0), \dots, Q_n(H)]^T. \quad (2.54)$$

The current through the nonlinear capacitor can be expressed by means of the derivative of the charge

$$i_{c,n}(t) = \frac{dq_n(t)}{dt} \leftrightarrow jh\omega_c Q_n(h). \quad (2.55)$$

In a compact form, expression (2.55) can also be written as:

$$\mathbf{I}_c = j\Omega \mathbf{Q}, \quad (2.56)$$

where $\mathbf{\Omega}$ is a diagonal matrix which includes N cycles of $(-H, \dots, 0, \dots, H)\omega_c$ through the main diagonal.

Similarly, the instantaneous current in a nonlinear conductance or a controlled current source can be expressed as

$$i_{g,n}(t) = g_n[v_1(t), v_2(t), \dots, v_N(t)] \leftrightarrow \mathbf{I}_{G,n} = \mathcal{F}[i_{g,n}(t)]. \quad (2.57)$$

A vector is also constructed with the harmonics of the nonlinear current at each port

$$\mathbf{I}_G = [\mathbf{I}_{G,1} \dots \mathbf{I}_{G,N}]^T, \text{ where } \mathbf{I}_{G,n} = [I_{G,n}(-H) \dots I_{G,n}(0) \dots I_{G,n}(H)]^T. \quad (2.58)$$

Substituting (2.56), (2.58) and (2.51) in (2.44) gives the following expression:

$$\mathbf{F}(\mathbf{V}) = \mathbf{I}_s + \mathbf{Y}_{N \times N} \mathbf{V} + j\mathbf{\Omega} \mathbf{Q} + \mathbf{I}_G = \mathbf{0}. \quad (2.59)$$

Note that if the vector \mathbf{V} is such that $\mathbf{F}(\mathbf{V}) = \mathbf{0}$, then \mathbf{V} is the solution of the HB analysis. $\mathbf{F}(\mathbf{V})$, called the *current-error vector*, represents the difference between the current calculated from the linear and nonlinear subcircuits, at each port and at each harmonic, for a trial-solution vector \mathbf{V} .

Regarding the linear subcircuit, there are many methods for generating the N -port admittance matrix of a linear circuit, although the simplest one is to generate an indefinite (modified) node admittance matrix and convert it into a port matrix. The process can be implemented readily on a computer. Of course, a matrix must be produced for each harmonic frequency in the analysis.

To convert the indefinite admittance matrix into a port admittance matrix, we must create a port impedance matrix and invert it. To obtain the impedance matrix, we first select the nodes corresponding to port 1, excite them with unity current, and measure the voltage between the nodes representing each of the ports. This produces the first column of the impedance matrix. Moving the excitation to port 2 produces the second column, and proceeding in this manner to the last port produces the entire matrix.

The conventional process for the formulation of HB analysis equations has been explained, based on the N -port admittance matrix of the linear circuit. Nevertheless, it is also possible to formulate the HB analysis simply by using the node admittance matrix. In this case, the principle of HB simply becomes a restatement of Kirchhoff's current law in the frequency domain. In a nodal formulation, each node voltage in the circuit becomes an independent variable. The number of variables in the HB analysis remains $N(2H + 1)$, but N is now the number of nodes, not the number of control voltages. In microwave and RF circuits, the number of nodes is likely to be greater than the number of nonlinear elements, so the nodal formulation increases the size of the Jacobian. However, this formulation is more robust regarding convergence, because the Jacobian is rarely ill conditioned.

2.4.3 Solution algorithms

The remaining part of the problem is to solve (2.59) to obtain \mathbf{V} . Each of the $2H + 1$ components of \mathbf{V} at each of the N ports is an unknown. Thus, there are $N(2H + 1)$ unknowns to determine. For example, the analysis of a FET amplifier usually includes nonlinear elements at three ports. Let assume that it has eight significant harmonics plus dc at each port. Thus, $N = 3$, $H = 8$, and there are 51 variables to obtain.

A number of algorithms have been proposed for solving (2.59), the most significant of which will be described. Today, there is a strong consensus that Newton's method is preferred for HB simulation and it is applied, possibly associated to some continuation method, in virtually all the commercial simulators.

2.4.3.1 Optimization methods

It is possible to apply nonlinear optimization techniques to solve (2.59). In this case, the magnitude squared of the current-error function $\varepsilon(\mathbf{V}) = \mathbf{F}^H(\mathbf{V}) \cdot \mathbf{F}(\mathbf{V})$ is treated as the cost function that we want to minimise, being $(\cdot)^H$ the Hermitian transpose. The chosen cost function has two important characteristics. First, each root of \mathbf{F} corresponds to a global minimum of $\varepsilon(\mathbf{V})$, and at these points, $\varepsilon(\mathbf{V}) = 0$. Second, at each \mathbf{V} that is a local minimum of $\varepsilon(\mathbf{V})$ but is not a root of \mathbf{F} , the Jacobian of \mathbf{F} is singular. If a $\hat{\mathbf{V}}$ is found such that $\varepsilon(\hat{\mathbf{V}}) = 0$, then $\hat{\mathbf{V}}$ satisfies (2.59), so we seek for a global minimum that must satisfy the following condition:

$$\nabla\varepsilon(\hat{\mathbf{V}}) = 0. \quad (2.60)$$

This problem can be solved by using different techniques, one of which is a Newton's method that uses Newton-Raphson to find the roots of (2.60). However, solving (2.60) with Newton-Raphson is more difficult than solving (2.59), because the equation involves the first derivative of the original function \mathbf{F} , so applying Newton-Raphson requires knowing the second derivatives of \mathbf{F} . In fact, the Newton-Raphson iteration used to solve (2.60) is

$$\nabla^2\varepsilon(\mathbf{V}^{(i)}) [\mathbf{V}^{(i+1)} - \mathbf{V}^{(i)}] = -\nabla\varepsilon(\mathbf{V}^{(i)}), \quad (2.61)$$

where $\nabla^2\varepsilon$ is the Hessian of ε , which can be written as:

$$\nabla^2\varepsilon(\mathbf{V}) = \frac{d\mathbf{J}_F(\mathbf{V})}{d\mathbf{V}}\mathbf{F}(\mathbf{V}) + \mathbf{J}_F^H(\mathbf{V})\mathbf{J}_F(\mathbf{V}), \quad (2.62)$$

and the gradient takes the form

$$\nabla\varepsilon(\mathbf{V}) = \mathbf{J}_F^H(\mathbf{F})\mathbf{F}(\mathbf{V}). \quad (2.63)$$

Clearly, the Hessian is denser than the Jacobian and it is therefore considerably more expensive to factor. Using (2.62) and (2.63), we can rewrite (2.61) as

$$\left[\frac{d\mathbf{J}_F(\mathbf{V}^{(i)})}{d\mathbf{V}} \mathbf{F}(\mathbf{V}^{(i)}) + \mathbf{J}_F^H(\mathbf{V}^{(i)}) \mathbf{J}_F(\mathbf{V}^{(i)}) \right] \cdot [\mathbf{V}^{(i+1)} - \mathbf{V}^{(i)}] = -\mathbf{J}_F^H(\mathbf{V}^{(i)}) \mathbf{F}(\mathbf{V}^{(i)}). \quad (2.64)$$

Applying nonlinear optimization techniques to solve the HB equations is expensive because there is a very large number of unknowns to be found and nonlinear optimization techniques are expensive for large problems. Furthermore, the considered cost function destroys a lot of information about the individual contribution of each variable to the error, so optimization routines may have convergence problems. For these reasons, the approaches presented subsequently are preferred over the optimization methods.

2.4.3.2 Relaxation methods

As the name implies, relaxation methods use simple algorithms that encourage the voltages to move gradually towards the solution. An advantage of these methods is that they are simple to implement, often not requiring the generation of I/V derivatives. Relaxation methods have been largely used, although their use has decreased recently. Their worst problems are unpredictable convergence characteristics and inapplicability to large systems.

Two different ways of applying relaxation methods are presented, the first uses a form of nonlinear relaxation called *splitting* similar to the approach taken by Gwarek, Kerr or Hicks [102] [103] [149] [150]. The second combines relaxation and Newton-Raphson [38].

2.4.3.2.1 Splitting

Splitting is a relaxation technique that was originally developed to solve linear systems of equations and was generalised to handle nonlinear systems [95]. Let consider the linear system $\mathbf{A}\mathbf{x} = \mathbf{b}$ and consider the splitting of \mathbf{A} into $\mathbf{A} = \mathbf{B} - \mathbf{C}$, where \mathbf{B} is a nonsingular matrix. Then a fixed-point iteration that can be applied to find its solution is $\mathbf{x}^{(i+1)} = \mathbf{B}^{-1}(\mathbf{C}\mathbf{x}^{(i)} + \mathbf{b})$, where $\mathbf{x}^{(i)}$ denotes the estimation of the unknown \mathbf{x} for the i -th iteration. The iterative algorithm converges if all the eigenvalues of $\mathbf{B}^{-1}\mathbf{C}$ are smaller in magnitude than one. In order to apply this result to the HB, let $\hat{\mathbf{I}}^{(i)} = -[j\Omega\mathbf{Q}(\mathbf{V}^{(i)}) + \mathbf{I}_G(\mathbf{V}^{(i)})]$ be the vector of the nonlinear current estimated after the i -th iteration. Taking into account that HB consists in finding \mathbf{V} such that $\mathbf{I} = -\hat{\mathbf{I}}$,

if we take $\mathbf{I}^{(i)} = -\hat{\mathbf{I}}^{(i)}$, it is possible to propose the following update for the voltage vector:

$$\mathbf{V}^{(i+1)} = \mathbf{Y}_{N \times N}^{-1} (\mathbf{I}^{(i)} - \mathbf{I}_s) \quad (2.65)$$

In practice, although the value $\mathbf{V}^{(0)}$ is close enough to the solution and the nonlinearities are weak, it is not possible to guarantee the convergence of this method. Because of that, the following alternative is preferred [149]:

$$\begin{aligned} \mathbf{U}^{(i)} &= \mathbf{Y}_{N \times N}^{-1} (\mathbf{I}^{(i)} - \mathbf{I}_s) \\ \mathbf{V}^{(i+1)} &= s\mathbf{U}^{(i)} + (1 - s)\mathbf{V}^{(i)} \end{aligned} \quad (2.66)$$

where s is a real constant ($0 < s < 1$) called the *splitting coefficient* which is determined heuristically. The values of s near zero help convergence, though slowly. As s tends to one, the convergence is accelerated, but it can even be lost. A typical value is $s = 0.2$, or even smaller if the initial guess is not good enough, the circuit is strongly nonlinear or the magnitude of the excitation is large. Note that, despite the resemblance in notation between splitting and continuation methods, they exhibit basic differences since the splitting coefficient is fixed through all the iterations whereas in continuation methods a sequence of values of the parameter are employed, generating a sequence of problems to be solved by means of iteration.

2.4.3.2.2 Gauss-Jacobi-Newton Harmonic Relaxation

The second relaxation approach to solve equation (2.59) is to use the block Gauss-Jacobi method with a one-step Newton inner loop, known as the block Gauss-Jacobi-Newton method. To apply this method, (2.59) is reformulated into a system of $2H + 1$ equations, each of which calculates the vector of node currents at one frequency given the node voltages at all frequencies. This can be done considering that the node admittance matrix for the linear portion of the circuit $\mathbf{Y}_{N \times N}$ is block diagonal, since linear devices are incapable of translating frequencies. Equation (2.59) can be written as:

$$\mathbf{Y}_{N \times N} \mathbf{V} = -\mathbf{I}_s - j\Omega \mathbf{Q} - \mathbf{I}_G, \quad (2.67)$$

and once the right-hand side of (2.67) has been evaluated, the task of finding \mathbf{V} can be broken into solving $2H + 1$ decoupled linear $N \times N$ systems of equations, one for each harmonic:

$$\mathbf{F}(\mathbf{V}, h) = \mathbf{I}_s(h) + \mathbf{Y}_{N \times N}(h, h)\mathbf{V}(h) + jh\omega_c \mathbf{Q}(\mathbf{V}, h) + \mathbf{I}_G(\mathbf{V}, h) = \mathbf{0}, \quad (2.68)$$

with $h = -H, \dots, -1, 0, 1, \dots, H$. In the block Gauss-Jacobi algorithm, there is an outer relaxation loop and an inner loop where each equation in (2.68) is solved by using Newton's method for $\mathbf{V}^{(i+1)}(h)$. Note that in this equation only $\mathbf{V}(h)$ is a variable, and $\mathbf{V}(l)$ with $l \neq h$ are constant and can be taken from the previous iteration.

Applying the Gauss-Jacobi-Newton method to (2.68) results in

$$\frac{\partial \mathbf{F}(\mathbf{V}^{(i)}, h)}{\partial \mathbf{V}(h)} [\mathbf{V}^{(i+1)}(h) - \mathbf{V}^{(i)}(h)] = -\mathbf{F}(\mathbf{V}^{(i)}, h), \quad h = -H, \dots, -1, 0, 1, \dots, H \quad (2.69)$$

or

$$\mathbf{V}^{(i+1)}(h) = \mathbf{V}^{(i)}(h) - \left(\frac{\partial \mathbf{F}(\mathbf{V}^{(i)}, h)}{\partial \mathbf{V}(h)} \right)^{-1} \mathbf{F}(\mathbf{V}^{(i)}, h), \quad (2.70)$$

where

$$\frac{\partial \mathbf{F}(\mathbf{V}, h)}{\partial \mathbf{V}(h)} = Y_{N \times N}(h, h) + jh\omega_c \frac{\partial \mathbf{Q}(\mathbf{V}, h)}{\partial \mathbf{V}(h)} + \frac{\partial \mathbf{I}_G(\mathbf{V}, h)}{\partial \mathbf{V}(h)}. \quad (2.71)$$

The term $\frac{\partial \mathbf{F}(\mathbf{V}, h)}{\partial \mathbf{V}(h)}$ can be viewed as the node admittance matrix of the circuit at the h -th harmonic where the circuit has been linearised about the solution.

Only the derivation of $\frac{\partial \mathbf{I}_G(\mathbf{V}, h)}{\partial \mathbf{V}(h)}$ will be developed, the derivation of $\frac{\partial \mathbf{Q}(\mathbf{V}, h)}{\partial \mathbf{V}(h)}$ is identical.

The Fourier series of the current at the n -th port is

$$i_{g_n}(t) = \sum_{h=-H}^H I_{G_n}(h) e^{jh\omega_c t}, \quad (2.72)$$

where the frequency coefficients are

$$I_{G_n}(h) = \frac{1}{T} \int_0^T i_{g_n}(t) e^{-jh\omega_c t} dt, \quad (2.73)$$

being $T = 2\pi/\omega_c$ the fundamental period. We can use the chain rule to differentiate and use a vector notation involving all the ports in the network

$$\frac{\partial I_{G_n}(h)}{\partial V_m(h)} = \frac{1}{T} \int_0^T \frac{\partial i_{g_n}(t)}{\partial V_m(h)} e^{-jh\omega_c t} dt = \frac{1}{T} \int_0^T \frac{\partial i_{g_n}(t)}{\partial v_m(t)} \frac{\partial v_m(t)}{\partial V_m(h)} e^{-jh\omega_c t} dt. \quad (2.74)$$

To compute the derivative of $v(t)$ we write it as a Fourier series

$$v_m(t) = \sum_{h=-H}^H V_m(h) e^{jh\omega_c t} \quad (2.75)$$

$$\frac{\partial v_m(t)}{\partial V_m(h)} = e^{jh\omega_c t}. \quad (2.76)$$

Then the derivative of $\mathbf{I}_G(\mathbf{V}, h)$ is formed by the elements

$$\frac{\partial I_{G_n}(h)}{\partial V_m(h)} = \frac{1}{T} \int_0^T \frac{\partial i_{g_n}(t)}{\partial v_m(t)} dt. \quad (2.77)$$

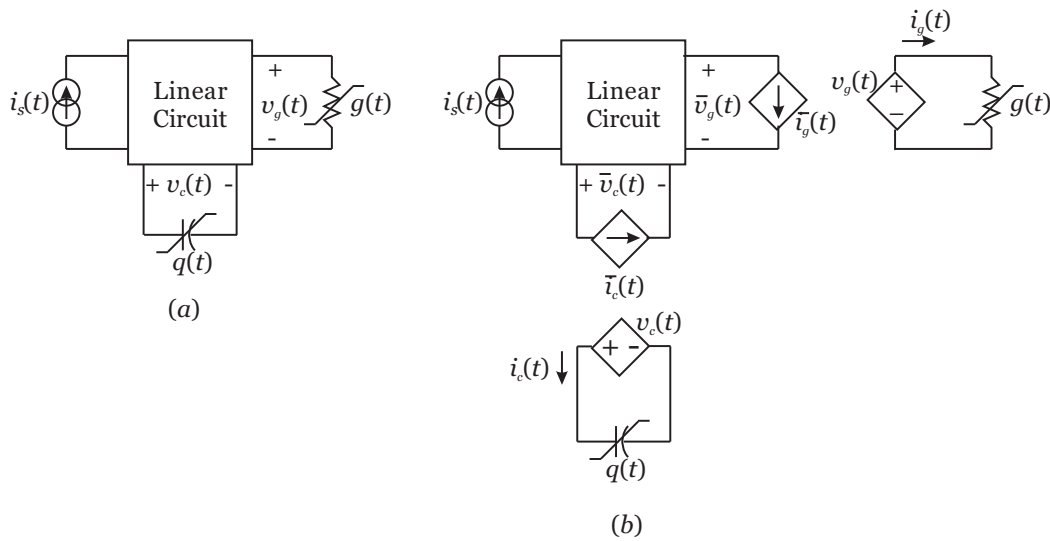


Figure 2.8: Circuit interpretation of the splitting method form of relaxation methods applied to the HB analysis.

Thus, the derivative is simply the average value of the derivative waveform over one period. Similarly, for the derivative of $\mathbf{Q}(\mathbf{V}, h)$ we have the elements

$$\frac{\partial Q_n(h)}{\partial V_m(h)} = \frac{1}{T} \int_0^T \frac{\partial q_n(t)}{\partial v_m(t)} dt. \quad (2.78)$$

Block Gauss-Jacobi-Newton algorithm is guaranteed to converge if $\mathbf{F}(\mathbf{V})$ is sufficiently linear and if $\mathbf{V}^{(0)}$ is sufficiently close to the solution $\hat{\mathbf{V}}$.

To illustrate how the two relaxation methods work, consider the network shown in Figure 2.8(a). In the splitting method, at each iteration the voltages of the nonlinear devices are fixed at the values of the previous iteration, which fixes the current passed by these devices. By means of the substitution theorem, in Figure 2.8(b) the nonlinear elements are replaced with current sources. This means that the analysed circuit is a linear subcircuit that never changes. Only the new current source values need to be calculated for the next iteration, which is done by applying the new node voltages to the nonlinear devices.

With block Gauss-Jacobi-Newton method, the circuit is linearised by dividing the nonlinear devices into two parts. One is the best linear approximation to the nonlinear device considering the signal present on the device. The other is the nonlinear residual that, when combined with the linear part gives the original nonlinear device. This division is illustrated in Figure 2.9(b). Comparing Figures 2.8 and 2.9 helps us to understand why Gauss-Jacobi-Newton method has better convergence properties than the splitting method; it has a better model of the nonlinear device in the linear subcircuit, and therefore less correction is needed on each iteration.

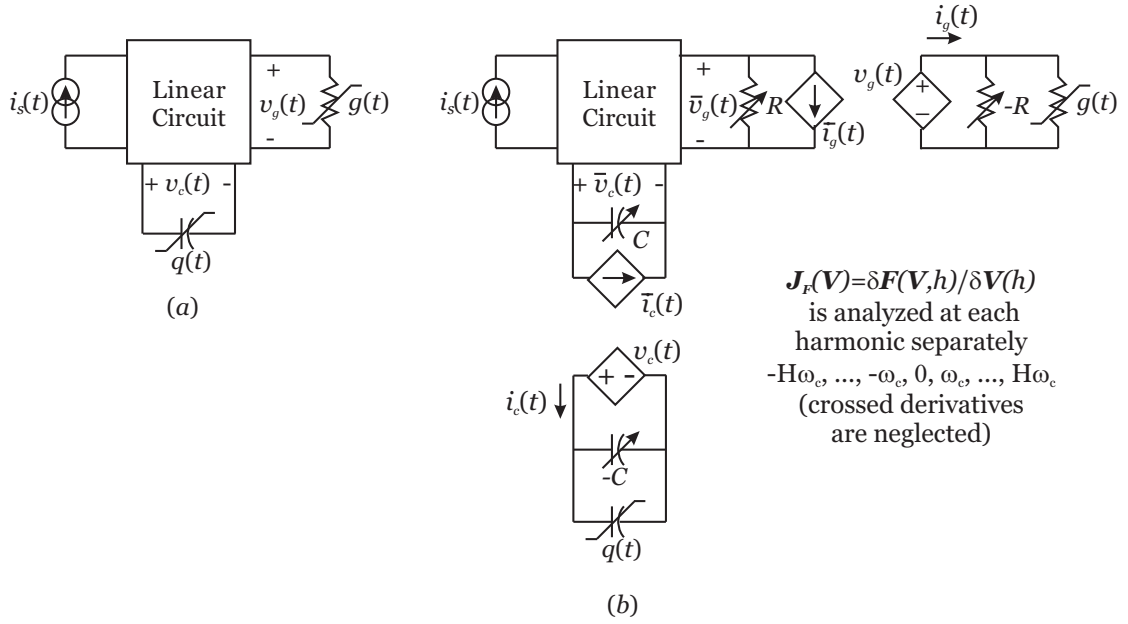


Figure 2.9: Circuit interpretation of the block Gauss-Jacobi-Newton method applied to the HB analysis.

The Gauss-Jacobi-Newton method presents the interesting feature that it uses very little memory. The circuit is analysed at only one frequency at a time, so space is needed for only the $N \times N$ node admittance matrix and the space is reused for each frequency. Nevertheless, it has severe convergence problems when circuits behave strongly nonlinearly. Another drawback of this method is that it is necessary to reevaluate the partial derivatives that represent the linearised circuit for each iteration, because the linear approximation of the nonlinear devices must be recalculated. Although the resultant matrix presents good sparsity features, this fact implies an additional computational cost compared to the splitting method.

2.4.3.3 Newton's methods or Harmonic Newton

Newton's method applied to (2.59) results in the following iteration:

$$\mathbf{V}^{(i+1)} = \mathbf{V}^{(i)} - \mathbf{J}_F^{-1}(\mathbf{V}^{(i)})\mathbf{F}(\mathbf{V}^{(i)}), \quad (2.79)$$

where $\mathbf{J}_F(\mathbf{V}^{(i)})$ is the Jacobian matrix of $\mathbf{F}(\mathbf{V}^{(i)})$, whose elements are given by the following definition:

$$\frac{\partial F_n(h)}{\partial V_m(l)} = Y_{n,m}(h, l) + jh\omega_c \frac{\partial Q_n(h)}{\partial V_m(l)} + \frac{\partial I_{G_n}(h)}{\partial V_m(l)}, \quad (2.80)$$

and where $Y_{m,n}(h, l)$ equals $Y_{m,n}(h\omega_c)$ if $h = l$, and zero otherwise. The partial derivatives are defined as follows:

$$\begin{aligned}\frac{\partial I_{G_n}(h)}{\partial V_m(l)} &= \frac{1}{T} \int_0^T \frac{\partial i_{g_n}(t)}{\partial V_m(l)} e^{-jh\omega_c t} dt \\ \frac{\partial Q_n(h)}{\partial V_m(l)} &= \frac{1}{T} \int_0^T \frac{\partial q_n(t)}{\partial V_m(l)} e^{-jh\omega_c t} dt\end{aligned}\quad (2.81)$$

being $T = 2\pi/\omega_c$ the fundamental period. The main advantage of this method is that a complete use of the error function derivatives with regard to each port variable is made. Because of that, it is able to achieve convergence even with a large number of variables. Its main disadvantage is the computational time that is required to generate the Jacobian, therefore it is largely advisable to have closed-form expressions for its elements if we want to avoid the calculation of the derivatives by means of finite differences [40], [151]. Applying the chain rule to the expressions in (2.81), we have

$$\begin{aligned}\frac{\partial I_{G_n}(h)}{\partial V_m(l)} &= \frac{1}{T} \int_0^T \frac{\partial i_{g_n}(t)}{\partial v_m(t)} \cdot \frac{\partial v_m(t)}{\partial V_m(l)} e^{-jh\omega_c t} dt \\ \frac{\partial Q_n(k)}{\partial V_m(l)} &= \frac{1}{T} \int_0^T \frac{\partial q_n(t)}{\partial v_m(t)} \cdot \frac{\partial v_m(t)}{\partial V_m(l)} e^{-jk\omega_c t} dt\end{aligned}\quad (2.82)$$

where

$$v_m(t) = \sum_{h=-\infty}^{\infty} V_m(h) e^{jh\omega_c t}, \quad (2.83)$$

and consequently

$$\frac{\partial v_m(t)}{\partial V_m(l)} = e^{jl\omega_c t}. \quad (2.84)$$

Let $G_{n,m}(k)$ and $C_{n,m}(k)$ be the Fourier coefficients of the first derivatives of the nonlinear conductance and capacitance, respectively

$$\begin{aligned}G_{n,m}(k) &= \frac{1}{T} \int_0^T \frac{\partial i_{g_n}(t)}{\partial v_m(t)} e^{-jk\omega_c t} dt \\ C_{n,m}(k) &= \frac{1}{T} \int_0^T \frac{\partial q_n(t)}{\partial v_m(t)} e^{-jk\omega_c t} dt\end{aligned}\quad (2.85)$$

Substituting (2.84) in (2.82), when we compare to (2.85) results

$$\begin{aligned}\frac{\partial I_{G_n}(h)}{\partial V_m(l)} &= G_{n,m}(h-l), \\ \frac{\partial Q_n(h)}{\partial V_m(l)} &= C_{n,m}(h-l).\end{aligned}\quad (2.86)$$

It can be written in a compact manner

$$\mathbf{J}_F = \begin{pmatrix} \mathbf{J}_{1,1} & \dots & \mathbf{J}_{1,N} \\ \vdots & \ddots & \vdots \\ \mathbf{J}_{N,1} & \dots & \mathbf{J}_{N,N} \end{pmatrix}, \quad (2.87)$$

where

$$\mathbf{J}_{n,m} = \mathbf{Y}_{n,m} + j\omega\mathbf{C}_{n,m} + \mathbf{G}_{n,m}. \quad (2.88)$$

$\mathbf{Y}_{n,m}$ presents the same form than in (2.48), and ω takes the form

$$\omega = \begin{pmatrix} -H\omega_c & 0 & \dots & 0 \\ 0 & (-H+1)\omega_c & \dots & 0 \\ \vdots & \vdots & \ddots & \vdots \\ 0 & 0 & \dots & H\omega_c \end{pmatrix}. \quad (2.89)$$

Taking into account the definition for the $G_{n,m}(h-l)$ and $C_{n,m}(h-l)$ elements given by (2.86), the resulting $\mathbf{G}_{n,m}$ and $\mathbf{C}_{n,m}$ matrices are Toeplitz matrices with the Fourier coefficients of the time-varying conductance and capacitance, respectively. That is to say, they are defined from the column vectors $[G(0), \dots, G(2H)]^T$ and $[C(0), \dots, C(2H)]^T$, respectively.

$$\mathbf{G}_{n,m} = \begin{pmatrix} G_{n,m}(0) & G_{n,m}(-1) & \dots & G_{n,m}(-2H) \\ G_{n,m}(1) & G_{n,m}(0) & \dots & G_{n,m}(-2H+1) \\ \vdots & \vdots & \ddots & \vdots \\ G_{n,m}(2H) & G_{n,m}(2H-1) & \dots & G_{n,m}(0) \end{pmatrix}, \quad (2.90)$$

$$\mathbf{C}_{n,m} = \begin{pmatrix} C_{n,m}(0) & C_{n,m}(-1) & \dots & C_{n,m}(-2H) \\ C_{n,m}(1) & C_{n,m}(0) & \dots & C_{n,m}(-2H+1) \\ \vdots & \vdots & \ddots & \vdots \\ C_{n,m}(2H) & C_{n,m}(2H-1) & \dots & C_{n,m}(0) \end{pmatrix}.$$

As it is shown in Figure 2.10, Newton's method applied to the HB analyses the circuit at all frequencies simultaneously, and so it needs more memory than the Gauss-Jacobi-Newton method. However, its convergence properties are better because the best model of the nonlinear devices is taken into account. Nevertheless, this advantage involves a significant additional computational cost to the Newton's method. This is because it is necessary to reevaluate the Jacobian of the linear subcircuit for each iteration and, for this method, the Jacobian matrix is not so sparse as in the case of Gauss-Jacobi-Newton.

The most computationally expensive part of Newton's method applied to HB is the factorization of \mathbf{J}_F , a $(N \times (2H+1))$ by $(N \times (2H+1))$ relatively sparse matrix. This requires $\mathcal{O}(N \times (2H+1)^3)$ operations. Simplified Newton's method can be employed to reduce the computation time required [95].

Newton's method is only guaranteed to converge if the initial guess is close enough to the solution. Thus, finding a good initial guess is a key issue in determining the like-

likelihood of convergence. For many circuits, a good initial guess is generated by linearising the circuit about the dc operating point, applying the stimulus, and performing a phasor analysis. Alternatively, continuation methods can be associated to Newton’s method in order to increase its region of convergence if necessary. After that, the Jacobian used for each iteration is the linearization of the circuit about its time-varying operating point.

A variant of Newton’s method proposed by Curtice [152] employs the following expression for updating the voltages vector:

$$\mathbf{V}^{(i+1)} = \mathbf{V}^{(i)} - \beta \mathbf{J}_F^{-1}(\mathbf{V}^{(i)}) \mathbf{F}(\mathbf{V}^{(i)}). \tag{2.91}$$

This method is also referred to as a *norm-reduction method*. The parameter β , which is $0 < \beta < 1$, reduces uniformly the changes suffered by the elements of \mathbf{V} at each iteration, thus improving the convergence properties. It is especially recommended for the cases in which the error function $\mathbf{F}(\mathbf{V})$ has an inflection point near the zero, where the Newton’s iterations can become trapped near the zero or even diverge. The usual process for adjusting β is to begin with a full Newton step, that is $\beta = 1$. If that step reduces the current error, it is retained; if not, β is reduced and the process is repeated until the error decreases. If we choose a value close to $\beta = 0.5$ the number of iterations needed to converge is minimised.

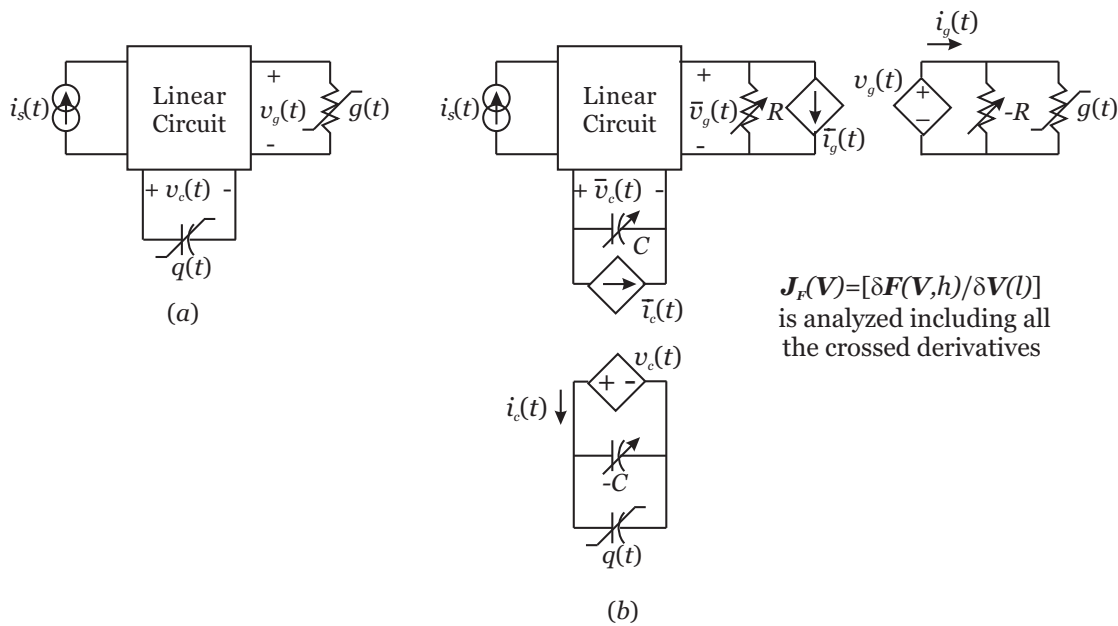


Figure 2.10: Circuit interpretation of the Newton’s method applied to the HB analysis.

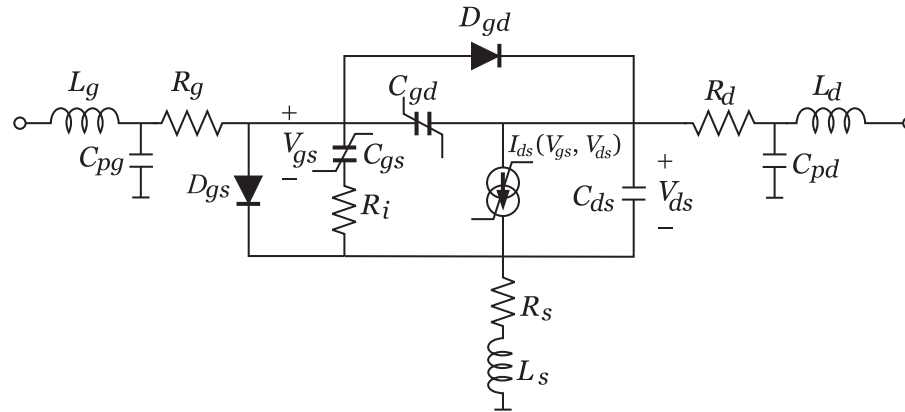


Figure 2.11: Equivalent circuit for the large-signal model of a FET.

2.4.4 Example: Harmonic Balance analysis of a FET amplifier

Through the last decades, several empirical models have been published describing the large-signal characteristics of MESFET and HEMT transistors, each of them being the best choice for a certain device and application. Figure 2.11 shows a lumped-element equivalent circuit of a FET device that can be used in a large-signal analysis. Two kinds of elements can be differentiated:

1. The elements of the intrinsic circuit (I_{ds} , C_{gs} , C_{gd} , C_{ds} , R_i , D_{gs} and D_{gd}), which are bias dependent and represent the elements that are specific to the operation of the device.
2. The access resistors, inductors and capacitors (R_g , R_s , R_d , L_g , L_s , L_d , C_{pg} and C_{pd}), parasitic elements that can be assumed to be constant and whose inclusion forms the extrinsic circuit.

The main nonlinear elements included in the large-signal models are:

- The drain-to-source current I_{ds} , which is a function of the voltages V_{gs} and V_{ds} and from which the transconductance $g_m = g_{10}$ and output conductance $g_d = g_{01}$ can be obtained.
- The gate-to-source capacitance C_{gs} .
- The gate-to-drain capacitance C_{gd} .
- The diodes D_{gs} and D_{gd} , which model the gate current under direct polarization of the gate-to-source union, and the avalanche drain-to-gate current, respectively.

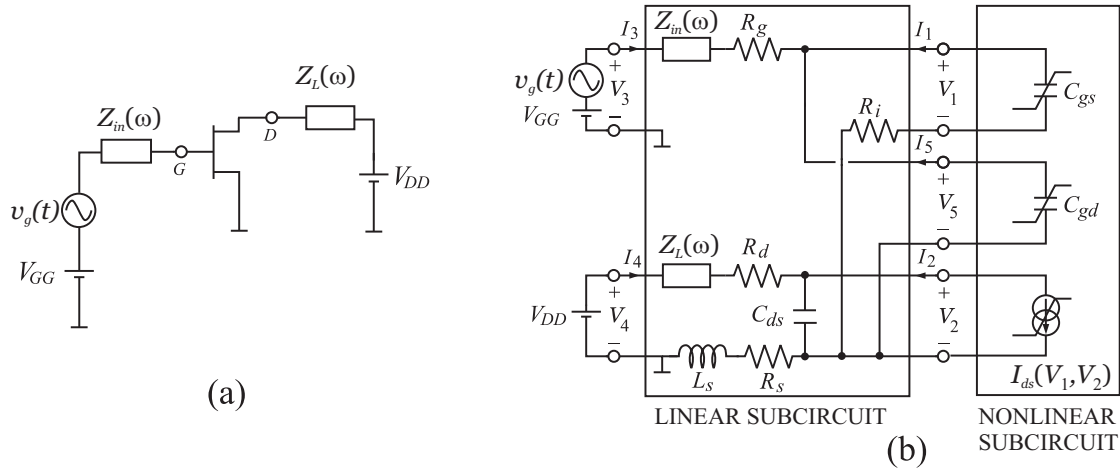


Figure 2.12: Equivalent circuit of a FET amplifier for the large-signal HB analysis.

It is generally accepted that the dominant source of nonlinearity in MESFET and HEMT transistors is the drain-to-source current $I_{ds}(V_{gs}, V_{ds})$ [9], [21], [28], [73], [74].

In this section, we will consider the example of a FET amplifier based on a single transistor, as shown in Figure 2.12(a). The excitation is applied at the gate port. A simplified model for the FET has been taken into account. In order to apply the HB analysis, it is convenient to separate the circuit in a linear subcircuit and another nonlinear subcircuit which includes the nonlinear elements. The circuit shown in Figure 2.12(b) is structured following the proposed methodology.

By means of nodal analysis, the following expressions can be obtained for the elements in the admittance matrix of the linear subcircuit, which is a five-port network:

$$\begin{aligned}
 \mathbf{Y}_{11} &= R_i^{-1} \\
 \mathbf{Y}_{22} &= R_i^{-1} + j\Omega C_{ds} + \left[\mathbf{Z}_s + (\mathbf{Z}_d^{-1} + \mathbf{Z}_g^{-1})^{-1} \right]^{-1} \\
 \mathbf{Y}_{33} &= \left[\mathbf{Z}_g + (\mathbf{Z}_d^{-1} + \mathbf{Z}_s^{-1})^{-1} \right]^{-1} \\
 \mathbf{Y}_{44} &= \left[\mathbf{Z}_d + (\mathbf{Z}_s^{-1} + \mathbf{Z}_g^{-1})^{-1} \right]^{-1} \\
 \mathbf{Y}_{55} &= \mathbf{Y}_{11} + \mathbf{Y}_{33} \\
 \mathbf{Y}_{12} &= -\mathbf{Y}_{11}, \quad \mathbf{Y}_{13} = \mathbf{Y}_{14} = \mathbf{0}, \quad \mathbf{Y}_{15} = \mathbf{Y}_{12} \\
 \mathbf{Y}_{23} &= -\mathbf{Z}_s^{-1} (\mathbf{Z}_d^{-1} + \mathbf{Z}_s^{-1})^{-1} \cdot \mathbf{Y}_{33} \\
 \mathbf{Y}_{24} &= -\mathbf{Z}_s^{-1} (\mathbf{Z}_s^{-1} + \mathbf{Z}_g^{-1})^{-1} \cdot \mathbf{Y}_{44} \\
 \mathbf{Y}_{25} &= \mathbf{Y}_{11} - \mathbf{Y}_{23} \\
 \mathbf{Y}_{34} &= -\mathbf{Z}_g^{-1} (\mathbf{Z}_s^{-1} + \mathbf{Z}_g^{-1})^{-1} \cdot \mathbf{Y}_{44}
 \end{aligned}$$

$$\begin{aligned} \mathbf{Y}_{35} &= -\mathbf{Y}_{33} \\ \mathbf{Y}_{45} &= -\mathbf{Y}_{34} \end{aligned} \quad (2.92)$$

where $\mathbf{Z}_g = \mathbf{Z}_{in} + \mathbf{R}_g$, $\mathbf{Z}_d = \mathbf{Z}_L + \mathbf{R}_d$ and $\mathbf{Z}_s = \mathbf{R}_s + j\Omega L_s$. The remaining elements in the admittance matrix are calculated by means of the reciprocity condition of the linear subcircuit, which implies $\mathbf{Y}_{ij} = \mathbf{Y}_{ji}$.

If the device is biased in the saturation region, it is a common practice to assume a linear behaviour of the capacitance C_{gd} . The number of ports in the linear subcircuit is reduced to four. Maintaining the references of the voltages and currents in Figure 2.12(b), the elements of the new admittance matrix (\mathbf{Y}'_{ij}) can be determined from (2.92) by applying the following rule:

$$\mathbf{Y}'_{ij} = \mathbf{Y}_{ij} - \mathbf{Y}_{i5} (\mathbf{Y}_{55} + j\Omega C_{gd})^{-1} \mathbf{Y}_{5j}. \quad (2.93)$$

The expression (2.59) can be written now as:

$$\mathbf{F}(\mathbf{V}) = \mathbf{I}_s + \mathbf{Y}_{2 \times 2} \mathbf{V} + j\Omega \mathbf{Q} + \mathbf{I}_G = \mathbf{0}, \quad (2.94)$$

where

$$\begin{aligned} \mathbf{Y}_{2 \times 2} &= \begin{pmatrix} \mathbf{Y}'_{11} & \mathbf{Y}'_{12} \\ \mathbf{Y}'_{21} & \mathbf{Y}'_{22} \end{pmatrix}, \\ \mathbf{I}_s &= \begin{bmatrix} \mathbf{I}_{s1} \\ \mathbf{I}_{s2} \end{bmatrix} = \begin{bmatrix} \mathbf{Y}'_{13} \mathbf{V}_3 + \mathbf{Y}'_{14} \mathbf{V}_4 \\ \mathbf{Y}'_{23} \mathbf{V}_3 + \mathbf{Y}'_{24} \mathbf{V}_4 \end{bmatrix}, \\ \mathbf{Q} &= \begin{bmatrix} \mathbf{Q}_{gs} \\ \mathbf{0} \end{bmatrix}, \\ \mathbf{I}_G &= \begin{bmatrix} \mathbf{0} \\ \mathbf{I}_{ds} \end{bmatrix}. \end{aligned} \quad (2.95)$$

As an example, the structure of the complete Jacobian \mathbf{J}_F for the circuit described in equations (2.95) will be detailed next:

$$\mathbf{J}_F = \begin{pmatrix} \mathbf{J}_{1,1} & \mathbf{J}_{1,2} \\ \mathbf{J}_{2,1} & \mathbf{J}_{2,2} \end{pmatrix} = \begin{pmatrix} \frac{\partial F_1(-H)}{\partial V_1(-H)} & \cdots & \frac{\partial F_1(-H)}{\partial V_1(H)} & \frac{\partial F_1(-H)}{\partial V_2(-H)} & \cdots & \frac{\partial F_1(-H)}{\partial V_2(H)} \\ \vdots & \ddots & \vdots & \vdots & \ddots & \vdots \\ \frac{\partial F_1(H)}{\partial V_1(-H)} & \cdots & \frac{\partial F_1(H)}{\partial V_1(H)} & \frac{\partial F_1(H)}{\partial V_2(-H)} & \cdots & \frac{\partial F_1(H)}{\partial V_2(H)} \\ \frac{\partial F_2(-H)}{\partial V_1(-H)} & \cdots & \frac{\partial F_2(-H)}{\partial V_1(H)} & \frac{\partial F_2(-H)}{\partial V_2(-H)} & \cdots & \frac{\partial F_2(-H)}{\partial V_2(H)} \\ \vdots & \ddots & \vdots & \vdots & \ddots & \vdots \\ \frac{\partial F_2(H)}{\partial V_1(-H)} & \cdots & \frac{\partial F_2(H)}{\partial V_1(H)} & \frac{\partial F_2(H)}{\partial V_2(-H)} & \cdots & \frac{\partial F_2(H)}{\partial V_2(H)} \end{pmatrix}, \quad \text{where}$$

$$\mathbf{J}_{1,1} = \begin{pmatrix} \mathbf{Y}'_{11}(-H\omega_c) - jH\omega_c C_{gs}(0) & \dots & -jH\omega_c C_{gs}(-H) & \dots & -jH\omega_c C_{gs}(-2H) \\ \vdots & \ddots & \vdots & \ddots & \vdots \\ 0 & \dots & \mathbf{Y}'_{11}(0) & \dots & 0 \\ \vdots & \ddots & \vdots & \ddots & \vdots \\ jH\omega_c C_{gs}(2H) & \dots & jH\omega_c C_{gs}(H) & \dots & \mathbf{Y}'_{11}(H\omega_c) + jH\omega_c C_{gs}(0) \end{pmatrix},$$

$$\mathbf{J}_{1,2} = \begin{pmatrix} \mathbf{Y}'_{12}(-H\omega_c) & \dots & 0 & \dots & 0 \\ \vdots & \ddots & \vdots & \ddots & \vdots \\ 0 & \dots & \mathbf{Y}'_{12}(0) & \dots & 0 \\ \vdots & \ddots & \vdots & \ddots & \vdots \\ 0 & \dots & 0 & \dots & \mathbf{Y}'_{12}(H\omega_c) \end{pmatrix},$$

$$\mathbf{J}_{2,1} = \begin{pmatrix} \mathbf{Y}'_{21}(-H\omega_c) + G_{10}(0) & \dots & G_{10}(-H) & \dots & G_{10}(-2H) \\ \vdots & \ddots & \vdots & \ddots & \vdots \\ G_{10}(H) & \dots & \mathbf{Y}'_{21}(0) + G_{10}(0) & \dots & G_{10}(-H) \\ \vdots & \ddots & \vdots & \ddots & \vdots \\ G_{10}(2H) & \dots & G_{10}(H) & \dots & \mathbf{Y}'_{21}(H\omega_c) + G_{10}(0) \end{pmatrix},$$

$$\mathbf{J}_{2,2} = \begin{pmatrix} \mathbf{Y}'_{22}(-H\omega_c) + G_{01}(0) & \dots & G_{01}(-H) & \dots & G_{01}(-2H) \\ \vdots & \ddots & \vdots & \ddots & \vdots \\ G_{01}(H) & \dots & \mathbf{Y}'_{22}(0) + G_{01}(0) & \dots & G_{01}(-H) \\ \vdots & \ddots & \vdots & \ddots & \vdots \\ G_{01}(2H) & \dots & G_{01}(H) & \dots & \mathbf{Y}'_{22}(H\omega_c) + G_{01}(0) \end{pmatrix}. \tag{2.96}$$

2.4.5 Matrix methods for solving the Harmonic Balance iteration

Working out the HB iteration (2.59) involves managing a set of linear equations. There are certain methods for solving linear equations that have been found especially useful for HB analysis. The first of them is LU decomposition. The principle behind LU decomposition is simple. Let us assume that the following matrix equations must be solved:

$$\mathbf{Ax} = \mathbf{b}. \tag{2.97}$$

We can factor the matrix \mathbf{A} into a lower triangular matrix \mathbf{L} , in which entries above the diagonal are zero, and an upper triangular matrix \mathbf{U} , in which the entries below the diagonal are zero. Then, we have $\mathbf{LUx} = \mathbf{b}$. Let $\mathbf{Ux} = \mathbf{m}$, where \mathbf{m} is a vector. Then we can solve, alternatively, in two steps:

$$\begin{aligned}\mathbf{Lm} &= \mathbf{b}, \\ \mathbf{Ux} &= \mathbf{m}.\end{aligned}\tag{2.98}$$

The two steps in (2.98) can be solved by back-substitution operations, which are computationally inexpensive. Furthermore, LU factorization can be performed without using more memory than that required to hold the original matrix, since \mathbf{A} is destroyed in the factorization and it is replaced by \mathbf{L} and \mathbf{U} . However, this method has the drawback that the time required to factor the matrix varies approximately as the cube of its dimension. Thus, this characteristic makes it impractical for analysis of large circuits.

Another option is to use sparse solvers. The Jacobian $\mathbf{J}_{\mathbf{F}}(\mathbf{V})$ consists of an $N \times N$ matrix of square submatrices, each of which has dimension $(2H+1)$, as shown in equations (2.87)-(2.90). Each submatrix represents the harmonic components for a particular nonlinear-element port; that is, if the current or charge at port n depends on the voltage at port m , the (n, m) submatrix is filled with Fourier terms $\mathbf{G}_{n,m} + j\omega\mathbf{C}_{n,m}$. Added to these terms, there is always a diagonal matrix $\mathbf{Y}_{n,m}$ at each harmonic, $-H\omega_c, \dots, -\omega_c, 0, \omega_c, \dots, H\omega_c$. Therefore, some submatrices are filled and some are diagonal, and it is even possible for some to be empty.

A sparse matrix is one that contains mostly zeros. Since the Jacobian matrix is rather sparse, it would be logical to use sparse solvers. Conventional sparse solvers use LU decomposition to factor the matrix but exploit the sparsity of the matrix to improve efficiency, by avoiding the need to multiply and add large numbers of zero entries. The zero entries are not stored, so a saving of memory results as well. Nevertheless, the Jacobian in HB problem is usually not sparse enough to benefit more than modestly from such methods.

Since it is usual that many of the elements of the Jacobian are very small and have little effect on the Newton update, a proposed technique to increase the sparsity of the Jacobian consists in eliminating all elements whose magnitudes are below some threshold or setting to zero selected entries on the basis of some predetermined physical criterion [122], [153]. These are invariably the farthest elements from the diagonals of the Jacobian's blocks.

Krylov-subspace techniques are a class of iterative methods for solving sparse linear systems of equations. There is now a general consensus that a technique called the

generalised minimum residual (GMRES) is the preferred one for HB analysis [8]. Iterative methods minimise the residual, \mathbf{r} of (2.97)

$$\mathbf{r} = \mathbf{b} - \mathbf{A}\hat{\mathbf{x}}, \quad (2.99)$$

where $\hat{\mathbf{x}}$ is an estimate of the solution. To employ GMRES, it is necessary that \mathbf{x} can be estimated with at least moderate accuracy, so that \mathbf{r} is not too large. To obtain such conditions, the matrix must be *preconditioned*; that is, multiplied by an estimate of the inverse called the preconditioner, $\mathbf{P} = \hat{\mathbf{A}}^{-1}$

$$\mathbf{P}\mathbf{A}\mathbf{x} = \mathbf{P}\mathbf{b}. \quad (2.100)$$

Generally, the preconditioner is chosen to be a close approximation to \mathbf{A} which is also easy to invert. In HB analysis, a suitable preconditioner is the inverse of the admittance matrix of the linear subcircuit, which is generated in the process of creating the port \mathbf{Y} matrix, and needs to be inverted only once in the solution process. For mildly nonlinear problems, constructing $\mathbf{P} = \mathbf{J}_{\mathbf{F}}^{-1}(\mathbf{V}^{(0)})$ by linearising about the dc operating point and performing a simple ac analysis at each mixing product is an effective and efficient choice. This preconditioner is not sufficient for strongly nonlinear problems, where it is necessary to adaptively prune the full harmonic Jacobian.

An advantage of Krylov techniques is that (2.59) do not have to be fully solved in each iteration, because the iterative process needs only proceed until

$$\|\mathbf{F}(\mathbf{V}) - \mathbf{J}_{\mathbf{F}}(\mathbf{V})\Delta\mathbf{V}\| < \alpha\|\mathbf{F}(\mathbf{V})\|, \quad (2.101)$$

where α is selected at the beginning of the i -th iteration to be

$$\alpha = \frac{\|\mathbf{F}(\mathbf{V}^{(i)}) - \mathbf{F}(\mathbf{V}^{(i-1)}) + \mathbf{J}_{\mathbf{F}}(\mathbf{V}^{(i-1)})\Delta\mathbf{V}^{(i-1)}\|}{\|\mathbf{F}(\mathbf{V}^{(i-1)})\|}. \quad (2.102)$$

This approach to the solution is called *Inexact Newton method*. Setting $\alpha = 0$ in (2.102) corresponds to ordinary, exact Newton iterations.

When using the Krylov-subspace methods, HB requires roughly $\mathcal{O}(N(2H+1))$ operations, where N is the number of circuit equations and $(2H+1)$ is the number of frequencies required. This does not include the necessary operations to precondition the system of equations, which may be far from negligible in strongly nonlinear problems. Therefore, this procedure can improve significantly the efficiency. However, it has some disadvantages. The main one is that Krylov solvers are distinctly inferior to direct solvers such as LU decomposition in handling poorly conditioned Jacobian matrices [8]. In addition to this, some precautions need to be taken when including these techniques in simulators. The simulator must be designed around the Krylov method, because it is not possible to simply replace the matrix solver. Furthermore, since a factored Jacobian is not created explicitly, methods like Simplified Newton or Samănskii's are not applicable in this case.

2.4.6 Multitone inputs in Harmonic Balance analysis

HB was formulated for the case of single-tone excitations, when the voltages and currents in the network are periodic and thus have a fundamental-frequency component and a number of harmonics. If several incommensurate excitations are applied, some modifications need to be made in order to generalise the HB concept. This modified method has been called *generalised Harmonic Balance analysis*, *Spectral Balance analysis* or *multitone Harmonic Balance analysis*.

Let us consider the case where the excitation may have two or more incommensurate frequencies, so the currents and voltages at each port have a set of K frequency components ω_k , $k = 0, 1, \dots, K - 1$. These frequency components are mixing products, not harmonics; each mixing product arises as a linear combination of the excitation frequencies. In the case of a two-tone excitation, $\omega_k = m\omega_1 + n\omega_2$, where ω_1 and ω_2 are the frequencies of the two excitations, and each (m, n) pair maps to a unique k . Taking into account the number of possible frequencies involved due to the mixing products, it becomes apparent that the size of the HB problem grows rapidly with the number of tones, and can easily become so large as to be impractical. This is a serious limitation of multitone HB analysis.

The goal of the HB analysis is to find a set of voltage components $V_n(k)$ at the frequencies ω_k that satisfy (2.44). In this case, however, the elements $I_n(k)$ of the current vector and $Q_n(k)$ of the charge vector represent the components at port n and at mixing frequency ω_k , where ω_k is not necessarily a harmonic of a single excitation frequency. The HB equations are still valid in the multitone case; it is necessary only to replace the harmonics $k\omega_c$ with ω_k and to include all excitation tones in the excitation voltage vectors. Finally, the voltage, current, charge, and similar components are components at the frequency ω_k , so they can no longer be determined by classical Fourier transform but must be found by an alternative time-to-frequency transform.

One possible method for creating a multitone Fourier transform is to adapt a discrete Fourier transform (DFT). We wish to express the time waveform $x(t)$, which may represent either a voltage or a current, as

$$x(t) = \frac{1}{K} \sum_{k=0}^{K-1} X(k) e^{j\omega_k t} \quad (2.103)$$

where ω_k are the set of mixing frequencies in the multitone problem. If the function $x(t)$ is sampled at the K time intervals $t_i = t_1, t_2, \dots, t_K$, the samples $x(t_i)$ can be

expressed by a set of linear equations

$$\begin{bmatrix} x(t_1) \\ x(t_2) \\ \vdots \\ x(t_K) \end{bmatrix} = \frac{1}{K} \cdot \begin{bmatrix} 1 & e^{j\omega_1 t_1} & \dots & e^{j\omega_{K-1} t_1} \\ 1 & e^{j\omega_1 t_2} & \dots & e^{j\omega_{K-1} t_2} \\ \vdots & \vdots & \ddots & \vdots \\ 1 & e^{j\omega_1 t_K} & \dots & e^{j\omega_{K-1} t_K} \end{bmatrix} \cdot \begin{bmatrix} X(0) \\ X(1) \\ \vdots \\ X(K-1) \end{bmatrix} \quad (2.104)$$

or, in simpler notation

$$\mathbf{x} = \frac{1}{K} \cdot \Gamma^{-1} \mathbf{X}, \quad (2.105)$$

and, by convention it is defined

$$\mathbf{X} = \Gamma \mathbf{x}. \quad (2.106)$$

Γ describes the transformation from the time domain to the frequency domain. In multitone analysis, the admittance matrix is evaluated at the mixing frequencies instead of the harmonic frequencies. The derivative matrices must be evaluated at those frequencies as well. Thanks to the representation of the DFT as a linear transform by means of Γ , the derivatives contained in the Jacobian can be obtained in the following simple way:

$$\mathbf{J}_F = \frac{\partial \mathbf{F}}{\partial \mathbf{V}} = \mathbf{Y}_{N \times N} + \frac{\partial \mathbf{I}_G}{\partial \mathbf{V}} + j\Omega \frac{\partial \mathbf{Q}}{\partial \mathbf{V}}, \quad (2.107)$$

with

$$\begin{aligned} \frac{\partial \mathbf{I}_G}{\partial \mathbf{V}} &= \frac{1}{K} \cdot \Gamma \frac{\partial \mathbf{i}_g}{\partial \mathbf{v}} \Gamma^{-1}, \\ \frac{\partial \mathbf{Q}}{\partial \mathbf{V}} &= \frac{1}{K} \cdot \Gamma \frac{\partial \mathbf{q}}{\partial \mathbf{v}} \Gamma^{-1}. \end{aligned} \quad (2.108)$$

In a classical DFT, the time samples involved in (2.104) are selected uniformly and the ω_k are harmonically related. The *Fast Fourier Transform* (FFT), which is commonly used in single-tone HB analysis, is just an algorithm that implements a DFT but minimises the number of repeated multiplications. The DFT generates little error in transforming between the time and frequency domains, because the rows of Γ^{-1} are orthogonal and the matrix is well conditioned. If the frequencies are not harmonics, the rows are not orthogonal, and it is possible for some rows to be nearly linearly dependent; then the matrix is ill conditioned and large errors result. Therefore, it is better to take nonuniformly spaced time samples and select the sample points so that they make the rows of Γ^{-1} orthogonal. Some methods for creating an optimum multitone DFT are the following:

- Almost-periodic Fourier transform (APFT) [109]
- Two-dimensional FFT [111]

- Quasiorthogonal matrix method and filter-balance DFT [139]
- Time-mapped Harmonic Balance [127]
- APFT and mapping techniques [140] [141]
- Artificial frequency mapping [10] [145]
- Determination of a low sampling frequency that prevents aliasing [143]
- Signal-Space representation of the spectral content of the device current [142]

We will describe here the two-dimensional FFT method, as it is an optimal method for the case of two-tone excitations. In this case, the $x(t)$ vector can be expressed as

$$x(t) = \sum_m \sum_n X(m, n) \cdot e^{j(m\omega_1 + n\omega_2)t} \quad (2.109)$$

where $X(m, n)$ are the complex phasor magnitudes of the components at their respective frequencies. It is possible to treat the time as two independent time variables, so we can define ν_1 and ν_2 as

$$\begin{aligned} \nu_1 &= \omega_1 t = (r - 1) \frac{2\pi}{N_m}, \\ \nu_2 &= \omega_2 t = (s - 1) \frac{2\pi}{N_n}, \end{aligned} \quad (2.110)$$

where N_m and N_n are the number of sample points for the m and n series, respectively. The number of samples must be at least twice the number of harmonics and these numbers must be powers of two in order to use the FFT algorithm. This results in a two-dimensional grid of time samples, which can be processed with a two-dimensional FFT resulting in a two-dimensional set of frequency components, in which the component at the pair $(m\omega_1, n\omega_2)$ is the frequency component $m\omega_1 + n\omega_2$.

Some disadvantages of this method are that a large number of samples are used, and this would be prohibitive without the use of the FFT. The restriction of the sample set to powers of two requires oversampling of the time waveform but can be otherwise beneficial, as it reduces aliasing in the transform. This method can be extended to any number of dimensions, but the time required to fill the multidimensional FFT matrix and to evaluate the transform increases exponentially with each dimension. The two-dimensional FFT is an optimal method in the sense that it achieves the same conditioning as an orthogonal DFT.

In addition to this, a different approach to the problem of transforming from the time domain to the frequency domain is presented by Soveiko in [146], where he proposes to use a wavelet transform instead of Fourier series. That is to say, to use matrices Γ and Γ^{-1} associated with the forward and inverse wavelet transform in $\mathbf{X} = \Gamma \mathbf{x}$

and $\mathbf{x} = \frac{1}{K} \cdot \Gamma^{-1} \mathbf{X}$, respectively. The main advantage of the use of bi-orthogonal wavelet basis functions is that they result in an increase in sparsity of the Jacobian, whereas Fourier basis functions (sines and cosines) have full support on an interval and matrices Γ and Γ^{-1} are essentially dense, producing the appearance of denser blocks in the Jacobian.

Despite the use of any of the aforementioned techniques, such as the two-dimensional FFT, APFT or aliasing control, the multitone HB becomes inefficient for input excitations containing a great number of tones. In practice, it is shown that these techniques stop being useful for more than three tones.

2.5 Volterra series

The functional expansion known as *Volterra series* is one of the most extended tools for the analysis of nonlinear circuits, as it is shown by the numerous research articles found in literature, from the first ones by Wiener [154], and Narayanan [155], to the most recent ones by Stauth [156], Tannir [157], Yamanouchi [158] or Roblin [159]. The main advantage of Volterra series representation is that it allows us to obtain closed-form expressions which provide insight into the operation of the circuit. However, these closed-form expressions are circuit specific.

Volterra showed that every functional ² $G[x]$, continuous in the field of continuous functions can be represented by the expansion

$$G[x] = \sum_{n=0}^{\infty} F_n[x] \quad (2.111)$$

where $F_n[x]$ is a regular homogeneous functional of the form

$$F_n[x] = \int_a^b \cdots \int_a^b h_n(\xi_1, \dots, \xi_n) x(\xi_1) x(\xi_2) \cdots x(\xi_n) d\xi_1 d\xi_2 \cdots d\xi_n. \quad (2.112)$$

The index n is said to be the degree of the functional.

Volterra series were introduced into nonlinear circuit analysis in 1942 by Wiener [154]. If the output $y(t)$ of a nonlinear system can be expressed by means of a functional of its input $x(t)$, then both can be related by means of a functional series. The method of analysis is primarily a frequency-domain method and uses appropriate nonlinear device models. Volterra series have been described as *power series with memory* which express the output of a nonlinear system in *powers* of the input $x(t)$. A substantial number of the systems encountered in communication problems

²A functional is an operation on a function for which the result is a number

can be represented as Volterra series, therefore Volterra series are particularly useful in calculating distortions in communications systems. Quoting Bedrosian and Rice:

In practice it appears that Volterra series do not enable us to do anything that cannot be done otherwise. However, [...] the Volterra series approach has the virtue that many such problems can be treated in an orderly way.

From the late 1950's there was a continuous effort in the application of Volterra series expansions to nonlinear system theory. In 1967, Narayanan applied the technique to the analysis of transistor amplifier distortion using a nonlinear T-model of the junction transistor [155], [160], [161]. Two significant papers that propelled the use of Volterra series for the nonlinear circuit analysis were those by Bussgang, Ehrman and Graham [13] and by Bedrosian and Rice [162]. Volterra representation has been successfully applied to the analysis of circuits including feedforward or IMPATT amplifiers, [163], [164], and GaAs FETs, being remarkable the contributions by Minasian [165] and Lambrinou [166] to the study of intermodulation in MESFET amplifiers. It is widely accepted that the current source I_{ds} is the main responsible for the nonlinear response in these kind of circuits [9], [21], [28], [73], [74]. Some characterization methods have been proposed for this current source, like the one in [97], though different studies have been made about the impact of other nonlinear elements in the circuit, such as the capacitances [74], on the overall nonlinear behaviour. In the last years, thanks to the availability of more powerful computational tools, the interest has been shifted to the analysis of multitone inputs [167], [28], continuous spectrum signals, the spectral regrowth phenomenon [8], [168], [43], or the analysis and design of linearisers [169], [159] and digital predistorters [158], [170]. In addition to this, Volterra series representation has been recently applied to get a better insight into the operation of circuits constructed with new transistor technologies, such as HBTs amplifiers [171], LDMOS high power amplifiers [172] or CMOS short-channel LNAs [173]. Other recent applications for Volterra series have been the analysis of new models for GaN HEMT devices taking into account dispersive effects such as thermal dependence [174] or trapping effects [175], and the optimization of termination impedances required to minimise the nonlinear distortion [176].

It is widely acknowledged that the main drawback of Volterra series representation is their considerable complexity for high-order nonlinearities. Because of this, it is usually applied under the weakly nonlinear assumption. To overcome this limitation of the classical Volterra series, a Volterra-like approach, called *modified Volterra series* ([136], [15], [177]) or *dynamic Volterra series* ([178]) was proposed, in which the input/output relationship for a nonlinear system with memory is described as a memoryless nonlinear term plus a purely dynamic contribution. Furthermore, by con-

trolling the order of the dynamics, the modified Volterra series can be truncated to a simpler version. However, this approach presents the disadvantage that the static part and the different order dynamics have to be extracted separately. This involves very complicated measurement procedures, especially when higher order dynamics are included.

Another extension based on Volterra series for strongly nonlinear systems where the classical Volterra series diverge is called *generalised Volterra series technique* and was proposed by Eijnde and Krozer in [179], [180], [181]. The generalised Volterra series technique consists basically in time-varying Volterra series. The level of the input signal is reduced sufficiently, up to a certain value for which the Volterra series converges. For this value, the output signal is calculated and a new Volterra series is obtained about the previously determined output value. Then the input signal is increased and the same process is repeated until the response to the original input signal is obtained. For those iterations in which the Volterra series cannot be determined because convergence is not achieved, the input signal is decreased. This technique can be seen as an association of the Volterra series to the Newton-Raphson HB techniques where continuation algorithms are considered.

In addition to this, an increasing interest in the use of Volterra representation as a base to obtain behavioural models for microwave power amplifiers has been recently developed [182], [183], [184], [185], [186], [187], [188], [189], [190], [86].

In this section, the fundamentals of Volterra series representation will be presented, paying special attention to the cases of bandpass nonlinear systems with memory and multitone inputs. We will follow the approaches of Weiner and Spina [191], Bussgang [13] and Maas [8]. Furthermore, the most common methods for determining the nonlinear transfer functions will be reviewed.

2.5.1 Volterra series representation

Let us consider a nonlinear system with an input $x(t)$ and an output $y(t)$. The input waveform can be approximated by a succession of elementary rectangular pulses $p(t)$ of width $\Delta\tau$, whose leading edges occur at $k\Delta\tau$, $k = 0, 1, 2, \dots$ and whose heights are $x_k = x(k\Delta\tau)$, as shown in Figure 2.13

$$x(t) \approx \sum_{k=0}^{\infty} x(k\Delta\tau) \Delta\tau p(t - k\Delta\tau). \quad (2.113)$$

Let K denote the number of rectangular pulses occurring between 0 and some positive time t . The expected response will be a function of the $K + 1$ input variables

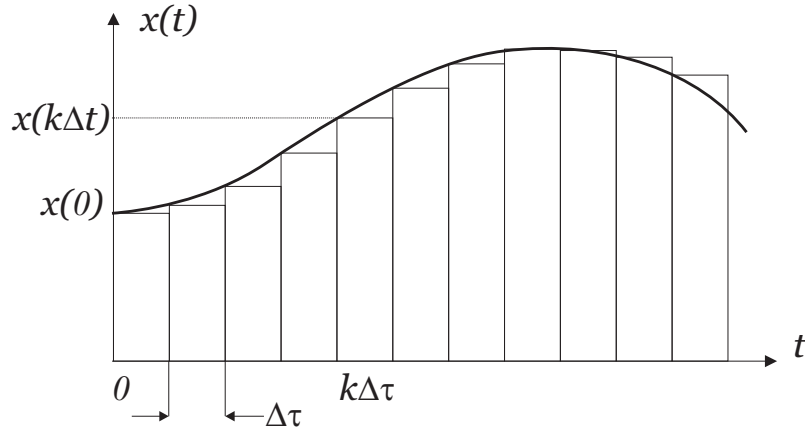


Figure 2.13: Approximation to $x(t)$ by a succession of rectangular pulses.

x_0, x_1, \dots, x_K , so that it can be written as:

$$y(t) = f(x_0, x_1, \dots, x_K), \quad (2.114)$$

where $f(\cdot)$ is a nonlinear function of the $K + 1$ input variables.

Assuming that $f(\cdot)$ can be expanded into a $(K + 1)$ -dimensional Taylor series expansion, and grouping terms having identical order, the response $y(t)$ can be expressed as

$$y(t) \approx \sum_{k_1=0}^K a_{k_1} x_{k_1} + \sum_{k_1=0}^K \sum_{k_2=0}^K a_{k_1 k_2} x_{k_1} x_{k_2} + \sum_{k_1=0}^K \sum_{k_2=0}^K \sum_{k_3=0}^K a_{k_1 k_2 k_3} x_{k_1} x_{k_2} x_{k_3} + \dots \quad (2.115)$$

Alternatively, the output may be written as:

$$y(t) = \sum_{n=1}^{\infty} y_n(t), \quad (2.116)$$

where the n -th order term is approximated by

$$y_n(t) \approx \sum_{k_1=0}^K \sum_{k_2=0}^K \dots \sum_{k_n=0}^K a_{k_1 k_2 \dots k_n} x_{k_1} x_{k_2} \dots x_{k_n}. \quad (2.117)$$

The term $y_n(t)$ is said to be of order n in the sense that, if the input $x(t)$ is multiplied by a constant A , then $y_n(t)$ depends on A as A^n .

If the system were linear, the Taylor series representation would be reduced to the first term of the expansion. In this case, superposition would apply and the total response would be the sum of the responses to each of the individual pulses. In the limit, as $\Delta\tau \rightarrow d\tau$, the pulse $p(t)$ tends to the unit impulse $\delta(t)$, so that the response

to $p(t)$ tends to the impulse response $h(t)$ and the summation becomes an integral. At time t , the linear response is given by

$$y_1(t) = \int_0^t x(\tau) h(t - \tau) d\tau. \quad (2.118)$$

The impulse response is considered a complete characterization of the linear part of the circuit.

The general term in the approximation to $y_n(t)$, given by $a_{k_1 k_2 \dots k_n} x_{k_1} x_{k_2} \dots x_{k_n}$, can be interpreted as the n -th order response to n elementary rectangular pulses applied at $k_1 \Delta\tau, k_2 \Delta\tau, \dots, k_n \Delta\tau$. Consequently, in analogy with the development of the convolution integral for the linear part, it results

$$y_n(t) = \int_0^t \int_0^t \dots \int_0^t h_n(t - \tau_1, t - \tau_2, \dots, t - \tau_n) x(\tau_1) x(\tau_2) \dots x(\tau_n) d\tau_1 d\tau_2 \dots d\tau_n. \quad (2.119)$$

The limits of integration can be extended from $-\infty$ to $+\infty$ if the input is assumed to be zero for negative time and the system is causal. An alternate form for $y_n(t)$ is obtained through of the change of variables $\tau_j \leftarrow t - \tau_j$

$$y_n(t) = \int_{-\infty}^{\infty} \int_{-\infty}^{\infty} \dots \int_{-\infty}^{\infty} h_n(\tau_1, \tau_2, \dots, \tau_n) x(t - \tau_1) x(t - \tau_2) \dots x(t - \tau_n) d\tau_1 d\tau_2 \dots d\tau_n. \quad (2.120)$$

Equations (2.116)-(2.120) allow us to express the response $y(t)$ by means of a functional series, known as Volterra functionals by their correspondence with (2.112), or simply Volterra series. The kernels of these functionals, $h_n(\tau_1, \tau_2, \dots, \tau_n)$, can be called the *nonlinear impulse responses of order n* . It can be shown that the series (2.116) converges and the magnitude of each successive term is inferior to that of the previous one. Therefore, this representation is more useful when the response can be approximated by the N first terms in the series, neglecting the higher order terms because they do not contribute significantly to the output, as in any series expansion

$$y(t) \approx \sum_{n=1}^N y_n(t). \quad (2.121)$$

This model consists in the parallel combination of N blocks with each block having, as a common input, the circuit excitation $x(t)$. The total response is obtained by adding the output of the individual blocks, as it is shown in Figure 2.14.

The Fourier transform of the n -th order kernel $h_n(\tau_1, \dots, \tau_n)$ can be called the *non-linear transfer function (NLTF) of order n*

$$H_n(f_1, f_2, \dots, f_n) = \int_{-\infty}^{\infty} \dots \int_{-\infty}^{\infty} h_n(\tau_1, \tau_2, \dots, \tau_n) e^{-j2\pi(f_1\tau_1 + f_2\tau_2 + \dots + f_n\tau_n)} \cdot d\tau_1 \cdot d\tau_2 \dots d\tau_n. \quad (2.122)$$

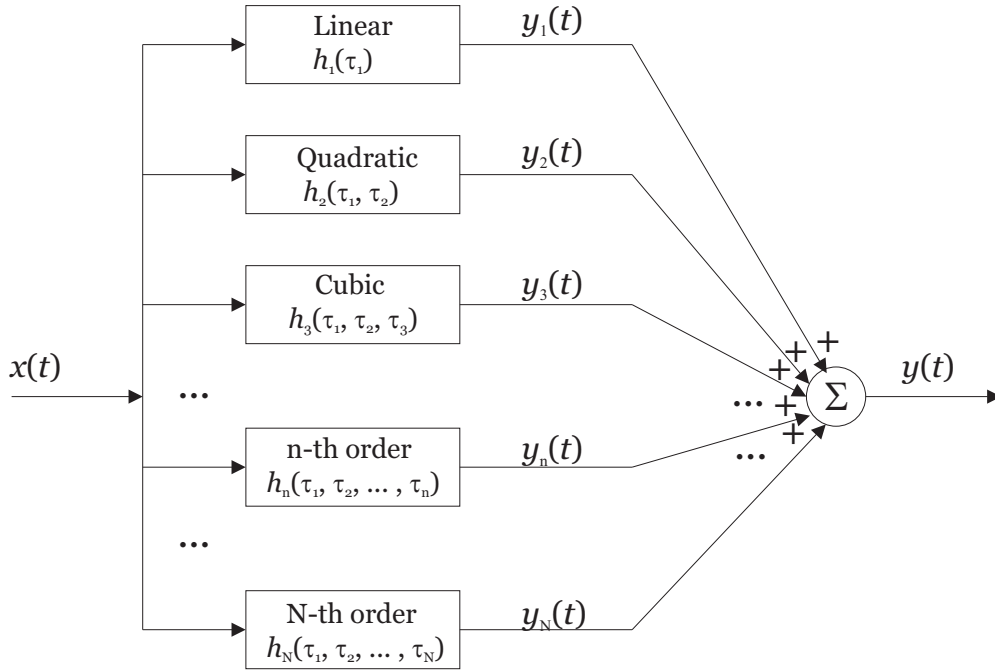


Figure 2.14: Model of nonlinear circuit suggested by the Volterra series representation.

Note that H_1 is the usual transfer function of a linear network. Volterra kernels are independent of the circuit excitation, which is a highly desirable feature of the approach.

Conversely, the nonlinear impulse response of order n follows from the nonlinear transfer function of order n by the inverse Fourier transform, i.e.,

$$h_n(\tau_1, \tau_2, \dots, \tau_n) = \int_{-\infty}^{\infty} \dots \int_{-\infty}^{\infty} H_n(f_1, f_2, \dots, f_n) e^{j2\pi(f_1\tau_1 + f_2\tau_2 + \dots + f_n\tau_n)} \cdot df_1 \cdot df_2 \dots df_n. \quad (2.123)$$

Substituting (2.123) into (2.120) and carrying out the multiple integrals that correspond to the Fourier transform of the inputs, we get

$$y_n(t) = \int_{-\infty}^{\infty} \dots \int_{-\infty}^{\infty} H_n(f_1, f_2, \dots, f_n) \cdot \prod_{i=1}^n X(f_i) e^{j2\pi f_i t} df_i. \quad (2.124)$$

At this point, it is convenient to generalise (2.120) by introducing an auxiliary multidimensional time function

$$y_n(t_1, \dots, t_n) = \int_{-\infty}^{\infty} \dots \int_{-\infty}^{\infty} H_n(f_1, f_2, \dots, f_n) \cdot \prod_{i=1}^n X(f_i) e^{j2\pi f_i t_i} df_i, \quad (2.125)$$

and its n -fold Fourier transform, or multispectral density,

$$Y_n(f_1, \dots, f_n) = \int_{-\infty}^{\infty} \cdots \int_{-\infty}^{\infty} y_n(t_1, \dots, t_n) e^{-j2\pi(f_1 t_1 + \cdots + f_n t_n)} dt_1 \cdots dt_n, \quad (2.126)$$

so that

$$y_n(t_1, \dots, t_n) = \int_{-\infty}^{\infty} \cdots \int_{-\infty}^{\infty} Y_n(f_1, \dots, f_n) e^{j2\pi(f_1 t_1 + \cdots + f_n t_n)} df_1 \cdots df_n. \quad (2.127)$$

It follows then by comparison of (2.125) and (2.127) that

$$Y_n(f_1, \dots, f_n) = H_n(f_1, \dots, f_n) \prod_{i=1}^n X(f_i), \quad (2.128)$$

and, in fact,

$$Y_n(f) = \int_{-\infty}^{\infty} \cdots \int_{-\infty}^{\infty} Y_n(f_1, \dots, f_n) \delta(f - f_1 - \cdots - f_n) df_1 \cdots df_n, \quad (2.129)$$

which states that $Y_n(f)$ is the integral of the multispectral density $Y_n(f_1, \dots, f_n)$, subject to the constraint $f = f_1 + \cdots + f_n$.

It will be assumed that the nonlinear transfer functions are symmetric functions of their arguments, i.e., the order of the arguments can be interchanged in $H_n(f_1, f_2, \dots, f_n)$. This is not true unless the impulse response $h_n(\tau_1, \tau_2, \dots, \tau_n)$ is itself a symmetric function of its arguments. It can be seen from (2.120) that the output $y_n(t)$ would be identical for any permutation of the arguments. All kernels which differ only by the permutation of arguments are equivalent in representing the system, therefore we can arbitrarily replace any kernel by $\frac{1}{n!}$ -th of the sum of all the $n!$ kernels resulting from all the permutations of the arguments, forcing the symmetry. Similarly, the symmetrised nonlinear transfer function is obtained by summing all the functions that can be generated by permutation of its arguments

$$\overline{H_n(f_1, f_2, \dots, f_n)} = \frac{1}{n!} \sum_{l=1}^{n!} H_n[P_l(\mathbf{f})], \quad (2.130)$$

where $P_l(\mathbf{f})$ denotes one of the vectors generated by the $n!$ permutations of the n components in the vector \mathbf{f} .

2.5.2 Multitone input analysis using Volterra series

Despite Volterra kernels enable the determination of the circuit response to any input, it is of particular interest the response of nonlinear circuits to purely sinusoidal inputs.

Consider an input formed by the linear combination of Q sinusoidal signals

$$x(t) = \sum_{q=1}^Q |V_q| \cos(2\pi f_q t + \theta_q) = \frac{1}{2} \sum_{q=-Q}^Q V_q e^{j2\pi f_q t} \quad (2.131)$$

where $V_q = |V_q| e^{j\theta_q}$ is the complex amplitude of the q -th sinusoid, and it is assumed that $V_{-q} = V_q^*$, with $V_0 = 0$. Substituting (2.131) into (2.120) results in

$$\begin{aligned} y_n(t) = & \frac{1}{2^n} \int_{-\infty}^{\infty} \int_{-\infty}^{\infty} \cdots \int_{-\infty}^{\infty} h_n(\tau_1, \tau_2, \dots, \tau_n) \sum_{q_1=-Q}^Q V_{q_1} e^{j2\pi f_{q_1}(t-\tau_1)} \cdot \\ & \cdot \sum_{q_2=-Q}^Q V_{q_2} e^{j2\pi f_{q_2}(t-\tau_2)} \cdots \sum_{q_n=-Q}^Q V_{q_n} e^{j2\pi f_{q_n}(t-\tau_n)} d\tau_1 d\tau_2 \cdots d\tau_n. \end{aligned} \quad (2.132)$$

Interchanging the order of summation and integration and rearranging terms, $y_n(t)$ becomes

$$\begin{aligned} y_n(t) = & \frac{1}{2^n} \sum_{q_1=-Q}^Q \sum_{q_2=-Q}^Q \cdots \sum_{q_n=-Q}^Q V_{q_1} V_{q_2} \cdots V_{q_n} e^{j2\pi(f_{q_1}+f_{q_2}+\cdots+f_{q_n})t} \cdot \\ & \cdot \int_{-\infty}^{\infty} \int_{-\infty}^{\infty} \cdots \int_{-\infty}^{\infty} h_n(\tau_1, \tau_2, \dots, \tau_n) e^{-j2\pi(f_{q_1}\tau_1+f_{q_2}\tau_2+\cdots+f_{q_n}\tau_n)} d\tau_1 d\tau_2 \cdots d\tau_n. \end{aligned} \quad (2.133)$$

If we identify the n -dimensional Fourier transform of the Volterra kernel $h_n(\tau_1, \tau_2, \dots, \tau_n)$ in this expression, we can write

$$y_n(t) = \frac{1}{2^n} \sum_{q_1=-Q}^Q \sum_{q_2=-Q}^Q \cdots \sum_{q_n=-Q}^Q V_{q_1} V_{q_2} \cdots V_{q_n} H_n(\mathbf{f}_n) e^{j2\pi(f_{q_1}+f_{q_2}+\cdots+f_{q_n})t} \quad (2.134)$$

where $\mathbf{f}_n = [f_{q_1}, f_{q_2}, \dots, f_{q_n}]$ and $H_n(\mathbf{f}_n)$ is the nonlinear transfer function of order n , relating the output at a frequency $(f_{q_1} + f_{q_2} + \dots + f_{q_n})$ with n inputs at frequencies $f_{q_1}, f_{q_2}, \dots, f_{q_n}$

$$H_n(\mathbf{f}_n) = \int_{-\infty}^{\infty} \int_{-\infty}^{\infty} \cdots \int_{-\infty}^{\infty} h_n(\tau_1, \tau_2, \dots, \tau_n) e^{-j2\pi(f_{q_1}\tau_1+f_{q_2}\tau_2+\cdots+f_{q_n}\tau_n)} d\tau_1 d\tau_2 \cdots d\tau_n. \quad (2.135)$$

This way, $y(t)$ contains frequency components which can be expressed as $(f_{q_1} + f_{q_2} + \dots + f_{q_n})$, where the indices q_1, q_2, \dots, q_n may vary from $-Q$ to Q . As $f_{-q} = -f_q$, there are also negative frequencies and frequency differences in (2.134). Since each summation includes $2Q$ non-zero terms, the total number of non-zero terms in (2.134) is $(2Q)^n$. This quantity increases rapidly as Q and n increase.

An important property of the nonlinear transfer functions, and thus of the nonlinear impulse responses, is their symmetry with respect to their arguments. In the

particular case of a pure sinusoidal input at a frequency f_q , the component $y_n(t)$ of the output contains all the input harmonics up to order n . Since nonlinear transfer functions are invariant to permutations of their arguments, the general term can be expressed by taking $Q = 1$ in (2.134) and grouping the mixes that generate the same output frequency

$$y_n(t) = \left(\frac{V_q}{2}\right)^n \sum_{\mu=0}^n \frac{n!}{(n-\mu)!\mu!} H_n [(f_q)_{n-\mu}, (-f_q)_\mu] e^{-j2\pi(n-2\mu)f_q t}. \quad (2.136)$$

Notation $(f)_\mu$ refers to a chain of μ arguments $\underbrace{f, f, \dots, f}_\mu$.

Intermodulation components generated in a nonlinear circuit have a notable interest, as they can be inside the desired bandpass of the system, even when the original excitations are out of band. Because of this, if the input of a system includes Q sinusoids, it is advisable to know the total response for a particular frequency mix. A frequency mix is characterised by the number of times the different frequencies appear, being irrelevant the order in which the frequencies appear. All possible frequency mixes can be represented by the frequency mix vector $\mathbf{m} = [m_{-Q}, \dots, m_{-1}, m_1, \dots, m_Q]$, where m_k denote the number of times the frequency f_k appears in the mix. The corresponding intermodulation frequency is

$$f_{\mathbf{m}} = \sum_{\substack{k=-Q \\ k \neq 0}}^Q m_k f_k = (m_1 - m_{-1})f_1 + \dots + (m_Q - m_{-Q})f_Q. \quad (2.137)$$

Each of the mixes involved in $y_n(t)$ contains exactly n frequencies. Therefore, the coefficients m_k must obey the constraint

$$\sum_{\substack{k=-Q \\ k \neq 0}}^Q m_k = m_{-Q} + \dots + m_{-1} + m_1 + \dots + m_Q = n. \quad (2.138)$$

Considering expression (2.134), the number of terms in $y_n(t)$ which contain the mix given by a particular vector \mathbf{m} is equivalent to the number of different ways the n indices q_1, \dots, q_n can be partitioned such that f_{-Q} appears m_{-Q} times, \dots , f_{-1} appears m_{-1} times, f_1 appears m_1 times, \dots , and f_Q appears m_Q times. This number is given by the permutations of the n indices grouped in classes of m_k elements

$$(n; \mathbf{m}) = \frac{(n!)}{(m_{-Q}!) \dots (m_{-1}!)(m_1!) \dots (m_Q!)}. \quad (2.139)$$

Each of the $(n; \mathbf{m})$ realizations yields the identical response

$$\frac{1}{2^n} (V_Q^*)^{m_{-Q}} \dots (V_1^*)^{m_{-1}} (V_1)^{m_1} \dots (V_Q)^{m_Q} H_n(\mathbf{f}_{\mathbf{m}}) e^{j2\pi f_{\mathbf{m}} t}, \quad (2.140)$$

where $\mathbf{f}_m = [(f_{-Q})_{m_{-Q}}, \dots, (f_{-1})_{m_{-1}}, (f_1)_{m_1}, \dots, (f_Q)_{m_Q}]$. Note the difference notation in \mathbf{f}_m and f_m . The former denotes a frequency vector of length n with the frequencies involved in the mix \mathbf{m} , while the latter denotes the intermodulation frequency corresponding to the mix \mathbf{m} (see (2.137)). Denoting the sum of the $(n; \mathbf{m})$ realizations by $y_n(t; \mathbf{m})$, we have

$$y_n(t; \mathbf{m}) = \frac{(n; \mathbf{m})}{2^n} (V_Q^*)^{m_{-Q}} \dots (V_1^*)^{m_{-1}} (V_1)^{m_1} \dots (V_Q)^{m_Q} H_n(\mathbf{f}_m) e^{j2\pi f_m t}. \quad (2.141)$$

The n -th order portion of $y(t)$ can now be written as:

$$y_n(t) = \sum_{\mathbf{m}} y_n(t; \mathbf{m}), \quad (2.142)$$

where the summation over \mathbf{m} is defined to be

$$\sum_{\mathbf{m}} = \sum_{m_{-Q}=0}^n \dots \sum_{m_{-1}=0}^n \sum_{m_1=0}^n \dots \sum_{m_Q=0}^n, \quad (2.143)$$

with

$$m_{-Q} + \dots + m_{-1} + m_1 + \dots + m_Q = n. \quad (2.144)$$

Note that the output $y_n(t)$ of a real system is real for real inputs, whereas $y_n(t; \mathbf{m})$ is a complex signal involving complex frequency terms which appear in conjugate pairs³.

When the excitation consists of Q sinusoidal inputs, it can be shown that the total number of different mixes contained in $y_n(t)$ is given by

$$M = \frac{(2Q + n - 1)!}{n!(2Q - 1)!} \quad (2.145)$$

In practice, the total response at a particular frequency can be approximated accurately enough when the terms corresponding to higher orders are neglected.

2.5.3 Volterra series representation of bandpass nonlinear systems with memory

Digital communication systems are usually operated over nonlinear channels with memory (see Section 4.1.4 for more details about the definition of a system with memory). In addition, for an efficient use of the frequency spectrum, only a restricted bandwidth is available around the carrier frequency. Therefore, it is convenient to introduce a form of Volterra series which is suitable to represent bandpass channels

³Except for $f_m = 0$, which generates by itself a real response.

with memory. In particular, a form of (2.120) will be derived in which the complex envelopes of input and output signals appear.

Consider a real narrowband⁴ bandpass signal $x(t)$. It can be written as:

$$x(t) = \frac{1}{2} [\tilde{x}(t)e^{j2\pi f_c t} + \tilde{x}^*(t)e^{-j2\pi f_c t}]. \quad (2.146)$$

The narrowband nature of the signal implies a low-pass complex envelope $\tilde{x}(t)$ modulating a carrier at the centre frequency f_c

$$x(t) = \text{Re} \{ \tilde{x}(t)e^{j2\pi f_c t} \} = x_I(t) \cos(2\pi f_c t) - x_Q(t) \sin(2\pi f_c t), \quad (2.147)$$

where the complex envelope is defined in terms of its in-phase $x_I(t)$ and quadrature $x_Q(t)$ components as

$$\tilde{x}(t) = x_I(t) + jx_Q(t). \quad (2.148)$$

In the frequency domain, the input signal spectrum is

$$X(f) = \frac{1}{2} [\tilde{X}(f - f_c) + \tilde{X}^*(f + f_c)], \quad (2.149)$$

where

$$\tilde{X}(f) = \int_{-\infty}^{\infty} \tilde{x}(t)e^{-j2\pi ft} dt, \quad (2.150)$$

$$\tilde{x}(t) = \int_{-\infty}^{\infty} \tilde{X}(f)e^{j2\pi ft} df. \quad (2.151)$$

Taking into account that the input signal spectrum can be expressed in terms of its complex envelope as showed in (2.149), the product of n input spectra becomes

$$\prod_{i=1}^n X(f_i) = \frac{1}{2^n} \prod_{i=1}^n [\tilde{X}(f_i - f_c) + \tilde{X}^*(f_i + f_c)]. \quad (2.152)$$

Let us change the variable f to ξ and denote $\tilde{X}_1(\xi) = \tilde{X}(\xi)$, $\tilde{X}_{-1}(\xi) = \tilde{X}^*(\xi)$, $\nu_1 = f_c$, and $\nu_{-1} = -f_c$. Then, when multiplied out, we get the sum of 2^n different terms for all possible combinations of $k_1 = \pm 1$, $k_2 = \pm 1$, ..., $k_n = \pm 1$, so that

$$\prod_{i=1}^n X(f_i) = \sum_{k_1=-1}^1 \cdots \sum_{k_n=-1}^1 \frac{1}{2^n} \prod_{i=1}^n \tilde{X}_{k_i}(\xi_i - \nu_{k_i}). \quad (2.153)$$

Therefore, we can substitute the result (2.153) in (2.124), and the component of order n of the output signal $y(t)$ can be expressed for a bandpass system as

$$y_n(t) = \sum_{k_1=-1}^1 \cdots \sum_{k_n=-1}^1 \frac{1}{2^n} \int_{-\infty}^{\infty} \cdots \int_{-\infty}^{\infty} H_n(\xi_1, \xi_2, \dots, \xi_n) \cdot \prod_{i=1}^n \tilde{X}_{k_i}(\xi_i - \nu_{k_i}) e^{j2\pi \xi_i t} d\xi_i, \quad (2.154)$$

⁴A narrowband signal has a bandwidth that is small compared to the carrier frequency. Virtually all practical communication signals, even those considered "wideband" in some other sense (e.g. wideband CDMA systems) are narrowband in the sense we consider here.

where $h_n(\tau_1, \tau_2, \dots, \tau_n)$ and $H_n(\xi_1, \xi_2, \dots, \xi_n)$ are assumed to be symmetric. Let m_i be the number of times that each distinct $k_i = 1$ or $k_i = -1$ occurs in the k_i set. The following constraints apply

$$\begin{aligned} m_i &= 0, 1, \dots, n, \\ m_1 + m_{-1} &= n, \end{aligned} \quad (2.155)$$

so that, if we denote $m_{-1} = m$ there are $\frac{n!}{m_{-1}!m_1!} = \frac{n!}{m!(n-m)!} = \binom{n}{m}$ identical integrals for each distinct set of k_i . Collecting them we get

$$y_n(t) = \sum_{\mathbf{k}} \frac{1}{2^n} \binom{n}{m} \int_{-\infty}^{\infty} \cdots \int_{-\infty}^{\infty} H_n(\xi_1, \xi_2, \dots, \xi_n) \cdot \prod_{i=1}^n \tilde{X}_{k_i}(\xi_i - \nu_{k_i}) e^{j2\pi\xi_i t} d\xi_i, \quad (2.156)$$

where \mathbf{k} denotes that the sum applies now only over all the distinct sets of k_1, \dots, k_n .

Considering the change of variables $f_i \leftarrow \xi_i - \nu_{k_i}$, we can write

$$\begin{aligned} y_n(t) &= \sum_{\mathbf{k}} \frac{1}{2^n} \binom{n}{m} \exp\left(j2\pi \sum_{i=1}^n \nu_{k_i} t\right) \cdot \\ &\int_{-\infty}^{\infty} \cdots \int_{-\infty}^{\infty} H_n(\nu_{k_1} + f_1, \nu_{k_2} + f_2, \dots, \nu_{k_n} + f_n) \cdot \prod_{i=1}^n \tilde{X}_{k_i}(f_i) e^{j2\pi f_i t} df_i, \end{aligned} \quad (2.157)$$

where the output component of order n is expressed around different frequency zones determined by the harmonics of the fundamental frequency

$$\nu = \sum_{i=1}^n \nu_{k_i} = m_{-1}\nu_{-1} + m_1\nu_1 = -mf_c + (n-m)f_c = (n-2m)f_c = hf_c. \quad (2.158)$$

Let represent the waveform in the h -th harmonic frequency zone as

$$\begin{aligned} y_n(h, t) &= \text{Re} \left\{ \frac{e^{j2\pi hf_c t}}{2^{n-1}} \binom{n}{\frac{n-h}{2}} \cdot \right. \\ &\left. \int_{-\infty}^{\infty} \cdots \int_{-\infty}^{\infty} H_n\left(\underbrace{f_c + f_1, \dots, f_c + f_{\frac{n+h}{2}}}_{m_1=(n-m)=\frac{n+h}{2} \text{ frequencies}}, \underbrace{-f_c + f_{\frac{n+h}{2}+1}, \dots, -f_c + f_n}_{m_{-1}=m=\frac{n-h}{2} \text{ frequencies}} \right) \cdot \prod_{i=1}^n \tilde{X}_{k_i}(f_i) e^{j2\pi f_i t} df_i \right\}, \end{aligned} \quad (2.159)$$

so that

$$y_n(t) = \sum_{\mathbf{k}} y_n(h, t). \quad (2.160)$$

The output component of order n is composed of narrowband zonal signals centered at all carrier harmonic frequencies. If we denote the complex envelope of the waveform at zone hf_c by $\tilde{y}_n(h, t)$ so that

$$y_n(h, t) = \text{Re} \left\{ \tilde{y}_n(h, t) e^{j2\pi hf_c t} \right\}, \quad (2.161)$$

then

$$\tilde{y}_n(h, t) = \frac{1}{2^{n-1}} \binom{n}{\frac{n-h}{2}} \int_{-\infty}^{\infty} \cdots \int_{-\infty}^{\infty} H_n(\underbrace{f_c + f_1, \dots, f_c + f_{\frac{n+h}{2}}}_{m_1 = \frac{n+h}{2} \text{ frequencies}}, \underbrace{-f_c + f_{\frac{n+h}{2}+1}, \dots, -f_c + f_n}_{m_{-1} = \frac{n-h}{2} \text{ frequencies}}) \cdot \prod_{i=1}^n \tilde{X}_{k_i}(f_i) e^{j2\pi f_i t} df_i. \quad (2.162)$$

Let $y(h, t)$ denote the component of $y(t)$ in the frequency zone centred at hf_c and $\tilde{y}(h, t)$ denote its complex envelope. Then

$$y(h, t) = \text{Re} \{ \tilde{y}(h, t) e^{j2\pi h f_c t} \}, \quad (2.163)$$

with

$$\tilde{y}(h, t) = \sum_{n=1}^{\infty} \tilde{y}_n(h, t). \quad (2.164)$$

Only the first N terms of this sum are usually considered for practical reasons. In particular, for the fundamental frequency zone where $h = 1$, the expression for the output complex envelope of $y(t)$ is given by

$$\tilde{y}(1, t) = \sum_{n=1}^{\infty} \frac{1}{2^{n-1}} \binom{n}{\frac{n-1}{2}} \int_{-\infty}^{\infty} \cdots \int_{-\infty}^{\infty} H_n(f_c + f_1, \dots, f_c + f_{\frac{n+1}{2}}, -f_c + f_{\frac{n+1}{2}+1}, \dots, -f_c + f_n) \cdot \prod_{r=1}^{\frac{n+1}{2}} \tilde{X}(f_r) e^{j2\pi f_r t} df_r \cdot \prod_{s=1}^{\frac{n-1}{2}} \tilde{X}^*(f_s) e^{-j2\pi f_s t} df_s. \quad (2.165)$$

Note that only odd-order terms contribute to the output for the fundamental frequency zone.

By inverse Fourier transforming, an expression that relates input and output complex envelopes is obtained

$$\tilde{y}(1, t) = \sum_{n=1}^{\infty} \frac{1}{2^{n-1}} \binom{n}{\frac{n-1}{2}} \int_{-\infty}^{\infty} \cdots \int_{-\infty}^{\infty} h_n(\tau_1, \dots, \tau_n) \cdot \prod_{r=1}^{\frac{n+1}{2}} \tilde{x}(t - \tau_r) e^{-j\omega_c \tau_r} d\tau_r \cdot \prod_{s=1}^{\frac{n-1}{2}} \tilde{x}^*(t - \tau_s) e^{j\omega_c \tau_s} d\tau_s. \quad (2.166)$$

Note that this relation is expressed in terms of the real Volterra kernels $h_n(\tau_1, \dots, \tau_n)$. In order to fully exploit the complex envelope representations, a further step can be advanced by defining low-pass equivalent Volterra kernels, as it is demonstrated

in [14]. Thus, an alternate expression relating input and output complex envelopes is

$$\tilde{y}(1, t) = \sum_{n=1}^{\infty} \frac{1}{2^n} \binom{n}{\frac{n-1}{2}} \int_{-\infty}^{\infty} \cdots \int_{-\infty}^{\infty} \tilde{h}_n(\tau_1, \dots, \tau_n) \cdot \prod_{r=1}^{\frac{n+1}{2}} \tilde{x}(t - \tau_r) d\tau_r \cdot \prod_{s=1}^{\frac{n-1}{2}} \tilde{x}^*(t - \tau_s) d\tau_s, \quad (2.167)$$

where the low-pass equivalent Volterra kernels are defined so that

$$h_n(\tau_1, \dots, \tau_n) = \frac{1}{2} \tilde{h}_n(\tau_1, \dots, \tau_n) \cdot \exp \left[-j\omega_c(\tau_1 + \tau_2 + \dots + \tau_{\frac{n-1}{2}} - \tau_{\frac{n-1}{2}+1} - \dots - \tau_n) \right]. \quad (2.168)$$

2.5.4 Nonlinear transfer functions determination

Keeping in mind the expressions obtained in the previous general developments, we can see that the response of a nonlinear system is determined by the NLTFs, in the sense that knowing $H_n(\mathbf{f}_n)$ suffices to obtain the response to any input. In this section, two methods employed to determine the NLTFs will be described. One of the main disadvantages of the Volterra series approach is that, in general, it is not easy to obtain an analytical closed-form expression of the nonlinear transfer functions, mainly for high orders. However, the recursive nature of these methods eases their programming so that we can calculate efficiently the nonlinear transfer functions with the help of a computer.

2.5.4.1 Probing or Harmonic Input method

In this section, a brief explanation of the Probing or Harmonic Input method proposed by Bedrosian in [162] will be presented. The approach followed in this method does not considerably differ from the process to determine the transfer function $H(f)$ of a linear system in the frequency domain: the simplest excitation is considered to be applied to the circuit, then its response is obtained, substituting both excitation and response in the input-to-output relation and, finally $H_n(f_n)$ is algebraically determined. This way, the transfer function of a linear circuit can be determined by assuming an input voltage $1 \cdot e^{j2\pi ft}$ is applied and rearranging the output so that it is expressed as $H(f) e^{j2\pi ft}$. The quotient between the input and the output is $H(f)$.

In the case of a nonlinear circuit, it is necessary to consider that the input to the system $x(t)$ is a sum of n exponentials

$$x(t) = e^{j2\pi f_1 t} + e^{j2\pi f_2 t} + \dots + e^{j2\pi f_n t}, \quad (2.169)$$

where the frequencies f_i are incommensurate. The Fourier transform of the input (2.169) is a sum of delta functions

$$X(f) = \delta(f - f_1) + \delta(f - f_2) + \cdots + \delta(f - f_n). \quad (2.170)$$

Note that the negative frequencies have not been included, since it is not necessary that excitation $x(t)$ be real because this is an analytical method. The sum of incommensurate exponentials can serve as an analytical probing signal, but not as a basis for real measurements. With this input, the Volterra expansion of the output becomes

$$y(t) = \sum_{n=1}^{\infty} \int_{-\infty}^{\infty} \cdots \int_{-\infty}^{\infty} H_n(f_1, f_2, \dots, f_n) \cdot \prod_{i=1}^n [\delta(f_i - f_1) + \cdots + \delta(f_i - f_n)] e^{j2\pi f_i t} df_i. \quad (2.171)$$

The product of the sum of delta functions generates a sum for all the different terms of the form

$$\delta(f_1 - f_{k_1}) \delta(f_2 - f_{k_2}) \cdots \delta(f_n - f_{k_n}) \quad (2.172)$$

with each index k_i ranging from 1 to n . If each f_{k_i} occurs in a product such as (2.172) m_i times, then there are $(n; \mathbf{m})$ identical terms but for the permutation of the factors. When integrals in (2.171) are carried out and identical terms have been collected, we get

$$y(t) = \sum_{n=1}^{\infty} \sum_{\mathbf{m}} (n; \mathbf{m}) H_n(f_1, f_2, \dots, f_n) e^{j2\pi(f_{k_1} + \cdots + f_{k_n})t}, \quad (2.173)$$

where \mathbf{m} under the sum indicates that it includes all the distinct sets $\{m_i\}$ such that $m_i < m_{i+1}$ and $\sum_{i=1}^n m_i = n$. The inequality $m_i < m_{i+1}$ orders the frequencies in $\{f_{m_i}\}$ by their indices so as not to repeat the sets of frequencies which differ only by permutation. It can be noticed that there is a term of order n in the expansion of $y(t)$ given by

$$n! \overline{H_n(f_1, f_2, \dots, f_n)} e^{j2\pi(f_1 + \cdots + f_n)t}. \quad (2.174)$$

Then, the symmetrised n th-order NLTF denoted as $\overline{H_n(f_1, f_2, \dots, f_n)}$ can be obtained analytically as the coefficient of $n! e^{j2\pi(f_1 + \cdots + f_n)t}$ in the output of the system when the input is the sum of n exponentials given by (2.169).

Thus, the Probing Method supplies a recursive method to determine all the NLTFs from the equation defining the behaviour of the system, when the input is given by (2.169). The system given by such an equation is first *probed* by a single exponential excitation. This permits the determination of $H_1(f)$. Then a sum of two exponentials is applied. This yields $H_2(f_1, f_2)$ in terms of $H_1(f)$. This procedure continues with one additional exponential being added to the input at each step until, at step n , the input consists of the sum of n exponentials at (f_1, \dots, f_n) . It then follows that the NLTF of order n is constructed from all the lower order NLTFs.

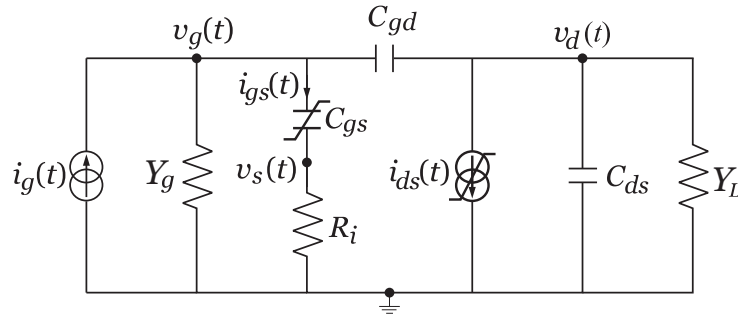


Figure 2.15: Simplified equivalent circuit of a FET amplifier.

It can be demonstrated that the expressions for the n -th order NLTF imply the multiplication of lower order NLTFs, or ultimately of the linear transfer function $H_1(f)$ evaluated at different combinations of frequencies. That way, if the linear transfer function $H_1(f)$ is that of a tuned circuit normalised to have a unit gain at a frequency, then

$$|H_n(f_1, \dots, f_n)| < \prod_{i=1}^n |H_1(f_i)| \quad (2.175)$$

so that the absolute values of the Volterra kernels become smaller and smaller with their order, as one would expect for convergence.

Next, the Harmonic Input method will be applied to the example of the circuit shown in Figure 2.15, which is the simplified equivalent circuit of a FET amplifier. In this three-node circuit, just the drain current source and the gate-to-source capacitance will be considered nonlinear. All the voltages and currents in the circuit will be assumed to be incremental variables and a nodal analysis of the circuit will be made, as it is explained in Section 2.3. Applying Kirchhoff's current law at each of the nodes in the circuit, the following equations are derived:

$$\begin{aligned} Y_g v_g(t) + i_{gs}(t) + \frac{d}{dt} C_{gd} [v_g(t) - v_d(t)] &= i_g(t) \\ -i_{gs}(t) + \frac{v_s(t)}{R_i} &= 0 \\ -\frac{d}{dt} C_{gd} [v_g(t) - v_d(t)] + i_{ds}(t) + \frac{d}{dt} C_{gs} v_d(t) + Y_L v_d(t) &= 0 \end{aligned} \quad (2.176)$$

The next step is to expand each of the currents through the nonlinear circuit elements in a power series, according to (2.40) and (2.41). It gives

$$\begin{aligned} i_{gs}(t) &= \sum_{k=0}^{\infty} c_k [v_g(t) - v_s(t)]^k \frac{d}{dt} [v_g(t) - v_s(t)], \\ i_{ds}(t) &= \sum_{k=0}^{\infty} \sum_{\substack{l=0 \\ k+l \geq 1}}^{\infty} g_{kl} [v_g(t) - v_s(t)]^k v_d^l(t). \end{aligned} \quad (2.177)$$

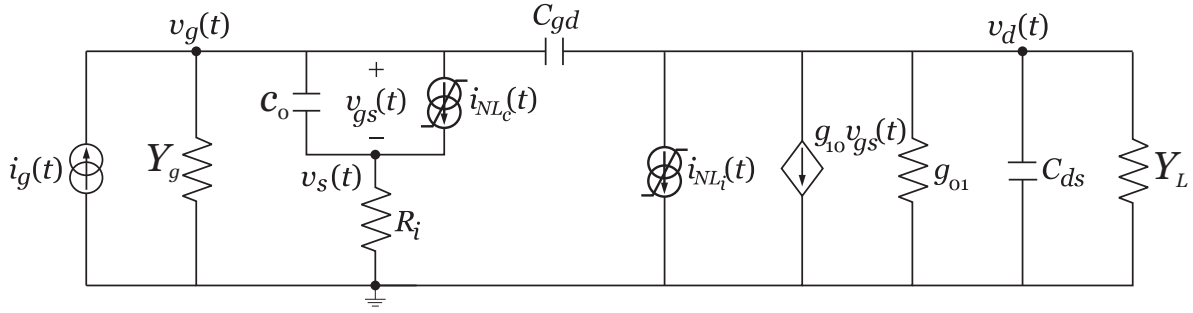


Figure 2.16: Alternative representation of the circuit shown in Figure 2.15, where the nonlinear circuit elements have been replaced by linear elements in parallel with nonlinear current sources.

Separating each power series in (2.177) into a linear term plus a higher order term suggests that each nonlinear circuit element may be replaced by a nonlinear voltage-controlled current source positioned in parallel with a linear circuit element. With this interpretation, an *augmented linear circuit* is built where the nonlinear elements play the role of current sources driving the linear part of the circuit, as it is shown in Figure 2.16. After substituting the power series expansions into (2.176), the equations are rearranged such that only terms that depend linearly on the node voltages appear on the left-hand side.

$$\begin{aligned}
 & \left[Y_g + \frac{d}{dt} (C_{gd} + c_0) \right] v_g(t) - \frac{d}{dt} C_{gd} v_d(t) - \frac{d}{dt} c_0 v_s(t) = \\
 & \quad = i_g(t) - \sum_{k=1}^{\infty} c_k [v_g(t) - v_s(t)]^k \frac{d}{dt} [v_g(t) - v_s(t)] \\
 -\frac{d}{dt} c_0 v_g(t) + \left[\frac{1}{R_i} + \frac{d}{dt} c_0 \right] v_s(t) &= \sum_{k=1}^{\infty} c_k [v_g(t) - v_s(t)]^k \frac{d}{dt} [v_g(t) - v_s(t)] \quad (2.178) \\
 \left[g_{10} - \frac{d}{dt} C_{gd} \right] v_g(t) + \left[g_{o1} + Y_L + \frac{d}{dt} (C_{gd} + C_{gs}) \right] v_d(t) - g_{10} v_s(t) &= \\
 & \quad = - \sum_{k=1}^{\infty} \sum_{l=1}^{\infty} g_{kl} [v_g(t) - v_s(t)]^k v_d^l(t)
 \end{aligned}$$

Using the gate-to-source voltage v_{gs} as a variable, the last equations result in

$$\begin{aligned}
 \left[Y_g + \frac{d}{dt} C_{gd} \right] v_g(t) - \frac{d}{dt} C_{gd} v_d(t) + \frac{d}{dt} c_0 v_{gs}(t) &= i_g(t) - \sum_{k=1}^{\infty} c_k v_{gs}^k(t) \frac{d}{dt} v_{gs}(t) \\
 \frac{1}{R_i} v_g(t) - \left[\frac{1}{R_i} + \frac{d}{dt} c_0 \right] v_{gs}(t) &= \sum_{k=1}^{\infty} c_k v_{gs}^k(t) \frac{d}{dt} v_{gs}(t) \quad (2.179) \\
 -\frac{d}{dt} C_{gd} v_g(t) + \left[g_{o1} + Y_L + \frac{d}{dt} (C_{gd} + C_{gs}) \right] v_d(t) + g_{10} v_{gs}(t) &= - \sum_{k=1}^{\infty} \sum_{l=1}^{\infty} g_{kl} v_{gs}^k(t) v_d^l(t)
 \end{aligned}$$

It can be written in matrix notation

$$\mathbf{Y}(\hat{p}) \mathbf{v}(t) = \mathbf{i}_s(t) + \mathbf{i}_{\text{NL}}(t), \quad (2.180)$$

where \hat{p} denotes the differential operator d/dt and

$$\mathbf{Y}(\hat{p}) = \begin{pmatrix} Y_g + \hat{p} C_{gd} & -\hat{p} C_{gd} & \hat{p} c_0 \\ \frac{1}{R_i} & 0 & -\left(\frac{1}{R_i} + \hat{p} c_0\right) \\ -\hat{p} C_{gd} & g_{01} + Y_L + \hat{p} (C_{ds} + C_{gd}) & g_{10} \end{pmatrix},$$

$$\mathbf{v}(t) = \begin{bmatrix} v_g(t) \\ v_d(t) \\ v_{gs}(t) \end{bmatrix}, \quad \mathbf{i}_s(t) = \begin{bmatrix} i_s(t) \\ 0 \\ 0 \end{bmatrix}, \quad (2.181)$$

$$\mathbf{i}_{\text{NL}}(t) = \begin{bmatrix} -\sum_{k=1}^{\infty} c_k v_{gs}^k(t) \hat{p} v_{gs}(t) \\ +\sum_{k=1}^{\infty} c_k v_{gs}^k(t) \hat{p} v_{gs}(t) \\ -\sum_{\substack{k=0 \\ k+l \geq 1}} \sum_{l=0}^{\infty} g_{kl} v_{gs}^k(t) v_d^l(t) \end{bmatrix},$$

with $\mathbf{Y}(\hat{p})$ being the matrix admittance of the augmented linear circuit; $\mathbf{v}(t)$ the vector with the unknown voltages; $\mathbf{i}_s(t)$ the vector with the independent current sources (excitations); and $\mathbf{i}_{\text{NL}}(t)$ a vector including all the nonlinearities in the circuit, which will be called from here on *nonlinear currents vector*.

Applying the Harmonic Input method, the independent current sources vector takes the following form to determine the linear (or first-order) transfer functions

$$\mathbf{i}_s(t) = \begin{bmatrix} e^{j2\pi f_1 t} \\ 0 \\ 0 \end{bmatrix}. \quad (2.182)$$

The circuit voltages can be expressed as a Volterra series and thus they can be written as:

$$\begin{aligned} v_g(t) &= \sum_{n=1}^{\infty} v_{gn}(t), \\ v_d(t) &= \sum_{n=1}^{\infty} v_{dn}(t), \\ v_{gs}(t) &= \sum_{n=1}^{\infty} v_{gsn}(t), \end{aligned} \quad (2.183)$$

where the components of order n are given by

$$\begin{aligned} v_{gn}(t) &= H_{gn}(f_1, \dots, f_1) e^{jn2\pi f_1 t} \\ v_{dn}(t) &= H_{dn}(f_1, \dots, f_1) e^{jn2\pi f_1 t} \\ v_{gsn}(t) &= H_{gsn}(\underbrace{f_1, \dots, f_1}_n) e^{jn2\pi f_1 t}. \end{aligned} \quad (2.184)$$

In order to get the linear transfer functions for each voltage in the network, expressions (2.182)-(2.184) with $n = 1$ are substituted in (2.180). We need to take into account that the differential operator \hat{p} is substituted by $j\omega$ in the frequency domain and equate the coefficients that multiply $e^{j2\pi f_1 t}$. The linear transfer functions satisfy the following matrix equation:

$$\begin{bmatrix} H_g(f_1) \\ H_d(f_1) \\ H_{gs}(f_1) \end{bmatrix} = \mathbf{Y}^{-1}(j2\pi f_1) \begin{bmatrix} 1 \\ 0 \\ 0 \end{bmatrix}. \quad (2.185)$$

Since only components at frequency f_1 can appear in the first-order terms, the nonlinear currents vector $\mathbf{i}_{\text{NL}}(t)$ does not contribute to the linear response and can thus be neglected.

In order to determine the second-order nonlinear transfer functions, the following independent current sources vector is considered:

$$\mathbf{i}_s(t) = \begin{bmatrix} e^{j2\pi f_1 t} + e^{j2\pi f_2 t} \\ 0 \\ 0 \end{bmatrix}. \quad (2.186)$$

Being a two-tone input, the n -th order components of the node voltages take the following expressions:

$$\begin{aligned} v_{gn}(t) &= \sum_{q_1=1}^2 \cdots \sum_{q_n=1}^2 H_{gn}(f_{q_1}, \dots, f_{q_n}) e^{j2\pi(f_{q_1} + \dots + f_{q_n})t} \\ v_{dn}(t) &= \sum_{q_1=1}^2 \cdots \sum_{q_n=1}^2 H_{dn}(f_{q_1}, \dots, f_{q_n}) e^{j2\pi(f_{q_1} + \dots + f_{q_n})t} \\ v_{gsn}(t) &= \sum_{q_1=1}^2 \cdots \sum_{q_n=1}^2 H_{gsn}(f_{q_1}, \dots, f_{q_n}) e^{j2\pi(f_{q_1} + \dots + f_{q_n})t}. \end{aligned} \quad (2.187)$$

Expressions (2.183), (2.186) and (2.187) are substituted into (2.180) and all the terms depending on $e^{j2\pi(f_1+f_2)t}$ are identified. Since frequencies f_1 and f_2 are assumed to be positive and incommensurate, the terms with frequency dependence $f_1 + f_2$ can only appear in the second-order components. If we develop any of the terms in (2.187) for $n = 2$, we get

$$v_{k2}(t) = H_{k2}(f_1, f_1) e^{j2 \cdot 2\pi f_1 t} + 2! H_{k2}(f_1, f_2) e^{j2\pi(f_1+f_2)t} + H_{k2}(f_2, f_2) e^{j2 \cdot 2\pi f_2 t}, \quad (2.188)$$

where H_{k2} is the second-order nonlinear transfer function for the node k . Note that there are so many identical terms at the frequency $f_1 + f_2$ as possible permutations of the indices q_1, q_2 such that f_1 and f_2 appear only once. Analysing the rest of the terms in the matrix equation, $\mathbf{i}_s(t)$ does not include terms at frequency $f_1 + f_2$, whereas the vector $\mathbf{i}_{NL}(t)$ may contribute to this frequency due to its nonlinear nature. Each of the elements in this vector can be expanded in a Volterra series, which is written as:

$$i_{NLk}(t) = \sum_{n=1}^{\infty} i_{NLkn}(t), \quad (2.189)$$

where

$$i_{NLkn}(t) = \sum_{q_1=1}^2 \cdots \sum_{q_n=1}^2 F_{kn}(f_{q_1}, \dots, f_{q_n}) e^{j2\pi(f_{q_1} + \dots + f_{q_n})t}. \quad (2.190)$$

Analogously to what happens in (2.188), the number of terms in $i_{NLkn}(t)$ depending on $e^{j2\pi(f_1+f_2)t}$ is equivalent to the possible permutations of the indices q_1, \dots, q_n , such that f_1 and f_2 appear only once. That is to say

$$i_{NLk}(t; f_1 + f_2) = 2! F_{k2}(f_1, f_2) e^{j2\pi(f_1+f_2)t}. \quad (2.191)$$

When the factors $2!$ are canceled in both sides of the matrix equation, the second-order NLTFs can be obtained

$$\begin{bmatrix} H_g(f_1, f_2) \\ H_d(f_1, f_2) \\ H_{gs}(f_1, f_2) \end{bmatrix} = \mathbf{Y}^{-1}[j2\pi(f_1 + f_2)] \begin{bmatrix} F_{g2}(f_1, f_2) \\ F_{d2}(f_1, f_2) \\ F_{gs2}(f_1, f_2) \end{bmatrix}. \quad (2.192)$$

The functions $F_{k2}(f_1, f_2)$ depend in turn on the NLTFs of lower orders. Regarding the first element of the vector $\mathbf{i}_{NL}(t)$, when (2.183) and (2.184) are substituted into the expression for i_{NLg} , it results

$$\begin{aligned} i_{NLg}(t) = & - \sum_{k=1}^{\infty} c_k v_{gs}^k(t) \hat{p} v_{gs}(t) = - \sum_{k=1}^{\infty} c_k \left\{ \sum_{n=1}^{\infty} \sum_{q_1=1}^2 \cdots \sum_{q_n=1}^2 H_{gsn}(f_{q_1}, \dots, f_{q_n}) \times \right. \\ & \left. \times e^{j2\pi(f_{q_1} + \dots + f_{q_n})t} \right\}^k \hat{p} \left\{ \sum_{m=1}^{\infty} \sum_{r_1=1}^2 \cdots \sum_{r_m=1}^2 H_{gsm}(f_{r_1}, \dots, f_{r_m}) e^{j2\pi(f_{r_1} + \dots + f_{r_m})t} \right\}. \end{aligned} \quad (2.193)$$

As mentioned before, terms with time dependence of the type $e^{j2\pi(f_1+f_2)t}$ can only be found among the second-order component. This is equivalent to particularise $k = 1$, $n = 1$ and $m = 1$ in the previous expression

$$\begin{aligned} i_{NLg2}(t) = & -c_1 \sum_{q=1}^2 \sum_{r=1}^2 H_{gs1}(f_q) H_{gs1}(f_r) j2\pi(f_r + f_q) e^{j2\pi(f_q+f_r)t} = \\ & -\frac{c_1}{2} \left\{ j4\pi f_1 H_{gs1}^2(f_1) e^{j4\pi f_1 t} + 2! j2\pi(f_1 + f_2) H_{gs1}(f_1) H_{gs1}(f_2) e^{j2\pi(f_1+f_2)t} + \right. \\ & \left. j4\pi f_2 H_{gs1}^2(f_2) e^{j4\pi f_2 t} \right\}. \end{aligned} \quad (2.194)$$

And comparing with (2.191) yields

$$F_{g2}(f_1, f_2) = -j2\pi(f_1 + f_2) \frac{c_1}{2} H_{gs1}(f_1) H_{gs1}(f_2). \quad (2.195)$$

Observe that $F_{g2}(f_1, f_2)$ can be interpreted as the Fourier coefficient of i_{NLg2} , evaluated at $f_1 + f_2$ and multiplied by a factor $\frac{1}{2!}$.

Taking into account the similarity between i_{NLg} and i_{NLd} , we have

$$F_{d2}(f_1, f_2) = j2\pi(f_1 + f_2) \frac{c_1}{2} H_{gs1}(f_1) H_{gs1}(f_2). \quad (2.196)$$

Regarding the nonlinearity dependent on i_{NLgs} , the second-order components are included in the following expression:

$$i_{NLgs2}(t) = -g_{20}v_{gs}^2(t) - g_{11}v_{gs}(t)v_d(t) - g_{02}v_d^2(t). \quad (2.197)$$

These three addends present a similar structure, so only the second will be studied in detail

$$\begin{aligned} v_{gs}(t)v_d(t) &= \sum_{n=1}^{\infty} \sum_{m=1}^{\infty} \sum_{q_1=1}^2 \cdots \sum_{q_n=1}^2 \sum_{r_1=1}^2 \cdots \sum_{r_m=1}^2 H_{gsn}(f_{q_1}, \dots, f_{q_n}) \cdot \\ &\quad \cdot H_{dm}(f_{r_1}, \dots, f_{r_m}) e^{j2\pi(f_{q_1} + \dots + f_{q_n} + f_{r_1} + \dots + f_{r_m})t}. \end{aligned} \quad (2.198)$$

Only the terms resulting when $n = 1$ and $m = 1$ are assumed to produce components at frequency $e^{j2\pi(f_1+f_2)t}$, that is to say

$$\begin{aligned} v_{gs1}(t)v_{d1}(t) &= \sum_{q=1}^2 \sum_{r=1}^2 H_{gs1}(f_q) H_{d1}(f_r) e^{j2\pi(f_1+f_2)t} = H_{gs1}(f_1) H_{d1}(f_1) e^{j4\pi f_1 t} + \\ &\quad + [H_{gs1}(f_1) H_{d1}(f_2) + H_{gs1}(f_2) H_{d1}(f_1)] e^{j2\pi(f_1+f_2)t} + H_{gs1}(f_2) H_{d1}(f_2) e^{j4\pi f_2 t}. \end{aligned} \quad (2.199)$$

Finally,

$$F_{gs2}(f_1, f_2) = -g_{20}H_{gs1}(f_1)H_{gs1}(f_2) - g_{11}\overline{H_{gs1}(f_1)H_{d1}(f_2)} - g_{02}H_{d1}(f_1)H_{d1}(f_2), \quad (2.200)$$

where

$$\overline{H_{gs1}(f_1)H_{d1}(f_2)} = \frac{1}{2} [H_{gs1}(f_1)H_{d1}(f_2) + H_{gs1}(f_2)H_{d1}(f_1)]. \quad (2.201)$$

Generalising, the following independent current sources vector will be considered in order to determine the NLTFs of order n :

$$\mathbf{i}_s(t) = \begin{bmatrix} e^{j2\pi f_1 t} + e^{j2\pi f_2 t} + \dots + e^{j2\pi f_n t} \\ 0 \\ 0 \end{bmatrix}, \quad (2.202)$$

and the process consists in identifying such terms with time dependence $e^{j2\pi(f_1 + \dots + f_n)t}$ in the matrix equation (2.180). These terms can only come from components of order

n and appear $n!$ times, which is the number of permutations in the indices q_1, \dots, q_n taken one by one. The NLTFs satisfy the following system of algebraic equations:

$$\begin{bmatrix} H_g(f_1, \dots, f_n) \\ H_d(f_1, \dots, f_n) \\ H_{gs}(f_1, \dots, f_n) \end{bmatrix} = \mathbf{Y}^{-1}[j2\pi(f_1 + \dots + f_n)] \begin{bmatrix} F_{gn}(f_1, \dots, f_n) \\ F_{dn}(f_1, \dots, f_n) \\ F_{gsn}(f_1, \dots, f_n) \end{bmatrix}, \quad (2.203)$$

where $F_{kn}(f_1, \dots, f_n)$ is the Fourier coefficient of the n -th order component of the nonlinear current $i_{NLk}(t)$ evaluated in $f_1 + \dots + f_n$ and multiplied by the factor $\frac{1}{n!}$.

This procedure can be continued indefinitely to find at each step higher and higher order NLTFs in terms of lower order NLTFs, or ultimately in terms of the linear transfer functions. However, since the $n!$ terms in each row of the nonlinear currents vector $\mathbf{i}_{NL}(t)$ are different, in general, their evaluation may be a very cumbersome process for orders higher than three.

2.5.4.2 Nonlinear Currents method

In this section, we will present an explanation of the Nonlinear Currents (NC) method proposed by Bussgang in [13] to determine the response of a nonlinear system with a power series type of nonlinearity. In order to illustrate this method with a simple notation but without losing generality, in [13] a single-node nonlinear circuit characterised by the following nonlinear equation is considered:

$$i(t) = L'[v(t)] + \sum_{n=1}^{\infty} K_n v^n(t) = L[v(t)] + \sum_{n=2}^{\infty} K_n v^n(t), \quad (2.204)$$

where $L'[\cdot]$ denotes a general linear integro-differential operator for the linear components of the circuit, and the nonlinear component is expressed as a power series of the node voltage. The linear coefficient K_1 of the nonlinear component is included in the *augmented linear circuit*, which is represented here by the linear integro-differential operator $L[\cdot]$.

The input-output relation for this nonlinear system can be represented by the following equation:

$$x(t) = L[y(t)] + \sum_{n=2}^{\infty} K_n y^n(t), \quad (2.205)$$

where an excitation of the form

$$x(t) = \alpha i(t) \quad (2.206)$$

will be considered. The dummy variable α is introduced so as to keep track of the order of different terms, since any term in α^n is of order n in $i(t)$.

Let $v(t)$ be the output of the nonlinear system when the input $i(t)$ is applied to the circuit. By definition of the Volterra expansion, we can write

$$v_n(t) = \int_{-\infty}^{\infty} \cdots \int_{-\infty}^{\infty} H_n(f_1, \dots, f_n) \prod_{i=1}^n I(f_i) \cdot e^{j2\pi f_i t} df_i, \quad (2.207)$$

so that

$$y(t) = \sum_{n=1}^{\infty} y_n(t) = \sum_{n=1}^{\infty} \alpha^n v_n(t). \quad (2.208)$$

Note that the excitation $i(t)$ and the response $v(t)$ are related by either of two different equations: (2.204), or the equation obtained by substituting (2.206) and (2.208) in (2.205)

$$\alpha \cdot i(t) = \sum_{n=1}^{\infty} \alpha^n L[v_n(t)] + \sum_{n=2}^{\infty} K_n \left[\sum_{s=1}^{\infty} \alpha^s v_s(t) \right]^n. \quad (2.209)$$

Thus, if we can solve (2.209) for the individual nonlinear response components of $v(t)$, denoted by $v_n(t)$, then the solution of (2.204) is obtained from the expansion

$$v(t) = \sum_{n=1}^{\infty} v_n(t). \quad (2.210)$$

The introduction of the dummy variable α is a helpful artifice when solving for the successive $v_n(t)$. This can be observed by solving (2.209) for $v_1(t)$, $v_2(t)$, and $v_3(t)$.

To solve for $v_1(t)$, both sides of (2.209) will be differentiated with respect to α and then $\alpha = 0$ will be substituted in the result. This procedure yields the following differential equation for $v_1(t)$:

$$i(t) = L[v_1(t)], \quad (2.211)$$

which simply entails the linear part of (2.209). Thus, the first-order response component $v_1(t)$ is solved as if the nonlinear element represented by the power series in $v^n(t)$ were removed from the circuit and only the current source $i(t)$ were applied to the linear part of the circuit.

To solve for the second-order nonlinear response $v_2(t)$, we repeat the process of differentiating both sides of (2.209) with respect to α , and then setting $\alpha = 0$. When this is done, we get the following differential equation satisfied by $v_2(t)$:

$$0 = L[v_2(t)] + K_2 v_1^2(t). \quad (2.212)$$

By comparing this equation to (2.211), $v_2(t)$ can be considered as the response of the linear part of the circuit driven by the second-order nonlinear current

$$i_2(t) = -K_2 v_1^2(t). \quad (2.213)$$

If we repeat the process of differentiating with respect to α three times, the following differential equation satisfied by $v_3(t)$ is obtained:

$$0 = L[v_3(t)] + 2K_2v_1(t)v_2(t) + K_3v_1^3(t). \quad (2.214)$$

Here again the nonlinear component $v_3(t)$ is the response of the linear circuit when driven by the third-order nonlinear current source

$$i_3(t) = -[2K_2v_1(t)v_2(t) + K_3v_1^3(t)]. \quad (2.215)$$

This process can be continued successively until the desired order of the nonlinear response is reached. In general, the n -th order current through the nonlinear element is defined as

$$i_n(t) = - \sum_{m=2}^{\infty} K_m \left[\frac{d}{d\alpha^n} \left[\sum_{s=1}^{\infty} \alpha^s v_s(t) \right]^m \right] \Big|_{\alpha=0}. \quad (2.216)$$

Note that $i_n(t)$ depends only on the already computed $n-1$ responses $v_1(t), \dots, v_{n-1}(t)$. Specifically, carrying out (2.216)

$$i_n(t) = - \sum_{m=2}^n K_m \sum_{\mathbf{p}} \frac{m!}{p_1! \cdots p_m!} v_1^{p_1}(t) \cdots v_m^{p_m}(t), \quad (2.217)$$

with \mathbf{p} under the summation sign indicating that the summation is on all such sets of p_1, \dots, p_m that satisfy

$$p_1 + 2p_2 + \cdots + mp_m = n, \quad m = 2, 3, \dots, n-1, \quad (2.218)$$

and where the exponent p_i can range from 0 to n . Since $v_1(t)$ depends on $i(t)$, $v_2(t)$ depends on $v_1(t)$, and $v_3(t)$ depends on $v_1(t)$ and $v_2(t)$, etc., all the nonlinear currents ultimately depend on $i(t)$. Specifically, $v_k^{p_k}$ is of the order kp_k in $i(t)$, and the total order of the dependence of $i_n(t)$ in $i(t)$ is n , as given by (2.218).

The NC method of determining the response of a nonlinear circuit with a power series type nonlinearity can be summarised as follows:

- Step 1:** Solve for the first-order response $v_1(t)$, which is simply the response of the linear part of the circuit to the excitation $i(t)$ as if the nonlinearity were removed from the circuit.
- Step 2:** When the first-order voltage across the nonlinearity $v_1(t)$ is found, compute the nonlinear current $i_2(t)$. Continuing in a recursive way, as each $v_{n-1}(t)$ is found, the nonlinear current $i_n(t)$ can be computed.

Step 3: Solve the linear differential equation

$$L[v_n(t)] = i_n(t), \quad n = 2, 3, \dots \quad (2.219)$$

for $v_n(t)$, in which $L[\cdot]$ denotes symbolically the augmented linear circuit operations and $i_n(t)$ is the nonlinear current source computed at step 2.

This is clearly a recursive method, as it requires the determination of all the lower order components before the higher order component is found. Finally, the total response is the sum of all the components

$$v(t) = \sum_{n=1}^{\infty} v_n(t), \quad (2.220)$$

but the sum can frequently be truncated for weakly nonlinear systems.

In short, instead of the nonlinear differential equation for the total response, in the NC method an augmented linear differential equation is solved repeatedly for the components of the nonlinear response, using each time an appropriate excitation. That appropriate excitation for the n -th iteration of the process is a function of the solutions for the lower order components of the nonlinear response obtained at the previous iterations. The sum of the components is the series expansion of the total response.

The process for the determination of the nonlinear currents has been presented for a general power series type of nonlinearity and will be now applied for the typical nonlinear elements in FET amplifiers.

For the nonlinear conductance, it is demonstrated in [13] that the expression for the nonlinear current component of order n can be obtained by the following recursion:

$$i_n(t) = - \sum_{m=2}^n g_m v_{n,m}, \quad (2.221)$$

where

$$v_{n,m} = \sum_{i=1}^{n-m+1} v_i(t) v_{n-i,m-1}, \quad (2.222)$$

and

$$v_{n,1} = v_n(t). \quad (2.223)$$

A similar procedure can be followed for the current generated by a dependent non-linearity, where the first two sums present similar expressions to those of a nonlinear conductance and their contribution can be obtained by means of (2.221) and (2.222).

The following recursive expression is obtained for the third of the sums accounting for the cross-terms g_{kl} :

$$i_n(t) = - \sum_{r=1}^{n-1} \sum_{s=1}^{n-r} g_{sr} \Phi_{s,r,n}, \quad (2.224)$$

where

$$\Phi_{s,r,n} = \sum_{j=1}^{n-1} v_{j,s} u_{n-j,r}, \quad n \geq r + s \quad (2.225)$$

and by analogy with (2.222)

$$v_{j,s} = \sum_{i=1}^{j-s+1} v_i(t) v_{j-i,s-1}, \quad j \geq s \quad (2.226)$$

in which

$$v_{j,1} = v_j(t). \quad (2.227)$$

The nonlinear current generated by a nonlinear capacitor is of the form

$$i(t) = \frac{d}{dt} \sum_{k=1}^{\infty} q_k v^k(t) = \sum_{k=1}^{\infty} q_k k v^{k-1}(t) \frac{dv(t)}{dt} = \sum_{k=0}^{\infty} c_k k v^k(t) \frac{dv(t)}{dt}, \quad (2.228)$$

which is a special case of the dependent nonlinearity considered in (2.41) with $u = \frac{dv(t)}{dt}$.

For example, we can follow the systematic procedure suggested for the aforementioned recursive expressions and obtain the following expressions for the nonlinear current components for a dependent nonlinearity:

$$\begin{aligned} i_2(t) &= - \{g_{20}v_1(t) + g_{11}v_1(t)u_1(t) + g_{20}u_1(t)\}, \\ i_3(t) &= - \{g_{30}v_1^3(t) + g_{03}v_1^3(t) + 2g_{20}v_1(t)v_2(t) + 2g_{02}u_1(t)u_2(t) + \\ &\quad g_{21}v_1^2(t)u_1(t) + g_{12}v_1(t)u_1^2(t) + g_{11}[v_1(t)u_2(t) + v_2(t)u_1(t)]\}, \\ i_4(t) &= - \{g_{40}v_1^4(t) + g_{04}u_1^4(t) + 3g_{30}v_1^2(t)v_2(t) + 3g_{03}u_1^2(t)u_2(t) + \\ &\quad 2g_{20}[v_1(t)v_3(t) + v_2^2(t)] + 2g_{02}[u_1(t)u_3(t) + u_2^2(t)] + \\ &\quad g_{11}[v_1(t)u_3(t) + v_2(t)u_2(t) + v_3(t)u_1(t)] + g_{21}[v_1^2(t)u_2(t) + 2v_1(t)v_2(t)u_1(t)] \\ &\quad + g_{31}v_1^3(t)u_1(t) + g_{12}[v_2(t)u_1^2(t) + 2v_1(t)u_1(t)u_2(t)] + g_{22}v_1^2(t)u_1^2(t) + g_{13}v_1(t)u_1^3(t)\} \\ &\quad \vdots \end{aligned} \quad (2.229)$$

The NC method can be combined efficiently with the Harmonic Input method to help the determination of the nonlinear transfer functions, by replacing the input $i(t)$ with sums of complex exponentials at incommensurate frequencies, as in (2.169).

Since we are analysing the frequency domain, the Fourier transform of the nonlinear currents of order n must be calculated in order to evaluate the NLTF of the same order. Given that $H_n(\mathbf{f}_n)$ is the factor that multiplies the term $n! e^{j2\pi(f_1+\dots+f_n)t}$, only the coefficient $F_n[i_{NLn}(t)]$ whose frequency component is $n! \delta[f - (f_1 + \dots + f_n)]$ must be known from the total spectrum $\mathcal{F}[i_{NLn}(t)]$. This coefficient can be expressed in terms of symmetrised products of lower-order nonlinear transfer functions. Therefore, it can be written as:

$$F_n[v_{k_1}^{m_1}(t) \cdots v_{k_s}^{m_s}(t)] = \frac{H_{k_1}(f_1, \dots, f_{k_1}) H_{k_1}(f_{k_1+1}, \dots, f_{2k_1}) \cdots H_{k_1}(f_{m_1 k_1 - k_1 + 1}, \dots, f_{m_1 k_1})}{\cdot H_{k_2}(f_{m_1 k_1 + 1}, \dots, f_{m_1 k_1 + k_2}) \cdots H_{k_s}(f_{n - m_s k_s + 1}, \dots, f_n)} \quad (2.230)$$

where $m_1 k_1 + m_2 k_2 + \dots + m_s k_s = n$ and H_{k_i} is the nonlinear transfer function of order k_i of the voltage $v(t)$. Recall that the symmetrization operation implies summing over all the different terms resulting from permutations of the f_i . This produces different sets of arguments and multiplying by a factor

$$N_0 = \frac{(k_1!)^{m_1} (k_2!)^{m_2} \cdots (k_s!)^{m_s} m_1! \cdots m_s!}{n!}. \quad (2.231)$$

Note that for any constant A

$$F_n[Av(t)] = A^n F_n[v(t)], \quad (2.232)$$

and, that in general,

$$F_n[u(t) + v(t)] \neq F_n[u(t)] + F_n[v(t)]. \quad (2.233)$$

In summary, the method to determine the nonlinear current sources of different orders for an exponentially driven circuit is as follows:

- Step 1:** Find the current of order n as a function of different order nonlinear voltage components, using the recursions (2.221)-(2.228).
- Step 2:** Apply (2.230) to find the coefficient of $n! \delta(f - f_1 - \dots - f_n)$ in $\mathcal{F}[i_n(t)]$, which here is denoted as $F_n[i_n(t)]$ for the n th-order when the input is the sum of n exponentials. This coefficient is expressed generally in terms of symmetric products of lower-order NLTFs.

Resuming the example of the FET amplifier, we will apply the NC method to obtain the second- and third-order NLTFs. Considering the circuit shown in Figure 2.16, the nonlinear currents vector takes the form

$$\mathbf{i}_{NL}(t) = \begin{bmatrix} i_{NLg}(t) \\ i_{NLd}(t) \\ i_{NLgs}(t) \end{bmatrix}, \quad (2.234)$$

where

$$\begin{aligned}
 i_{NLg}(t) &= -\frac{d}{dt} \sum_{k=2}^{\infty} \frac{c_{k-1}}{k} v_{gs}^k(t) = -\sum_{k=1}^{\infty} c_k v_{gs}^k(t) \frac{dv_{gs}(t)}{dt} \\
 i_{NLd}(t) &= \frac{d}{dt} \sum_{k=2}^{\infty} \frac{c_{k-1}}{k} v_{gs}^k(t) = \sum_{k=1}^{\infty} c_k v_{gs}^k(t) \frac{dv_{gs}(t)}{dt} \\
 i_{NLgs}(t) &= -\sum_{k=2}^{\infty} g_{k0} v_{gs}^k(t) - \sum_{l=2}^{\infty} g_{0l} v_d^l(t) - \sum_{k=1}^{\infty} \sum_{l=1}^{\infty} g_{kl} v_{gs}^k(t) v_d^l(t)
 \end{aligned} \tag{2.235}$$

The resulting second- and third-order nonlinear currents take the following expressions:

- For the second-order:

- For the case of the nonlinear capacitance:

$$i_{NLg2}(t) = -i_{NLd2}(t) = -\frac{d}{dt} \left[\frac{c_1}{2} v_{gs1}^2(t) \right] \tag{2.236}$$

- For the case of the dependent nonlinearity:

$$i_{NLgs2}(t) = -\left[g_{20} v_{gs1}^2(t) + g_{02} v_{d1}^2(t) + g_{11} v_{gs1}(t) v_{d1}(t) \right] \tag{2.237}$$

- The Fourier coefficient $F_2[i_{NLk2}(t)]$ of the spectral components at frequency $f_1 + f_2$ are:

$$F_2[i_{NLg2}(t)] = F_{g2}(f_1, f_2) = -j2\pi(f_1 + f_2) \frac{c_1}{2} H_{gs1}(f_1) H_{gs1}(f_2)$$

$$F_2[i_{NLd2}(t)] = F_{d2}(f_1, f_2) = -F_{g2}(f_1, f_2) \tag{2.238}$$

$$\begin{aligned}
 F_2[i_{NLgs2}(t)] &= F_{gs2}(f_1, f_2) = -\left[g_{20} H_{gs1}(f_1) H_{gs1}(f_2) \right. \\
 &\quad \left. + g_{11} \overline{H_{gs1}(f_1) H_{d1}(f_2)} + g_{02} H_{d1}(f_1) H_{d1}(f_2) \right]
 \end{aligned}$$

- For the third-order:

- For the case of the nonlinear capacitance:

$$i_{NLg3}(t) = -i_{NLd3}(t) = -\frac{d}{dt} \left[\frac{c_1}{2} v_{gs1}(t) v_{gs2}(t) + \frac{c_2}{3} v_{gs1}^3(t) \right] \tag{2.239}$$

- For the case of the dependent nonlinearity:

$$\begin{aligned}
 i_{NLgs3}(t) &= -\left[2g_{20} v_{gs1}(t) v_{gs2}(t) + g_{30} v_{gs1}^3(t) + 2g_{02} v_{d1}(t) v_{d2}(t) + g_{03} v_{d1}^3(t) \right. \\
 &\quad \left. + g_{11} [v_{gs1}(t) v_{d2}(t) + v_{gs2}(t) v_{d1}(t)] + g_{21} v_{gs1}^2(t) v_{d1}(t) + g_{12} v_{gs1}(t) v_{d1}^2(t) \right]
 \end{aligned} \tag{2.240}$$

- The Fourier coefficient $F_3[i_{NLk3}(t)]$ of the spectral components at frequency $f_1 + f_2 + f_3$ are:

$$F_3[i_{NLg3}(t)] = F_{g3}(f_1, f_2, f_3) = -j2\pi(f_1 + f_2 + f_3) \times \left[c_1 \overline{H_{gs1}(f_1)H_{gs2}(f_2, f_3)} + \frac{c_2}{3} H_{gs1}(f_1)H_{gs1}(f_2)H_{gs1}(f_3) \right]$$

$$F_3[i_{NLd3}(t)] = F_{d3}(f_1, f_2, f_3) = -F_{g3}(f_1, f_2, f_3)$$

$$\begin{aligned} F_3[i_{NLgs3}(t)] = F_{gs3}(f_1, f_2, f_3) = & - \left[2g_{20} \overline{H_{gs1}(f_1)H_{gs2}(f_2, f_3)} + \right. \\ & + g_{30} H_{gs1}(f_1)H_{gs1}(f_2)H_{gs1}(f_3) + 2g_{02} \overline{H_{d1}(f_1)H_{d2}(f_2, f_3)} + \\ & + g_{03} H_{d1}(f_1)H_{d1}(f_2)H_{d1}(f_3) + g_{11} \left[\overline{H_{gs1}(f_1)H_{d2}(f_2, f_3)} + \right. \\ & \left. \left. + \overline{H_{gs2}(f_1, f_2)H_{d1}(f_3)} \right] + g_{21} \overline{H_{gs1}(f_1)H_{gs1}(f_2)H_{d1}(f_3)} + \right. \\ & \left. + g_{12} \overline{H_{gs1}(f_1)H_{d1}(f_2)H_{d1}(f_3)} \right] \end{aligned} \quad (2.241)$$

2.6 Brief overview of envelope-based methods

In this section, a brief overview of the principles governing the envelope-based methods for the simulation of circuits will be presented so that a comparison of the usual techniques for nonlinear circuits can be made. A detailed explanation of efficient methods for the analysis of nonlinear circuits excited with wireless communication signals will be presented in Chapter 3. The most relevant advantage of envelope-based methods is their efficiency, which is especially notable when digitally modulated excitations are used [192].

The envelope simulation process consist of the following steps [87]:

1. Representation of the input signal in terms of its complex envelope.

Each modulated signal can be represented as a carrier at frequency f_c modulated by an envelope $\tilde{x}(t) = A(t)e^{j\phi(t)}$, that is $x(t) = \text{Re}\{\tilde{x}(t)e^{j2\pi f_c t}\}$. In the envelope-based methods, the values of amplitude and phase of the sampled envelope are normally used as input signals for frequency-domain methods.

2. Transformation into the frequency domain and analysis using a frequency-domain method.

In most of the cases, HB analysis is performed at each time step. This process creates a succession of spectra that characterise the response of the circuit at the different time steps.

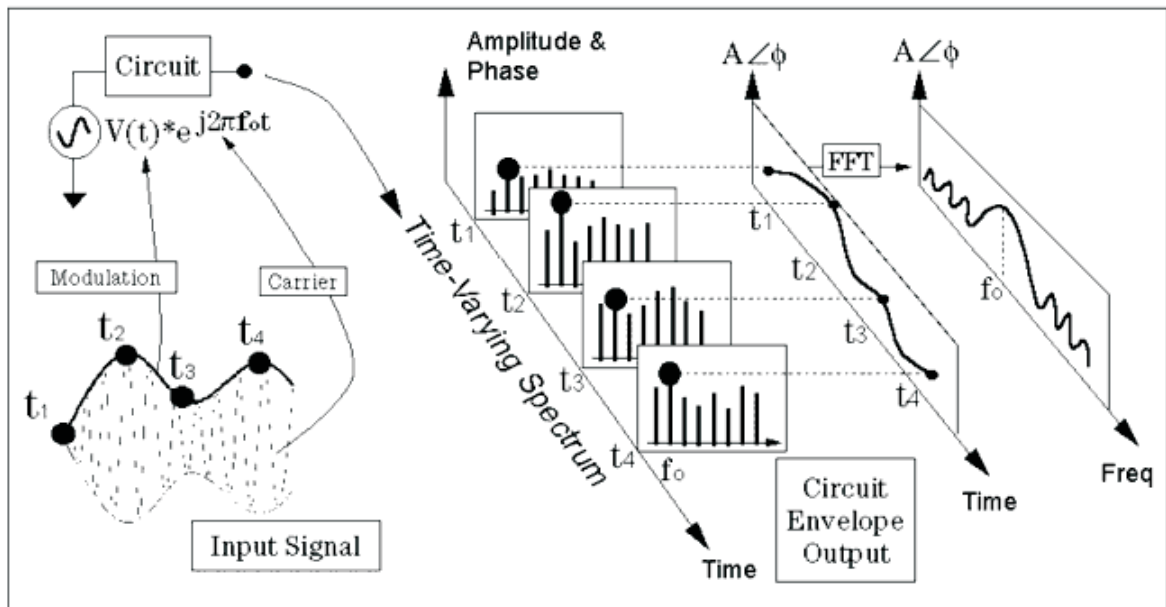


Figure 2.17: Envelope-based simulation process. Picture taken from [87].

3. Time-domain analysis.

The previous step provides a complete non steady-state solution of the circuit through a Fourier series with time-varying coefficients. We can obtain an envelope response for each harmonic formed with the Fourier coefficients obtained at each time step.

4. Extraction of data from the time domain.

Selecting the desired harmonic spectral line, normally the fundamental frequency f_c , it is possible to carry out transient simulations and predict amplitude and/or phase versus time.

5. Extraction of data from the frequency domain.

By Fourier transforming the selected time-varying spectral line it is possible to obtain the output spectrum and predict spectral regrowth, Adjacent Channel Power Ratio (ACPR), Noise to Power Ratio (NPR), AM/AM and AM/PM distortion or any kind of distortion in the signal constellation.

2.7 Comparison of analysis techniques

In order to sum up the main advantages and disadvantages of the techniques for the analysis of nonlinear microwave circuits presented in this chapter, a comparison

is shown in Table 2.1. Although envelope-based techniques will be thoroughly explained in Chapter 3, they have also been included for comparison purposes.

As it was stated in Chapter 1, the basic aim of this Thesis is the study and development of new analysis techniques for weakly nonlinear systems under narrowband digitally-modulated communications signals. Therefore, considering the advantages and disadvantages shown in Table 2.1 we can conclude that the recommended techniques are envelope-based techniques or, in those cases where we seek a better comprehension of the implications of design parameters, Volterra series representation. Time-domain simulation, classical Harmonic Balance and multitone Harmonic Balance techniques result inefficient when dealing with wireless communications signals.

Table 2.1: Comparison of techniques for the analysis of nonlinear microwave circuits.

Advantages	Disadvantages
Time-domain simulation	
<ul style="list-style-type: none"> - Allows transient analysis - Any kind of nonlinear function in the time domain can be used - Allows the analysis of strongly nonlinear systems 	<ul style="list-style-type: none"> - Long convergence times - Inefficient for circuits with very different time constants - Difficult to include distributed elements
Classic Harmonic Balance	
<ul style="list-style-type: none"> - Faster convergence than time-domain - Easy to include distributed elements - General purpose method, including strong nonlinearities 	<ul style="list-style-type: none"> - Requires periodic solutions - Possible convergence problems
Multitone Harmonic Balance	
<ul style="list-style-type: none"> - Quasiperiodic input signals can be considered - Easy to include distributed elements - Allows the analysis of strongly nonlinear systems 	<ul style="list-style-type: none"> - It can be computationally expensive - Possible convergence problems
Envelope-Based techniques	
<ul style="list-style-type: none"> - Allows envelope transient analysis - Considerable reduction in computation time - Deals naturally with modulated signals 	<ul style="list-style-type: none"> - Approximated method - Input modulated signals have to be narrowband - Distributed elements need consideration - Possible convergence problems
Volterra series representation	
<ul style="list-style-type: none"> - Provides closed-form expressions, which gives a better insight for design implications 	<ul style="list-style-type: none"> - Only for weakly nonlinear behaviour, since high order expressions are cumbersome - Difficult to systematise - Nonlinear functions have to be approximated by power series

ENVELOPE-BASED METHODS FOR THE ANALYSIS OF NONLINEAR WIRELESS COMMUNICATIONS SYSTEMS

3.1 Introduction

In this chapter, a number of methods for the analysis of nonlinear distortion produced in circuits for modern wireless communications is presented. The signals employed in these circuits show complex digital modulations which force the search for more specific simulation techniques. On the other hand, it is in the wireless communications field where efficiency and linearity of active devices have become most significant. Considerable optimization efforts when designing such systems are necessary, for which accurate and efficient simulation techniques are demanded.

Traditionally, power amplifiers or mixers for communications systems are designed to meet specifications like the 1-dB gain-compression output power (P_{1dB}) or the third-order intercept point (IP_3). Such tests can be performed with one or two sinusoidal input tones. Nowadays, however, these power amplifiers or mixers are usually required to meet a certain Adjacent Channel Power Ratio specification or satisfy a spectral mask at a particular output power. These results may not be obtained by using sinusoidal input signals.

A very important issue when transmitting digitally modulated signals is the Adjacent Channel Power (ACP). A transmitter should only emit power within its designated channel. Any power emitted in adjacent channels can interfere with the proper operation of nearby receivers that are attempting to receive signals from other transmitters. As such, transmitters have strict adjacent channel interference or ACP requirements that must be satisfied. Moreover, if mixers or power amplifiers are nonlinear, intermodulation distortion can cause the bandwidth to grow. This effect is

referred to as *spectral regrowth*. The adjacent channel power is characterised by means of the figure of merit called Adjacent Channel Power Ratio (ACPR), usually defined as¹

$$ACPR = \frac{P_{adj}}{P_{inband}}, \quad (3.1)$$

where P_{adj} is the total power in the adjacent channel and P_{inband} is the power in the desired channel. The simulation of this figure of merit is clearly impractical for conventional transient analysis.

The main difficulty when applying circuit simulation techniques to communication signals is that, due to the random nature of the digital data which modulate the carriers, it is necessary to consider long symbol sequences in order to reduce the variations that can be observed from one realization to the other. Therefore, it is necessary to take into account a large number of frequency components in standard HB techniques and to carry out the circuit equations integration for large time intervals when using time-domain techniques. Iterative approximation techniques have been applied to the solution of the Newton-Raphson iteration step by using Krylov subspace techniques in HB analysis. It results in a decrease of computational complexity and reduced memory requirements. However, conventional HB simulation of large RFICs with digitally-modulated waveforms applied is not practical yet. Instead, the best choice is using envelope-based methods such as those presented in [20], [17] or [18], which will be explained in this section. Nevertheless, ACPR simulations are very expensive even for the known methods, therefore some new and more efficient simulation techniques will be proposed that allow their use in design and optimization processes.

All the analysis methods presented in this chapter will be circuit-level approaches, since they provide more accurate results at the cost of larger simulation times. In contrast to circuit-level approaches we can find the system-level ones, also referred to as *behavioural methods*, which model the input-output relationship for the desired variables neglecting all the internal details of the nonlinear circuit structure. System-level methods are the simplest representation and allow a fast estimation of the nonlinear effects, but they usually result less accurate. Due to their more rigorous approach and to the fact that they are suitable to analyse the memory effects produced by the nonlinearities of the different circuit components, in this Thesis the use of a circuit-level approach has been chosen.

The approaches that will be presented in this chapter aim at the efficient simulation of nonlinear circuits whose excitations are digitally-modulated signals. These

¹The alternate definition $ACPR = \frac{P_{inband}}{P_{adj}}$ can also be found in the literature, although the selected one is more commonly implemented in experimental characterization equipment. In addition, this concept is termed Adjacent Channel Leakage Power Ratio (ACLR) in 3GPP W-CDMA systems.

specialised approaches are enveloped-based methods, which are approximate techniques. Although it is also possible to use multitone HB in a more exact manner, it would be considerably less efficient. The main drawback of the envelope-based techniques is that they cannot be applied to broadband signals where the envelope frequency is close to the carrier frequency. However, this is not the case for most practical digitally-modulated signals.

First, several outstanding envelope-based approaches that take into account communications signals will be presented: the Envelop [sic] Transient analysis [17], where a time-domain integration of the complex envelopes equations is proposed; a modulation-oriented HB technique [20], which is an approximate form of the piecewise HB technique for circuits driven by narrowband modulated signals; and the Envelope Currents method [18], which is based on an envelope formulation and on the NC method, and takes advantage of the common weakly nonlinear behaviour in communication signals to speed up simulation. In order to overcome the limitations of the Envelope Currents method, an extension proposed in [19] will be presented where a time-varying linear circuit is analysed resulting a more accurate approach at the expense of a slightly higher computational cost. Finally, three simplified methods will be presented as a part of the original contribution of this Thesis. The first of them is a simplified method to evaluate weakly nonlinear circuits where a significant reduction of the simulation time is achieved while maintaining an appropriate accuracy. This method will be related to the use of a simplified Newton-Raphson algorithm to solve the system of equations of the nonlinear circuit. Then, two methods will be presented for the analysis of a mixer with communications signals, which are extensions of the Envelope Currents and the Simplified Newton approaches taking into account the particularities of mixers.

3.1.1 Modulated signals

A narrowband modulated waveform, $x(t)$, can be represented as

$$x(t) = \text{Re} \{ \tilde{x}(t) e^{j\omega_c t} \}, \quad (3.2)$$

where $\tilde{x}(t)$ is the complex envelope of the signal, containing information about the magnitude and phase of the modulated waveform. When such a waveform is distorted by a nonlinear circuit, harmonics of the carrier and mixing products between the individual frequency components of the spectrum are generated. The bandwidth of the modulated signal is broadened by odd-order nonlinearities, which generate frequency components adjacent to the linear spectrum that fall outside the intended channel causing interference. This phenomenon is referred to as *spectral regrowth*.

However, not only adjacent-channel distortion is generated but also co-channel distortion due to the mixing products that fall inside the intended channel.

Taking into account that each carrier harmonic is surrounded by modulation components, the distorted waveform can be represented as

$$x(t) = \frac{1}{2} \sum_{h=-\infty}^{\infty} \tilde{x}(h, t) e^{jh\omega_c t}. \quad (3.3)$$

$\tilde{x}(h, t)$ represents the envelope around the h -th harmonic, whose frequency representation is

$$X(\omega) = \frac{1}{2} \sum_{h=-\infty}^{\infty} \tilde{X}(h, \omega - h\omega_c) = \frac{1}{2} \sum_{h=-\infty}^{\infty} \tilde{X}(h, \Omega). \quad (3.4)$$

That is to say, the spectrum of a signal consists of clusters of frequency components centred at the different carrier harmonics, as it is shown in Figure 3.1. Nonlinear RF circuit simulators exploit the “spars” nature of this spectrum in different ways and with varying degrees of success. If we assume that the modulation signal is quasi-periodic and deterministic, $\tilde{x}(h, t)$ can be expressed by the Fourier series

$$\tilde{x}(h, t) = \sum_{m=-\infty}^{\infty} \tilde{X}(h, m) e^{jm\omega_m t}, \quad (3.5)$$

and (3.3) becomes

$$x(t) = \frac{1}{2} \sum_{h=-\infty}^{\infty} \sum_{m=-\infty}^{\infty} \tilde{X}(h, m) e^{j(h\omega_c + m\omega_m)t}. \quad (3.6)$$

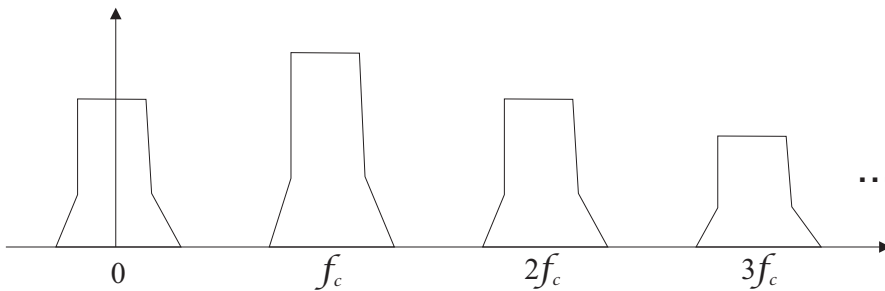


Figure 3.1: Spectrum of a narrowband RF signal centred at a carrier frequency f_c after passing through a nonlinear circuit.

3.2 Envelop Transient method

The *Envelop [sic] Transient Method* (ET) [17] was first proposed by Ngoya and Larchevèque in 1996 as an efficient and general purpose technique for the simulation of communications microwave circuits and systems, aimed at the analysis of both the transient and the steady-state solutions.

In the ET method, any signal is considered to be a combination of a low-frequency dynamic (the envelope or modulation) and a high-frequency dynamic (the carrier), which are processed separately. The high-frequency dynamic is treated by HB, while the low-frequency dynamic is solved by time-domain integration.

The considered excitation signal is a modulated carrier with a limited bandwidth, whose spectrum is centred at a frequency ω_c . Then, any circuit signal can be written as:

$$\begin{aligned} x(t) &= \frac{1}{2} \sum_{h=-H}^{h=H} \tilde{x}(h, t) e^{jh\omega_c t} \\ \tilde{x}(h, t) &= \frac{1}{2\pi} \int_{-\frac{B}{2}}^{\frac{B}{2}} \tilde{X}(h, \Omega) e^{j\Omega t} d\Omega, \end{aligned} \quad (3.7)$$

where $\tilde{x}(h, t)$ is the time-varying complex envelope (or modulating signal) of the h -th harmonic of the carrier frequency ω_c , and B is the largest bandwidth of the envelopes in the carrier harmonics. Note that, in this method, the time-varying complex envelope of the signal is not necessarily a periodic signal, since it is treated in the time-domain.

In order to carry out an ET analysis, two time dimensions t_1 and t_2 are considered in the signals expressions

$$x(t) \Rightarrow \bar{x}(t_1, t_2) = \frac{1}{2} \sum_{h=-H}^{h=H} \tilde{x}(h; t_1) e^{jh\omega_c t_2}. \quad (3.8)$$

As it is quite common when analysing microwave circuits, it is proposed to consider the circuit divided into two parts, a purely linear subcircuit and another non-linear subcircuit, and then substitute the nonlinear subcircuit with excitation current sources with the same value as the electrical variables in this subcircuit ports. This way, a linear circuit is analysed, excited by both the real sources, $s(t)$, and those obtained from the nonlinear elements, which are defined by the intrinsic characteristic of the nonlinear subcircuit $y(t) = f(x(t))$. Therefore, any circuit equation can be expressed in the frequency domain as

$$X(\omega) = A(\omega)Y(\omega) + B(\omega)S(\omega), \quad (3.9)$$

where $X(\omega)$ is the spectrum of the state variables of the circuit $x(t)$, $Y(\omega)$ is the spectrum of the equivalent sources of the nonlinear subcircuit $y(t)$, $S(\omega)$ is the spectrum of the original driving sources, and $A(\omega)$ and $B(\omega)$ are the transfer functions that characterise the linear subcircuit.

Taylor series expansion of the transfer functions inside the bandwidth of the modulation are considered, as a function of a variable Ω

$$A(h\omega_c + \Omega) = a_{h,0} + \sum_{p=1}^P a_{h,p}(\Omega)^p = \alpha_{h,0} + \sum_{p=1}^P \alpha_{h,p}(j\Omega)^p, \quad (3.10)$$

$$B(h\omega_c + \Omega) = b_{h,0} + \sum_{p=1}^P b_{h,p}(\Omega)^p = \beta_{h,0} + \sum_{p=1}^P \beta_{h,p}(j\Omega)^p. \quad (3.11)$$

Recalling that the spectrum of a signal consists of clusters of frequency components centred at the different carrier harmonics, these expansions depend on which harmonic h is considered.

We can express (3.9) as a function of the complex envelopes spectra and introduce the series expansions of the transfer functions. If an inverse Fourier transform is applied, then the following set of differential equations of order P is obtained for the ET, with an equation for every carrier harmonic:

$$\begin{aligned} \tilde{x}(h; t_1) = \alpha_{h,0}\tilde{y}(h; t_1) + \beta_{h,0}\tilde{s}(h; t_1) + \sum_{p=1}^P \alpha_{h,p} \frac{d^p \tilde{y}(h; t_1)}{dt_1^p} + \sum_{p=1}^P \beta_{h,p} \frac{d^p \tilde{s}(h; t_1)}{dt_1^p}, \quad (3.12) \\ -H \leq h \leq H. \end{aligned}$$

In these equations, the variables of the nonlinear subcircuit and the intrinsic equation are expressed as a function of two temporal indices $\tilde{y}(t_1, t_2) = f(\tilde{x}(t_1, t_2))$, in the same way than the rest of the signals.

When narrowband signals are considered, first-order Taylor series ($P = 1$) are sufficient to achieve a good accuracy, resulting a first-order differential equation for the ET method

$$\begin{aligned} \tilde{x}(h; t_1) = \alpha_{h,0}\tilde{y}(h; t_1) + \beta_{h,0}\tilde{s}(h; t_1) + \alpha_{h,1} \frac{d\tilde{y}(h; t_1)}{dt_1} + \beta_{h,1} \frac{d\tilde{s}(h; t_1)}{dt_1}, \quad (3.13) \\ -H \leq h \leq H. \end{aligned}$$

It can be seen that, for a fixed value of t_1 , equations (3.12) and (3.13) correspond to the HB analysis of the circuit, since the complex envelope is constant. This makes possible to obtain the time-varying complex envelope response, $\tilde{x}(h, t)$, by means of successively solving a steady-state quasi-periodic problem for each time instant t_1 of the envelope. When the envelopes $\tilde{x}(h; t_1)$ at all H harmonics for all time instants t_1 are known, the real signal $x(t)$ can be calculated. This process is inherently more efficient than multitone HB analysis, as it replaces a dimension of the multitone problem with a sequence of analyses. In order to obtain the solution at any instant, the differential equations in (3.12) or (3.13) are integrated in the time domain from an initial time until the desired value $t_{1,max}$ or until the transient dies out.

As it is shown in [17], the ET method implies a considerable reduction in the computation time compared to the time-domain integration methods used in several commercial simulators such as SPICE. Its efficiency is due to the achieved reduction in the time samples to be employed, since the sampling interval is chosen in accordance with the variation rate of the envelope. However, it maintains an accuracy similar to that of the direct time-integration methods. This method is especially indicated for the realization of transient analysis of microwave circuits. Among its application examples we can include the transient analysis of oscillators and circuits with modulated carriers shown by its authors in [17] and [178], developing in the latter a thorough calculation of the phase noise in microwave oscillators. Other more recent works which apply and extend the ET method are: [193], in which PLL-based systems are analysed using ET with three time scales; [194], in which the ET method is used to analyse auto-oscillating mixers, both autonomous and sub-synchronised; and [195], where ET is applied to analyse phase variation in oscillators arrays produced by control voltage. Another interesting example of application for ET analysis is determining the turn-on and turn-off behaviour of Time-Division Multiple Access (TDMA) transmitters [196]. In TDMA, transmitters broadcast during a narrow slice of time, during which they must power up, stabilise, send the message, and then power down. The transmitter can neither power up and down too slowly, because it would not work properly, or too quickly, because the resulting spectrum would be too wide to fit in the allotted channel. Simulating with traditional transient analysis would be considerably expensive because the reference time lasts on the order of milliseconds (e.g., 0.577 ms for mobile communications GSM systems and 2 ms for satellite communications Intelsat or Eutelsat systems) and the carrier frequency is typically over 1 GHz.

Nevertheless, the ET method presents some limitations. First, it is assumed that the complex envelope is a modulating signal which varies slowly. Furthermore, this method was created for excitations composed by only one carrier frequency modulated by baseband signals that are expressed in the time domain. Therefore, its usefulness is limited to excitation signals which occupy a small percentage of the nonlinear circuit bandwidth, not being appropriate to deal with multi-carrier excitations.

3.2.1 Multi-rate partial differential equation methods

The separation of signals with two very different time scales which has been made in the ET method is addressed by other authors by means of the property of latency [134], [135], [197], [198], [199]. Slowly-varying state-variables in a circuit are said to be latent, while fastly-varying state-variables are considered active. Latency refers to the fact that there are long periods over which the value of a given signal remains constant.

The property of latency can be viewed as a subset of the more general property of multi-rate behavior, which refers to signal values changing at different rates over the same interval of time. The possibility of solving the differential equations governing the behaviour of nonlinear circuits with dual or multiple time steps is termed latency exploitation. In this sense, multi-rate partial differential equation (MPDE) methods can be viewed as a generalization of the ET method, where multiple time scales are considered. These methods are intuitively formulated in the time domain.

MPDE approaches represent a family of methods based on the idea of replacing the single time variable with a sum of time variables, one for each of the time scales in the circuit. The underlying ordinary differential equations that describe the circuit are reformulated as partial differential equations in the different time scales t_1, \dots, t_n . The various MPDE methods are formulated by applying particular boundary conditions and numerical methods to the different time dimensions. For example, ET analysis is a MPDE method that applies HB analysis (implying a periodic boundary condition) to the t_2 dimension corresponding to the carrier frequency or high-frequency dynamic signal, and an initial condition and transient analysis to the t_1 dimension corresponding to the envelope signal or low-frequency dynamic. Another example of MPDE method is [199], a recently proposed time-domain method suitable for highly heterogeneous nonlinear RF circuits. In this case, the periodicity of the problem for the t_2 dimension is exploited and the periodic boundary value problem that arises is solved by using a shooting algorithm (a common time-domain technique used for steady-state circuit simulation) based on multi-rate Runge-Kutta numerical methods.

3.3 Modulation-oriented Harmonic Balance

The theoretical foundations for the Modulation-oriented Harmonic Balance (MHB) method were first proposed by Rizzoli in 1996 [20]. MHB is aimed at the analysis of nonlinear microwave circuits driven by narrowband modulated RF signals. In this method, it is considered that any variable in a nonlinear circuit under a multitone excitation can be written in the form

$$x(t) = \sum_{h=-\infty}^{\infty} \sum_{s=-\infty}^{\infty} X_{h,s} e^{j(\Omega_h + \Omega_s)t} = \sum_{h=-\infty}^{\infty} X_h(t) e^{j\Omega_h t}, \quad (3.14)$$

where

$$X_h(t) = \sum_{s=-\infty}^{\infty} X_{h,s} e^{j\Omega_s t}, \quad (3.15)$$

Ω_s accounts for the low-frequency mixing products, and Ω_h accounts for the high-frequency mixing products. The complex quantity $X_h(t)$ is the modulation law of the

h -th mixing product of the high-frequency components, and is slowly varying with time. $X_h(t)$ is also referred to as the time-dependent h -th harmonic of $x(t)$. Therefore, in the MHB method, the unknowns are the time-dependent harmonics $X_h(t)$ instead of the regular harmonics.

If we reformulate the aforementioned expressions to consider a modulated excitation instead of a multitone excitation, they can be written as:

$$x(t) = \frac{1}{2} \sum_{h=-\infty}^{\infty} \sum_{m=-\infty}^{\infty} \tilde{X}(h, m) e^{j(h\omega_c + m\omega_m)t} = \frac{1}{2} \sum_{h=-\infty}^{\infty} \tilde{x}(h, t) e^{jh\omega_c t}, \quad (3.16)$$

where

$$\tilde{x}(h, t) = \frac{1}{2} \sum_{m=-\infty}^{\infty} \tilde{X}(h, m) e^{jm\omega_m t}, \quad (3.17)$$

and ω_m accounts for the low-frequency variation of the baseband signal while ω_c is the carrier frequency. Note that it is necessary to assume quasi-periodic complex envelopes $\tilde{x}(h, t)$ so that their Fourier series can be defined and used in (3.16)-(3.17). However, the discussion made in the MHB method is also applicable to generic complex envelopes of finite duration, as long as the formulation is made in terms of time-domain expressions of the complex envelopes and does not include their Fourier coefficients. In this case, the unknowns are the complex envelopes $\tilde{x}(h, t)$ of all the harmonics of the carrier frequency. Moreover, the complex envelopes are sampled at a finite number of uniformly spaced time instants t_k , with $1 \leq k \leq K$, and the complex quantities $\tilde{x}(h, t_k)$ are taken as the problem unknowns.

In order to perform an HB analysis, balancing of the linear and nonlinear currents now leads to the following expression in terms of complex envelopes:

$$\sum_{h=-\infty}^{\infty} \left[\tilde{\mathbf{i}}_{\text{LIN}}(h, t) + \tilde{\mathbf{i}}_{\text{NL}}(h, t) \right] e^{jh\omega_c t} = 0. \quad (3.18)$$

The summation (3.18) looks like a Fourier series, but its terms are not orthogonal because the coefficients in brackets are time dependent. However, the slow dependence on time of the complex envelopes can be used in order to obtain orthogonal terms. Considering this property, it is assumed that $\tilde{x}(h, t)$ remains virtually unchanged in the time interval required to sweep the high-frequency components given for the carrier harmonics, since the complex envelope is a slowly varying signal. On this basis, the terms $\tilde{\mathbf{i}}_{\text{LIN}}(h, t_k)$ and $\tilde{\mathbf{i}}_{\text{NL}}(h, t_k)$ are kept fixed over the time dimension corresponding to the high-frequency. Therefore, (3.18) can be rewritten as:

$$\tilde{\mathbf{i}}_{\text{LIN}}(h, t_k) + \tilde{\mathbf{i}}_{\text{NL}}(h, t_k) = \tilde{\mathbf{f}}(h, t_k) \approx \mathbf{0}, \quad (3.19)$$

for all values of h and k . Note that the complex envelopes are only approximately balanced. This approximation becomes worse as the complex envelopes become faster.

Regarding the expressions for the currents of the linear subcircuit, if we consider that the $m\omega_m$ components are small, the admittance matrix of the circuit $\mathbf{Y}(\omega)$ can be approximated by a low-order Taylor series expansion about each harmonic of the carrier

$$\mathbf{Y}(\omega) = \mathbf{Y}(h\omega_c + m\omega_m) = \mathbf{Y}(h\omega_c) + \sum_{n=1}^N \frac{1}{n!} \Omega^n \left. \frac{d^n \mathbf{Y}(\omega)}{d\omega^n} \right|_{\omega=h\omega_c} + \mathcal{O}(\Omega^n), \quad (3.20)$$

$$\Omega = \text{diag}(\omega - h\omega_c) = \text{diag}(m\omega_m),$$

with N sufficiently small. Taking into account (3.20), the frequency-domain equation for the linear subcircuit can be written as:

$$\tilde{\mathbf{I}}(h, m\omega_m) = \tilde{\mathbf{I}}_s(h, m\omega_m) + \left[\mathbf{Y}(h\omega_c) + \sum_{n=1}^N \frac{1}{n!} \Omega^n \left. \frac{d^n \mathbf{Y}(\omega)}{d\omega^n} \right|_{\omega=h\omega_c} \right] \tilde{\mathbf{V}}(h, m\omega_m), \quad (3.21)$$

and the following time-domain equation is obtained by inverse Fourier transform:

$$\tilde{\mathbf{i}}(h, t) = \tilde{\mathbf{i}}_s(h, t) + \mathbf{Y}(h\omega_c) \tilde{\mathbf{v}}(h, t) + \sum_{n=1}^N \frac{(-j)^n}{n!} \left. \frac{d^n \mathbf{Y}(\omega)}{d\omega^n} \right|_{\omega=h\omega_c} \frac{d^n \tilde{\mathbf{v}}(h, t)}{dt^n}. \quad (3.22)$$

On the other hand, the time derivatives contained in the implicit time-domain equations which define the nonlinear elements of the circuit must also be expressed in terms of the complex envelopes. For example,

$$\frac{dx(t)}{dt} = \sum_{h=-\infty}^{\infty} \left[jh\omega_c \tilde{x}(h, t) + \frac{d\tilde{x}(h, t)}{dt} \right] e^{jh\omega_c t}. \quad (3.23)$$

The derivatives of the complex envelopes included in (3.22) and (3.23) are usually evaluated numerically by using a discretization rule, as the ones presented in Section 2.2.5.

Rizzoli remarks in [20] that the entire procedure breaks down if the bandwidth of the modulation law is not small enough with respect to the high-frequency fundamentals. More relevantly, the Jacobian matrix obtained when solving by a Newton iteration is actually a band matrix where only a number of submatrices given by the kind of discretization rule employed are nonzero, instead of the full matrix required by a conventional multitone HB. Furthermore, the diagonal submatrices in the Jacobian are often dominant with respect to the off-diagonal ones, allowing us to reduce it to a block-diagonal form with a strong increase in numerical efficiency. Therefore, the MHB is much faster than the conventional multitone HB.

3.4 Envelope Currents method

The *Envelope Currents (EC) method* [18] was first presented by Borich in 1999 as an efficient tool for the simulation of weakly nonlinear communications circuits. This method is oriented to the analysis of the spectral regrowth suffered by nonlinear circuits when they are excited by digitally-modulated narrowband signals. It can be considered as an efficient extension of the Nonlinear Currents (NC) method for digital communications signals.

In order to achieve a considerable reduction of the simulation time, in this method a weakly nonlinear behaviour of the circuits is assumed. Despite the microwave amplifiers are employed closer and closer to saturation to obtain higher output power levels and efficiency, a high linearity is still necessary to get a better performance of the system. Because of this the wireless communications circuits are often operated in a weakly nonlinear regime. The HB techniques usually converge faster for weakly nonlinear circuits than for strongly nonlinear circuits, due to the smaller number of iterations needed. However, these methods do not directly exploit the quasi-linear characteristic. In the EC method, a significant improvement of the simulation time is achieved by assuming a narrowband excitation and a weak nonlinearity.

In order to apply this method, the problem is formulated in terms of the modified nodal analysis equations of the equivalent circuit for the device to be analysed, as it was explained in Section 2.3.1. The nodal voltages of the circuit are considered to be given by a sum of incremental voltages

$$v(t) = V_0 + v_1(t) + \dots + v_n(t), \quad (3.24)$$

where the voltage V_0 represents the dc component. The nonlinear elements are represented by means of power series about the bias point, as it has been detailed in Section 2.3.2, with a finite number of terms. According to the weakly nonlinear approximation, it is assumed that the incremental currents and voltages are small enough, that is, that the nonlinearities of the elements are mild enough for the currents of the conductances, capacitances and dependent sources to be approximated by the first terms of their power series expansions. In the EC method, all the summations are extended up to $N = 3$

$$\begin{aligned} i_g(t) &= \sum_{k=1}^3 g_k v^k(t), \\ i_c(t) &= \sum_{k=0}^3 c_k v^k(t) \frac{dv_c(t)}{dt}, \\ i(t) &= \sum_{k=1}^3 g_{k0} v^k(t) + \sum_{l=1}^3 g_{0l} u^l(t) + \sum_{k=1}^3 \sum_{l=1}^3 g_{kl} v^k(t) u^l(t). \end{aligned} \quad (3.25)$$

The EC method is based on the application of the NC method described in Section 2.5.4.2 to a circuit whose excitation currents are narrowband modulated signals expressed as

$$i_s(t) = \text{Re} \{ \tilde{i}_s(t) e^{j\omega_c t} \}. \quad (3.26)$$

In this case, any circuit variable takes the following form for the n -th iteration:

$$x_n(t) = \frac{1}{2} \sum_{h=-n}^n \tilde{x}_n(h, t) e^{jh\omega_c t}, \quad (3.27)$$

where $\tilde{x}_n(h, t)$ is the complex envelope of the signal about the h -th harmonic of ω_c . Note that all the summations are limited to $|h| < n$, since the NC method is applied and the nonlinear currents used do not exceed order n , agreeing with the number of the iteration. Taking into account that the components of $x_n(h, t)$ which are centred at $-\omega_c, \dots, -n\omega_c$ are the complex conjugates of those centred at $\omega_c, \dots, n\omega_c$, it is usual to consider only positive frequencies

$$\hat{x}_n(t) = \sum_{h=0}^n \tilde{x}_n(h, t) e^{jh\omega_c t}. \quad (3.28)$$

Two basic assumptions are made in the EC method: the first one is based on a quasi-periodic treatment of the complex envelopes about each harmonic of ω_c , i.e., to treat them as periodic signals, representing each complex envelope $\tilde{x}_n(h, t)$ by a discrete number of sinusoids and introducing a Fourier series representation.

Under this assumption, the system of frequency-domain equations corresponding to that solved in the NC method can be expressed as

$$\begin{aligned} \mathbf{Y}(\omega) \tilde{\mathbf{V}}_{n,h}(\omega - h\omega_c) &= \tilde{\mathbf{I}}_{n,h}(\omega - h\omega_c) \\ n &= 1, \dots, N, \quad h = 0, \dots, H, \end{aligned} \quad (3.29)$$

where $\mathbf{Y}(\omega)$ is the node admittance matrix of the augmented linear subcircuit. $\tilde{\mathbf{V}}_{n,h}(\omega - h\omega_c)$ and $\tilde{\mathbf{I}}_{n,h}(\omega - h\omega_c)$ are the vectors containing the complex envelopes of the node voltages and the excitation currents for the n -th iteration, evaluated around the h -th harmonic.

In principle, it is possible to directly solve the system of equations (3.29) in order to find $\tilde{\mathbf{V}}_{n,h}(\omega - h\omega_c)$, although this approach is not efficient. The envelopes need to be sampled during long time intervals, what usually generates several thousands of frequency components and would imply to evaluate and factorise $\mathbf{Y}(\omega)$ for several thousands of frequency points.

Because of this, the second assumption made is based on the fact that, if the excitation is narrowband, the spectrum corresponding to the waveforms in the circuit will

be concentrated in narrow frequency bands around $h\omega_c$. Therefore, it is possible to use a low-order Taylor series expansion for the frequency representation of the admittance matrix about each harmonic ω_c without a significant error. In the EC method, a first-order expansion is considered enough for the general case, that is,

$$\mathbf{Y}(\omega) \simeq \mathbf{Y}(h\omega_c) + \mathbf{\Omega}\mathbf{Y}'(h\omega_c), \quad h = 0, \dots, n \quad (3.30)$$

with

$$\mathbf{\Omega} = \text{diag}(\omega - h\omega_c), \quad \text{and} \quad \mathbf{Y}'(h\omega_c) = \left. \frac{d\mathbf{Y}(\omega)}{d\omega} \right|_{\omega=h\omega_c}, \quad (3.31)$$

although higher-order series expansions can be taken into account if a better accuracy is desired when predicting the changes with modulation frequency experienced by distortion components, i.e., to deal with the memory effects more rigorously.

If (3.30) is substituted into (3.29) and an inverse Fourier transform is applied to recover the node voltage waveforms, the following expression is obtained:

$$\left[\mathbf{Y}(h\omega_c) - j\mathbf{Y}'(h\omega_c) \frac{d}{dt} \right] \tilde{\mathbf{v}}_n(h, t) = \tilde{\mathbf{i}}_n(h, t), \quad (3.32)$$

$$n = 1, \dots, N, \quad h = 0, \dots, n$$

where $\tilde{\mathbf{v}}_n(h, t)$ is the solution vector with the complex envelopes of the voltage waveforms around $h\omega_c$ for the n -th order nonlinear current. Equation (3.32) summarises the EC method. For each n and each h , (3.32) is a system of linear differential equations expressed in terms of the complex envelopes of the node voltages. When this algorithm is applied up to $N = H = 3$, twelve systems of equations will appear on the whole, although some of them present trivial solutions and others are of no interest. Finally, it is only necessary to solve four systems of equations.

The *current envelopes* appearing at the right-hand side of (3.32) are obtained by substituting the adopted representation in terms of the complex envelopes of the node voltages, (3.27), in the nonlinear current expressions obtained in 2.5.4.2, and then collecting all the terms centred at the frequency $h\omega_c$. The results of this procedure are as follows:

- For the first-order solution ($n = 1$), the current envelope is the envelope of the original current source of the circuit.
- For the second order ($n = 2$), there are two current envelopes corresponding to the baseband component and the second-harmonic zone, $2\omega_c$. The expressions taken by the second-order current envelopes for the different types of nonlinear elements are the following:

– For a nonlinear conductance:

$$\begin{aligned}\tilde{i}_2(0, t) &= -\frac{g_2}{2}|\tilde{v}_1(1, t)|^2 \\ \tilde{i}_2(2, t) &= -\frac{g_2}{2}\tilde{v}_1^2(1, t)\end{aligned}\quad (3.33)$$

– For a nonlinear current source controlled by two voltages:

$$\begin{aligned}\tilde{i}_2(0, t) &= -\left[\frac{g_{20}}{2}|\tilde{v}_1(1, t)|^2 + \frac{g_{02}}{2}|\tilde{u}_1(1, t)|^2 + \frac{g_{11}}{2}\Re\{\tilde{v}_1(1, t)\tilde{u}_1^*(1, t)\}\right] \\ \tilde{i}_2(2, t) &= -\left[\frac{g_{20}}{2}\tilde{v}_1^2(1, t) + \frac{g_{02}}{2}\tilde{u}_1^2(1, t) + \frac{g_{11}}{2}\tilde{v}_1(1, t)\tilde{u}_1(1, t)\right]\end{aligned}\quad (3.34)$$

– In the case of a nonlinear capacitance, it has been considered that the derivatives appearing in its power series expansion can be approximated by the derivatives acting on the carrier signals only (neglecting the envelopes variation compared to that of the carrier), so their action is multiplication by $j\hbar\omega_c$. Therefore, the expressions obtained when nonsignificant terms are neglected are:

$$\begin{aligned}\tilde{i}_2(0, t) &= -\frac{c_1}{4}\frac{d}{dt}(|\tilde{v}_1(1, t)|^2) \approx 0 \\ \tilde{i}_2(2, t) &\approx -j\omega_c\frac{c_1}{2}\tilde{v}_1^2(1, t)\end{aligned}\quad (3.35)$$

- For the third order ($n = 3$), there are also two current envelopes corresponding to the fundamental and third-harmonic zone, $3\omega_c$. However, it is the fundamental frequency on which the main practical interest is focused. The expressions of the current envelopes for the third order are the following:

– For a nonlinear conductance:

$$\begin{aligned}\tilde{i}_3(1, t) &= -\left[\frac{3g_3}{4}\tilde{v}_1^2(1, t)\tilde{v}_1^*(1, t) + 2g_2\tilde{v}_1(1, t)\tilde{v}_2(0, t) + g_2\tilde{v}_1^*(1, t)\tilde{v}_2(2, t)\right] \\ \tilde{i}_3(3, t) &= -\left[\frac{g_3}{4}\tilde{v}_1^3(1, t) + g_2\tilde{v}_1(1, t)\tilde{v}_2(2, t)\right]\end{aligned}\quad (3.36)$$

– For a nonlinear current source controlled by two voltages:

$$\begin{aligned}\tilde{i}_3(1, t) &= -\left\{\frac{3g_{30}}{4}\tilde{v}_1^2(1, t)\tilde{v}_1^*(1, t) + \frac{3g_{03}}{4}\tilde{u}_1^2(1, t)\tilde{u}_1^*(1, t) + \right. \\ &\quad \left. 2g_{20}\left[\frac{1}{2}\tilde{v}_1^*(1, t)\tilde{v}_2(2, t) + \tilde{v}_1(1, t)\tilde{v}_2(0, t)\right] + \right. \\ &\quad \left. 2g_{02}\left[\frac{1}{2}\tilde{u}_1^*(1, t)\tilde{u}_2(2, t) + \tilde{u}_1(1, t)\tilde{u}_2(0, t)\right] + \right. \\ &\quad \left. g_{11}\left[\frac{1}{2}\tilde{v}_1^*(1, t)\tilde{u}_2(2, t) + \tilde{v}_1(1, t)\tilde{u}_2(0, t) + \frac{1}{2}\tilde{u}_1^*(1, t)\tilde{v}_2(2, t) + \tilde{u}_1(1, t)\tilde{v}_2(0, t)\right]\right\} +\end{aligned}$$

$$\frac{g_{21}}{4} [\tilde{v}_1^2(1, t) \tilde{u}_1^*(1, t) + 2|\tilde{v}_1(1, t)|^2 \tilde{u}_1(1, t)] + \quad (3.37)$$

$$\frac{g_{12}}{4} [\tilde{u}_1^2(1, t) \tilde{v}_1^*(1, t) + 2|\tilde{u}_1(1, t)|^2 \tilde{v}_1(1, t)] \Big\}$$

$$\tilde{i}_3(3, t) = - \left\{ \frac{g_{30}}{4} \tilde{v}_1^3(1, t) + \frac{g_{03}}{4} \tilde{u}_1^3(1, t) + \frac{g_{21}}{4} \tilde{v}_1^2(1, t) \tilde{u}_1(1, t) + \right.$$

$$\frac{g_{12}}{4} \tilde{u}_1^2(1, t) \tilde{v}_1(1, t) + g_{20} \tilde{v}_1(1, t) \tilde{v}_2(2, t) + g_{02} \tilde{u}_1(1, t) \tilde{u}_2(2, t) + \quad (3.38)$$

$$\left. \frac{g_{11}}{2} [\tilde{v}_1(1, t) \tilde{u}_2(2, t) + \tilde{u}_1(1, t) \tilde{v}_2(2, t)] \right\}$$

– For a nonlinear capacitance:

$$\tilde{i}_3(1, t) \approx -j\omega_c \left[\frac{c_2}{4} \tilde{v}_1^2(1, t) \tilde{v}_1^*(1, t) + c_1 \tilde{v}_1(1, t) \tilde{v}_2(0, t) + \frac{c_1}{2} \tilde{v}_1^*(1, t) \tilde{v}_2(2, t) \right]$$

$$\tilde{i}_3(3, t) \approx -j3\omega_c \left[\frac{c_2}{12} \tilde{v}_1^3(1, t) + \frac{c_1}{2} \tilde{v}_1(1, t) \tilde{v}_2(2, t) \right] \quad (3.39)$$

In order to solve the system of linear differential equations of the complex envelopes in (3.32), the waveforms of the complex envelopes are sampled at M points through the time interval $(M - 1)\Delta t$, where the time step Δt is chosen appropriately. When, for example, the Backward-Euler discretization method is applied, the following iterative process results:

$$[j\mathbf{Y}'(h\omega_c) - \Delta t \cdot \mathbf{Y}(h\omega_c)] \tilde{\mathbf{v}}_n(h, t_{k+1}) = \quad (3.40)$$

$$j\mathbf{Y}'(h\omega_c) \tilde{\mathbf{v}}_n(h, t_k) - \Delta t \cdot \tilde{\mathbf{i}}_n(h, t_{k+1}),$$

$$\tilde{\mathbf{v}}_n(h, t_0) = 0,$$

$$n = 1, \dots, N, \quad h = 0, \dots, n.$$

Other higher-order integration formula can be employed with similar results, as long as the time step Δt is maintained constant. The coefficient matrices $[j\mathbf{Y}'(h\omega_c) - \Delta t \cdot \mathbf{Y}(h\omega_c)]$ are sparse and it is necessary to factorise them only once for the initial iteration. It can be observed that only four of these matrices need to be stored and factorised. Therefore, once the coefficient matrices are factorised, almost the complete simulation time is devoted to solve triangular sparse linear systems of equations. This produces a considerable reduction of the simulation time.

As it can be observed in (3.40), a constraint has been imposed that the envelope waveform starts with a zero value, without implying any loss of accuracy or generality in the distortion analysis. Since the envelope waveform presents a smooth slope and the original data sequence is usually long enough, the transient is not likely to introduce non-negligible errors in the spectral regrowth calculation.

The main limitation of this method arises from the weakly nonlinear approximation that has been made, the dynamic range of application for the EC method being affected. If we considered an amplifier circuit driven by a sinusoidal signal, it can be analysed using HB in a direct way and a very accurate prediction of the real solution will be obtained. When comparing the results with the EC method to those obtained with HB, it is observed that they show a good agreement for low input power levels, but the EC method starts to depart from the solution as the amplifier goes into the saturation region and its gain starts to compress. This happens because in the saturation region the low-order power series expansions used do not describe adequately the device behaviour. In order to overcome this limitation, Borich proposed to extend the power series expansions up to $N = 5$ in the EC method described, to increase the dynamic range and achieve a better agreement with the HB simulations at the cost of nearly doubling the computation time and storage space.

3.5 Envelope currents method with extended dynamic range

The aforementioned limitations of the EC method regarding its dynamic range may prevent the use of this efficient technique to wireless communications circuits operated with signal levels near the 1 dB compression point, for which the analysis of nonlinear distortion is really significant. In addition to this, the previous method presents a second disadvantage: due to the fact that it is based on the NC method, it presents poor convergence properties in the same manner than the latter and becomes an impractical technique when the order n increases.

In order to overcome these disadvantages and to improve the accuracy of the EC method in [18], a new current envelopes method with extended dynamic range was proposed in [19]. In the same way that in EC and NC methods, this approach is based on writing the output of the circuit as a sum of incremental voltages, but now each of these voltages is the solution of a time-varying linear circuit excited by a nonlinear current. At each step of the iterative process it is necessary to update the values of the elements of the circuit (whose topology remains unchanged), together with the nonlinear current sources. The main advantages of this technique are the good convergence properties and better accuracy than [18] that it presents. The theoretical base of this technique will be reviewed next.

For the sake of clarity, in [19] a simple circuit with a single node is considered, as it is shown in Figure 3.2. This circuit consists of a nonlinear conductance, a nonlinear capacitance, and a current source $I_s + i_s(t)$. The corresponding integro-differential

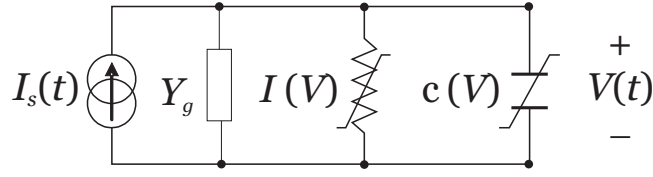


Figure 3.2: Single-node nonlinear circuit.

equation can be expressed in a symbolic way as

$$L[V(t)] + I[V(t)] + c[V(t)] \frac{dv(t)}{dt} = I_s + i_s(t), \quad (3.41)$$

where $v(t)$ is the node voltage, $I(V)$ and $I_C(V) = c(V) \frac{dv}{dt}$ are the currents flowing through the nonlinear conductance and capacitance, respectively, and $L[\cdot]$ represents an integro-differential operator accounting for the linear elements of the circuit. As in the previous section, $V(t)$ is a summation of incremental voltages plus the corresponding residual voltage

$$V = V_0 + v_1 + \dots + v_n + \delta v_n = \bar{v}_n + \delta v_n, \quad (3.42)$$

where explicit temporal dependence has been neglected to simplify notation. First, the dc voltage V_0 is calculated taking into account only the current I_s in (3.41). By expanding $I(V)$ and $c(V)$ in Taylor series about V_0 and substituting them in (3.41), the following linear equation is obtained for the first incremental voltage v_1 :

$$L[v_1] + \left[g(V_0) + c(V_0) \frac{d}{dt} \right] v_1 = i_s. \quad (3.43)$$

Note that the NC method leads to the same equation for the linear term v_1 . Therefore, the first residual voltage δv_1 satisfies the following equation:

$$L[\delta v_1] + I(v) + c(v) \frac{dv}{dt} = I(V_0) + g(V_0)v_1 + c(V_0) \frac{dv_1}{dt}. \quad (3.44)$$

Taking into account that $\delta v_1 = v_2 + \delta v_2$, the previous process is repeated, expressing the Taylor series expansions of $I(v)$ and $c(v)$ about $\bar{v}_1 = V_0 + v_1$. Similarly, the second incremental voltage v_2 can be evaluated by solving the following linear equation, which is now a time-varying equation:

$$L[v_2] + \left[g(\bar{v}_1) + c(\bar{v}_1) \frac{d}{dt} \right] v_2 = i_2, \quad (3.45)$$

with

$$i_2 = - \left[I(\bar{v}_1) + c(\bar{v}_1) \frac{d\bar{v}_1}{dt} - I(V_0) \right] + \left[g(V_0) + c(V_0) \frac{d}{dt} \right] v_1. \quad (3.46)$$

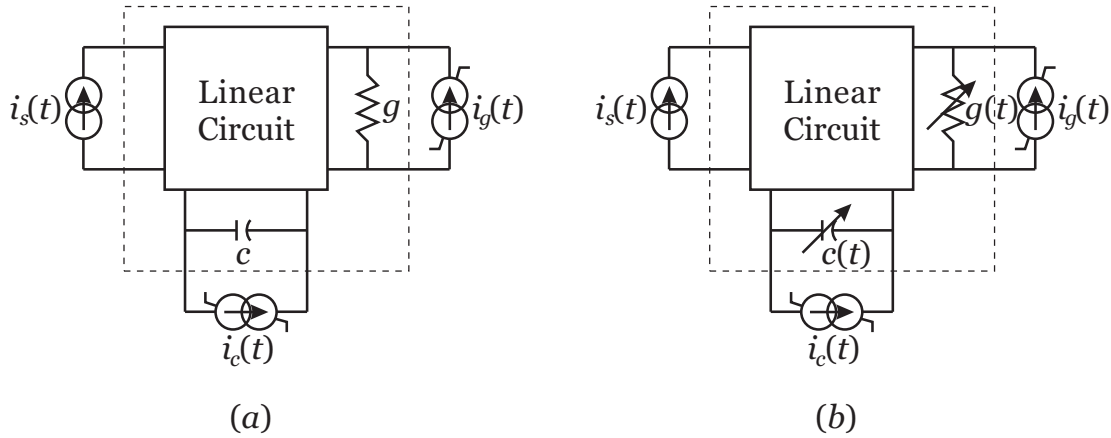


Figure 3.3: Different approaches for the simulation of microwave nonlinear circuits. (a) NC method. (b) NEC method.

It is not difficult to generalise these results, proving that each incremental voltage v_n can be calculated by solving the corresponding time-varying linear equation

$$L[v_n] + \left[g(\bar{v}_{n-1}) + c(\bar{v}_{n-1}) \frac{d}{dt} \right] v_n = i_n, \quad (3.47)$$

with

$$i_n = - \left[I(\bar{v}_{n-1}) + c(\bar{v}_{n-1}) \frac{d\bar{v}_{n-1}}{dt} - I(\bar{v}_{n-2}) - c(\bar{v}_{n-2}) \frac{d\bar{v}_{n-2}}{dt} \right] + \left[g(\bar{v}_{n-2}) + c(\bar{v}_{n-2}) \frac{d}{dt} \right] v_{n-1}. \quad (3.48)$$

Assuming that this iterative process converges, the residual voltage δv_n becomes negligible for a sufficiently high order n .

Note that this approach shares several aspects with the NC method presented in 2.5.4.2. As it is shown in Figure 3.3(a), in the NC method the components of order n are determined by solving a linear circuit with constant coefficients, extended with the linear terms of the nonlinear elements and excited by the appropriate nonlinear currents which depend on the voltages of orders lower than n . The approach followed in the NEC method is illustrated in Figure 3.3(b). With the NEC method, the same linear circuit is solved, but it is now extended with time-varying conductances and capacitances. These time-varying elements come from the linear terms of the Taylor series expansions of the nonlinearities, which are evaluated about the waveforms of the voltages computed in the previous iteration. The resulting time-varying linear circuit is excited by nonlinear currents which take into account the residuals coming from the overall current balance in the nonlinear circuit.

When the input signal is a continuous wave (CW), for each iteration, all the signals in the time-varying circuit are periodic signals. Therefore, they can be expressed as a

Fourier series and (3.47) can be rewritten in matrix notation

$$[\mathbf{Y}_g + \mathbf{G} + j\Omega\mathbf{C}] \mathbf{v}_n = \mathbf{i}_n, \quad (3.49)$$

where \mathbf{v}_n and \mathbf{i}_n are vectors containing the Fourier coefficients of $v_n(t)$ and $i_n(t)$, usually truncated for a small number of harmonics. \mathbf{G} and \mathbf{C} are Toeplitz matrices with the Fourier coefficients of the time-varying conductance and capacitance, respectively. These matrices, accounting for the relationship between the frequency-domain currents and voltages in a time-varying circuit element, are also referred to as a *conversion matrices* [8]. \mathbf{Y}_g is the admittance matrix of the linear circuit and Ω is a diagonal matrix whose elements are $[-H\omega_c, \dots, 0, \dots, H\omega_c]$ when H harmonics plus the dc component are considered. It can be observed that (3.49) is equivalent to make an iteration of HB using the Newton-Raphson algorithm, therefore it presents quadratic convergence as the latter.

For the case of digital communications signals, the signals in the circuit are quasi-periodic and can be expressed as a function of their time-varying complex envelopes. Thus, following a similar development to that presented in 3.4, the n -th incremental voltage can be expressed as

$$v_n(t) = \frac{1}{2} \sum_{h=-\infty}^{\infty} \tilde{v}_n(h, t) e^{jh\omega_c t}, \quad (3.50)$$

where both positive and negative frequencies have been considered. The rest of the variables in the circuit present similar expressions, and the admittance matrix of the circuit can be approximated by the following term:

$$\left[Y_g(h\omega_c) - jY'_g(h\omega_c) \frac{d}{dt} \right]. \quad (3.51)$$

With this, (3.47) can be rewritten as:

$$\begin{aligned} & \sum_{l=-\infty}^{\infty} e^{jl\omega_c t} \sum_{h=-\infty}^{\infty} \left\{ Y_g(h\omega_c) \delta_{hl} + \tilde{g}(l-h, t) + jh\omega_c \tilde{c}(l-h, t) + \right. \\ & \left. + [\tilde{c}(l-h, t) - jY'_g(h\omega_c) \delta_{hl}] \frac{d}{dt} \right\} \tilde{v}_n(h, t) = \sum_{l=-\infty}^{\infty} e^{jl\omega_c t} \tilde{i}_n(l, t), \end{aligned} \quad (3.52)$$

where δ_{hl} is the Kronecker delta function.

Being H the number of significant harmonics, we can define the vectors $\mathbf{v}_n(t) = [\tilde{v}_n(-H, t), \dots, \tilde{v}_n(H, t)]^T$ and $\mathbf{i}_n(t) = [\tilde{i}_n(-H, t), \dots, \tilde{i}_n(H, t)]^T$. Then, taking into account the linear independence of the exponential functions $e^{jl\omega_c t}$, it is possible to rewrite (3.52) in matrix notation as

$$\left\{ \mathbf{Y}_g + \mathbf{G}(t) + j\Omega\mathbf{C}(t) + [\mathbf{C}(t) - j\mathbf{Y}'_g] \frac{d}{dt} \right\} \mathbf{v}_n(t) = \mathbf{i}_n(t), \quad (3.53)$$

where the Toeplitz matrix $\mathbf{G}(t)$ is now time-varying and is defined from the column vector $[\tilde{g}(0, t), \dots, \tilde{g}(2H, t)]^T$. Matrix $\mathbf{C}(t)$ is analogously defined. These results can be derived alternatively by using two temporal dimensions t_1 and t_2 , following the reasoning presented in [17].

Finally, the envelope waveforms can be sampled with a time step Δt and the differential operator in (3.53) can be discretised using the Backward-Euler rule, resulting the update procedure of this method

$$\begin{aligned} \{[\mathbf{Y}_g + \mathbf{G}(k) + j\Omega\mathbf{C}(k)] \Delta t + [\mathbf{C}(k) - j\mathbf{Y}'_g]\} \mathbf{v}_n(k) = \\ = \mathbf{i}_n(k)\Delta t + [\mathbf{C}(k) - j\mathbf{Y}'_g] \mathbf{v}_n(k-1), \end{aligned} \quad (3.54)$$

where $\mathbf{C}(k)$, $\mathbf{G}(k)$ and the term in the right-hand side of the equation $\mathbf{i}_n(k)$ depend on the node voltages of the previous iterations, and all the harmonics in $\mathbf{v}_n(k-1)$ have been evaluated for $k-1$.

From equation (3.54) it can be seen that the NEC method gives slightly more complex expressions than the EC method for the incremental voltages involved in an accurate prediction of the spectral regrowth experienced by communications signals. Therefore, this method implies a trade-off between the accuracy of simulations and the computational cost. However, the complexity of solving time-varying systems is partially compensated with the reduction in the number of equations involved.

3.6 Simplified Newton method for weakly nonlinear communications circuits

One of the original contributions presented in this Thesis is the Simplified Newton method (SN) proposed in [32] for the efficient analysis of weakly nonlinear circuits driven by communications signals, which is based on the EC method. The main advantage of the proposed method is that it implies a reduction of the computation time while a good adjustment with experimental measurements is achieved. This necessity of speeding up the simulations of nonlinear communications circuits stems from the requirement of ACPR predictions, which are of great interest in design and optimization processes, but also results a very time consuming task because they are swept-power simulations. To predict ACPR, an accurate prediction of the spectral regrowth for the modulated input signal is required at each input power level. Therefore, the proposed efficient method is appropriate for the simulation of ACPR and output power of an amplifier versus input power (with a digitally-modulated input signal.)

As it has been explained in previous sections, during the last decades several techniques for the evaluation of nonlinearities in microwave circuits have been developed which can also be used for the prediction of ACPR. HB techniques using the Newton-Raphson algorithm (HB-N) or the relaxation methods (HB-R) presented in Section 2.4 are examples of very efficient simulation methods when periodic or quasi-periodic signals and general nonlinear circuits are considered [37], [38], [39]. However, in wireless communications systems the circuits are usually driven in a weakly nonlinear mode and this fact can be exploited to perform fast simulations even considering the high number of spectral lines contained in digitally modulated signals. The methods explained in Sections 3.4 and 3.5 present different approaches based on the complex envelopes of the variables of the circuit and make the approximation of a weakly nonlinear behaviour to use first-order Taylor series expansions, each of them in a different way. Both methods are more efficient for communications signals than conventional multitone HB techniques, since the use of large multidimensional frequency-domain matrices is replaced by a limited number of time-domain integrations of the complex envelopes. The EC method stands out because of its simplicity and presents better simulation times, but with a lower accuracy and more limited dynamic range.

In this section, a new approach for distortion analysis of weakly nonlinear circuits excited with RF narrowband signals will be presented, maintaining the simplicity of the reduced number of linear systems of equations employed in the EC method and achieving a further reduction in computation time. In addition to this, the proposed method can be easily extended to include fifth-order terms in order to improve the accuracy of predictions.

Following an analogous explanation to that presented in Section 3.5, let us consider the same simple nonlinear circuit with a single node used there, which contains a nonlinear conductance and a nonlinear capacitance with currents expressed in terms of the node voltage, and is driven by a single current source. The aforementioned circuit is shown again in Figure 3.4 for convenience. The voltage $V(t)$ at the node of the circuit is an incremental voltage

$$V(t) = V_0 + v_1(t) + \dots + v_n(t) + \delta v_n(t), \quad (3.55)$$

where voltage V_0 corresponds to the dc term. The power series expansions of the nonlinear current, $I(V)$, and the nonlinear charge, $q(V)$, are expressed about the dc bias point, in this case. These series expansions will be maintained for all the successive iterations. As a result, it is possible to distinguish two terms in each of the nonlinear elements: a first term which is linear to the node voltages and a second term with a nonlinear dependence on such voltages:

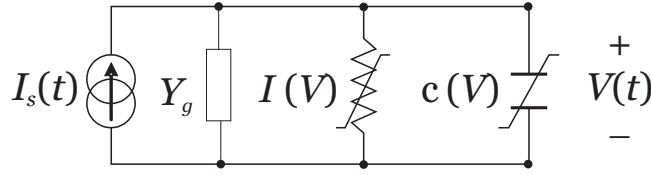


Figure 3.4: Single-node nonlinear circuit.

- For a nonlinear conductance:

$$i[v(t)] = \sum_{k=1}^{\infty} g_k v^k(t) = g_1 v(t) + i_{NL}[v(t)] \quad (3.56)$$

- For a nonlinear current source controlled by two voltages:

$$i[v(t), u(t)] = \sum_{\substack{k, l \\ k+l \geq 1}}^{\infty} g_{kl} v^k(t) u^l(t) = g_{10} v(t) + g_{01} u(t) + i_{NL}[v(t), u(t)] \quad (3.57)$$

- For a nonlinear capacitance:

$$i_c[v(t)] = \frac{d}{dt} \sum_{k=1}^{\infty} q_k v^k(t) = c_0 \frac{dv(t)}{dt} + \frac{dq_{NL}[v(t)]}{dt} \quad (3.58)$$

The node voltage in the example circuit satisfies the equation

$$L[V(t)] + I[V(t)] + \frac{dq[V(t)]}{dt} = I_s + i_s(t), \quad (3.59)$$

with $L[\cdot]$ an integro-differential operator which accounts for the linear elements of the circuit. For the dc voltage (3.59) can be solved as

$$L[V_0] + I[V_0] = I_s, \quad (3.60)$$

while the following equation applies on the rest of the incremental voltage:

$$L[v_1(t) + \delta v_1(t)] + I[v_1(t) + \delta v_1(t)] + \frac{dq[v_1(t) + \delta v_1(t)]}{dt} = i_s(t). \quad (3.61)$$

If explicit time dependence is omitted to simplify notation, the following linear equation is obtained for the first incremental voltage v_1 :

$$L[v_1] + g_1 v_1 + c_0 \frac{dv_1}{dt} = i_s. \quad (3.62)$$

Again, v_1 is calculated in the same way than the linear term of the NC method and the NEC method. The first residual voltage δv_1 satisfies the equation

$$L[\delta v_1] + g_1 \delta v_1 + i_{NL}(v) + c_0 \frac{d\delta v_1}{dt} + \frac{dq_{NL}(v)}{dt} = 0. \quad (3.63)$$

Taking into account that $\delta v_1 = v_2 + \delta v_2$, the second incremental voltage v_2 can be evaluated by solving the linear equation

$$L[v_2] + g_1 v_2 + c_0 \frac{dv_2}{dt} = i_2(\bar{v}_1) \quad (3.64)$$

with

$$i_2(\bar{v}_1) = -i_{NL}(\bar{v}_1) - \frac{dq_{NL}(\bar{v}_1)}{dt} \quad (3.65)$$

When these results are generalised, the following equation is obtained to calculate the n -th incremental voltage:

$$L[v_n] + g_1 v_n + c_0 \frac{dv_n}{dt} = i_n(\bar{v}_{n-1}) \quad (3.66)$$

with

$$i_n(\bar{v}_{n-1}) = -[i_{NL}(\bar{v}_{n-1}) - i_{NL}(\bar{v}_{n-2})] - \left[\frac{dq_{NL}(\bar{v}_{n-1})}{dt} - \frac{dq_{NL}(\bar{v}_{n-2})}{dt} \right] \quad (3.67)$$

Note that, for each iteration, the Taylor series expansions are calculated about the bias point. Therefore, for all of them the same time-invariant linear circuit is being solved, consisting of the linear elements together with the linear part of the nonlinear elements, as in the EC method. In contrast to this, the applied nonlinear currents differ from that of the NC method, because in that case the nonlinear currents expressions are obtained by neglecting all the terms with a order higher than the present iteration. The reason for this is that the NC method was proposed for the obtention of the NLTFs involved in Volterra series representations. Thus, the nonlinear currents used in the proposed approach are a better approximation to the real nonlinear currents than those of the NC method, since they consider higher order terms.

In order to obtain the incremental voltages for a general circuit with more than one node it is necessary to solve the following system of equations:

$$\bar{L}[\mathbf{v}_n] = \mathbf{i}_n, \quad n = 1, 2, \dots, N. \quad (3.68)$$

where $\bar{L}[\cdot]$ represents a general linear operator in matrix notation. This system of integro-differential equations is obtained by means of a nodal analysis of the augmented linear subcircuit. The current sources \mathbf{i}_n applied to the time-invariant linear circuit in (3.68) are as follows:

1. For the first iteration ($n = 1$), the excitation current is the original current source.
2. The nonlinear current source for the second iteration ($n = 2$) in the example of the single-node circuit of Figure 3.4 is

$$i_2 = -i_{NL}(v_1) - \frac{dq_{NL}(v_1)}{dt} = -\sum_{k=2}^{\infty} g_k v_1^k - \frac{d}{dt} \sum_{k=2}^{\infty} \frac{c_{k-1}}{k} v_1^k. \quad (3.69)$$

In a more realistic case, such as the equivalent circuit model for a FET amplifier shown in Figure 2.11 of Section 2.4.4, it is necessary to consider the nonlinear currents associated to all of the nodes, each of them involving different contributions. The term corresponding to the drain-to-source nonlinear current (I_{ds}) depends on the gate-to-source (v) and drain-to-source (u) voltages and is given by the expression

$$i_2 = -i_{NL}(v_1, u_1) = -\sum_{k=2}^{\infty} g_{k0}v_1^k - \sum_{l=2}^{\infty} g_{0l}u_1^l - \sum_{k,l=1}^{\infty} g_{kl}v_1^k u_1^l, \quad (3.70)$$

and those corresponding to the nonlinear capacitances C_{gs} and C_{gd} , which depend on a single voltage, are given by

$$i_2 = -\frac{dq_{NL}(v_1)}{dt} = -\frac{d}{dt} \sum_{k=2}^{\infty} \frac{c_{k-1}}{k} v_1^k = -\sum_{k=1}^{\infty} c_k v_1^k \frac{dv_1}{dt}. \quad (3.71)$$

These power series expansions can be extended up to the desired K -th power in order to achieve the appropriate accuracy in results.

3. In order to obtain the nonlinear current sources for the third iteration in the circuit with a single node, we recall that

$$i_3 = -[i_{NL}(v_2 + v_1) - i_{NL}(v_1)] - \left[\frac{dq_{NL}(v_2 + v_1)}{dt} - \frac{dq_{NL}(v_1)}{dt} \right]. \quad (3.72)$$

Considering that the incremental voltage $v_2(t)$ is small compared to the linear term $v_1(t)$, the exciting current can be approximated by its first-order Taylor expansion

$$\begin{aligned} i_{NL}(v_1 + v_2) &\approx i_{NL}(v_1) + \left. \frac{di_{NL}(v)}{dv} \right|_{v=v_1} \cdot v_2, \\ \frac{dq_{NL}(v_1 + v_2)}{dt} &\approx \frac{dq_{NL}(v_1)}{dt} + \frac{d}{dt} \left[\left. \frac{dq_{NL}(v)}{dv} \right|_{v=v_1} \cdot v_2 \right]. \end{aligned} \quad (3.73)$$

Therefore,

$$i_3 = -\left. \frac{di_{NL}(v)}{dv} \right|_{v=v_1} \cdot v_2 - \frac{d}{dv} \left. \frac{dq_{NL}(v)}{dt} \right|_{v=v_1} \cdot v_2 - \left. \frac{dq_{NL}(v)}{dv} \right|_{v=v_1} \cdot \frac{dv_2}{dt}. \quad (3.74)$$

4. We could generalise this procedure to obtain the nonlinear current sources for the n -th iteration

$$i_n = -\left. \frac{di_{NL}(v)}{dv} \right|_{v=v_{n-2}} \cdot v_{n-1} - \frac{d}{dv} \left. \frac{dq_{NL}(v)}{dt} \right|_{v=v_{n-2}} \cdot v_{n-1} - \left. \frac{dq_{NL}(v)}{dv} \right|_{v=v_{n-2}} \cdot \frac{dv_{n-1}}{dt}. \quad (3.75)$$

In the proposed SN method, the number of iterations for the algorithm in (3.68) are restricted to $N = 3$, relying on a weakly nonlinear behaviour.

In case a narrowband RF modulated excitation signal is applied, a procedure similar to that of [18] can be put into practice to obtain, for the n -th iteration and the h -th harmonic, the following system of linear equations for the complex envelopes of the incremental node voltages

$$\left[\mathbf{Y}(h\omega_c) - j\mathbf{Y}'(h\omega_c) \frac{d}{dt} \right] \tilde{\mathbf{v}}_n(h, t) = \tilde{\mathbf{i}}_n(h, t). \quad (3.76)$$

The expressions for $\tilde{\mathbf{i}}_n(h, t)$ in (3.76) include contributions of each nonlinear element of the circuit. As it was previously stated, for the equivalent circuit of a FET amplifier the nonlinear envelope currents include the contributions of the nonlinear current I_{ds} and the nonlinear capacitances C_{gs} and C_{gd} , being the first one the main source of nonlinear distortion [9], [21], [28], [73], [74]. Close-form expressions for the second and n -th order nonlinear envelope currents are obtained in detail in Appendix B. Since narrowband signals are being considered, we are interested in the expressions for the currents around the most significant harmonics of the carrier. For example, when the power series expansions are truncated with $K = 3$, the second-order nonlinear envelope current due to I_{ds} can be expressed around the harmonics as

$$\tilde{i}_2(0, t) = - \left[\frac{g_{20}}{2} |\tilde{v}_1(t)|^2 + \frac{g_{02}}{2} |\tilde{u}_1(t)|^2 + \frac{g_{11}}{2} \text{Re}\{\tilde{v}_1(t)\tilde{u}_1^*(t)\} \right] \quad (3.77)$$

$$\begin{aligned} \tilde{i}_2(1, t) = - \left[\frac{3g_{30}}{4} |\tilde{v}_1(t)|^2 \tilde{v}_1(t) + \frac{3g_{03}}{4} |\tilde{u}_1(t)|^2 \tilde{u}_1(t) + \frac{g_{21}}{4} \tilde{v}_1^2(t) \tilde{u}_1^*(t) + \right. \\ \left. \frac{g_{21}}{2} |\tilde{v}_1(t)|^2 \tilde{u}_1(t) + \frac{g_{12}}{4} \tilde{u}_1^2(t) \tilde{v}_1^*(t) + \frac{g_{12}}{2} |\tilde{u}_1(t)|^2 \tilde{v}_1(t) \right] \end{aligned} \quad (3.78)$$

$$\tilde{i}_2(2, t) = - \left[\frac{g_{20}}{2} \tilde{v}_1^2(t) + \frac{g_{02}}{2} \tilde{u}_1^2(t) + \frac{g_{11}}{2} \tilde{v}_1(t) \tilde{u}_1(t) \right] \quad (3.79)$$

$$\tilde{i}_2(3, t) = - \left[\frac{g_{30}}{4} \tilde{v}_1^3(t) + \frac{g_{03}}{4} \tilde{u}_1^3(t) + \frac{g_{21}}{4} \tilde{v}_1^2(t) \tilde{u}_1(t) + \frac{g_{12}}{4} \tilde{u}_1^2(t) \tilde{v}_1(t) \right] \quad (3.80)$$

And the analogous expressions due to the nonlinear capacitances C_{gs} and C_{gd} truncated with $K = 2$ (corresponding to third order) are

$$\tilde{i}_2(0, t) \approx 0 \quad (3.81)$$

$$\tilde{i}_2(1, t) \approx -j\omega \frac{C_2}{4} |\tilde{v}_1(t)|^2 \tilde{v}_1(t) \quad (3.82)$$

$$\tilde{i}_2(2, t) \approx -j\omega \frac{C_1}{2} \tilde{v}_1^2(t) \quad (3.83)$$

$$\tilde{i}_2(3, t) \approx -j\omega \frac{C_2}{4} \tilde{v}_1^3(t) \quad (3.84)$$

where the non-significant terms have been neglected.

Once the complex envelopes of the nonlinear currents have been determined, all the waveforms can be sampled with a time step Δt and the Backward-Euler discretization method can be used to solve the system of equations (3.76) for each iteration and each harmonic

$$[j\mathbf{Y}'(h\omega_c) - \Delta t \cdot \mathbf{Y}(h\omega_c)] \tilde{\mathbf{v}}_{\mathbf{n}}(h, t_{k+1}) = j\mathbf{Y}'(h\omega_c)\tilde{\mathbf{v}}_{\mathbf{n}}(h, t_k) - \Delta t \cdot \tilde{\mathbf{i}}_{\mathbf{n}}(h, t_{k+1}). \quad (3.85)$$

Furthermore, this procedure can be extended to include more harmonics and higher-order terms in the power series expansions of the nonlinear currents by applying (3.85) for $n = 1, \dots, N-1$ and $h = 0, \dots, H$, whereas in the last iteration ($n = N$), it is necessary to apply (3.85) only for $h = 1$, since just the fundamental frequency needs to be considered for in-band responses.

In order to illustrate the efficiency of the proposed approach, a comparison with the EC method can be made in a theoretical way. In terms of the algebraic set of equations to solve, the EC method can be considered a suboptimal method, since those terms with an order higher than n are being neglected in the right-hand side of the equation. However, the proposed method implements an iterative process based on a Simplified Newton algorithm, where the Jacobian is determined for the initial dc iteration and then reused for the rest of iterations. The reutilization of the Jacobian relies on the fact that, if the circuit is behaving near-linearly as it has been assumed, the Jacobian does not vary much from iteration to iteration. Therefore, the convergence of the proposed method results slightly slower than in the Newton-Raphson algorithm, but the computational cost of each iteration is much smaller, so on the whole a reduction in the computation time is accomplished.

On the other hand, the Simplified Newton approach presents as its main drawback a reduced convergence region causing that, if the initial solution of the iterative process is not close enough to the actual solution, there is a possibility that the method will not converge. That is, if the nonlinear circuit being studied presents a strongly nonlinear behaviour, the convergence of this method is not guaranteed. Nevertheless, some results will be shown in Chapter 4 in which a satisfactory prediction of the nonlinear behaviour of an amplifier has been achieved with a power level near the 1 dB compression point, where it exhibits a mildly nonlinear behaviour, demonstrating that this restriction is not excessively strict.

Comparing also in terms of the circuit to be analysed, the idea of reusing the Jacobian results in the fact that both approaches solve the same time-invariant linear subcircuit with different exciting current sources for each iteration. For the first iteration, both approaches use the original sources, therefore the voltages obtained in the

first iteration are the same for the proposed method and the EC method. The main difference between both approaches are the expressions for the second-iteration nonlinear sources. In the EC method the second-iteration nonlinear current sources are given by the power series expansions in (3.70) with $K = 2$, whereas the proposed method extends these power series expansions for several orders. In other words, the nonlinear current sources used in the proposed method are a better approximation for the real nonlinearity, which leads to a solution for the second iteration closer to the final solution than the one produced by the EC method. In addition to this, subsequent iterations for both approaches will produce a further reduction of the error, so that the advantage of the proposed method, obtained in the solution of the second iteration, is expected to be increased for the remainder iterations.

For example, a comparison of the expressions proposed for the second-order nonlinear currents in the EC and SN methods are presented in Table 3.1 for the case of the nonlinear contribution of the I_{ds} current of a FET amplifier. It can be observed that the SN method includes higher-order terms, which gives a better approximation of the real nonlinearity for the envelope currents.

Finally, it is worth noticing that, in this method, an incremental node voltage for the complex envelope in the fundamental frequency zone can be obtained from the second iteration. Consequently, it is necessary to solve only two linear systems of equations to get a first correction to the linear prediction for the in-band complex envelope response. Furthermore, the good agreement between calculated and measured spectral regrowth allows a reliable prediction of ACPR, even with only two iterations.

Table 3.1: Comparison between the second-order nonlinear currents for the EC method and SN approach

Frequency zone	EC method	SN approach
$h = 0$	$\tilde{i}_2(0, t) = \frac{g_{20}}{2} \tilde{v}_{gs_1}(t) ^2 + \frac{g_{02}}{2} \tilde{v}_{ds_1}(t) ^2 + \frac{g_{11}}{2} \text{Re} [\tilde{v}_{gs_1}(t) \tilde{v}_{ds_1}^*(t)]$	$\tilde{i}_2(0, t) = \frac{g_{20}}{2} \tilde{v}_{gs_1}(t) ^2 + \frac{g_{02}}{2} \tilde{v}_{ds_1}(t) ^2 + \frac{g_{11}}{2} \text{Re} [\tilde{v}_{gs_1}(t) \tilde{v}_{ds_1}^*(t)]$
$h = 1$	-	$\tilde{i}_2(1, t) = \frac{3g_{30}}{4} \tilde{v}_{gs_1}(t) ^2 v_{gs_1} + \frac{3g_{03}}{4} \tilde{v}_{ds_1}(t) ^2 v_{ds_1} + \frac{g_{21}}{4} [\tilde{v}_{gs_1}^2(t) v_{ds_1}^*(t) + 2 \tilde{v}_{gs_1}(t) ^2 v_{ds_1}(t)] + \frac{g_{12}}{4} [\tilde{v}_{ds_1}^2(t) v_{gs_1}^*(t) + 2 \tilde{v}_{ds_1}(t) ^2 v_{gs_1}(t)]$
$h = 2$	$\tilde{i}_2(2, t) = \frac{g_{20}}{2} \tilde{v}_{gs_1}^2(t) + \frac{g_{02}}{2} \tilde{v}_{ds_1}^2(t) + \frac{g_{11}}{2} \tilde{v}_{gs_1}(t) \tilde{v}_{ds_1}(t)$	$\tilde{i}_2(2, t) = \frac{g_{20}}{2} \tilde{v}_{gs_1}^2(t) + \frac{g_{02}}{2} \tilde{v}_{ds_1}^2(t) + \frac{g_{11}}{2} \tilde{v}_{gs_1}(t) \tilde{v}_{ds_1}(t)$
$h = 3$	-	$\tilde{i}_2(3, t) = \frac{g_{30}}{4} \tilde{v}_{gs_1}^3(t) + \frac{g_{03}}{4} \tilde{v}_{ds_1}^3(t) + \frac{g_{21}}{4} \tilde{v}_{gs_1}^2(t) v_{ds_1}(t) + \frac{g_{12}}{4} \tilde{v}_{gs_1}(t) v_{ds_1}^2(t)$

3.7 Envelope Currents methods for communications signals in mixers

3.7.1 Introduction

In this section, we will present two new methods proposed in [46] and [33] to evaluate nonlinear distortion in mixers to which communication signals are applied as excitations. Similarly to other methods previously treated in this chapter, these approaches are based on complex envelope representation. The main difference is that they are particularised for mixers, which are strongly nonlinear devices.

The nonlinear analysis of mixers is one of the most demanding tasks in microwave circuits simulations. These difficulties are attributed to two common characteristics of mixers. First, mixers are strongly nonlinear devices regarding the local oscillator source; the mixing process itself involves a strongly nonlinear behaviour. Secondly, the spectra of the signals appearing in mixers are complicated. Therefore, the algorithms used to solve the nonlinear equations of these circuits usually converge slowly, each iteration implies a high computational cost and storage necessities are significant. In addition to this, the need for computational resources increases for the case of mixers excited by modulated RF signals, making standard HB techniques inefficient.

For microwave mixers, the local oscillator (LO) power is usually much higher than the input signal power. This situation leads to the idea that the input excitation can be considered as a perturbation about the response to the LO; therefore, each of the nonlinear elements of the circuit can be described by means of a low-order power series expansion about the LO solution. This is similar to say that the incremental I/V or Q/V characteristics of the nonlinear elements are weakly nonlinear. Note that it does not imply assuming that the nonlinear device is weakly nonlinear; instead, it means that the element is weakly nonlinear for small deviations from its instantaneous large-signal voltage. Virtually all nonlinear solid-state devices meet this condition, as long as they are not driven into saturation by the small-signal excitation.

An example of these procedures applied to the analysis of mixers is that proposed in the landmark paper [40], where Egami employed a first-order expansion to study the response of a mixer to a single tone signal. Later, Maas [41] extended Egami's method for two-tone intermodulation analysis. In [41], HB is used for the analysis of the LO and time-varying Volterra series (TV-VS) for the small-signal analysis. This procedure was also used in [200] to calculate two-tone intermodulation in a FET mixer. A generalization of the TV-VS for the analysis of systems with two input ports was presented in [42], and an extension to the TV-VS was presented in [43] for the

analysis of narrowband modulated signals in mixers considering a discretised input with 61 components. However, the random nature of the digital data recommends simulating long symbol sequences and, consequently, about hundreds of thousands frequency components are involved. In [44], Borich proposed a method to efficiently analyse mixers with narrowband modulated signals following the principles of his EC method. In [45], Thodesen proposed a method referred to as *Parametric Harmonic Balance* that presents important savings in time and memory with respect to HB using a Newton algorithm, yet showing a strong convergence.

The technique based on seeking only the small-signal output in problems where the input excitation can be considered as a perturbation about the response to a large sinusoidal signal is referred to as *large-signal/small-signal analysis* or *conversion matrix analysis* [8]. The large-signal/small-signal analysis involves first analysing the non-linear device under large-signal excitation only, usually by the HB method. The non-linear elements in the equivalent circuit of the device are then linearised to create small-signal, time-varying elements, and finally a small-signal analysis is performed.

3.7.1.1 Parametric Harmonic Balance

Parametric Harmonic Balance (PHB) is a variant of standard HB proposed by Thodesen in [45], which retains the advantages of standard HB but also exploits the weakly nonlinear behaviour usually presented by the mixer with respect to one of its input signals. PHB employs the technique of large-signal/small-signal analysis and splits HB into two stages: one to compute the response to the large periodic signal of the LO alone, and a second stage to compute the response to the input viewed as a perturbation from the solution previously computed in the first stage. Different HB algorithms are employed for each stage, exploiting the strongly nonlinear nature for the large signal and the weakly nonlinear nature for the small signal. The advantage of this method is that equations are solved for significantly fewer frequencies in the first stage when the convergence is more difficult. In addition, the information generated in the first stage can be used to accelerate the second one.

The PHB method is used to solve the usual system of equations that stems from a HB analysis

$$\mathbf{F}(\mathbf{V}) = \mathbf{I} + \mathbf{YV} + j\Omega\mathbf{Q} + \mathbf{I}_G = \mathbf{0}. \quad (3.86)$$

where two inputs are considered

$$\mathbf{I} = \mathbf{I}_0 + \mathbf{I}_s, \quad (3.87)$$

\mathbf{I}_0 representing the LO signal to which the circuit responds in a strongly nonlinear way, and \mathbf{I}_s representing the input signal to which the circuit responds in a weakly

nonlinear fashion. The circuit is considered to produce the output voltage $\mathbf{V} = \mathbf{V}_0 + \mathbf{V}_s$, and each of these two contributions is calculated in a different stage.

For the first stage, the input signal is neglected and the circuit responds with \mathbf{V}_0 when only \mathbf{I}_0 is applied. It is assumed that \mathbf{I}_0 , and therefore \mathbf{V}_0 , are periodic. The problem at this stage is solved by using an HB-N method, where the Jacobian matrix $\mathbf{J}_F(\mathbf{V})$ is updated for each iteration, being its elements

$$\frac{\partial F_n(h)}{\partial V_m(l)} = Y_{n,m}(h, l) + jh\omega_c \frac{\partial Q_n(h)}{\partial V_m(l)} + \frac{\partial I_{G_n}(h)}{\partial V_m(l)}, \quad (3.88)$$

with h and l indices for the harmonics. In the first stage of PHB, the double of the usual number of harmonics, $2H$, is considered in order to achieve less aliasing error in the DFT and a better convergence for subsequent steps in the analysis.

For the second stage, a two-tone signal is considered with a total of M harmonics. The response to the LO voltage \mathbf{V}_0 is assumed to be known, therefore the expressions for the nonlinear elements in the circuit are linearised about this known voltage

$$\bar{\mathbf{Q}}(\mathbf{V}_s, m) = \bar{\mathbf{Q}} \left(\begin{bmatrix} V_1 \\ V_2 \\ \vdots \\ V_M \end{bmatrix}, m \right) = \mathbf{Q} \left(\begin{bmatrix} V_0 + V_1 \\ V_2 \\ \vdots \\ V_M \end{bmatrix}, m \right) - \mathbf{Q} \left(\begin{bmatrix} V_0 \\ 0 \\ \vdots \\ 0 \end{bmatrix}, m \right) \quad (3.89)$$

and the same applies to $\bar{\mathbf{I}}_G(\mathbf{V}_s, m)$. This change causes the circuit to become a parametric circuit. The HB error function in the second stage can be written as:

$$\mathbf{F}(\mathbf{V}_s, m) = \mathbf{I}(m) + \mathbf{Y}(m, m)\mathbf{V} + jm\omega_m \bar{\mathbf{Q}}(\mathbf{V}_s, m) + \bar{\mathbf{I}}_G(\mathbf{V}_s, m) = \mathbf{0}, \quad (3.90)$$

$$m = 1, \dots, M,$$

where a block Gauss-Seidel relaxation method is applied, which implies that each harmonic is analysed separately. In addition to this, the Jacobian matrix is reused for the second stage by using a Simplified Newton algorithm. The motivation for doing these simplifications is the assumption that the circuit is weakly nonlinear for the small signal. Finally, the algorithm that describes the second stage is given by

$$\mathbf{V}_m^{(i+1)} = \mathbf{V}_m^{(i)} - \mathbf{J}_F^{-1} \left(\mathbf{V}_s^{(0)}, m, m \right) \cdot \mathbf{F} \left(\begin{bmatrix} V_1^{(i+1)} & \dots & V_{m-1}^{(i+1)} & V_m^{(i)} & \dots & V_M^{(i)} \end{bmatrix}^T, m \right), \quad (3.91)$$

$$m = 1, \dots, M,$$

where

$$\mathbf{J}_F \left(\mathbf{V}_s^{(0)}, m, m \right) = \mathbf{Y}(m, m) + jm\omega_m \frac{\partial \bar{\mathbf{Q}} \left(\mathbf{V}_s^{(0)}, m \right)}{\partial \mathbf{V}(m)} + \frac{\partial \bar{\mathbf{I}}_G \left(\mathbf{V}_s^{(0)}, m \right)}{\partial \mathbf{V}(m)}. \quad (3.92)$$

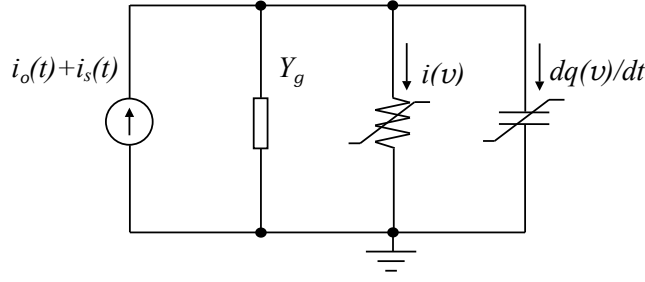


Figure 3.5: Single-node nonlinear circuit driven as a mixer.

The required memory to store the Jacobian matrix of a circuit with N nodes when using the HB-N algorithm is $\mathcal{O}(N \times ((2H + 1)(2M + 1))^2)$, whilst that of PHB is $\mathcal{O}(N \times (2H + 1)^2(2M + 1))$. Furthermore, the number of operations needed for factoring the Jacobian matrix in HB-N is $\mathcal{O}(KN \times ((2H + 1)(2M + 1))^3)$, being K the number of times the Jacobian has to be loaded and factorised, whereas that of the PHB is $\mathcal{O}(N \times (2H + 1)^3(2M + 1))$. Therefore, a significant reduction of the computational cost can be achieved compared to that of the standard two-tone HB, particularly if we consider the operations needed for factoring the Jacobian and the need to recalculate it for each iteration. This is the reason why one of the proposed approaches is based on the PHB method.

3.7.2 Description of the procedure

In order to explain the theoretical foundations of the proposed method, the simple single-node nonlinear circuit shown in Figure 3.5 will be considered. This circuit represents an hypothetical mixer and is analogous to the example employed in Section 3.5, consisting of a nonlinear conductance and a nonlinear capacitance. In contrast to the aforementioned example, the mixer circuit is driven by two independent current sources: the LO signal $i_o(t)$ including dc bias, which is assumed to be sinusoidal, and the RF signal $i_s(t)$. In that case, the node voltage $v(t)$ must satisfy the following equation

$$L[v(t)] + i[v(t)] + \frac{dq[v(t)]}{dt} = i_o(t) + i_s(t), \quad (3.93)$$

where the operator $L[\cdot]$ stands for the integro-differential equation representing the linear subcircuit, denoted in the frequency domain by admittance Y_g in Figure 3.5.

First, as it was considered in Sections 3.5 and 3.6, the node voltage $v(t)$ will be expressed as a sum of incremental voltages

$$v(t) = v_0(t) + v_1(t) + \cdots + v_n(t) + \delta v_n(t) = \bar{v}_n(t) + \delta v_n(t), \quad (3.94)$$

where $\bar{v}_n(t)$, $v_n(t)$ and $\delta v_n(t)$, for $n \geq 1$, are the approximate node voltage, the incremental voltage and the residual voltage in the n -th iteration, respectively. Voltage $v_0(t)$ is the solution of (3.93) when only the LO source $i_o(t)$ is present, i.e.

$$L[v_0] + i(v_0) + \frac{dq(v_0)}{dt} = i_o. \quad (3.95)$$

The explicit temporal dependence has been omitted for simplicity. This way, the number of frequencies to be considered is drastically reduced and the convergence using HB-N does not require an special effort. Let us suppose that v_0 is known. If we substitute $v = v_0 + v_1 + \delta v_1$ in (3.93) and expand $i(v)$ and $q(v)$ in Taylor series about v_0 retaining only the linear terms, $g(v_0) = di/dv|_{v=v_0}$ and $c(v_0) = dq/dv|_{v=v_0}$ respectively, the following equation for the first incremental voltage is obtained:

$$L[v_1] + g(v_0)v_1 + \frac{d}{dt} [c(v_0)v_1] = i_s. \quad (3.96)$$

It is worth noticing that the assumption of a very large LO with respect to the RF input is not necessary. Equation (3.96) represents a quasi-periodically time-varying linear system, for which the solution can be obtained by using the concept of conversion matrix [8]. Since this is a well-known method, v_1 and $\bar{v}_1 = v_0 + v_1$ are assumed to be known.

In the following sections, two different approaches will be presented in order to carry out the subsequent iterations for $n \geq 2$, originating two different methods to evaluate nonlinear distortion in mixers to which communication signals are applied as excitations.

3.7.2.1 NEC method for communications signals in mixers

The new method explained in this section was proposed in [46] and comes from an analogous development to that of Borich in [44] in order to extend the NEC method presented in 3.5 to the analysis of digitally-modulated signals in mixers, exploiting its good convergence properties. In the following explanation, this method will be referred to as NEC-M. The main advantage of this method versus multitone HB or the method proposed by Borich is a reduction in simulation time and a more efficient use of the computational resources.

For iterations from the second incremental voltage on, the NEC-M method differs from previously used methods for the analysis of time-varying circuits [41], [200], [43]. As mentioned in Section 3.5, the NEC method consists in updating the node voltage, $\bar{v}_1 = v_0 + v_1$, and expanding $I(v)$ and $c(v)$ in Taylor series about this voltage. Then, the second incremental voltage satisfies the equation

$$L[v_2] + g(\bar{v}_1)v_2 + \frac{d}{dt} [c(\bar{v}_1)v_2] = i_2(\bar{v}_1), \quad (3.97)$$

where

$$\begin{aligned} i_2(\bar{v}_1) &= i_0 + i_s - L[\bar{v}_1] - i(\bar{v}_1) - \frac{dq(\bar{v}_1)}{dt} = \\ &= \left\{ g(v_0)v_1 + \frac{d}{dt} [c(v_0)v_1] \right\} - \left[i(\bar{v}_1) - i(v_0) + \frac{dq(\bar{v}_1)}{dt} - \frac{dq(v_0)}{dt} \right]. \end{aligned} \quad (3.98)$$

Repeating this steps for each subsequent iteration, the following equation can be deduced for the n -th incremental voltage:

$$L[v_n] + g(\bar{v}_{n-1})v_n + \frac{d}{dt} [c(\bar{v}_{n-1})v_n] = i_n(\bar{v}_{n-1}), \quad (3.99)$$

where

$$\begin{aligned} i_n(\bar{v}_{n-1}) &= i_0 + i_s - L[\bar{v}_{n-1}] - i(\bar{v}_{n-1}) - \frac{dq(\bar{v}_{n-1})}{dt} = \\ &= \left\{ g(\bar{v}_{n-2})v_{n-1} + \frac{d}{dt} [c(\bar{v}_{n-2})v_{n-1}] \right\} - \left[i(\bar{v}_{n-1}) - i(\bar{v}_{n-2}) + \frac{dq(\bar{v}_{n-1})}{dt} - \frac{dq(\bar{v}_{n-2})}{dt} \right]. \end{aligned} \quad (3.100)$$

Equivalently, node voltage \bar{v}_n can be calculated by solving

$$L[\bar{v}_n] + g(\bar{v}_{n-1})\bar{v}_n + \frac{d}{dt} [c(\bar{v}_{n-1})\bar{v}_n] = \bar{i}_n(\bar{v}_{n-1}), \quad (3.101)$$

if the circuit is excited with the current

$$\bar{i}_n(\bar{v}_{n-1}) = i_0 + i_s + \left\{ g(\bar{v}_{n-2})\bar{v}_{n-1} + \frac{d}{dt} [c(\bar{v}_{n-2})\bar{v}_{n-1}] \right\} - \left[i(\bar{v}_{n-1}) + \frac{dq(\bar{v}_{n-1})}{dt} \right]. \quad (3.102)$$

The problem of computing v_2 consist in solving the same time-varying linear equation of the iteration given by (3.96), linearised about the new node voltage waveform \bar{v}_1 . However, this problem cannot be solved by directly using conversion matrices because now the updated voltage is not periodic in contrast to v_0 .

In the case of a RF modulated input, the exciting current has the form

$$i_s(t) = \text{Re}\{\tilde{i}_s(t)e^{j(\omega_c+\omega_o)t}\} \quad (3.103)$$

where ω_c and ω_o , which are assumed to be incommensurate frequencies, are the LO and intermediate (IF) frequencies, respectively. It is considered that the bandwidth of $i_s(t)$ is small compared to its carrier frequency. The circuit variables are quasi-periodic waveforms, being a multivariate representation of all the waveforms. In this case, the samples of the waveforms and their Fourier coefficients are related by a two-dimensional DFT. Moreover, the Fourier coefficients are time-varying, representing complex modulation of the frequency components. Therefore, the n -th incremental voltage v_n can be written as:

$$v_n(t) = \frac{1}{2} \sum_{h,m} \tilde{v}_n(h, m, t) e^{j(h\omega_c+m\omega_o)t}, \quad (3.104)$$

and similar expressions are valid for \bar{v}_{n-1} , $I(\bar{v}_{n-1})$, $g(\bar{v}_{n-1})$ and $c(\bar{v}_{n-1})$. Substituting in (3.99) and following a similar procedure to that of the single-input case, the solution can be obtained by solving the following matrix equation:

$$\left\{ \mathbf{Y}_g + \mathbf{G}(t) + j\Omega\mathbf{C}(t) + [\mathbf{C}(t) - j\mathbf{Y}'_g] \frac{d}{dt} \right\} \mathbf{v}_n(t) = \mathbf{i}_n(t). \quad (3.105)$$

For the proposed method, the weakly nonlinear approximation will be assumed. In this case, sufficient convergence will be achieved with a few iterations. For instance, in [33] good results have been obtained with only $n = 2$. Although equation (3.105) is similar to the one obtained for a single input, the differences are important. Here $\mathbf{v}_n(t)$ is defined as

$$\mathbf{v}_n = \begin{bmatrix} \tilde{v}_n(-H, -M, t), & \dots, & \tilde{v}_n(-H, M, t) \\ \tilde{v}_n(-H + 1, -M, t), & \dots, & \tilde{v}_n(-H + 1, M, t) \\ \vdots & & \vdots \\ \tilde{v}_n(H, -M, t), & \dots, & \tilde{v}_n(H, M, t) \end{bmatrix}^T, \quad (3.106)$$

and a similar definition is made for $\mathbf{i}_2(t)$, thus they are column vectors with $(2H + 1) \times (2M + 1)$ rows, where H and M refer to the relevant LO and IF harmonics, respectively. Another difference is that $\mathbf{G}(t)$ is a time-varying matrix which is constructed as a Toeplitz-likewise matrix

$$\mathbf{G}(t) = \begin{pmatrix} \mathbf{G}(0, t) & \mathbf{G}(-1, t) & \dots & \mathbf{G}(-2M, t) \\ \mathbf{G}(1, t) & \mathbf{G}(0, t) & \dots & \mathbf{G}(-M + 1, t) \\ \vdots & \vdots & \ddots & \vdots \\ \mathbf{G}(2M, t) & \mathbf{G}(2M - 1, t) & \dots & \mathbf{G}(0, t) \end{pmatrix} \quad (3.107)$$

whose elements $\mathbf{G}(m, t)$ are original Toeplitz matrices defined from the column vectors $[\tilde{g}(0, m, t), \dots, \tilde{g}(2H, m, t)]^T$, for $m = 0, \dots, 2M$. Matrix $\mathbf{C}(t)$ is constructed in a similar way. Besides, \mathbf{Y}_g and Ω are block diagonal matrices defined as

$$\mathbf{Y}_g = \text{diag}\{\mathbf{Y}_g(-M), \dots, \mathbf{Y}_g(M)\}, \quad (3.108)$$

$$\Omega = \text{diag}\{\Omega(-M), \dots, \Omega(M)\}. \quad (3.109)$$

Evaluation of $\mathbf{i}_n(t)$ in (3.105) requires a two-dimensional inverse discrete transformation, IDFT, in order to obtain samples of \bar{v}_{n-1} in a bi-dimensional grid (t_1, t_2) , at each instant t . Evaluating $i(\bar{v}_{n-1})$ and $q(\bar{v}_{n-1})$ at these points and recalling that these functions can also be expressed by means of similar expressions to (3.104), the corresponding coefficients $\tilde{i}(h, m, t)$ and $\tilde{q}_n(h, m, t)$ are derived with a two-dimensional discrete Fourier transform. That is to say, for each instant t ,

$$\begin{aligned} \mathbf{i}(\bar{\mathbf{v}}_n) &= \mathcal{F}_D\{i(\mathcal{F}_D^{-1}\{\bar{\mathbf{v}}_n\})\}, \\ \mathbf{q}(\bar{\mathbf{v}}_n) &= \mathcal{F}_D\{q(\mathcal{F}_D^{-1}\{\bar{\mathbf{v}}_n\})\}. \end{aligned} \quad (3.110)$$

The increase in complexity with respect to the single input case is evident. Nevertheless, we should clarify that the weakly nonlinear approximation allows to consider only a few IF harmonics and, in consequence, M is not high. Finally, equation (3.105) need to be solved discretising the differential operator with the Backward-Euler rule in order to obtain the update procedure of the proposed method.

3.7.2.2 Extended PHB approach for communication signals in mixers

In this section, an extension of the Parametric Harmonic Balance (E-PHB) proposed in [33] to efficiently analyse mixers excited by communications signals will be explained. The aim of this new approach is to achieve a further reduction of the computational cost with respect to the method presented in the previous section.

The E-PHB approach is based on the consideration that, from the second incremental voltage on, iterations can be carried out by maintaining the expansion of $i(v)$ and $q(v)$ about v_0 . This implies that the same time-varying linear equation (3.96), with an appropriate excitation current, is solved to obtain the corresponding incremental voltage. This procedure is equivalent to a Simplified Newton algorithm in which the Jacobian matrix of the first iteration is reused in the following steps, so that it can be conceived as an extension of PHB [45] for the case of signals with time-varying Fourier coefficients in a quasiperiodic manner.

Substraction of (3.95) and (3.96) from (3.93) yields the equation of the residual voltage δv_1

$$L[\delta v_1] + g(v_0)\delta v_1 + i_{NL}(v) + \frac{d}{dt}[c(v_0)\delta v_1] + \frac{dq_{NL}(v)}{dt} = 0, \quad (3.111)$$

where $i_{NL}(v)$ and $\frac{dq_{NL}(v)}{dt}$ are the residual nonlinear terms in the expansion of $i(v)$ and $\frac{dq(v)}{dt}$ about v_0 . Recalling that $\delta v_1 = v_2 + \bar{v}_1$, after substitution in (3.111) and some rearrangement of terms dependent on \bar{v}_1 , the following equation for the incremental voltage v_2 is derived:

$$L[v_2] + g(v_0)v_2 + i_{NL}(\bar{v}_1) + \frac{d}{dt}[c(v_0)v_2] + \frac{dq_{NL}(\bar{v}_1)}{dt} = 0. \quad (3.112)$$

Expansion of $i(\bar{v}_1)$ and $\frac{dq(\bar{v}_1)}{dt}$ about v_0 allows to write

$$L[v_2] + g(v_0)v_2 + \frac{d}{dt}[c(v_0)v_2] = i_2(\bar{v}_1), \quad (3.113)$$

with

$$i_2(\bar{v}_1) = i_0 + i_s - L[\bar{v}_1] - i(\bar{v}_1) - \frac{dq(\bar{v}_1)}{dt} = \quad (3.114)$$

$$= \left\{ g(v_0)v_1 + \frac{d}{dt} [c(v_0)v_1] \right\} - \left[i(\bar{v}_1) - i(v_0) + \frac{dq(\bar{v}_1)}{dt} - \frac{dq(v_0)}{dt} \right].$$

Adding the contributions of equations (3.95) and (3.96), an alternative procedure to the previous expressions can be found which solves directly the node voltage \bar{v}_2 by using the following equations:

$$L[\bar{v}_2] + g(v_0)\bar{v}_2 + \frac{d}{dt} [c(v_0)\bar{v}_2] = \bar{i}_2(\bar{v}_1), \quad (3.115)$$

$$\bar{i}_2(\bar{v}_1) = i_0 + i_s + \left\{ g(v_0)\bar{v}_1 + \frac{d}{dt} [c(v_0)\bar{v}_1] \right\} - \left[i(\bar{v}_1) + \frac{dq(\bar{v}_1)}{dt} \right]. \quad (3.116)$$

These results can be generalised concluding that, for each iteration, the incremental voltage v_n (with $n > 1$) is obtained by exciting the time-varying linear circuit described by (3.96) and (3.113) with the current

$$\begin{aligned} i_n(\bar{v}_{n-1}) &= i_0 + i_s - L[\bar{v}_{n-1}] - i(\bar{v}_{n-1}) - \frac{dq(\bar{v}_{n-1})}{dt} = \\ &= \left\{ g(v_0)v_{n-1} + \frac{d}{dt} [c(v_0)v_{n-1}] \right\} - \left[i(\bar{v}_{n-1}) - i(\bar{v}_{n-2}) + \frac{dq(\bar{v}_{n-1})}{dt} - \frac{dq(\bar{v}_{n-2})}{dt} \right]. \end{aligned} \quad (3.117)$$

Equivalently, node voltage \bar{v}_n can be calculated if the same circuit is excited with the current

$$\bar{i}_n(\bar{v}_{n-1}) = i_0 + i_s + \left\{ g(v_0)\bar{v}_{n-1} + \frac{d}{dt} [c(v_0)\bar{v}_{n-1}] \right\} - \left[i(\bar{v}_{n-1}) + \frac{dq(\bar{v}_{n-1})}{dt} \right]. \quad (3.118)$$

The excitation (3.118) of the augmented time-varying linear circuit is calculated with the difference between the current sources and the currents through the remaining nonlinearities evaluated at the previous node voltage. Alternatively, the incremental voltage can be computed instead if the excitation current is calculated with (3.117), i.e. the difference between the current sources and the current through the original nonlinear circuit, evaluated at the same previous node voltage. In both cases $i(v)$ and $q(v)$ should be updated.

In the case of an RF modulated input, the exciting current has the form of (3.103). Using a two-dimensional DFT like in the previous section, all variables can be written in terms of time-varying Fourier coefficients. Some simplifications can be made with respect to the procedure proposed in the NEC-M method. Variables $g(v_0)$ and $c(v_0)$ have constant coefficients with nonzero values only for $m = 0$, which represents the LO fundamental and harmonic frequencies. Recalling (3.96), the spectrum of the incremental voltage v_1 is proportional to the spectrum of $i_s(t)$ shifted by the LO harmonics and the coefficients are nonzero only for frequencies $h\omega_c \pm \omega_o$. Actually, it is just necessary to consider a subset of the coefficients involved in (3.104), i.e. those terms with $|h| \leq H$ and $0 \leq m \leq M$, since the rest of the terms can be obtained by complex

conjugation. This alternative represents taking the upper-sideband terms regarding the IF. Accordingly, the coefficients of v_n are obtained by solving the matrix equation

$$\left\{ \mathbf{Y}_g(m) + \mathbf{G} + j\Omega(m)\mathbf{C} + [\mathbf{C} - j\mathbf{Y}'_g(m)] \frac{d}{dt} \right\} \mathbf{v}_n(m, t) = \mathbf{i}_n(m, t), \quad (3.119)$$

for $m = 0, \dots, M$. Note that a relaxation algorithm has been employed producing a similar approach to the block Gauss-Jacobi-Newton method, where each harmonic m of the IF is analysed independently. The following definitions have been used:

$$\mathbf{v}_n(m, t) = [\tilde{v}_n(-H, m, t), \tilde{v}_n(-H + 1, m, t), \dots, \tilde{v}_n(H, m, t)]^T, \quad (3.120)$$

similarly for $\mathbf{i}_n(m, t)$,

$$\mathbf{Y}_g(m) = \text{diag}\{Y_g(-H, m, t), \dots, Y_g(H, m, t)\}, \quad (3.121)$$

and

$$\Omega(m) = \text{diag}\{-H\omega_c + m\omega_o, \dots, H\omega_c + m\omega_o\}. \quad (3.122)$$

\mathbf{G} is a Toeplitz matrix defined from the vector of the Fourier coefficients of $g(v_0)$, with a similar definition for \mathbf{C} . Recall that evaluation of $\mathbf{i}(\bar{\mathbf{v}}_n)$ requires two-dimensional inverse and direct DFTs as follows:

$$\mathbf{i}(\bar{\mathbf{v}}_n) = \mathcal{F}_D\{i(\mathcal{F}_D^{-1}\{\bar{\mathbf{v}}_n\})\} \quad (3.123)$$

and for $\mathbf{q}(\bar{\mathbf{v}}_n)$ likewise. Finally, equation (3.119) is solved discretising the differential operator with the Backward-Euler rule in order to obtain the update procedure of the present method. Again the weakly nonlinear condition allows to consider only a few IF harmonics and, in consequence, M is not high.

3.7.3 Comparison of NEC-M and E-PHB with other methods

It is possible to establish the differences of the two proposed approaches with other widely used modulation-oriented HB methods in terms of memory requirements, computational load and convergence. Starting with the EC method proposed in [44], it is an extension of transient envelopes to the case of mixers. Consequently the algorithm is reduced to the analysis of a periodically time-varying linear circuit excited by appropriate nonlinear currents. The Jacobian matrix in this method is the nodal-admittance conversion matrix, and remains the same for all the iterations. The NEC-M method presented in Section 3.7.2.1 is an implementation of HB-N with transient envelopes. As in [44], it can be reduced to the analysis of a time-varying circuit with nonlinear currents. The difference is that the waveforms of the time-varying elements are not periodical and do not remain constant for all the iterations; instead, the Jacobian

matrix is updated in each iteration. Finally, E-PHB of Section 3.7.2.2 is a particularly efficient implementation that reuses the first Jacobian. Like in the other approaches, the LO steady-state is taken as the starting solution.

In terms of memory requirements, this property is dominated by the cost of storing the Jacobian matrix. It is the same in [44] and E-PHB, since it represents a periodically time-varying linear circuit, using $(2H + 1)^2$ elements per circuit node. With regard to the NEC-M method, with the exception of the first Jacobian matrix, which is the same as that of E-PHB and [44], for the next iterations the analysis of a non-periodically time-varying circuit is needed. Hence, the size of the matrix requires $(2H + 1)^2 \times (2M + 1)^2$ elements per circuit node.

Concerning the computational cost, the number of operations required by [44] and E-PHB is nearly the same, while for the NEC-M method it is higher, as it can be observed when comparing the set of $(M + 1)$ independent equations in (3.119) to the coupled system of equations (3.105), where the structure of Toeplitz-wise matrices $\mathbf{G}(t)$ and $\mathbf{C}(t)$ is considerably more complex than that of the authentic Toeplitz matrices \mathbf{G} and \mathbf{C} .

In terms of convergence, both the rate and range are better in E-PHB than in [44], if we consider that the former is a Simplified Newton approach, and the latter a sub-optimal method. Compared with NEC-M, E-PHB yields the correct solution but its range of convergence is not as large as in NEC-M. However, it can be considered wide enough to analyse weakly and moderately nonlinear circuits with input levels over 10 dB above the 1-dB compression point. The NEC-M method requires less iterations than E-PHB to reach the correct solution for a fixed tolerance, but this is compensated with a higher number of operations per iteration, what results in an overall reduction of CPU time in favor of E-PHB.

The two proposed methods, NEC-M and E-PHB, represent an alternative solution with respect to TV-VS [41] and do not require a significant increase of computational cost.

3. ENVELOPE-BASED METHODS FOR NONLINEAR WIRELESS SYSTEMS

COMPARISON WITH EXPERIMENTAL MEASUREMENTS

In order to demonstrate some of the methods described in Chapter 3, they have been applied to the analysis of simple amplifier and mixer circuits implemented with a single MESFET or HEMT device. This way, the performance of each of the methods has been proved and simulations have been satisfactorily compared with experimental measurements.

This chapter will start with a description of the basic characterization techniques commonly used for nonlinear devices. After that, we will describe the experimental setup employed in this Thesis for the automated or semi-automated characterization of the constructed nonlinear circuits. Some measurement results obtained by means of this setup will be shown as examples. Next, diverse nonlinear models for the employed solid-state devices will be presented, including large-signal models and parameter extraction techniques applicable for MESFET and HEMT devices. Making use of these nonlinear circuit models, comparisons between the measurements carried out and simulations following the previously described analysis methods will be presented. The most relevant aspects for each of the methods will be remarked. Finally, a new experimental method to characterise the phase of the third-order (IM3) and fifth-order (IM5) intermodulation products with non-sophisticated communications equipment will be presented together with some results obtained with it.

4.1 Basic nonlinear characterization techniques

Electronic devices are specified by some figures of merit representing the observable properties of the device, which are determined by characterization procedures. For a power amplifier, for instance, widely used figures of merit are its gain, power-added

efficiency, and some quantitative measurements of the nonlinear distortion such as the 1-dB compression point and third-order intercept point.

While figures of merit for linear behaviour are already well-established, their nonlinear counterparts still continue to be developed and debated [26]. The main property of nonlinear devices is that they do not comply with the superposition principle; therefore, the system's response to a certain input may vary depending on the kind of input tested. Considering this, it seems advisable to use input signals which are similar to the excitation expected in real operation. The most useful probing signals for nonlinear devices employed in communication circuits are those with a band-limited power spectral density (PSD) containing a large number of spectral lines.

In this way, single-tone tests with sinusoidal inputs can be viewed as the simplest approximation for the recommended probing signals, in which all the power is concentrated in a single spectral line. However, the one-tone test results a very poor characterization tool for nonlinear systems, since it can only produce output spectral components that are harmonically related to the input frequency. To overcome this difficulty, the two-tone test is used, where the input signal is composed by two tones of equal amplitude and located inside the bandwidth of the channel of interest. The advantage of two-tone tests is that there are a large number of odd-order mixing products that produce in-band distortion. Their main drawback is the difficulty in evaluating distortion in the fundamental frequencies. Considering that some of the odd-order mixing terms fall exactly at the same frequencies as the fundamentals but with a much weaker amplitude than the linear output components, there is no possibility of independently measuring distortion in the fundamental frequencies. Because of this, multitone or band-limited modulated signals are adopted when attempting to measure co-channel distortion.

4.1.1 One-tone characterization tests

A linear device is identified by its frequency-domain transfer function $H(f)$. To measure it, a sinusoid $x(t) = A_i \cos(2\pi ft)$ is applied as excitation signal to the device under test (DUT), and the output is measured at the same input frequency f , referred to as the fundamental frequency. Due to the linearity of the device, a frequency sweep of the sinusoidal stimulus can only produce output changes in amplitude and phase, i.e. $y_{LIN}(t) = A_o(f) \cos[2\pi ft + \phi_o(f)]$. When this sinusoidal test is extended to a nonlinear DUT, the output amplitude A_o and phase ϕ_o will also vary nonlinearly with the stimulus level. Furthermore, the DUT will also generate new frequency components

located at the harmonics of the input

$$y_{NL}(t) = \sum_{h=0}^{\infty} A_{oh}(f, A_i) \cos[2\pi hft + \phi_{oh}(f, A_i)]. \quad (4.1)$$

The main figures of merit associated to one-tone tests are the following:

- **AM-AM conversion:**

The output amplitude variations versus input drive present in nonlinear devices manifest themselves as if the device could transform input amplitude variations into output amplitude variations or, in other words, as if it could transform a possible amplitude modulation (AM) associated to its input into an output amplitude modulation. This property is referred to as *AM-AM conversion* and describes the relation between the output amplitude of the fundamental frequency with the input amplitude at a fixed input frequency (the same frequency as in the output for power amplifiers, but a different one for mixers). Thus, it characterises gain compression of a nonlinear device versus the input level.

- **1-dB compression point:**

The *1-dB compression point*, P_{1dB} , is defined as the power level at which the signal output is 1 dB below the output that would be obtained extrapolating the linear small-signal characteristic of the system. The 1-dB compression point may be referred to the input or the output power level. A gain plot provides an immediate way for evaluating the 1-dB compression point, since it is simply the power at which the gain has already tailed off 1 dB from its small-signal value.

- **AM-PM conversion:**

Analogously to AM-AM conversion, the capability of the nonlinear DUT to transform a possible input amplitude modulation for a constant frequency into an output phase modulation (PM) of the fundamental is referred to as *AM-PM conversion*. In nonlinear systems, vector addition of the output fundamental with distortion components also determines a phase variation of the resultant output, when the input level varies. It is important to note that AM-AM behaviour would be visible whether or not the nonlinear system presented memory effects. However, AM-PM conversion is exclusive of dynamic nonlinear systems or nonlinearities with memory, included those usually called quasi-memoryless systems [47] (See Section 4.1.4 for details).

- **Total Harmonic Distortion:**

The DUT's capability for generating new harmonic components is characterized by the ratio between the square root of the total harmonic output power and the

square root of the output power at the fundamental frequency, a figure of merit called *total harmonic distortion* (THD) [26], [201]:

$$THD = \frac{\sqrt{\frac{1}{T} \int_0^T \left[\sum_{h=2}^{\infty} A_{oh}(f, A_i) \cos [2\pi hft + \phi_{oh}(f, A_i)] \right]^2 dt}}{\sqrt{\frac{1}{T} \int_0^T [A_{o1}(f, A_i) \cos [2\pi ft + \phi_{o1}(f, A_i)]]^2 dt}}. \quad (4.2)$$

An usual amplitude controlled sinusoidal or CW generator connected to a Vector Network Analyser (VNA) are sufficient to accomplished one-tone tests. The VNA simultaneously measures the DUT's gain and phase, therefore it is possible to characterise both AM-AM and AM-PM conversion with a single power sweep [48], [49]. Alternatively and less expensive, if only AM-AM conversion is needed, we can make use of a Scalar Network Analyser (SNA) or a Spectrum Analyser (SA) [50], [51]. The setup based on a SA shows the advantage that a THD characterization can be performed with it an not with a VNA, as the measured output includes frequency components that are different from the input excitation. Because of that, a setup based on a SA is employed for the automated characterization tool used in this Thesis.

There are simpler characterizations that use, for example, a power meter for measuring the DUT's input and output powers for AM-AM conversion, or a calibrated phase shifter and a SA for AM-PM conversion. In the latter, a shifted sample of the input is added to the output of the DUT trying to cancel the output fundamental signal. Nevertheless, these setups require special care not to measure other quantities different from the desired ones. For example, AM-PM measurements may be corrupted if the employed phase shifter generated distortion components which were mixed with the DUT's ones [26].

Other one-tone characterization setups relying on dedicated or special laboratory equipment are possible. Among them, Microwave Transition Analysers (MTAs) deserve to be mentioned since they combine the VNA operation with a spectrum analyser. They include a two-port high-speed sampling oscilloscope with built-in Fourier transform software, which provides them with phase measurement capabilities [202]. In addition to it, Nonlinear Network Vector Analysers (NVNAs) are powerful but expensive equipment for nonlinear component characterization. These instruments are able to measure and display both the amplitude and phase of the full output spectra — fundamental, harmonics and cross-frequency products — in time, frequency, power or user-defined custom domains. They extend the concept of linear scattering parameters to the nonlinear field by means of new nonlinear scattering parameters called X-parameters [203]. The NVNA also provides a nonlinear pulse-envelope domain measurement. However, they are not yet available in most laboratories.

4.1.2 Two-tone characterization tests

The use of two-tone stimulus not only allows the characterization of generated harmonics, but also enables the identification of new mixing components close to the fundamentals which constitute distortion components. If a two-tone excitation $x(t) = A_{i1} \cos(2\pi f_1 t) + A_{i2} \cos(2\pi f_2 t)$ were applied to our nonlinear model, the output would be given by a very large number of mixing terms involving all possible combinations of $\pm f_1$ and $\pm f_2$:

$$y_{NL}(t) = \sum_{r=1}^{\infty} A_{or} \cos(2\pi f_r t + \phi_{or}), \text{ where } f_r = m f_1 + n f_2 \text{ and } m, n \in \mathbb{Z}. \quad (4.3)$$

Referring to a usual narrowband RF subsystem, two types of information can be extracted from a two-tone test:

- **In-band distortion:**

In-band distortion products are the mixing components falling in the output fundamental frequencies zone. According to (4.3), the in-band distortion frequencies are those satisfying $m + n = 1$. For example, for a general nonlinear system represented by a power series, in-band measurements would include the fundamental frequencies, f_1 and f_2 , third-order components ($|m| + |n| = 3$) at $2f_1 - f_2$ and $2f_2 - f_1$, fifth-order components ($|m| + |n| = 5$) at $3f_1 - 2f_2$ and $3f_2 - 2f_1$, seventh-order components ($|m| + |n| = 7$) at $4f_1 - 3f_2$ and $4f_2 - 3f_1$, and so forth. These distortion products are referred to as n -th order intermodulation products (IM $_n$) and constitute the intermodulation distortion (IMD). They form a group of lower and upper sidebands, separated from the signals and from each other by the tones' frequency difference, $\Delta f = f_2 - f_1$.

The *signal-to-intermodulation distortion ratio*, or simply the *intermodulation ratio* (IMR), is defined as the ratio between the fundamental and IM3 output power, $IMR = \frac{P_{f_{1,2}}}{P_{IM3}}$. There are some cases in which lower and upper IMR are different. Those situations, often called IMD asymmetries, require the specification of lower or upper IMR.

The *third-order intercept point*, IP_3 , is a fictitious point obtained when the extrapolated 1-dB/dB slope line of the output fundamental power intersects the extrapolated 3-dB/dB slope line of the IM3 power. Since IP_3 is determined by the system's third-order distortion behaviour, it must be guaranteed that no large-signal effects are involved when measuring it. The intercept point can be referred to the input or the output of the DUT. Despite rarely being seen, some other intercept figures of merit could be defined for the fifth-order (IP_5) or seventh-order

(IP_7) distortion. As it will be detailed in Section 4.1.4, it must be noted that the existence of memory effects can cause an imbalance of the IM_n levels from the lower to the upper sideband frequencies. Most specifications of IMD level will measure the worst case of the two.

Restricted to the small-signal region, there is a relationship between the IP_3 and IMR values which allows the obtention of one of them from the other:

$$\begin{aligned} IP_{3o}(dB) &= P_o(f_{1,2})(dB) + \frac{IMR(dB)}{2}, & \text{or} \\ IMR(dB) &= 2[P_o(f_{1,2})(dB) - IP_{3o}(dB)], \end{aligned} \quad (4.4)$$

where $P_o(f_{1,2})$ is the fundamental output power per tone at which IMR was measured.

Because IMD generally increases with increasing signal levels, IP_3 may be used to establish the *dynamic range* of a system. The signal level at which the IMD level meets the noise floor is employed to define the *spurious free dynamic range* (SFDR), which is the ratio of the output power level for the fundamental frequency to the noise or IMD power level.

- **Out-of-band distortion:**

Out-of-band components are the mixing products of (4.3) obeying $m + n \neq 1$. These include harmonics of each of the tones, but also new mixing products at $mf_1 + nf_2$ that fall, either near dc ($n + m = 0$), or close to the various harmonics ($m + n = 2, 3, 4, \dots$). As their name indicates, out-of-band distortion components appear at zones of the output spectrum quite far from the fundamental signals; therefore, they are simple to be filtered in narrowband systems. The mixing product located at dc describes the bias point shift from the quiescent point, when input driving level increases.

Additionally, a two-tone signal can be viewed as a carrier at $f_c = \frac{f_1+f_2}{2}$ with a double-sideband suppressed-carrier (DSB-SC) amplitude modulation where the envelope or modulation frequency varies with the frequency separation between the two tones, $f_m = \frac{\Delta f}{2}$, as it can be observed from the following equations:

$$\begin{aligned} \tilde{x}(t) &= 2A \cos(2\pi f_m t + \phi_m) \\ x(t) &= \text{Re}\{\tilde{x}(t)e^{j2\pi f_c t}\} = 2A \cos(2\pi f_m t + \phi_m) \cos(2\pi f_c t) = \\ &= A \cos[2\pi(f_c - f_m)t - \phi_m] + A \cos[2\pi(f_c + f_m)t + \phi_m] = \\ &= A \cos(2\pi f_1 t + \phi_{0,1}) + A \cos(2\pi f_2 t + \phi_{0,2}). \end{aligned} \quad (4.5)$$

Note that the inclusion of an arbitrary phase ϕ_m in the modulation signal accounts for the situation encountered when using non-coherent signal generators. The existing

relationship between the two-tones separation and the envelope or baseband frequencies makes two-tone IMD measurements appropriate for nonlinear characterization taking into account memory effects, as it will be detailed in Section 4.1.4.

The usual equipment to accomplish two-tone tests is a SA, since mixing products involving a combination of both f_1 and f_2 have frequencies different from either of the inputs. The most commonly used arrangement for such a setup employs two signal generators, each one providing an input tone which is applied to the DUT by means of a power combiner or a directional coupler. Phases of the two tones generated in this way are uncorrelated [26].

The combination of the two input signals should be made in such a way that it guarantees port matching and adjacent port isolation, preventing each signal to mix with the other in the nonlinear output stages of the generators. Moreover, harmonics of the generated signals can also mix with the other fundamental to produce residual distortion in the DUT, the signal generators' output stages, or both. Therefore, a good signal spectral purity of the generated outputs should be assured. A final recommendation is to take advantage, as much as possible, of the available Spectrum Analyser's dynamic range so as not to mask the measurements with noise when the Spectrum Analyser's attenuation or resolution bandwidth is high, or to add undesired distortion mixing components because of the Spectrum Analyser's nonlinearity [51].

4.1.3 Band-limited continuous spectra characterization tests

Although one-tone and two-tone techniques still represent the industry standards in nonlinear distortion characterization, nowadays, engineers seek for alternative test procedures closer to the final operation regime of the system, which involve communication signals composed of one or more digitally-modulated carriers with band-limited continuous spectra, or even signals that mimic them such as multitones (with discrete spectrum) and band-limited noise.

As it was stated in Section 3.1.1, the spectrum of a nonlinearly distorted signal consists of clusters of frequency components centred at the different carrier harmonics. If we focus on the in-band distortion, we can clearly observe that the output contains many more frequency components which generate spectral regrowth. In addition to this, the output spectrum of a nonlinear DUT also includes co-channel distortion components whose frequencies fall inside the signal channel.

• **Multitone Intermodulation Ratio:**

If a multitone signal is used as the stimulus, the output of a nonlinear system is given by a large number of line-clusters placed near dc, located next to the output fundamentals and close to them, and near the harmonics:

$$y_{NL}(t) = \sum_{r=1}^R A_r \cos(2\pi f_r t + \phi_r), \quad (4.6)$$

where, $f_r = m_0 f_0 + \dots + m_q f_q + \dots + m_{Q-1} f_{Q-1}$ is the given mixing product of the Q input frequencies $f_0, \dots, f_q, \dots, f_{Q-1}$ and N is the maximum order of the mixing product under consideration, being $|m_0| + \dots + |m_q| + \dots + |m_{Q-1}| \leq N$.

In general, multitone signals showing random phase present a lower peak to average power ratio than phase-aligned multitone signals, which may be considered a worst case condition [204]. Furthermore, as the number of tones increases, and if their phases are uncorrelated, the Central Limit Theorem predicts that the distribution of the peak to average power ratio approaches that of white Gaussian random noise. This is the reason why multitone signals are employed to mimic communications modulated signals in the same way as noise signals.

The *multitone intermodulation ratio* (MIMR) is a generalization of the IMR concept introduced with two-tone tests for the case in which multitone signals are being employed as a first approximation of a band-limited continuous spectrum signal. It is defined as the ratio of the common fundamental power per tone, $P_{o/tone}$, to the power of the f_r distortion component present in the lower or upper adjacent bands, $P_{l/u}(f_r)$:

$$MIMR(r) = \frac{P_{o/tone}}{P_{l/u}(f_r)}. \quad (4.7)$$

• **Adjacent Channel Power and Adjacent Channel Power Ratio:**

Among the mixing products which compose the spectral regrowth components, those located adjacent to the signal channel are referred to as adjacent-channel distortion and constitute an interference to a possible adjacent-channel. Because of the youth of this subject, various proposed figures of merit are still accepted and investigated to characterise this form of distortion.

One of them is the *total adjacent-channel power ratio* ($ACPR_T$), defined as the ratio of the total power integrated in the lower, $P_{adj,L}$, and upper, $P_{adj,U}$, adjacent-channel bands, to the total output power measured in the fundamental zone, P_o , as shown in Figure 4.1. Thus, if $Y_o(f)$ is taken as the power spectral density

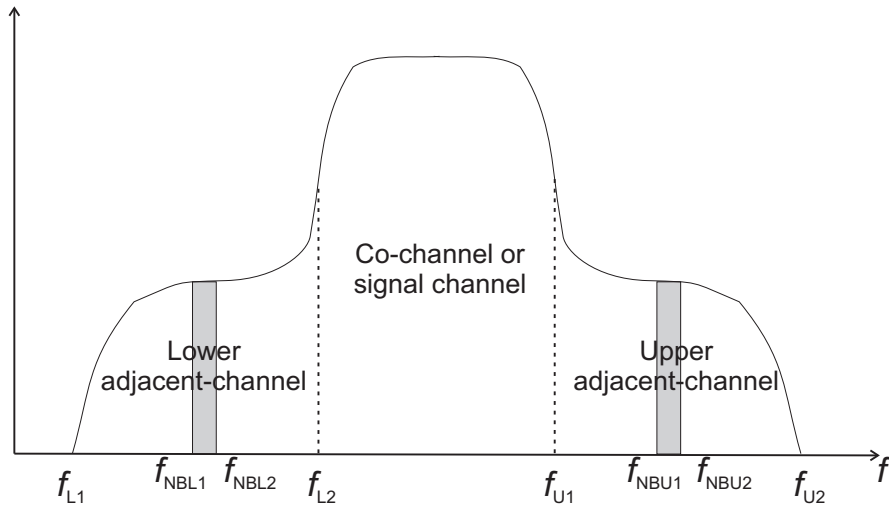


Figure 4.1: Spectral regrowth observed in a nonlinear system excited by a narrowband modulated stimulus.

function of the system's output, total ACPR is expressed as

$$ACPR_T = \frac{P_{adj,L} + P_{adj,U}}{P_o} = \frac{\int_{f_{L1}}^{f_{L2}} Y_o(f) df + \int_{f_{U1}}^{f_{U2}} Y_o(f) df}{\int_{f_{L2}}^{f_{U1}} Y_o(f) df}. \quad (4.8)$$

If the excitation were a multitone signal, the output spectrum would be discrete, and the integrals of (4.8) would become summations of spectral regrowth line powers.

If only the lower or upper adjacent-channels are of concern, then we can use the *adjacent-channel power ratio (lower or upper)*, defined as the ratio between the lower or upper adjacent-channel power, $P_{adj,L/U}$, to the total output power measured in the fundamental zone, P_o :

$$ACPR_L = \frac{P_{adj,L}}{P_o} = \frac{\int_{f_{L1}}^{f_{L2}} Y_o(f) df}{\int_{f_{L2}}^{f_{U1}} Y_o(f) df}, \quad (4.9)$$

$$ACPR_U = \frac{P_{adj,U}}{P_o} = \frac{\int_{f_{U1}}^{f_{U2}} Y_o(f) df}{\int_{f_{L2}}^{f_{U1}} Y_o(f) df}. \quad (4.10)$$

An alternative definition, particularly used in the wireless equipment industry, is herein called *spot adjacent-channel power*, (ACP_{SP}), to distinguish it from the

previously referred ACPR. According to Figure 4.1, ACP_{SP} is given by the ratio of the power integrated in a band of predefined bandwidth and distance from the centre frequency of operation $P_{SPL/U}$, to the total output power measured in the fundamental zone, P_o :

$$ACP_{SP,L} = \frac{P_{SP,L}}{P_o} = \frac{\int_{f_{NBL_1}}^{f_{NBL_2}} Y_o(f) df}{\int_{f_{L_2}}^{f_{U_1}} Y_o(f) df}, \quad (4.11)$$

$$ACP_{SP,U} = \frac{P_{SP,U}}{P_o} = \frac{\int_{f_{NBU_1}}^{f_{NBU_2}} Y_o(f) df}{\int_{f_{L_2}}^{f_{U_1}} Y_o(f) df}. \quad (4.12)$$

Finally, simply the power integrated in those bands corresponding to the first, second, and so on, lower and upper adjacent-channels can be measured and denoted by $ACP_{nl/w}$, where n represents the distance of the adjacent-channel to the one of interest.

- **Noise Power Ratio:**

Noise power ratio (NPR) was proposed as an indirect means of characterising co-channel distortion. A noise power ratio test eliminates the fundamental components from the zone where the test is made. Because of that, the DUT is excited by a noise spectrum in which a slice has been previously deleted, usually by passing the excitation through a very narrow notch filter before being applied to the DUT. If the notch bandwidth is sufficiently narrow, it is believed that no significant perturbation has been caused in the test conditions, then any frequency component observed at the output within the notch position constitutes the co-channel distortion.

A sample output for a typical noise power ratio test is shown in Figure 4.2. Noise power ratio is defined as the ratio of the output power spectral density function measured in the vicinity of the test window position, f_T , $Y_o(f_T)$, to the power spectral density observed within that window, $Y_{wd}(f_T)$:

$$NPR(f_T) = \frac{Y_o(f_T)}{Y_{wd}(f_T)}. \quad (4.13)$$

- **Error Vector Magnitude:**

Digitally modulated signals employed in wireless communications are often expressed as a *constellation* plot, with the in-phase component envelope plotted

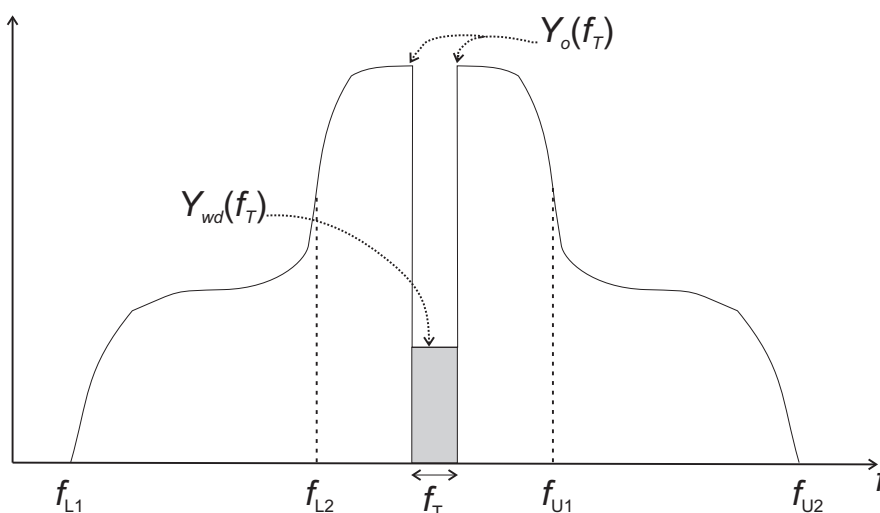


Figure 4.2: Illustration of the output power spectral density of a noise power ratio test.

against the quadrature component. The observed effect that nonlinear systems cause in the constellation of digitally modulated signals is that the envelope is clipped and/or phase rotated. As previously mentioned, it has been stated that the level of the in-band distortion is difficult to measure directly because it is superimposed on the channel spectrum. However, when the signal is demodulated, the effects of in-band distortion cause errors in the sample points of the output constellation that result in a false decision, and hence bit errors. The *error vector magnitude* (EVM) is a figure of merit that provides an indication of signal distortion for digitally-modulated signals. EVM is defined as the root mean squared sum of vector error divided by the number of samples:

$$EVM = \frac{1}{M} \sqrt{\sum_{m=0}^{M-1} [|x_I(t_m) - s_{Im}|^2 + |x_Q(t_m) - s_{Qm}|^2]}, \quad (4.14)$$

where the envelope sample points at the m -th sample windows are given by $x_I(t_m)$ and $x_Q(t_m)$, and the m -th symbol location point in-phase and quadrature components are given by s_{Im} and s_{Qm} , respectively.

Depending on the objective of the characterization, the excitation source employed may be a multitone generator, a noise-like continuous spectrum source, or even a specific real telecommunications signal. Test signals for digitally-modulated signals are usually synthesized according to system standards using an *arbitrary waveform generator*, for which the envelope waveforms may be created using commonly available communications engineering software and then fed to the RF modulator [205].

Except for special cases of very small number of tones, where they can be created independently and then added with a power combiner, RF multitone excitations are generally built up by upconverting a baseband multitone signal to the desired spectral location. This baseband multitone signal needs to be complex when it is desired that the modulated signal presents different power levels for each tone and a certain phase distribution. Furthermore, a sufficient mixer rejection must be guaranteed or the leaking carrier may perturb observation of very weak distortion components [26].

Adjacent-channel distortion tests can use a setup basically composed by an appropriate excitation source and a SA [52]. An NPR test may be performed with a digitally produced multitone or a noise signal. In the first situation, a multitone signal is made from an arbitrary waveform generator, at the desired RF centre frequency. The notch is made by selective elimination of one of these tones. Alternatively, if the NPR test is to be performed with band-limited noise, then a narrowband limited notch filter must be provided between the RF noise generator and the input of the DUT. The main difficulty stems from finding an appropriate notch filter due to the high Q values required [206].

Measurement of EVM is usually done with a Vector Signal Analyser (VSA). This instrument is essentially a receiver that is flexible enough to handle a variety of frequencies and modulation formats [53]. Specialised software is often included to directly measure EVM for well-known standards used in wireless communications.

A final remark on continuous spectra distortion tests should be how to address the problem of measuring power with a SA. Measuring total power within a user-defined bandwidth requires the integration of the power spectral density function, which, in turn, can be obtained by dividing the SA power spot readings by the utilized resolution bandwidth, RBW. Alternatively, total power can be simply measured by dividing the sought bandwidth in the corresponding number of bandwidth segments of RBW width, and then adding the SA power readings one by one. This calculation is usually automatically performed by SAs by means of special firmware functions implemented on them. Beyond that, special attention must be paid to the correct definition of fundamental and distortion band-limits.

4.1.4 Memory effects

In the context of nonlinear systems, the term *memory* was proposed by Chua [54], to describe the influence on the output of a system at a time t of the input signal not only at time t , but also spanning a finite history of the input signal, to some time in the past, $t - \tau$. The largest time delay, τ , determines the *length of the memory* of

the system. This is known as a *fading memory*, as the influence of the input signals deep in the past fades to zero. In general, a nonlinear memoryless system may only cause an amplitude, never a phase, distortion. If a phase distortion is present, the system must possess a certain amount of memory. Essentially, by memory effects we are describing the dynamical behaviour of the system. Thus, amplifiers with reactive components introducing phase shifts have memory, with characteristic times that are generally either of the same timescale as the signal frequency — *short-term memory* — or at much slower rates — *long-term memory*. Because of that, nonlinear systems that only exhibit short-term memory effects are considered by many authors as *quasi-memoryless systems* [24], for which the amount of amplitude and phase distortions are modelled by *static* AM-AM and AM-PM conversions or, equivalently, complex-valued but constant NLTFs. By contrast, nonlinear systems exhibiting long-term memory effects are usually considered to present *dynamic* AM-AM and AM-PM characteristics which are modelled by frequency-dependent NLTFs.

Memory effects can be detected as shifts in the amplitude and phase of IMD components caused by changes in the modulation frequency [24], or also by hysteresis in the AM-AM and AM-PM plots [55]. In the literature, these phenomena are also referred to as *bandwidth-dependent IMD behaviour* [25], *dynamic system effects* [56], *rate-dependent effects* [57] or *non-quasi-static (NQS) effects* [9], [58]. A difference between the upper and lower IM products for a two-tone input or between the upper and lower adjacent channels for a modulated input is referred to as an *asymmetry*, and it is another indication of memory effects. When we talk of memory effects in RF power amplifiers, the major sources of these effects are [27], [58]:

- **Short-term memory effects:**

The high-frequency dynamics of the amplifiers are determined by the reactances associated with the transistor. In the usual description of a transistor model, these reactances comprise the capacitances and inductances associated with the parasitic elements of the extrinsic model, and also the nonlinear charge storage within the transistor's active region, in the intrinsic model.

For small-signal characterization, the short-term memory effects are simply the frequency response of the transistor, which is bias-dependent and requires that the capacitances describing the linearized charge storage behaviour in the transistor are also bias-dependent. Under large-signal conditions, the voltage- or current-dependence of the charge storage functions becomes important. The changing dynamical behaviour with signal drive manifests when measuring AM-AM and AM-PM characteristics of the system. The AM-PM effects are essentially the nonlinear behaviour that is often referred to as short-term memory effects.

The matching networks are also a source of short-term memory effects, since they are built from reactive components or transmission lines whose frequency dependence contribute to the short-term dynamics.

- **Long-term memory effects:**

The three main causes of long-term memory effects are:

- **Thermal effects:**

The transistor channel can heat up nonuniformly when driven by modulated signals. Because of this local change of temperature, some of the transistor's parameters will be slightly different, for example a reduction of the gain from the equilibrium-temperature value is common. The time constants associated with thermal transients are generally of the order of milliseconds, which is close to the timescale of low modulation frequencies, in the range of 100 KHz and below. These long-term memory effects can be seen in the AM-AM characteristics of RF power amplifiers as a spread around the mean gain compression curve.

- **Charge trapping:**

Imperfections and defects in the semiconductor occur in several locations at the internal structure of the transistors. These imperfections often manifest themselves as available states that can capture and release electrons and holes, a mechanism governed by local potentials and temperature. The action of trapping or releasing an electron is effectively changing the charge density in the channel of the transistor, and its rate is on a timescale of kilohertz through megahertz, depending on the nature of the trapping centre. Therefore, charge trapping is a mechanism causing long-term memory effects. GaAs and GaN FETs display several trap-related phenomena, while other transistors like LDMOS do not suffer from them.

- **Dc bias networks:**

The dc bias network provides a low impedance path for the dc bias connections that is simultaneously a high impedance for the RF signal. This path has inductance and capacitance that control the frequency response from the dc to a few tens of MHz. Therefore, any signal components in this frequency range will experience memory effects. The signal components appearing in this baseband frequency range will mix with the RF components as a result of the even-order nonlinearities in the active device. This is the most usual cause of asymmetries in IMD responses.

The aforementioned measurement consisting in two-tone tests, where a sweep of the tone spacing is performed, reveals the presence of long-term memory effects if the

IM products vary with the tone spacing. However, the identification of the origins of the long-term memory is more difficult. Thermal effects can be observed by making pulsed dc measurements and varying the pulse width and duty cycle.

Traditionally, technical datasheets of commercial RF and microwave circuits show the behaviour of the different forms of nonlinear performance (like spectral regrowth, two-tone IMD, ACP) using an arbitrary modulation bandwidth. However, IMD levels can experience significant variations when excitations with different bandwidths are tested. This phenomenon is the result of complex interactions among the active devices and the rest of the circuit, which make distortion strongly dependent on the characteristics of the modulation signal. These effects represent a challenge to the success of linearization methods, specially for those trying to accomplish IMD reduction by applying the excitation signal corrupted by a similar distortion with opposite phase, as it is the case for a simplified view of digital predistortion.

A one-tone power sweep measurement is very helpful during the design of power amplifiers, but it does not provide enough information about the system's memory. On the contrary, a two-tone intermodulation characterization with a varying frequency separation between the tones is a widespread measurement in nonlinear characterization which provides memory information and the comprehension of its peculiarities has centred the interest of researchers. Examples of this concern are the classification of amplifiers regarding its memory effects [24], the study of asymmetries in third-order IM products revealing that terminating impedances at baseband or difference frequencies are the main cause for distortion sideband asymmetries [28], [21], and the relation between two-tone IMD measurement and the spectrum of a W-CDMA signal [31].

However, the characterization of memory effects is not a widespread practice outside the research field nowadays. Because of that, only a reduced number of figures of merit for the quantification of memory effects have been proposed and they are not well-established yet:

- **Figures of merit based on behavioural modelling:**

In [207] and [208], two different figures of merit are proposed for the quantification of the contribution of memory effects in the context of the extraction of behavioural models for power amplifiers. Therefore, their definitions require the use of a certain model for the DUT's output signal.

In [207], the proposed model is based on certain frequency-dependent coefficients $a_{2k-1}(\omega_m)$ of order $2k - 1$ that vary with the modulation frequency ω_m . The constant coefficient $a_{2k-1,1}$ corresponds to the memoryless case. To quantify

the frequency dependence of each coefficient, \hat{a}_{2k-1} is defined as

$$\hat{a}_{2k-1} = \sqrt{\frac{1}{\Delta\omega} \int_{\omega_1}^{\omega_2} \left| \frac{a_{2k-1}(\omega_m) - a_{2k-1,1}}{a_{2k-1,1}} \right|^2 d\omega_m}, \quad (4.15)$$

where $\Delta\omega = \omega_2 - \omega_1$ is the difference between the upper and lower frequencies. The coefficients \hat{a}_{2k-1} quantify the contribution of the memory effect terms relative to the memoryless terms in the frequency zones affected by IMD of order $2k - 1$.

In addition to this, the *memory effect ratio* (MER) is defined in [208] as the ratio of the root-mean-square error that cannot be predicted with a memoryless model to the root-mean-square value of the output signal:

$$MER = \frac{\sqrt{\sum_{k=0}^K |y_o(k) - y_{o, modelled}(k)|^2}}{\sqrt{\sum_{k=0}^K |y_o(k)|^2}}. \quad (4.16)$$

Large values of the MER or the coefficients \hat{a}_{2k-1} indicate that the device has significant memory effects. Although such figures of merit may be used to quantify the relative strength of memory effects between different amplifiers, these metrics are difficult to apply in the industrial environment because they are conditioned by a previous model extraction.

- **Power amplifier linearizability under static conditions:**

This figure of merit was proposed in [209] considering a two-tone excitation. In this case, for the IMD at the DUT's output, $Y_{IM3}(f')$, a one-dimensional frequency-dependence on the tone spacing $f' = \Delta f$ is assumed. Firstly, the best memoryless lineariser is defined in this case as the static auxiliary device that produces a constant two-tone IMD response C that minimises the distortion power in the considered operation bandwidth W , i.e.

$$C : \left[\int_{-W}^{+W} |C - Y_{IM3}(f')|^2 df' \right] \text{ is minimum.} \quad (4.17)$$

That way, the optimum memoryless lineriser of a certain power amplifier is the system whose constant response is the vectorial mean of the response of that power amplifier to a two-tone test where the tone spacing is swept within the bandwidth of interest.

$$C = \frac{1}{2W} \int_{-W}^{+W} Y_{IM3}(f') df' = \int_0^\infty y_{IM3}(\tau) \frac{\sin(W\tau)}{W\tau} d\tau. \quad (4.18)$$

Taking this into account, the *power amplifier linearizability* under static conditions is defined as the ratio between the unlinearised IMD integrated power in the desired bandwidth and the total IMD integrated power after memoryless linearization in the same bandwidth:

$$L_M = \frac{\int_{-W}^{+W} |Y_{IM3}(f')|^2 df'}{\int_{-W}^{+W} |Y_{IM3}(f') - C|^2 df'}. \quad (4.19)$$

When seen in the time domain for the whole power amplifier IMD bandwidth characteristics ($W \rightarrow \infty$), this memory figure of merit is a metric of the power contained only in the power amplifier dynamic IMD, normalized to the total IMD power.

- **Memory Effect Intensity:**

In [210], a very intuitive memory figure of merit is defined for power amplifiers driven by modulated signals. In this case, it is considered that memory effects prevent conventional memoryless linearisers from effectively suppress the out-of-band emission in the output spectrum after linearisation, $Y_{o,ml}(f)$. Since the residual spectral regrowth is primarily caused by memory effects, the proposed quantification of the memory effects' intensity is defined as the ratio of the integrated power in the out-of-band spectrum to that of the in-band spectrum. Expressed in dBc, *memory effect intensity* (MEI) is:

$$MEI = 10 \log \left(\frac{\int_{f_c-5B/2}^{f_c-B/2} Y_{o,ml}(f) df + \int_{f_c+B/2}^{f_c+5B/2} Y_{o,ml}(f) df}{\int_{f_c-B/2}^{f_c+B/2} Y_{o,ml}(f) df} \right), \quad (4.20)$$

where B is the bandwidth of the modulated signal. In that work, only the third- and fifth-order IM products are included to represent the out-of-band spectrum regrowth since they are the most significant.

4.2 Measurement setup description

The automatic setup for the characterization of nonlinear circuits employed in this Thesis is shown in Figure 4.3. With this equipment, different standard nonlinear figures of merit have been evaluated for one-tone and two-tone tests, such as the $P_{1\text{ dB}}$ or the level of IM3. In addition to this, band-limited continuous spectra communication

4. COMPARISON WITH EXPERIMENTAL MEASUREMENTS

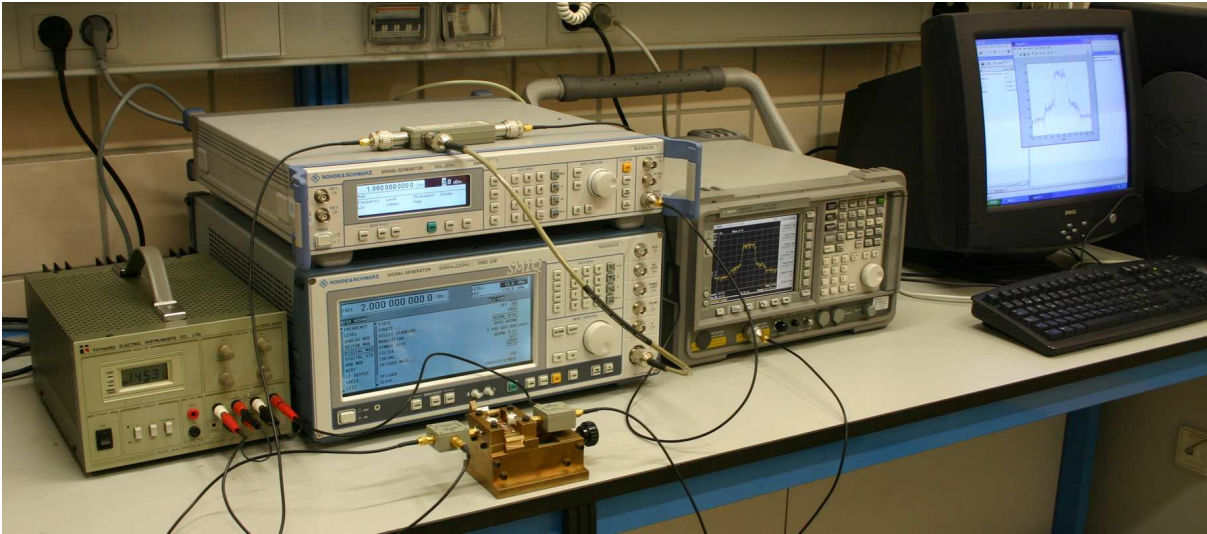


Figure 4.3: Photograph of the equipment setup for the characterization of non-linear circuits.

signals corresponding to the digital standard 3GPP UMTS W-CDMA have been generated and ACPR has been quantified and output power spectrum traces have been captured where spectral regrowth can be observed. A diagram of the implemented automated characterization setup is shown in Figure 4.4. The most notable elements in the setup are the following:

- Spectrum analyser ESA E4407B of Agilent, with a modulation analysis option.
- Signal generator SMIQ02B of Rhode & Schwarz, with built-in arbitrary waveform facility.
- Signal generator SMR20 of Rhode & Schwarz.
- Two dc power supplies: a 6622A of Agilent and a TPS-4000D of Topward Electric Instruments.

The instruments are controlled by a commercial software installed in a PC, via a GPIB (General Purpose Interface Bus) interface. A test-fixture is also included in the setup to place the different microwave circuits to be characterised. For each particular measurement other elements may be necessarily included, such as commercial bias networks, filters, attenuators, power splitters or combiners, directional couplers, etc. It is also possible to add more signal generators for multitone signals by means of directional couplers or power combiners.

The main advantages of the employed setup are the speed achieved due to measurement automation and the simplicity attained with the user-friendly graphic interface of the designed software, which makes the sometimes complex and repetitive

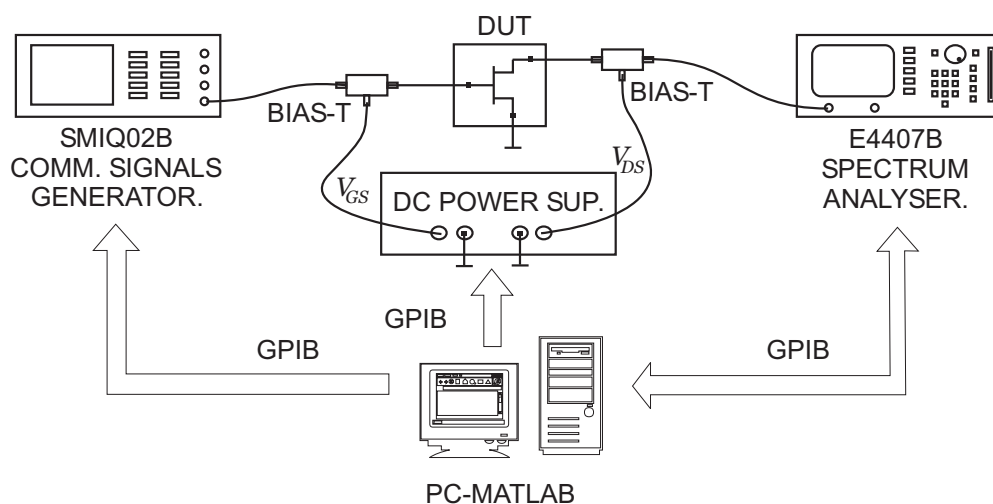


Figure 4.4: Diagram of the equipment setup for the characterization of nonlinear circuits.

configurations of parameters transparent to users. Another positive issue is the possibility of having all the measurement results immediately available in the PC, both in graphical and numeric format, so that it is easier to integrate experimental data into modelling and simulation techniques. The design of this software tool has been carried out by following a modular philosophy in order to simplify its future extensions with new measurement procedures and functionalities. A library of custom-designed functions is the base of the software. These functions are used to establish the measurement conditions in the instruments, create the desired arbitrary waveforms, export them to the signal generator SMIQ02B, store them in its internal memory, and recover in the PC the measurement data, which can be automatically processed.

Figure 4.5 shows a screenshot of the software's main window, where it can be noted that the possible control and configuration actions for each instrument are determined by the type of measurement to be done, so that the user needs to specify the smallest number of parameters. Moreover, in order to protect the devices against inappropriate dc supplies, i.e., with wrong polarity or values over the maximum recommended ones, the tool includes an extendable database with the acceptable voltage and current ranges for the commonly used devices and an undetermined device for which it is the user who establishes the desired range.

4.2.1 Illustrative examples of nonlinear distortion characterization

With the described setup, the commercial amplifier MAX2430, manufactured by MAXIM Integrated Products, has been automatically characterised. According to the manufacturer's datasheet, this is a silicon medium power amplifier, with 16-pin QSOP

4. COMPARISON WITH EXPERIMENTAL MEASUREMENTS

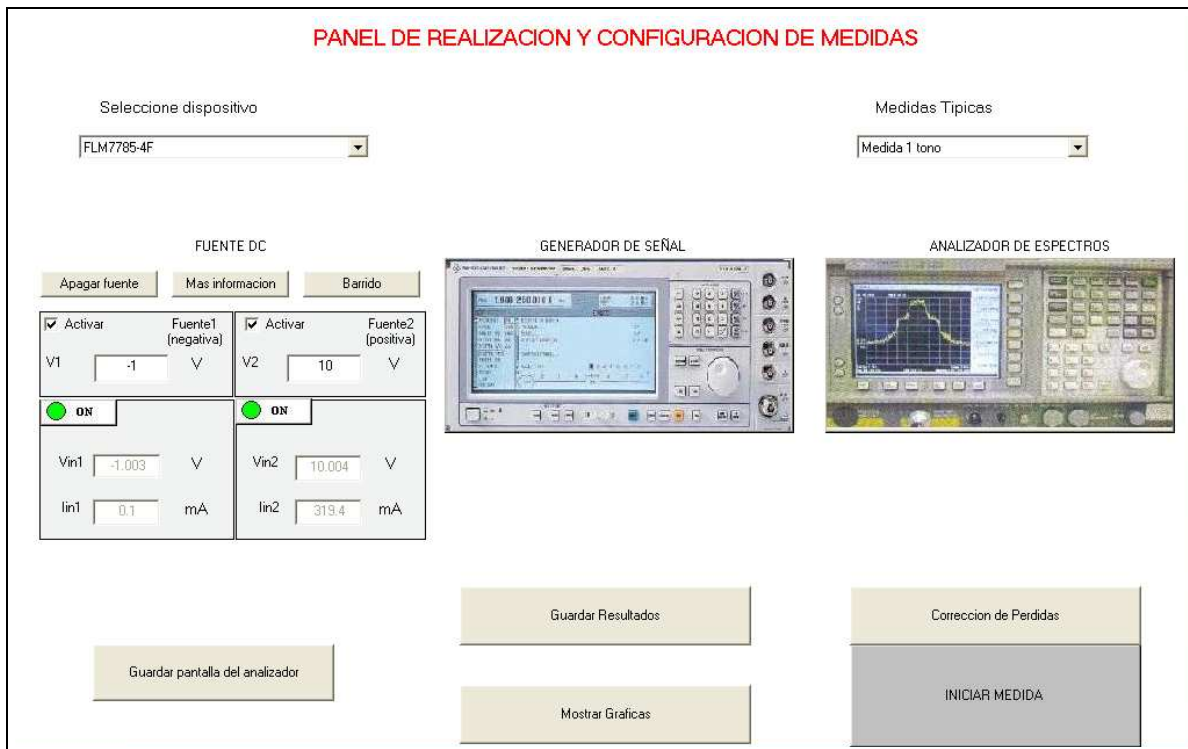


Figure 4.5: Main window of the implemented software controlling the automated measurement setup.

package, operating in the frequency range between 800 and 1000 MHz, delivering 100 mW of output power at 915 MHz and exhibiting a gain over 30 dB with 3 V dc voltage and 60 mA current supply. For 0.6 V dc voltage the circuit operates as a class C amplifier. Above 2 V, the output stage is biased in class AB. The selected operation regime is a dc voltage of 3.6 V and a fundamental frequency of 915 MHz. It must be noted that, for this device, the operation point varies with the amplitude of the excitation signal, as it is shown in Figure 4.6 where the current consumption is depicted versus the input power level for a CW signal.

Among the measurements carried out, firstly a one-tone test was performed, in which the output power levels for the fundamental frequency and the first harmonics have been registered. This measurement allows us to represent the power gain versus the input level and determine the 1 dB compression point. Figure 4.7 illustrates the typical output amplitude characteristic of a nonlinear DUT versus the input power or AM-AM characterization for the fundamental and first harmonics for an input level of $P_{in} = -10$ dBm, above the 1-dB compression point. Corresponding to it, in Figure 4.8 the gain of the studied power amplifier is depicted, together with its estimated 1-dB compression point of about -12 dBm at the input and 22.1 dBm at the output.

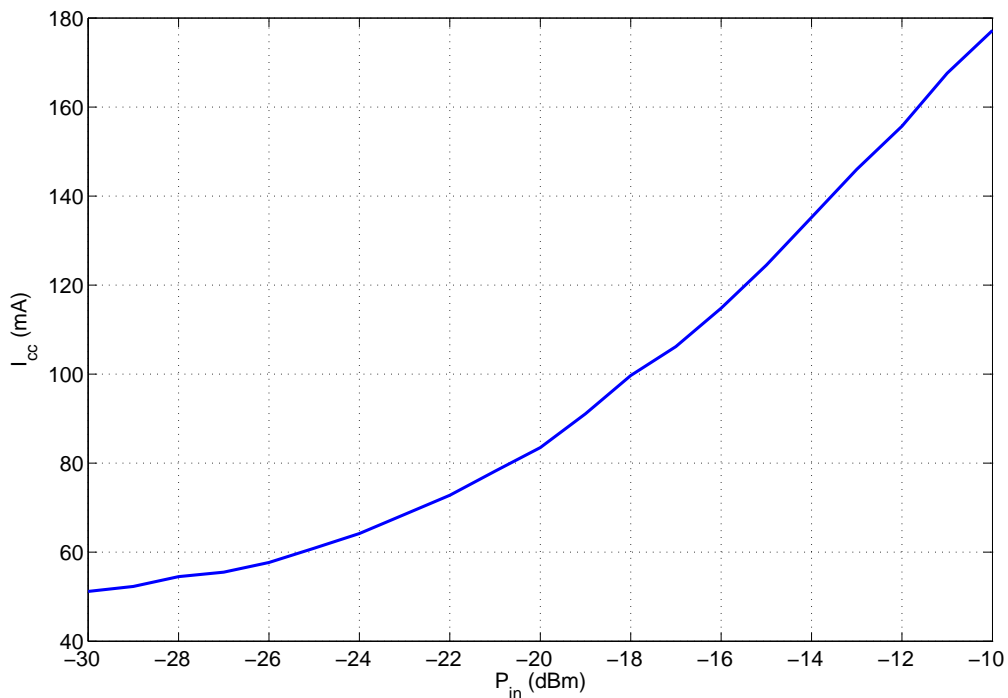


Figure 4.6: Current consumption for a MAXIM 2430 power amplifier versus input power level.

Next, a two-tone test was performed with fundamental frequencies $f_1 = 914$ MHz and $f_2 = 916$ MHz, for which Figure 4.9 presents a plot of the DUT's output power at the fundamental signals and IM3 versus input power. At sufficiently small-signal levels, the fundamental output power increases 1 dB for each decibel rise of input power, while a 3 dB per decibel rate is observable for the IM3 power. However, at very large-signal levels where the contribution of the higher order terms is no longer negligible, both curves tend to compress towards constant fundamental and IM3 output power values. A direct reading of this plot immediately provides IMR as a function of input drive level. Note that, in this case, a notable asymmetry can be observed between the upper and lower IM3 products, making difficult the obtention of the IP_3 .

In addition to this, the in-band power and ACP in the first, second and third adjacent channels (both upper and lower) were measured for the MAX2430 power amplifier excited with a 3GPP UMTS W-CDMA signal varying the input power level. The measurement results are shown in Figure 4.10. The averaged output PSD of the power amplifier for two different input power levels is depicted in Figure 4.11, where spectral regrowth can be observed due to the nonlinear distortion for the highest input power level $P_{in} = -10$ dBm. This spectral regrowth is the cause for the observed increase of the ACP in the previous figure.

4. COMPARISON WITH EXPERIMENTAL MEASUREMENTS

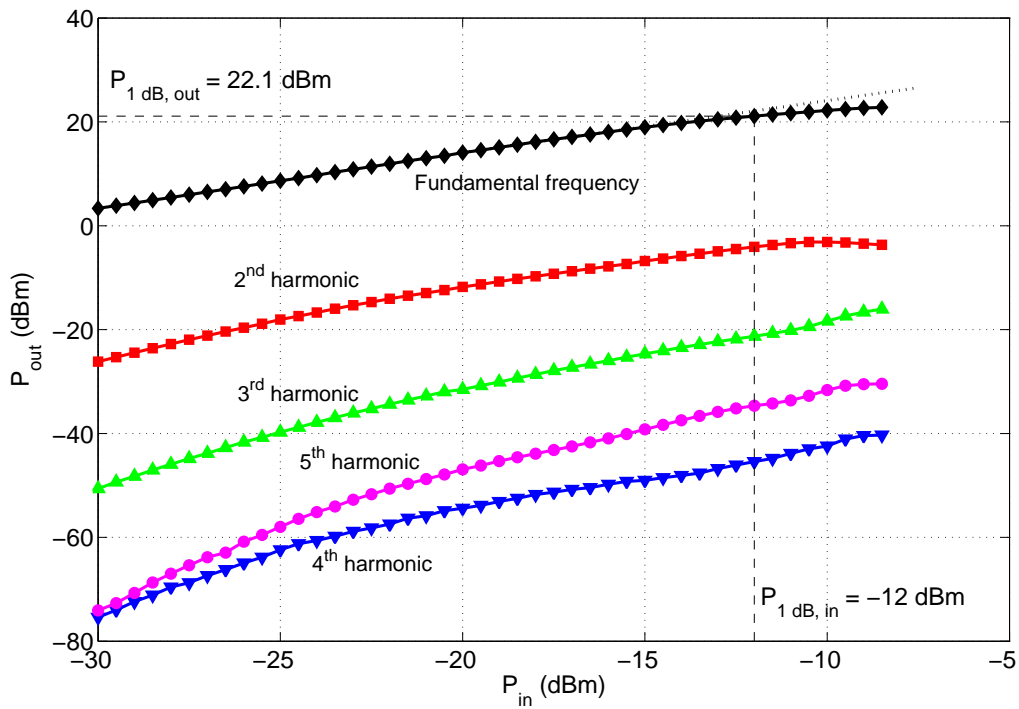


Figure 4.7: Output power for the fundamental frequency and first harmonics for a MAXIM 2430 power amplifier illustrating AM-AM characterization.

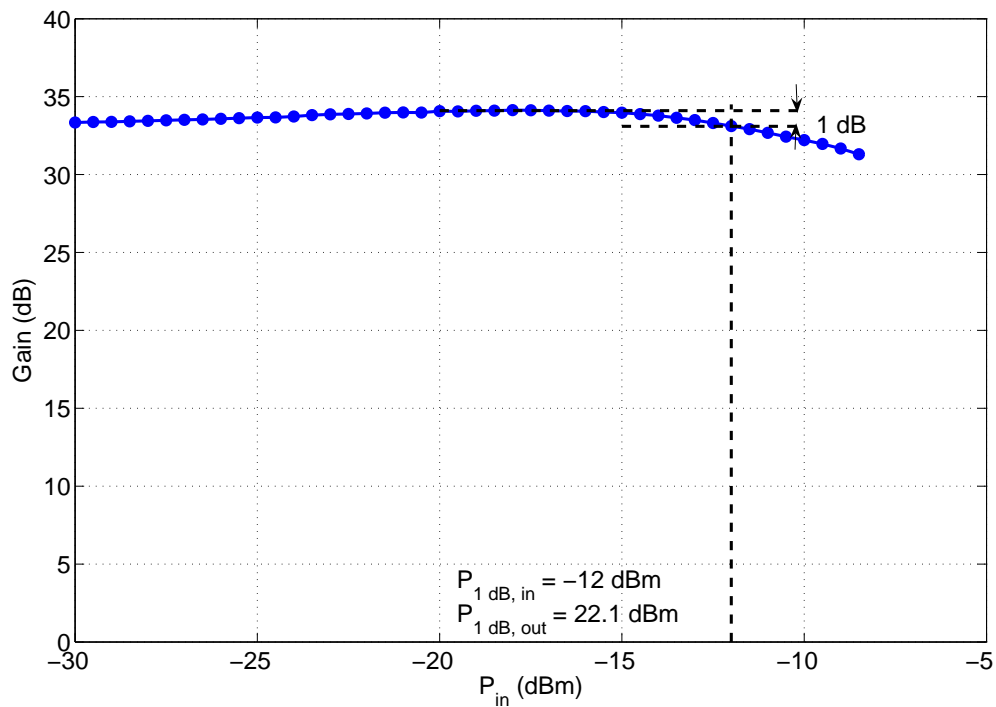


Figure 4.8: Conversion gain measurement for a MAXIM 2430 power amplifier.

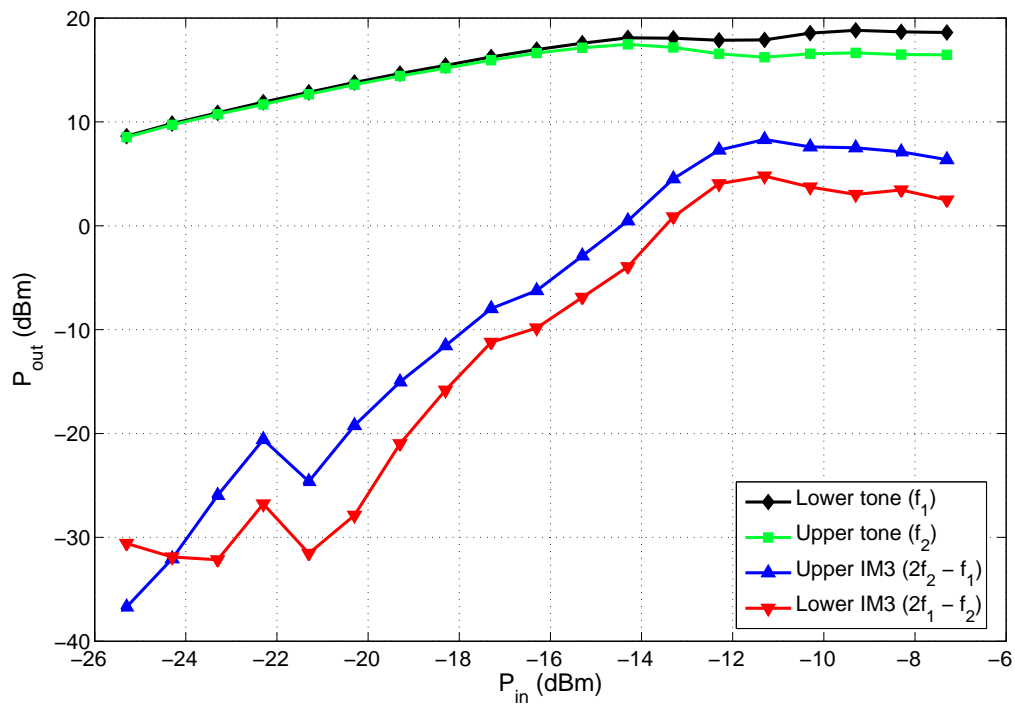


Figure 4.9: Output power at fundamentals and IM3 components versus input level for a MAXIM 2430 power amplifier for a two-tone excitation with $\Delta f = 2$ MHz.

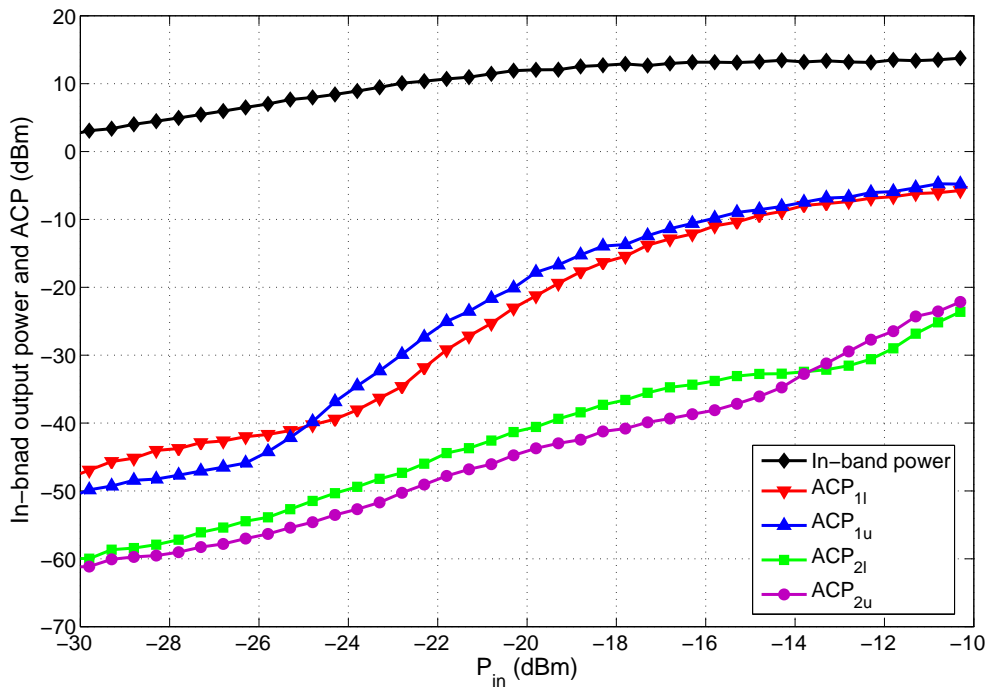


Figure 4.10: Measurements of in-band power and ACP in both upper and lower first and second adjacent channels of a MAXIM 2430 power amplifier with a 3GPP UMTS W-CDMA signal.

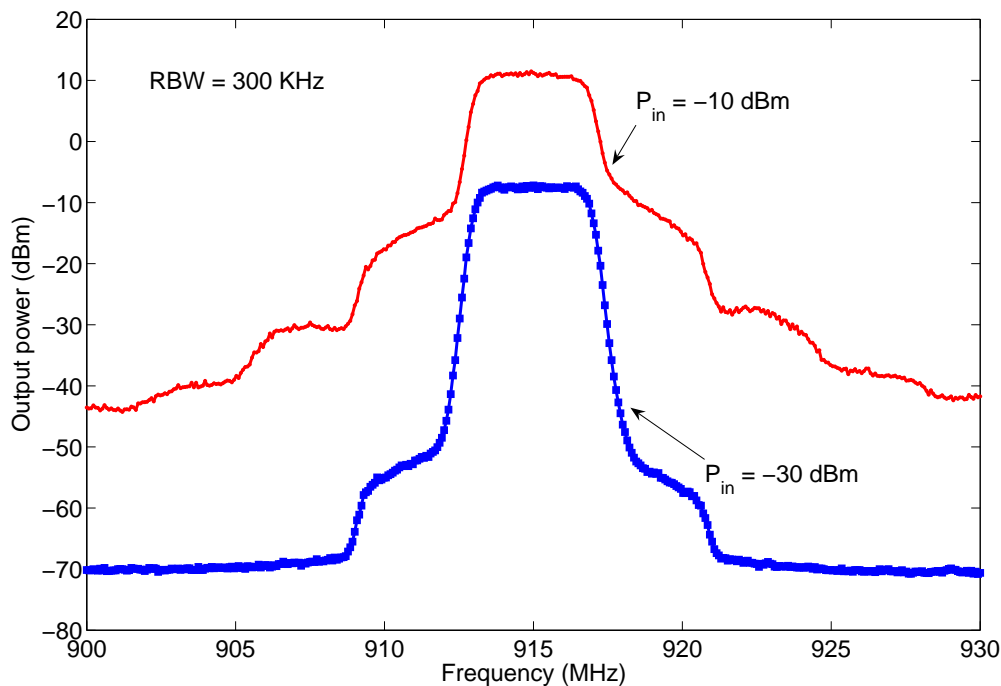


Figure 4.11: Output PSD traces for a MAXIM 2430 power amplifier with a QPSK 3GPP UMTS W-CDMA signal employing a root raised cosine filter and two power input levels.

4.3 Results for envelope-based analysis methods

In order to verify performance of the analysis methods described in Chapter 3, some simple amplifiers and mixers have been constructed based on two active devices: MESFET CFB0301 of Celeritek and a HEMT EPB018A5-70 of Excellics. Before the results of predictions provided by these methods are compared with measurements, a detailed explanation of the followed modelling procedure will be presented.

4.3.1 Employed large-signal models for MESFET and HEMT devices

In order to model the active MESFET and HEMT devices employed, the compact equivalent three-node circuit shown in Figure 4.12 will be used. It can be noticed that it is a simplification of that shown in Figure 2.11, where the diodes and extrinsic capacitances have been neglected. In the last decades, several large-signal models for MESFET and HEMT devices have been proposed. Well-known examples of compact models are the *Curtice* [211] and *Statz* or *Raytheon* [212] models for GaAs IC FETs, the *Curtice-cubic* [71] model for FETs used in power amplifiers, the *Angelov* [72] model suitable for both MESFET and HEMT devices, and more general-purpose models such as the *Materka* [213] model. Many of these compact models are extensions of the small-

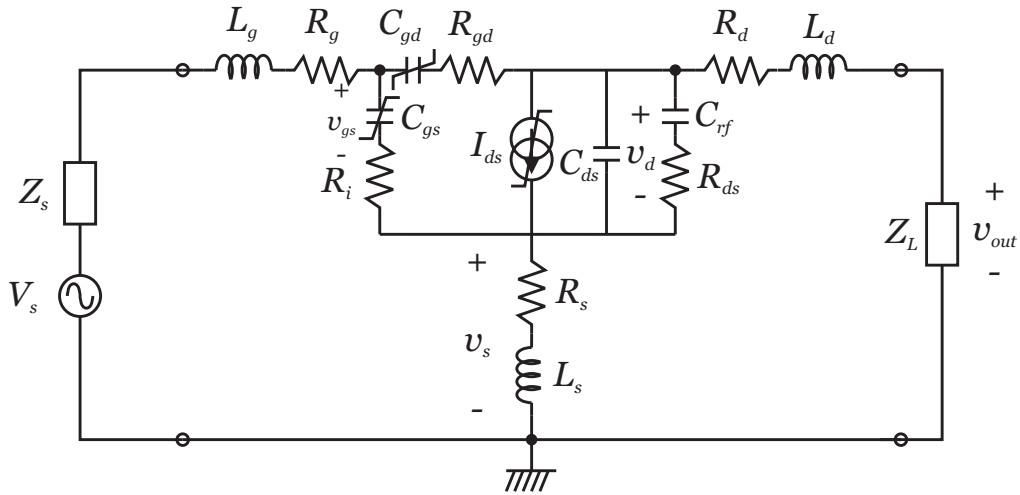


Figure 4.12: Equivalent three-node circuit employed to analyse the MESFET CFB0301 of Celeritek and the HEMT EPB018A5-70 of Excellics.

signal equivalent circuit model, based on the intuitive association of the circuit elements with the physical structure of the transistor, and describing the large-signal behaviour by curve fitting the dc $I_d - V_{ds}$ characteristics and the capacitance-voltage relationships of the transistor.

Among the elements of the equivalent circuit, R_g , R_s , R_d , L_g , L_s , and L_d form the extrinsic circuit. Regarding the intrinsic circuit, R_i is the intrinsic resistance or the resistance of the semiconductor region under the gate, between the source and channel. C_{ds} is the drain-to-source capacitance, which is dominated by metallization capacitance, and is therefore often treated as a constant. C_{gs} and C_{gd} are the gate-to-channel capacitances. Note that the branches containing $R_i - C_{gs}$ and $R_{ds} - C_{rf}$ introduce a filter-like frequency dependence, since they account for NQS or memory effects. I_{ds} is the nonlinear channel-current source.

Solid-state device models are used in circuit simulators based on Harmonic Balance or transient analysis, where the dominant implementations employ Newton iteration in their solution. Because of that, convergence of both methods requires continuous first and second derivatives of the $I - V$ and $Q - V$ expressions proposed by models. Furthermore, for accurate n -th order IM simulations, the modelling functions must reproduce not only the $I - V$ characteristic, but also its first n derivatives.

Since it is generally accepted that the dominant source of nonlinearity in MESFET and HEMT transistors is the drain-to-source current $I_{ds}(V_{gs}, V_{ds})$ [9], [21], [28], [73], [74], we will pay special attention to modelling the drain current characteristics and the models employed in this work will be reviewed. Furthermore, some remarks will be presented about modelling the gate capacitances, being the second source of nonlinearity.

- **Models for the drain current characteristics:**

- **Quadratic Curtice model:**

The description for the nonlinear drain current proposed in [211] takes the analytic form:

$$I_{ds}(V_{gs}, V_{ds}) = \beta(V_{gs} - V_T)^2 \cdot (1 + \lambda V_{ds}) \tanh(\alpha V_{ds}). \quad (4.21)$$

This model involves four parameters to be fitted with measurements: α , β , λ , and the threshold voltage V_T . Each of the terms whose multiplication gives rise to (4.21) emphasises a different feature of the $I - V$ characteristic. For example, the term $\beta(V_{gs} - V_T)^2$ models the approximately quadratic dependence of the drain current on voltage V_{ds} . The β parameter is related to the maximum drain current. The following term, $(1 + \lambda V_{ds})$, is employed to describe the finite output conductance, whose slope depends on the λ parameter. Finally, both saturation and knee regions in the $I - V$ characteristic are modelled by means of a \tanh function. The α parameter controls the sharpness of the knee region; the higher α is, the faster the saturation effects will be noticed. Note, that (4.21) describe the drain current as a separable function on the variables V_{gs} and V_{ds} , that is, $I_{ds} = I_{dA}(V_{gs}) \cdot I_{dA}(V_{ds})$.

In order to get the transconductance and output conductance, equation (4.21) is differentiated with respect to V_{gs} and V_{ds} , respectively. Note that this model predicts that all the transconductance derivatives are zero for orders higher than 3, that is, $g_{k0} = 0$ for $k \geq 3$, being this one of the main drawbacks for the use of this model in strongly nonlinear circuits.

In order to include the transit-time effects, it is suggested that the current dependence on V_{gs} be on the form $I_{ds}[V_{gs}(t - \tau), V_{ds}]^1$.

- **Curtice-Ettenberg or Curtice-cubic model:**

Curtice and Ettenberg [71] modified the original *Curtice model* by using a cubic approximation in order to get a better adjustment in the drain current as a function of the gate-to-source voltage, which provides an additional degree of freedom to fit the characteristics of the device:

$$I_{ds} = (A_0 + A_1 V_1 + A_2 V_1^2 + A_3 V_1^3) \cdot \tanh(\gamma V_{ds}), \quad (4.22)$$

¹In more recent works, such as [58], it has been stated that the τ parameter usually found in small-signal nonlinear models is not originated by transit-time effects or channel delay. Its physical meaning is related with the fact that the real drain-to-source conductance in the device depends on both V_{gs} and V_{ds} , which generates a transcapacitance term in the small-signal equivalent circuit. This term is usually added to the transconductance g_m and their sum is approximated by the voltage-controlled current source $g_m \exp[-j\omega\tau]v_{gs}$.

where V_1 is the input voltage. A_i coefficients are extracted from measurements in the saturation region by means of an adjustment in the least-square error sense. In order to include the increment experimented on the pinch-off voltage with an increasing voltage V_{ds} , it is considered that

$$V_1 = V_{gs}(t - \tau) \cdot [1 + \beta(V_{ds}^0 - V_{ds}(t))], \quad (4.23)$$

where β is the parameter controlling the change rate of the pinch-off voltage and V_{ds}^0 is the drain-to-source voltage (in saturation) for which the A_i coefficients have been extracted. Because of that, the drain current is no longer described as a separable function on the variables V_{gs} and V_{ds} .

– **Angelov model:**

Models previously presented were designed to describe the large-signal behaviour of MESFET devices and, despite they can also fit the $I - V$ characteristic for HEMT devices, there are certain features of HEMTs which are not sufficiently stressed with them. The transconductance is one of the most critical aspects for large-signal predictions. The transconductance of a HEMT device exhibits a peak value that is not present in MESFET devices. The *Angelov* or *Chalmers University model* [72] takes into account this phenomenon by means of a separable expression for the drain current $I_{ds}(V_{gs}, V_{ds}) = I_{dA}(V_{gs}) \cdot I_{dB}(V_{ds})$. The term $I_{dB}(V_{ds})$ is the same as the one used in the Curtice model. However, a gate control function $I_{dA}(V_{gs})$ is proposed wherein the first derivative has the same generic shape as the transconductance curve:

$$\begin{aligned} I_{ds} &= I_{pk}(1 + \tanh \psi) \cdot (1 + \lambda V_{ds}) \tanh(\alpha V_{ds}), \\ \psi &= P_1(V_{gs} - V_{pk}) + P_2(V_{gs} - V_{pk})^2 + P_3(V_{gs} - V_{pk})^3 + \dots \end{aligned} \quad (4.24)$$

where I_{pk} and V_{pk} are the drain current and gate voltage corresponding to the peak transconductance, respectively. In these expressions, the various P_i coefficients are empirical polynomial fitting parameters describing the dependence on an effective gate potential, ψ . The model is sufficiently accurate even if ϕ is approximated by a linear function. Note that this drain current function has well defined derivatives with respect to the gate voltage, which enables the identification of the higher-order derivative terms with the order of the distortion components.

• **Models for the gate capacitances:**

Whereas many of the remaining components in the large-signal equivalent circuit exhibit little or no voltage dependence, the input capacitances C_{gs} and C_{dg}

can vary significantly with bias in a nonlinear fashion. Early large-signal MES-FET models, such as the Curtice model, incorporate a voltage dependence for the model capacitors based on that of the ideal metal-semiconductor junction:

$$C_{gs}(V_{gs}) = \frac{C_{gs0}}{\sqrt{1 - \frac{V_{gs}}{V_{bi}}}}, \quad (4.25)$$

where C_{gs0} is the zero-bias capacitance, and V_{bi} is the built-in voltage of the Schottky barrier. The gate-to-drain capacitance can be described by means of the same analytic expression, although its value is significantly smaller under usual bias condition.

In the *Materka model*, the same expression is applied for the gate-to-source capacitance, as long as $V_{gs} < 0.8V_{bi}$. Nevertheless, for higher voltage values, the capacitance is approximated by a linear function with a slope calculated as $\left. \frac{dC_{gs}}{dV_{gs}} \right|_{V_{gs}=0.8V_{bi}}$.

However, since a close inspection of the measured capacitance-voltage dependence for the capacitors C_{gs} and C_{gd} indicates that the form of the relationship in several cases is different from that predicted by the aforementioned expressions, newly proposed models are functions of both V_{gs} and V_{ds} as well as they are fully charge-conservative [58].

For instance, in the Angelov model the same tanh functions employed in the drain current expression are used to model gate-to-source and gate-to-drain capacitances, and a certain cross-coupling of both V_{gs} and V_{ds} is taken into account in C_{gs} :

$$C_{gs} = C_{gs0} [1 + \tanh(\psi_1)] \cdot [1 + \tanh(\psi_2)], \quad (4.26)$$

$$C_{gd} = C_{gd0} [1 + \tanh(\psi_3)] \cdot [1 - \tanh(\psi_4)], \quad (4.27)$$

where

$$\begin{aligned} \psi_1 &= P_{0gs} + P_{1gs}V_{gs} + P_{2gs}V_{gs}^2 + P_{3gs}V_{gs}^3 + \dots \\ \psi_2 &= P_{0gsd} + P_{1gsd}V_{ds} + P_{2gsd}V_{ds}^2 + P_{3gsd}V_{ds}^3 + \dots \\ \psi_3 &= P_{0gd} + P_{1gd}V_{gs} + P_{2gd}V_{gs}^2 + P_{3gd}V_{gs}^3 + \dots \\ \psi_4 &= P_{0gdd} + (P_{1gdd} + P_{1cc}V_{gs})V_{ds} + P_{2gdd}V_{ds}^2 + P_{3gdd}V_{ds}^3 + \dots \end{aligned} \quad (4.28)$$

4.3.1.1 Illustrative examples of large-signal modelling

As it was explained in Chapter 3, the common features of both the EC and the SN methods are that they analyse the same augmented linear circuit for all the iterations.

Therefore, they can be summarised in the following iterative process:

$$[j\mathbf{Y}'(h\omega_c) - \Delta t \cdot \mathbf{Y}(h\omega_c)] \tilde{\mathbf{v}}_{\mathbf{n}}(h, t_{k+1}) = j\mathbf{Y}'(h\omega_c) \tilde{\mathbf{v}}_{\mathbf{n}}(h, t_k) - \Delta t \cdot \tilde{\mathbf{i}}_{\mathbf{n}}(h, t_{k+1}), \quad (4.29)$$

where a number N of nonlinear iterations will be considered for each case. In the example of Figure 4.12, the admittance matrix and its first derivative with respect to ω take the following expressions:

$$\mathbf{Y}(h\omega_c) = \begin{pmatrix} Y_{11}(h\omega_c) & Y_{12}(h\omega_c) & Y_{13}(h\omega_c) \\ Y_{21}(h\omega_c) & Y_{22}(h\omega_c) & Y_{23}(h\omega_c) \\ Y_{31}(h\omega_c) & Y_{32}(h\omega_c) & Y_{33}(h\omega_c) \end{pmatrix}, \quad (4.30)$$

with

$$\begin{aligned} Y_{11}(h\omega_c) &= \frac{1 + jh\omega_c R_i C_{gs}}{Z_s + R_g + jh\omega_c L_g} + \frac{jh\omega_c C_{gd} (1 + jh\omega_c R_i C_{gs})}{1 + jh\omega_c R_{gd} C_{gd}} + jh\omega_c C_{gs}, \\ Y_{12}(h\omega_c) &= -\frac{jh\omega_c C_{gd}}{1 + jh\omega_c R_{gd} C_{gd}}, \\ Y_{13}(h\omega_c) &= \frac{1}{Z_s + R_g + jh\omega_c L_g}, \\ Y_{21}(h\omega_c) &= g_{10} - \frac{jh\omega_c C_{gd} (1 + jh\omega_c R_i C_{gs})}{1 + jh\omega_c R_{gd} C_{gd}}, \\ Y_{22}(h\omega_c) &= g_{01} + \frac{1}{Z_L + R_d + jh\omega_c L_d} + \frac{jh\omega_c C_{gd}}{1 + jh\omega_c R_{gd} C_{gd}} + jh\omega_c C_{ds} + \frac{jh\omega_c C_{rf}}{1 + jh\omega_c R_{ds} C_{rf}}, \\ Y_{23}(h\omega_c) &= \frac{1}{Z_L + R_d + jh\omega_c L_d}, \\ Y_{31}(h\omega_c) &= -g_{10} - jh\omega_c C_{gs}, \\ Y_{32}(h\omega_c) &= -g_{01} - jh\omega_c C_{ds} - \frac{jh\omega_c C_{rf}}{1 + jh\omega_c R_{ds} C_{rf}}, \\ Y_{33}(h\omega_c) &= \frac{1}{R_s + jh\omega_c L_s}, \end{aligned} \quad (4.31)$$

and

$$\mathbf{Y}'(h\omega_c) = \begin{pmatrix} Y'_{11}(h\omega_c) & Y'_{12}(h\omega_c) & Y'_{13}(h\omega_c) \\ Y'_{21}(h\omega_c) & Y'_{22}(h\omega_c) & Y'_{23}(h\omega_c) \\ Y'_{31}(h\omega_c) & Y'_{32}(h\omega_c) & Y'_{33}(h\omega_c) \end{pmatrix}, \quad (4.32)$$

with

$$\begin{aligned} Y'_{11}(h\omega_c) &= \frac{jR_i C_{gs}}{Z_s + R_g + jh\omega_c L_g} - \frac{jL_g (1 + jh\omega_c R_i C_{gs})}{(Z_s + R_g + jh\omega_c L_g)^2} + \\ &+ \frac{jC_{gd} (1 + jh\omega_c R_i C_{gs})}{(1 + jh\omega_c R_{gd} C_{gd})^2} - \frac{h\omega_c R_i C_{gs} C_{gd}}{1 + jh\omega_c R_{gd} C_{gd}} + jC_{gs}, \\ Y'_{12}(h\omega_c) &= -\frac{jC_{gd}}{(1 + jh\omega_c R_{gd} C_{gd})^2}, \end{aligned}$$

$$\begin{aligned}
 Y'_{13}(h\omega_c) &= -\frac{jL_g}{(Z_s + R_g + jh\omega_c L_g)^2}, \\
 Y'_{21}(h\omega_c) &= -\frac{jC_{gd}(1 + jh\omega_c R_i C_{gs})}{(1 + jh\omega_c R_{gd} C_{gd})^2} + \frac{h\omega_c R_i C_{gs} C_{gd}}{1 + jh\omega_c R_{gd} C_{gd}}, \\
 Y'_{22}(h\omega_c) &= -\frac{jL_d}{(Z_L + R_d + jh\omega_c L_d)^2} + \frac{jC_{gd}}{(1 + jh\omega_c R_{gd} C_{gd})^2} + jC_{ds} + \frac{jC_{rf}}{(1 + jh\omega_c R_{ds} C_{rf})^2}, \\
 Y'_{23}(h\omega_c) &= -\frac{jL_d}{(Z_L + R_d + jh\omega_c L_d)^2}, \\
 Y'_{31}(h\omega_c) &= -jC_{gs}, \\
 Y'_{32}(h\omega_c) &= -jC_{ds} - \frac{jC_{rf}}{(1 + jh\omega_c R_{ds} C_{rf})^2}, \\
 Y'_{33}(h\omega_c) &= -\frac{jL_s}{(R_s + jh\omega_c L_s)^2}.
 \end{aligned} \tag{4.33}$$

The problem unknowns are the complex envelopes of the voltages as expressed in the following vector:

$$\tilde{\mathbf{v}}_{\mathbf{n}}(h, t) = \begin{bmatrix} \tilde{v}_{gs,n}(h, t) \\ \tilde{v}_{ds,n}(h, t) \\ \tilde{v}_{s,n}(h, t) \end{bmatrix}, \tag{4.34}$$

and the output voltage is:

$$\tilde{v}_{out,n}(h, t) = \frac{Z_L [\tilde{v}_{ds,n}(h, t) + \tilde{v}_{s,n}(h, t)]}{Z_L + R_d + jh\omega_c L_d}. \tag{4.35}$$

Note that constant generator (Z_s) and load (Z_L) impedances have been taken into account, since bias-Tees with ideally flat frequency response have been considered.

The only elements that still need to be modelled are the nonlinear ones, for which two different approaches have been followed for each active device:

- **Modelling of a MESFET device CFB0301 of Celeritek:**

In order to verify performance of the analysis methods described in Chapter 3, a simple amplifier has been constructed at 2 GHz based on a MESFET CFB0301 of Celeritek. Special care has been devoted to the following procedure in order to get an accurate model representing the nonlinearities of the device.

The active device has been biased under $V_{DS} = 2$ V and $I_D = 25$ mA, and the elements of the small-signal circuit have been obtained from S -parameter measurements with a VNA. Fukui method has been employed for the extraction of access resistors and Dambrine-Cappy method for determining the elements of the intrinsic circuit, following an overall optimization with Agilent's Advanced Design System (ADS) software.

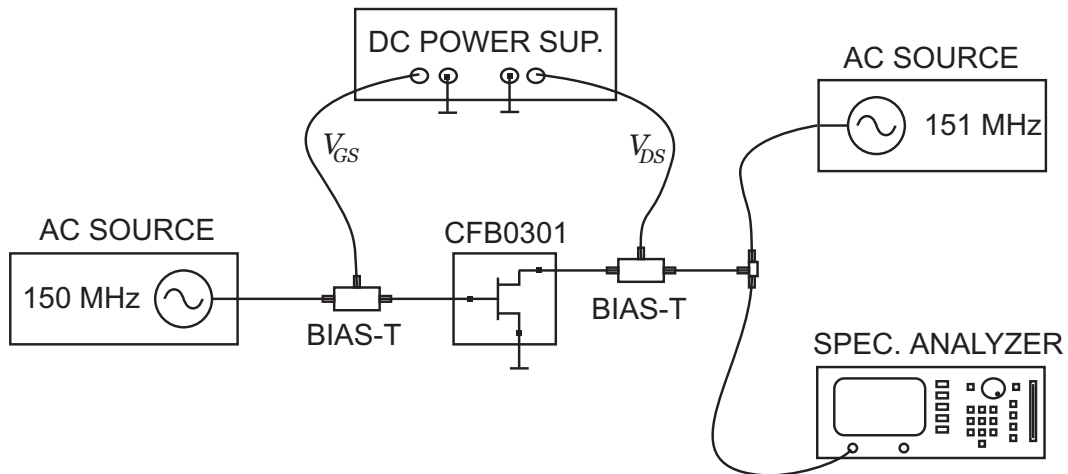


Figure 4.13: Measurement setup for large-signal characterization of a MESFET amplifier.

Regarding the large-signal model, only the nonlinear drain current source has been taken into consideration, since C_{gd} and C_{gs} have been considered linear capacitances. The drain current parameters have been fitted to an Angelov [72] model with only six coefficients ($P_2 = 0$) using the measurement setup shown in Figure 4.13. Two signals at incommensurate VHF frequencies (150 and 151 MHz) were injected into the source and drain ports and the different IM products were measured with a spectrum analyser. Extraction of the large-signal parameters was accomplished through a double Volterra-series approach [42] by comparing measurements of each product with the predicted IM in terms of nonlinear transfer functions of order $n + m$. The accuracy of the achieved adjustment is depicted in Figure 4.14, showing a good agreement.

- **Modelling of a HEMT device EPB018A5 of Excellics:**

Another single-FET amplifier has been constructed and modelled, apart from the previously presented MESFET amplifier. The active device in this case is the HEMT EPB018A5 of Excellics Semiconductor Inc., encapsulated in a 70-mil package and mounted on a 2×2 cm PTFE substrate for in-fixture measurements. The dc bias has been applied to the gate and drain ports by using two ZFBT-6G bias-Tees of Minicircuits Inc. The active device has been biased at $V_{GS} = -0.245$ V and $V_{DS} = 2$ V, in order to have a drain current of 15 mA.

The manufacturer of the active device provides both small-signal and package equivalent circuits, together with the typical parameters of a Curtice-cubic large-signal model [71]. The large-signal model includes a Curtice-cubic model for the nonlinear gate-to-source capacitance, considering to be linear the gate-to-drain capacitance. However, in order to accomplish the simulations, the nonlinear pa-

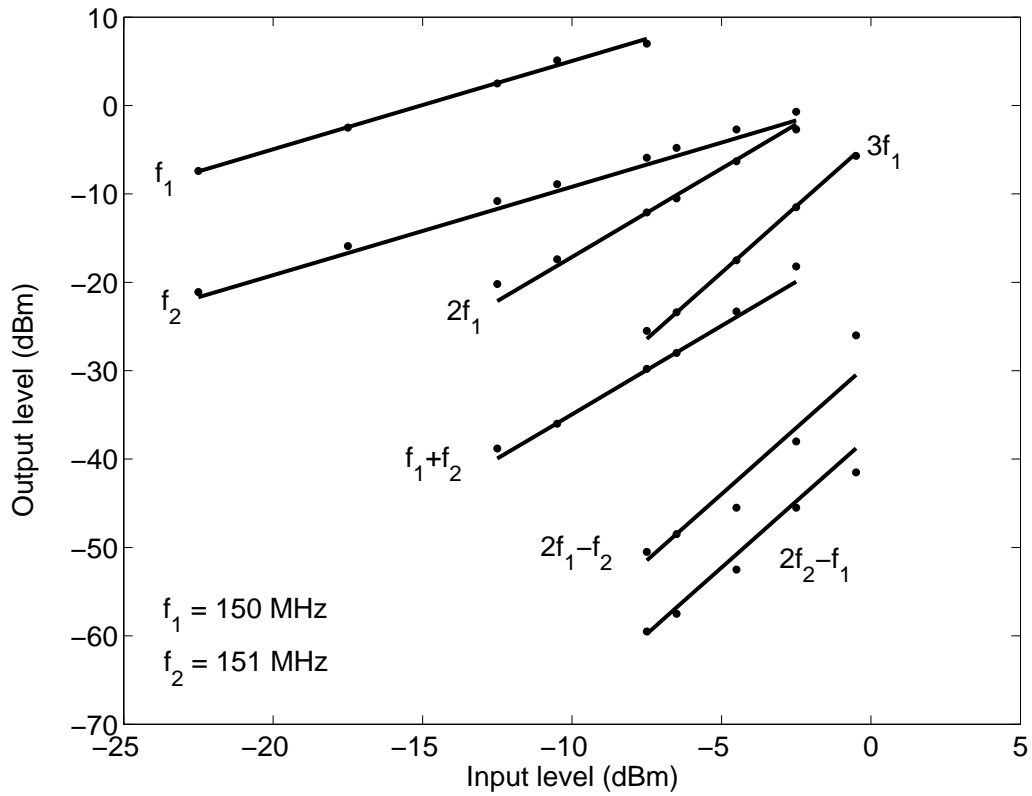


Figure 4.14: IM products level measured at the input of the spectrum analyser: dots, measurements; solid line, predictions employing Angelov’s model.

rameters provided by the manufacturer resulted in non-negligible inaccuracies that made necessary a careful re-modelling of the main nonlinearity I_{ds} . This re-modelling procedure consisted in adjusting new parameters optimised for an Angelov model using six coefficients (with $\lambda = 1$).

Furthermore, a mixer has been constructed using the aforementioned HEMT device EPB018A5-70 of Excellics, which has been biased as a gate mixer. The same equivalent circuit as in the case of an amplifier has been employed, in which a different bias has been taken and two excitation signals have been injected. The optimum bias point has been obtained experimentally resulting in a gate voltage $V_{GS} = -0.45$ V for the recommended drain voltage $V_{DS} = 2$ V. These voltages have been applied through two bias-Tees used to decouple the dc from LO and RF signals in the input and from the IF signal in the output. The RF signal at $f_{RF} = 2$ GHz and the LO signal at $f_{LO} = 1.86$ GHz have been applied by using a directional coupler and the LO level has been also experimentally fixed at $P_{LO} = -4.5$ dBm, in order to obtain the maximum gain.

4.3.2 Envelope Currents method

In order to verify the performance of the EC method described in Section 3.4 the simple amplifier constructed with the MESFET CFB0301 of Celeritek has been employed. The performance of the amplifier has been widely characterised at 2 GHz and measurements have been compared with the predictions of the EC method. The following nonlinear envelope currents have been taken into consideration, since we were interested in predicting the output for the fundamental frequency zone and the second and third harmonics after three iterations:

- For the linear case, $n = 1$, only the fundamental frequency zone with $h = 1$ was taken into account:

$$\tilde{\mathbf{i}}_1(1, t) = \begin{bmatrix} \frac{\tilde{v}_g(t)}{Z_s + R_g + j\omega_c L_g} \\ 0 \\ 0 \end{bmatrix}. \quad (4.36)$$

- For the second iteration, $n = 2$, two envelope current components for $h = 0$ and $h = 2$ need to be considered:

$$\tilde{\mathbf{i}}_2(0, t) = \begin{bmatrix} 0 \\ -\tilde{i}_{d,2}(0, t) \\ \tilde{i}_{d,2}(0, t) \end{bmatrix}, \quad (4.37)$$

$$\tilde{\mathbf{i}}_2(2, t) = \begin{bmatrix} 0 \\ -\tilde{i}_{d,2}(2, t) \\ \tilde{i}_{d,2}(2, t) \end{bmatrix}, \quad (4.38)$$

with

$$\tilde{i}_{d,2}(0, t) = \frac{g_{20}}{2} |\tilde{v}_{gs,1}(1, t)|^2 + \frac{g_{02}}{2} |\tilde{v}_{ds,1}(1, t)|^2 + \frac{g_{11}}{2} \text{Re}\{\tilde{v}_{gs,1}(1, t)\tilde{v}_{ds,1}^*(1, t)\}, \quad (4.39)$$

$$\tilde{i}_{d,2}(2, t) = \frac{g_{20}}{2} \tilde{v}_{gs,1}^2(1, t) + \frac{g_{02}}{2} \tilde{v}_{ds,1}^2(1, t) + \frac{g_{11}}{2} \tilde{v}_{gs,1}(1, t)\tilde{v}_{ds,1}(1, t). \quad (4.40)$$

- For the third iteration, $n = 3$, again two envelope current components for $h = 1$ and $h = 3$ are considered, although the latter is just necessary because a prediction of the third harmonic is sought:

$$\tilde{\mathbf{i}}_3(1, t) = \begin{bmatrix} 0 \\ -\tilde{i}_{d,3}(1, t) \\ \tilde{i}_{d,3}(1, t) \end{bmatrix}, \quad (4.41)$$

$$\tilde{\mathbf{i}}_3(3, t) = \begin{bmatrix} 0 \\ -\tilde{i}_{d,3}(3, t) \\ \tilde{i}_{d,3}(3, t) \end{bmatrix}, \quad (4.42)$$

with

$$\begin{aligned}
 \tilde{i}_{d,3}(1, t) = & \frac{3g_{30}}{4} \tilde{v}_{gs,1}^2(1, t) \tilde{v}_{gs,1}^*(1, t) + \frac{3g_{03}}{4} \tilde{v}_{ds,1}^2(1, t) \tilde{v}_{ds,1}^*(1, t) + \\
 & 2g_{20} \left[\frac{1}{2} \tilde{v}_{gs,1}^*(1, t) \tilde{v}_{gs,2}(2, t) + \tilde{v}_{gs,1}(1, t) \tilde{v}_{gs,2}(0, t) \right] + \\
 & 2g_{02} \left[\frac{1}{2} \tilde{v}_{ds,1}^*(1, t) \tilde{v}_{ds,2}(2, t) + \tilde{v}_{ds,1}(1, t) \tilde{v}_{ds,2}(0, t) \right] + \\
 & g_{11} \left[\frac{1}{2} \tilde{v}_{gs,1}^*(1, t) \tilde{v}_{ds,2}(2, t) + \tilde{v}_{gs,1}(1, t) \tilde{v}_{ds,2}(0, t) + \right. \\
 & \left. + \frac{1}{2} \tilde{v}_{ds,1}^*(1, t) \tilde{v}_{gs,2}(2, t) + \tilde{v}_{ds,1}(1, t) \tilde{v}_{gs,2}(0, t) \right] + \\
 & \frac{g_{21}}{4} [\tilde{v}_{gs,1}^2(1, t) \tilde{v}_{ds,1}^*(1, t) + 2|\tilde{v}_{gs,1}(1, t)|^2 \tilde{v}_{ds,1}(1, t)] + \\
 & \frac{g_{12}}{4} [\tilde{v}_{ds,1}^2(1, t) \tilde{v}_{gs,1}^*(1, t) + 2|\tilde{v}_{ds,1}(1, t)|^2 \tilde{v}_{gs,1}(1, t)], \tag{4.43}
 \end{aligned}$$

$$\begin{aligned}
 \tilde{i}_{d,3}(3, t) = & \frac{g_{30}}{4} \tilde{v}_{gs,1}^3(1, t) + \frac{g_{03}}{4} \tilde{v}_{ds,1}^3(1, t) + \frac{g_{21}}{4} \tilde{v}_{gs,1}^2(1, t) \tilde{v}_{ds,1}(1, t) + \\
 & \frac{g_{12}}{4} \tilde{v}_{ds,1}^2(1, t) \tilde{v}_{gs,1}(1, t) + g_{20} \tilde{v}_{gs,1}(1, t) \tilde{v}_{gs,2}(2, t) + g_{02} \tilde{v}_{ds,1}(1, t) \tilde{v}_{ds,2}(2, t) + \\
 & \frac{g_{11}}{2} [\tilde{v}_{gs,1}(1, t) \tilde{v}_{ds,2}(2, t) + \tilde{v}_{ds,1}(1, t) \tilde{v}_{gs,2}(2, t)] \tag{4.44}
 \end{aligned}$$

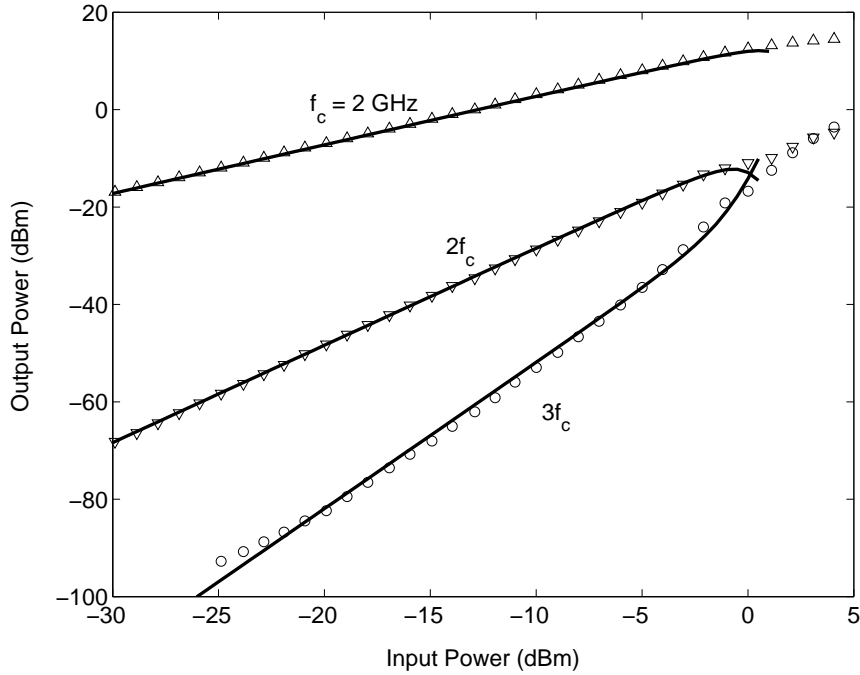


Figure 4.15: Output power for a MESFET amplifier at the fundamental frequency, second and third harmonics. Dots, measurements; solid line, simulations using the EC method.

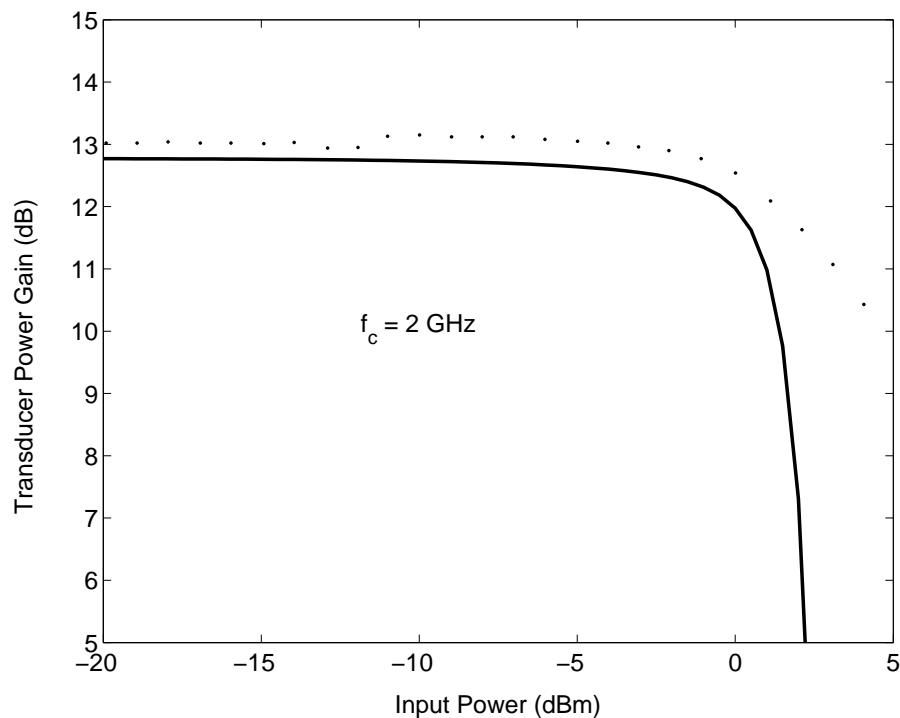


Figure 4.16: Power gain of a MESFET amplifier at 2 GHz. Dots, measurements; solid line, simulations using the EC method.

Simulations have been accomplished by using the adjusted Angelov model to obtain the coefficients g_{kl} used in the nonlinear current source expressions as defined in (2.43). Figure 4.15 shows the first, second and third harmonics at the output in a wide range of input power levels. The amplifier gain is depicted in Figure 4.16, demonstrating a good correspondence.

The amplifier has also been tested with a 2 GHz 3GPP QPSK W-CDMA signal at a rate of 3.84 Mcps using raised-cosine (RC) and root-raised-cosine (RRC) pulse-shaping filters. For the simulations, 256 symbols of a QPSK sequence were generated, taking eight samples per symbol and using pulse-shaping filters with a length equivalent to 24 symbols and a 0.22 roll-off factor. Figure 4.17 compares the measured spectrum at the output port with the simulated PSD following the EC method for a RC filter. Two different input levels are used, the first one low enough for the nonlinearities of the amplifier not to be appreciable and the second one closer to the 1 dB compression point, where a notable spectral regrowth causing adjacent-channel interference can be observed. For the sake of comparison, Figure 4.18 depicts the same information using a RRC filter, with predictions obtained with the EC method. A greater spectral regrowth in the second case is clearly noticeable due to the pulse-shaping filter applied. In both cases, the simulations agree with measurements satisfactorily. Considering the small computation times necessary to achieve this appropriate agreement, it can

4. COMPARISON WITH EXPERIMENTAL MEASUREMENTS

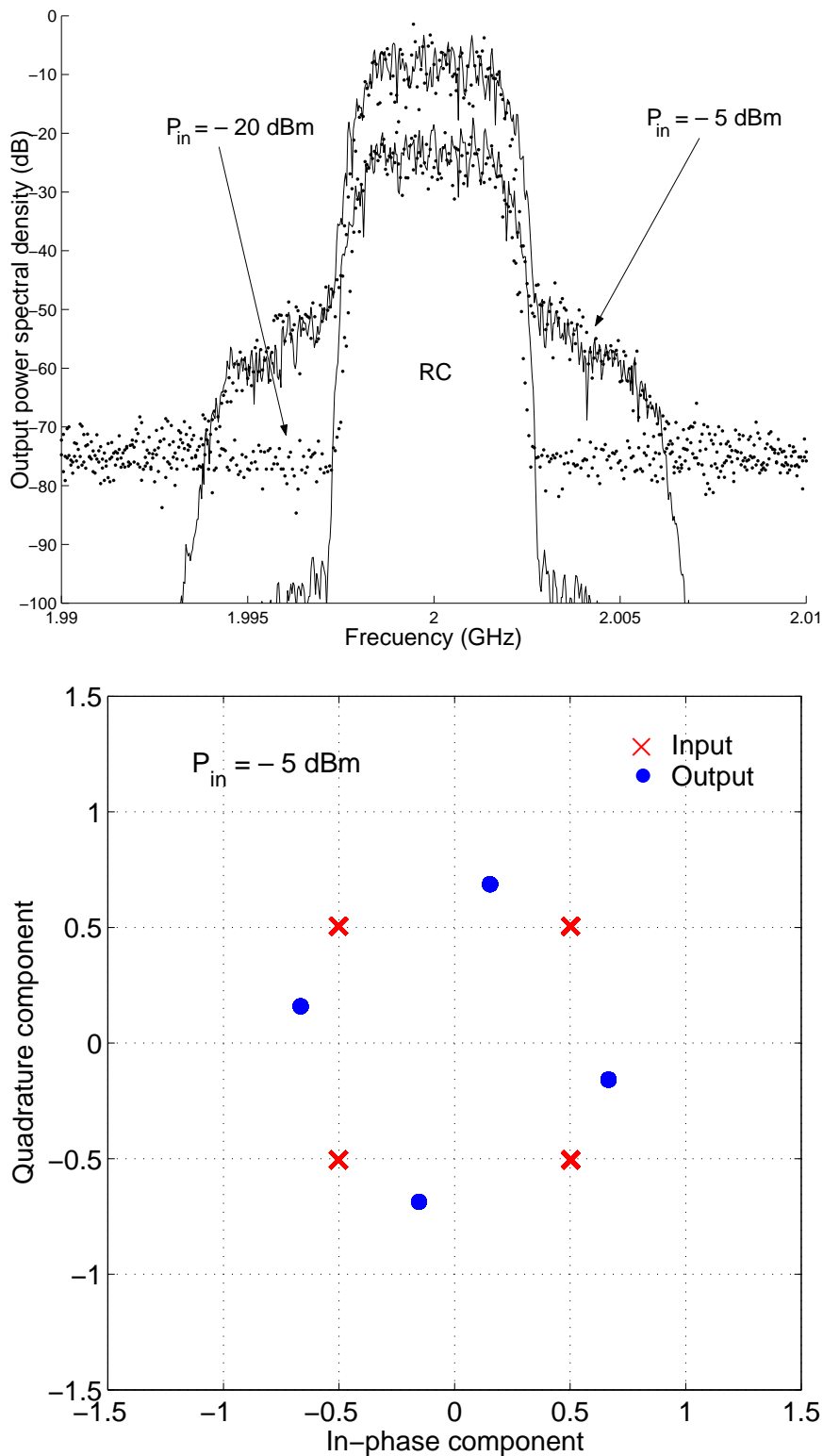


Figure 4.17: Constellation and output PSD of a MESFET amplifier for two input power levels with a raised-cosine pulse shaping filter. Dots, measurements; solid line, predictions with the EC method.

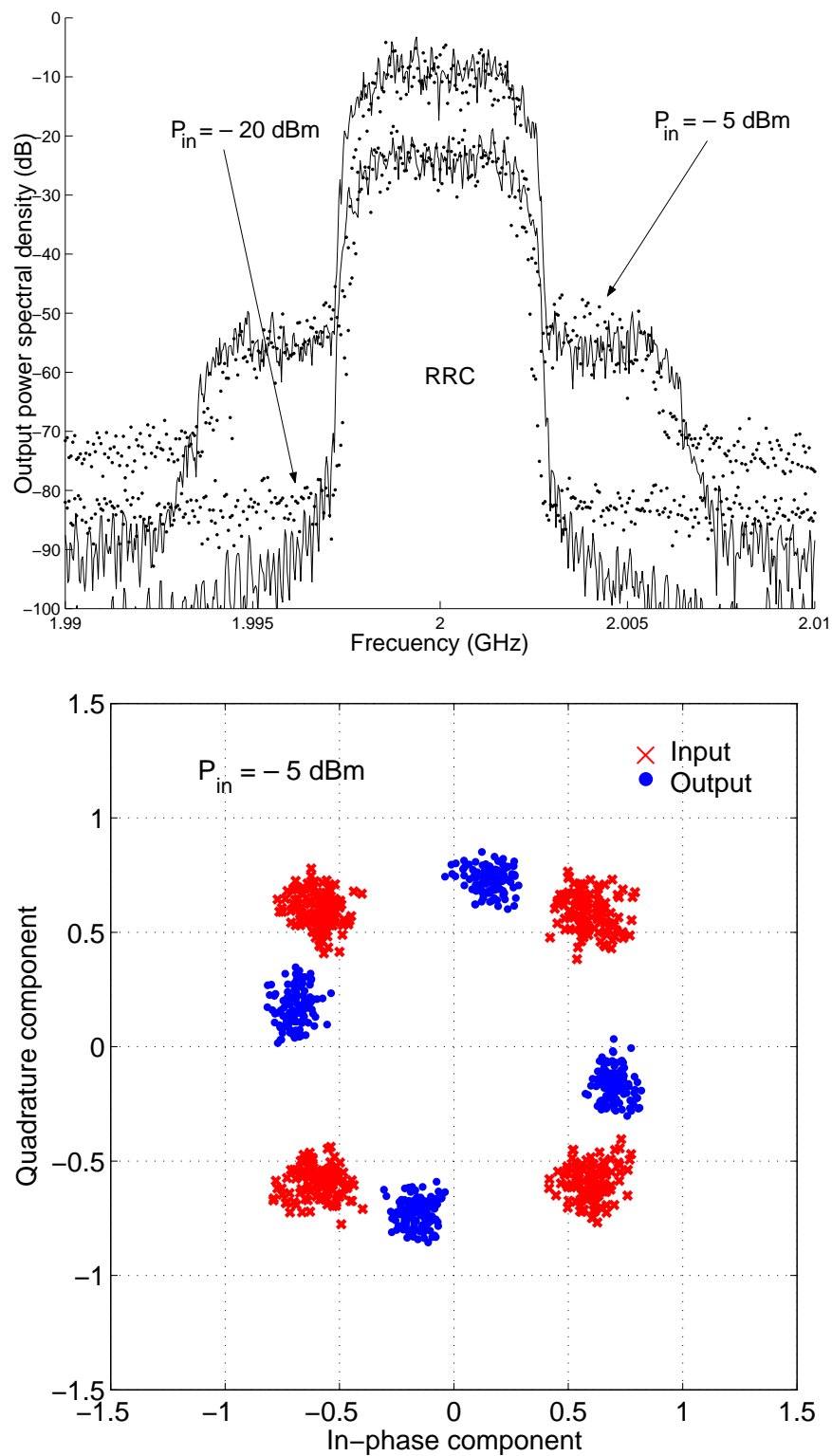


Figure 4.18: Constellation and output PSD of a MESFET amplifier for two input power levels with a root-raised-cosine pulse shaping filter. Dots, measurements; solid line, predictions with the EC method.

be concluded that envelope-based approaches such as the EC method are appropriate to predict spectral regrowth and ACPR for nonlinear devices. Nevertheless, in the next section it will be shown that a greater reduction in computation times while maintaining a satisfactory agreement with measurements can be achieved by using a SN approach.

4.3.3 Simplified Newton approach for weakly nonlinear communication circuits

In order to demonstrate the SN approach proposed in Section 3.6, the amplifier constructed with the HEMT EPB018A5 of Excelics has been used. The following nonlinear envelope currents have been taken into consideration for predicting the output for the fundamental frequency zone, and the second and third harmonics. For the simulations with the SN method, coefficients of both the nonlinear drain current source and the nonlinear gate-to-source capacitance up to the second order are taken into account:

- For the linear case, $n = 1$, only the fundamental frequency zone with $h = 1$ was taken into account:

$$\tilde{\mathbf{i}}_1(1, t) = \begin{bmatrix} \frac{\tilde{v}_g(t)}{Z_s + R_g + j\omega_c L_g} \\ 0 \\ 0 \end{bmatrix}. \quad (4.45)$$

- For the second iteration, $n = 2$, four envelope current components for $h = 0, 1, 2$, and 3 need to be considered:

$$\tilde{\mathbf{i}}_2(h, t) = \begin{bmatrix} -\tilde{i}_{c,2}(h, t) \\ -\tilde{i}_{d,2}(h, t) \\ \tilde{i}_{d,2}(h, t) + \tilde{i}_{c,2}(h, t) \end{bmatrix}, \quad (4.46)$$

with

$$\tilde{i}_{d,2}(0, t) = \frac{g_{20}}{2} |\tilde{v}_{gs,1}(t)|^2 + \frac{g_{02}}{2} |\tilde{v}_{ds,1}(t)|^2 + \frac{g_{11}}{2} \text{Re}\{\tilde{v}_{gs,1}(t)\tilde{v}_{ds,1}^*(t)\} \quad (4.47)$$

$$\begin{aligned} \tilde{i}_{d,2}(1, t) = & \frac{3g_{30}}{4} |\tilde{v}_{gs,1}(t)|^2 \tilde{v}_{gs,1}(t) + \frac{3g_{03}}{4} |\tilde{v}_{ds,1}(t)|^2 \tilde{v}_{ds,1}(t) + \frac{g_{21}}{4} \tilde{v}_{gs,1}^2(t) \tilde{v}_{ds,1}^*(t) + \\ & + \frac{g_{21}}{2} |\tilde{v}_{gs,1}(t)|^2 \tilde{v}_{ds,1}(t) + \frac{g_{12}}{4} \tilde{v}_{ds,1}^2(t) \tilde{v}_{gs,1}^*(t) + \frac{g_{12}}{2} |\tilde{v}_{ds,1}(t)|^2 \tilde{v}_{gs,1}(t) \end{aligned} \quad (4.48)$$

$$\tilde{i}_{d,2}(2, t) = \frac{g_{20}}{2} \tilde{v}_{gs,1}^2(t) + \frac{g_{02}}{2} \tilde{v}_{ds,1}^2(t) + \frac{g_{11}}{2} \tilde{v}_{gs,1}(t) \tilde{v}_{ds,1}(t) \quad (4.49)$$

$$\tilde{i}_{d,2}(3, t) = \frac{g_{30}}{4} \tilde{v}_{gs,1}^3(t) + \frac{g_{03}}{4} \tilde{v}_{ds,1}^3(t) + \quad (4.50)$$

$$+ \frac{g_{21}}{4} \tilde{v}_{gs,1}^2(t) \tilde{v}_{ds,1}(t) + \frac{g_{12}}{4} \tilde{v}_{ds,1}^2(t) \tilde{v}_{gs,1}(t)$$

$$\tilde{i}_{c,2}(0, t) = 0 \quad (4.51)$$

$$\tilde{i}_{c,2}(1, t) = j\omega \frac{C_2}{4} |\tilde{v}_{gs,1}(t)|^2 \tilde{v}_{gs,1}(t) \quad (4.52)$$

$$\tilde{i}_{c,2}(2, t) = j\omega \frac{C_1}{2} \tilde{v}_{gs,1}^2(t) \quad (4.53)$$

$$\tilde{i}_{c,2}(3, t) = j\omega \frac{C_2}{4} \tilde{v}_{gs,1}^3(t) \quad (4.54)$$

The amplifier has been widely characterised at 2 GHz, including one- and two-tone tests and measurements of ACPR under a 3GPP UMTS W-CDMA input signal. Figure 4.19 shows the gain compression as a function of the input level for a two-tone excitation with a separation of 1 MHz between the tones. It can be observed that the SN approach shows a good dynamic range, even when only the first and second iteration (solid line) are computed and it is necessary to solve only two systems of equations. These conclusions are also evident in Figure 4.20, where both the output upper tone and IM3 levels are depicted. Simulation time for these data was below 2 seconds in a Pentium IV PC. Performance is enhanced by using a communications signal, as shown in Figs. 4.21 and 4.22, where spectral regrowth is successfully compared with measurements for a 3GPP UMTS W-CDMA signal with 3.84 Mchip/s. To simulate this signal, 4096 samples of a QPSK complex envelope with root-raised-cosine pulse-shaping filter were generated. The correspondence between the EC method, the SN approach and the measured spectrum is very good, and a close agreement with measurements is accomplished even when only two systems of equations are solved, i.e., computing only up to the second iteration for the SN approach (see Figure 4.21). With regard to simulation times, the computation of three iterations took approximately the same time with the EC method than with the SN approach, while in Figure 4.21 a reduction over 50 % of the time was achieved. Despite the theoretical restriction of weakly nonlinear behaviour, in practice the SN approach is able to predict spectral regrowth fairly accurately even with an input power level close to the 1-dB compression point, as it is shown in Figure 4.23.

The aforementioned accuracy in the prediction of spectral regrowth for a wide dynamic range and the reduced simulation times allows us to perform ACPR simulations as the one shown in Figure 4.24, where the EC method is compared with the SN approach up to the second and third iteration.

As it was explained in Section 3.6, although nonlinearities above third order have been neglected for these examples, the SN approach can be easily extended to higher orders and, simply from the second iteration, nonlinear effects can be predicted in a cost-efficient simulation time.

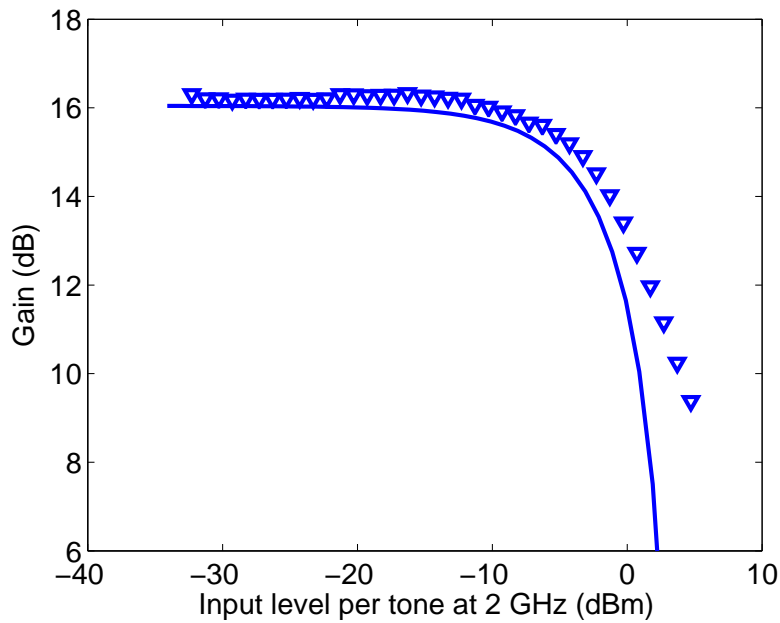


Figure 4.19: Power gain of a HEMT amplifier for an input of two-tones. Measurements (triangles) are compared to the prediction using the SN approach up to the second iteration (solid line).

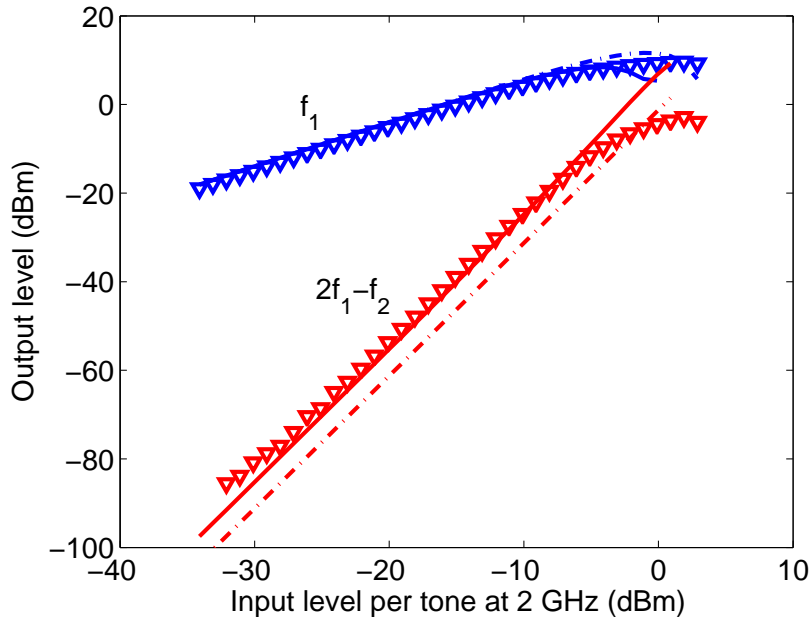


Figure 4.20: IM products for a HEMT amplifier as a function of input power level. Obtained values for the SN approach (solid line), and considering only up to the second iteration (dashed-dotted line). Measurements at 2 GHz (triangles).

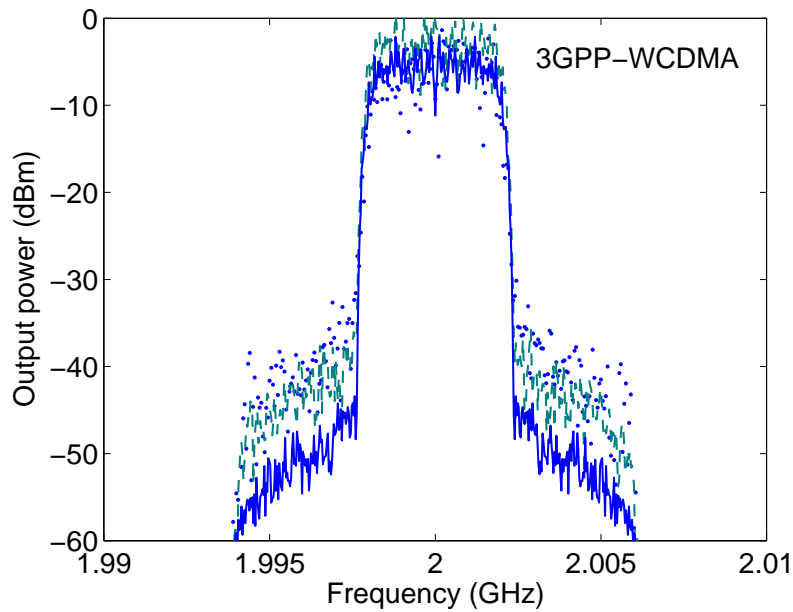


Figure 4.21: Spectral regrowth prediction for a HEMT amplifier with a 3GPP UMTS W-CDMA signal. Measurements (dots) are compared to the SN approach up to the second iteration (solid line) and to the EC method up to the third iteration (dotted line).

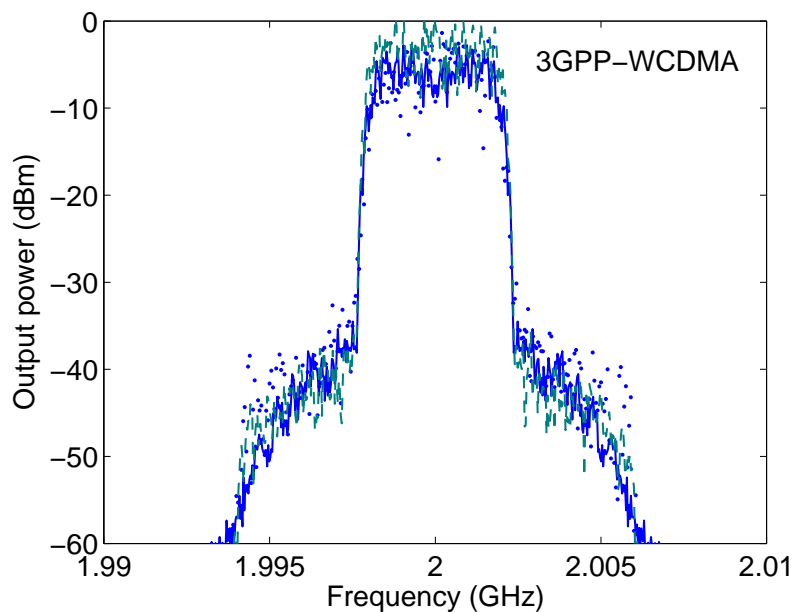


Figure 4.22: Spectral regrowth prediction for a HEMT amplifier with a 3GPP UMTS W-CDMA signal. Measurements (dots) are compared to the SN approach (solid line) and to the EC method (dotted line), in both cases up to the third iteration.

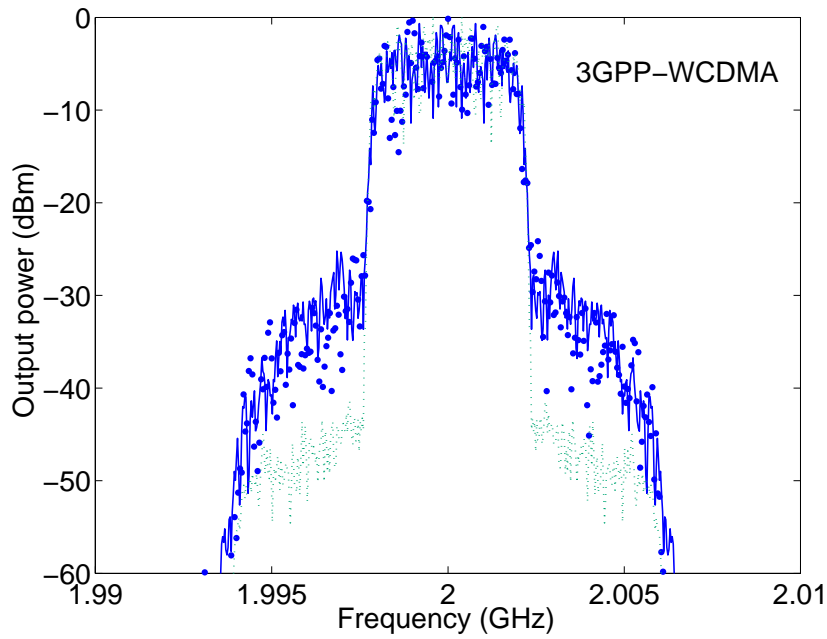


Figure 4.23: Spectral regrowth prediction for a HEMT amplifier with a 3GPP W-CDMA signal and an input level near the 1-dB compression point. Measurements (dots) are compared to the SN approach up to the third (solid line) and second (dotted line) iteration.

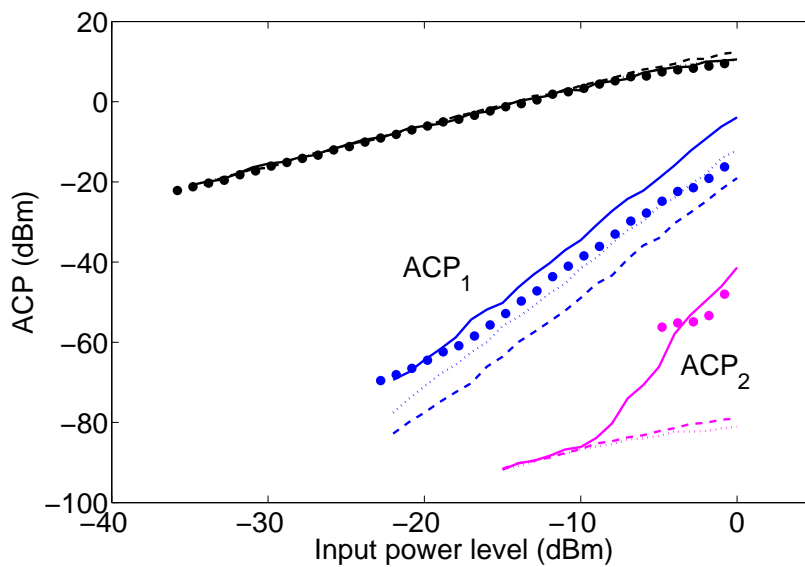


Figure 4.24: In-band power and ACP prediction in the first and second adjacent channels for a HEMT amplifier with a 3GPP UMTS W-CDMA signal versus the input level. Measurements (dots) are compared with the SN approach up to the third (solid line) and second (dashed line) iteration and to the EC method (dotted line).

4.3.4 Two alternate Envelope Currents approaches for communication signals in mixers

To demonstrate and compare the performance of the NEC and E-PHB approaches described in Sections 3.7.2.1 and 3.7.2.2, respectively, the simple mixer constructed with the HEMT EPB018A5-70 of Excellics has been employed. A set of measurements were performed to empirically characterise the mixer, and in all cases the corresponding simulations were implemented according to the experimental conditions.

First, a one-tone test was performed and the resulting conversion gain was compared satisfactorily with the calculated results. The mixer was also tested with two RF tones at 2 and 2.001 GHz, varying the power level. Figure 4.25 shows the measured conversion gain (marks) and it is possible to observe that the characteristics calculated with the E-PHB, depicted in the same figure with a solid line, and the NEC method, depicted with a dashed line, are very close to the experimental results, even for levels well beyond the 1-dB compression point. Besides this, the output power level of the two intermediate frequencies and of the IMD are shown in Figure 4.26. Good agreement of the calculated IMD in approximately the same level range is evident.

Finally, a 2 GHz 3GPP UMTS W-CDMA RF signal was generated at a rate of 3.84 Mchips/s and the IF output was measured for different levels of input power. In all cases the spectra were recorded and the corresponding spectral regrowth could be observed. Under this condition Figure 4.27 depicts the IF output spectrum showing the spectral regrowth that appears when a RRC pulse-shaping filter is used and even in this case the coincidence between computed and measured data with the E-PHB approach is remarkable. Notice that low level measurements were limited by the noise floor of the analyser, about -80 dBm in this case. Furthermore, it should be noticed that the calculated output spectra with both NEC and E-PHB approaches presented close-fitting characteristics in a high dynamic range. In fact, only for a high signal level above 1-dB compression point, unrealistic in wireless communication systems, the discrepancy was distinct, as Figure 4.28 reveals.

In addition to this, measurements of the output power level within the channel of interest and the ACP in two lower- and upper-adjacent channels were made for a wide range of input power levels using the same 2 GHz 3GPP UMTS W-CDMA signal. Figure 4.29 shows a comparison of measured and computed in-band power as well as ACP. Agreement is very good in all measured range validating the approach presented in this communication. Moreover, E-PHB employed about five minutes per power point in this simulation when each harmonic of the IF was computed separately to reduce the CPU time.

4. COMPARISON WITH EXPERIMENTAL MEASUREMENTS

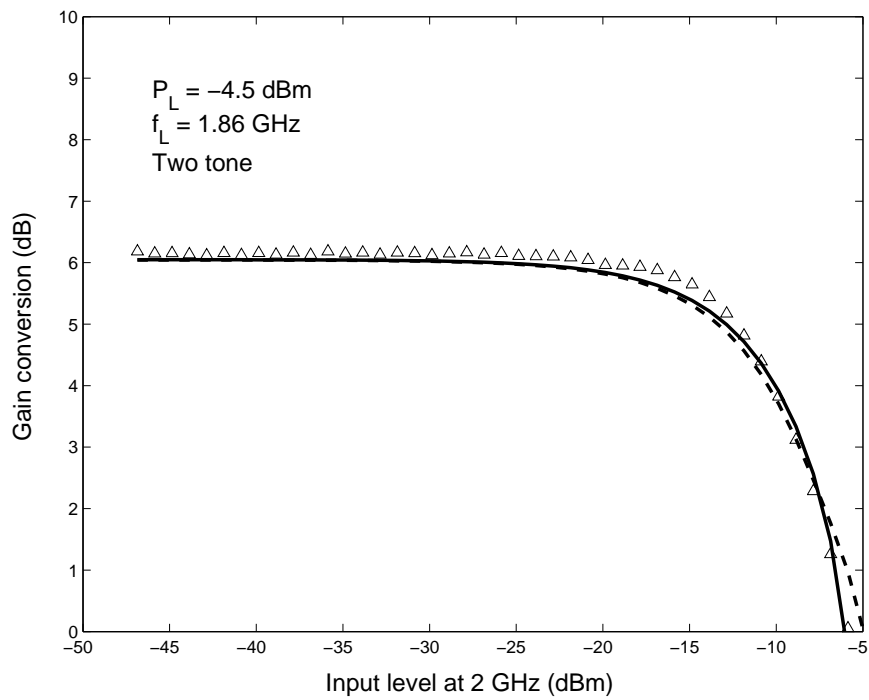


Figure 4.25: Conversion gain of the HEMT gate mixer for two-tone input. Measurements (marks) and results computed with the proposed methods (E-PHB: solid line; NEC: dashed line)

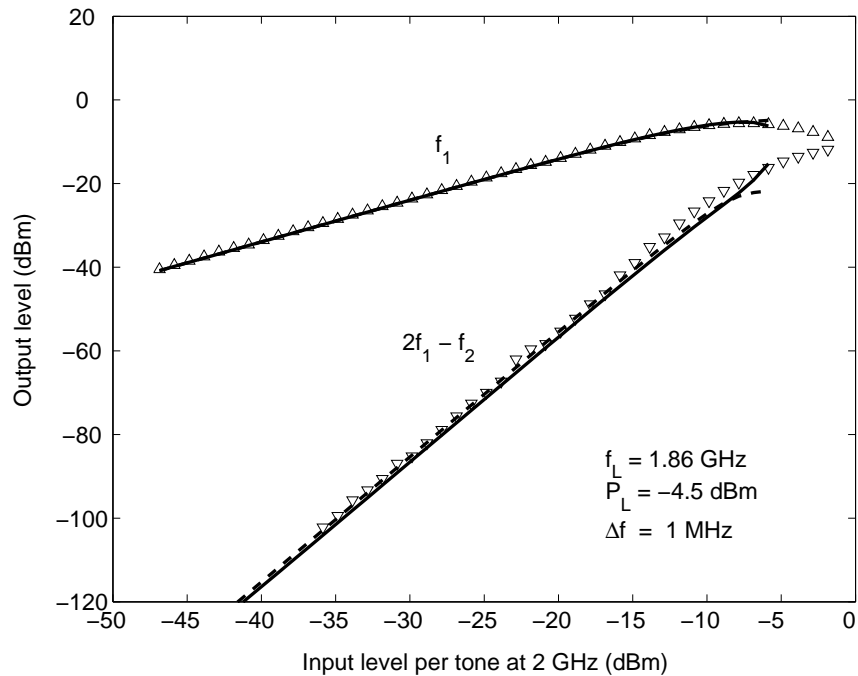


Figure 4.26: Two-tone IMD of the HEMT gate mixer versus input power. Measurements at $f_{RF} = 2$ GHz (marks) and results computed with the proposed methods (E-PHB: solid line; NEC: dashed line).

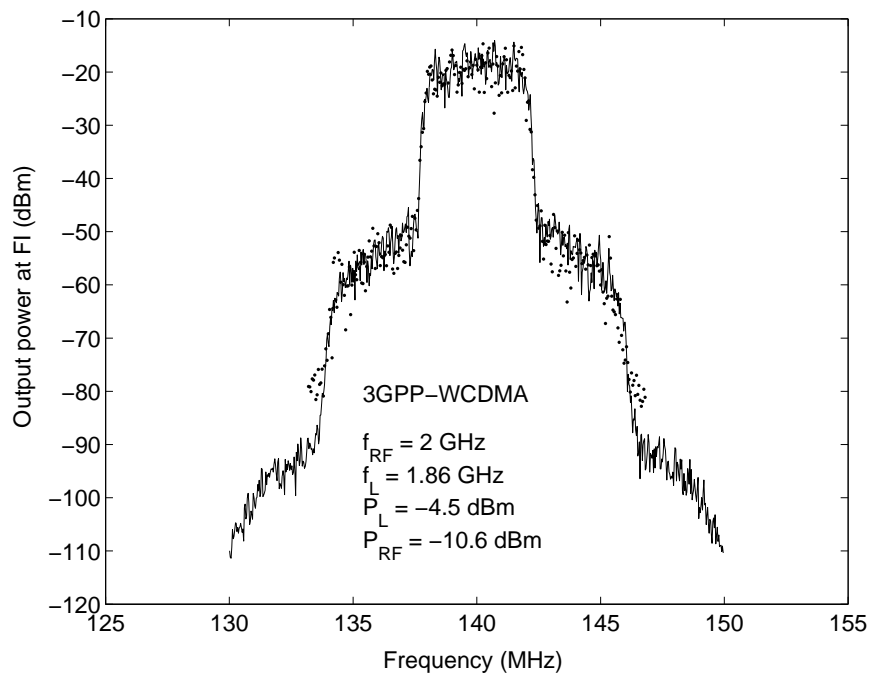


Figure 4.27: Spectral regrowth prediction for a 3GPP UMTS W-CDMA signal (solid line) and measurements at $f_{RF} = 2$ GHz (dots). Resolution bandwidth: 100 kHz.

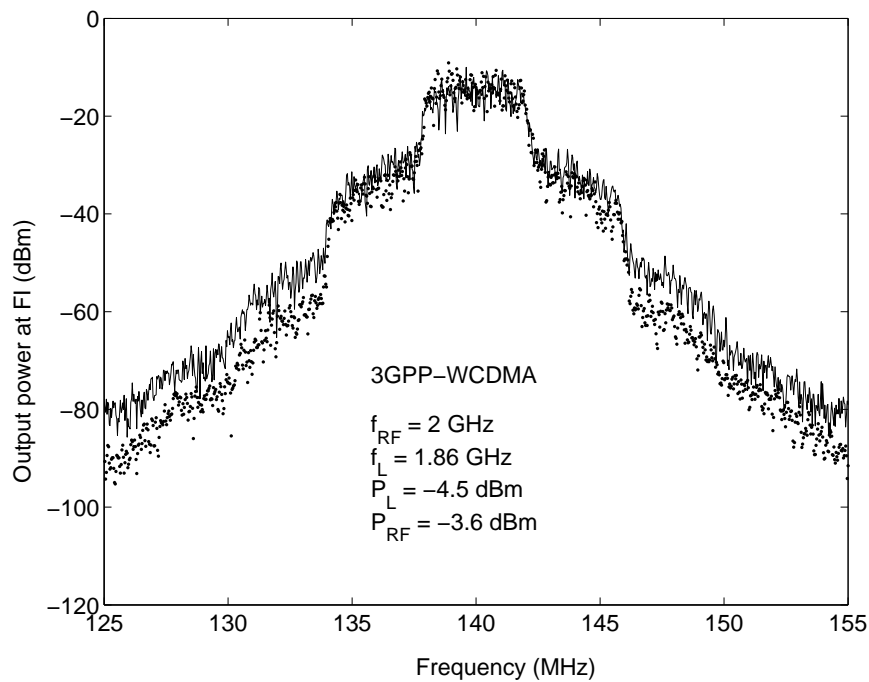


Figure 4.28: Spectral regrowth prediction of a 3GPP UMTS W-CDMA strong signal applied to a HEMT gate mixer. Computed with E-PHB (dots) and with NEC (solid line). Resolution bandwidth: 300 kHz.

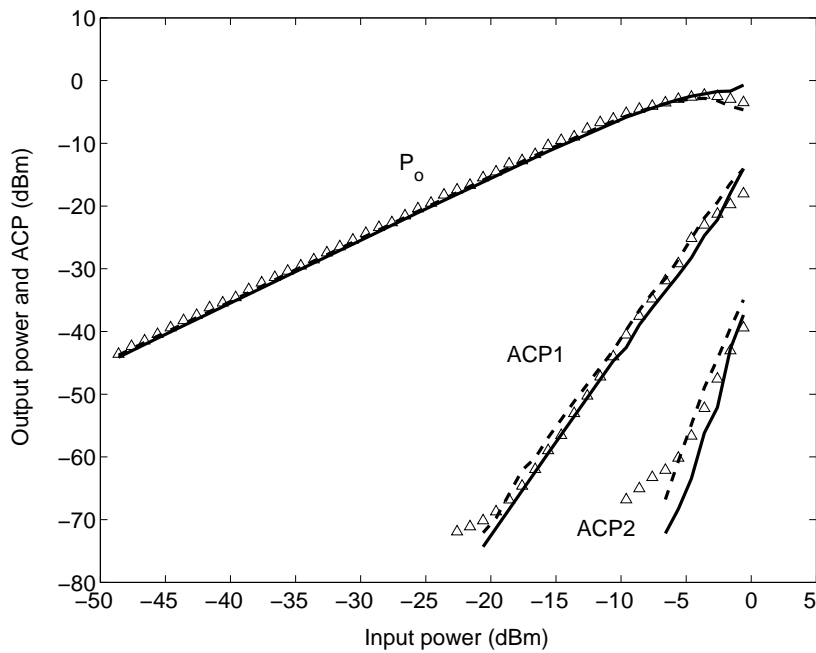


Figure 4.29: In-band power and adjacent channel power prediction for a 3GPP UMTS W-CDMA signal (E-PHB: solid line and NEC: dashed line) and measurements at $f_{RF} = 2$ GHz (marks). Calculation bandwidth: 3.84 MHz.

4.4 Phase characterization of intermodulation products IM3 and IM5

A complete two-tone IMD characterization requires not only the measurement of magnitude using a SA but also phase, varying the frequency separation Δf between the two tones, as several specialists have recommended.

Different methods for measurement of IMD phase using synchronised generators and several VNAs have been proposed [27]-[59], [60], or a Vector Signal Generator (VSG) and a NVNA [61]. Their main disadvantage is that they require sophisticated and highly-developed setups. The setup proposed in [27] is shown in Figure 4.30. It is based on the idea that an IM distortion signal is applied together with a two-tone signal to the input. By adjusting the amplitude and phase of the test signal, the output IM3 can be canceled and memory effects can be measured by sweeping the tone separation over a range of modulation frequencies. Nevertheless, this setup presents the drawback that a complicated calibration process must be carried out. A similar setup is proposed in [59] and shown in Figure 4.31. It is based on a modified VNA used in receiver mode and calibrated, which is used to measure ratios in amplitude and phase between input and output of the DUT at frequencies of the IM products with the help

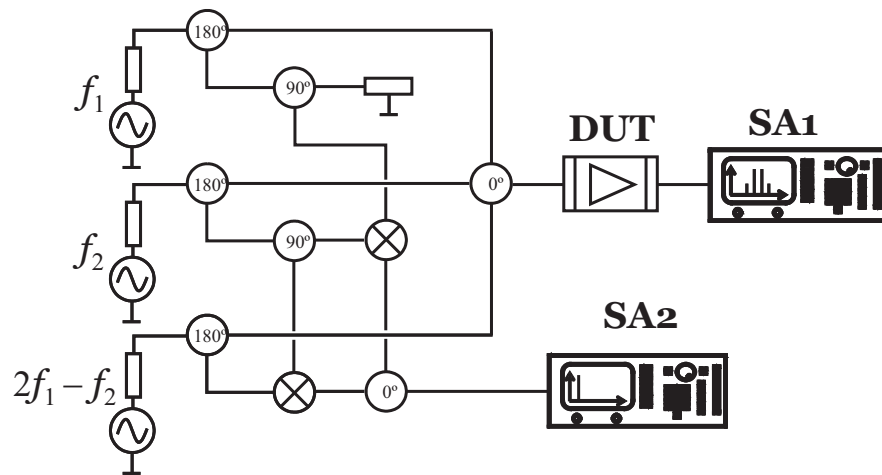


Figure 4.30: Proposed setup in [27] for measuring amplitude and phase responses of IM products.

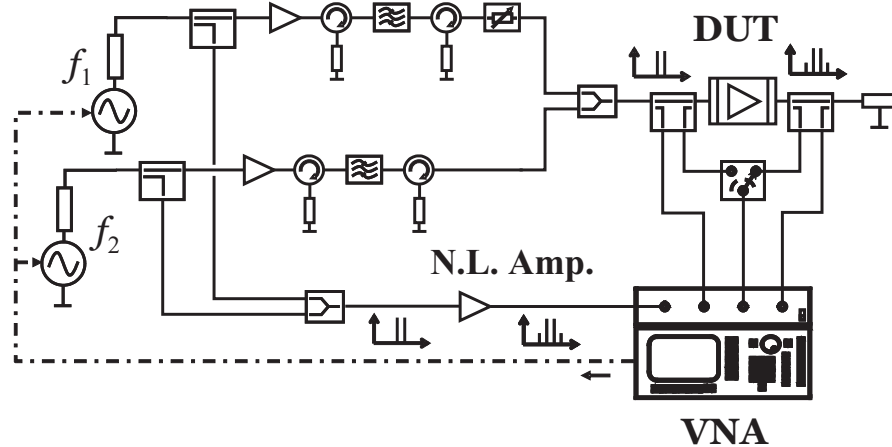


Figure 4.31: Proposed setup in [59] for measuring amplitude and phase responses of IM products.

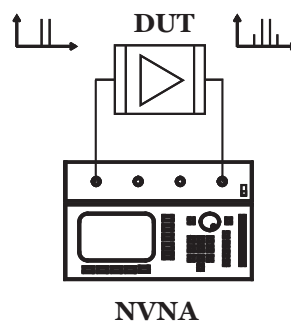


Figure 4.32: Proposed setup in [61] for measuring amplitude and phase responses of IM products.

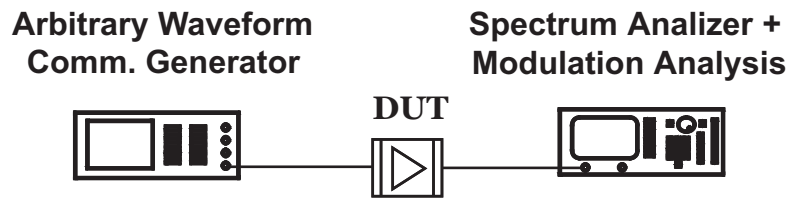


Figure 4.33: Equipment setup for two-tone IMD characterization

of a constant reference signal. The use of a NVNA, as shown in Figure 4.32, allows the accurate measurement of the magnitude and phase of all distortion products at the input and output of a device with a calibrated instrument. In [61] a technique was used to overcome the bandwidth limitation of NVNAs.

In addition to this, other methods for phase characterization of IM products have been recently proposed. Employing standard uncorrelated two-tone and multitone excitations, [62] is based on statistical averages of signal windows captured by a MTA, and [63] applies a spectral filtering approach, with a topology similar to that of a superheterodyne receiver which relies on the use of a nonlinear reference device for phase measurements calibration. On the contrary, [64], also based on spectral filtering, is devoted to correlated signals and avoids the need for a nonlinear reference. Other widely accepted methods are based on the used of signal generators with arbitrary modulation facility which allow time-domain operation, either by means of the acquisition of samples with a Digital Oscilloscope [65], a VSA [66] or a SA [69], for two-tone or digitally modulated signals [214]. In other cases, the input and output of the amplifier under test are connected to a VSA with two channels [67] or with a single switched channel [68].

Following this trend of broadband sampling, a simplified method to measure the phase of IM products relative to the tones using non-sophisticated communications equipment was presented in [70], with the collaboration of the author of this Thesis in the experimental setup. Figure 4.33 presents a simplified schematic of the employed setup, shown in Figure 4.4. The two tones are formed by using a DSB-SC signal modulated by a sinusoidal baseband waveform with frequency f_m , producing two coherent tones with the same level and an exactly constant separation $\Delta f = 2f_m$. The advantage of this method is not simply the use of only one signal generator to produce the two tones, but also that the relative phase between tones can be controlled by software definition of the modulating signal. A restriction of the method is the existence of responses generated by the digital processing of the signal. However, these responses are more than 65 dB below the tones and allow margin enough to measure IM in practical situations without appreciable error.

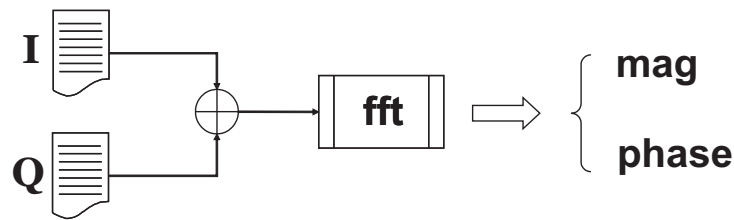


Figure 4.34: Schematic diagram of the post-process carried out with the acquired baseband samples.

In the case of magnitude, standard spectrum analyser level measurement facilities were used, but in the case of the phase the built-in modulation analysis option of the spectrum analyser was employed to acquire the baseband signal of the amplifier's output using a sampling rate of 10 samples per symbol. These samples contain all the information, i.e. magnitude and phase, of the original modulating signal and also of the generated IM products. Therefore, after a Fourier transform to the frequency domain, the relative phases corresponding to each IM product with respect to the tones could be evaluated. The maximum separation possible between tones is about 10 MHz according to the spectrum analyser specifications. However, taking into account that the IM3 and IM5 products have wider separations, $3\Delta f$ and $5\Delta f$ in each case, the maximum frequency separation between the tones should be circumscribed to 3.3 MHz and 2 MHz, respectively. As long as the narrowband condition is satisfied, any frequency dependence introduced by the spectrum analyser to the relative phase measurement can be neglected.

In order to obtain the relative phases corresponding to each IM product, it is necessary to process the acquired samples in the following way (see Figure 4.34):

1. Form the complex envelope with the acquired in-phase \hat{x}_i and quadrature \hat{x}_q baseband samples, i.e. $\tilde{x} = \hat{x}_i + j \cdot \hat{x}_q$, and Fourier transform it $\tilde{X} = \mathcal{F}\{\tilde{x}\}$.
2. Find the indices of the frequency-domain vector corresponding to each of the two tones, r_1 y r_2 , and use them to find the IM products, $m \cdot r_1 \pm n \cdot r_2$.
3. Determine magnitude and phase of the tones and IM products directly in the frequency domain.
4. Correct the recovered phase in order to take into account that the acquired signal experiments a certain delay while propagating from the device under test to the spectrum analyser.

4.4.1 Phase correction considering delay

The signal at the output of the nonlinear device under test presents a certain delay when it reaches the spectrum analyser. This phenomenon produces a different shift in phase for each of the frequency components in the output signal, i.e. the two tones and the IM products, which is added to the phase that we want to measure. If the signal's delay is denoted by τ and we considered the acquired two tones and third order products, the phases obtained directly from the frequency-domain representation are

$$\begin{aligned}
 \text{Upper tone:} & \quad \psi_u + 2\pi k_u = 2\pi f_u \tau + \phi_u \\
 \text{Lower tone:} & \quad \psi_l + 2\pi k_l = 2\pi f_l \tau + \phi_l \\
 \text{Upper IM3:} & \quad \psi_{3u} + 2\pi k_{3u} = 2\pi(2f_u - f_l)\tau + \phi_{3u} \\
 \text{Lower IM3:} & \quad \psi_{3l} + 2\pi k_{3l} = 2\pi(2f_l - f_u)\tau + \phi_{3l}
 \end{aligned} \tag{4.55}$$

where the terms $2\pi k_u$, $2\pi k_l$, $2\pi k_{3u}$ and $2\pi k_{3l}$ account for the number of completed cycles during the delayed time for each sinusoid, since the phase obtained from the frequency-domain representation of the recovered signal is between -180° and 180° .

It is necessary to estimate the delay in order to correct these phases. A procedure will be applied based on finding the instant corresponding to the initial zero phase of the tones, which is defined by software. With the time elapsed from the initial condition until the tones are separated a certain absolute phase, the relative phases of the IM products with respect to the tone phases can be evaluated.

Furthermore, this procedure was based on the assumption that the tone phases, ϕ_l and ϕ_u , are equal since their frequency separation is small enough and the devices under test is weakly nonlinear. It has been checked that this assumption does not imply a considerable loss in accuracy for the studied devices. Taking into account this assumption and recalling that $f_u = f_c + f_m$, $f_l = f_c - f_m$ and $\Delta f = 2f_m$, the experimented delay from the initial condition can be worked out as follows:

$$\begin{aligned}
 \psi_u &= 2\pi(f_c + f_m)\tau + \phi_u - 2\pi k_u, \\
 \psi_l &= 2\pi(f_c - f_m)\tau + \phi_l - 2\pi k_l, \\
 \Delta\psi &= \psi_u - \psi_l = 2 \cdot 2\pi f_m \tau + \phi_u - \phi_l - 2\pi k_u + 2\pi k_l = \\
 &= 2\pi \Delta f \tau - 2\pi k - (\phi_u - \phi_l) \simeq 2\pi \Delta f \tau - 2\pi k, \\
 \tau &= \frac{1}{\Delta f} \left(\frac{\Delta\psi}{2\pi} + k \right), \quad \text{where } k, k_u, k_l \in \mathbb{Z}.
 \end{aligned} \tag{4.56}$$

In order to know the delay following (4.56), it is necessary to determine the number of complete cycles k that the phase ψ_u overtakes the phase ψ_l . An iterative method is implemented to find k , starting from $k = 0$. First, τ is calculated and it is checked if

the assumed condition $|\psi_u - \psi_l| < \epsilon$ is fulfilled. Otherwise, k is incremented until the condition is fulfilled.

Once the delay τ is known, it is possible to determine the numbers of complete cycles k_u and k_l , and the corrected phases for the two tones are

$$\begin{aligned} \text{Upper tone:} \quad \phi_u &= \psi_u - 2\pi f_u \tau + 2\pi k_u \\ \text{Lower tone:} \quad \phi_l &= \psi_l - 2\pi f_l \tau + 2\pi k_l \end{aligned} \quad (4.57)$$

In order to correct the phases of the IM3, the following reasoning is made:

$$\begin{aligned} \text{Upper IM3:} \quad \psi_{3u} &= 2\pi(2f_u - f_l)\tau + \phi_{3u} = 2\pi(f_u + \Delta f)\tau + \phi_{3u} = \\ &= 2\pi f_u \tau + 2\pi \Delta f \tau + \phi_{3u} = (\psi_u - \phi_u) + 2\pi \Delta f \tau + \phi_{3u} \\ \phi_{3u} &= 2\pi - 2\pi \Delta f \tau + \phi_u - \psi_u + \psi_{3u} \end{aligned} \quad (4.58)$$

$$\begin{aligned} \text{Lower IM3:} \quad \psi_{3l} &= 2\pi(2f_l - f_u)\tau + \phi_{3l} = 2\pi(f_l - \Delta f)\tau + \phi_{3l} = \\ &= 2\pi f_l \tau - 2\pi \Delta f \tau + \phi_{3l} = (\psi_l - \phi_l) - 2\pi \Delta f \tau + \phi_{3l} \\ \phi_{3l} &= 2\pi \Delta f \tau + \phi_l - \psi_l + \psi_{3l} \end{aligned} \quad (4.59)$$

On the other hand, the described procedure can be easily extended in order to account for the case in which the upper and lower tone differ in a known quantity. This extension requires only an additional measurement with a Vector Network Analyser of the phase difference at the output of the device between the limits of the desired frequency range. For the general case in which $\psi_u \neq \psi_l$, the aforementioned expressions change in the following way:

$$\begin{aligned} \Delta\psi &= \psi_u - \psi_l = 2 \cdot 2\pi f_m \tau + \phi_u - \phi_l - 2\pi k_u + 2\pi k_l = \\ &= 2\pi \Delta f \tau - 2\pi k - (\phi_u - \phi_l) = 2\pi \Delta f \tau - 2\pi k - \Delta\phi \\ \tau &= \frac{1}{\Delta f} \left(\frac{(\Delta\psi - \Delta\phi)}{2\pi} + k \right) \\ \phi_u &= \psi_u - 2\pi f_u \tau + 2\pi k_u - \frac{\Delta\phi}{2} \\ \phi_l &= \psi_l - 2\pi f_l \tau + 2\pi k_l + \frac{\Delta\phi}{2} \end{aligned} \quad (4.60)$$

To confirm the reliability of the described method, the phase was checked with an alternate procedure. For a test amplifier constructed with the HEMT EPB018A5-70 of Excelics and biased with an arbitrary network, the relative phase of the IM3 products was measured. Once this result was known, the IM3 products were referred to the amplifier's input and a new signal "predistorted" with two products of the same magnitude but with opposite phase, was loaded in the internal memory of the generator. The new signal is defined as

$$x_I(t) = 2A \cos \omega_m t - 2A_I \cos \phi_r \cos\left(3\omega_m t + \frac{\Delta\phi}{2}\right), \quad (4.61)$$

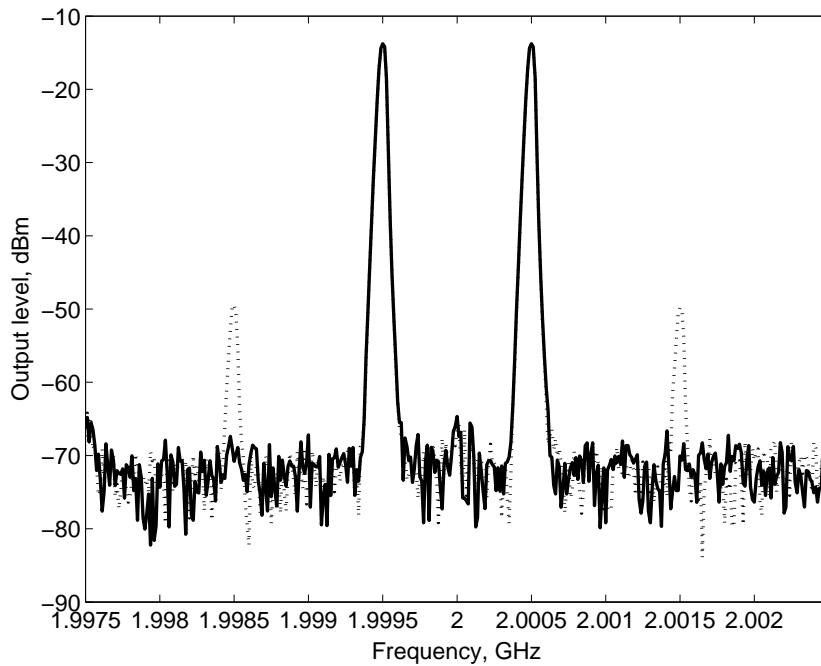


Figure 4.35: IM characteristic of a HEMT amplifier without (dotted line) and with predistortion using the measured phase (solid line).

for the in-phase component and

$$x_Q(t) = -2A_I \sin \phi_r \cos\left(3\omega_m t + \frac{\Delta\phi}{2}\right), \quad (4.62)$$

for the quadrature component. The phase ϕ_r is the average relative phase of the IM products with respect to the two-tones and $\Delta\phi$ is the phase difference between the upper and lower IM products. Applying this new signal to the amplifier's input, a perfect cancelation of the IM products was achieved, as can be observed in Figure 4.35, a result that demonstrated the convenience of the proposed method.

The main advantages of this simplified method are the following:

- Phase synchronization of the two tones is ensured.
- Negligible non-systematic errors.
- Measurements of IM3 phase can be accomplished automatically in seconds.
- Measurements of IM5 phase have been possible.

On the other hand, it also presents some drawbacks:

- Accuracy limited by quantization noise of the synthesised signal (65 dB dynamic margin).

- Bandwidth limited by the available equipment (10 MHz).
- Limited tone spacing: 3.3 MHz in IM3 and 2 MHz in IM5.
- Measurement of phase with respect to the tones phase, not absolute values.

4.4.2 Measurement results

The described method was used to measure the magnitude and phase of the third- and fifth-order IM products for the HEMT EPB018A5-70 amplifier biased with a commercial bias-Tee (ZFBT-6GW of Minicircuits) at different V_{GS} voltages and with several excitation levels of the input signal. The results of magnitude measurements are presented in Figure 4.36 for $V_{GS} = -0.24$ V and $V_{GS} = -0.4$ V for an input level $P_{in} = -7$ dBm. The magnitude is similar for lower and upper products, presenting no asymmetries and dependence with frequency is evident only for very low values. The corresponding phase measurements are plotted in Figure 4.37, where it is possible to clearly observe memory effects and difference between upper and lower products for small frequency separations. In other cases, the IM3 is approximately opposite in phase with respect to the fundamental tones, for both biasing conditions. However, the IM5 is in phase with the fundamental tones for $V_{GS} = -0.24$ V and suffers a 180° shift at $V_{GS} = -0.4$ V. This can also be observed in Figure 4.39 by means of the phase inversion that is produced at $V_{GS} = -0.4$ V with respect to higher voltages. Figure 4.38 shows the magnitude of the IM3 products for the same V_{GS} sweep.

A new amplifier was constructed using a bias network designed with a resonance near 130 kHz in order to observe some dependence on frequency of both IM3 and IM5 relative phase and phase difference. An approximate model of the new bias network was deduced from its measured S -parameters and used to calculate the phases to be compared with experimental data. Its schematic is depicted in Figure 4.40.

Magnitude and phase of the IM3 products for the HEMT amplifier biased at $V_{GS} = -0.4$ V and and input level $P_{in} = -7$ dBm, together with magnitude and phase differences between the upper and lower IM products are shown in Figs. 4.41 and 4.42. These measurements are a clear example of asymmetries in the IM products, a clear evidence that memory effects are present in this amplifier as it will be theoretically demonstrated in the next chapter.

Finally, Figure 4.43 shows magnitude and phase of IM3 versus the power input at $V_{GS} = -0.4$ V. In this case, the measurement of magnitude display several input levels for which the asymmetry is greater pointing out some non-desirable operation conditions for which memory effects will be more notable and thus predistortion may be inefficient.

4. COMPARISON WITH EXPERIMENTAL MEASUREMENTS

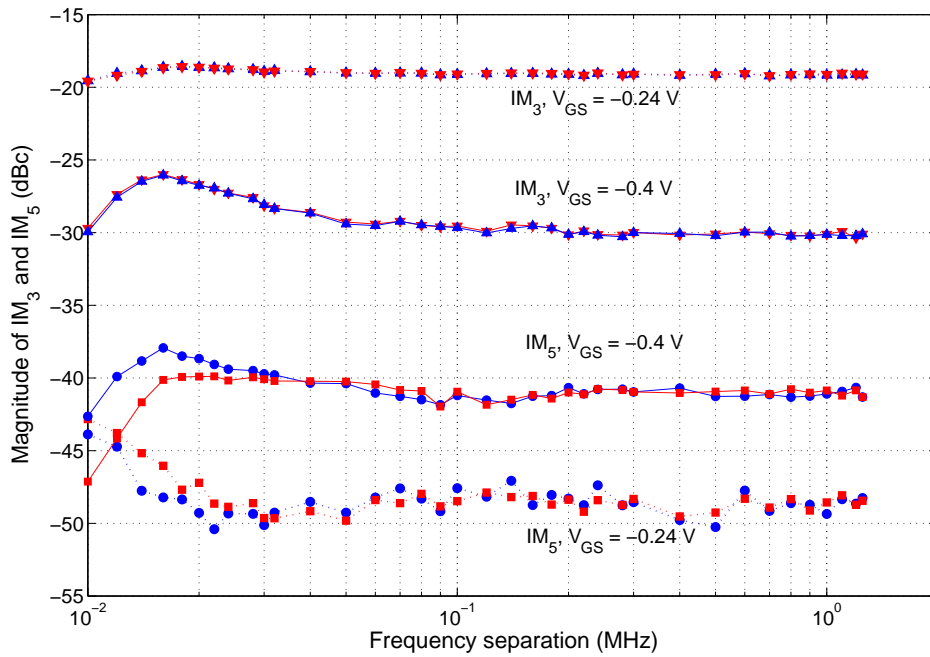


Figure 4.36: Measured magnitude of third-order IM products (triangles) and fifth-order IM products (circles and squares). Commercial bias-Tee.

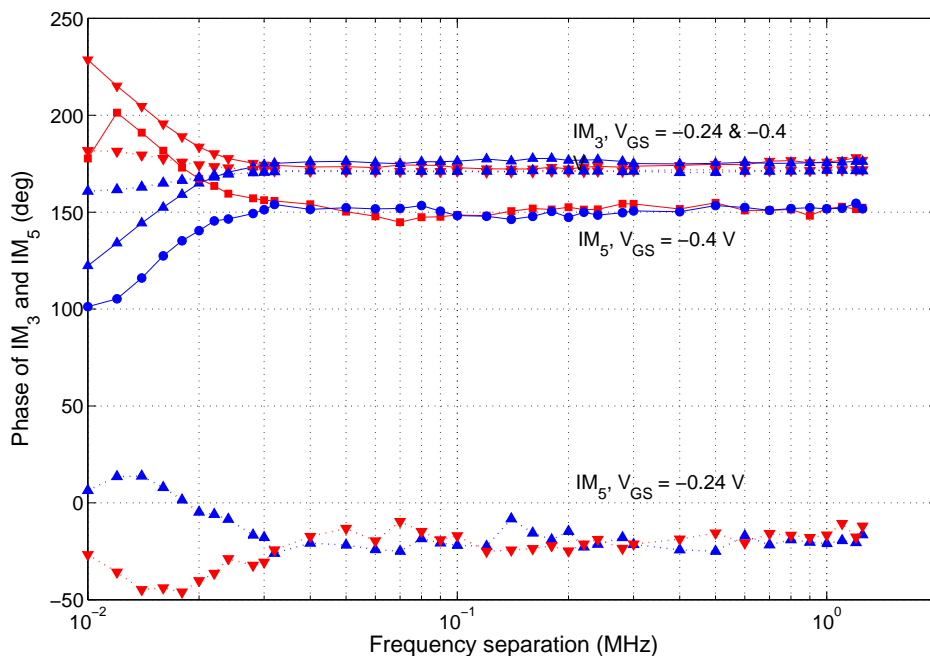


Figure 4.37: Measured phase of third-order IM products (triangles) and fifth-order IM products (circles and squares). Commercial bias-Tee.

4.4. PHASE CHARACTERIZATION OF INTERMODULATION PRODUCTS IM3 AND IM5

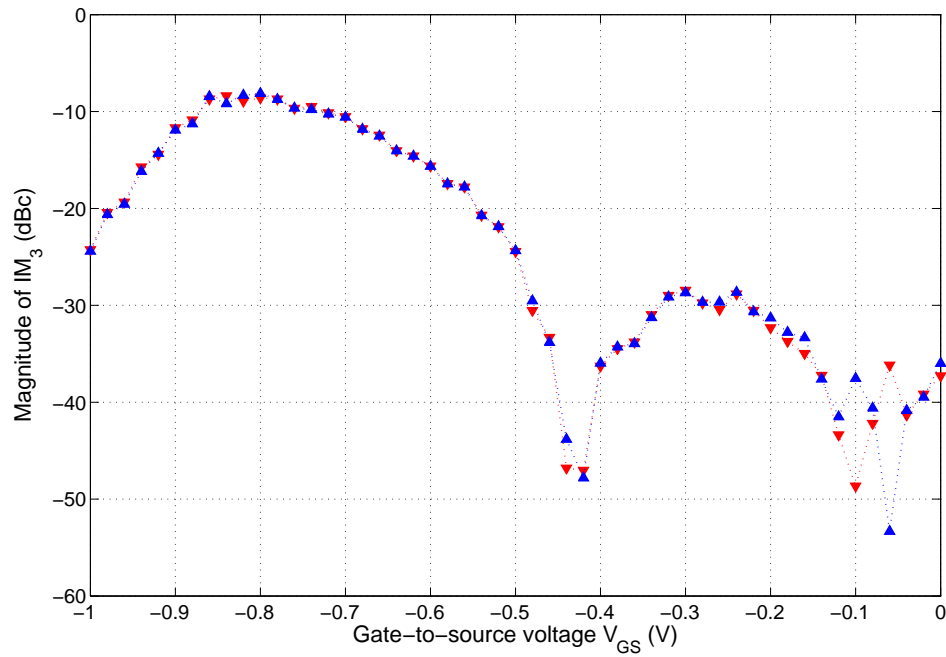


Figure 4.38: Measured magnitude of third-order IM products versus the gate-to-source voltage applied to the FET. Commercial bias-Tee.

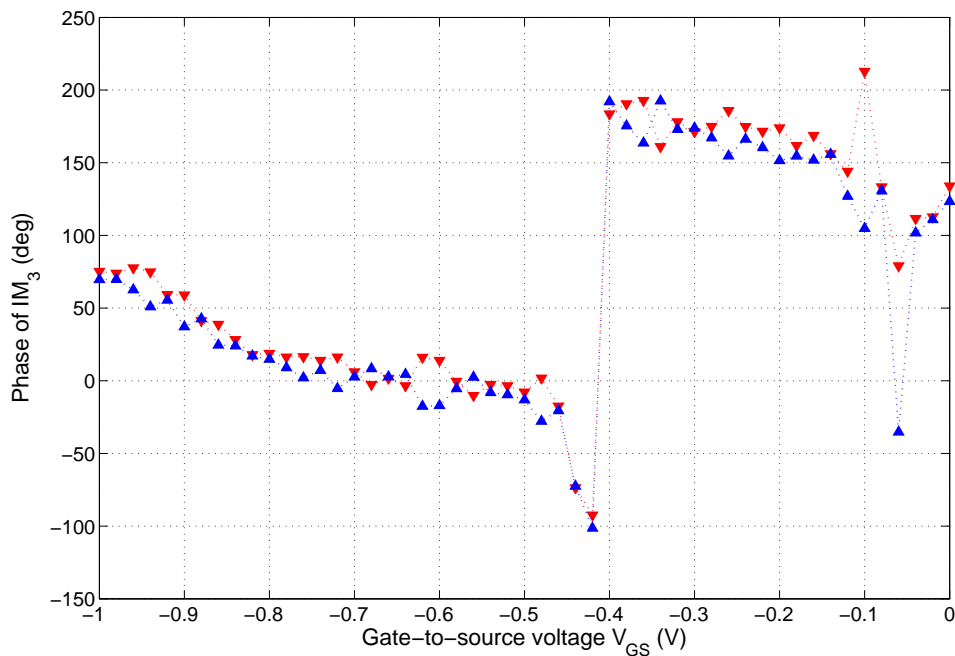


Figure 4.39: Measured phase of third-order IM products versus the gate-to-source voltage applied to the FET. Commercial bias-Tee.

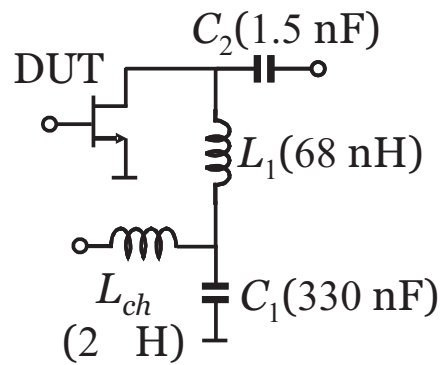


Figure 4.40: Circuit model for the constructed resonant bias network.

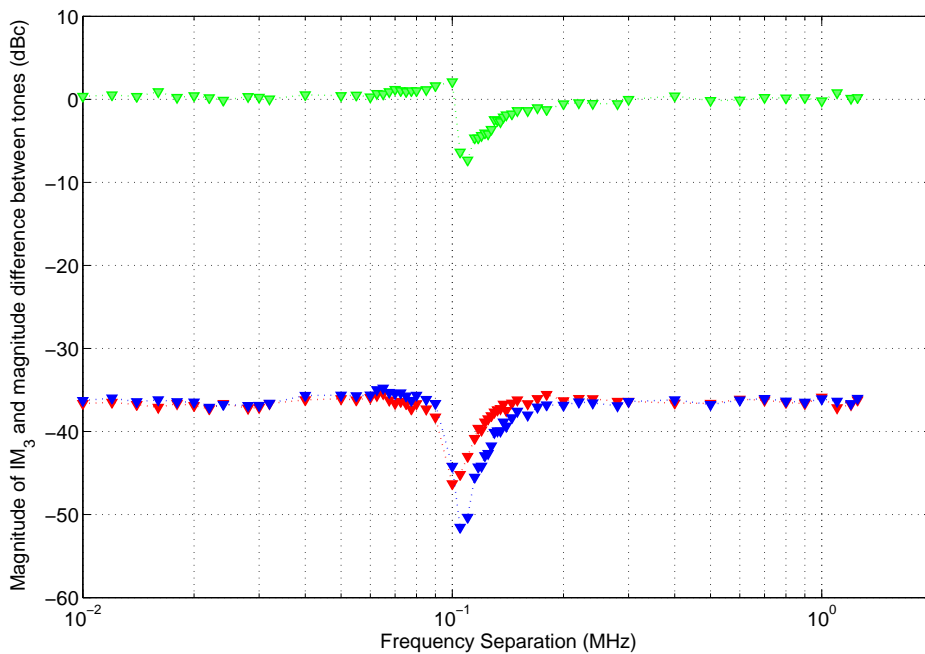


Figure 4.41: Measured magnitude of third-order IM products (red and blue) and magnitude difference between tones (green). Resonant bias network.

4.4. PHASE CHARACTERIZATION OF INTERMODULATION PRODUCTS IM3 AND IM5

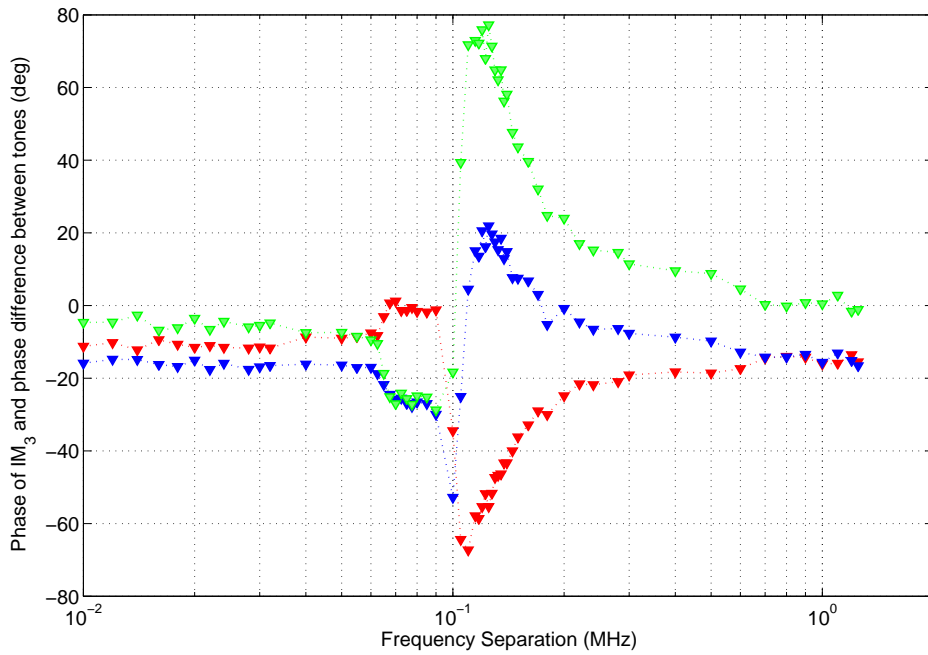


Figure 4.42: Measured phase of third-order IM products (red and blue) and phase difference between tones (green). Resonant bias network.

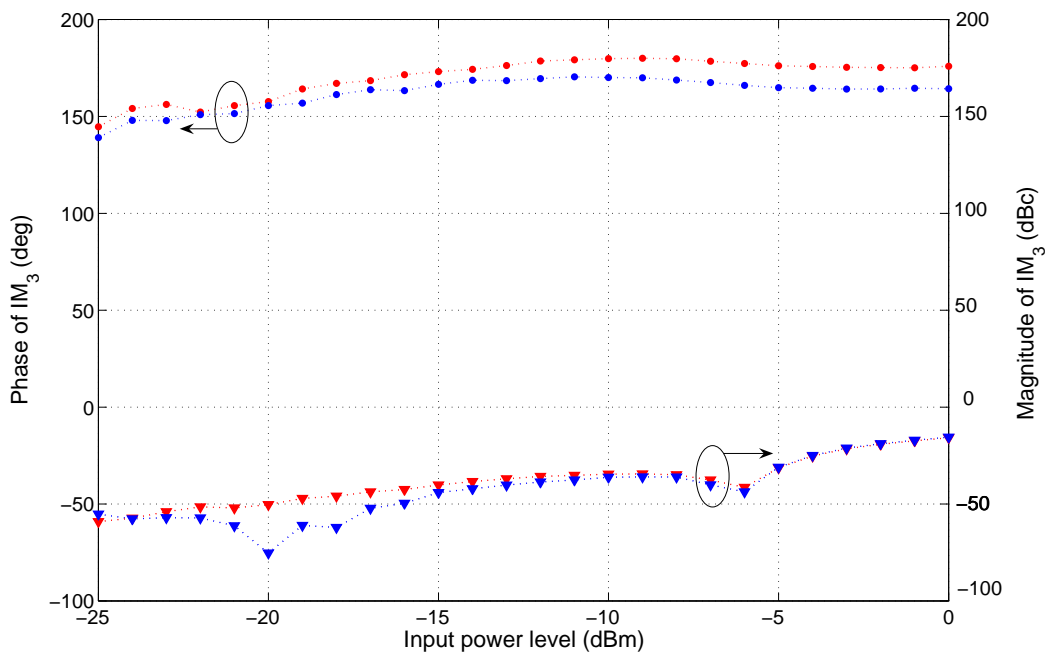


Figure 4.43: Measured magnitude (triangles) and phase (circles) of third-order IM products versus the tones input power level. Resonant bias network.

4. COMPARISON WITH EXPERIMENTAL MEASUREMENTS

MODELLING OF INTERMODULATION DISTORTION

5.1 Introduction

Traditional modelling methods do not have the capability to estimate the dependence of IMD on bandwidth. As it has been explained in Section 4.1.4, this phenomenon arises as a consequence of memory effects and causes a strong dependence of nonlinear distortion on the characteristics of the modulation signal. Wireless engineers have to account for these effects when designing high efficiency amplifiers in order to satisfy the strict requirements demanded over increasingly growing bandwidths. The need for models that allow the prediction of memory effects is thus fully justified. Among the current trends, behavioural modelling techniques are placed at an outstanding position [23], [29], [184], [86], [215], [216]. The aim of behavioural modelling is to obtain a prediction of the circuit's output with no knowledge about the internal structure of the nonlinear device, by using a reduced-order expression generally formulated in the time domain. However, the prevalent method for theoretical analysis of weakly nonlinear behaviour is Volterra series representation, both conventional [28], [21], [75], [76], or dynamic [59]. The main reason for this is that, although numerical methods such as HB are clearly oriented towards computational simulation, their results cannot be written in closed-form expressions that contribute to the comprehension of the IMD phenomenon. As it is shown in [28], using a two-tone test it can be concluded that the baseband termination impedances are the main causes for the asymmetries between the sidebands in distortion. Furthermore, in [21] a theoretical study of a unilateral FET amplifier was made following an approach based on Volterra series. This study demonstrated the IMD dependence on the load impedance, using closed-form expressions to appropriately predict asymmetries in the magnitude of the IM products.

Following this trend, in Section 5.2 the SN approach will be applied to the analysis of two-tone IMD in HEMT amplifiers under a narrowband assumption and including fifth-order terms. Closed-form expressions will be presented for IM3 and IM5. Based on the obtained expressions, Section 5.2.1 will contain a discussion about the theoretical results. The concepts of memory effects and asymmetries will be reviewed, as well as the circumstances that need to be met so that an asymmetry in magnitude and/or phase can be observed between the IM products. Predicted simulation results will be compared to the measured data shown in Section 4.4.2, with a special interest in those conditions where the asymmetry is more significant. Results for different excitation levels, bias points or load impedances will be shown in Section 5.3. After that, in order to improve the adjustment for low-frequency modulated measurements where thermal memory effects prevail, a simplified model will be presented in Section 5.4. It will be based on finding an equivalent hypothetical load impedance that can explain discrepancies between measurements and circuit-level predictions. To conclude this section, the results obtained in this analysis will be related to large-signal FET models where dispersive phenomena are taken into account. Finally, the impedance-based approach will be generalised in Section 5.5, where it will be applied to model asymmetries in magnitude and phase of IM3 for commercial amplifiers, without prior knowledge of the internal structure of the circuit.

5.2 Simplified Newton approach applied to the analysis of two-tone IM products under the narrowband assumption

Closed-form expressions obtained in [28], [21] and [70] for the analysis of IMD in FET devices are limited to third-order terms. In all cases, a Volterra series representation was used. When the Volterra series are combined with the NC method, the augmented linear subcircuit is excited with different nonlinear currents for the successive iterations, throughout which the NLTFs and the terms involved in the final IMD expression are obtained. A significant drawback of the method based on Volterra series is the unavoidable complexity associated to the derivation of higher-order terms, hence it is very attractive to explore another strategy. In Section 3.6, some interesting characteristics of the SN method were examined. For example, the region of convergence of the SN method is often smaller than with standard Newton and it requires a greater number of iterations, however it can be faster because each iteration is less expensive [32]. When the dc bias point of the circuit is selected as the initial approximation of the SN method, the Jacobian matrix calculated for the first iteration is the admittance

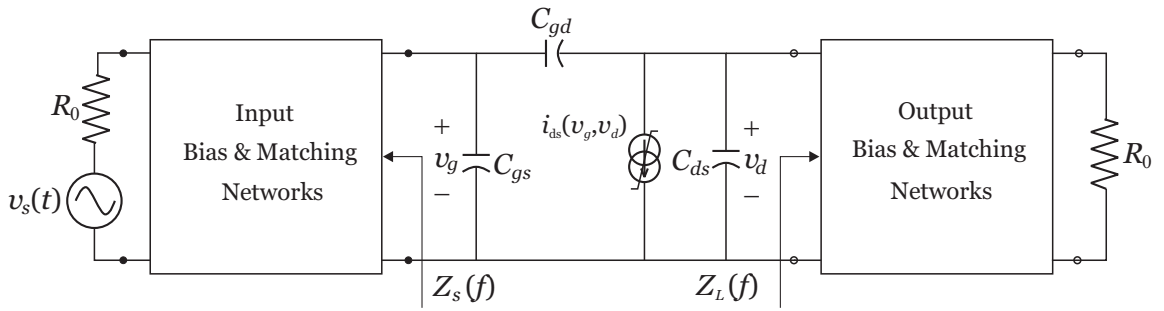


Figure 5.1: Simplified two-node equivalent model used in the two-tone intermodulation analysis of a HEMT amplifier, where only the most significant nonlinearity has been considered.

matrix of the augmented linear circuit, and this same admittance is used to deduce the incremental voltages in the following iterations. In that form, the problem is reduced to the reiterated solution of exactly the same circuit analysed in the NC approach. The only difference consists in the selection of the circuit driving currents for each iteration: while in the NC method higher-order terms are truncated for the computation of the n -th order NLTF, in this SN procedure the exciting currents are derived considering all the terms of the nonlinearity describing function. Therefore, in each n -th iteration this approach deals with contributions from terms with orders higher than n . It is possible to conclude that under the same assumption of convergence considered in the Volterra series approach and in a weakly nonlinear context, closed-form expressions for the IMD accounting for higher-order terms can be obtained in an orderly way by applying this SN method.

Let us consider the simplified two-node equivalent circuit of an elementary amplifier based on a HEMT in common-source configuration, as it is shown in Figure 5.1. In the present analysis, the nonlinear terms of capacitances C_{gs} and C_{gd} will be neglected and only the drain current source I_{ds} will be considered, since it is widely accepted that good results can be obtained considering the drain current source as the only nonlinear element in the circuit ([9], [21], [28], [73], [74]). Note that $Z_s(f)$ and $Z_L(f)$, which are the source and load impedances, include the elements for both the bias and matching networks. The SN approach presented in 3.6 will be applied to the analysis of two-tone intermodulation products for this circuit.

Recall that the drain current source can be written as a double Taylor-series expansion around the dc voltages

$$i_{ds}(t) = g_{10}v_g(t) + g_{01}v_d(t) + i_{NL}[v_g(t), v_d(t)] \quad (5.1)$$

where g_{10} and g_{01} are the linear conductances of the current source included in the

augmented linear circuit, and the term

$$i_{NL}[v_g(t), v_d(t)] = \sum_{k=2}^{\infty} g_{k0} v_g^k(t) + \sum_{l=2}^{\infty} g_{0l} v_d^l(t) + \sum_{k,l=1}^{\infty} g_{kl} v_g^k(t) v_d^l(t), \quad (5.2)$$

is the nonlinear contribution of the current source. Considering previous experimental results and simulations, in the present analysis the summations will be truncated assuming that $g_{k0} = 0$, $g_{0l} = 0$ for $k, l > 5$ and $g_{kl} = 0$ for $k + l > 3$. Recall that the coefficients g_{kl} , defined in (2.43), are constants that vary with bias.

For the two-node circuit under analysis, equations can be formulated in terms of the unknown frequency-domain voltages $V_g(f)$ and $V_d(f)$. A nodal analysis of the augmented linear circuit results in

$$\mathbf{Y}(f)\mathbf{V}(f) = \mathbf{I}(f), \quad (5.3)$$

where

$$\mathbf{Y}(f) = \begin{bmatrix} Y_s(f) + j2\pi f(C_{gs} + C_{gd}) & -j2\pi f C_{gd} \\ -j2\pi f C_{gd} + g_{10} & Y_L(f) + j2\pi f(C_{ds} + C_{gd}) + g_{01} \end{bmatrix},$$

$$\mathbf{V}(f) = \begin{bmatrix} V_g(f) \\ V_d(f) \end{bmatrix}, \quad (5.4)$$

$$\mathbf{I}(f) = \begin{bmatrix} Y_s(f)V_s(f) \\ -\mathcal{F}\{i_{ds}(t)\} \end{bmatrix}.$$

The following definitions have been made to simplify notation:

$$\bar{Y}_L(f) = Y_L(f) + j2\pi f(C_{ds} + C_{gd}) + g_{01}, \quad (5.5)$$

$$Y_{md}(f) = -j2\pi f C_{gd} + g_{10}, \quad (5.6)$$

and

$$\bar{Y}_s(f) = Y_s(f) + j2\pi f(C_{gs} + C_{gd}). \quad (5.7)$$

Therefore, the admittance matrix will be written as:

$$\mathbf{Y}(f) = \begin{bmatrix} \bar{Y}_s(f) & -j2\pi f C_{gd} \\ Y_{md}(f) & \bar{Y}_L(f) \end{bmatrix}. \quad (5.8)$$

Let us assume that a two-tone RF small-signal $v_s(t)$ is applied and express it by means of its complex envelope

$$v_s(t) = \frac{1}{2} \tilde{v}_s(t) e^{j2\pi f_c t} + \frac{1}{2} \tilde{v}_s^*(t) e^{-j2\pi f_c t}, \quad (5.9)$$

where

$$\tilde{v}_s(t) = A e^{j2\pi f_m t} + A e^{-j2\pi f_m t} = 2A \cos(2\pi f_m t), \quad (5.10)$$

with A real and $\Delta f = 2f_m$ the frequency spacing between the tones. We will also assume the weakly nonlinear approximation and a narrowband RF modulated signal, that is, with $mf_m \ll f_c$ for $m \leq 5$.

With (5.9) as the driving source, at any step of the SN algorithm the circuit variables, such as the gate and drain voltages, take the general form

$$v_{gn}(t) = \frac{1}{2} \sum_{h=-\infty}^{\infty} \tilde{v}_{gn}(h, t) e^{j2\pi h f_c t} = \frac{1}{2} \sum_{h,m=-\infty}^{\infty} \tilde{v}_{gn}(h, m) e^{j2\pi(hf_c + mf_m)t}, \quad (5.11)$$

$$v_{dn}(t) = \frac{1}{2} \sum_{h=-\infty}^{\infty} \tilde{v}_{dn}(h, t) e^{j2\pi h f_c t} = \frac{1}{2} \sum_{h,m=-\infty}^{\infty} \tilde{v}_{dn}(h, m) e^{j2\pi(hf_c + mf_m)t}, \quad (5.12)$$

for the n -th iteration, with $n \geq 1$.

For computational purposes, it is convenient to approximate (5.11) and (5.12) by quasi-periodic signals, i.e., to represent each complex envelope by a finite number of discrete sinusoids. For the case of two-tone signals, a finite number of harmonics, H , will be considered.

In quasi-periodic steady-state, the SN method has a frequency-domain equivalent

$$\mathbf{Y}(hf_c + f) \tilde{\mathbf{V}}_n(h, f) = \tilde{\mathbf{I}}_n(h, f) \quad (5.13)$$

for each iteration n and harmonic h , being $\mathbf{Y}(f)$ the admittance matrix of the augmented linear circuit.

A detailed explanation for the obtention of the incremental envelope voltages arising from the application of the SN approach to the case of a two-tone excitation is presented in Appendix C. Nevertheless, a summary will be included here.

Once the quiescent point of the circuit has been calculated and all the expansion coefficients in (5.1) and (5.2) have been determined, all dc voltage sources are short-circuited, all dc current sources are open-circuited and the augmented linear circuit characterised by the admittance matrix of (5.8) is solved in the first-order iteration.

The linear iteration ($n = 1$) produces output terms only at frequencies for $h = 1$ and $m = \pm 1$

$$\begin{aligned} \tilde{v}_{g1}(1, \pm 1) &= H_{g1}A \\ \tilde{v}_{d1}(1, \pm 1) &= H_1A. \end{aligned} \quad (5.14)$$

where H_{g1} and H_1 are the linear transfer functions relating input voltages with gate and drain voltages, respectively, both evaluated at the carrier frequency f_c .

From the second iteration, the external signal source is short circuited and the excitation NCs are applied instead. In the second iteration, the employed nonlinear driving source is $i_2(t) = -i_{NL}[v_{g1}(t), v_{d1}(t)]$. From this expression, the nonlinear envelope current components $\tilde{i}_2(h, m)$ are obtained. It must be noticed that, while in the NC method the second-order exciting current is $-[g_{20}v_{g1}^2(t) + g_{02}v_{d1}^2(t) + g_{11}v_{g1}(t)v_{d1}(t)]$ and generates components exclusively at dc, $f_2 \pm f_1$, $2f_1$ and $2f_2$, in the SN approach $i_2(t)$ produces terms at all harmonics and IM products of all orders considered. The most relevant components of $i_2(t)$ are those corresponding to the dc zone

$$\begin{aligned}\tilde{i}_2(0, \pm 2) &= -[\gamma_{20}A^2 + 3\gamma_{40}A^4], \\ \tilde{i}_2(0, \pm 4) &= -\frac{3}{4}\gamma_{40}A^4,\end{aligned}\tag{5.15}$$

and to the fundamental frequency zone

$$\begin{aligned}\tilde{i}_2(1, \pm 1) &= -\left[\frac{9}{4}\gamma_{31}A^3 + \frac{25}{4}\gamma_{51}A^5\right], \\ \tilde{i}_2(1, \pm 3) &= -\left[\frac{3}{4}\gamma_{31}A^3 + \frac{25}{8}\gamma_{51}A^5\right], \\ \tilde{i}_2(1, \pm 5) &= -\frac{5}{8}\gamma_{51}A^5.\end{aligned}\tag{5.16}$$

The recursive expressions used to calculate $\tilde{i}_2(h, m)$ and the definitions of the coefficients γ are shown in Appendix C. The corresponding incremental voltage components at $hf_c + mf_m$ can be expressed as

$$\begin{aligned}\tilde{v}_{g2}(h, m) &= Z_g(hf_c + mf_m)\tilde{i}_2(h, m) \approx Z_{gh}\tilde{i}_2(h, m), \\ \tilde{v}_{d2}(h, m) &= Z(hf_c + mf_m)\tilde{i}_2(h, m) \approx Z_h\tilde{i}_2(h, m),\end{aligned}\tag{5.17}$$

where $Z_g(f)$ and $Z(f)$ are impedances relating components of the nonlinear currents with the components of $v_g(t)$ and $v_d(t)$, respectively. In particular, $Z_g(f)$ accounts for the feedback across C_{gd} and can be neglected for components in the dc zone. Furthermore, in this special zone the narrowband assumption does not apply. However, we can consider $Z(mf_m) = \bar{Z}_L(mf_m)$, which represents the load impedance seen by the drain source at baseband frequencies. Then, the following relations are satisfied:

$$\begin{aligned}\tilde{v}_{g2}(0, m) &= 0, \\ \tilde{v}_{d2}(0, m) &= \bar{Z}_L(mf_m)\tilde{i}_2(0, m),\end{aligned}\tag{5.18}$$

for m even. Without loss of generality, it is assumed that $\bar{Z}_L(0) = 0$, since a bias-Tee is contained in the load impedance block. At other frequency zones, the approximations $Z_g(hf_c + mf_m) \approx Z_g(hf_c) = Z_{gh}$ and $Z(hf_c + mf_m) \approx Z(hf_c) = Z_h$ have been made.

Note that we are assuming that the drain-node impedance is flat for the fundamental and harmonic frequencies and can be represented by a constant value at the

central frequency of the band hf_c^1 , while it presents some variations for baseband frequencies taken into account by means of different values of $\bar{Z}_L(mf_m)$ for each m . This assumption is based on the typical characteristics of the load, bias networks and matching networks for RF circuits, which rule the frequency behaviour of the load impedance. Near dc, the impedance is a very small resistance corresponding to the resistance of the inductor or RF choke in the dc current path. At high frequencies, the impedance is the load impedance transformed by the matching network. In between those two extremes, there is a region where the impedance and transfer characteristics are changing. At these frequencies, the impedance and transfer characteristics are complex. Although a constant bias network impedance in the range of envelope frequencies can not be guaranteed, it is a common practice for comercial bias networks to place the corner frequency of the bias-Tee low enough so that the drain impedance presents no changes for the fundamental and higher-harmonic frequencies [25]. This is the reason why impedances are considered varying with frequency for the baseband but constant for the fundamental and higher-harmonic frequencies.

As a result, the following second incremental voltage contributions to the fundamental frequency zone have been obtained:

$$\begin{aligned}\tilde{v}_{d2}(1, \pm 1) &= - \left[\frac{9}{4} \gamma_{31} Z_1 A^3 + \frac{25}{4} \gamma_{51} Z_1 A^5 \right], \\ \tilde{v}_{d2}(1, \pm 3) &= - \left[\frac{3}{4} \gamma_{31} Z_1 A^3 + \frac{25}{8} \gamma_{51} Z_1 A^5 \right], \\ \tilde{v}_{d2}(1, \pm 5) &= - \frac{5}{8} \gamma_{51} Z_1 A^5.\end{aligned}\quad (5.19)$$

Similar expressions are obtained for the remaining products, as shown in Appendix C.

For the third iteration, it is necessary to evaluate the excitation nonlinear current $i_3(t) = - \left[i_{NL} [v_{g1}(t) + v_{g2}(t), v_{d1}(t) + v_{d2}(t)] - i_{NL} [v_{g1}(t), v_{d1}(t)] \right]$. Considering that the incremental voltages $v_{g2}(t)$ and $v_{d2}(t)$ are small compared to the linear terms $v_{g1}(t)$ and $v_{d1}(t)$, the exciting current can be approximated by its first-order Taylor expansion and keeping only the most significant terms, linear in v_{g2} and v_{d2} , this results in

$$i_3(t) = - \left\{ 2g_{20}v_{g1}(t)v_{g2}(t) + g_{11} [v_{d1}(t)v_{g2}(t) + v_{g1}(t)v_{d2}(t)] + 2g_{02}v_{d1}(t)v_{d2}(t) \right\}. \quad (5.20)$$

Proceeding in an analogous way to that of the second iteration, the incremental drain voltage contributions in the fundamental frequency zone can be derived: first, obtaining the components of $\tilde{i}_3(1, m)$, and then recalling that $\tilde{v}_{d3}(1, m) = Z_1 \tilde{i}_3(1, m)$.

¹In case even-order harmonic impedances change over the possible bandwidths of the signals, it can be shown that additional frequency-dependent terms need to be included in order to predict the IMD variation with tone spacing. However, this scenario of rapidly changing even-order harmonic impedances is not usually observed, unless harmonic trap networks are employed [217].

Table 5.1: Incremental drain voltage terms for the fundamental frequency zone ($h = 1$)

	$m = \pm 1$
$n = 1$	$H_1 A$
$n = 2$	$-\frac{9}{4}\gamma_{31}Z_1 A^3 - \frac{25}{4}\gamma_{51}Z_1 A^5$
$n = 3$	$\frac{3}{2}\gamma'_{22}Z_1 A^3 + \gamma'_{20}\bar{Z}_L(\pm\Delta f)A^3 +$ $+ [5\gamma'_{42}Z_1 + 3\gamma'_{40}\bar{Z}_L(\pm\Delta f)] A^5$
	$m = \pm 3$
$n = 1$	0
$n = 2$	$-\frac{3}{4}\gamma_{31}Z_1 A^3 - \frac{25}{8}\gamma_{51}Z_1 A^5$
$n = 3$	$\frac{1}{2}\gamma'_{22}Z_1 A^3 + \gamma'_{20}\bar{Z}_L(\pm\Delta f)A^3 +$ $+ [\frac{5}{2}\gamma'_{42}Z_1 + 3\gamma'_{40}\bar{Z}_L(\pm\Delta f) + \frac{3}{4}\gamma'_{40}\bar{Z}_L(\pm 2\Delta f)] A^5$
	$m = \pm 5$
$n = 1$	0
$n = 2$	$-\frac{5}{8}\gamma_{51}Z_1 A^5$
$n = 3$	$[\frac{1}{2}\gamma'_{42}Z_1 + \frac{3}{4}\gamma'_{40}\bar{Z}_L(\pm 2\Delta f)] A^5$

Incremental distortion in drain voltage at fundamental tones ($f = f_c \pm f_m$), and incremental voltages for third- and fifth-order IM products ($f = f_c \pm 3f_m$, and $f = f_c \pm 5f_m$, respectively) can be expressed as

$$\begin{aligned}\tilde{v}_{d3}(1, \pm 1) &= \frac{3}{2}\gamma'_{22}Z_1A^3 + \gamma'_{20}\bar{Z}_L(\pm\Delta f)A^3 + [5\gamma'_{42}Z_1 + 3\gamma'_{40}\bar{Z}_L(\pm\Delta f)]A^5, \quad (5.21) \\ \tilde{v}_{d3}(1, \pm 3) &= \frac{1}{2}\gamma'_{22}Z_1A^3 + \gamma'_{20}\bar{Z}_L(\pm\Delta f)A^3 + \left[\frac{5}{2}\gamma'_{42}Z_1 + 3\gamma'_{40}\bar{Z}_L(\pm\Delta f) + \frac{3}{4}\gamma'_{40}\bar{Z}_L(\pm 2\Delta f) \right] A^5, \\ \tilde{v}_{d3}(1, \pm 5) &= \left[\frac{1}{2}\gamma'_{42}Z_1 + \frac{3}{4}\gamma'_{40}\bar{Z}_L(\pm 2\Delta f) \right] A^5.\end{aligned}$$

In summary, the incremental drain voltage products in the fundamental frequency zone are presented in Table 5.1. Summing up the incremental voltages obtained for all the iterations considered, the drain voltage components at tone frequencies $f = f_c \pm f_m$ can be expressed as

$$V_{d_{u,l}} = H_1A + \left[\frac{9}{4}\gamma_3 + \gamma'_{20}\bar{Z}_L(\pm\Delta f) \right] A^3 + \left[\frac{25}{4}\gamma_5 + 3\gamma'_{40}\bar{Z}_L(\pm\Delta f) \right] A^5, \quad (5.22)$$

where the notation V_{d_l}/V_{d_u} has been used to denote the lower/upper tone frequency, respectively; and the used γ 's are defined in Appendix C. Note that these coefficients γ change with bias and with gate and drain impedances at the fundamental and second harmonic, but are independent of the baseband frequency.

Similarly, third-order IM products at frequencies $f = f_c \pm 3f_m$ are calculated as

$$V_{d_{3u,3l}} = \left[\frac{3}{4}\gamma_3 + \gamma'_{20}\bar{Z}_L(\pm\Delta f) \right] A^3 + \left[\frac{25}{8}\gamma_5 + 3\gamma'_{40}\bar{Z}_L(\pm\Delta f) + \frac{3}{4}\gamma'_{40}\bar{Z}_L(\pm 2\Delta f) \right] A^5, \quad (5.23)$$

and fifth-order IM products at frequencies $f = f_c \pm 5f_m$ are calculated as

$$V_{d_{5u,5l}} = \left[\frac{5}{8}\gamma_5 + \frac{3}{4}\gamma'_{40}\bar{Z}_L(\pm 2\Delta f) \right] A^5. \quad (5.24)$$

Since we have made the assumption that node impedances Z_g and Z can be considered constant with Δf for the fundamental and second-harmonic frequency zones, then the output IM3 and IM5 variations only depend on the baseband load impedance variations with Δf and, thus, this term will be the exclusive source for the device memory effects.

It can be observed in (5.22)- (5.24) that output voltages for the tones and IM products present a different expression for the upper and lower frequencies, mainly due to the fact that the load impedance \bar{Z}_L can take a different value for baseband positive and negative frequencies Δf and $2\Delta f$. Therefore, considering that $\bar{Z}_L(-k\Delta f) =$

$\bar{Z}_L^*(k\Delta f)$, the following expressions for IM3 and IM5 asymmetries can be obtained:

$$A_3 = \frac{1 + \frac{4\gamma'_{20}}{3\gamma_3} \bar{Z}_L(\Delta f) + \left[\frac{25}{6} \frac{\gamma_5}{\gamma_3} + 4 \frac{\gamma'_{40}}{\gamma_3} \bar{Z}_L(\Delta f) + \frac{\gamma'_{40}}{\gamma_3} \bar{Z}_L(2\Delta f) \right] A^2}{1 + \frac{4\gamma'_{20}}{3\gamma_3} \bar{Z}_L^*(\Delta f) + \left[\frac{25}{6} \frac{\gamma_5}{\gamma_3} + 4 \frac{\gamma'_{40}}{\gamma_3} \bar{Z}_L^*(\Delta f) + \frac{\gamma'_{40}}{\gamma_3} \bar{Z}_L^*(2\Delta f) \right] A^2}, \quad (5.25)$$

$$A_5 = \frac{1 + \frac{6\gamma'_{40}}{5\gamma_5} \bar{Z}_L(2\Delta f)}{1 + \frac{6\gamma'_{40}}{5\gamma_5} \bar{Z}_L^*(2\Delta f)}. \quad (5.26)$$

Note that, in spite of their resemblance, γ_2 and γ_5 are not the original NLTFs of a Volterra series analysis and only when fifth-order terms are neglected, (5.23) reduces to a conventional Volterra series approximation [21]. In addition to this, (5.23) takes into account that optimization is signal-level dependent, showing that the optimum bias point for low-level signals, for which the second term can be neglected, is not necessarily the same as that for high level signals. In order to emphasise these observations coincident with [21], the herein proposed results include fifth-order effects, leading to a more detailed description of IM3, which incorporate input level dependence to IM3 asymmetry, and allowing the prediction of IM5 in a similar way.

5.2.1 Discussion about theoretical results

Asymmetries observed in real microwave devices subjected to two-tone or multitone tests have been the object of several research works ([21], [24], [28], [75], [217], [218], [219]). However, these asymmetries are often sought only in the amplitudes of IM products, while no attention is paid to asymmetries in their phase. Moreover, the concepts of memory effects and asymmetries are misleadingly exchanged sometimes, thus a clarification on their relation is not out of place here. If asymmetries are not considered in predistortion linearisers, there is a severe limit to sideband reduction. Indeed, asymmetries in phase present the same significance as in magnitude regarding linearisation and predistortion techniques [217].

As a general comment on the obtained expressions, it can be said that, in addition to static AM-AM and AM-PM conversion, equations (5.22)-(5.24) demonstrate the dependence on envelope frequency introduced by the baseband load impedance $\bar{Z}_L(\pm\Delta f)$, a characteristic of dynamic AM-AM and AM-PM functions that are a sign of memory effects, as it was stated in Section 4.1.4. Recall that, in the context of two-tone and multitone tests, memory effects can be detected as changes in the amplitude and phase of IMD components with frequency spacing, whereas a difference between the upper and lower IM products is referred to as an asymmetry. Therefore, any system

that presents a frequency-dependent baseband load impedance is a nonlinear system with memory. Despite asymmetry is another indication of memory effects, not all the nonlinear systems with memory exhibit spectral asymmetries. The theoretical analysis performed in this section leads to an intuitive understanding of the circumstances that need to be met in order to observe asymmetries in magnitude and/or phase between the upper and lower IM products in two-tone tests. Let us analyse the following expression, which retains the main dependence on baseband load impedance \bar{Z}_L shown in the closed-form expressions (5.25) and (5.26), for a fixed value of the tone spacing:

$$F_{asym} = \frac{1 + \gamma\bar{Z}_L}{1 + \gamma\bar{Z}_L^*}. \quad (5.27)$$

The necessary condition for the IM products to present an asymmetry in magnitude is

$$|F_{asym}| = \frac{|1 + \gamma\bar{Z}_L|}{|1 + \gamma\bar{Z}_L^*|} \neq 1, \quad (5.28)$$

and it is necessary that

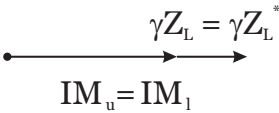
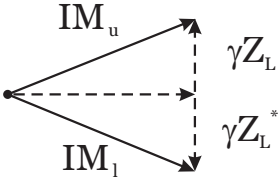
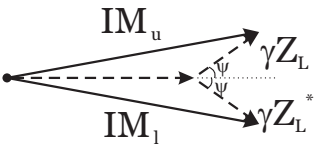
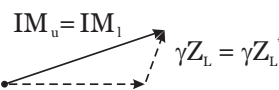
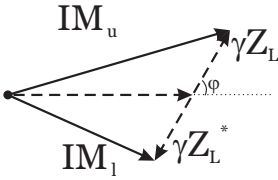
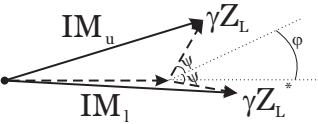
$$\phi_{asym} = \angle(1 + \gamma\bar{Z}_L) - \angle(1 + \gamma\bar{Z}_L^*) \neq 0 \quad (5.29)$$

so that an asymmetry in phase can be observed. Different scenarios for the values of γ and \bar{Z}_L are graphically illustrated in Table 5.2, where the nonlinear contributions are represented with vectors to highlight their interactions. It can be concluded that, if the baseband load impedance \bar{Z}_L is real, both the upper and lower IM products will have the same magnitude and phase for all the possible values of γ . Therefore, unless the baseband load impedance presents a non-negligible complex part, no asymmetry will be observed. By contrast, if \bar{Z}_L is complex, the device will always exhibit an asymmetry in phase. Nevertheless, only when γ is also complex, an asymmetry in magnitude will appear. This situation can easily be encountered when the gate and drain impedances at the fundamental and second harmonic frequencies are complex.

The shown vector diagrams also point to the fact that, if the coefficient γ is negligible, the constant term will dominate the final resultant vectors, being both the upper and lower IM products almost equal in magnitude and phase. In this case, we can be misled by the fact that the variation of IMD with Δf may not be evident, although the power amplifier still presents memory effects. The opposite situation explains why it is common to observe large IMD changes with tone spacing and asymmetries in low intermodulation amplifiers, since power amplifier designs for minimum IMD typically bias the transistors to the point where the third-order terms in the nonlinearity are negligible. However, for this bias point the even-order effects which produce the $\bar{Z}_L(\pm\Delta f)$ dependence will achieve more significance.

The aforementioned comments and other similar conclusions found in literature have helped RF designers to gain an insight into the mechanisms which can minimise

Table 5.2: Different asymmetry situations with respect to γ and \bar{Z}_L .

$\gamma \in \mathbb{R}$		
$\bar{Z}_L \in \mathbb{R}$	\bar{Z}_L is purely imaginary	$\bar{Z}_L \in \mathbb{C}, \bar{Z}_L = Z e^{j\psi}$
$\bar{Z}_L^* = \bar{Z}_L$ $ F_{asym} = 1, \phi_{asym} = 0$	$\bar{Z}_L^* = -\bar{Z}_L$ $ F_{asym} = 1, \phi_{asym} \neq 0$	$\bar{Z}_L^* = Z e^{-j\psi}$ $ F_{asym} = 1, \phi_{asym} \neq 0$
 <p>Symmetry</p>	 <p>Symmetry in magnitude Asymmetry in phase</p>	 <p>Symmetry in magnitude Asymmetry in phase</p>
$\gamma \in \mathbb{C}, \gamma = \gamma e^{j\varphi}$		
$\bar{Z}_L \in \mathbb{R}$	\bar{Z}_L is purely imaginary	$\bar{Z}_L \in \mathbb{C}, \bar{Z}_L = Z e^{j\psi}$
$\gamma \bar{Z}_L^* = \gamma \bar{Z}_L$ $ F_{asym} = 1, \phi_{asym} = 0$	$\gamma \bar{Z}_L^* = -\gamma \bar{Z}_L$ $ F_{asym} \neq 1, \phi_{asym} \neq 0$	$\gamma \bar{Z}_L = \gamma Z e^{j(\varphi+\psi)}$ $\gamma \bar{Z}_L^* = \gamma Z e^{j(\varphi-\psi)}$ $ F_{asym} \neq 1, \phi_{asym} \neq 0$
 <p>Symmetry</p>	 <p>Asymmetry in magnitude and phase</p>	 <p>Asymmetry in magnitude and phase</p>

the IMD asymmetry and power levels, leading to more linear and efficient power amplifiers. Two recent examples of this can be found in [220], where conditions related to the second-harmonic load selection are applied, and [221], where a circuit technique is proposed to decrease the baseband termination by including a short-circuit condition over a wide frequency range.

Regarding the subject of the relation between memory and asymmetries, notice that if the characteristic observed in a SA has (magnitude) asymmetry, then it is possible to say that the amplifier has memory, since the condition of a complex \bar{Z}_L can only be met for those bias and matching networks in which the baseband load impedance is also frequency-dependent, $\bar{Z}_L(\Delta f)$. But the converse is not true, as it is depicted in Figure 5.2. Even in the case of a spectrum with symmetric magnitude, it is possible to observe memory in an amplifier if its memory were related with phase asymmetry, or if its memory effects were concealed by dominant third-order nonlinearities.

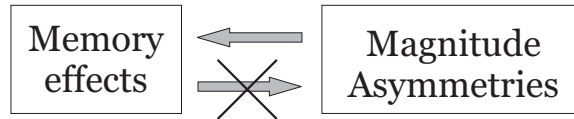


Figure 5.2: Asymmetries imply memory effects, but the converse is not true.

5.3 Correspondence of the predicted IM asymmetries with experimental results

In Section 4.4.2, measurements of relative phase of the IM products in an amplifier constructed with the HEMT EPB018A5-70 of Excelics have been presented. In this section, these measurements will be compared to the theoretical predictions obtained with the SN approach given in (5.22)-(5.26).

As it has been mentioned before, the manufacturer of the active device provides the typical parameters of a Curtice-cubic large-signal model. As this model is truncated to three terms, the coefficients g_{kl} are zero for $k + l > 3$ and it is unable to predict the appearance of IM5 products. This is the reason why a five-terms Curtice model (see Section 4.3.1 for more details) will be used in this chapter

$$\begin{aligned} I_{ds} &= (A_0 + A_1 V_1 + A_2 V_1^2 + A_3 V_1^3 + A_4 V_1^4 + A_5 V_1^5) \cdot \tanh(\gamma V_{ds}), \\ V_1 &= V_{gs}(t - \tau) \cdot [1 + \beta(V_{ds}^0 - V_{ds})], \end{aligned} \quad (5.30)$$

where V_{ds}^0 is the drain-to-source voltage for which A_0, A_1, A_2, A_3, A_4 and A_5 are evaluated. The parameters were obtained by merely fitting the new dc $I_{ds} - V_{gs}$ characteris-

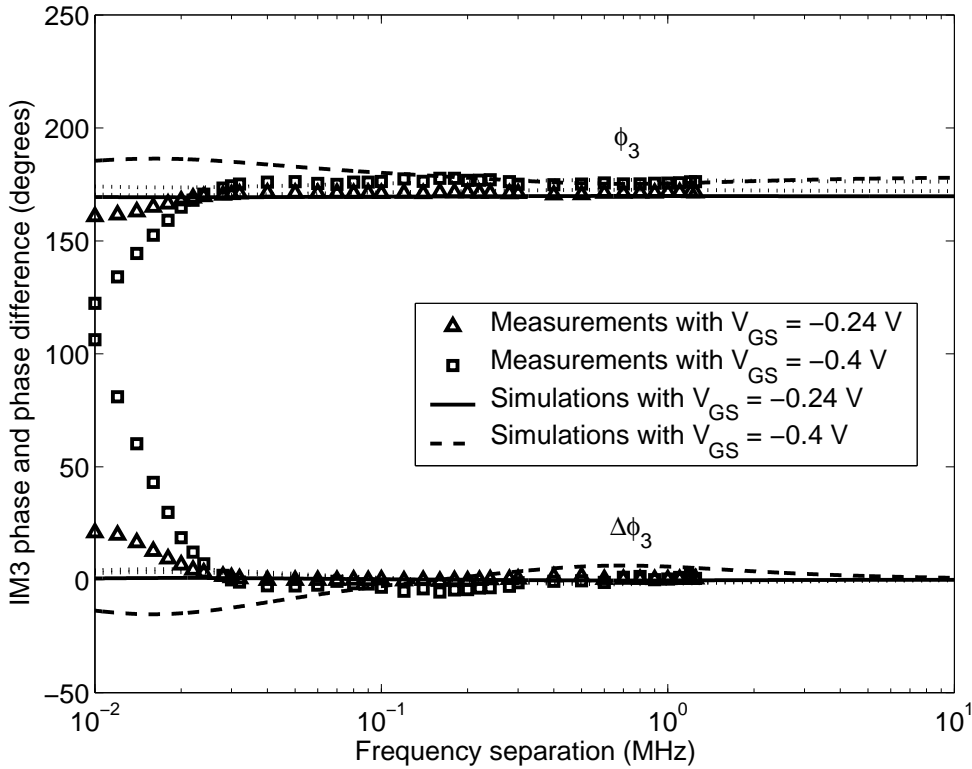


Figure 5.3: Measured and calculated phase of lower IM3 and phase difference at two bias points using a commercial bias-Tee.

tic curve to the original three-terms function given by the manufacturer, considering a drain voltage of 2 V. Considering that the large-signal model has been obtained from dc measurements, we could advance that the predicted behaviour will not be able to account for thermal or charge trapping memory effects.

In Figure 5.3 the results for the measured lower IM3 phase and phase difference of the amplifier biased with a commercial bias-Tee (ZFBT-6GW of Minicircuits) for $V_{GS} = -0.24$ V (triangles) and for $V_{GS} = -0.4$ V (squares), are shown. In both cases, the relative phase of the lower IM3 product ϕ_3 is near 180° with respect to the tones and almost no dependence with frequency spacing is observed except for very low frequencies, below approximately 30 kHz. In the same figure, theoretical results obtained by calculating the phase with expressions (5.22), (5.23) and (5.24) are also plotted in solid line for $V_{GS} = -0.24$ V and in dashed line for $V_{GS} = -0.4$ V. The results obtained with a Volterra series approach similar to that in [21] are also represented in a thinner dotted line. The model of the commercial bias-Tee used in the computations was extracted from S_{11} measurements in a VNA. A good fit to experimental data can be observed, although in the low frequency range the deviation is evident, indicating that, in this region, the frequency dependence could be caused by thermal or charge trapping memory effects. The measured phase difference between the up-

per IM3 and lower IM3, or phase asymmetry, $\Delta\phi_3$, is also depicted in Figure 5.3 for the same bias points indicating that no asymmetry is present for frequency spacings over 30 kHz. Again, the coincidence of calculated results with measurements is good except where the possible thermal or charge trapping memory effects, not included in the HEMT model, are important. A model to improve the adjustment in this zone will be presented in Section 5.4.

A new amplifier, using the resonant bias network whose model was shown in Figure 4.40, was measured in order to observe some dependence on frequency of both IM3 and IM5 relative phase and phase difference. In Figures 5.4 and 5.5, the relative phase and phase difference of IM3 products are shown, respectively, for a weakly nonlinear condition where the amplifier is biased in saturation with $V_{GS} = -0.24$ V. It is clearly observed the frequency dependence which motivates a change in the relative phase around the resonant frequency of about 130 kHz. At the same frequency, there is a nonzero phase difference indicating a phase asymmetry between tones. In both cases, the measured out-of-resonance values are predicted by the closed-form expressions presented in Section 5.2 and the general behaviour around resonance is also anticipated revealing a clear jump in phase when Δf varies, as it is shown in Figure 5.5. The calculated characteristic exhibits another jump in phase at $\frac{\Delta f}{2}$ that indicates the contribution of fifth-order terms to IM3 products, a second resonance also suggested by the measurements. This fact is more distinctly observed in Figure 5.6 where the excitation has been increased 5 dB giving rise to a more accentuated asymmetry, specially that caused by the fifth-order terms at $\frac{\Delta f}{2}$. While the proposed procedure (dashed line) can describe in an approximate form this effect, it is evident that the VS approach applied in [21] (dotted line), which does not include such terms, cannot explain this behaviour. Despite the good coincidence between theory and measurements in the flat segment of the curves, and the coarse agreement in the resonance zone, the discrepancy in this part does not permit an exact explanation of the frequency-dependent effect. The difference can be attributed to the nonlinear HEMT model and to the approximated equivalent circuit of the bias network. The estimations were repeated using a more detailed equivalent circuit of the bias network, including the Q factor of its elements, with a modest improvement in the shape. However, it was not sufficient to accomplish a satisfactory description of the quantitative phase behaviour, indicating the need of a more precise HEMT nonlinear model. To illustrate this deduction, the γ coefficients of equation (5.23) were varied using a least-squares optimization algorithm, in order to adjust the theoretical data to the measurements. The results, shown with solid line in the same Figure 5.6, demonstrate a very satisfactory agreement with the measured phase asymmetry, reinforcing the validation of the present procedure and the need of a more elaborated nonlinear model for the HEMT.

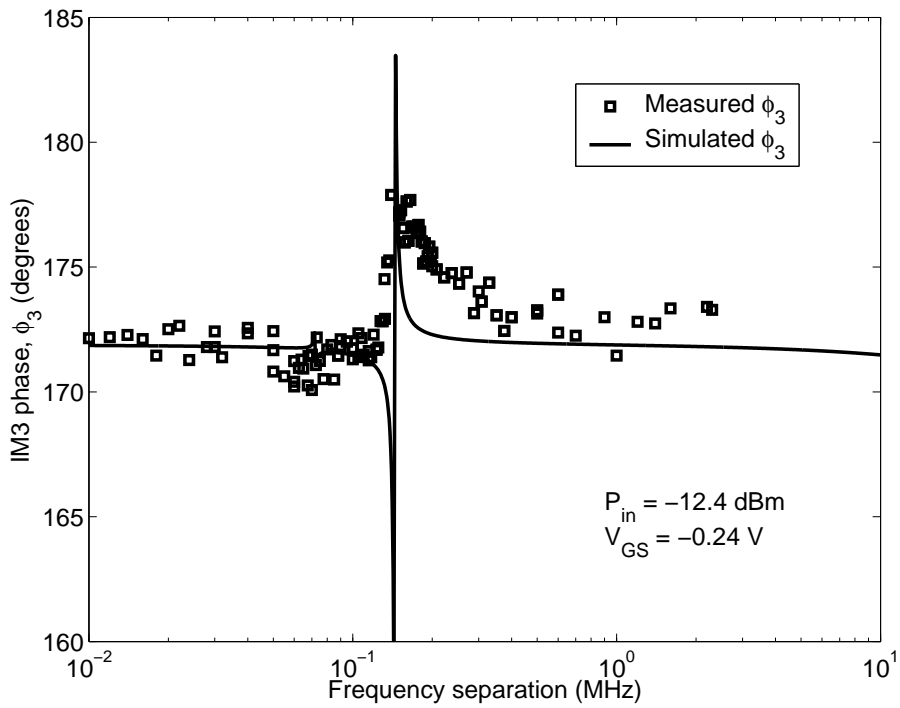


Figure 5.4: Measured and calculated phase of IM3 lower product when a resonant network is used for dc bias of the HEMT amplifier. Results calculated with the SN approach are plotted with a solid line.

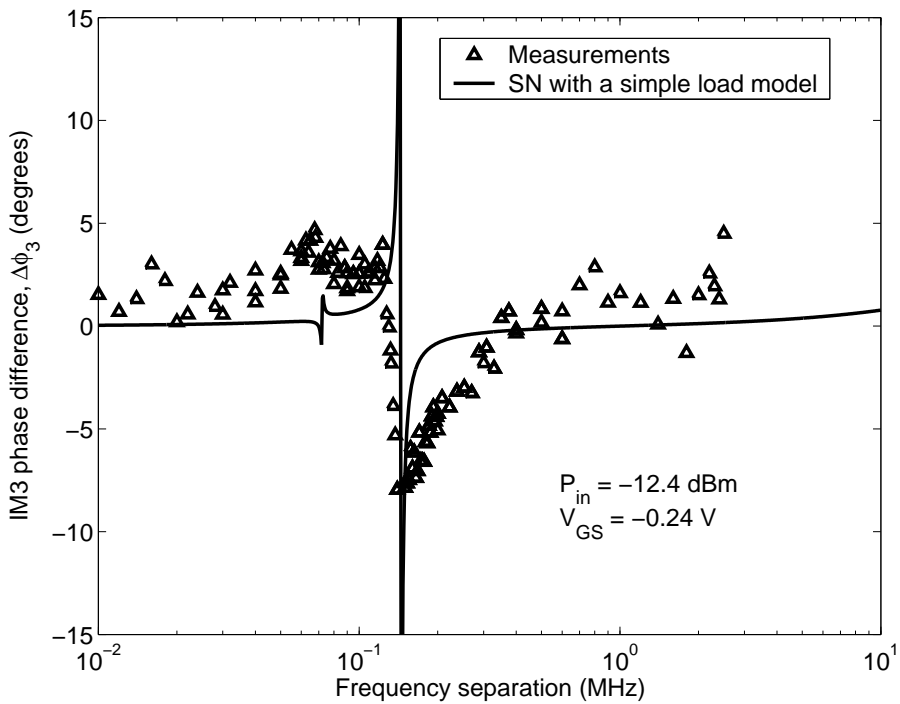


Figure 5.5: Detail of measured and calculated phase difference between IM3 products. Resonant bias network.

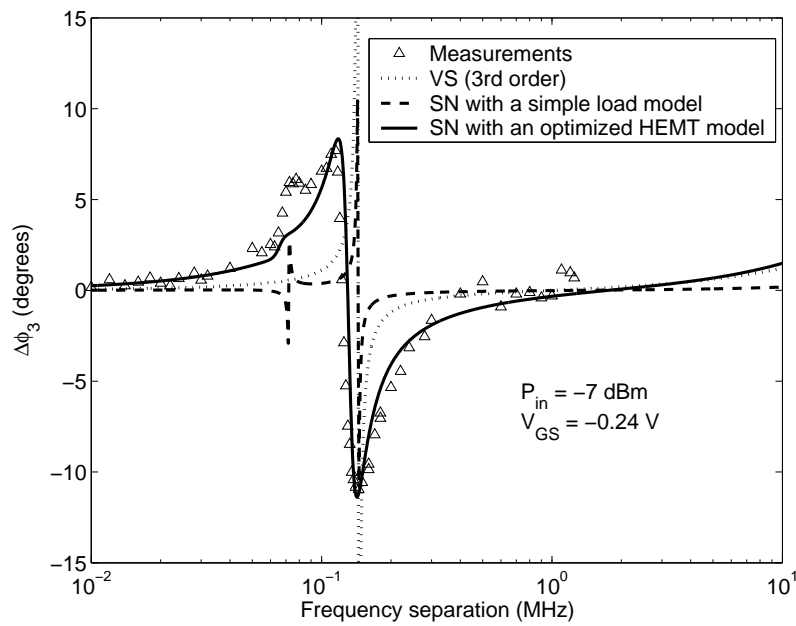


Figure 5.6: Measured phase difference of IM3 in the same conditions as Figure 5.5 but with an increment of 5 dB in the input signal level. Dotted line: conventional VS approach. Dashed line: SN approach with a basic load model. Solid line: SN approach with an optimised HEMT model.

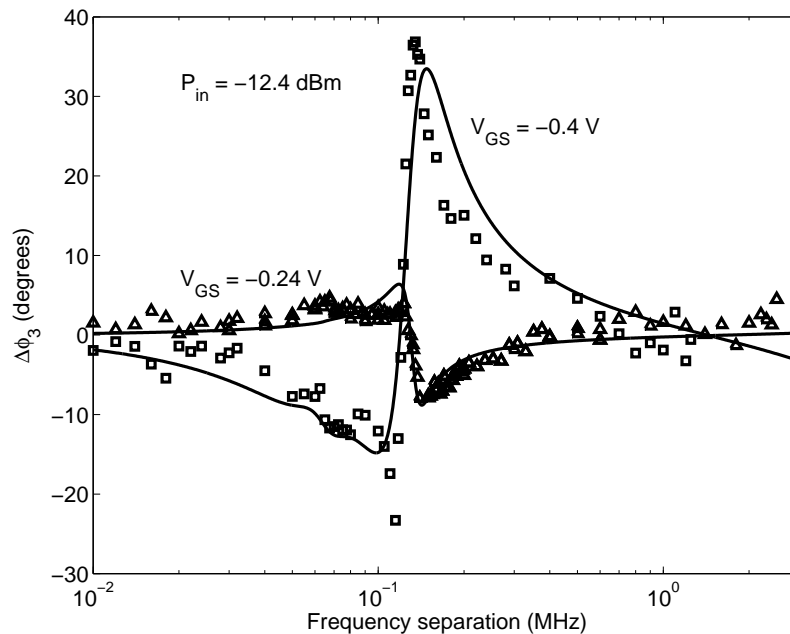


Figure 5.7: Measured phase difference of IM3 for the recommended bias point (triangles) and for $V_{GS} = -0.4$ V (squares). Solid lines represent the simulation with the SN approach and an optimised HEMT model. A phase inversion is clearly observed.

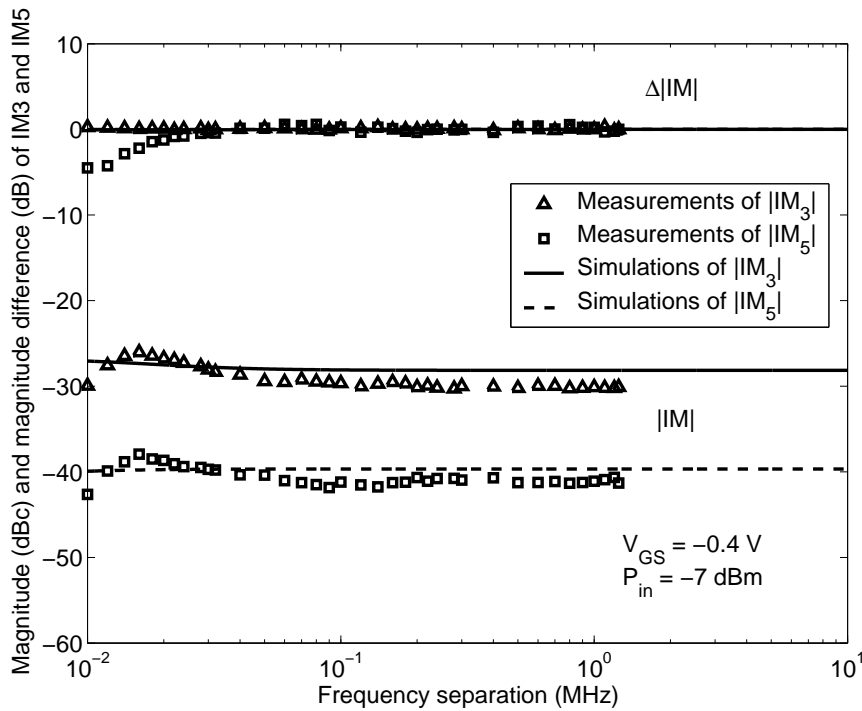


Figure 5.8: Measured magnitude and magnitude difference of IM3 (triangles) and IM5 (squares) using a commercial bias-Tee. The simulations using SN approach are represented with lines.

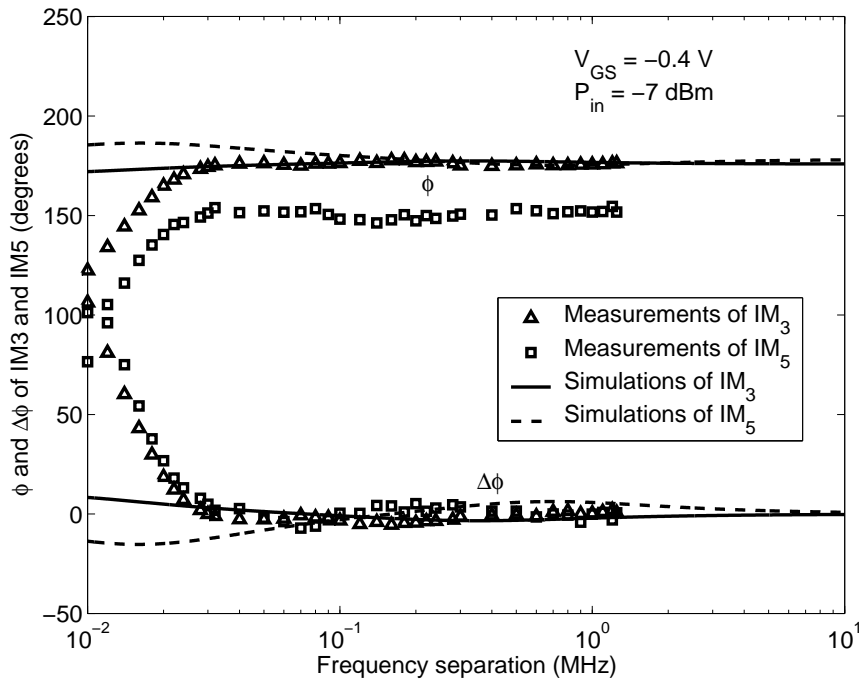


Figure 5.9: Measured phase and phase difference of IM3 (triangles) and IM5 (squares) using a commercial bias-Tee. The simulations using the SN approach are represented with lines.

Measurements of the phase of IM3 were also performed as a function of the dc gate voltage V_{GS} for an input level $P_{in} = -12.4$ dBm and a clear jump of 180° could be observed in the phase asymmetry as it is shown in Figure 5.7. The asymmetry predicted by the proposed method using the previously optimised coefficients for the bias point recommended by manufacturer, $V_{GS} = -0.24$ V, is represented with a solid line in the same figure and presents a quite good coincidence with the measured asymmetry. On the other hand, for $V_{GS} = -0.4$ V, the asymmetry is more pronounced and the polarity is inverted with respect to the case of normal operation. Taking into account that the γ 's are bias dependent, a new optimised set was found for $V_{GS} = -0.4$ V. The theoretical data were computed using these new coefficients and the results were also plotted with solid line in the same figure, demonstrating again a notable correspondence.

Magnitude and phase of IM5 were also measured with the present method for the amplifier biased at different V_{GS} voltages via the commercial bias-Tee and with several excitation levels. The results of IM3 (triangles) and IM5 (squares) magnitude and phase measurements for $V_{GS} = -0.24$ V and $P_{in} = -7$ dBm are depicted in Figures 5.8 and 5.9, where thermal or charge trapping memory effects are suggested in the phase and phase difference between upper and lower products for small frequency spacings. The deduced closed-form expressions (5.22)-(5.24) allowed to calculate voltages for IM3 and IM5 products and to represent the corresponding magnitudes and phases in the same figures with solid and dashed lines, respectively. The phase difference of IM3 and IM5 and the relative phase of IM3 were estimated with accuracy in all the cases. However, the estimated IM5 phase exhibits a deviation of about 25° with respect to the experimental values. Considering the simplifications that have been introduced in order to obtain closed-form expressions, the agreement between measurements and simulations is good. The differences suggest once more the need of a better drain source modelling for a further precision in IM5 phase characterization.

5.4 Impedance-based IM3 model for FET amplifiers including electrothermal memory effects

As it can be observed from the results of the previous section, the derived theoretical expressions presented some discrepancies with the measured IM3 for small tone separations. Traditional modelling methods do not have the capability to fully estimate the dependence of IMD on bandwidth unless they include some models for the thermal, impact ionization or charge trapping memory effects. These long-term memory effects have to be taken into account when designing high efficiency amplifiers so that they can comply with the strict requirements demanded for modern wireless commu-

nications bandwidths. In order to obtain an appropriate prediction for the variation of IM products with tone spacing, a simplified model based on finding an equivalent hypothetical load impedance that can explain discrepancies between measurements and circuit-level simulations was proposed by the author of this Thesis in [77].

The majority of recent works on nonlinear modelling techniques including memory have been focused on purely electrical memory effects. Among the approaches that account for thermal memory effects, we can mention the inclusion of thermal elements in transistor models to be able to correctly reproduce thermal effects, either by means of simple RC stages which describe self-heating [78], different RC stages for die and package temperature responses [79], distributed RC models [80], [81], or even RC stages with diodes in order to independently control charge and discharge time constants. Unlike these approaches, in [222] a Wiener behavioural thermal model is coupled to a temperature-dependent electrical device model, leading to a full-dynamic electrothermal model. Other long-term memory effects whose study have been recently undertaken are those caused by charge trapping mechanisms. These charge trapping effects are usually modelled by means of transfer functions showing a dependence on both the modulation frequency Δf and the bias voltages [82], [83].

Similar to Volterra-based IM analyses, the method proposed in Section 5.2 lends a leading role in generating memory effects to the load impedance. Consequently, the extraction of an appropriate hypothetical load impedance should provide a good adjustment with two-tone IM measurements, regardless the asymmetry is caused by electrical, thermal, impact ionization or charge trapping memory effects. In this section, we will explain the obtention of this hypothetical load impedance expressed in terms of electrical parameters, and test several circuit models for it in order to predict electrical and thermal memory effects by means of a circuit-level simulation method. These models have been derived from comparison between the experimental measurements of IM products presented in Section 5.3 and the theoretical expressions obtained in Section 5.2.

Figure 5.10(a) shows the equivalent two-node circuit model of the elemental HEMT amplifier used in the analysis presented in Section 5.2. Recall that, if the Taylor-series expansion for the nonlinear drain current is truncated up to third-order terms ($g_{kl} = 0$ for $k + l > 3$), the following closed-form expressions can be obtained for the drain voltage components at the fundamental tone frequencies and third-order IM product:

$$\begin{aligned} V_{d_{u,l}} &= H_1 A + \left[\frac{9}{4} \gamma_3 + \gamma'_{20} \bar{Z}_L(\pm \Delta f) \right] A^3, \\ V_{d_{3u,3l}} &= \left[\frac{3}{4} \gamma_3 + \gamma'_{20} \bar{Z}_L(\pm \Delta f) \right] A^3, \end{aligned} \quad (5.31)$$

with $\bar{Z}_L(\pm \Delta f)$ the load impedance seen by the drain source at baseband frequencies,

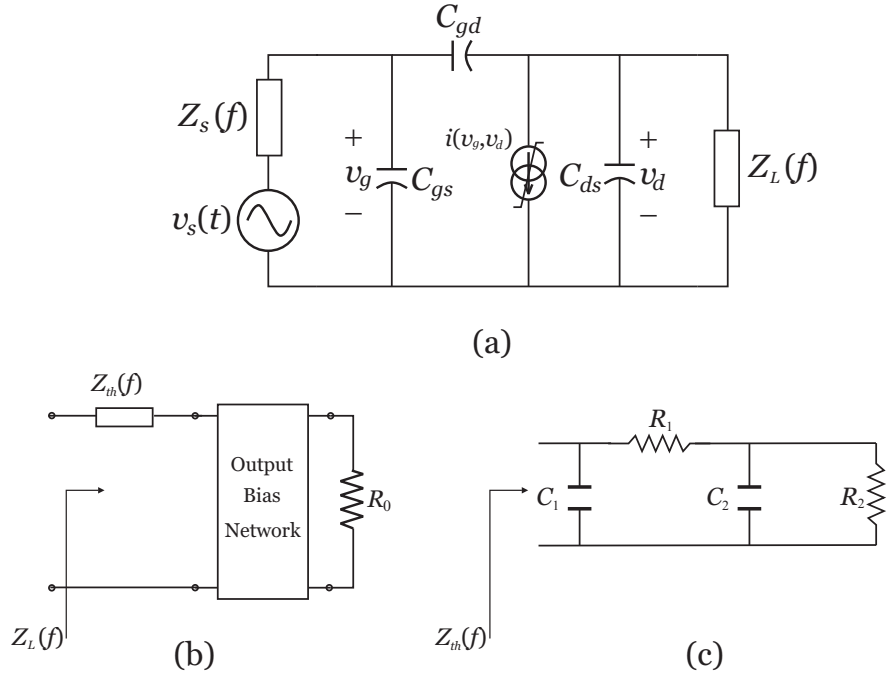


Figure 5.10: Equivalent circuit of a HEMT amplifier used in the analysis (a). Proposed model for the equivalent load impedance \bar{Z}_L (b) and the hypothetical impedance Z_{th} (c).

and the coefficients γ expressed in terms of the gate and drain linear transfer functions, and the gate and drain impedances at the fundamental and second-harmonic frequency zones. Therefore, for a given carrier frequency, the values γ'_{20} and γ_3 are bias-dependent constants.

As it was remarked in Section 5.2, none of the terms in (5.31) depends on frequency except for $\bar{Z}_L(\pm\Delta f)$, thus the load impedance plays a predominant role in the generation of memory effects. Furthermore, the only difference between the expression for the lower IM3 (IM_{3l}), expressed by the component $V_{d_{3l}}$, and the upper IM3 (IM_{3u}), expressed by the component $V_{d_{3u}}$, is the presence of $\bar{Z}_L(\Delta f)$ in the latter and $\bar{Z}_L(-\Delta f) = \bar{Z}_L^*(\Delta f)$ in the former.

Since the experimental setup used for IM3 characterization in this work provides phase measurements relative to the tones, the expressions for the voltages of IM_{3l} and IM_{3u} relative to the lower and upper tones, respectively, will be considered

$$F_{3u} = \frac{\left[\frac{3}{4}\gamma_3 + \gamma'_{20}\bar{Z}_L(\Delta f) \right] A^2}{H_1 + \left[\frac{9}{4}\gamma_3 + \gamma'_{20}\bar{Z}_L(\Delta f) \right] A^2} \quad (5.32)$$

$$F_{3l} = \frac{\left[\frac{3}{4}\gamma_3 + \gamma'_{20}\bar{Z}_L^*(\Delta f) \right] A^2}{H_1 + \left[\frac{9}{4}\gamma_3 + \gamma'_{20}\bar{Z}_L^*(\Delta f) \right] A^2}. \quad (5.33)$$

Following (5.32) and (5.33), a prediction of the IM3 variation with tone spacing can be determined by using $\bar{Z}_L(\Delta f)$, which must include all the intrinsic and extrinsic elements in the circuit connected to the drain node. However, if the amplifier shows low-frequency dispersive effects (including dispersion due to self-heating, impact ionization, or trapping effects), circuit-level simulations accomplished by using the SN approach will not fit measurements for the lower tone separations. Therefore, the basic idea under the proposed approach is that the extraction of an appropriate hypothetical load impedance, using measurements of both magnitude and phase, must be able to provide a good agreement with two-tone IM measurements, regardless the nature of the memory effects that cause the asymmetry. Furthermore, a part of the load impedance seen by the drain node will be known, that is, the elements of the intrinsic model of the HEMT connected to the drain node, the impedance of the bias network, and the impedance placed at the output of the amplifier. Once the values for the equivalent load impedance that fit measurements have been obtained, all known elements can be de-embedded and the remaining term will be a hypothetical electrical impedance Z_{th} , which accounts for electrothermal effects and is not included in the device model. In Section 5.4.1, a circuit model for the impedance Z_{th} will be obtained and discussed for a certain group of measurements.

5.4.1 HEMT amplifier experimental results

A simple amplifier constructed with the HEMT EPB018A5-70 of Excelics was used to demonstrate the good correspondence with measurements obtained by the proposed impedance-based model. Two different biasing voltages, $V_{GS} = -0.24$ V and $V_{GS} = -0.4$ V, being $V_{DS} = 2$ V, and different input power levels were applied using a commercial bias-Tee ZFBT-6GW of Minicircuits. Results for some of these measurements were shown in Figures 5.3, 5.8 and 5.9 of Section 5.3, where we can observe that circuit-level simulations accomplished under the SN approach only fit measurements for tone separations over 30 or 100 kHz, while the observed variations for lower tone spacings cannot be explained by purely electrical memory effects taking into account the load impedance given by the employed commercial Bias-Tee.

The methodology previously described was applied to the measurements of IM_{3l} in order to extract the values of the equivalent load impedance \bar{Z}_L , whose inclusion in simulation leads to a perfect agreement with measurements even for small tone

separations, between 10 and 30 kHz. Then, part of the intrinsic model of the HEMT, the bias network, and the termination impedance were de-embedded and the best results were obtained when the hypothetical impedance Z_{th} was modelled as a series impedance placed between the intrinsic model of the amplifier and the bias network, as it is shown in Figure 5.10(b). Finally, several simple circuit topologies for Z_{th} were tested and the best agreement was obtained for a parallel RC circuit. The model shown in Figure 5.10(c) was employed to achieve a more precise fit. For all the studied conditions with this HEMT amplifier, the same configuration of \bar{Z}_L and the same topology of Z_{th} produced the best adjustment. The optimised parameters for the elements of Z_{th} in some of the cases were the following:

- $R_1 = 444.9 \Omega$, $C_1 = 0.25 \mu\text{F}$, $R_2 = 541.8 \Omega$, and $C_2 = 0.22 \text{ nF}$, for $V_{GS} = -0.24 \text{ V}$ and $P_{in} = -7 \text{ dBm}$.
- $R_1 = 267 \Omega$, $C_1 = 0.26 \mu\text{F}$, $R_2 = 318.3 \Omega$, and $C_2 = 0.31 \text{ nF}$, for $V_{GS} = -0.24 \text{ V}$ and $P_{in} = -5 \text{ dBm}$.
- $R_1 = 966 \text{ K}\Omega$, $C_1 = 0.23 \mu\text{F}$, $R_2 = 976.2 \text{ K}\Omega$, and $C_2 = 0.023 \text{ pF}$, for $V_{GS} = -0.4 \text{ V}$ and $P_{in} = -5 \text{ dBm}$.

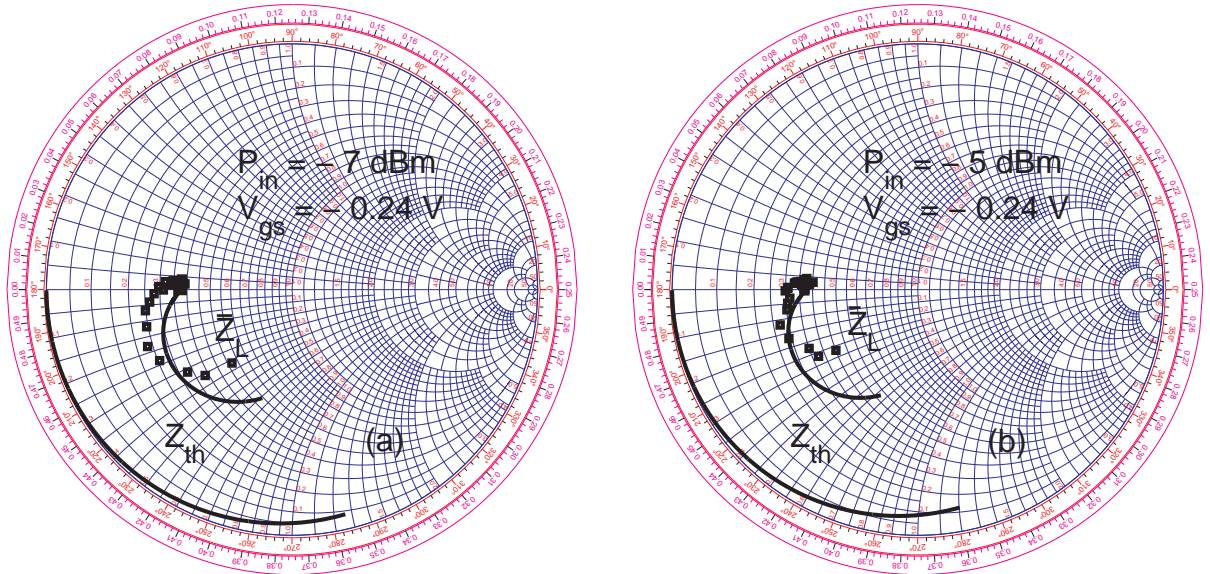


Figure 5.11: Smith Chart with the extracted values of Z_{th} at baseband frequencies (marks) for a HEMT amplifier at input levels of -7 dBm (a) and -5 dBm (b) for a bias voltage $V_{GS} = -0.24 \text{ V}$. Solid lines represent the impedance of a parallel resonant RC circuit that best approximates the extracted values in least-squares sense and the equivalent load impedance including this RC circuit (\bar{Z}_L).

The models for the equivalent load impedance \bar{Z}_L and the hypothetical impedance Z_{th} for a biasing voltage of $V_{GS} = -0.24$ V and input power levels of -7 dBm and -5 dBm are shown in the Smith Charts of Figure 5.11. The only moderate adjustment of circuit models with the equivalent load impedance could be explained by the simplicity of their topology. However, acceptable results are obtained including them in magnitude and phase simulations of the IM products.

A good correspondence with measurements can be observed for the magnitude of IM_{3u} in the simulations at all frequency spacings. This agreement is shown in Figure 5.12 for a bias voltage of $V_{GS} = -0.24$ V, where results including the equivalent load impedance \bar{Z}_L are depicted in dotted line while solid line is employed for the results using the adjusted model of Z_{th} . We can observe that, increasing the input power level from -7 dBm to -5 dBm, the measured IM_3 does not follow the typical 3 dB/dB slope for the linear behaviour because the input level is very close to the 1-dB compression point. However, the use of the equivalent load impedance gives an appropriate agreement even for a mild nonlinear behaviour.

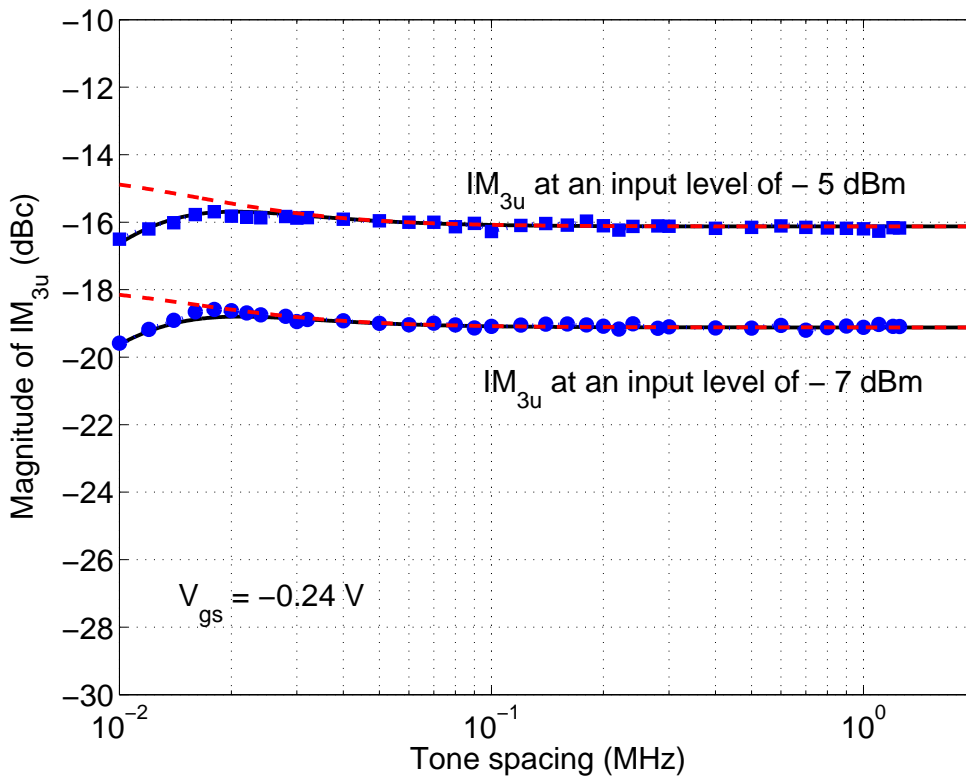


Figure 5.12: Measured magnitude of upper IM_3 products for a HEMT amplifier at input levels of -7 dBm (circles) and -5 dBm (squares) and a bias voltage $V_{GS} = -0.24$ V. Predictions without Z_{th} (dashed line), with the extracted values of Z_{th} (dotted line) and with the chosen circuit model (solid line).

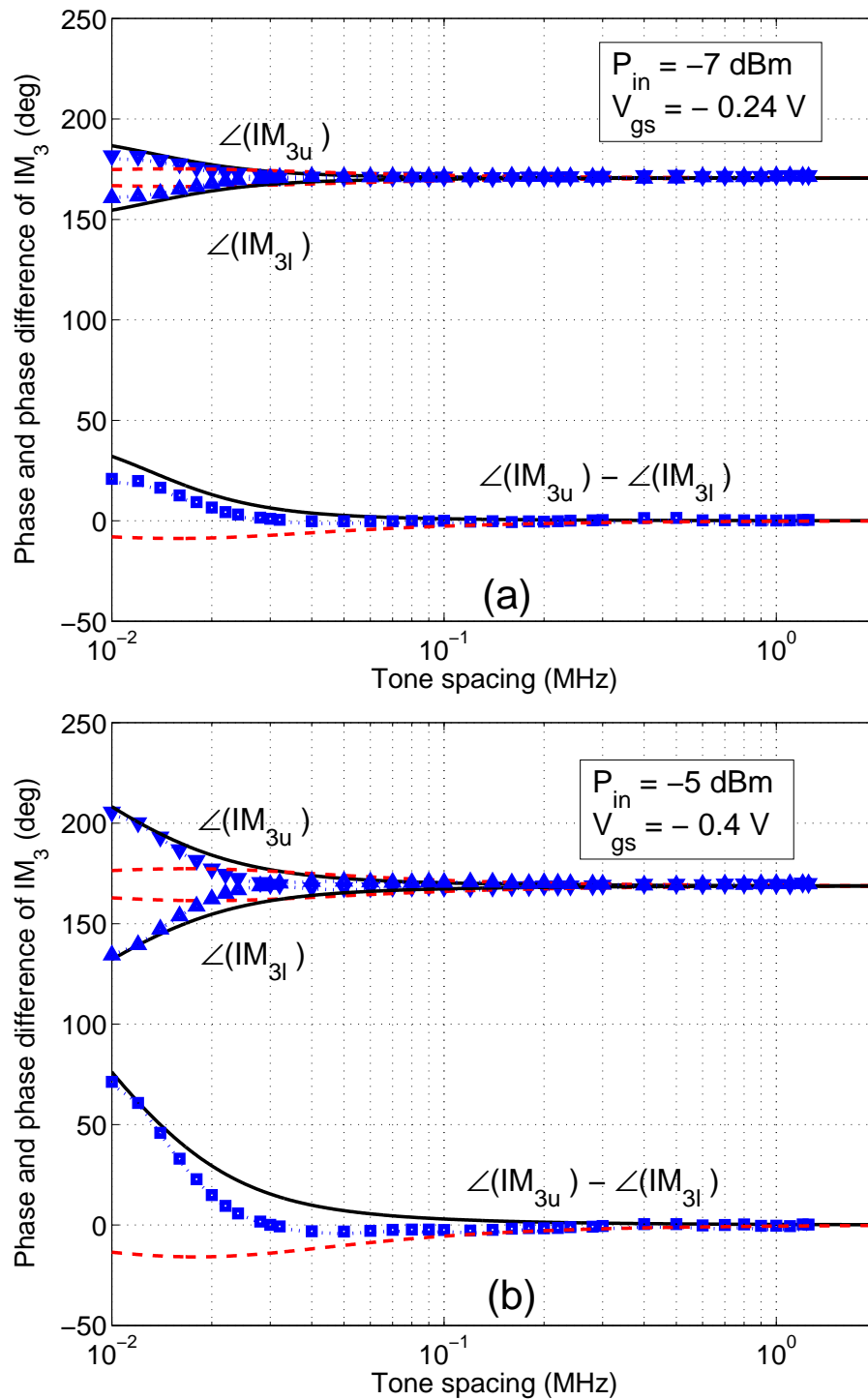


Figure 5.13: Measured phase (triangles) of upper and lower IM3 products and phase difference (squares) for a HEMT amplifier with $P_{in} = -7$ dBm and $V_{GS} = -0.24$ V (a) and $P_{in} = -5$ dBm and $V_{GS} = -0.4$ V (b). Predictions without Z_{th} (dashed line), with the extracted values of Z_{th} (dotted line) and with the chosen circuit model (solid line).

Figure 5.13 shows the phases of IM_{3u} and IM_{3l} and their phase difference for: (a) a bias point of $V_{GS} = -0.24$ V and an input level of -7 dBm, and (b) a bias point of $V_{GS} = -0.4$ V and an input level of -5 dBm. It should be noticed that changes with frequency produced by memory effects can be observed more clearly in phase than in magnitude. Furthermore, it is more relevant for the bias voltage $V_{GS} = -0.4$ V, which is nearer the pinch-off voltage and produces a stronger nonlinearity in the amplifier. Again, a good agreement with measurements is achieved with a simple circuit model for Z_{th} , even when a different bias condition and a higher input level are applied, increasing the importance of memory effects.

The close correspondence between the measured and modelled data demonstrates the ability of this approach to capture memory effects using a simple impedance-based model, even when the amplifier is driven near saturation. This corresponds to a common situation in the real practice, for which the impact of memory effects is critical and requires a careful modelling. We can remark that, in the case of the employed HEMT device, the modelled circuit is a low-pass filter placed between the drain and source nodes. Therefore, the proposed Z_{th} , although electrical, plays an analogous role to that of a thermal impedance [78]. As it is stated in [27], the thermal impedance of the active device is not purely resistive, but forms a distributed low-pass filter, which means that the temperature changes caused by the dissipated power are frequency-dependent and cause thermal memory effects.

5.4.2 Memory effects in FET amplifiers including dispersive phenomena

Large-signal model coefficients of GaAs MESFET/HEMT devices such as drain conductance or transconductance can be found from dc measurements, RF measurements with a VNA or pulsed measurements. Research has shown that there are significant differences between static (dc) and dynamic (RF or pulsed) I/V characteristics [175], [57], [223], [224], [225], [226]. These differences have been a cause of considerable difficulty in large-signal modelling, which must accurately predict both static and dynamic performance. This phenomenon is usually referred to as *dispersion* of FET characteristics, and it is attributed mainly to self-heating, impact ionization, and trapping effects. At frequencies where the transconductance or drain conductance is changing, the parameter has an imaginary component [25]. At high frequencies, it settles to a constant value. Evidence of dispersion can be observed both in the time and frequency domains. When it is observed in the frequency domain, for example over a frequency sweep, dispersion typically occurs between 100 Hz and 10 MHz. Therefore conventional VNAs are not suitable for these measurements in most cases, because

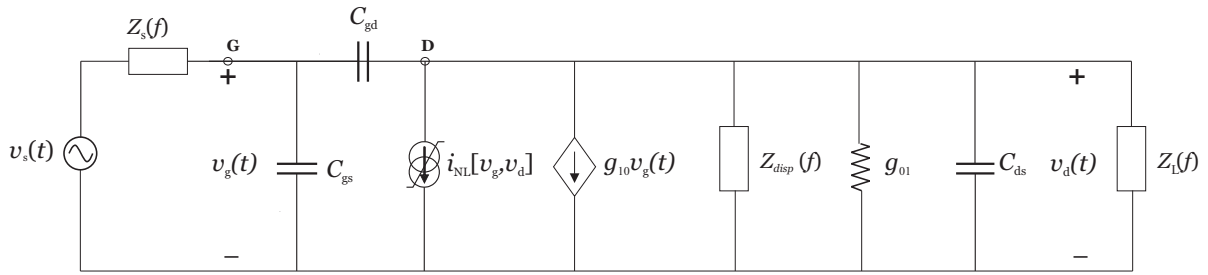


Figure 5.14: Equivalent circuit of a model including dispersive phenomena.

they cannot measure at the low frequencies required. Pulsed $I - V$ measurements are recommended, since the physical mechanisms causing dispersion have low-pass characteristics, i.e., they involve large time constants. Dispersive phenomena have been proved to cause bandwidth-dependent distortion, therefore they are an important source of memory effects. In this section, it will be briefly shown that they can be included in the SN analysis of IMD in a quite straightforward way.

In general, dispersive effects have been included in electrical models by adding either extra current sources to the gate and drain of the FET in parallel with the dc nonlinear elements [227], extrinsic series voltage sources which are linearly controlled by the voltages at the device ports [228], or a RC branch with a time-constant consistent with the measured characteristics [223], [229], [230], [231]. Note that the RC networks employed in the last approaches are selected in such a way that they do not influence the small- or large-signal parameters in the GHz range, as they have high impedance at these frequencies. In order to improve these methods, other alternatives that have been proposed are the employment of equivalent circuits with four terminals [232], the inclusion of a feedback voltage from drain to gate terminals [233], and the addition of more complex multi-pole RC filter networks at the gate and drain to model the multi-time constant transition from dc to RF and separate the static and dynamic components of the intrinsic voltages [234].

Following the trend presented in [223], [229], [231], and [234], a two-node linear augmented circuit as shown in Figure 5.14 will be considered, similar to the one analysed in Section 5.2. Recall that it was a simplified FET model in common-source configuration where nonlinear terms of the capacitances C_{gs} and C_{gd} were neglected, and only the nonlinearity in the drain current source was considered. The source and load impedances, $Z_s(f)$ and $Z_L(f)$, include the elements for both the bias and matching networks. The difference is the inclusion of a frequency-dependent network whose equivalent impedance $Z_{disp}(f)$ models the dispersive phenomena. Note that, for a general formulation, this impedance does not need to be an actual circuit, even theoretically. With this formulation of the problem, closed-form expressions (5.22)-(5.26),

obtained in Section 5.2, are still applicable provided that the following new baseband equivalent load impedance is considered:

$$\bar{Z}_L(\Delta f) = \frac{1}{Z_L^{-1}(\Delta f) + g_{01} + Z_{disper}^{-1}(\Delta f)}. \quad (5.34)$$

As it can be observed, it includes the effects of the dispersive network $Z_{disper}(\Delta f)$, as well as those originated by the bias network impedance $Z_L(\Delta f)$ at baseband frequencies. The effect of the intrinsic model capacitors connected to the drain node are neglected at baseband frequencies.

In this way, observed changes in IM3 products with the lower frequency spacings can be conveniently treated by the inclusion of the proper dispersive networks within large-signal circuit models in order to accomplish accurate predictions for measurements showing low-frequency dispersion. Therefore, closed-form expressions (5.22)-(5.26) could additionally be employed for the parameter extraction of the dispersive networks in [223], [229], [231], and [234], by means of the comparison between IMD predictions and measurements for the lower values of modulation frequency, where dispersion typically occurs.

5.5 Extension of the impedance-based model for commercial amplifiers

The theoretical results obtained for a HEMT device in Section 5.4 can be generalised to more complex circuits provided that they exhibit a moderate gain, and high reverse isolation at low frequencies. These assumptions are common in amplifiers, for which we propose the following extension [84]:

$$V_{3u,3l} = \sum_{\substack{n=3 \\ n\text{-odd}}} [a_n + b_n Z_{eq}(\pm \Delta f)] A^n. \quad (5.35)$$

Parameters a_n and b_n depend on carrier frequency, while Z_{eq} retains the dependence of IMD with modulation frequencies. In order to extract the model parameters and the frequency response of the impedance, the measurement setup presented in Chapter 4 can be used for the characterization of IM3, in magnitude and phase, varying both the input level and the tones separation. Measurements can be fitted to the proposed model through a nonlinear least-squares optimization procedure provided that the set of measurements is wide enough. The main difference with the case of the HEMT amplifier is the extraction of model parameters, which was done assuming a prior knowledge of the internal circuit structure, i.e. the coefficients γ in (5.32) and (5.33)

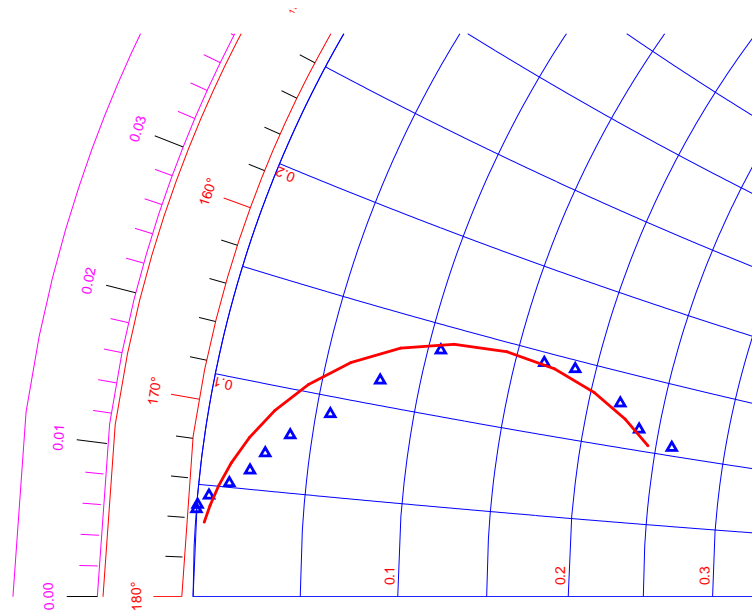


Figure 5.15: Zoom in the Smith Chart with the extracted values of $Z_{eq}(\Delta f)$ (marks) for a commercial amplifier. The solid line represents the impedance of a parallel resonant RLC circuit that best approximates the extracted values in least-squares sense.

were derived from the large-signal model of a HEMT transistor by using closed-form expressions. However, for a more complex commercial amplifier, there is no such knowledge about a_n and b_n .

5.5.1 Commercial amplifier results

In order to demonstrate the suitability of the impedance-based model approach not only for a HEMT circuit, the commercial amplifier MAX2430 of MAXIM has been modelled. This device is the same employed to illustrate the nonlinear distortion characterization capabilities of the proposed setup in Section 4.2.1. Although the device under test is a wideband amplifier at 915 MHz, the experimental characterization showed an asymmetry in the IM products, a clear indication of the existence of nonlinear memory effects.

Four values of the input power per tone ranging from -25 to -10 dBm, were applied using a bias voltage of 3.6 V, and a sweep of 15 tone spacings per level, around 915 MHz was performed to provide a grid of 60 complex values. First, measurements were fitted to a model with 4 coefficients plus the unknown impedance.

Figure 5.15 shows the extracted impedance values $Z_{eq}(\Delta f)$ that minimise the square error. Considering the resemblance of this curve in the Smith Chart with that

of a parallel resonant circuit, the hypothetical impedance was approximated by the impedance of an equivalent RLC circuit, depicted in solid line in the same figure. The parameter values of the parallel resonator were $R = 14.5 \Omega$, $L = 5.4 \mu\text{H}$, and $C = 5.4 \mu\text{F}$. The model with the resonant circuit and calculated coefficients $\{a_n, b_n\}$ was then tested to simulate IM3 products and asymmetries. Figures 5.16 and 5.17 represent the predicted values of magnitude and phase at the highest measured power level (above the 1-dB compression point), as a function of tone spacing, showing a very good correspondence despite the simplicity of the model.

Although it showed a satisfactory agreement for the highest measured power level, the concordance was not as good for low power levels, due to the high dynamic range of the IMD values used for the adjustment. Using 6 coefficients, the dynamic range of the model was increased accordingly, as Figure 5.18 shows, which compares predicted and measured IM3 phase asymmetry in the full range of input levels and tone spacings. Magnitude levels of $\text{IM}_{3\text{u}}$ for this model are also depicted in Figure 5.19. Simulated $\text{IM}_{3\text{l}}$ exhibits a similar correspondence with measurement data. Despite it has been observed that the applied optimization procedure is affected by the dynamic range of the measurements, the measured to model agreement is very good when the amplifier is driven near saturation, which corresponds to a common situation in the real practice, for which the impact of memory effects is critical and requires a careful modelling.

Further work is needed to extend the model to other modulation formats, although the impedance impulse response seems a promising approach to develop an equivalent signal-independent behavioural model in the time domain. This approach can make possible some contributions to the large-signal modelling of devices, including thermal or charge trapping memory effects that affect low modulation frequencies.

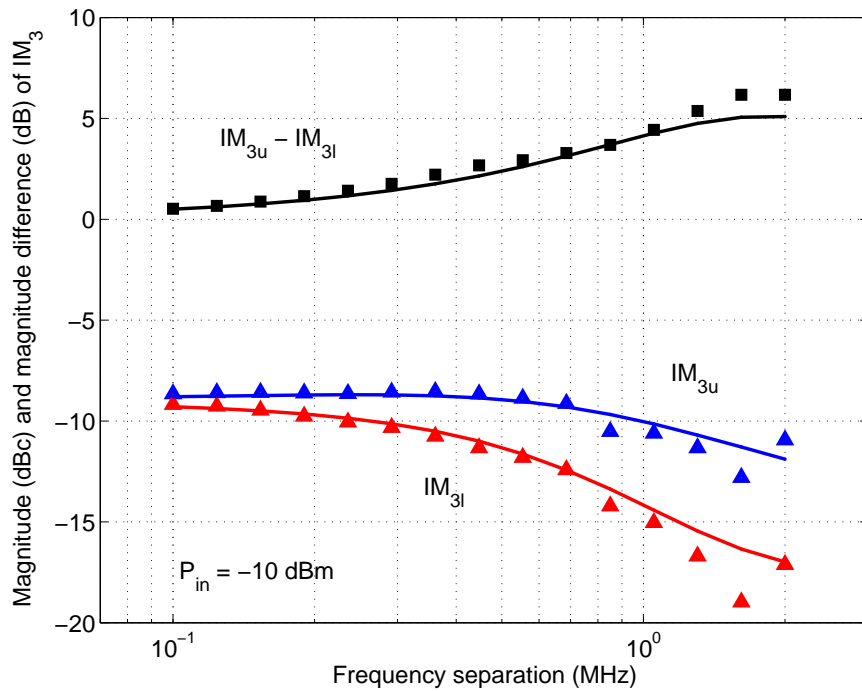


Figure 5.16: Measured magnitude (triangles) and magnitude difference (squares) of IM3 at an input level of -10 dBm. Predictions with the proposed model using the equivalent resonant RLC circuit load (solid line).

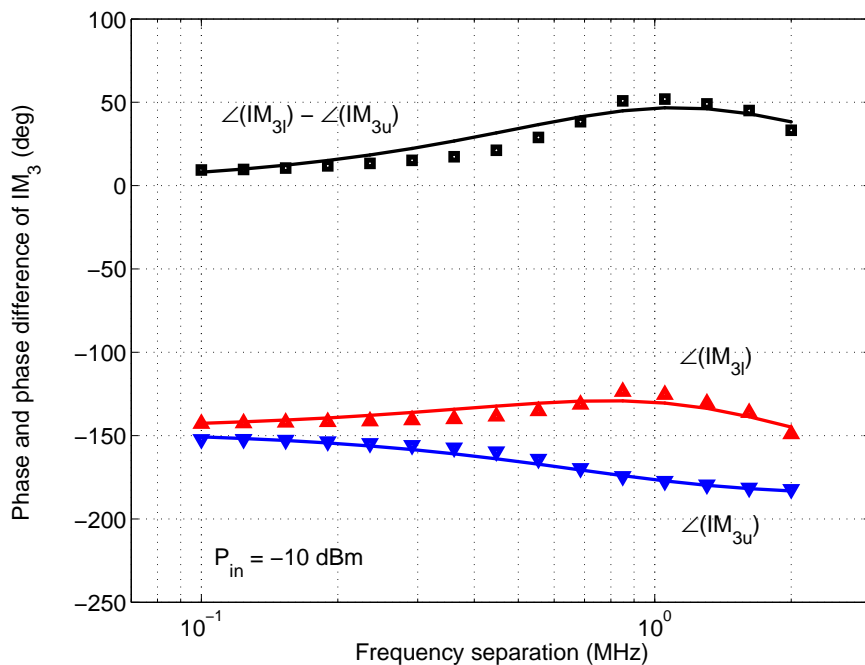


Figure 5.17: Measured phase (triangles) and phase difference (squares) of IM3 at an input level of -10 dBm. Predictions with the proposed model using the equivalent resonant RLC circuit load (solid line).

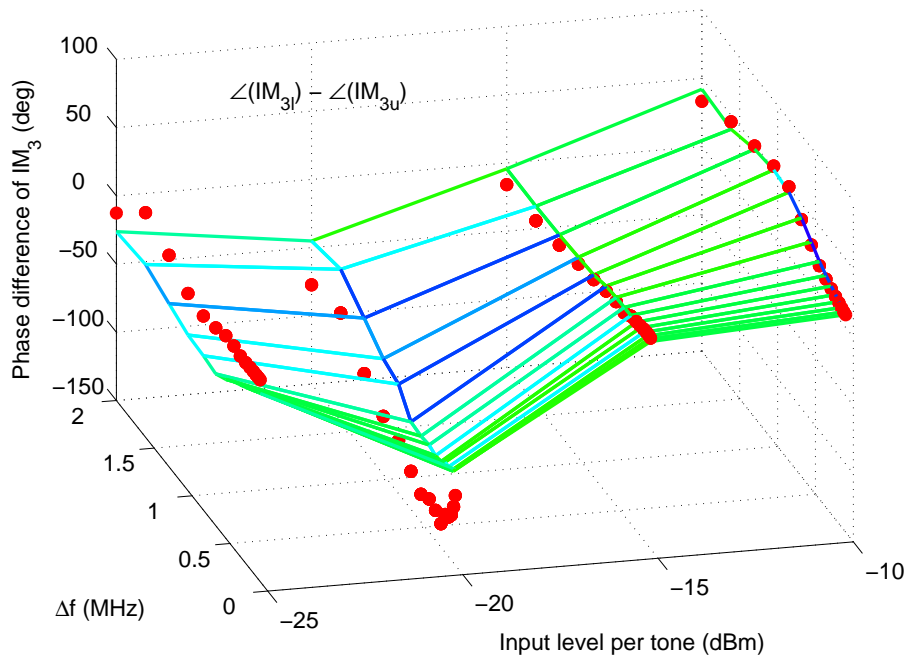


Figure 5.18: Measured two-tone IM3 phase asymmetries between lower and upper products (marks) and prediction (wireframe) with the extracted values of the equivalent load impedance using a model with 6 parameters for a commercial amplifier.

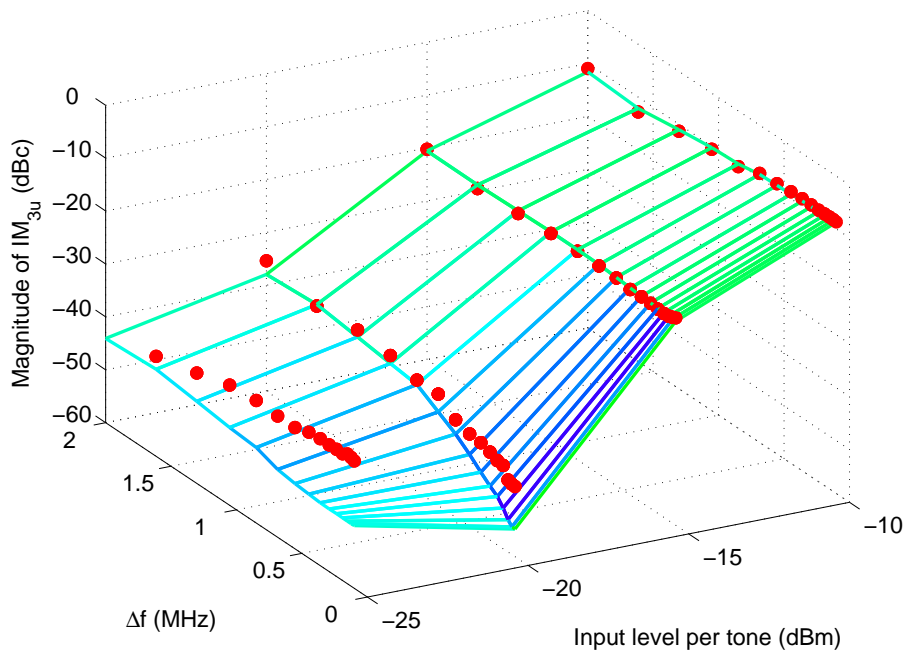


Figure 5.19: Measured magnitude of upper IM3 products (marks) and prediction (wireframe) with the extracted values of the equivalent load impedance using a model with 6 parameters for a commercial amplifier.

CONCLUSIONS AND SUGGESTIONS FOR FUTURE WORK

6.1 Conclusions

This Thesis was begun by exposing the current interest in the study of the nonlinear characterization in wireless communications systems and, particularly, in the modelling of memory effects in power amplifiers. After the research carried out in this Thesis, three fundamental ideas can be derived:

1. A new Simplified Newton method can be applied to analyse the distortion phenomena in weakly nonlinear circuits excited by wireless communications signals. The proposed method allows time competitive ACPR simulations for a wide range of input power levels. An specific application of this method can be made for mixers, where the more complex output spectra advise some additional simplifications to reduce the computational cost and storage necessities.
2. This Simplified Newton approach can also be used to obtain closed-form expressions for the intermodulation distortion in power amplifiers. These theoretical expressions can be employed to gain an insight into the behaviour of input level dependence and the impact of the baseband termination impedance on the memory effects and asymmetries observed. This analysis leads to some useful hints to optimise the intermodulation behaviour.
3. More work needs to be done in large-signal circuit modelling in order to account for low-frequency dispersion effects in the theoretical expressions for the intermodulation distortion. The extraction of an impedance-based model for both FET and commercial amplifiers is a potential approach that should be examined.

The use of an equivalent impedance provides the model with a structural significance, since it identifies a circuit element playing a major role in the generation of memory effects, regardless their nature.

In order to provide an overview of the important results, we would like to extend some of the aforementioned conclusions. The Simplified Newton approach could be seen as the common thread of all the proposed techniques. Classical techniques such as standard Harmonic Balance turn to be inefficient for circuits excited with digital modulations. This is the reason why the more efficient envelope-based methods have been studied. The usefulness of the Simplified Newton approach for the analysis of nonlinear distortion is remarked by the fact that it can be applied to both amplifiers and mixers, two of the key elements of any circuit used in wireless communications. Similarly to other envelope-based methods, such as the Envelope Currents method, this iterative approach is based on solving an augmented linear subcircuit driven by different nonlinear current sources for each iteration. As it has been mentioned, its main advantage relies on the fact that the nonlinear currents derived from the Simplified Newton method are a better approximation for the real nonlinearity, since they include higher-order terms. Despite the reduced convergence region of the Simplified Newton algorithm, satisfactory predictions of a mildly nonlinear amplifier characteristics have been achieved. On the whole, a reduction of the computational time may be achieved, allowing efficient ACPR simulations for a wide range of input power levels.

In the analogous Simplified Newton approach devoted to the study of communications signals in mixers, the input excitation is considered as a perturbation about the response to the LO large sinusoidal signal, which leads to the solution of a periodically time-varying augmented linear subcircuit by means of its nodal-admittance conversion matrix. The computational and storage cost of the Simplified Newton technique are significantly more demanding for mixers than for amplifiers, due to the higher number of frequency lines needed. For this reason, some additional simplifications have been proposed to include in the recursive procedure only a subset of the Fourier coefficients involved in the solution, and obtain the rest by complex conjugation. The performance of the Simplified Newton approach has been compared to that of a standard Newton-Raphson method, in which a non-periodically time-varying circuit that must be updated for each iteration is needed. The latter presents better convergence properties at the cost of a higher computational cost.

The same Simplified Newton approach has allowed the obtention of closed-form expressions that can be employed to gain an insight into the impact of the baseband termination impedance on the memory effects and asymmetries observed in the intermodulation products of power amplifiers. This new theoretical approximation is an

alternative to the conventional Volterra series method and has the attribute of being a faster convergent algorithm without losing the possibility of generating closed-form expressions. This quality grants not only inclusion of higher order terms in the expression of IM3 which incorporates input level dependence to IM3 asymmetry, but even the possibility of IM5 magnitude and phase evaluation.

Some important observations can be gathered from the deduced closed-form expressions for IM3 and IM5, that can be summarised as:

- If the baseband load impedance \bar{Z}_L of the power amplifier is real, no memory effects or asymmetries are possible between the upper and lower IM products, either in magnitude or phase.
- If the baseband load impedance \bar{Z}_L presents a non-negligible complex part, the device will always exhibit an asymmetry in phase.
- Only when the coefficients γ and the baseband load impedance \bar{Z}_L are complex, an asymmetry in both magnitude and phase will appear. This situation can easily be encountered when the gate and drain impedances at the fundamental and second harmonic frequencies are complex.
- If the coefficients γ are negligible, the constant term will dominate the final resultant vectors and no asymmetries will be observed. In this case, we can be misled by the fact that the variation of IMD with Δf may not be evident, although the power amplifier still presents memory effects.
- If the characteristic observed in a spectrum analyser has (magnitude) asymmetry, then it is possible to say that the amplifier has memory, but the converse is not true.

An automated setup for the characterization of nonlinear devices has been proposed using standard communications laboratory equipment, with capabilities for relative magnitude and phase measurements in two-tone tests. The experimental method is based on the generation of two tones by means of a double-sideband suppressed-carrier modulated signal, the acquisition of baseband samples of the output signal in order to recover its spectrum, which contains all the magnitude and phase information, and finally, a post-processing for phase correction so as to eliminate the transit delay. Experimental measurements for IM3 and IM5 of an elemental HEMT amplifier have been compared to the theoretical predictions obtained with the proposed Simplified Newton approach. Phase measurements proved to be more appropriate in several cases for the detection of frequency-dependent effects or asymmetries, emphasising the importance of phase characterization of IMD.

Regarding the modelling of thermal and charge trapping effects, the extracted equivalent hypothetical impedance provides the model with an structural significance, since it identifies a circuit element playing a major role in the generation of memory effects, regardless their nature. It is worth noticing that the modelled hypothetical impedance circuit takes an analogous form to some of the dispersive networks found in literature, which are included within large-signal circuit models in order to account for low-frequency dispersion phenomena. Therefore, the obtained closed-form expressions could help to extract the parameters of the dispersive networks.

As far as the proposed extension of the impedance-based model for commercial amplifiers is concerned, the reduced-order model is obtained by comparing the device's input and output waveforms, no knowledge of the internal circuit structure being required. Although the optimization procedure is affected by the dynamic range of the measurements, the good measured to model agreement demonstrates the proposed model suitability for capturing memory effects.

6.2 Suggestions for future work

Some of the results presented in this Thesis are subjected to future extensions, while new research lines are opened:

- The strategies for achieving a higher efficiency of the analysis approaches presented in this Thesis are focused on single-carrier modulated signals. The proliferation of modern wireless communication standards based on multi-carrier signals, such as WiMAX or the IEEE 802.11 family, recommends their study in order to extend or adapt the proposed Simplified Newton approach for their specific characteristics. On the other hand, in this Thesis mainly single-transistor amplifiers have been employed as illustrative examples, in order to demonstrate the good performance of the analysis techniques in a simple way. The use of the proposed techniques to reduce the computational time when analysing very large circuits or complete communications systems suggests another promising extension of the Simplified Newton approach.
- The automated setup proposed in Chapter 4 for the experimental characterization of nonlinear distortion and memory effects presents some limitations regarding its maximum sampling rate and dynamic range. Some signal processing techniques have recently been proposed in order to extend the bandwidth of RF power amplifier test beds [85]. It should be advisable to investigate in the application of these or some alternative techniques to improve the quality of the measurements accomplished with the designed characterization tool.

- It might be interesting to evaluate how the obtained results would change if the narrowband assumption were not considered. This analysis could result of the utmost importance for systems in which the bandwidth of the modulated signal is comparable to the the centre frequency as occurs, for instance, in ultra-wideband technology.
- The assumption made in this work, for which the node impedances in the FET amplifier are considered flat over the narrow bandwidths of communications signals around the fundamental and second-harmonic frequencies, has been successfully applied in [86] for the Volterra-based deduction of a reduced-order behavioural model for wideband RF amplifiers. This assumption has led to a significant reduction in the number of the coefficients involved in the behavioural model. This simplification has been achieved by considering the physical characteristics of the nonlinear system, its equivalent circuit model and the kind of signals with which it is excited; and produces a specific out-of-diagonal structure for the coefficients matrix. This fact has opened a new research line aimed at the study of the implications that the different behavioural models' structures present regarding their accuracy, their effectiveness in handling memory effects, or the suitability of their associated kernels identification procedures. In addition to this, some research is being currently done for the application of the proposed behavioural model to digital predistortion.
- There are various avenues to be explored in relation to the incorporation of memory effects modelling capabilities in large-signal circuit models. More detailed equivalent circuit models could be considered with the help of CAD software and establish a comparison between intermodulation distortion predictions for the given dispersive models (accounting for thermal effects, impact ionization and charge trapping, among other dispersive phenomena) and measurements, in order to asses the suitability of the models. It would also be useful to take advantage of the deduced knowledge about the dispersive networks so as to devise efficient linearisers.
- Another interesting research field could consist in the study of the nonlinear distortion in power amplifiers based on different types of active devices, with the subsequent search for appropriate device models. Some recent technologies, such as LDMOS transistors, and materials, like GaN, could be highlighted due to their widespread application in base stations for mobile communications.

6. CONCLUSIONS AND SUGGESTIONS FOR FUTURE WORK

LIST OF PUBLICATIONS

The scientific publications and conference communications related with the present Thesis are list below.

International Journals

- M. J. Madero-Ayora, J. Reina-Tosina, and C. Crespo-Cadenas, "An Impedance-Based Model for the Evaluation of IM3 in Nonlinear Amplifiers Showing Memory Effects," *Microwave and Optical Technology Letters*, Vol. 50, No. 3, pp. 568–573, Mar. 2008.
- C. Crespo-Cadenas, J. Reina-Tosina, and M. J. Madero-Ayora, "IM3 and IM5 Phase Characterization and Analysis Based on a Simplified Newton Approach," *IEEE Transactions on Microwave Theory and Techniques*, Vol. 54, No. 1, pp. 321–328, Jan. 2006.
- C. Crespo-Cadenas, J. Reina-Tosina, and M. J. Madero-Ayora, "Evaluation of ACPR in Mixers Based on a Parametric Harmonic-Balance Approach," *IEEE Transactions on Microwave Theory and Techniques*, Vol. 54, No. 1, pp. 445–450, Jan. 2006.
- M. J. Madero-Ayora, J. Reina-Tosina, R. Freire-Pérez, and C. Crespo-Cadenas, "Circuit-Level Simulation of W-CDMA Communications Systems Applied to the Analysis of Nonlinear Distortion," *Microwave and Optical Technology Letters*, Vol. 43, No. 4, pp. 310–314, Nov. 2004.

International Conferences

- J. Reina-Tosina, M. J. Madero-Ayora, and C. Crespo-Cadenas, "An Impedance-Based Model for the Evaluation of IM3 in Commercial Amplifiers with Memory," in *2006 IEEE Wireless and Microwave Technology Conference Proceedings (Florida, USA)*, Dec. 2006.
- M. J. Madero-Ayora, J. Reina-Tosina, and C. Crespo-Cadenas, "Phase Characterization of Intermodulation Products Including Electrothermal Memory Effects," in *2006 International Workshop on Integrated Nonlinear Microwave and Millimeter-wave Circuits Proceedings (Aveiro, Portugal)*, p. 56-59, Jan. 2006.
- M. J. Madero-Ayora, J. Reina-Tosina, and C. Crespo-Cadenas, "Simplified Method to Evaluate Weakly Nonlinear Communication Circuits," in *Proceedings of the 35th European Microwave Conference (Paris, France)*, p. 119-122, Oct. 2005.
- C. Crespo-Cadenas, J. Reina-Tosina, and M. J. Madero-Ayora, "Phase Characterization of Two-tone Intermodulation Distortion," in *IEEE MTT-S International Microwave Symposium Digest (Long Beach, USA)*, p. 1505-1508, Jun. 2005.
- C. Crespo-Cadenas, J. Reina-Tosina, and M. J. Madero, "New Envelope Currents Method to Evaluate Distortion of Communication Signals in Mixers," in *Proceedings of the 34th European Microwave Conference (Amsterdam, The Netherlands)*, pp. 852-856, Oct. 2004.
- J. Reina, M. J. Madero, R. Freire, and C. Crespo, "Simulation of Nonlinear Distortion in W-CDMA Communications Circuits," in *Proceedings of SPIE. International Symposium on Microwave and Optical Technology 2003 (Ostrava, Czech Republic)*, p. 47-50, Aug. 2003.

Other publications of the author not directly related to this work are:

- C. Crespo-Cadenas, J. Reina-Tosina, and M. J. Madero-Ayora, "Amplifiers Non-linear Modelling with RF Pulses," scheduled for publication in *IEEE Transactions on Microwave Theory and Techniques*, Vol. 56, No. 11, Nov. 2008.
- C. Crespo-Cadenas, J. Reina-Tosina, and M. J. Madero-Ayora, "Volterra Behavioral Model for Wideband RF Amplifiers," *IEEE Transactions on Microwave Theory and Techniques*, Vol. 55, No. 3, pp. 449-457, Mar. 2007.

EXPRESSIONS FOR THE NONLINEAR ENVELOPE CURRENTS IN THE SIMPLIFIED NEWTON METHOD

The Simplified Newton method applied to RF modulated excitation signals was presented in Section 3.6. The procedure to obtain the complex envelopes of the incremental node voltages for a general circuit consists in solving the following system of linear equations:

$$\left[\mathbf{Y}(h\omega_c) - j\mathbf{Y}'(h\omega_c) \frac{d}{dt} \right] \tilde{\mathbf{v}}_n(h, t) = \tilde{\mathbf{i}}_n(h, t), \quad (\text{B.1})$$

for the n -th iteration and the h -th harmonic, where $\mathbf{Y}(\omega)$ is the node admittance matrix of the extended linear subcircuit. This system of equations must be solved for $n = 1, \dots, N$ and $h = 0, \dots, H$. The current sources $\tilde{\mathbf{i}}_n(h, t)$ applied to the time-invariant linear circuit in (B.1) for the example of the equivalent circuit model for a FET amplifier shown in Figure 2.11 of Section 2.4.4 can be obtained as follows:

1. For the first iteration ($n = 1$), the excitation envelope current is the original envelope current source.
2. The obtention of the nonlinear current source for the second iteration ($n = 2$) requires considering contributions originated by the drain-to-source nonlinear current (I_{ds}) and the nonlinear capacitances C_{gs} and C_{gd} , being the first one the main source of nonlinear distortion [74], [73]. If we take into account (3.70), the contribution of the drain-to-source nonlinear current is given by

$$\tilde{i}_2(h, t) = \tilde{i}_{2I}(h, t) + \tilde{i}_{2II}(h, t) + \tilde{i}_{2III}(h, t), \quad (\text{B.2})$$

where

$$\tilde{i}_{2I}(h, t) = - \sum_{r=\lceil \frac{h}{2} + 1 \rceil}^{\infty} \frac{1}{2^{2r-h-1}} g_{2r-h,0} \binom{2r-h}{r} |\tilde{v}_1(t)|^{2(r-h)} \tilde{v}_1^h(t), \quad (\text{B.3})$$

B. EXPRESSIONS FOR THE NONLINEAR ENVELOPE CURRENTS IN THE SN METHOD

$$\tilde{i}_{2II}(h, t) = - \sum_{r=\lceil \frac{h}{2} + 1 \rceil}^{\infty} \frac{1}{2^{2r-h-1}} g_{0,2r-h} \binom{2r-h}{r} |\tilde{u}_1(t)|^{2(r-h)} \tilde{u}_1^h(t), \quad (\text{B.4})$$

and

$$\tilde{i}_{2III}(h, t) = - \sum_{k,l=1}^{\infty} \frac{1}{2^{k+l-1}} g_{k,l} \cdot \left[\sum_{r=0}^k \binom{k}{r} \binom{l}{\frac{l+h+k}{2}-r} |\tilde{v}_1(t)|^{2(k-r)} \tilde{v}_1^{2r-k}(t) |\tilde{u}_1(t)|^{l-h-k+2r} \tilde{u}_1^{h+k-2r}(t) \right]. \quad (\text{B.5})$$

For equation (B.5), the even harmonics are obtained when $k + l$ is even and the odd harmonics are obtained when $k + l$ is an odd number.

On the other hand, the contribution of the nonlinear capacitances is given by the following expression:

$$\tilde{i}_2(h, t) = -j\hbar\omega \sum_{r=\lceil \frac{h}{2} + 1 \rceil}^{\infty} \frac{1}{2^{2r-h-1}} \frac{1}{2r-h} c_{2r-h-1} \binom{2r-h}{r} |\tilde{v}_1(t)|^{2(r-h)} \tilde{v}_1^h(t). \quad (\text{B.6})$$

It should be clarified that the case $h = 0$ is a special one, since the given expressions account for $2\tilde{i}_2(0, t)$ as long as definition (3.3) for the signals in terms of their complex envelopes is considered. If we use equations (B.2) -(B.6), closed-form expressions for the second-order nonlinear envelope currents can be obtained.

3. For the n -th iteration in the equivalent circuit model for a FET amplifier, the contribution of the drain-to-source nonlinear current is given by $i_n(t) = - \left[i_{NL}[v_{n-2}(t) + v_{n-1}(t), u_{n-2}(t) + u_{n-1}(t)] - i_{NL}[v_{n-2}(t), u_{n-2}(t)] \right]$. Considering that the incremental voltages $v_{n-1}(t)$ and $u_{n-1}(t)$ are small compared to the linear terms $v_{n-2}(t)$ and $u_{n-2}(t)$, the exciting current can be approximated by its first-order Taylor expansion

$$i_{NL}[v_{n-2}(t) + v_{n-1}(t), u_{n-2}(t) + u_{n-1}(t)] \approx i_{NL}[v_{n-2}(t), u_{n-2}(t)] + \frac{\partial i_{NL}[v(t), u(t)]}{\partial v(t)} \Big|_{v_{n-2}(t), u_{n-2}(t)} v_{n-1}(t) + \frac{\partial i_{NL}[v(t), u(t)]}{\partial u(t)} \Big|_{v_{n-2}(t), u_{n-2}(t)} u_{n-1}(t). \quad (\text{B.7})$$

From (2.41) the derivatives can be obtained

$$\frac{\partial i_{NL}[v(t), u(t)]}{\partial v(t)} \Big|_{v_{n-2}(t), u_{n-2}(t)} v_{n-1}(t) = \sum_{k=1}^{\infty} \left[(k+1)g_{k+1,0}v_{n-2}^k(t) + \sum_{l=1}^{\infty} kg_{kl}v_{n-2}^{k-1}(t)u_{n-2}^l(t) \right] v_{n-1}(t), \quad (\text{B.8})$$

$$\left. \frac{\partial i_{NL}[v(t), u(t)]}{\partial u(t)} \right|_{v_{n-2}(t), u_{n-2}(t)} u_{n-1}(t) = \sum_{l=1}^{\infty} \left[(l+1)g_{0,l+1}u_{n-2}^l(t) + \sum_{k=1}^{\infty} l g_{kl} v_{n-2}^k(t) u_{n-2}^{l-1}(t) \right] u_{n-1}(t). \quad (\text{B.9})$$

Therefore, the exciting nonlinear current can be expressed as

$$i_n(t) = - \left[\sum_{k=1}^{\infty} (k+1)g_{k+1,0}v_{n-2}^k(t)v_{n-1}(t) + \sum_{l=1}^{\infty} (l+1)g_{0,l+1}u_{n-2}^l(t)u_{n-1}(t) + \sum_{k=1}^{\infty} \sum_{l=1}^{\infty} g_{kl} [k v_{n-2}^{k-1}(t)v_{n-1}(t)u_{n-2}^l(t) + l v_{n-2}^k(t)u_{n-2}^{l-1}(t)u_{n-1}(t)] \right], \quad (\text{B.10})$$

where we will treat each term separately in order to find the envelope currents more conveniently

$$\begin{aligned} i_{nI}(t) &= - \sum_{k=1}^{\infty} (k+1)g_{k+1,0}v_{n-2}^k(t)v_{n-1}(t), \\ i_{nII}(t) &= - \sum_{l=1}^{\infty} (l+1)g_{0,l+1}u_{n-2}^l(t)u_{n-1}(t), \\ i_{nIII}(t) &= - \sum_{k=1}^{\infty} \sum_{l=1}^{\infty} g_{kl} [k v_{n-2}^{k-1}(t)v_{n-1}(t)u_{n-2}^l(t) + l v_{n-2}^k(t)u_{n-2}^{l-1}(t)u_{n-1}(t)]. \end{aligned} \quad (\text{B.11})$$

The contribution of the drain-to-source nonlinear current in terms of the current envelopes is given by

$$\tilde{i}_n(h, t) = \tilde{i}_{nI}(h, t) + \tilde{i}_{nII}(h, t) + \tilde{i}_{nIII}(h, t), \quad (\text{B.12})$$

where

$$\begin{aligned} \tilde{i}_{nI}(h, t) &= - \sum_{r=\lceil \frac{h}{2} \rceil}^{\infty} \frac{2r-h+2}{2^{2r-h-1}} g_{2r-h+2,0} |\tilde{v}_{n-2}(t)|^{2(r-h)} \tilde{v}_{n-2}^{2(h-1)}(t) \cdot \\ &\left[\binom{2r-h+1}{r} |\tilde{v}_{n-2}(t)|^2 \tilde{v}_{n-1}(t) + \binom{2r-h+1}{r+1} \tilde{v}_{n-2}^4(t) \tilde{v}_{n-1}^*(t) \right], \end{aligned} \quad (\text{B.13})$$

$$\begin{aligned} \tilde{i}_{nII}(h, t) &= - \sum_{r=\lceil \frac{h}{2} \rceil}^{\infty} \frac{2r-h+2}{2^{2r-h-1}} g_{0,2r-h+2} |\tilde{u}_{n-2}(t)|^{2(r-h)} \tilde{u}_{n-2}^{2(h-1)}(t) \cdot \\ &\left[\binom{2r-h+1}{r} |\tilde{u}_{n-2}(t)|^2 \tilde{u}_{n-1}(t) + \binom{2r-h+1}{r+1} \tilde{u}_{n-2}^4(t) \tilde{u}_{n-1}^*(t) \right], \end{aligned} \quad (\text{B.14})$$

B. EXPRESSIONS FOR THE NONLINEAR ENVELOPE CURRENTS IN THE SN METHOD

$$\begin{aligned}
\tilde{i}_{nIII}(h, t) = & - \sum_{k,l=1}^{\infty} \frac{1}{2^{k+l}} g_{k,l} \cdot \left\{ \sum_{r=0}^k 2(k-r) \binom{k}{r} |\tilde{v}_{n-2}|^{2(k-r)} \tilde{v}_{n-2}^{2r-k} |\tilde{u}_{n-2}|^{l+h+k-2r-1} \cdot \right. \\
& \cdot \tilde{u}_{n-2}^{h+k-2r-1} \left[\binom{l}{\frac{l+h+k-1}{2}-r} \tilde{v}_{n-1} + \binom{l}{\frac{l+h+k-1}{2}-r+1} \tilde{v}_{n-1}^* |\tilde{u}_{n-2}(t)|^2 \tilde{u}_{n-2}^2(t) \right] + \\
& + \sum_{r=0}^l 2(l-r) \binom{l}{r} |\tilde{v}_{n-2}|^{l+h+k-2r-1} \tilde{v}_{n-2}^{h+k-2r-1} |\tilde{u}_{n-2}|^{2(k-r)} \tilde{u}_{n-2}^{2r-k} \cdot \\
& \cdot \left. \left[\binom{k}{\frac{l+h+k-1}{2}-r} \tilde{u}_{n-1} + \binom{k}{\frac{l+h+k-1}{2}-r+1} \tilde{u}_{n-1}^* |\tilde{v}_{n-2}(t)|^2 \tilde{v}_{n-2}^2(t) \right] \right\}. \quad (\text{B.15})
\end{aligned}$$

And finally, the contribution of the nonlinear capacitances to the envelope currents is

$$\begin{aligned}
\tilde{i}_n(h, t) = & -j\omega \sum_{r=\lceil \frac{h-1}{2} \rceil}^{\infty} \frac{2r-h+3}{2^{2r-h+3}} c_{2r-h+3} \binom{2r-h+2}{r+1} |\tilde{v}_{n-2}(t)|^{2(r-h+1)} \tilde{v}_{n-2}^{h-1}(t) \cdot \\
& \cdot \left[\frac{h-1}{r-h+2} |\tilde{v}_{n-2}(t)|^2 \tilde{v}_{n-1}(t) + \frac{h+1}{r+2} \tilde{v}_{n-2}^2(t) \tilde{v}_{n-1}^*(t) \right] + \\
& + \omega^2 \sum_{r=\lceil \frac{h}{2} \rceil}^{\infty} \frac{1}{2^{2r-h+3}} c_{2r-h+2} |\tilde{v}_{n-2}(t)|^{2(r-h+1)} \tilde{v}_{n-2}^{h-1}(t) \cdot \\
& \cdot \left\{ |\tilde{v}_{n-2}(t)|^2 \tilde{v}_{n-1}(t) \binom{2r-h+1}{r-1} \left[1 - \frac{(r-h+2)(r-h+1)}{(r+1)(r)} \right] \right. \\
& \quad \left. - \tilde{v}_{n-1}^*(t) \binom{2r-h+1}{r} \left[1 - \frac{(r-h+1)(r-h)}{(r+2)(r+1)} \right] \right\}. \quad (\text{B.16})
\end{aligned}$$

INCREMENTAL ENVELOPE VOLTAGES IN THE SIMPLIFIED NEWTON ANALYSIS OF TWO-TONE INTERMODULATION PRODUCTS

The Simplified Newton method applied to the analysis of two-tone intermodulation products was presented in Section 5.2. It was stated that, in quasi-periodic steady-state, the SN method has a frequency-domain equivalent

$$\mathbf{Y}(hf_c + mf_m) \tilde{\mathbf{V}}_n(h, m) = \tilde{\mathbf{I}}_n(h, m) \quad (\text{C.1})$$

for each iteration n and harmonic h , being the admittance matrix of the augmented linear circuit written as

$$\mathbf{Y}(f) = \begin{bmatrix} \bar{Y}_s(f) & -j2\pi f C_{gd} \\ Y_{md}(f) & \bar{Y}_L(f) \end{bmatrix}, \quad (\text{C.2})$$

and

$$\begin{aligned} \tilde{\mathbf{V}}_n(h, m) &= \begin{bmatrix} \tilde{v}_g(h, m) \\ \tilde{v}_d(h, m) \end{bmatrix}, \\ \tilde{\mathbf{I}}_n(h, m) &= \begin{bmatrix} Y_s(hf_c + mf_m) \tilde{v}_s(h, m) \\ -\mathcal{F}\{i_{ds}(t)\}(h, m) \end{bmatrix}. \end{aligned} \quad (\text{C.3})$$

The first step consists in calculating the quiescent point of the circuit and determining all the Taylor-series expansion coefficients g_{k0} and g_{0l} for $k, l \leq 5$ and g_{kl} for $k + l \leq 3$. Then, all dc voltage sources are short-circuited and all dc current sources are open-circuited and the augmented linear circuit characterised by the admittance matrix of (C.2) is solved.

C.1 First-order iteration: linear iteration

For $n = 1$ there are terms only at frequencies for $h = 1$ and $m = \pm 1$. In that case,

$$\begin{bmatrix} \tilde{v}_{g1}(1, \pm 1) \\ \tilde{v}_{d1}(1, \pm 1) \end{bmatrix} = \mathbf{Y}^{-1}(f_c \pm f_m) \begin{bmatrix} Y_s(f_c \pm f_m)A \\ 0 \end{bmatrix}. \quad (\text{C.4})$$

Recall that, with the narrow-band assumption, the linear transfer functions or equivalently the NLTFs of order $n = 1$ are

$$\begin{aligned} H_{g1}(f_c \pm f_m) &\approx H_{g1}(f_c) = \mathbf{Y}_{11}^{-1}(f_c)Y_s(f_c) = \frac{\bar{Y}_L(f_c)Y_s(f_c)}{\bar{Y}_L(f_c)\bar{Y}_s(f_c) + j2\pi f_c C_{gd}Y_{md}(f_c)}, \\ H_1(f_c \pm f_m) &\approx H_1(f_c) = \mathbf{Y}_{21}^{-1}(f_c)Y_s(f_c) = \frac{-Y_{md}(f_c)Y_s(f_c)}{\bar{Y}_L(f_c)\bar{Y}_s(f_c) + j2\pi f_c C_{gd}Y_{md}(f_c)}. \end{aligned} \quad (\text{C.5})$$

Let define $H_{g1} = H_{g1}(f_c)$ and $H_1 = H_1(f_c)$. Then

$$\begin{aligned} \tilde{v}_{g1}(1, \pm 1) &= H_{g1}A, \\ \tilde{v}_{d1}(1, \pm 1) &= H_1A. \end{aligned} \quad (\text{C.6})$$

C.2 Second-order iteration

From the second iteration on, the original driving sources are not considered and the nonlinear currents sources are applied instead. In the second iteration, the incremental voltage is obtained evaluating the nonlinear current (5.2) and then using the driving source $i_2(t) = -i_{NL}[v_{g1}(t), v_{d1}(t)]$ expressed as

$$i_2(t) = \frac{1}{2} \sum_{h,m=-\infty}^{\infty} \tilde{i}_2(h, m) e^{j2\pi(hf_c + mf_m)t}. \quad (\text{C.7})$$

Separating (5.2) in the same three terms than those considered in (B.2)

$$\begin{aligned} i_{NL_I}[v_{g1}(t)] &= \sum_{k=2}^{\infty} g_{k0} v_{g1}^k(t), \\ i_{NL_{II}}[v_{d1}(t)] &= \sum_{l=2}^{\infty} g_{0l} v_{d1}^l(t), \\ i_{NL_{III}}[v_{g1}(t), v_{d1}(t)] &= \sum_{k,l=1}^{\infty} g_{kl} v_{g1}^k(t) v_{d1}^l(t). \end{aligned} \quad (\text{C.8})$$

C. INCREMENTAL ENVELOPE VOLTAGES IN THE SN ANALYSIS OF TWO-TONE IM PRODUCTS

and recalling that the sums will be truncated for $g_{k0} = 0$, $g_{0l} = 0$ for $k, l > 5$ and $g_{kl} = 0$ for $k + l > 3$, the following expressions for the nonlinear envelope currents can be obtained

$$\tilde{i}_{2I}(h, m) = - \sum_{r=\lceil \frac{h}{2} + 1 \rceil}^{\infty} \frac{1}{2^{2r-h-1}} \binom{2r-h}{r} \binom{2r-h}{r + \frac{m-h}{2}} g_{2r-h,0} |H_{g1}|^{2(r-h)} H_{g1}^h A^{2r-h} \quad (C.9)$$

$$\tilde{i}_{2II}(h, m) = - \sum_{r=\lceil \frac{h}{2} + 1 \rceil}^{\infty} \frac{1}{2^{2r-h-1}} \binom{2r-h}{r} \binom{2r-h}{r + \frac{m-h}{2}} g_{0,2r-h} |H_1|^{2(r-h)} H_1^h A^{2r-h} \quad (C.10)$$

and a similar expression for $\tilde{i}_{2III}(h, m)$.

Using these results it is possible to obtain the components of $i_2(t)$ for the different harmonics:

- For dc zone:

$$\begin{aligned} \tilde{i}_2(0, 0) &= - \left[2\gamma_{20} A^2 + \frac{9}{2} \gamma_{40} A^4 \right], \\ \tilde{i}_2(0, \pm 2) &= - \left[\gamma_{20} A^2 + 3\gamma_{40} A^4 \right], \\ \tilde{i}_2(0, \pm 4) &= - \frac{3}{4} \gamma_{40} A^4, \end{aligned} \quad (C.10)$$

where the following definitions have been used

$$\gamma_{20} = g_{20} |H_{g1}|^2 + g_{02} |H_1|^2 + \frac{1}{2} g_{11} (H_{g1} H_1^* + H_{g1}^* H_1), \quad (C.11)$$

$$\gamma_{40} = g_{40} |H_{g1}|^4 + g_{04} |H_1|^4. \quad (C.12)$$

- For the fundamental frequency zone, $h = 1$:

$$\begin{aligned} \tilde{i}_2(1, \pm 1) &= - \left[\frac{9}{4} \gamma_{31} A^3 + \frac{25}{4} \gamma_{51} A^5 \right], \\ \tilde{i}_2(1, \pm 3) &= - \left[\frac{3}{4} \gamma_{31} A^3 + \frac{25}{8} \gamma_{51} A^5 \right], \\ \tilde{i}_2(1, \pm 5) &= - \frac{5}{8} \gamma_{51} A^5, \end{aligned} \quad (C.12)$$

where the following definitions have been used

$$\begin{aligned} \gamma_{31} &= g_{30} |H_{g1}|^2 H_{g1} + g_{03} |H_1|^2 H_1 + \frac{2}{3} [g_{21} (2 |H_{g1}|^2 H_1 + H_{g1}^2 H_1^*) + \\ &\quad g_{12} (2 |H_1|^2 H_{g1} + H_1^2 H_{g1}^*)], \\ \gamma_{51} &= g_{50} |H_{g1}|^4 H_{g1} + g_{05} |H_1|^4 H_1. \end{aligned} \quad (C.13)$$

C. INCREMENTAL ENVELOPE VOLTAGES IN THE SN ANALYSIS OF TWO-TONE IM PRODUCTS

- For the second harmonic frequency zone, $h = 2$:

$$\begin{aligned}\tilde{i}_2(2, 0) &= -[\gamma_{22}A^2 + 3\gamma_{42}A^4], \\ \tilde{i}_2(2, \pm 2) &= -\left[\frac{1}{2}\gamma_{22}A^2 + 2\gamma_{42}A^4\right], \\ \tilde{i}_2(2, \pm 4) &= -\frac{1}{2}\gamma_{42}A^4,\end{aligned}\tag{C.14}$$

where the following definitions have been used

$$\gamma_{22} = g_{20}H_{g1}^2 + g_{02}H_1^2 + g_{11}H_{g1}H_1,\tag{C.15}$$

$$\gamma_{42} = g_{40}|H_{g1}|^2H_{g1}^2 + g_{04}|H_1|^2H_1^2.\tag{C.16}$$

- For the third harmonic frequency zone, $h = 3$:

$$\begin{aligned}\tilde{i}_2(3, \pm 1) &= -\left[\frac{3}{4}\gamma_{33}A^3 + \frac{25}{8}\gamma_{53}A^5\right], \\ \tilde{i}_2(3, \pm 3) &= -\left[\frac{1}{4}\gamma_{33}A^3 + \frac{25}{16}\gamma_{53}A^5\right], \\ \tilde{i}_2(3, \pm 5) &= -\frac{5}{16}\gamma_{53}A^5,\end{aligned}\tag{C.16}$$

where the following definitions have been used

$$\gamma_{33} = g_{30}H_{g1}^3 + g_{03}H_1^3 + 2(g_{21}H_{g1}^2H_1 + g_{12}H_1^2H_{g1}),\tag{C.17}$$

$$\gamma_{53} = g_{50}|H_{g1}|^2H_{g1}^3 + g_{05}|H_1|^2H_1^3.\tag{C.18}$$

For the second-order iteration (5.13) gives

$$\begin{bmatrix} \tilde{v}_{g2}(h, m) \\ \tilde{v}_{d2}(h, m) \end{bmatrix} = \mathbf{Y}^{-1}(hf_c + mf_m) \begin{bmatrix} 0 \\ -\tilde{i}_2(h, m) \end{bmatrix} \approx \mathbf{Y}^{-1}(hf_c) \begin{bmatrix} 0 \\ \tilde{i}_2(h, m) \end{bmatrix}.\tag{C.18}$$

For $h > 0$, we can write the second-order voltage contributions in the following form:

$$\begin{aligned}\tilde{v}_{g2}(h, m) &= Z_{gh}\tilde{i}_2(h, m), \\ \tilde{v}_{d2}(h, m) &= Z_h\tilde{i}_2(h, m),\end{aligned}\tag{C.19}$$

where

$$\begin{aligned}Z_g(hf_c + mf_m) &\approx Z_g(hf_c) = \mathbf{Y}_{12}^{-1}(hf_c) = \frac{j2\pi hf_c C_{gd}}{\bar{Y}_L(hf_c)\bar{Y}_s(hf_c) + j2\pi hf_c C_{gd}\bar{Y}_{md}(hf_c)} = Z_{gh} \\ Z(hf_c + mf_m) &\approx Z(hf_c) = \mathbf{Y}_{22}^{-1}(hf_c) = \frac{\bar{Y}_s(hf_c)}{\bar{Y}_L(hf_c)\bar{Y}_s(hf_c) + j2\pi hf_c C_{gd}\bar{Y}_{md}(hf_c)} = Z_h.\end{aligned}\tag{C.20}$$

C. INCREMENTAL ENVELOPE VOLTAGES IN THE SN ANALYSIS OF TWO-TONE IM PRODUCTS

However, for dc zone the narrowband assumption does not apply since, for $h = 0$, $mf_m > hf_c = 0$. However, we can consider $Z_g(mf_m) = 0$ and $Z(mf_m) = \bar{Z}_L(mf_m)$, which can be justified by the following reasoning. At baseband frequencies, the capacitances in the equivalent circuit model can be considered to be open circuits and the terms involved in (5.8) take the next form:

$$\bar{Y}_L(f) = Y_L(f) + g_{01}, \quad (\text{C.21})$$

$$Y_{md}(f) = g_{10}, \quad (\text{C.22})$$

$$\bar{Y}_s(f) = Y_s(f), \quad (\text{C.23})$$

resulting in the following inverse for the admittance matrix:

$$\mathbf{Y}^{-1}(f) = \frac{1}{\bar{Y}_s(f)\bar{Y}_L(f)} \begin{bmatrix} \bar{Y}_L(f) & 0 \\ -Y_{md}(f) & \bar{Y}_s(f) \end{bmatrix} = \begin{bmatrix} \frac{\bar{Z}_s(f)}{\bar{Y}_s(f)\bar{Y}_L(f)} & 0 \\ -\frac{Y_{md}(f)}{\bar{Y}_s(f)\bar{Y}_L(f)} & \bar{Z}_L(f) \end{bmatrix}. \quad (\text{C.22})$$

Recalling the definitions $Z_g(hf_c + mf_m) = \mathbf{Y}_{12}^{-1}(hf_c + mf_m)$ and $Z(hf_c + mf_m) = \mathbf{Y}_{22}^{-1}(hf_c + mf_m)$, and considering $h = 0$, the aforementioned expressions $Z_g(mf_m) = 0$ and $Z(mf_m) = \bar{Z}_L(mf_m)$ can be obtained. Then, the following values for the second-order incremental envelope voltages are obtained for the different harmonics:

- For the dc zone with $h = 0$:

$$\begin{aligned} \tilde{v}_{g2}(0, m) &= 0, \\ \tilde{v}_{d2}(0, m) &= \bar{Z}_L(mf_m)\tilde{i}_2(0, m), \end{aligned} \quad (\text{C.23})$$

with m even. If it is assumed that $\bar{Z}_L(0) = 0$,

$$\begin{aligned} \tilde{v}_{d2}(0, 0) &= 0, \\ \tilde{v}_{d2}(0, \pm 2) &= -[\gamma_{20}\bar{Z}_L(\pm\Delta f)A^2 + 3\gamma_{40}\bar{Z}_L(\pm\Delta f)A^4], \\ \tilde{v}_{d2}(0, \pm 4) &= -\frac{3}{4}\gamma_{40}\bar{Z}_L(\pm 2\Delta f)A^4. \end{aligned} \quad (\text{C.24})$$

- For the fundamental frequency zone, $h = 1$:

$$\begin{aligned} \tilde{v}_{g2}(1, \pm 1) &= -\left[\frac{9}{4}\gamma_{31}Z_{g1}A^3 + \frac{25}{4}\gamma_{51}Z_{g1}A^5\right], \\ \tilde{v}_{g2}(1, \pm 3) &= -\left[\frac{3}{4}\gamma_{31}Z_{g1}A^3 + \frac{25}{8}\gamma_{51}Z_{g1}A^5\right], \\ \tilde{v}_{g2}(1, \pm 5) &= -\frac{5}{8}\gamma_{51}Z_{g1}A^5, \end{aligned} \quad (\text{C.25})$$

C. INCREMENTAL ENVELOPE VOLTAGES IN THE SN ANALYSIS OF TWO-TONE IM PRODUCTS

and

$$\begin{aligned}\tilde{v}_{d2}(1, \pm 1) &= - \left[\frac{9}{4} \gamma_{31} Z_1 A^3 + \frac{25}{4} \gamma_{51} Z_1 A^5 \right], \\ \tilde{v}_{d2}(1, \pm 3) &= - \left[\frac{3}{4} \gamma_{31} Z_1 A^3 + \frac{25}{8} \gamma_{51} Z_1 A^5 \right], \\ \tilde{v}_{d2}(1, \pm 5) &= - \frac{5}{8} \gamma_{51} Z_1 A^5.\end{aligned}\tag{C.26}$$

- For the second harmonic frequency zone, $h = 2$:

$$\begin{aligned}\tilde{v}_{g2}(2, 0) &= - \left[\gamma_{22} Z_{g2} A^2 + 3 \gamma_{42} Z_{g2} A^4 \right], \\ \tilde{v}_{g2}(2, \pm 2) &= - \left[\frac{1}{2} \gamma_{22} Z_{g2} A^2 + 2 \gamma_{42} Z_{g2} A^4 \right], \\ \tilde{v}_{g2}(2, \pm 4) &= - \frac{1}{2} \gamma_{42} Z_{g2} A^4,\end{aligned}\tag{C.27}$$

and

$$\begin{aligned}\tilde{v}_{d2}(2, 0) &= - \left[\gamma_{22} Z_2 A^2 + 3 \gamma_{42} Z_2 A^4 \right], \\ \tilde{v}_{d2}(2, \pm 2) &= - \left[\frac{1}{2} \gamma_{22} Z_2 A^2 + 2 \gamma_{42} Z_2 A^4 \right], \\ \tilde{v}_{d2}(2, \pm 4) &= - \frac{1}{2} \gamma_{42} Z_2 A^4.\end{aligned}\tag{C.28}$$

- For the third harmonic frequency zone, $h = 3$:

$$\begin{aligned}\tilde{v}_{g2}(3, \pm 1) &= - \left[\frac{3}{4} \gamma_{33} Z_{g3} A^3 + \frac{25}{8} \gamma_{53} Z_{g3} A^5 \right], \\ \tilde{v}_{g2}(3, \pm 3) &= - \left[\frac{1}{4} \gamma_{33} Z_{g3} A^3 + \frac{25}{16} \gamma_{53} Z_{g3} A^5 \right], \\ \tilde{v}_{g2}(3, \pm 5) &= - \frac{5}{16} \gamma_{53} Z_{g3} A^5,\end{aligned}\tag{C.29}$$

and

$$\begin{aligned}\tilde{v}_{d2}(3, \pm 1) &= - \left[\frac{3}{4} \gamma_{33} Z_3 A^3 + \frac{25}{8} \gamma_{53} Z_3 A^5 \right], \\ \tilde{v}_{d2}(3, \pm 3) &= - \left[\frac{1}{4} \gamma_{33} Z_3 A^3 + \frac{25}{16} \gamma_{53} Z_3 A^5 \right], \\ \tilde{v}_{d2}(3, \pm 5) &= - \frac{5}{16} \gamma_{53} Z_3 A^5.\end{aligned}\tag{C.30}$$

C.3 Third-order iteration

For the third iteration it is necessary to evaluate the excitation nonlinear current $i_3(t) = -\left[i_{NL}[v_{g1}(t) + v_{g2}(t), v_{d1}(t) + v_{d2}(t)] - i_{NL}[v_{g1}(t), v_{d1}(t)] \right]$. Considering that the incremental voltages $v_{g2}(t)$ and $v_{d2}(t)$ are small compared to the linear terms $v_{g1}(t)$ and $v_{d1}(t)$, the exciting current can be approximated by its first-order Taylor expansion

$$\frac{i_{NL}[v_{g1}(t) + v_{g2}(t), v_{d1}(t) + v_{d2}(t)]}{\partial v_g(t)} \Big|_{v_{g1}(t), v_{d1}(t)} v_{g2}(t) + \frac{\partial i_{NL}[v_g(t), v_d(t)]}{\partial v_d(t)} \Big|_{v_{g1}(t), v_{d1}(t)} v_{d2}(t). \quad (\text{C.31})$$

From (5.2) we can obtain the derivatives

$$\frac{\partial i_{NL}[v_g(t), v_d(t)]}{\partial v_g(t)} \Big|_{v_{g1}(t), v_{d1}(t)} v_{g2}(t) = \sum_{k=1}^{\infty} \left[(k+1)g_{k+1,0}v_{g1}^k(t) + \sum_{l=1}^{\infty} kg_{kl}v_{g1}^{k-1}(t)v_{d1}^l(t) \right] v_{g2}(t), \quad (\text{C.32})$$

$$\frac{\partial i_{NL}[v_g(t), v_d(t)]}{\partial v_d(t)} \Big|_{v_{g1}(t), v_{d1}(t)} v_{d2}(t) = \sum_{l=1}^{\infty} \left[(l+1)g_{0,l+1}v_{d1}^l(t) + \sum_{k=1}^{\infty} lg_{kl}v_{g1}^k(t)v_{d1}^{l-1}(t) \right] v_{d2}(t). \quad (\text{C.33})$$

Considering only the most significant terms, linear in v_{g2} and v_{d2} , respectively

$$\frac{\partial i_{NL}[v_g(t), v_d(t)]}{\partial v_g(t)} \Big|_{v_{g1}(t), v_{d1}(t)} v_{g2}(t) \approx 2g_{20}v_{g1}(t)v_{g2}(t) + g_{11}v_{d1}(t)v_{g2}(t), \quad (\text{C.34})$$

$$\frac{\partial i_{NL}[v_g(t), v_d(t)]}{\partial v_d(t)} \Big|_{v_{g1}(t), v_{d1}(t)} v_{d2}(t) \approx 2g_{02}v_{d1}(t)v_{d2}(t) + g_{11}v_{g1}(t)v_{d2}(t), \quad (\text{C.35})$$

the exciting current can be expressed as

$$i_3(t) = -\left[2g_{20}v_{g1}(t)v_{g2}(t) + g_{11}[v_{d1}(t)v_{g2}(t) + v_{g1}(t)v_{d2}(t)] + 2g_{02}v_{d1}(t)v_{d2}(t) \right], \quad (\text{C.36})$$

where we will treat each term separately in order to find the components for the IM product frequencies in an easier way

$$\begin{aligned} i_{3_I}(t) &= -2g_{20}v_{g1}v_{g2}, \\ i_{3_{II}}(t) &= -g_{11}(v_{d1}v_{g2} + v_{g1}v_{d2}), \\ i_{3_{III}}(t) &= -2g_{02}v_{d1}v_{d2}. \end{aligned} \quad (\text{C.37})$$

C. INCREMENTAL ENVELOPE VOLTAGES IN THE SN ANALYSIS OF TWO-TONE IM PRODUCTS

- For the first term $i_{3I}(t)$, let us consider the product $v_{g1}(t)v_{g2}(t)$ and use (5.11) to obtain

$$\begin{aligned}
 v_{g1}(t)v_{g2}(t) &= \frac{1}{4} \sum_{h=-\infty}^{\infty} \tilde{v}_{g2}(h, t)\tilde{v}_{g1}(1, t)e^{j2\pi(h+1)f_c t} + \frac{1}{4} \sum_{h=-\infty}^{\infty} \tilde{v}_{g2}(h, t)\tilde{v}_{g1}(-1, t)e^{j2\pi(h-1)f_c t} = \\
 &\frac{1}{4} \sum_{h,m=-\infty}^{\infty} \tilde{v}_{g2}(h, m)\tilde{v}_{g1}(1, \pm 1)e^{j2\pi[(h+1)f_c+(m\pm 1)f_m]t} + \\
 &\frac{1}{4} \sum_{h,m=-\infty}^{\infty} \tilde{v}_{g2}(h, m)\tilde{v}_{g1}(-1, \pm 1)e^{j2\pi[(h-1)f_c+(m\pm 1)f_m]t} .
 \end{aligned} \tag{C.38}$$

The interesting terms are those in the fundamental frequency zone, with $h = 0$ and $h = 2$ for the first and second sum, respectively. Then $i_{3I}(t)$ can be written as:

$$i_{3I}(t) = \frac{1}{2} \sum_{h,m=-\infty}^{\infty} \tilde{i}_{3I}(h, m)e^{j2\pi(hf_c+m f_m)t} = -2g_{20}v_{g1}(t)v_{g2}(t), \tag{C.39}$$

and

$$\begin{aligned}
 \frac{1}{2} \sum_{m=-\infty}^{\infty} \tilde{i}_{3I}(1, m)e^{j2\pi m f_m t} &= -\frac{1}{2}g_{20} [\tilde{v}_{g2}(0, t)\tilde{v}_{g1}(1, t) + \tilde{v}_{g2}(2, t)\tilde{v}_{g1}(-1, t)] = \\
 -\frac{1}{2}g_{20} [\tilde{v}_{g2}(0, m)\tilde{v}_{g1}(1, \pm 1)e^{j2\pi(m\pm 1)f_m t} &+ \tilde{v}_{g2}(2, m)\tilde{v}_{g1}(-1, \pm 1)e^{j2\pi(m\pm 1)f_m t}] ,
 \end{aligned} \tag{C.40}$$

$$\begin{aligned}
 \tilde{i}_{3I}(1, m) &= -g_{20} [\tilde{v}_{g2}(0, m+1)\tilde{v}_{g1}(1, -1) + \tilde{v}_{g2}(0, m-1)\tilde{v}_{g1}(1, 1) + \\
 &\tilde{v}_{g2}(2, m+1)\tilde{v}_{g1}(-1, -1) + \tilde{v}_{g2}(2, m-1)\tilde{v}_{g1}(-1, 1)] .
 \end{aligned} \tag{C.41}$$

Recall that $\tilde{v}_{g2}(0, m) = 0$ for any value of m and $\tilde{v}_{g1}(-1, \pm 1) = H_{g1}^* A$, then (C.41) can be reduced to

$$\tilde{i}_{3I}(1, m) = -g_{20}H_{g1}^* A [\tilde{v}_{g2}(2, m+1) + \tilde{v}_{g2}(2, m-1)] . \tag{C.42}$$

- Distortion at fundamental tones, $m = \pm 1$, can be obtained by substituting $\tilde{v}_{g2}(2, 2)$, $\tilde{v}_{g2}(2, 0)$ for $m = 1$ and $\tilde{v}_{g2}(2, 0)$, $\tilde{v}_{g2}(2, -2)$ for $m = -1$ from (C.27) in (C.42)

$$\tilde{i}_{3I}(1, \pm 1) = \frac{3}{2}\gamma_{22}g_{20}H_{g1}^* Z_{g2}A^3 + 5\gamma_{42}g_{20}H_{g1}^* Z_{g2}A^5 . \tag{C.43}$$

- Third-order IM terms, $m = \pm 3$, can be obtained by substituting $\tilde{v}_{g2}(2, 4)$, $\tilde{v}_{g2}(2, 2)$ for $m = 3$ and $\tilde{v}_{g2}(2, -2)$, $\tilde{v}_{g2}(2, -4)$ for $m = -3$ from (C.27) in (C.42)

$$\tilde{i}_{3I}(1, \pm 3) = \frac{1}{2}\gamma_{22}g_{20}H_{g1}^* Z_{g2}A^3 + \frac{5}{2}\gamma_{42}g_{20}H_{g1}^* Z_{g2}A^5 . \tag{C.44}$$

- Fifth-order IM terms, $m = \pm 5$, can be obtained by substituting $\tilde{v}_{g2}(2, 4)$ for $m = 5$ and $\tilde{v}_{g2}(2, -4)$ for $m = -5$ from (C.27) in (C.42)

$$\tilde{i}_{3I}(1, \pm 5) = \frac{1}{2} \gamma_{42} g_{20} H_{g1}^* Z_{g2} A^5. \quad (\text{C.45})$$

- For the second term $i_{3II}(t)$, let consider the products $v_{d1}(t)v_{g2}(t)$ and $v_{g1}(t)v_{d2}(t)$ and use (5.11) and (5.12) to obtain

$$\begin{aligned} v_{d1}(t)v_{g2}(t) &= \frac{1}{4} \sum_{h=-\infty}^{\infty} \tilde{v}_{g2}(h, t) \tilde{v}_{d1}(1, t) e^{j2\pi(h+1)f_c t} + \frac{1}{4} \sum_{h=-\infty}^{\infty} \tilde{v}_{g2}(h, t) \tilde{v}_{d1}(-1, t) e^{j2\pi(h-1)f_c t} = \\ &\quad \frac{1}{4} \sum_{h,m=-\infty}^{\infty} \tilde{v}_{g2}(h, m) \tilde{v}_{d1}(1, \pm 1) e^{j2\pi[(h+1)f_c + (m\pm 1)f_m]t} + \\ &\quad \frac{1}{4} \sum_{h,m=-\infty}^{\infty} \tilde{v}_{g2}(h, m) \tilde{v}_{d1}(-1, \pm 1) e^{j2\pi[(h-1)f_c + (m\pm 1)f_m]t}, \end{aligned} \quad (\text{C.46})$$

$$\begin{aligned} v_{g1}(t)v_{d2}(t) &= \frac{1}{4} \sum_{h=-\infty}^{\infty} \tilde{v}_{d2}(h, t) \tilde{v}_{g1}(1, t) e^{j2\pi(h+1)f_c t} + \frac{1}{4} \sum_{h=-\infty}^{\infty} \tilde{v}_{d2}(h, t) \tilde{v}_{g1}(-1, t) e^{j2\pi(h-1)f_c t} = \\ &\quad \frac{1}{4} \sum_{h,m=-\infty}^{\infty} \tilde{v}_{d2}(h, m) \tilde{v}_{g1}(1, \pm 1) e^{j2\pi[(h+1)f_c + (m\pm 1)f_m]t} + \\ &\quad \frac{1}{4} \sum_{h,m=-\infty}^{\infty} \tilde{v}_{d2}(h, m) \tilde{v}_{g1}(-1, \pm 1) e^{j2\pi[(h-1)f_c + (m\pm 1)f_m]t}. \end{aligned} \quad (\text{C.47})$$

The interesting terms are those in the fundamental frequency zone, with $h = 0$ and $h = 2$ for the first and second sum, respectively. Then the second term of (C.36) can be written as:

$$i_{3II}(t) = \frac{1}{2} \sum_{h,m=-\infty}^{\infty} i_{3II}(h, m) e^{j2\pi(hf_c + mf_m)t} = -g_{11} [v_{d1}(t)v_{g2}(t) + v_{g1}(t)v_{d2}(t)], \quad (\text{C.48})$$

and

$$\begin{aligned} \frac{1}{2} \sum_{m=-\infty}^{\infty} i_{3II}(1, m) e^{j2\pi mf_m t} &= -\frac{1}{4} g_{11} [\tilde{v}_{g2}(0, t) \tilde{v}_{d1}(1, t) + \tilde{v}_{g2}(2, t) \tilde{v}_{d1}(-1, t) + \\ &\quad \tilde{v}_{d2}(0, t) \tilde{v}_{g1}(1, t) + \tilde{v}_{d2}(2, t) \tilde{v}_{g1}(-1, t)] = \\ &= -\frac{1}{4} g_{11} [\tilde{v}_{g2}(0, m) \tilde{v}_{d1}(1, \pm 1) e^{j2\pi(m\pm 1)f_m t} + \tilde{v}_{g2}(2, m) \tilde{v}_{d1}(-1, \pm 1) e^{j2\pi(m\pm 1)f_m t} + \\ &\quad \tilde{v}_{d2}(0, m) \tilde{v}_{g1}(1, \pm 1) e^{j2\pi(m\pm 1)f_m t} + \tilde{v}_{d2}(2, m) \tilde{v}_{g1}(-1, \pm 1) e^{j2\pi(m\pm 1)f_m t}], \end{aligned} \quad (\text{C.49})$$

C. INCREMENTAL ENVELOPE VOLTAGES IN THE SN ANALYSIS OF TWO-TONE IM PRODUCTS

$$\begin{aligned}
\tilde{i}_{3II}(1, m) = & -\frac{1}{2}g_{11} [\tilde{v}_{g2}(0, m+1)\tilde{v}_{d1}(1, -1) + \tilde{v}_{g2}(0, m-1)\tilde{v}_{d1}(1, 1) + \\
& \tilde{v}_{g2}(2, m+1)\tilde{v}_{d1}(-1, -1) + \tilde{v}_{g2}(2, m-1)\tilde{v}_{d1}(-1, 1) + \\
& \tilde{v}_{d2}(0, m+1)\tilde{v}_{g1}(1, -1) + \tilde{v}_{d2}(0, m-1)\tilde{v}_{g1}(1, 1) + \\
& \tilde{v}_{d2}(2, m+1)\tilde{v}_{g1}(-1, -1) + \tilde{v}_{d2}(2, m-1)\tilde{v}_{g1}(-1, 1)] .
\end{aligned} \tag{C.50}$$

Recall that $v_{g1}(1, \pm 1) = H_{g1}A$, $v_{g1}(-1, \pm 1) = H_{g1}^*A$, $v_{d1}(1, \pm 1) = H_1A$, and $v_{d1}(-1, \pm 1) = H_1^*A$, then (C.50) can be reduced to

$$\begin{aligned}
\tilde{i}_{3II}(1, m) = & -\frac{1}{2}g_{11}A \left\{ H_1[\tilde{v}_{g2}(0, m+1) + \tilde{v}_{g2}(0, m-1)] + \right. \\
& H_1^*[\tilde{v}_{g2}(2, m+1) + \tilde{v}_{g2}(2, m-1)] + H_{g1}[\tilde{v}_{d2}(0, m+1) + \tilde{v}_{d2}(0, m-1)] \\
& \left. H_{g1}^*[\tilde{v}_{d2}(2, m+1) + \tilde{v}_{d2}(2, m-1)] \right\}.
\end{aligned} \tag{C.51}$$

- Distortion at fundamental tones, $m = \pm 1$, can be obtained by substituting $\tilde{v}_{d2}(0, 2)$, $\tilde{v}_{d2}(0, 0) = 0$, $\tilde{v}_{d2}(2, 2)$, and $\tilde{v}_{d2}(2, 0)$ for $m = 1$, and $\tilde{v}_{d2}(0, 0) = 0$, $\tilde{v}_{d2}(0, -2)$, $\tilde{v}_{d2}(2, 0)$, and $\tilde{v}_{d2}(2, -2)$ for $m = -1$ from (C.24), (C.28), (C.23) and (C.27) in (C.51)

$$\begin{aligned}
\tilde{i}_{3II}(1, \pm 1) = & \frac{3}{4}\gamma_{22}g_{11}(H_1^*Z_{g2} + H_{g1}^*Z_2)A^3 + \frac{1}{2}\gamma_{20}g_{11}H_{g1}\bar{Z}_L(\pm\Delta f)A^3 + \\
& \left[\frac{5}{2}\gamma_{42}g_{11}(H_1^*Z_{g2} + H_{g1}^*Z_2) + \frac{3}{2}\gamma_{40}g_{11}H_{g1}\bar{Z}_L(\pm\Delta f) \right] A^5.
\end{aligned} \tag{C.52}$$

- Third-order IM terms, $m = \pm 3$, can be obtained by substituting $\tilde{v}_{d2}(0, 4)$, $\tilde{v}_{d2}(0, 2)$, $\tilde{v}_{d2}(2, 4)$, and $\tilde{v}_{d2}(2, 2)$ for $m = 3$, and $\tilde{v}_{d2}(0, -2)$, $\tilde{v}_{d2}(0, -4)$, $\tilde{v}_{d2}(2, -2)$, and $\tilde{v}_{d2}(2, -4)$ for $m = -3$ from (C.24), (C.28), (C.23) and (C.27) in (C.51)

$$\begin{aligned}
\tilde{i}_{3II}(1, \pm 3) = & \frac{1}{4}\gamma_{22}g_{11}(H_1^*Z_{g2} + H_{g1}^*Z_2)A^3 + \frac{1}{2}\gamma_{20}g_{11}H_{g1}\bar{Z}_L(\pm\Delta f)A^3 + \\
& \left[\frac{5}{4}\gamma_{42}g_{11}(H_1^*Z_{g2} + H_{g1}^*Z_2) + \frac{3}{2}\gamma_{40}g_{11}H_{g1}\bar{Z}_L(\pm\Delta f) + \frac{3}{8}\gamma_{40}g_{11}H_{g1}\bar{Z}_L(\pm 2\Delta f) \right] A^5.
\end{aligned} \tag{C.53}$$

- Fifth-order IM terms, $m = \pm 5$, can be obtained by substituting $\tilde{v}_{d2}(0, 4)$, and $\tilde{v}_{d2}(2, 4)$ for $m = 5$, and $\tilde{v}_{d2}(0, -4)$, and $\tilde{v}_{d2}(2, -4)$ for $m = -5$ from (C.24), (C.28), (C.23) and (C.27) in (C.51)

$$\tilde{i}_{3II}(1, \pm 5) = \frac{1}{4}\gamma_{42}g_{11}(H_1^*Z_{g2} + H_{g1}^*Z_2)A^5 + \frac{3}{8}\gamma_{40}g_{02}H_{g1}\bar{Z}_L(\pm 2\Delta f)A^5. \tag{C.54}$$

C. INCREMENTAL ENVELOPE VOLTAGES IN THE SN ANALYSIS OF TWO-TONE IM PRODUCTS

- For the third term $i_{3III}(t)$, let us consider the product $v_{d1}(t)v_{d2}(t)$ and use (5.12) to obtain

$$\begin{aligned}
 v_{d1}(t)v_{d2}(t) &= \frac{1}{4} \sum_{h=-\infty}^{\infty} \tilde{v}_{d2}(h, t) \tilde{v}_{d1}(1, t) e^{j2\pi(h+1)f_c t} + \frac{1}{4} \sum_{h=-\infty}^{\infty} \tilde{v}_{d2}(h, t) \tilde{v}_{d1}(-1, t) e^{j2\pi(h-1)f_c t} = \\
 &\quad \frac{1}{4} \sum_{h,m=-\infty}^{\infty} \tilde{v}_{d2}(h, m) \tilde{v}_{d1}(1, \pm 1) e^{j2\pi[(h+1)f_c + (m\pm 1)f_m]t} + \\
 &\quad \frac{1}{4} \sum_{h,m=-\infty}^{\infty} \tilde{v}_{d2}(h, m) \tilde{v}_{d1}(-1, \pm 1) e^{j2\pi[(h-1)f_c + (m\pm 1)f_m]t} .
 \end{aligned} \tag{C.55}$$

The interesting terms are those in the fundamental frequency zone, with $h = 0$ and $h = 2$ for the first and second sum, respectively. Then the third term of (C.36) can be written as:

$$i_{3III}(t) = \frac{1}{2} \sum_{h,m=-\infty}^{\infty} i_{3III}(h, m) e^{j2\pi(hf_c + mf_m)t} = -2g_{02}v_{d1}(t)v_{d2}(t), \tag{C.56}$$

and

$$\begin{aligned}
 \frac{1}{2} \sum_{m=-\infty}^{\infty} i_{3III}(1, m) e^{j2\pi mf_m t} &= -\frac{1}{2} g_{02} [\tilde{v}_{d2}(0, t) \tilde{v}_{d1}(1, t) + \tilde{v}_{d2}(2, t) \tilde{v}_{d1}(-1, t)] = \\
 &= -\frac{1}{2} g_{02} [\tilde{v}_{d2}(0, m) \tilde{v}_{d1}(1, \pm 1) e^{j2\pi(m\pm 1)f_m t} + \tilde{v}_{d2}(2, m) \tilde{v}_{d1}(-1, \pm 1) e^{j2\pi(m\pm 1)f_m t}] ,
 \end{aligned} \tag{C.57}$$

$$\begin{aligned}
 \tilde{i}_{3III}(1, m) &= -g_{02} [\tilde{v}_{d2}(0, m+1) \tilde{v}_{d1}(1, -1) + \tilde{v}_{d2}(0, m-1) \tilde{v}_{d1}(1, 1) + \\
 &\quad \tilde{v}_{d2}(2, m+1) \tilde{v}_{d1}(-1, -1) + \tilde{v}_{d2}(2, m-1) \tilde{v}_{d1}(-1, 1)] .
 \end{aligned} \tag{C.58}$$

Recall that $v_{d1}(1, \pm 1) = H_1 A$, and $v_{d1}(-1, \pm 1) = H_1^* A$, then (C.58) can be reduced to

$$\begin{aligned}
 \tilde{i}_{3III}(1, m) &= -g_{20} A [H_1 (\tilde{v}_{d2}(0, m+1) + \tilde{v}_{d2}(0, m-1)) + \\
 &\quad H_1^* (\tilde{v}_{d2}(2, m+1) + \tilde{v}_{d2}(2, m-1))] .
 \end{aligned} \tag{C.59}$$

- Distortion at fundamental tones, $m = \pm 1$, can be obtained by substituting $\tilde{v}_{d2}(0, 2)$, $\tilde{v}_{d2}(0, 0) = 0$, $\tilde{v}_{d2}(2, 2)$, $\tilde{v}_{d2}(2, 0)$ for $m = 1$ and $\tilde{v}_{d2}(0, 0) = 0$, $\tilde{v}_{d2}(0, -2)$, $\tilde{v}_{d2}(2, 0)$, $\tilde{v}_{d2}(2, -2)$ for $m = -1$ from (C.24) and (C.28) in (C.59)

$$\begin{aligned}
 \tilde{i}_{3III}(1, \pm 1) &= \frac{3}{2} \gamma_{22} g_{02} H_1^* Z_2 A^3 + \gamma_{20} g_{02} H_1 \bar{Z}_L(\pm \Delta f) A^3 + \\
 &\quad [5\gamma_{42} g_{02} H_1^* Z_2 + 3\gamma_{40} g_{02} H_1 \bar{Z}_L(\pm \Delta f)] A^5 .
 \end{aligned} \tag{C.60}$$

C. INCREMENTAL ENVELOPE VOLTAGES IN THE SN ANALYSIS OF TWO-TONE IM PRODUCTS

- Third-order IM terms, $m = \pm 3$, can be obtained by substituting $\tilde{v}_{d2}(0, 4), \tilde{v}_{d2}(0, 2), \tilde{v}_{d2}(2, 4), \tilde{v}_{d2}(2, 2)$ for $m = 3$ and $\tilde{v}_{d2}(0, -2), \tilde{v}_{d2}(0, -4), \tilde{v}_{d2}(2, -2), \tilde{v}_{d2}(2, -4)$ for $m = -3$ from (C.24) and (C.28) in (C.59)

$$\tilde{i}_{3III}(1, \pm 3) = \frac{1}{2}\gamma_{22}g_{02}H_1^*Z_2A^3 + \gamma_{20}g_{02}H_1\bar{Z}_L(\pm\Delta f)A^3 + \left[\frac{5}{2}\gamma_{42}g_{02}H_1^*Z_2 + 3\gamma_{40}g_{02}H_1\bar{Z}_L(\pm\Delta f) + \frac{3}{4}\gamma_{40}g_{02}H_1\bar{Z}_L(\pm 2\Delta f) \right] A^5. \quad (\text{C.61})$$

- Fifth-order IM terms, $m = \pm 5$, can be obtained by substituting $\tilde{v}_{d2}(0, 4), \tilde{v}_{d2}(2, 4)$ for $m = 5$ and $\tilde{v}_{d2}(0, -4), \tilde{v}_{d2}(2, -4)$ for $m = -5$ from (C.24) and (C.28) in (C.59)

$$\tilde{i}_{3III}(1, \pm 5) = \frac{1}{2}\gamma_{42}g_{02}H_1^*Z_2A^5 + \frac{3}{4}\gamma_{40}g_{02}H_1\bar{Z}_L(\pm 2\Delta f)A^5. \quad (\text{C.62})$$

Once the components of $\tilde{i}_3(1, m)$ have been obtained for the main IM products frequencies, third-order incremental voltages $\tilde{v}_{g3}(t)$ and $\tilde{v}_{d3}(t)$ can be found, recalling the following expressions:

$$\begin{aligned} \tilde{v}_{g3}(1, m) &= Z_{g1}\tilde{i}_3(1, m), \\ \tilde{v}_{d3}(1, m) &= Z_1\tilde{i}_3(1, m). \end{aligned} \quad (\text{C.63})$$

Third-order iteration is the last iteration in the proposed approach. Since we are interested in getting some closed-expressions for the output voltage, only expressions for $\tilde{v}_{d3}(t)$ in the fundamental frequency will be given. The reason why both drain and gate voltages at the main harmonic frequencies were obtained in the second-order iteration was that they were necessary to get the expressions for third-order nonlinear current.

Incremental distortion in drain voltage at fundamental tones, $f = f_c \pm f_m$ can be expressed as

$$\tilde{v}_{d3}(1, \pm 1) = \frac{3}{2}\gamma'_{22}Z_1A^3 + \gamma'_{20}\bar{Z}_L(\pm\Delta f)A^3 + [5\gamma'_{42}Z_1 + 3\gamma'_{40}\bar{Z}_L(\pm\Delta f)] A^5. \quad (\text{C.64})$$

Incremental distortion in drain voltage at the frequencies for third-order IM products, $f = f_c \pm 3f_m$ can be expressed as

$$\tilde{v}_{d3}(1, \pm 3) = \frac{1}{2}\gamma'_{22}Z_1A^3 + \gamma'_{20}\bar{Z}_L(\pm\Delta f)A^3 + \left[\frac{5}{2}\gamma'_{42}Z_1 + 3\gamma'_{40}\bar{Z}_L(\pm\Delta f) + \frac{3}{4}\gamma'_{40}\bar{Z}_L(\pm 2\Delta f) \right] A^5. \quad (\text{C.65})$$

C. INCREMENTAL ENVELOPE VOLTAGES IN THE SN ANALYSIS OF TWO-TONE IM PRODUCTS

And last, incremental distortion in drain voltage at the frequencies for fifth-order IM products, $f = f_c \pm 5f_m$ can be expressed as

$$\tilde{v}_{d3}(1, \pm 5) = \left[\frac{1}{2} \gamma'_{42} Z_1 + \frac{3}{4} \gamma'_{40} \bar{Z}_L(\pm 2\Delta f) \right] A^5. \quad (\text{C.66})$$

In the previous expressions we have used the following definitions:

$$\begin{aligned} \gamma'_{22} &= \gamma_{22} \left[g_{20} H_{g1}^* Z_{g2} + \frac{1}{2} g_{11} (H_1^* Z_{g2} + H_{g1}^* Z_2) + g_{02} H_1^* Z_2 \right], \\ \gamma'_{42} &= \gamma_{42} \left[g_{20} H_{g1}^* Z_{g2} + \frac{1}{2} g_{11} (H_1^* Z_{g2} + H_{g1}^* Z_2) + g_{02} H_1^* Z_2 \right], \\ \gamma'_{20} &= \gamma_{20} Z_1 \left(\frac{1}{2} g_{11} H_{g1} + g_{02} H_1 \right), \\ \gamma'_{40} &= \gamma_{40} Z_1 \left(\frac{1}{2} g_{11} H_{g1} + g_{02} H_1 \right). \end{aligned} \quad (\text{C.67})$$

And simplifying,

$$\gamma'_{40} = \frac{\gamma'_{20}}{\gamma_{20}} \gamma_{40}, \quad (\text{C.68})$$

$$\gamma'_{42} = \frac{\gamma'_{22}}{\gamma_{22}} \gamma_{42}. \quad (\text{C.69})$$

Finally, the additional coefficients that follow are defined in order to simplify notation in drain voltage expressions:

$$\gamma_3 = - \left(\gamma_{31} - \frac{2}{3} \gamma'_{22} \right) Z_1, \quad (\text{3.69})$$

$$\gamma_5 = - \left(\gamma_{51} - \frac{4}{5} \gamma'_{42} \right) Z_1. \quad (\text{3.70})$$

C. INCREMENTAL ENVELOPE VOLTAGES IN THE SN ANALYSIS OF TWO-TONE IM PRODUCTS

BIBLIOGRAPHY

- [1] J. G. Proakis, *Digital Communications*. McGraw-Hill, 4th. Ed., 2001.
- [2] R. Steele, *Mobile Radio Communications*. London Pentech Press, 1994.
- [3] M. Golio, *Low Voltage/Low Power Microwave Electronics*, Chap. 3.6. CRC Press, 2001.
- [4] C. K. Chen, P. C. Tseng, Y. C. Chang, and L. G. Chen, "A digital signal processor with programmable correlator array architecture for third generation wireless communication system," *IEEE Transactions on Circuits and Systems II: Analog and Digital Signal Processing*, Vol. 48, No. 12, pp. 1110–1120, Dec. 2001.
- [5] P. Asbeck, L. E. Larson, and I. G. Galton, "Synergistic design of DSP and power amplifiers for wireless communications," *IEEE Transactions on Microwave Theory and Techniques*, Vol. 49, No. 11, pp. 2163–2169, Nov. 2001.
- [6] B. Maham and R. Ali-Hemmati, "DSP implementation aspects of an OFDM based wireless MAN modem," in *International Conference on Wireless Communications, Networking and Mobile Computing*, pp. 1–4, 2006.
- [7] B. Razavi, "Challenges in portable RF transceiver design," *IEEE Circuits and Devices Magazine*, Vol. 12, No. 5, pp. 12–25, Sep. 1996.
- [8] S. A. Maas, *Nonlinear Microwave and RF Circuits*. Artech House, 2nd Ed., 2003.
- [9] T. J. Brazil, "Simulating circuits and devices," *IEEE Microwave Magazine*, Vol. 4, No. 1, pp. 42–50, Mar. 2003.
- [10] K. Kundert, J. K. White, and A. Sangiovanni-Vincentelli, *Steady-State Methods for Simulating Analog and Microwave Circuits*. Kluwer Academic Publishers, 1990.
- [11] C. Camacho-Peñalosa, "Numerical steady-state analysis of nonlinear microwave circuits with periodic excitation," *IEEE Transactions on Microwave Theory and Techniques*, Vol. 31, No. 9, pp. 724–730, Sep. 1983.

BIBLIOGRAPHY

- [12] V. Rizzoli, A. Lipparini, D. Masotti, and F. Mastri, "Efficient circuit-level analysis of large microwave systems by Krylov-subspace Harmonic Balance," in *IEEE MTT-S International Microwave Symposium Digest*, Vol. 1, pp. 25–28, 2001.
- [13] J. J. Bussgang, L. Ehrman, and J. W. Graham, "Analysis of nonlinear systems with multiple inputs," *Proceedings of the IEEE*, Vol. 62, No. 8, pp. 1088–1119, Aug. 1974.
- [14] S. Benedetto, E. Biglieri, and R. Daffara, "Modeling and performance evaluation of nonlinear satellite links - A Volterra series approach," *IEEE Transactions on Aerospace and Electronic Systems*, Vol. 15, No. 4, pp. 494–506, Apr. 1979.
- [15] D. Mirri, G. Ioculano, F. Filicori, G. Pasini, G. Vannini, and G. P. Gualtieri, "A modified Volterra series approach for nonlinear dynamic systems modeling," *IEEE Transactions on Circuits and Systems I: Fundamentals, Theory and Applications*, Vol. 49, No. 8, pp. 1118–1128, Aug. 2002.
- [16] J. Reina Tosina, *MMIC Mixers Design and Analysis Techniques by Means of Volterra Series (in Spanish)*. PhD. Thesis, Universidad de Sevilla, 2002.
- [17] E. Ngoya and R. Larchevèque, "Envelope Transient Analysis: A new method for the transient and steady state analysis of microwave communication circuits and systems," in *1996 IEEE MTT-S International Microwave Symposium Digest*, Vol. 3, pp. 1365–1368, Jun. 1996.
- [18] V. Borich, J. East, and G. Haddad, "The Method of Envelope Currents for rapid simulation of weakly nonlinear communications circuits," in *1999 IEEE MTT-S International Microwave Symposium Digest*, pp. 981–984, Jun. 1999.
- [19] C. Crespo-Cadenas and J. Reina-Tosina, "New envelope-currents method for the simulation of weakly nonlinear communication circuits," *IEEE Transactions on Microwave Theory and Techniques*, Vol. 52, No. 4, pp. 1339–1342, Apr. 2004.
- [20] V. Rizzoli, A. Neri, and F. Mastri, "A modulation-oriented piecewise Harmonic-Balance technique suitable for transient analysis and digitally modulated signals," in *Proceedings of the 26th European Microwave Conference*, pp. 546–550, 1996.
- [21] J. Brinkhoff and A. E. Parker, "Effect of baseband impedance on FET intermodulation," *IEEE Transactions on Microwave Theory and Techniques*, Vol. 51, No. 3, pp. 1045–1051, Mar. 2003.
- [22] A. Katz, "Linearization: reducing distortion in power amplifiers," *IEEE Microwave Magazine*, Vol. 2, No. 4, No. 4, pp. 37–49, 2001.

- [23] D. R. Morgan, Z. MA, J. Kim, M. G. Zierdt, and J. Pastalan, "A generalized memory polynomial model for digital predistortion of RF power amplifiers," *IEEE Transactions on Signal Processing*, Vol. 54, No. 10, pp. 3852–3860, Oct. 2006.
- [24] W. Bosch and G. Gatti, "Measurement and simulation of memory effects in predistortion linearizers," *IEEE Transactions on Microwave Theory and Techniques*, Vol. 37, No. 12, pp. 1885–1890, Dec. 1989.
- [25] J. Brinkhoff, *Bandwidth-Dependent Intermodulation Distortion in FET Amplifiers*. PhD. Thesis, Macquarie University, Sydney, Australia, 2004.
- [26] J. C. Pedro and N. B. Carvalho, *Intermodulation Distortion in Microwave and Wireless Circuits*. Norwood, MA, USA: Artech House, 1st Ed., 2003.
- [27] J. H. K. Vuolevi, T. Rahkonen, and J. P. A. Manninen, "Measurement technique for characterizing memory effects in RF power amplifiers," *IEEE Transactions on Microwave Theory and Techniques*, Vol. 49, No. 8, pp. 1383–1389, Aug. 2001.
- [28] N. B. de Carvalho and J. C. Pedro, "A comprehensive explanation of distortion sideband asymmetries," *IEEE Transactions on Microwave Theory and Techniques*, Vol. 50, No. 9, pp. 2090–2101, Sep. 2002.
- [29] A. Walker, M. Steer, and K. G. Gard, "A vector intermodulation analyzer applied to behavioral modeling of amplifiers with memory," *IEEE Transactions on Microwave Theory and Techniques*, Vol. 54, No. 5, pp. 1991–1999, May 2006.
- [30] J. P. Martins, N. B. Carvalho, and J. C. Pedro, "Intermodulation distortion of third-order nonlinear systems with memory under multisine excitations," *IEEE Transactions on Microwave Theory and Techniques*, Vol. 55, No. 6, pp. 1264–1271, Jun. 2007.
- [31] S. Yi *et al.*, "Prediction of a CDMA output spectrum based on intermodulation products of two-tone tests," *IEEE Transactions on Microwave Theory and Techniques*, Vol. 49, No. 5, pp. 938–946, May 2001.
- [32] M. J. Madero-Ayora, J. Reina-Tosina, and C. Crespo-Cadenas, "Simplified method to evaluate weakly nonlinear communication circuits," in *Proceedings of the 35th European Microwave Conference*, Oct. 2005.
- [33] C. Crespo-Cadenas, J. Reina-Tosina, and M. J. Madero-Ayora, "Evaluation of ACPR in mixers based on a Parametric Harmonic-Balance approach," *IEEE Transactions on Microwave Theory and Techniques*, Vol. 54, No. 1, pp. 445–450, Jan. 2006.

BIBLIOGRAPHY

- [34] C. Crespo-Cadenas, J. Reina-Tosina, and M. J. Madero-Ayora, "IM3 and IM5 phase characterization and analysis based on a Simplified Newton approach," *IEEE Transactions on Microwave Theory and Techniques*, Vol. 54, No. 1, pp. 321–328, Jan. 2006.
- [35] M. J. Madero-Ayora, J. Reina-Tosina, and C. C. Cadenas, "An impedance-based model for the evaluation of IM3 in nonlinear amplifiers showing memory effects," *Microwave and Optical Technology Letters*, Vol. 50, No. 3, pp. 568–573, Mar. 2008.
- [36] C. Crespo-Cadenas and J. Reina-Tosina, "Envelope currents method with extended dynamic range for the simulation of nonlinear communication circuits," in *Proc. 33rd EuMC European Microwave Conference*, pp. 769–772, Oct. 2003.
- [37] V. Rizzoli, A. Liparini, and E. Marazzi, "A general-purpose program for nonlinear microwave circuit design," *IEEE Transactions on Microwave Theory and Techniques*, Vol. 31, No. 9, pp. 762–770, Sep. 1983.
- [38] K. S. Kundert and A. Sangiovanni-Vincentelli, "Simulation of nonlinear circuits in the frequency domain," *IEEE Transactions on Computer-Aided Design*, Vol. 5, No. 4, pp. 521–535, Oct. 1986.
- [39] P. L. Heron and M. B. Steer, "Jacobian calculation using the multidimensional Fast Fourier Transform in the Harmonic Balance analysis of nonlinear circuits," *IEEE Transactions on Microwave Theory and Techniques*, Vol. 38, No. 4, pp. 429–431, Apr. 1990.
- [40] S. Egami, "Nonlinear, linear analysis and computer-aided design of resistive mixers," *IEEE Transactions on Microwave Theory and Techniques*, Vol. 21, No. 3, pp. 270–275, Mar. 1973.
- [41] S. A. Maas, "Two-tone intermodulation in diode mixers," *IEEE Transactions on Microwave Theory and Techniques*, Vol. 35, No. 3, pp. 307–314, Mar. 1987.
- [42] C. Crespo-Cadenas and J. Reina-Tosina, "Analysis of FET resistive mixers with a double Volterra series approach," in *Proc. 32nd EuMC European Microwave Conference*, pp. 255–258, Sep. 2002.
- [43] J. A. García, M. L. de la Fuente, J. C. Pedro, N. B. Carvalho, Y. Newport, A. Mediavilla, and A. Tazón, "Time-varying Volterra-series analysis of spectral regrowth and noise power ratio in FET mixers," *IEEE Transactions on Microwave Theory and Techniques*, Vol. 49, No. 3, pp. 545–548, Mar. 2001.

- [44] V. Borich, *Analysis and Optimization of Solid-State Microwave Circuits for Digital Communications*. PhD. Thesis, University of Michigan, Ann Arbor, United States, 2001.
- [45] Y. Thodesen and K. Kundert, "Parametric Harmonic Balance," in *1996 IEEE MTT-S International Microwave Symposium Digest*, pp. 1361–1364, Jun. 1996.
- [46] C. Crespo-Cadenas, J. Reina-Tosina, and M. J. Madero, "New envelope currents method to evaluate distortion of communication signals in mixers," in *Proc. 34th EuMC European Microwave Conference*, pp. 853–856, Oct. 2004.
- [47] Y. Ding and A. Sano, "Time-domain adaptive predistortion for nonlinear amplifiers," in *Proceedings of the International Conference on Acoustics, Speech, and Signal Processing*, Vol. 2, pp. 865–868, 2004.
- [48] Agilent Technologies, *Understanding the Fundamental Principles of Vector Network Analysis*, 2000. Application Note 1287-1.
- [49] Agilent Technologies, *Network Analyzer Measurements: Filter and Amplifier Examples*, 2000. Application Note 1287-4.
- [50] Agilent Technologies, *Agilent Spectrum Analysis Basics*, 2006. Application Note 150.
- [51] Agilent Technologies, *8 Hints for Better Spectrum Analysis*, 2005. Application Note 1286-1.
- [52] Agilent Technologies, *Agilent Technologies Wireless Test Solutions*, 2002. Application Note 1313.
- [53] Agilent Technologies, *Agilent Vector Signal Analysis Basics*, 2004. Application Note 150-15.
- [54] L. O. Chua, C. A. Desoer, and E. S. Kuh, *Linear and Nonlinear Circuits*. McGraw-Hill, 1987.
- [55] P. M. Cabral, J. C. Pedro, and N. B. Carvalho, "Dynamic AM-AM and AM-PM behavior in microwave PA circuits," in *2005 Asia Pacific Microwave Conference Proceedings*, IEEE Asia Pacific Microwave Conference, 2005.
- [56] J. C. Pedro, N. B. de Carvalho, and P. M. Lavrador, "Modeling nonlinear behavior of band-pass memoryless and dynamic systems," in *IEEE MTT-S International Microwave Symposium Digest*, pp. 2133–2136, 2003.

BIBLIOGRAPHY

- [57] A. E. Parker and J. G. Rathmell, "Bias and frequency dependence of FET characteristics," *IEEE Transactions on Microwave Theory and Techniques*, Vol. 51, No. 2, pp. 588–592, Feb. 2003.
- [58] P. H. Aaen, J. A. Plá, and J. Wood, *Modeling and Characterization of RF and Microwave Power FETs*. Cambridge University Press, 2007.
- [59] N. Le Gallou *et al.*, "An improved behavioral modeling technique for high power amplifiers with memory," in *2001 IEEE MTT-S International Microwave Symposium Digest*, pp. 983–986, 2001.
- [60] H. Ku, M. D. McKinley, and J. S. Kenney, "Extraction of accurate behavioral models for power amplifiers with memory effects using two-tone measurements," in *IEEE MTT-S International Microwave Symposium Digest*, pp. 139–142, 2002.
- [61] K. A. Remley, D. F. Williams, D. M. M.-P-Schreurs, and J. Wood, "Simplifying and interpreting two-tone measurements," *IEEE Transactions on Microwave Theory and Techniques*, Vol. 52, No. 11, pp. 2576–2584, Nov. 2004.
- [62] J. C. Pedro, J. Martins, and P. Cabral, "New method for phase characterization of nonlinear distortion products," in *IEEE MTT-S International Microwave Symposium Digest*, pp. 971–974, 2005.
- [63] J. P. Martins and N. B. Carvalho, "Multitone phase and amplitude measurement for nonlinear device characterization," *IEEE Transactions on Microwave Theory and Techniques*, Vol. 53, No. 6, pp. 1982–1989, Jun. 2005.
- [64] J. P. Martins, N. B. Carvalho, and J. C. Pedro, "Practical multitone amplitude and phase characterization," in *2005 Asia Pacific Microwave Conference Proceedings*, IEEE Asia Pacific Microwave Conference, 2005.
- [65] A. Soury *et al.*, "Measurement based modeling of power amplifiers for reliable design of modern communication systems," in *2003 IEEE MTT-S International Microwave Symposium Digest*, pp. 795–798, 2003.
- [66] P. Draxler, I. Langmore, T. P. Hung, and P. M. Asbeck, "Time domain characterization of power amplifiers with memory effects," in *IEEE MTT-S International Microwave Symposium Digest*, Vol. 2, pp. 803–806, 2003.
- [67] S. Boumaiza and F. M. Ghannouchi, "Dynamic nonlinear distortion characterization of wireless radio transmitters," in *Proc. 12th International Symposium Electron Devices for Microwave and Optoelectronic Applications (EDMO)*, pp. 92–95, 2004.

- [68] A. Ahmed, B. Bunz, E. R. Srinidhi, and G. Kompa, "Measurements of envelope frequency dependent nonlinearity in GaN HEMT power device," in *Proc. Integrated Nonlinear Microwave and Millimetre-Wave Circuits*, pp. 48–51, 2006.
- [69] M. D. McKinley, Y. Park, J. S. Kenney, and H. Ku, "Obtaining accurate IMD variation and imbalance measurements for identifying memory effects in high-power amplifiers," in *Proc. 62nd ARFTG Microwave Measurements Conference*, pp. 77–80, 2003.
- [70] C. Crespo-Cadenas, J. Reina-Tosina, and M. J. Madero-Ayora, "Phase characterization of two-tone intermodulation distortion," in *IEEE MTT-S International Microwave Symposium Digest*, pp. 1505–1508, 2005.
- [71] W. R. Curtice and M. Ettenberg, "A nonlinear GaAs FET model for use in the desing of output circuits for power amplifiers," *IEEE Transactions on Microwave Theory and Techniques*, Vol. 33, No. 12, pp. 1383–1394, Dec. 1985.
- [72] I. Angelov, H. Zirath, and N. Rorsman, "A new empirical nonlinear model for HEMT and MESFET devices," *IEEE Transactions on Microwave Theory and Techniques*, Vol. 40, No. 12, pp. 2258–2266, Dec. 1992.
- [73] J. C. Pedro and J. Pérez, "A novel nonlinear GaAs FET model for intermodulation analysis in general purpose Harmonic Balance simulators," in *Proc. 23rd EuMC European Microwave Conference*, pp. 714–716, Sep. 1993.
- [74] J. A. García, A. Mediavilla, J. C. Pedro, N. B. de Carvalho, A. Tazón, and J. L. García, "Characterizing the gate to source nonlinear capacitor role on GaAs FET IMD performance," *IEEE Transactions on Microwave Theory and Techniques*, Vol. 46, No. 12, pp. 2344–2355, Dec. 1998.
- [75] J. F. Sevic, K. L. Burger, and M. B. Steer, "A novel envelope-termination load-pull method for ACPR optimization of RF/microwave power amplifiers," in *IEEE MTT-S International Microwave Symposium Digest*, pp. 723–726, 1998.
- [76] V. Aparin and C. Perisco, "Effect of out-of-band terminations on intermodulation distortion in common-emitter circuits," in *IEEE MTT-S International Microwave Symposium Digest*, pp. 977–980, 1999.
- [77] M. J. Madero-Ayora, J. Reina-Tosina, and C. Crespo-Cadenas, "Phase characterization of intermodulation products including electrothermal memory effects," in *Proc. Integrated Nonlinear Microwave and Millimetre-Wave Circuits*, pp. 56–59, 2006.

- [78] S. Boumaiza and F. M. Ghannouchi, "Thermal memory effects modelling and compensation of RF power amplifiers and predistortion linearizers," *IEEE Transactions on Microwave Theory and Techniques*, Vol. 51, No. 12, pp. 2427–2433, Dec. 2003.
- [79] O. Tornblad, B. Wu, W. Dai, C. Blair, G. Ma, and R. W. Dutton, "Modeling and measurements of electrical and thermal memory effects for RF power LDMOS," in *2007 IEEE MTT-S International Microwave Symposium Digest*, pp. 2015–2018, 2007.
- [80] W. Dai, P. Roblin, and M. Frei, "Distributed and multiple time-constant electro-thermal modeling and its impact on ACPR in RF predistortion," in *Proc. 62nd ARFTG Microwave Measurements Conference*, Vol. 1, pp. 89–98, 2003.
- [81] Y. Takahashi, R. Ishikawa, and K. Honjo, "Precise modelling of thermal memory effect for power amplifier using multi-stage thermal rc-ladder network," in *Proc. Asia-Pacific Microwave Conference*, pp. 287–290, 2006.
- [82] J. Brinkhoff and A. E. Parker, "Charge trapping and intermodulation in HEMTs," in *2004 IEEE MTT-S International Microwave Symposium Digest*, pp. 799–802, 2004.
- [83] A. E. Parker and J. G. Rathmell, "Dispersion of linearity in broadband FET circuits," in *Proceedings of the 1st European Microwave Integrated Circuits Conference*, pp. 320–323, 2006.
- [84] J. Reina-Tosina, M. J. Madero-Ayora, and C. Crespo-Cadenas, "An impedance-based model for the evaluation of IM3 in commercial amplifiers with memory," in *IEEE Wireless and Microwave Technology Conference Proc.*, 2006.
- [85] D. Wisell, D. Rönnow, and P. Händel, "A technique to extend the bandwidth of an RF power amplifier test bed," *IEEE Transactions on Instrumentation and Measurement*, Vol. 56, No. 4, pp. 1488–1494, Aug. 2007.
- [86] C. Crespo-Cadenas, J. Reina-Tosina, and M. J. Madero-Ayora, "Volterra behavioral model for wideband RF amplifiers," *IEEE Transactions on Microwave Theory and Techniques*, Vol. 55, No. 3, pp. 449–457, Mar. 2007.
- [87] Agilent Technologies, *Circuit Envelope Simulation*, May 2003.
- [88] D. D'Amore, P. Maffezzoni, and M. Pillan, "A Newton-Powell modification algorithm for Harmonic Balance-based circuit analysis," *IEEE Transactions on Circuits and Systems I: Fundamental Theory and Applications*, Vol. 41, No. 2, pp. 177–180, Feb. 1994.

- [89] F. Seydou, T. Seppanen, and R. Duraiswami, "A Simplified Newton method for the inverse orthotopic problem," in *IEEE Antennas and Propagation Society International Symposium*, Vol. 1, pp. 535–538, 2003.
- [90] C. Barbulescu, S. Kilyrni, A. Ceclan, D. D. Micu, and G. Vuc, "Power flow calculation for ill-conditioned systems. Simplified Newton method with SVD partial regularization," in *The International Conference on "Computer as a Tool", EUROCON 2007*, pp. 1481–1484, 2007.
- [91] A. Suarez and R. Quéré, *Stability Analysis of Nonlinear Microwave Circuits*. Artech House, 2003.
- [92] F. Giannini and G. Leuzzi, *Nonlinear Microwave Circuit Desing*. John Wiley and Sons, 2004.
- [93] L. R. Petzold, "An efficient numerical method for highly oscillatory ordinary differential equations," *SIAM Journal on Numerical Analysis*, Vol. 18, No. 3, pp. 455–479, Jun. 1981.
- [94] K. S. Kundert, J. White, and A. Sangiovanni-Vincentelli, "An envelope-following method for the efficient transient simulation of switching power and filter circuits," in *ICCAD-88 Digest of Technical Papers*, pp. 446–449, IEEE International Conference on Computer-Aided Design, Nov. 1988.
- [95] J. M. Ortega and W. C. Rheinboldt, *Iterative Solution of Nonlinear Equations in Several Variables*. Academic Press, 1970.
- [96] J. Stoer and R. Bulirsch, *Introduction to Numerical Analysis*. Springer-Verlag, 1980.
- [97] J. C. Pedro and J. Pérez, "Accurate simulation of GaAs MESFET's intermodulation distortion using a new drain-source current model," *IEEE Transactions on Microwave Theory and Techniques*, Vol. 42, No. 1, pp. 25–33, Jan. 1994.
- [98] I. Sarkas, D. Mavridis, M. Papamichail, and G. Papadopoulos, "Volterra analysis using Chebyshev series," in *IEEE International Symposium on Circuits and Systems*, pp. 1931–1934, 2007.
- [99] W. J. Cunningham, *Introduction to Nonlinear Analysis*. McGraw-Hill, 1958.
- [100] E. M. Baily, *Steady-State Harmonic Analysis of Nonlinear Networks*. PhD. Thesis, Stanford University, Palo Alto, United States, 1969.
- [101] S. Egami, "Nonlinear, linear analysis and computer-aided desing of resistive mixers," *IEEE Transactions on Microwave Theory and Techniques*, Vol. 22, No. 3, pp. 270–275, Mar. 1974.

BIBLIOGRAPHY

- [102] W. K. Gwarek, "Nonlinear analysis of microwave mixers," Masters Thesis, Massachusetts Institute of Technology, 1974.
- [103] A. R. Kerr, "A technique for determining the local oscillator waveforms in a microwave mixer," *IEEE Transactions on Microwave Theory and Techniques*, Vol. 23, No. 10, pp. 828–831, Oct. 1975.
- [104] M. S. Nakhla and J. Vlach, "A piecewise Harmonic Balance technique for determination of the periodic response of nonlinear systems," *IEEE Transactions on Circuits and Systems*, Vol. 23, No. 2, pp. 85–91, Feb. 1976.
- [105] A. Ushida and L. O. Chua, "Frequency-domain analysis of nonlinear circuits driven by multi-tone signals," *IEEE Transactions on Circuit and Systems*, Vol. 31, No. 9, pp. 766–778, Sep. 1984.
- [106] R. J. Gilmore and F. J. Rosenbaum, "Modeling of nonlinear distortion in GaAs MESFETs," in *IEEE MTT-S International Microwave Symposium Digest*, pp. 430–431, May. 1984.
- [107] R. Gilmore, "Nonlinear circuit desing using the modified Harmonic Balance algorithm," *IEEE Transactions on Microwave Theory and Techniques*, Vol. 34, No. 12, pp. 1294–1307, Dec. 1986.
- [108] K. S. Kundert, G. B. Sorkin, and A. Sangiovanni-Vincentelli, "Applying Harmonic Balance to almost-periodic circuits," *IEEE Transactions on Microwave Theory and Techniques*, Vol. 36, No. 2, pp. 366–378, Feb. 1988.
- [109] G. B. Sorkin, K. S. Kundert, and A. Sangiovanni-Vincentelli, "An almost-periodic Fourier transform for use with Harmonic Balance," in *IEEE MTT-S International Microwave Symposium Digest*, Vol. 2, pp. 717–720, Jun. 1987.
- [110] G. P. Bava, S. Benedetto, E. Biglieri, F. Fillicori, V. A. Monaco, C. Naldi, U. Pisani, and V. Pozzolo, "Modeling and performance simulation techniques of GaAs MESFET's for microwave power amplifiers," tech. rep., ESA-ESTEC REPORT, Mar. 1982.
- [111] V. Rizzoli, C. Cecchetti, and A. Lipparini, "A general-purpose program for the analysis of nonlinear microwave circuits under multitone excitation by multi-dimensional Fourier transform," in *Proceedings of the 17th European Microwave Conference*, pp. 635–640, Sep. 1987.
- [112] V. Rizzoli, C. Cecchetti, A. Lipparini, and F. Matri, "General-purpose Harmonic Balance analysis of nonlinear microwave circuits under multitone excitation,"

- IEEE Transactions on Microwave Theory and Techniques*, Vol. 36, No. 12, pp. 1650–1660, Dec. 1988.
- [113] A. Ushida, L. O. Chua, and T. Sugawara, “A substitution algorithm for solving nonlinear circuits with multi-frequency components,” *International Journal on Circuits Theory and Application*, Vol. 15, pp. 327–355, 1987.
- [114] M. Gayral, E. Ngoya, R. Quere, J. Rousset, and J. Obregon, “The Spectral Balance: A general method for analysis of nonlinear microwave circuits driven by non-harmonically related generators,” in *IEEE MTT-S International Microwave Symposium Digest*, pp. 119–121, 1987.
- [115] E. Ngoya, M. Gayral, and J. Rousset, “Application of Spectral-Balance to the design of non-linear microwave circuits: Steady-state response, sensitivity analysis and optimization,” in *IEEE International Symposium on Circuits and Systems*, pp. 2283–2285, 1988.
- [116] M. B. Steer and P. J. Khan, “An algebraic formula for the output of a system with large-signal, multifrequency excitation,” *Proceedings of the IEEE*, Vol. 71, No. 1, pp. 177–179, Jan. 1983.
- [117] G. W. Rhyne, M. B. Steer, and B. D. Bates, “Frequency-domain nonlinear circuit analysis using generalized power series,” *IEEE Transactions on Microwave Theory and Techniques*, Vol. 36, No. 2, pp. 379–387, Feb. 1988.
- [118] J. H. Haywood and Y. L. Chow, “Intermodulation distortion analysis using a frequency-domain Harmonic Balance technique,” *IEEE Transactions on Microwave Theory and Techniques*, Vol. 36, No. 8, pp. 1251–1257, Aug. 1988.
- [119] C. Chang, M. B. Steer, and G. W. Rhyne, “Frequency-domain spectral balance using the arithmetic operator method,” *IEEE Transactions on Microwave Theory and Techniques*, Vol. 37, No. 11, pp. 1681–1688, Nov. 1989.
- [120] C. Chang, P. L. Heron, and M. B. Steer, “Harmonic Balance and frequency-domain simulation of nonlinear microwave circuits using the block Newton method,” *IEEE Transactions on Microwave Theory and Techniques*, Vol. 38, No. 4, pp. 431–434, Apr. 1990.
- [121] T. Narhi, “Frequency-domain analysis of strongly nonlinear circuits using a consistent large-signal model,” *IEEE Transactions on Microwave Theory and Techniques*, Vol. 44, No. 2, pp. 182–192, Feb. 1996.
- [122] V. Rizzoli, F. Mastri, F. Sgallari, and V. Frontini, “The exploitation of sparse-matrix techniques in conjunction with the piecewise Harmonic-Balance method

BIBLIOGRAPHY

- for nonlinear microwave circuit analysis," in *IEEE MTT-S International Microwave Symposium Digest*, pp. 1295–1298, 1990.
- [123] H. G. Brachtendorf, G. Welsch, and R. Laur, "Fast simulation of the steady-state of circuits by the Harmonic Balance technique," in *IEEE International Symposium on Circuits and Systems*, Vol. 2, pp. 1388–1391, 1995.
- [124] R. Telichevesky, K. Kundert, I. Elfadel, and J. White, "Fast simulation algorithms for RF circuits," in *IEEE Custom Integrated Circuits Conference*, pp. 437–444, 1996.
- [125] V. Rizzoli, F. Mastri, C. Cecchetti, and F. Sgallari, "Fast and robust inexact Newton approach to the Harmonic-Balance analysis of nonlinear microwave circuits," *IEEE Microwave and Guided Wave Letters*, Vol. 7, No. 10, pp. 359–362, Oct. 1997.
- [126] V. Rizzoli, F. Mastri, and C. Cecchetti, "Signal and noise analysis of large microwave front-ends by the inexact-Newton Harmonic-Balance technique," in *IEEE MTT-S International Microwave Symposium Digest*, pp. 1599–1602, 1998.
- [127] O. Nastov and J. K. White, "Time-mapped Harmonic Balance," in *Proceedings of the 36th Design Automation Conference*, pp. 641–646, 1999.
- [128] O. J. Nastov and J. K. White, "Grid selection strategies for time-mapped Harmonic Balance simulation of circuits with rapid transitions," in *IEEE Custom Integrated Circuits Conference*, pp. 13–16, 1999.
- [129] M. M. Gourary, S. G. Rusakov, S. L. Ulyanov, M. M. Zharov, K. K. Gullapalli, and B. J. Mulvaney, "Adaptive preconditioners for the simulation of extremely nonlinear circuits using Harmonic Balance," in *IEEE MTT-S International Microwave Symposium Digest*, Vol. 2, pp. 779–782, 1999.
- [130] V. Rizzoli, A. Neri, F. Mastri, and A. Lipparini, "Modulation-oriented Harmonic Balance based on Krylov-subspace methods," in *IEEE MTT-S International Microwave Symposium Digest*, pp. 771–774, 1999.
- [131] V. Rizzoli, E. Montanari, A. Liparini, D. Masotti, and F. Mastri, "A fully automatic domain partitioning technique for the efficient circuit-level simulation of large nonlinear microwave subsystems," *IEEE Microwave and Wireless Components Letters*, Vol. 14, No. 7, pp. 349–351, Jul. 2004.
- [132] W. Dong and P. Li, "Hierarchical Harmonic-Balance methods for frequency-domain analog-circuit analysis," *IEEE Transactions on Computer-Aided Design of Integrated Circuits and Systems*, Vol. 26, No. 12, pp. 2089–2101, Dec. 2007.

- [133] E. Gad, R. Khazaka, M. S. Nakhla, and R. Griffith, "A circuit reduction technique for finding the steady-state solution of nonlinear circuits," *IEEE Transactions on Microwave Theory and Techniques*, Vol. 48, No. 12, pp. 2389–2396, Dec. 2000.
- [134] H. Asai and H. Makino, "Frequency domain latency and relaxation-based Harmonic Balance analysis of nonlinear circuits," in *IEEE Proceedings of the Midwest Symposium on Circuits and Systems*, Vol. 1, pp. 202–205, 1991.
- [135] H. Makino and H. Asai, "Acceleration techniques for the circuit simulation in the frequency domain," in *IEEE International Symposium on Circuits and Systems*, Vol. 2, pp. 903–903, 1992.
- [136] F. Filicori and G. Vannini, "Mathematical approach to large-signal modeling of electron devices," *Electronic Letters*, Vol. 27, No. 4, pp. 357–359, 1991.
- [137] C. P. Silva, "Efficient and reliable numerical algorithms for nonlinear microwave computer-aided design," in *Proceedings of the Midwest Symposium on Circuits and Systems*, Vol. 1, pp. 422–428, 1991.
- [138] P. Li and L. Pileggi, "A linear-centric modeling approach to Harmonic Balance analysis," in *Proceedings of the 2002 Design, Automation and Test in Europe Conference*, 2002.
- [139] E. Ngoya, J. Rousset, M. Gayral, R. Quere, and J. Obregon, "Efficient algorithms for spectra calculations in nonlinear microwave circuits simulators," *IEEE Transactions on Circuits and Systems*, Vol. 37, No. 11, pp. 1339–1355, Nov. 1990.
- [140] P. Rodrigues, "An orthogonal almost-periodic Fourier transform for use in nonlinear circuit simulation," *IEEE Microwave and Guided Wave Letters*, Vol. 4, No. 3, pp. 74–76, Mar. 1994.
- [141] P. Rodrigues, "A general mapping technique for Fourier transform computation in nonlinear circuit analysis," *IEEE Microwave and Guided Wave Letters*, Vol. 7, No. 11, pp. 374–377, Nov. 1997.
- [142] D. Elad and A. Madjar, "Signal space and its implementation for microwave nonlinear-network analysis," *IEEE Transactions on Microwave Theory and Techniques*, Vol. 46, No. 10, pp. 1577–1582, Oct. 1998.
- [143] V. Borich, J. East, and G. Haddad, "An efficient Fourier transform algorithm for multitone Harmonic Balance," *IEEE Transactions on Microwave Theory and Techniques*, Vol. 47, No. 2, pp. 182–188, Feb. 1999.
- [144] A. Brambilla, "Multitone signal Harmonic Balance method," *IEEE Electronic Letters*, Vol. 35, No. 21, pp. 1809–1810, Oct. 1999.

BIBLIOGRAPHY

- [145] J. C. Pedro and N. B. de Carvalho, "Artificial frequency mapping techniques for multitone Harmonic Balance," in *IEEE MTT-S International Microwave Symposium Digest, Workshops*, 2000.
- [146] N. Soveiko and M. Nakhla, "Wavelet Harmonic Balance," *IEEE Microwave and Wireless Components Letters*, Vol. 13, No. 6, pp. 232–235, Jun. 2003.
- [147] V. Borich, J. East, and G. Haddad, "A fixed-point Harmonic Balance approach for circuit simulation under modulated carrier excitation," in *Proceedings of the IEEE International Symposium on Circuits and Systems*, Vol. 6, pp. 346–349, 1999.
- [148] N. B. Carvalho, J. C. Pedro, W. Jang, and M. B. Steer, "Nonlinear RF circuits and systems simulation when driven by several modulated signals," *IEEE Transactions on Microwave Theory and Techniques*, Vol. 54, No. 2, pp. 572–579, Feb. 2000.
- [149] R. G. Hicks and P. J. Khan, "Numerical analysis of nonlinear solid-state device excitation in microwave circuits," *IEEE Transactions on Microwave Theory and Techniques*, Vol. 30, No. 3, pp. 251–259, Mar. 1982.
- [150] R. G. Hicks and P. J. Khan, "Numerical analysis of subharmonic mixers using accurate and approximate models," *IEEE Transactions on Microwave Theory and Techniques*, Vol. 30, No. 12, pp. 2113–2120, Dec. 1982.
- [151] C. Camacho-Peñalosa and C. S. Aitchison, "Analysis and design of MESFET gate mixers," *IEEE Transactions on Microwave Theory and Techniques*, Vol. 35, No. 7, pp. 643–652, Jul. 1987.
- [152] W. R. Curtice, "Nonlinear analysis of GaAs MESFET amplifiers, mixers, and distributed amplifiers using the Harmonic Balance technique," *IEEE Transactions on Microwave Theory and Techniques*, Vol. 35, No. 4, pp. 441–447, Apr. 1987.
- [153] V. Rizzoli, A. Lipparini, A. Costanzo, F. Mastri, C. Cecchetti, A. Neri, and D. Masotti, "State-of-the-art Harmonic-Balance simulation of forced nonlinear microwave circuits by the piecewise technique," *IEEE Transactions on Microwave Theory and Techniques*, Vol. 40, No. 1, pp. 12–28, Jan. 1992.
- [154] N. Wiener, "Response of a nonlinear device to noise," technical report v-16s, M.I.T. Radiation Lab, 1942.
- [155] S. Narayanan, "Transistor distortion analysis using Volterra series representation," *Bell Syst. Tech. Journal*, Vol. 46, p. 991, 1967.
- [156] J. T. Stauth and S. R. Sanders, "Power supply rejection for RF power amplifiers: Theory and measurements," *IEEE Transactions on Microwave Theory and Techniques*, Vol. 55, No. 10, pp. 2043–2052, Oct. 2007.

- [157] D. Tannir and R. Khazaka, "Moments-based computation of intermodulation distortion of RF circuits," *IEEE Transactions on Microwave Theory and Techniques*, Vol. 55, No. 10, pp. 2135–2146, Oct. 2007.
- [158] S. Yamanouchi, Y. Aoki, K. Kunihiro, T. Hirayama, T. Miyazaki, and H. Hida, "Analysis and desing of a dynamic predistorter for WCDMA handset power amplifiers," *IEEE Transactions on Microwave Theory and Techniques*, Vol. 55, No. 3, pp. 493–593, Mar. 2007.
- [159] P. Roblin, S. K. Myoung, D. Chaillot, Y. G. Kim, A. Fathimulla, J. Strahler, and S. Bibyk, "Frequency-selective predistortion linearization of RF power amplifiers," *IEEE Transactions on Microwave Theory and Techniques*, Vol. 56, No. 1, pp. 65–76, Jan. 2008.
- [160] S. Narayanan, "Application of Volterra series to intermodulation distortion analysis of transistor feedback amplifiers," *IEEE Transactions on Circuit Theory*, Vol. 17, No. 4, pp. 518–527, Nov. 1970.
- [161] S. Narayanan and H. C. Poon, "An analysis of distortion in bipolar transistors using integral charge control model and Volterra series," *IEEE Transactions on Circuit Theory*, Vol. 20, No. 4, pp. 341–351, Jul. 1973.
- [162] E. Bedrosian and S. O. Rice, "The output properties of Volterra systems driven by harmonic and gaussian inputs," *Proceedings of the IEEE*, Vol. 59, No. 12, pp. 1688–1707, Aug. 1971.
- [163] A. Javed, P. A. Goud, and B. A. Syrett, "Analysis of a microwave feedforward amplifier using Volterra series representation," *IEEE Transactions on Communications*, pp. 355–360, Mar. 1977.
- [164] A. Javed, B. A. Syrett, and P. A. Goud, "Intermodulation distortion analysis of reflection-type IMPATT amplifiers using Volterra series representation," *IEEE Transactions on Microwave Theory and Techniques*, Vol. 25, No. 9, pp. 729–734, Sep. 1977.
- [165] R. A. Minasian, "Intermodulation distortion analysis of MESFET amplifiers using the Volterra series representation," *IEEE Transactions on Microwave Theory and Techniques*, Vol. 28, No. 1, pp. 1–8, Jan. 1980.
- [166] G. M. Lambrinou and C. S. Aitchison, "Optimization of third-order intermodulation product and output power from an X-band MESFET amplifier using Volterra series analysis," *IEEE Transactions on Microwave Theory and Techniques*, Vol. 33, No. 12, pp. 1395–1403, Dec. 1985.

BIBLIOGRAPHY

- [167] N. B. de Carvalho and J. C. Pedro, "Multitone frequency-domain simulation of nonlinear circuits in large- and small-signal regimes," *IEEE Transactions on Microwave Theory and Techniques*, Vol. 46, No. 12, pp. 2016–2023, Dec. 1998.
- [168] S. A. Maas, "Volterra analysis of spectral regrowth," *IEEE Microwave and Guided Waves Letters*, Vol. 7, No. 7, pp. 192–193, Jul. 1997.
- [169] S. Kusunoki, K. Kawakami, and T. Hatsigai, "Load-impedance and bias-network dependence of power amplifier with second harmonic injection," *IEEE Transactions on Microwave Theory and Techniques*, Vol. 52, No. 9, pp. 2169–2176, Sep. 2004.
- [170] Z. Peng, Z. Qin, and W. Siliang, "A novel adaptive digital predistortion for RF power amplifier linearization based on simplified Volterra series," in *IEEE International Symposium on Microwave, Antenna, Propagation, and EMC Technologies For Wireless Communications*, pp. 327–331, 2007.
- [171] A. Samelis and D. Pavlidis, "Mechanisms determining third order intermodulation distortion in AlGaAs/GaAs heterojunction bipolar transistors," *IEEE Transactions on Microwave Theory and Techniques*, Vol. 40, No. 12, pp. 2374–2380, Dec. 1992.
- [172] J. Aikio and T. Rahkonen, "Detailed distortion analysis technique based on simulated large-signal voltage and current spectra," *IEEE Transactions on Microwave Theory and Techniques*, Vol. 53, No. 10, pp. 3057–3066, Oct. 2005.
- [173] R. A. Baki, T. K. K. Tsang, and M. N. El-Gamal, "Distortion in RF CMOS short-channel low-noise amplifiers," *IEEE Transactions on Microwave Theory and Techniques*, Vol. 54, No. 1, pp. 46–56, Jan. 2006.
- [174] A. Ahmed, S. S. Islam, and A. F. M. Anwar, "A temperature-dependent nonlinear analysis of GaN/AlGaIn HEMTs using Volterra series," *IEEE Transactions on Microwave Theory and Techniques*, Vol. 49, No. 9, pp. 1518–1524, Sep. 2001.
- [175] S. S. Islam and A. F. M. Anwar, "Nonlinear analysis of GaN MESFETs with Volterra series using large-signal models including trapping effects," *IEEE Transactions on Microwave Theory and Techniques*, Vol. 50, No. 11, pp. 2474–2479, Nov. 2002.
- [176] E. R. Srinidhi, R. Ma, and G. Kompa, "Volterra-series-based distortion analysis for optimization of out-of-band terminations in GaN HEMT devices," *IEEE Electron Devices Letters*, Vol. 29, No. 1, pp. 24–27, Jan. 2008.

- [177] D. Mirri, F. Filicori, G. Ioculano, and G. Pasini, "A non-linear dynamic model for performance analysis of large-signal amplifiers in communication systems," *IEEE Transactions on Instrumentation and Measurement*, Vol. 53, No. 4, pp. 341–350, Apr. 2004.
- [178] E. N. and, "Accurate RF and microwave system level modeling of wideband nonlinear circuits," in *IEEE MTT-S International Microwave Symposium Digest*, Vol. 1, pp. 79–82, 2000.
- [179] E. Van Den Eijnde and J. Schoukens, "Steady-state analysis of a periodically excited nonlinear system," *IEEE Transactions on Circuits and Systems*, Vol. 37, No. 2, pp. 232–242, Feb. 1990.
- [180] E. Van Den Eijnde and J. Schoukens, "Parameter estimation in strongly nonlinear circuits," *IEEE Transactions on Instrumentation and Measurement*, Vol. 39, No. 12, pp. 853–859, Dec. 1990.
- [181] V. Krozer and H. L. Hartnagel, "Large-signal analysis of nonlinear microwave circuits using modified Volterra series," in *1st International Workshop of the Integrated Nonlinear Microwave and Millimetre Wave Circuits Digest*, pp. 197–211, 1990.
- [182] T. Wang and T. J. Brazil, "Volterra-mapping-based behavioral modeling of nonlinear circuits and systems for high frequencies," *IEEE Transactions on Microwave Theory and Techniques*, Vol. 51, No. 5, pp. 1433–1440, May 2003.
- [183] A. Zhu and T. J. Brazil, "Behavioral modeling of RF power amplifiers based on pruned Volterra series," *IEEE Microwave and Wireless Components Letters*, Vol. 14, No. 12, pp. 563–565, Dec. 2004.
- [184] J. C. Pedro and S. A. Maas, "A comparative overview of microwave and wireless power-amplifier behavioral modeling approaches," *IEEE Transactions on Microwave Theory and Techniques*, Vol. 53, No. 4, pp. 1150–1163, Apr. 2005.
- [185] K. M. Gharaibeh and M. B. Steer, "Modeling distortion in multichannel communication systems," *IEEE Transactions on Microwave Theory and Techniques*, Vol. 53, No. 5, pp. 1682–1692, May 2005.
- [186] A. Zhu, J. C. Pedro, and T. J. Brazil, "Dynamic deviation reduction-based Volterra behavioral modeling of RF power amplifiers," *IEEE Transactions on Microwave Theory and Techniques*, Vol. 54, No. 12, pp. 4323–4332, Dec. 2006.
- [187] A. Zhu, J. C. Pedro, and T. R. Cunha, "Pruning the Volterra series for behavioral modeling of power amplifiers using physical knowledge," *IEEE Transactions on Microwave Theory and Techniques*, Vol. 55, No. 5, pp. 813–821, May 2007.

BIBLIOGRAPHY

- [188] T. R. Cunha, J. C. Pedro, and P. M. Cabral, "Desing of a power-amplifier feed-forward RF model with physical knowledge considerations," *IEEE Transactions on Microwave Theory and Techniques*, Vol. 55, No. 12, pp. –, Dec. 2007.
- [189] D. D. Silveira and G. Magerl, "Extraction and improvements of a behavioral model based on the Wiener-Bose structure used for baseband Volterra kernels extraction," in *IEEE MTT-S International Microwave Symposium*, pp. 2007–2010, 2007.
- [190] Z. Madini, A. Bennadji, and E. Ngoya, "A novel extraction technique of long term memory effects in solid state amplifiers based on compund dynamic Volterra models structure," in *IEEE International Symposium on Wireless Communication Systems*, pp. 529–532, 2007.
- [191] D. D. Weiner and J. F. Spina, *Sinusoidal Analysis and Modeling of Weakly Nonlinear Circuits*. Van Nostrand Reinhold, 1980.
- [192] M. J. Madero-Ayora, J. Reina-Tosina, R. Freire-Pérez, and C. Crespo-Cadenas, "Circuit-level simulation of W-CDMA communication systems applied to the analysis of nonlinear distortion," *Microwave and Optical Technology Letters*, Vol. 43, No. 4, pp. 310–314, Nov. 2004.
- [193] S. Sancho, A. Suarez, and J. Chuan, "General Envelope-Transient formulation of phase-locked loops using three time scales," *IEEE Transactions on Microwave Theory and Techniques*, Vol. 52, No. 4, pp. 1310–1320, Apr. 2004.
- [194] E. de Cos, A. Suarez, and S. Sancho, "Envelope Transient analysis of self-oscillating mixers," *IEEE Transactions on Microwave Theory and Techniques*, Vol. 52, No. 4, pp. 1090–1100, Apr. 2004.
- [195] A. Collado, F. Ramirez, A. Suarez, and J. P. Pascual, "Harmonic-Balance analysis and synthesis of coupled-oscillator arrays," *IEEE Microwave and Wireless Components Letters*, Vol. 14, No. 5, pp. 192–194, May 2004.
- [196] K. Kundert, "Simulation methods for the RF integrated circuits," in *Digest of Technical Papers of the IEEE/ACM International Conference on Computer-Aided Design*, pp. 752–765, 1997.
- [197] N. B. G. Rabbat, A. L. Sangiovanni-Vincentelli, and H. Y. Hsieh, "A multilevel Newton algorithm with macromodeling and latency for the analysis of large-scale nonlinear circuits in the time domain," *IEEE Transactions on Circuits and Systems*, Vol. 26, No. 9, pp. 733–742, Sep. 1979.

- [198] M. M. Gourary, S. G. Rusakov, S. L. Ulyanov, M. M. Zharov, K. K. Gullapalli, and B. J. Mulvaney, "A new technique to exploit frequency domain latency in Harmonic Balance simulators," in *Proceedings of the Asia and South Pacific Design Automation Conference*, Vol. 1, pp. 65–68, 1999.
- [199] J. F. Oliveira and J. C. Pedro, "An efficient time-domain simulation method for multirate RF nonlinear circuits," *IEEE Transactions on Microwave Theory and Techniques*, Vol. 55, No. 11, pp. 2384–2391, Nov. 2007.
- [200] P. Peng, P. J. McCleer, and G. I. Haddad, "Nonlinear models for the intermodulation analysis of FET mixers," *IEEE Transactions on Microwave Theory and Techniques*, Vol. 43, No. 5, pp. 1037–1045, May 1995.
- [201] D. Shmilovitz, "On the definition of Total Harmonic Distortion and its effects on measurement interpretation," *IEEE Transactions on Power Delivery*, Vol. 20, No. 1, pp. 526–528, Jan. 2005.
- [202] Agilent Technologies, *The Microwave Transition Analyzer: A versatile Measurement Set for Bench and Test*, 1991. Product Note 70820-1.
- [203] Agilent Technologies, *Agilent Nonlinear Vector Network Analyzer (NVNA)*, 2008. Brochure.
- [204] N. B. Carvalho, K. A. Remley, D. Schreurs, and K. G. Gard, "Multisine signals for wireless system test and design," *IEEE Microwave Magazine*, Vol. 9, No. 3, pp. 122–138, Jun. 2008.
- [205] Rohde & Schwarz, *R&S Transfer Toolbox for Matlab*, 2005. Application Note 1GP60-1E.
- [206] J. S. Kenney, *Nonlinear Microwave Measurement and Characterization*, Chap. 4.4. CRC Press, 2001.
- [207] H. C. Ku, M. D. McKinley, and J. S. Kenney, "Quantifying memory effects in RF power amplifiers," *IEEE Transactions on Microwave Theory and Techniques*, Vol. 50, No. 12, pp. 2843–2849, Dec. 2002.
- [208] H. C. Ku and J. S. Kenney, "Behavioral modelling of nonlinear RF power amplifiers considering memory effects," *IEEE Transactions on Microwave Theory and Techniques*, Vol. 51, No. 12, pp. 2495–2504, Dec. 2003.
- [209] J. P. Martins, P. M. Cabral, N. B. Carvalho, and J. C. Pedro, "A metric for the quantification of memory effects in power amplifiers," *IEEE Transactions on Microwave Theory and Techniques*, Vol. 54, No. 12, pp. 4432–4439, Dec. 2006.

BIBLIOGRAPHY

- [210] T. Liu, S. Boumaiza, A. B. Sesay, and F. M. Ghannouchi, "Quantitative measurements of memory effects in wideband RF power amplifiers driven by modulated signals," *IEEE Microwave and Wireless Components Letters*, Vol. 17, No. 1, pp. 79–81, Jan. 2007.
- [211] W. R. Curtice, "A MESFET model for use in the desing of GaAa integrated circuits," *IEEE Transactions on Microwave Theory and Techniques*, Vol. 28, No. 5, pp. 448–456, May 1980.
- [212] H. Statz, P. Newman, I. W. Smith, R. A. Pucel, and H. A. Haus, "GaAa FET device and circuit simulation in SPICE," *IEEE Transactions on Electron Devices*, Vol. 34, No. 2, pp. 160–168, Feb. 1980.
- [213] A. Materka and T. Kacprzak, "Computer calculation of large-signal GaAs FET amplifier characteristics," *IEEE Transactions on Microwave Theory and Techniques*, Vol. 33, No. 2, pp. 129–135, Feb. 1985.
- [214] T. Liu, S. Boumaiza, and F. M. Ghannouchi, "Deembedding static nonlinearities and accurately identifying and modeling memory effects in wide-band RF transmitters," *IEEE Transactions on Microwave Theory and Techniques*, Vol. 53, No. 11, pp. 3578–3587, Nov. 2005.
- [215] D. Wisell and M. Isaksson, "Derivation of a behavioral RF power amplifier model with low normalized mean-square error," in *Proceedings of the 37th. European Microwave Conference*, 2007.
- [216] O. Hammi, F. M. Ghannouchi, and B. Vassilakis, "A compact envelope-memory polinomial for RF transmitters modeling with application to baseband and RF-digital predistortion," *IEEE Microwave and Wireless Components Letters*, Vol. 18, No. 5, pp. 359–361, May 2008.
- [217] J. Vuolevi, J. Manninen, and T. Rahkonen, "Cancelling the memory effects in RF power amplifiers," in *IEEE International Circuits and Systems Symposium*, pp. 57–60, 2001.
- [218] P. M. McIntosh and C. M. Snowden, "The effect of a variation in tone spacing on the intermodulation performance of class A and class AB HBT power amplifiers," in *IEEE MTT-S International Microwave Symposium Digest*, pp. 371–374, 1997.
- [219] N. B. Carvalho and J. C. Pedro, "Two-tone IMD asymmetry in microwave power amplifiers," in *2000 IEEE MTT-S International Microwave Symposium Digest*, pp. 445–448, 2000.

- [220] P. Colantonio, F. Giannini, E. Limiti, A. Nanni, V. Camarchia, V. Teppati, and M. Pirola, "Linearity and efficiency optimization in microwave power amplifier desing," in *Proceedings of the 37th European Microwave Conference*, pp. 1081–1084, 2007.
- [221] I. Takenaka, K. Ishikura, H. Takahashi, K. Hasegawa, K. Asano, and N. Iwata, "Improvement of intermodulation distortion asymmetry characteristics with wideband microwave signals in high power amplifiers," *IEEE Transactions on Microwave Theory and Techniques*, Vol. 56, No. 6, pp. 1355–1363, Jun. 2008.
- [222] V. Camarchia, F. Cappelluti, M. Pirola, S. D. Guerrieri, and G. Ghione, "Self-consistent electrothermal modeling of class A, AB, and b power GaN HEMTs under modulated RF excitation," *IEEE Transactions on Microwave Theory and Techniques*, Vol. 55, No. 9, pp. 1824–1831, Sep. 2007.
- [223] C. Camacho-Peñalosa and C. S. Aitchison, "Modeling frequency dependence of output impedance of a microwave MESFET at low frequencies," *Electronic Letters*, Vol. 21, No. 12, pp. 528–529, Jun. 1985.
- [224] Y. Hasumi, N. Matsanaga, T. Oshima, and H. Kodera, "Characterization of the frequency dispersion of transconductance and drain conductance of GaAs MESFET," *IEEE Transactions on Electron Devices*, Vol. 50, No. 10, pp. 2032–2038, Oct. 2003.
- [225] A. E. Parker and J. G. Rathmell, "Measurement and characterization of HEMT dynamics," *IEEE Transactions on Microwave Theory and Techniques*, Vol. 49, No. 11, pp. 2105–2111, Nov. 2001.
- [226] S. S. Islam and A. F. M. Anwar, "Temperature-dependent nonlinearities in GaN/AlGaN HEMTs," *IEEE Transactions on Electron Devices*, Vol. 49, No. 5, pp. 710–717, May. 2002.
- [227] T. Fernández, Y. Newport, J. M. Zamanillo, A. Tazón, and A. Mediavilla, "Extracting a bias-dependent large signal MESFET model from pulsed I/V measurements," *IEEE Transactions on Microwave Theory and Techniques*, Vol. 44, No. 3, pp. 372–378, Mar. 1996.
- [228] A. Santarelli, G. Zucchelli, R. Paganelli, G. Vannini, and F. Filicori, "Equivalent-voltage approach for modelling low-frequency dispersive effects in microwave FETs," *IEEE Microwave and Wireless Components Letters*, Vol. 12, No. 9, pp. 339–341, Sep. 2002.

BIBLIOGRAPHY

- [229] V. J. Cojocaru and T. J. Brazil, "A scalable general-purpose model for microwave FETs including DC/AC dispersion effects," *IEEE Transactions on Microwave Theory and Techniques*, Vol. 45, No. 12, pp. 2248–2255, Dec. 1997.
- [230] J. M. Golio, M. G. Miller, G. N. Maracas, and D. A. Johnson, "Frequency-dependent electrical characteristics of GaAs MESFET's," *IEEE Transactions on Electron Devices*, Vol. 37, No. 5, pp. 1217–1227, May. 1990.
- [231] G. Rafael-Valdivia, R. Brady, and T. J. Brazil, "Single function drain current model for MESFET/HEMT devices including pulsed dynamic behavior," in *IEEE MTT-S International Microwave Symposium Digest*, pp. 473–476, 2006.
- [232] M. Lee and L. Forbes, "A self-backgating GaAs MESFET model for low frequency anomalies," *IEEE Transactions on Electron Devices*, Vol. 37, No. 10, pp. 2148–2156, Oct. 1990.
- [233] I. Angelov, A. Inoue, T. Hirayama, D. Schreurs, and J. Verspecht, "On the modelling of high frequency and high power limitations of FETs," in *Workshop on Integrated Nonlinear Microwave and Millimetre-Wave Circuits Proc.*, 2004.
- [234] R. Brady, G. Rafael-Valdivia, and T. J. Brazil, "Single function drain current model for MESFET/HEMT devices including pulsed dynamic behavior," in *IEEE MTT-S International Microwave Symposium Digest*, pp. 593–596, 2007.

LIST OF ABBREVIATIONS AND SYMBOLS

3GPP	3rd Generation Partnership Project
\angle	Phase of a complex quantity
$\Re[\cdot]$	Real part
Δf	Frequency spacing between tones
α	Dummy variable, large-signal current model parameter
β, λ	Large-signal current model parameters
$\delta(\cdot)$	Dirac's delta function
$\varepsilon(V)$	Error function
γ	Coefficients for the IMD modelling following a SN approach
ν, ξ	Frequency variables
ϕ, φ, ψ	Phases
Γ	Transformation matrix from time domain to frequency domain
τ	Time delay or Bound variable
ω	Angular frequency in radians
Ω	Vector of angular frequencies in radians
ac	Alternating Current
ACLR	Adjacent Channel Leakage Power Ratio
ACP	Adjacent Channel Power
$ACP_{nl/u}$	Lower or Upper n-th Adjacent Channel Power
ACPR	Adjacent Channel Power Ratio
$ACPR_T$	Total Adjacent Channel Power Ratio
$ACPR_L$	Adjacent Channel Power Ratio Lower
$ACPR_U$	Adjacent Channel Power Ratio Upper
ACP_{SP}	Spot Adjacent Channel Power
ADS	Advanced Design System (Agilent's software)
AM	Amplitude Modulation

AM-AM	Amplitude Modulation to Amplitude Modulation Conversion
AM-PM	Amplitude Modulation to Phase Modulation Conversion
APFT	Almost-Periodic Fourier Transform
B	Bandwidth
C_{ds}	Drain-to-source capacitance
C_{gd}	Gate-to-drain capacitance
C_{gs}	Gate-to-source capacitance
C_{pg}	Gate parasitic capacitance
C_{pd}	Drain parasitic capacitance
CAD	Computer Aided Design
CDMA	Code Division Multiple Access
CPU	Central Processing Unit
CW	Continuous Wave
D	Drain node in a FET
dc	Direct Current
D_{gd}	Gate-to-drain diode
D_{gs}	Gate-to-source diode
DFT	Discrete Fourier Transform
DSB-SC	Double-sideband Suppressed-Carrier
DSP	Digital Signal Processor
DUT	Device Under Test
EC	Envelope Currents
E-PHB	Extended Parametric Harmonic Balance
ET	Envelop [sic] Transients
EVM	Error Vector Magnitude
f	Frequency
f_c	Carrier frequency
f_m, f_o	Modulation frequency
f_m	Result frequency from the frequency mix \mathbf{m}
\mathbf{f}_m	Frequency vector for the frequency mix \mathbf{m}
\mathbf{f}_n	Frequency vector with length n
$(f)_\mu$	Chain with μ arguments $\underbrace{f, f, \dots, f}_\mu$
f_T	Test window frequency position
$f(x)$	Generic Function of x
$\mathcal{F}[\cdot]$	Fourier transform
$\mathcal{F}_D[\cdot]$	Discrete Fourier transform
$\mathbf{F}(\mathbf{V})$	Current-Error Vector in Harmonic Balance
FET	Field Effect Transistor

FFT	Fast Fourier Transform
G	Gate node in a FET
g_{ds}, g_{01}	Output conductance
g_k	Coefficients of the power series expansion of an element depending on one voltage
g_{kl}	Coefficients of the power series expansion of an element depending on two voltages
\mathbf{G}_{kl}	Conversion matrix associated to g_{kl}
g_m, g_{10}	Transconductance
GaAs	Gallium Arsenide
GaN	Gallium Nitride
GPIB	General Purpose Interface Bus
GSM	Global System for Mobile Communications
h	Harmonic under consideration
H	Total number of harmonics
$H(f)$	Linear transfer function
$H_n(\mathbf{f}_n)$	Nonlinear transfer function of order n
$\overline{H_n(\mathbf{f}_n)}$	Symmetrised nonlinear transfer function of order n
HB	Harmonic Balance
HB-N	Harmonic Balance using Newton Raphson algorithm or Harmonic Newton
HB-R	Harmonic Balance using relaxation methods or Harmonic Relaxation
HEMT	High Electron Mobility Transistor
HFET	Heterostructure FET (Field Effect Transistor)
I_d, i_d	Drain current
IDFT	Inverse Discrete Fourier Transform
I_{ds}, i_{ds}	Drain-to-source current
I_{dss}	Maximum drain-to-source current
IF	Intermediate Frequency
$i_L(t)$	Linear subcircuit current in the time domain
$I_L(f)$	Linear subcircuit current in the frequency domain
IM	Intermodulation
IM3	Third-order Intermodulation Product
IM _{3l}	Third-order Lower Intermodulation Product
IM _{3u}	Third-order Upper Intermodulation Product
IM5	Fifth-order Intermodulation Product
IM _n	n -th order Intermodulation Product
IMl	Lower Intermodulation Product

IMD	Intermodulation Distortion
$I_n(h)$	h -th harmonic component of the linear current for the n -th iteration
$\hat{I}_n(h)$	h -th harmonic component of the nonlinear current for the n -th iteration
IMR	Intermodulation Ratio or Signal-to-Intermodulation Distortion Ratio
IMu	Upper Intermodulation Product
$i_{NL}(t)$	Nonlinear subcircuit current in the time domain
\mathbf{i}_{NL}, \hat{I}	Nonlinear currents vector in the time domain
$I_{NL}(f)$	Nonlinear subcircuit current in the frequency domain
\mathbf{I}_{NL}	Nonlinear currents vector in the frequency domain
$i_{NLn}(t)$	n -th order nonlinear current in the time domain
$I_{NLn}(f)$	n -th order nonlinear current in the frequency domain
IP ₃	Third-order Intercept Point
IP ₂	Second-order Intercept Point
IP ₅	Fifth-order Intercept Point
IP ₇	Seventh-order Intercept Point
I_s, i_s	Source current
$\mathbf{J}(\mathbf{V}), \mathbf{J}$	Jacobian matrix
k	Derivative order and bound variable
l	Derivative order and bound variable
LDMOS	Laterally-diffused MOS (Metal-Oxide-Semiconductor)
L_d	Drain inductance
L_g	Gate inductance
L_s	Source inductance
L _M	Power Amplifier Linearizability under static conditions
LNA	Low Noise Amplifier
LO	Local Oscillator
m	Intermodulation product index and sequence index
\mathbf{m}	Frequency mix vector
M	Total number of terms in Fourier series
MEI	Memory Effect Intensity
MER	Memory Effect Ratio
MESFET	Metal Epitaxial Semiconductor Field Effect Transistor
MHB	Modulation-oriented Harmonic Balance
MIMR	Multitone Intermodulation Ratio
MPDE	Multi-rate Partial Differential Equation
MTA	Microwave Transition Analyser

n	Order, number of iteration, sequence index
NC	Nonlinear Currents
NEC	New Envelope Currents
NEC-M	New Envelope Currents for mixers
NLTF	Nonlinear Transfer Function
NPR	Noise to Power Ratio
NQS	Non-Quasi-Static
NVNA	Nonlinear Vector Network Analyser
\hat{p}	Differential operator
P_{1dB}	1-dB Gain-Compression Power
$P_{adj,L/U}$	Lower or Adjacent Channel Power
P_{in}	Input Power
$P_{l/u}$	Lower or Upper Intermodulation Product Power
P_o, P_{out}	Output Power
$P_{SP,L/U}$	Lower or Upper Spot Power
PC	Personal Computer
PHB	Parametric Harmonic Balance
PLL	Phase Locked Loop
PM	Phase Modulation
PSD	Power Spectral Density
q	Charge
QPSK	Quadrature Phase Shift Keying
R_d	Drain resistance
R_{ds}	Drain-to-source resistance
R_g	Gate resistance
R_{gs}	Gate-to-source resistance
R_i, R_{in}	Intrinsic resistance
R_s	Source resistance
RBW	Resolution Bandwidth
RC	Raised-cosine filter
RC	Resistor Capacitor
RLC	Resistor Inductor Capacitor
RRC	Root-raised-cosine filter
RF	Radio Frequency
RFIC	Radio Frequency Integrated Circuit
S	Source node in a FET
SA	Spectrum Analyser
SNA	Scalar Network Analyser
SFDR	Spurious Free Dynamic Range

SN	Simplified Newton
SNA	Scalar Network Analyser
t	Time variable
T	Time period
TDMA	Time Division Multiple Access
THD	Total Harmonic Distortion
TV-VS	Time-Varying Volterra series
UMTS	Universal Mobile Telecommunications System
$V(t), v(t)$	Voltage in the time domain
$V(f)$	Voltage in the frequency domain
V_d, v_d	Drain voltage
V_{DC}, V_0	Bias or dc voltage
V_{DS}, V_{ds}, v_{ds}	Drain-to-source voltage
V_g, v_g	Gate voltage
V_{GS}, V_{gs}, v_{gs}	Gate-to-source voltage
V_s, v_s	Source voltage
V_t	Threshold voltage
VS	Volterra series
VNA	Vector Network Analyser
VSA	Vector Signal Analyser
VSG	Vector Signal Generator
$x(t), y(t)$	Input and output variables in the time domain
$\tilde{x}(t), \tilde{y}(t)$	Input and output complex envelopes in the time domain
$\tilde{x}(h, t), \tilde{y}(h, t)$	Input and output complex envelopes for the h -th harmonic in the time domain
$X(f), Y(f)$	Input and output variables in the frequency domain
$X_n(f), Y_n(f)$	n -th order nonlinear input and output variables in the frequency domain
$x_n(t), y_n(t)$	n -th order nonlinear input and output variables in the time domain
$\tilde{x}_n(t), \tilde{y}_n(t)$	n -th order nonlinear input and output complex envelopes in the time domain
$\tilde{x}_n(h, t), \tilde{y}_n(h, t)$	n -th order nonlinear input and output complex envelopes for the h -th harmonic in the time domain
$\tilde{X}_n(h, m), \tilde{Y}_n(h, m)$	n -th order nonlinear input and output envelope components for the frequency $h.f_c + m.f_m$
Y	Admittance matrix
$Y_{IM3}(f)$	Output Intermodulation Distortion Power Spectral Density Function

$Y_o(f)$	Output Power Spectral Density Function
$Y_{o,ml}(f)$	Output Power Spectral Density Function after memoryless linearization
$Y_{wd}(f)$	Window Power Spectral Density Function
W	Operation bandwidth
W-CDMA	Wideband CDMA (Code Division Multiple Access)
Z_0	Characteristic impedance
$Z_{eq}, Z_{eq}(\Delta f)$	(Baseband) equivalent impedance
$Z_{g,h}$	Gate impedance for the h -th harmonic
Z_h	Drain impedance for the h -th harmonic
$Z_L, Z_L(f)$	Load impedance
$\bar{Z}_L, \bar{Z}_L(\Delta f)$	Baseband load impedance
$Z_s, Z_s(f)$	Source impedance
Z_{th}	Hypothetical thermal impedance

